IChF
Institute of Physical Chemistry PAS

Host–guest complexes and assemblies based on calix[*n*]arenes: structural diversity and transformations

PhD thesis by

Kateryna Kravets

Prepared under the supervision of

dr hab. Oksana Danylyuk, prof. IPC PAS

A thesis submitted in fulfillment of the requirements for the degree of Doctor of Philosophy

under

Warsaw PhD School in Natural and BioMedical Sciences [Warsaw-4-PhD]

at the Institute of Physical Chemistry, Polish Academy of Sciences

Kasprzaka 44/52,

01-224, Warsaw, Poland

Warsaw, February 2026

The work was financed by the National Science Centre (NCN), under the **PRELUDIUM BIS-1 grant no. 2019/35/O/ST4/01865**

NARODOWE CENTRUM NAUKI

and by the Polish National Agency for Academic Exchange (NAWA) within the Programme for Foreign Doctoral Internships **NAWA PRELUDIUM BIS 1**

NAWA NARODOWA AGENCJA WYMIANY AKADEMICKIEJ

The project was developed within the **Warsaw PhD School in Natural and BioMedical Sciences** (Warsaw-4-PhD Doctoral School) at the Institute of Physical Chemistry, Polish Academy of Sciences

Warsaw-4-PhD Warsaw Doctoral School in Natural and BioMedical Sciences

Dedicated to

My biggest motivation, my husband, Mykola Kravets

ACKNOWLEDGMENT

I extend my heartfelt thanks to my supervisor, **Prof. Oksana Danylyuk**, for her scientific inspiration, valuable advice, continuous encouragement, and patience throughout my doctoral studies. Her constant help and support have had a profound impact on both my research and my personal development.

My deepest thanks go to **Prof. Volodymyr Sashuk**, from the Institute of Physical Chemistry, Polish Academy of Sciences, for his invaluable help with the interpretation of experimental results, insightful discussions, guidance, and inspiring new ideas.

I wish to thank **Dr. Karolina Kędra** (Institute of Physical Chemistry, Polish Academy of Sciences) for performing the TGA–DSC measurements and for her assistance in interpreting the experimental results.

It is my pleasure to thank **Dr. Helena Butkiewicz** from the Faculty of Chemistry, University of Warsaw, for her "unofficial" assistance, valuable advice, and the many happy moments we shared at conferences.

My sincere appreciation goes to all members of **Team 1** at the Institute of Physical Chemistry, Polish Academy of Sciences, for sharing coffee breaks, sweets, and positive energy, which made my time in the laboratory truly enjoyable.

Finally, I wish to express my sincere gratitude to my beloved husband, **Mykola**, who has been a constant source of unwavering motivation, emotional support, and faith in my abilities, even during moments of self-doubt and challenging times. I am also deeply grateful to my parents who always supported my scientific interests and made an initial contribution to their development.

DECLARATION OF ORIGINALITY

I hereby declare that the research included within this thesis was carried out by myself or with the support of others included in the acknowledgments.

I state that I have exercised care to ensure that the work is original and contains no previously published material or was not written by another person, except where citations have been made in the text. To the best of my knowledge, the content provided here does not violate any copyrights.

I accept that the Polish Academy of Sciences has the right to use plagiarism detection software to ensure the thesis's legitimacy.

I certify that no part of my thesis has been or will be submitted for obtaining a degree or diploma by the Institute of Physical Chemistry, Polish Academy of Science, or any other educational institution.

This thesis's copyright rests with the author, and no information derived from it may be published without the author's consent.

Warsaw, February 2026

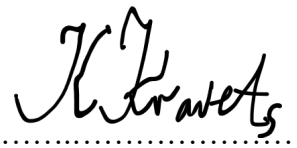

.....

(signature)

LIST OF SCIENTIFIC PUBLICATIONS:

1. **Kravets, K.**; Kravets, M.; Danylyuk, O. Host–Guest Conformational Adaptation in the Crystal Complexes of Pentamidine and *p*-Sulfonatocalix[*n*]arenes. *CrystEngComm* **2025**, *27* (40), 6611–6622. **Featured on the journal cover**.
2. **Kravets, K.**; Kravets, M.; Sashuk, V.; Perret, F.; Maskani, W.; Albertini, D.; Lazar, A. N.; Zimnicka, M.; Danylyuk, O. Alexidine and Pentamidine Fold inside the Bowl-Shaped Cavity of *p*-Sulfonatocalix[4]arene. *Chem. Eur. J.* **2025**, *31* (16), e202404625. **Featured on the journal cover**.
3. **Kravets, K.**; Kravets, M.; Danylyuk, O. Host–Guest Complexes of *p*-Sulfonatocalix[4]arene and Benzamidine: A Matter of Counterion and Aging in the Mother Liquor. *Cryst. Growth Des.* **2024**, *24* (24), 10338–10349.
4. **Kravets, K.**; Kravets, M.; Kędra, K.; Danylyuk, O. *p*-Sulfonatocalix[8]arene Coordinates Sodium Cations and Forms a Host–Guest Complex with Berberine: Insight from the Crystal Structure. *Supramol. Chem.* **2023**, *33* (12), 666–676.
5. **Kravets, K.**; Kravets, M.; Butkiewicz, H.; Kosiorek, S.; Sashuk, V.; Danylyuk, O. Electrostatic Co-Assembly of Pillar[*n*]pyridiniums and Calix[4]arene in Aqueous Media. *CrystEngComm* **2022**, *24* (12), 2213–2216. **Featured on the journal cover**.

LIST OF SCIENTIFIC PRESENTATIONS:

Oral presentations:

1. **Kravets, K.**; Contini, L.; Grepioni, F.; Danylyuk, O. Diversity of the host–guest crystalline assemblies of *p*-sulfonatocalix[*n*]arenes with benzamidines. Young Crystallographers Satellite Meeting, 34th European Crystallography Meeting, University of Padova, 26 August **2024**, Padova, Italy.
2. **Kravets, K.**; Contini, L.; Grepioni, F.; Danylyuk, O. Host–guest assemblies of *p*-sulfonatocalix[*n*]arenes with benzamidines: solution versus slurry crystallization. Sesja Młodych Krystalografów PTKryst, 65th Konwersatorium Krystalograficzne, 26 July **2024**, Wrocław, Poland.
3. **Kravets, K.**; Danylyuk, O. Structural studies of host–guest complexes of sulfonated calixarenes. Sesja Młodych Krystalografów PTKryst, 64th Konwersatorium Krystalograficzne, 6 July **2023**, Wrocław, Poland.
4. **Kravets, K.**; Coleman, A. W.; Suwinska, K.; Danylyuk, O. Host–guest crystals with a flexible structure. Young Crystallographers Satellite Meeting, 33rd European Crystallographic Meeting, Palais des Congrès de Versailles, 23 August **2022**, Versailles, France.
5. **Kravets, K.**; Kravets, M.; Butkiewicz, H.; Kosiorek, S.; Sashuk, V.; Danylyuk, O. Crystalline host–guest complexes of pillar[*n*]pyridiniums and *p*-sulfonatocalix[4]arene. Summer School for PhD Students – Modern Research Techniques for Physicochemical Characterization of the Potential Application Systems, Maria Curie-Skłodowska University, 18–20 May **2022**, Lublin, Poland.

Poster presentations:

1. **Kravets, K.**; Danylyuk, O. Conformational folding of alexidine and pentamidine molecules within the bowl-shaped cavity of *p*-sulfonatocalix[4]arene. 35th European Crystallography Meeting , The Poznań Congress Center,, 25–29 August **2025**, Poznań, Poland.
2. **Kravets, K.**; Danylyuk, O. Diversity of *p*-sulfonatocalix[*n*]arene complexes caused by counterion and crystal “aging” in the mother liquor. The 17th International Seminar on Inclusion Compounds and Porous Materials, Adam Mickiewicz University in Poznań, 2–6 September **2024**, Poznań, Poland.
3. **Kravets, K.**; Contini, L.; Grepioni, F.; Danylyuk, O. Diversity of the host–guest crystalline assemblies of *p*-sulfonatocalix[*n*]arenes with benzamidines. 34th European Crystallography Meeting, University of Padova, 26–30 August **2024**, Padova, Italy.
4. **Kravets, K.**; Contini, L.; Grepioni, F.; Danylyuk, O. Host–guest assemblies of *p*-sulfonatocalix[*n*]arenes with benzamidines: solution versus slurry crystallization. 65th

Konwersatorium Krystalograficzne, Instytut Niskich Temperatur i Badań Strukturalnych PAN (INTiBS PAN), 27–28 January **2024**, Wrocław, Poland.

5. **Kravets, K.**; Danylyuk, O. Host–guest crystals of *p*-sulfonatocalix[*n*]arenes with pentamidine. CrystalForms@Bo, Aula Magna, Department of Chemistry "G. Ciamician", 10–12 September **2023**, Bologna, Italy.

6. **Kravets, K.**; Danylyuk, O. Supramolecular host–guest complexes of pentamidine with *p*-sulfonatocalix[*n*]arenes. 64th Konwersatorium Krystalograficzne, Centrum Kongresowe Politechniki Wrocławskiej, 6–7 July **2023**, Wrocław, Poland.

7. **Kravets, K.**; Danylyuk, O. Supramolecular host–guest complexes of pentamidine with *p*-sulfonatocalix[*n*]arenes. ChemSession'24, Cardinal Stefan Wyszyński University, 23 June **2023**, Warsaw, Poland.

8. **Kravets, K.**; Coleman, A. W.; Suwinska, K.; Danylyuk, O. Host–guest crystals with a flexible structure. 33th European Crystallographic Meeting, Palais des Congrès de Versailles, 23–27 August **2022**, Versailles, France.

9. **Kravets, K.**; Kravets, M.; Butkiewicz, H.; Kosiorek, S.; Sashuk, V.; Danylyuk, O. Crystalline host–guest complexes of pillar[*n*]pyridiniums and *p*-sulfonatocalix[4]arene. 2nd International Conference on Noncovalent Interactions, University of Strasbourg, 18–22 July **2022**, Strasbourg, France.

10. **Kravets, K.**; Kravets, M.; Butkiewicz, H.; Kosiorek, S.; Sashuk, V.; Danylyuk, O. Electrostatic self-assembly of organic crystals from charged macrocycles. Summer School for PhD Students – Modern Research Techniques for Physicochemical Characterization of Potential Application Systems, Maria Curie-Skłodowska University, 18–20 May **2022**, Lublin, Poland.

11. **Kravets, K.**; Kravets, M.; Sashuk, V.; Danylyuk, O. Electrostatic self-assembly of *p*-sulfonatocalix[4]arene and pillar[*n*]pyridiniums into organic crystals. 30th Annual Meeting of the German Crystallographic Society, Ludwig Maximilians Universität, 14–17 March **2022**, Munich, Germany (online).

12. **Kravets, K.**; Sashuk, V.; Danylyuk, O. Electrostatic self-assembly of organic crystals from charged macrocycles. 25th Congress of the International Union of Crystallography, Prague Congress Centre, 14–22 August **2021**, Prague, Czech Republic (online).

Scientific schools:

1. Zurich School of Crystallography, 19–30 June **2022**, Zurich, Switzerland.
2. 6th European Crystallographic School, 4–10 July **2021**, Budapest, Hungary (online).

ABSTRACT

p-Sulfonatocalix[*n*]arenes have long been studied for their host–guest complexation behavior and have found applications in drug delivery, molecular sensing, supramolecular catalysis, and protein crystal engineering, etc. Their attractiveness stems from high aqueous solubility, oligo-anionic charge, conformational flexibility, and low toxicity. In the solid state, multiple sulfonate groups at the macrocyclic rim promote charge-assisted hydrogen bonding and electrostatic interactions, leading to diverse supramolecular synthons and extended multidimensional assemblies. The presence of inner cavities further enables porous material design, including molecular sieving and guest-permeable frameworks. Despite substantial progress in recent decades, many aspects of *p*-sulfonatocalix[*n*]arene complexation and crystallization remain poorly understood due to their pronounced conformational flexibility, especially in larger homologues, and sensitivity to crystallization conditions.

This dissertation aims to establish how host size and flexibility, guest functionalization, solvent composition, and counterions determine the solid-state structure of *p*-sulfonatocalix[*n*]arene complexes. The selected guest molecules include various benzamidine derivatives, which enable highly directional charge-assisted hydrogen bonding via amidinium–sulfonate synthons. Another group of guests comprises species devoid of classical hydrogen-bond donors, including pillar[*n*]pyridiniums and berberine. Structural characterization of host–guest complexes and assemblies was performed by single-crystal X-ray diffraction, supported by PXRD, TGA–DSC, and selected NMR studies in solution.

Across all benzamidine complexes, charge-assisted *N–H···O* hydrogen bonding to anionic sulfonate groups is the dominant host–guest interaction. Host size and conformational freedom strongly influence the complexation mode. Larger calix[6]arene and calix[8]arene adopt multiple conformations that create pseudo-cavities and grooves. These features support multi-guest inclusion, external surface binding, and cooperative host–guest–solvent assemblies. Calixarene counterions, particularly sodium ions, play an important role in determining stoichiometry and supramolecular connectivity. Pronounced guest–solvent competition is observed, and the binding mode (inclusion versus exclusion) can be switched by changing the complexation or crystallization medium. Although many *p*-sulfonatocalix[*n*]arene complexes lose crystallinity upon dehydration, selected frameworks exhibit notable stability and even single-crystal-to-single-crystal transformations, suggesting potential for porous or guest-permeable materials. These outcomes establish design principles for calixarene assemblies and emphasize the usefulness of sulfonated calixarenes as building blocks for supramolecular materials and crystal engineering.

STRESZCZENIE

p-Sulfonatokaliks[*n*]areny oraz ich kompleksy gość–gospodarz są intensywnie badane jako układy supramolekularne, m.in. w dostarczaniu leków, czujnikach molekularnych, katalizie, oraz inżynierii krystalicznej protein. Ich atrakcyjność wynika z dobrej rozpuszczalności w wodzie, giętkości konformacyjnej i niskiej toksyczności. W kontekście inżynierii krystalicznej, liczne grupy sulfonowe osadzone na obrzeżu makrocyklicznym sprzyjają wiązaniom wodorowym (jako ich akceptory) i oddziaływaniom elektrostatycznym, prowadząc do złożonych struktur supramolekularnych. Obecność luk makrocyklicznych potencjalnie umożliwia projektowanie materiałów porowatych. Pomimo znacznych postępów w chemii supramolekularnej *p*-sulfonatokaliks[*n*]arenów, wiele aspektów ich kompleksowania i krystalizacji pozostaje słabo poznanych. Powodem trudności skutecznego projektowania czy przewidywania struktury kompleksów kaliks[*n*]arenów jest ich wysoka giętkość konformacyjna (zwłaszcza większych homologów), jak i wysoka wrażliwość na warunki krystalizacji.

Celem przedstawianej rozprawy jest ustalenie, jak wielkość, giętkość konformacyjna oraz przeciw-jony cząsteczek gospodarza, wraz z funkcjonalizacja cząsteczek gościa, wpływają na strukturę kompleksów *p*-sulfonatokaliks[*n*]arenów. W badaniach przebiegu krystalizacji uwzględniono też wpływ składu rozpuszczalnika. Jako cząsteczki gości wybrano liczne pochodne benzamidyny (tworzące kierunkowe wiązania wodorowe), oraz cząsteczki bez klasycznych donorów wiązań wodorowych, jak pillar[*n*]pirydyny i berberyna. Charakterystyka strukturalna opierała się na metodzie dyfrakcji promieniowania rentgenowskiego na monokryształe, wspieranej rentgenowską dyfrakcją proszkową, analizą termiczna, i spektroskopią NMR w roztworze.

Badania strukturalne pokazały, że we wszystkich kompleksach kaliks[*n*]arenów z pochodnymi benzamidyny dominują wiązania wodorowe *N–H···O* dodatkowo wspomagane ładunkiem. Wykazano, że większe cząsteczki kaliks[6]arenów i kaliks[8]arenów tworzą *pseudo*-wnęki czy rowki na powierzchni, umożliwiając inkluzję wielu gości, kompleksowanie płytkie („powierzchniowe”), czy ansamble potrójne gość–gospodarz–rozpuszczalnik. Przeciw-jony (np. jony sodu) mogą wpływać na stechiometrię i strukturę supramolekularną kompleksów, wbudowując się do sieci krystalicznej. Zaobserwowano konkurencję gość–rozpuszczalnik w stosunku do luki makrocyklicznej kaliks[*n*]arenu, a także wykazano możliwość drastycznej zmiany sposobu kompleksowania poprzez modyfikacje rozpuszczalnika. Chociaż wiele kompleksów na bazie kaliks[*n*]arenów traci krystaliczność pod czas utraty cząsteczek rozpuszczalnika z sieci krystalicznej, wybrane struktury są stabilne, a nawet wykazują przemiany strukturalne typu z kryształu-do-kryształu, co wskazuje na ich potencjał w materiałach

porowatych. Wyniki te stanowią podstawy dla bardziej precyzyjnego projektowania kryształów i układów supramolekularnych na bazie kaliks[*n*]arenów, oraz podkreślają ich wartość jako elementów budulcowych w chemii supramolekularnej i inżynierii krystalicznej.

SHORTCUTS

C*n*S	*p*-sulfonatocalix[*n*]arene
C4S	*p*-sulfonatocalix[4]arene
C6S	*p*-sulfonatocalix[6]arene
C8S	*p*-sulfonatocalix[8]arene
CSD	Cambridge Structural Database
CCDC	Cambridge Crystallographic Data Centre
BNZ	benzamidine
M–BNZ	4-methylbenzamidine
H–BNZ	4-hydroxybenzamidine
A–BNZ	4-aminobenzamidine
IPR	iproniazid
PT	pentamidine
ALEX	alexidine
P[*n*]Ps	pillar[*n*]pyridiniums
P4P	pillar[4]pyridinium
P6P	pillar[6]pyridinium
Berb	berberine
SXRD	Single Crystal X-ray Diffraction
S.O.F	site occupancy factor
TGA–DSC	Thermogravimetric Analysis – Differential Scanning Calorimetry
PXRD	Powder X-Ray Diffraction
NMR	Nuclear Magnetic Resonance
BPE	1,2-bis(4-pyridyl)ethane
bpdo	4,4-dipyridine-N,N-dioxide
SCSC	single-crystal-to-single-crystal transformations
EtOH	ethanol
MeOH	metanol
IPA	isopropanol
Ace	acetone

OUTLINE

1. INTRODUCTION 19
2. LITERATURE REVIEW 22
2.1 Supramolecular host–guest chemistry – "chemistry beyond the molecules" 22
2.2 Intermolecular interactions 23
2.2.1 Electrostatic interactions 23
2.2.1.1 Van der Waals forces 24
2.2.2 π···π Interactions 24
2.2.3 Hydrophobic effect 25
2.2.4 Hydrogen bond 26
2.2.4.1 Crystal engineering 28
2.2.4.2 Supramolecular synthons 29
2.2.5 Coordination complexes 30
2.3 Macrocyclic hosts 31
2.4 Calix[*n*]arenes 32
2.5 *p*-Sulfonatocalix[*n*]arenes 33
2.5.1 Crystal structure of the *p*-sulfonatocalix[4]arene complexes and assemblies 35
2.5.2 Crystal structure of the *p*-sulfonatocalix[6]arene complexes and assemblies 41
2.5.3 Crystal structure of the *p*-sulfonatocalix[8]arene complexes and assemblies 45
2.6 Structural transformations in the macrocycle-based complexes 49
2.7 Guest molecules 51
3. EXPERIMANTAL PART 54
3.1 Single Crystal X-Ray Diffraction (SXRD) 54
3.1.1 Preparation of crystalline complexes 54
3.1.2 Single crystal X-ray diffraction 55
3.1.3 Structure solution and refinement 56
3.1.4 Details on the structure refinement 57
3.1.5 Structural disorder 59
3.1.6 Graphical representation of results 59
3.2 Thermogravimetric Analysis and Differential Scanning Calorimetry (TGA–DSC) 60
3.3 Powder X-Ray Diffraction (PXRD) 61
3.4 Nuclear Magnetic Resonance (NMR) spectroscopy 62
4. RESULTS AND DISCUSSION 63

4.1 *p*-Sulfonatocalix[*n*]arene complexes with benzamidine derivatives 63
4.1.1 C4S complexes with benzamidine: Forms I–V 65
4.1.2 C6S complex with benzamidine 91
4.1.3 C4S complex with 4-methylbenzamidine 97
4.1.4 C6S complex with 4-methylbenzamidine 101
4.1.5 C4S complexes with 4-aminobenzamidine 110
4.1.6 C6S complexes with 4-hydroxybenzamidine 119
4.2 *p*-Sulfonatocalix[*n*]arene complexes with alexidine and pentamidine 126
4.2.1 C4S complex with alexidine 126
4.2.2 C4S complexes with pentamidine 134
4.2.3 C6S complex with pentamidine 156
4.2.4 C8S complex with pentamidine 162
4.3 *p*-Sulfonatocalix[4]arene complexes with pillar[*n*]pyridiniums 174
4.3.1 C4S complex with pillar[4]pyridinium 174
4.3.2 C4S complex with pillar[6]pyridinium 180
4.4 *p*-Sulfonatocalix[8]arene complexes with sodium cations and berberine 185
4.4.1 C8S complex with sodium cations 186
4.4.2 C8S complex with berberine 191
4.5 *p*-Sulfonatocalix[8]arene complexes with iproniazid 199
5. CONCLUSIONS 213
6. REFERENCES 216
7. ANNEX I – the parameters of intermolecular interactions 228

1. INTRODUCTION

Synthetic chemistry traditionally builds molecules by forming strong covalent bonds in a controlled manner. In contrast, living systems assemble functional structures using weak and reversible non-covalent forces. Interactions such as hydrogen bonding, electrostatic attraction, aromatic stacking, hydrophobic effects, and van der Waals forces allow biomolecules to organize into precise architectures. This dynamic assembly is essential for biological functions, including protein folding, enzyme activity, selective recognition, and signal transmission.

Supramolecular chemistry adopts this biological strategy and applies it to synthetic molecules. The field focuses on designing components that can recognize and bind each other through non-covalent interactions, producing organized complexes and larger assemblies. Molecular recognition and assembly are therefore not only a matter of shape complementarity but also the result of a balanced combination of interactions. Modern artificial supramolecular systems often show flexibility, meaning that both the host and the guest may change shape during binding. This adaptive behavior is described by models such as lock-and-key, induced fit, and conformational selection. In synthetic systems, conformational selection is difficult to observe directly because host and guest structures can interconvert rapidly, making kinetic and structural studies essential for understanding binding mechanisms.

Host–guest complexes are a central concept in supramolecular chemistry. A host provides a defined environment that selectively accommodates a guest, either by fully enclosing it (inclusion) or by interacting at the surface (exclusion). The binding mode depends on the size, shape, and chemical compatibility of the components, as well as the balance of non-covalent forces. Macrocyclic hosts such as cyclodextrins, cucurbiturils, pillararenes, and calixarenes are widely used because their cavities offer predictable and versatile binding behavior. These systems have practical applications in drug delivery, sensing, separation, catalysis, promotion of protein assembly, and as crystallization chaperones.

The structure, stability, and selectivity of host–guest complexes arise from a combination of non-covalent forces. Electrostatic interactions between charges or dipoles can provide strong attraction, while van der Waals forces and aromatic stacking contribute additional stabilization. In water, the hydrophobic effect is particularly important, as nonpolar guests are driven into hydrophobic cavities to reduce unfavorable interactions with the solvent. Hydrogen bonding adds directionality and specificity, often determining the final geometry of the complex. Solvent and temperature further influence these interactions, making supramolecular binding highly context-dependent.

In the solid state, crystal engineering applies the same principles to build ordered materials. Crystals are treated as assemblies of molecules arranged through predictable interaction patterns. Hydrogen bonds are typically the most reliable driving force, but electrostatic and π–π interactions also shape the final packing arrangement. The concept of supramolecular synthons – repeating interaction motifs – allows chemists to design crystals with desired structures and properties.

Among water-soluble macrocycles, *p*-sulfonatocalix[*n*]arenes (C4S, C6S, C8S) are particularly attractive due to their high aqueous solubility, oligo-anionic charge, significant conformational flexibility, and low toxicity. The sulfonate groups enable strong electrostatic binding of cationic guests, while the aromatic cavity supports π–π interactions and the hydrophobic effect. C4S is the smallest and most rigid member, exhibiting affinity toward small cationic guests and forming well-defined assemblies through hydrogen bonding, metal coordination, and inclusion. C6S offers a larger cavity and greater flexibility, enabling medium-sized guests to form extended hydrogen-bond networks. C8S, the largest and most flexible macrocycle, can accommodate bulky or multiple guests and form potentially porous architectures with channels or voids, enabling encapsulation and transport of large multicationic molecules.

The solid-state structural chemistry of the smallest homologue, C4S, is relatively well-explored, ranging from simple inclusion and coordination complexes with organic and inorganic cations to large multicomponent assemblies. In contrast, the solid-state structural chemistry of the larger C6S and C8S macrocycles remains scarce, as their high conformational flexibility presents significant challenges for crystallization. At the same time, the high charge of C6S and C8S, and their ability to adapt their conformation to external variables are advantageous for multivalent complexation and hierarchical assembly. Nevertheless, many aspects of complexation and crystallization of *p*-sulfonatocalix[*n*]arene complexes – even for C4S – remain insufficiently understood. These include the role of the calixarene counterion, the influence of the solvent system on inclusion scenarios and host–guest–solvent assemblies, and the navigation of crystallization landscapes governed by kinetic and thermodynamic pathways.

This dissertation describes solid-state supramolecular complexes and assemblies formed by *p*-sulfonatocalix[*n*]arenes (n = 4, 6, 8) with the aim of addressing these knowledge gaps in supramolecular and crystal engineering based on these macrocyclic hosts. The central objective was to determine how host size and conformational flexibility, guest functionalization (through the introduction of various supramolecular synthons), solvent composition, and crystallization pathways dictate the final solid-state structure. The selected guest molecules include various benzamidine and bis-benzamidine derivatives (such as pentamidine), which enable highly directional charge-assisted

hydrogen bonding via amidinium–sulfonate synthons. Another group of guests comprises species devoid of classical hydrogen-bond donors, including pillar[*n*]pyridiniums and berberine.

Structural characterization of the studied host–guest complexes and supramolecular assemblies relied primarily on single-crystal X-ray diffraction for atomic-level structural elucidation, complemented by microscopic observations of crystal morphology and additional analytical methods such as powder X-ray diffraction and TGA–DSC analysis. For selected host–guest systems, solution complexation studies were also performed using NMR spectroscopy.

The structural studies presented in this dissertation reveal dominant interaction motifs that govern host–guest inclusion versus exclusion complexation, as well as the roles of the calixarene counterion and solvent system in directing supramolecular assembly. These results expand the understanding of structure–property relationships in *p*-sulfonatocalix[*n*]arene systems and highlight their potential for applications in supramolecular crystal engineering, with relevance to (bio)molecular recognition, drug delivery, and the development of porous or permeable supramolecular materials.

2. LITERATURE REVIEW

2.1 Supramolecular host–guest chemistry – "chemistry beyond the molecules"

The central principle of supramolecular chemistry – selective molecular recognition – originates from Emil Fischer's lock-and-key model (1894), which described how enzymes (hosts) specifically bind their substrates (guests) based on complementary shapes.[1] Building on this concept, supramolecular chemistry was formally conceptualized in the late 1960s by Jean-Marie Lehn and co-workers as the "chemistry beyond the molecule", focusing on structures formed *via* non-covalent interactions between molecules or ions.[2] This principle became the basis of modern supramolecular chemistry, where molecules are designed to recognize and bind each other through non-covalent interactions in synthetic systems, such as host–guest complexes and self-assembled structures.[3]

Induced fit and conformational selection are two major mechanisms of molecular recognition, as illustrated in Figure 1. In induced fit, the ligand binds to a receptor in a non-ideal conformation and then induces the receptor to adopt the optimal conformation, so binding precedes structural change. In conformational selection, the receptor exists in a pre-existing equilibrium of conformations, and the ligand selectively binds the conformation that best fits. Conformational selection is well established in biology, where it explains allostery, signal transduction, and the behavior of proteins as conformational ensembles. In synthetic supramolecular systems, induced fit is often assumed, while detailed studies of conformational selection are rare, partly because fast host and guest dynamics often exceed experimental detection limits. Kinetic experiments are therefore critical to distinguish these mechanisms, as conformational selection requires that conformational interconversion occurs independently of ligand binding.[4]

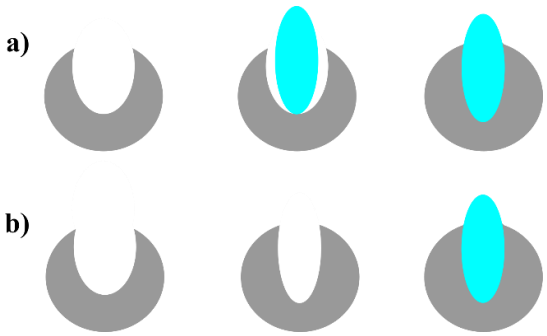

Figure 1. Two pathways of ligand binding: (a) induced fit and (b) conformational selection. Receptor is colored grey, ligand – light blue.

Within the general context of host–guest complexes, the definition proposed by Donald Cram is commonly adopted, describing them as "complexes composed of two or more molecules or ions organized in a unique structural arrangement through intermolecular forces".[5] In such systems, a

larger host molecule provides a well-defined environment capable of selectively accommodating a smaller guest molecule.

The nature of host–guest interactions varies depending on the mode of binding. In *inclusion* complexes, the guest is fully enclosed within the host cavity, whereas in *exclusion* complexes, the guest interacts with the host's external surface without being completely encapsulated. The preference for a particular binding mode is dictated by the geometric and chemical complementarity between host and guest, as well as the combined effects of non-covalent interactions.[6] As an example, among the most extensively studied macrocyclic hosts are cyclodextrins,[7] cucurbiturils,[8] calixarenes[9,10] and pillararenes[11,12] constitute established supramolecular macrocycles capable of encapsulating both organic and inorganic guest species within their cavities, as exampled in Figure 2. Owing to their well-defined and tunable binding properties, host–guest systems based on macrocyclic hosts are currently applied across a wide range of areas, including molecular sensing,[13,14] supramolecular catalysis,[15,16] and targeted drug delivery[17,18].

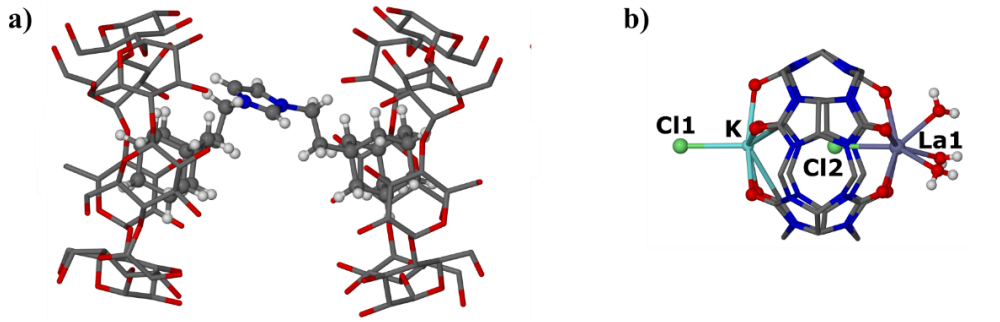

Figure 2. (a) Encapsulation of the organic cation 1,3-bis(2-(adamantan-1-yl)ethyl)imidazolium by β-cyclodextrin (refcode FADFIC)[19]; (b) Chloride anion encapsulated by cucurbit[5]uril molecule capped by two different metal cations (refcode QAGHUD)[20].

2.2 Intermolecular interactions

The formation and behavior of host–guest complexes are determined by a variety of non-covalent forces, including van der Waals and electrostatic attractions, $\pi\cdots\pi$ stacking, hydrophobic effect and hydrogen bonding, among others. The balance and combination of these forces dictate the stability, selectivity, and functionality of the complex, while environmental factors such as solvent and temperature, etc. can additionally influence binding.

2.2.1 Electrostatic interactions

Unlike covalent bonding, which involves electron sharing, electrostatic forces arise from Coulombic attraction between opposite charges or between dipoles. Because the electric field surrounding a charge is uniform in every direction, these interactions lack a specific geometric orientation and are therefore considered non-directional. Depending on the degree of polarization, electrostatic interactions can be categorized into ion–ion (ionic bonds), ion–dipole, and dipole–dipole types. Ion–ion interactions, also referred to as ionic bonds, are the strongest among non-covalent

forces, typically ranging from 200 to 350 kJ·mol^{-1}. They occur widely in inorganic materials such as sodium chloride, as well as in organic structures like carboxylate or amino acid salts. Although non-directional, ionic species often assemble into orderly crystal lattices, driven by the energetic benefit of optimal packing, known as lattice energy. Ion–dipole interactions arise between charged ions and polar molecules – for instance, sodium cations solvated by water and generally fall within 50 to 200 kJ·mol^{-1} in strength. Dipole–dipole interactions are weaker, typically around 5–50 kJ·mol^{-1}, due to the limited extent of polarization involved. The influence of these weak forces can be observed in properties such as the melting point of acetone.[21] Even though a single non-covalent interaction is much weaker than a covalent bond, the combined effect of many such interactions can produce a strong overall binding energy and lead to stable molecular assemblies.

2.2.1.1 Van der Waals forces

Van der Waals forces are weak attractive interactions that act between neutral atoms or molecules, making them a particular set of electrostatic interactions. While classical electrostatic forces arise from permanent charges or dipoles, van der Waals interactions occur when at least one of the interacting partners possesses a temporary dipole. Their average interaction energy is approximately 5 kJ/mol. These forces can be categorized into three types: Keesom interactions (between two permanent dipoles), Debye interactions (between a permanent dipole and an induced dipole), and London dispersion forces (between fluctuating induced dipoles). Keesom interactions arise from the attraction between two permanent, re-orientable dipoles. Their strength decreases with the inverse sixth power of the distance; however, if the dipoles are fixed in space, the interaction energy instead scales with the inverse third power of the distance. Debye interactions occur when a molecule bearing a permanent dipole approaches another molecule lacking one. The permanent dipole distorts the electron distribution of the second molecule, generating an induced dipole that then attracts the first. London dispersion forces occur between molecules that initially lack a permanent dipole moment. Random fluctuations in electron density induce transient dipoles, which interact in a manner analogous to the permanent dipoles in Debye interactions, leading to an attractive force. The strength of these interactions depends largely on the polarizability of the molecular species involved.[22]

2.2.2 π···π Interactions

The Hunter–Sanders model is a fundamental framework for understanding interactions between aromatic systems. According to this model, $\pi\cdots\pi$ interactions come mainly from attractive forces between the electrical quadrupoles of aromatic rings, which reduce the repulsion between their π-electron clouds. These $\pi\cdots\pi$ stacking interactions usually occur between electron-rich and electron-poor aromatic rings.[23]

The strength and properties of $\pi\cdots\pi$ interactions depend on several factors. These include the molecular structure and shape of the molecules, the size and arrangement of their π-electron clouds, the distance between the rings, aromaticity, and the type of substituents present. For strong interactions, the molecules must be arranged so that the π-electron clouds overlap effectively, which makes the interaction stable. Larger π-electron clouds generally lead to stronger interactions because they allow more overlap and attraction.[24–27]

Based on the relative geometry, interactions between two aromatic species can be broadly classified into three main categories: *face-to-face* (sandwiched), *edge-to-face* (T-shaped), and *offset* (parallel displaced) as shown in Figure 3.[28] In the *face-to-face*, the rings are stacked directly on top of each other, resulting in full overlap of the π-electron clouds and consequently strong electrostatic repulsion. In contrast, *edge-to-face* interactions occur when the edge of one ring approaches the face of another at an angle close to 90°, such that the π-electron clouds barely overlap and repulsion is minimal. In this geometry, the partially positive hydrogen atoms at the ring edge interact with the electron-rich π-cloud of the adjacent ring. A phenomenon often described as a $C{-}H\cdots\pi$ interaction. Finally, in offset (parallel displaced) stacking, the rings are laterally shifted, reducing the direct overlap of the π-electron clouds and decreasing repulsion, which makes this arrangement energetically more stable.[29–31] Environmental conditions such as solvent polarity, temperature, and pressure also affect $\pi\cdots\pi$ interactions. In general, non-polar solvents and lower temperatures promote stronger and more stable stacking.[32–34]

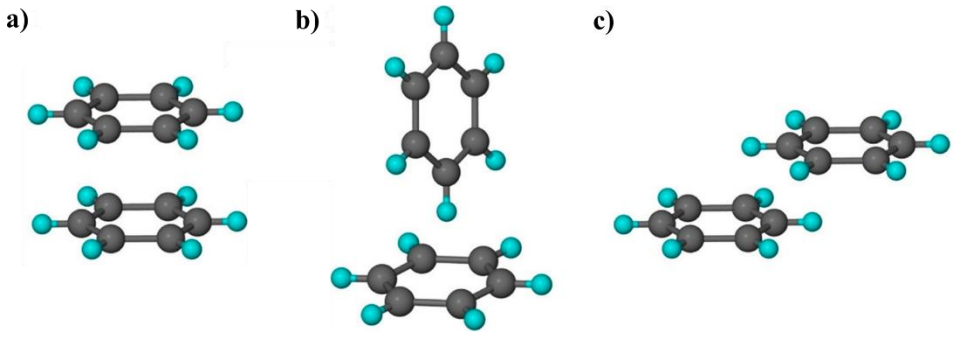

Figure 3. Schematic representation of different types of interactions between aromatic rings (taking benzene rings as an example): (a) face-to-face (sandwich); (b) edge-to-face (T-shaped) and (c) offset interactions.[26]

2.2.3 Hydrophobic effect

The hydrophobic effect is a fundamental thermodynamic principle that significantly influences the formation and stability of host–guest complexes, particularly in aqueous environments. It arises from the tendency of nonpolar molecules to aggregate in water to minimize exposure, driven by their exclusion from the structured water network. In host–guest systems, the host molecule typically provides a hydrophobic cavity that can encapsulate a guest molecule. Upon binding, the guest displaces water molecules from the host cavity, leading to an increase in the entropy of the

surrounding water molecules as they are freed from ordering around the nonpolar guest. Moreover, the presence of both host and guest molecules introduces two distinct "spaces" within the solvent structure. The formation of a host–guest complex reduces the disruption of the solvent network by merging these spaces, thereby lowering the system's free energy and further stabilizing the complex.[35] Figure 4 shows the schematic example of the hydrophobic action during host–guest binding.

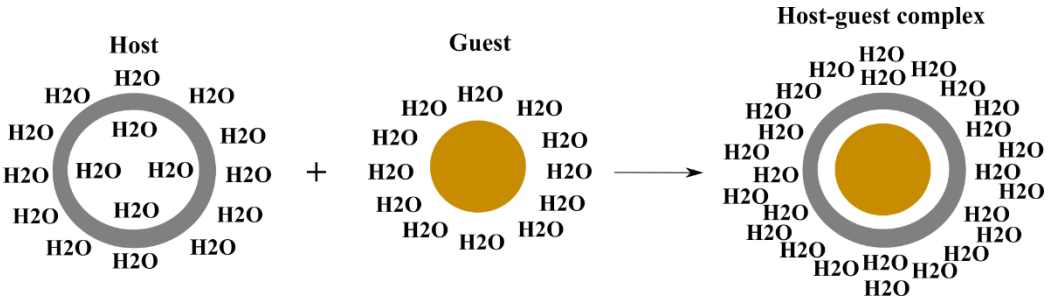

Figure 4. Schematic representation of the hydrophobic effect during host–guest binding.

2.2.4 Hydrogen bond

Hydrogen bond has long been recognized as one of the most important noncovalent interactions, crucial for determining the arrangement and stability of molecules, ions, and supramolecular assemblies.[36–38] The most widely accepted modern definition, recommended by IUPAC, describes the hydrogen bond as "an attractive interaction between a hydrogen atom from a molecule or a molecular fragment *X–H*, in which X is more electronegative than H, and an atom or a group of atoms in the same or a different molecule, in which there is evidence of bond formation." According to this definition, the hydrogen atom is more strongly associated with the donor atom (X) than with the acceptor atom (Y), and the interaction is denoted as *X–H···Y*.[39]

Six criteria are listed that could be used as evidence for the presence of a hydrogen bond. A hydrogen bond of the type *X–H···Y–Z* is formed through electrostatic interactions, charge transfer between the donor and acceptor, and dispersion forces. The X–H bond is covalent and polarized, and the strength of the hydrogen bond increases with the electronegativity of X. Hydrogen bonds are usually nearly linear, with angles close to 180º, and a more linear bond corresponds to a stronger interaction and a shorter *H···Y* distance. Formation of the hydrogen bond often lengthens the X–H bond, leading to a red shift in its infrared stretching frequency and the appearance of new vibrational modes. In NMR spectroscopy, hydrogen bonding causes proton deshielding and may produce spin–spin couplings and nuclear Overhauser enhancements. For the hydrogen bond to be observed experimentally, its Gibbs energy of formation must be larger than the thermal energy of the system.[40] According to the model introduced by Gilli (2000), the known strong and very strong H-bonds can be classified into three fundamental types: negative charge-assisted H-bond [(−)CAHB], positive charge-assisted H-bond [(+)CAHB], and resonance-assisted H-bond [RAHB].[41] There are instances

in which the H-bonding pattern may include more than one donor or acceptor. Such bonds are known as bifurcated H bonds and may describe an instance in which one H-bond donor is bound to two H-bond acceptors (e.g., *C=O···H···O=C*). Another possibility entails the opposite configuration, in which two H-bond donors are bound to a single H-bond acceptor (e.g., *N–H···O···H–N*).[42] The types of geometries of the hydrogen bonding are summarized in Figure 5.

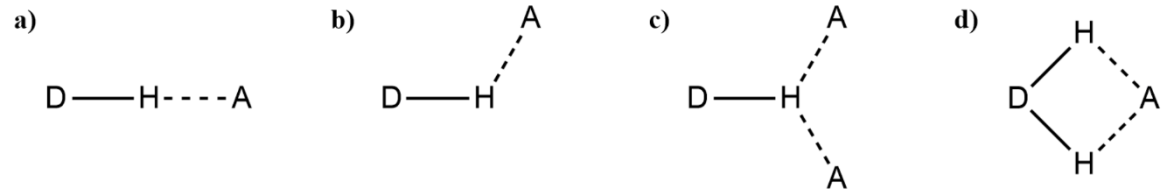

Figure 5. Different types of hydrogen bond geometries: (a) linear; (b) bent; (c) donating bifurcated; (d) accepting bifurcated. D is a donor, A is acceptor.

Hydrogen bonding plays a critical role in determining the structure and properties of many real systems, including water, DNA, and proteins. In water, each molecule can form up to four hydrogen bonds, creating a dynamic three-dimensional network. This network is responsible for many of water's unique properties, such as its high boiling and melting points, large heat capacity, high surface tension, and the unusual density behavior of ice. These properties are essential for life, providing stable aqueous environments for biochemical processes. The cooperative nature of hydrogen bonding in water amplifies these effects, while other interactions, such as van der Waals forces, also contribute to its overall behavior.[43]

Hydrogen bonds between complementary bases in the DNA double helix (adenine–thymine and guanine–cytosine) provide the molecular recognition necessary for accurate genetic information storage and transmission. Although these bonds determine base-pairing specificity, the stability of the helix also relies on base stacking interactions and the surrounding hydration shell. Water molecules positioned in the major and minor grooves form hydrogen-bonded networks that support the helical architecture and influence its conformation, highlighting the cooperative nature of the forces that maintain DNA integrity. Hydration also affects the binding of small molecules, including groove binders and intercalators, by mediating key contacts that influence both affinity and specificity.[44]

A similar interplay of forces is observed in proteins. Hydrogen bonds mainly stabilize secondary structures, such as α-helices and β-sheets, through interactions between backbone NH and C=O groups. While these bonds provide the framework for protein folding, overall stability is determined largely by hydrophobic interactions, van der Waals forces, and the organization of water in the hydration shell. Hydrogen bonds between the protein backbone and surrounding water molecules further regulate folding, flexibility, and stability, demonstrating that the impact of hydrogen

bonding extends beyond the macromolecule to include its dynamic interaction with the solvent environment.[45]

Hydrogen bonding, however, is not always easy to classify strictly. Phrases like "evidence of bond formation" are context-dependent, and electronegativity can vary depending on the local chemical environment. Desiraju described the hydrogen bond as an "interaction without borders" emphasizing that these interactions exist on a continuum, ranging from strong, almost covalent bonds to very weak, van der Waals–like contacts.[46] In host–guest supramolecular chemistry, moderate hydrogen bonds are usually dominant (Table 1).[47]

Table 1. The properties of the strong, moderate and weak hydrogen bonds.

Strength of bond	**Strong**	**Moderate**	**Weak**
Covalency	Pronounced	Weak	Vanishing
Electrostatics	Significant	Dominant	Moderate
Bond energy (kJ/mol)	63–167	17–63	<17
H···A range (Å)	1.2–1.5	1.5–2.2	2.0–3.0
D···A range (Å)	2.2–2.5	2.5–3.2	3.0–4.0
D–H···A bond angle range (˚)	175–180	130–180	90–180
Examples of the bonds	$[F\cdots H\cdots F]^-$ $[N\cdots H\cdots N]^+$ P–OH···O=P	O–H···O=S O–H···O=C N–H···O=C O–H···O–H	C–H···O N–H···F–C O–H···π

2.2.4.1 Crystal engineering

The term *"crystal engineering"* was first introduced by G. M. J. Schmidt in solid-state organic photochemistry.[48] It represents a shift in thinking, seeing crystals not just as packed molecules but as structures formed through specific molecular recognition and self-assembly.

Later developments showed a close connection between crystal engineering and supramolecular chemistry, which studies how discrete molecules organize through non-covalent interactions. In this context, crystalline solids can be seen as unified chemical objects and, in some cases, as supramolecular assemblies or *"supermolecules"*. This view highlights that the properties of crystals depend not only on the molecules themselves but also on the intermolecular interactions that arrange them in three-dimensional space.[49]

Crystallization can be seen as a self-assembly process in which molecules or ions meet and recognize one another, usually in solutions, and pack according to their steric and electronic properties. Aggregates that reach sufficient stability form a nucleus, which then grows by adding more components from the solution. It is important to distinguish this crystal self-assembly from

solution self-assembly, as the two processes differ in their thermodynamic and kinetic characteristics.[50]

Since its early beginnings,[51] crystal engineering has grown into a mature and widely used discipline. Its goals go beyond practical or economic purposes, including aesthetic and scientific curiosity. Today, the field allows both, the rational design of functional solids and the study of structural diversity in the solid state, increasing its scientific and technological importance. Advances in crystal engineering have improved control over structure, stability, porosity, and reactivity, enabling the development of functional materials for applications in chemistry, pharmaceuticals, optics, catalysis, and electronics.

2.2.4.2 Supramolecular synthons

Crystal engineering is the rational design of supramolecular structures through self-assembly, using the principles of supramolecular synthesis. Similar to classical covalent synthesis, which relies on synthons, crystal engineering makes use of supramolecular synthons. According to Desiraju, these are structural units within a crystal (or supermolecule) that can be assembled through known or plausible intermolecular interactions. The main goal of crystal engineering is to identify and design synthons that are reliable enough to be transferred between systems, providing generality and predictability.[52]

Supramolecular synthons are commonly classified as homosynthons, formed between identical functional groups, or heterosynthons, formed between different functional groups (Figure 6). The work of Desiraju, along with studies by Russel *et al.*, established libraries and hierarchical classifications of such synthons in solid-state organic chemistry.[53,54]

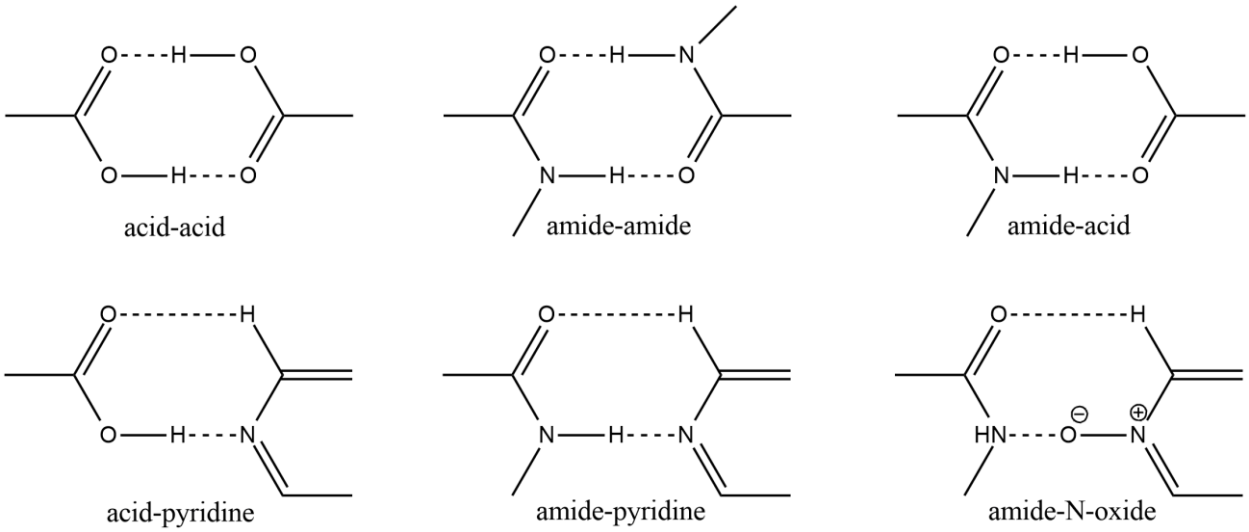

Figure 6. Examples of common strong hydrogen-bonded homo- and hetero-synthons.

Among the noncovalent interactions used in crystal engineering, hydrogen bonding is the most common. Other important interactions include halogen bonding and $\pi\cdots\pi$ interactions between

aromatic rings. In general, molecules in the crystalline state adopt the strongest feasible noncovalent bonds. Overall, supramolecular synthons remain the key design elements for controlling the assembly and structure of organic solids.[52]

The most frequently observed synthons in this study are between the amidinium cations and the sulfonate anions (as seen in benzamidine and pentamidine guests). Amidine is basic and readily protonates even in the presence of weak acids, forming amidinium cations. These cations then interact with oppositely charged functional groups, including carboxyl, phosphate, nitro, or sulfonate groups. The presence of water can also influence synthon formation.[55] Figure 7 illustrates the amidinium formed synthons.

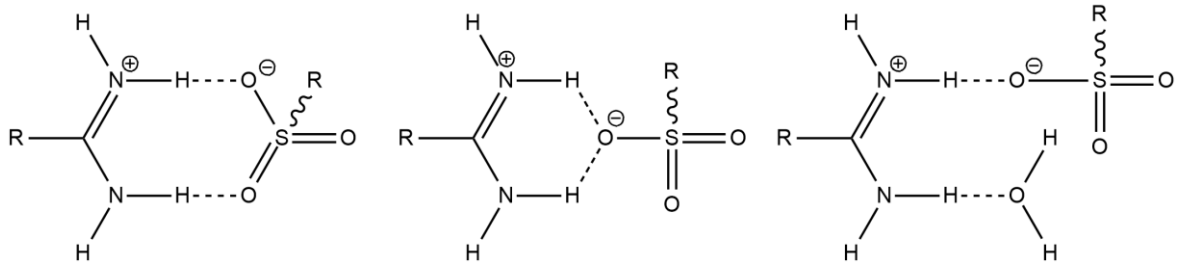

Figure 7. Supramolecular synthons formed by an amidinium cation with (a,b) sulfonate anion, and (c) a ternary synthon involving the sulfonate anion and water.

2.2.5 Coordination complexes

Selective binding occurs when a host and a guest attract each other or have mutual affinity. One important type of selective interaction is coordination binding, which can be traced back to Alfred Werner's 1893 theory of coordination chemistry. This theory describes how metal ions bind to surrounding ligands in regular geometric arrangements through coordinate (dative) bonds. Coordinate bonding occurs when an electron-rich atom donates a lone pair of electrons to a metal ion. These interactions are direction-specific and range from moderate to strong in strength depending on the atom nature, making them essential for the formation of complex ions and coordination compounds. Coordination bonding is widely used in designing ordered structures both in the solid state and in solution.

The nature of bonding in coordination complexes varies. At one extreme, the interaction is mostly ionic, where the ligand's lone pair stabilizes a positively charged metal center without strong orbital overlap. At the other extreme, it can be more covalent, with significant sharing of electron density between metal and ligand orbitals. Most real systems lie between these extremes and contain some non-covalent character. The degree of covalency depends on factors such as the metal ion's charge and size and the ligand's properties. Small, highly charged metal ions, including those with closed-shell configurations like Na^+ or Al^{3+}, tend to form more ionic complexes. The coordination

number and geometry are then determined by how many ligands can effectively surround the metal ion.[56]

Supramolecular coordination complexes (SCCs) are discrete, self-assembled structures formed through highly directional and stoichiometric metal–ligand coordination bonds.[57] They are also called coordination-driven self-assemblies and belong to the broader class of supramolecular structures known as metal-organic complexes (MOCs).[58] SCCs overcome problems associated with supramolecular structures that form through the accumulation of weak noncovalent interactions, such as hydrogen bonds, ion–ion or ion–dipole interactions, donor–acceptor interactions, $\pi\cdots\pi$ stacking, van der Waals forces, or hydrophobic interactions. These problems include instability in various environments, the absence of defect-free final structures, and insufficient control over directionality, which is necessary to form complex, symmetrical, or highly specific architectures.[59,60] SCCs have a wide range of applications, including molecular and guest recognition, supramolecular catalysis, separation, host–guest chemistry, drug delivery, diagnostic and therapeutic agents, sensor systems, stimuli-responsive materials, and many others.[61–63]

2.3 Macrocyclic hosts

Macrocyclic compounds are central to supramolecular chemistry because they can form stable, non-covalent host–guest complexes. Among the most studied macrocyclic hosts are cyclodextrins (CD[*n*]), cucurbit[*n*]urils (CB[*n*]), pillar[*n*]arenes and crown ethers, each distinguished by their unique structures, binding properties, and practical applications. The interactions including hydrogen bonding, electrostatic forces, and hydrophobic effects enable precise molecular recognition and underpin applications in drug delivery[64], sensing, catalysis[15], and materials science[65].

Cyclodextrins are cyclic oligosaccharides composed of glucose units linked *via* α-1,4-glycosidic bonds (Figure 8a). Their truncated cone-shaped structure features a hydrophobic cavity and a hydrophilic exterior, allowing the encapsulation of hydrophobic molecules in aqueous environments. CDs are widely used in pharmaceuticals[66], food[67], and environmental applications[68]. Recent studies also emphasize their role in supramolecular assemblies and recognition.[69,70]

Cucurbit[*n*]urils are rigid macrocycles, symmetrical hosts consist of *n* glycoluril units linked by methylene bridges, forming a hollow cavity with carbonyl-lined portals (Figure 8b).[71] CB[*n*]s bind cationic or neutral guests through hydrophobic effects and ion–dipole interactions, showing exceptional affinity and selectivity. Recent research highlights their applications in molecular recognition[72], drug delivery and stimuli-responsive systems[73,74]

Pillar[*n*]arenes consists of aromatic units linked *via* methylene bridges at the para positions, forming a rigid, pillar-shaped structure (Figure 8c). The cavity size, defined by *n*, controls selectivity

and complexation geometry. These electron rich macrocycles can host a variety of guests through hydrophobic effects, π–stacking, and electrostatic interactions.[75] Recent studies highlight their applications in molecular recognition,[76] drug delivery,[77] smart materials, and sensing[78].

Crown ethers are cyclic polyether's consisting of repeating *–CH₂–CH₂–O–* units arranged in a ring (Figure 8d). Their oxygen atoms coordinate selectively with metal cations, and the ring size determines ion selectivity. Crown ethers are widely applied in phase-transfer catalysis,[79] ion sensing,[80] and molecular recognition[81]. The binding properties of crown ethers arise primarily from ion–dipole interactions between the ether oxygens and guest cations, complemented by conformational flexibility that allows the host to adapt to the guest size.

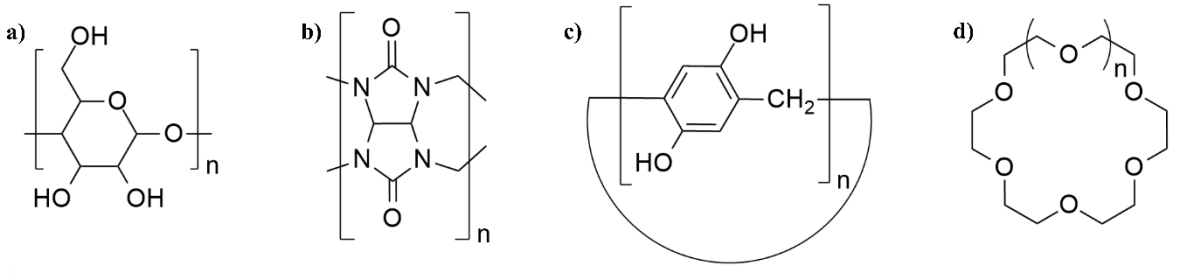

Figure 8. Structure of the macrocyclic hosts: (a) cyclodextrins; (b) cucurbit[n]urils; (c) pillar[n]arenes; (d) crown ethers.[82]

2.4 Calix[*n*]arenes

Over recent decades, calixarenes are the third generation of supramolecular hosts succeeding cyclodextrins and crown ethers, have attracted extensive attention due to their special structures, ease of functionalization, and broad applications.[83]

In the 1940s, Zinke and Ziegler discovered that base-induced reactions of *p*-alkylphenols with formaldehyde produce cyclic oligomers.[84] Then, the synthesis of cyclic oligomers (now known as calix[*n*]arenes) was reported and their structures established by C. David Gutsche and co-workers in the late 1970s.[85] The phenol units in calixarenes are linked by methylene bridges at the meta-positions, typically forming 4, 5, 6, or 8 units (n = 4–8), which results in basket-like macrocyclic structures with well-defined cavities (Figures 9a,b). These cup-shaped calix[*n*]arenes can be conceptually divided into two distinct regions: the lower and upper rims (Figure 9c). The upper rim, located opposite the hydroxyl groups, can be functionalized with a variety of substituents, such as sulfonate, carboxylate, or other polar groups, to modulate the physicochemical properties of the calixarene. Functionalization at this rim primarily enhances water solubility, enabling the formation of aqueous host–guest complexes, and provides additional recognition sites for interactions such as hydrogen bonding, ionic interactions, etc. Furthermore, the size and nature of the substituents on the upper rim regulate the accessibility and steric environment of the cavity, thereby influencing both binding affinity and selectivity.[86]

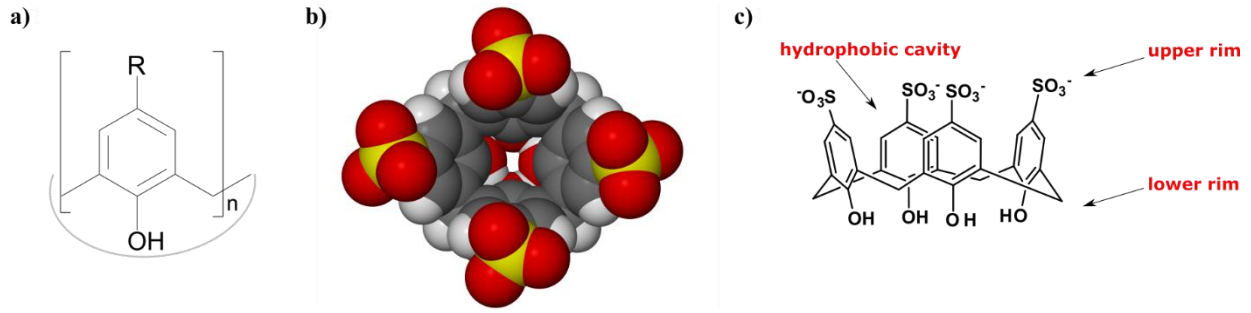

Figure 9. (a) Calix[n]arene structures with R = H, SO_3H, t-C_4H_9, i-C_3H_7, adamantyl, C_6H_5, etc.; (b) hydrophobic basket-like cavity and (c) upper and lower rims positions on the example of the p-sulfonatocalix[4]arene.

In contrast, the lower rim contains phenolic hydroxyl groups (–OH) that form intramolecular hydrogen bonds stabilizing the macrocycle, as well as alkyl or aryl substituents. Phenolic hydroxyl groups (–OH) establish a network of intramolecular hydrogen bonds that sterically influence the macrocyclic conformation (cone, partial cone, 1,2- or 1,3-alternate) and modulate the cavity's shape, flexibility, and host–guest interactions (Figure 10). The hydrophobic interior of the cavity allows calixarenes to encapsulate small molecules, ions, or even neutral organic compounds, facilitating selective host–guest complexation.

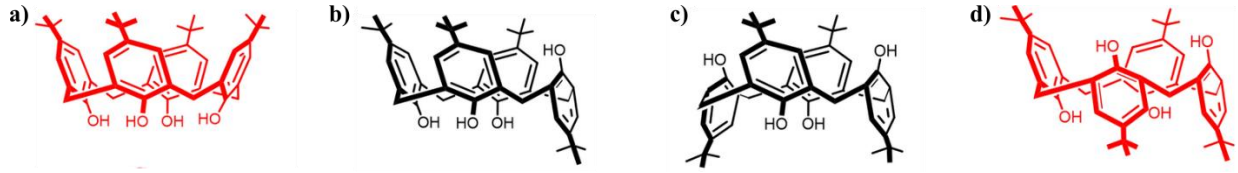

Figure 10. Different conformations of calix[4]arene: (a) cone; (b) partial cone; (c) 1,3-alternate; (d) 1,2-alternate.[87,88]

Together, the complementary roles of the lower and upper rims – structural stabilization and hydrogen bonding at the lower rim, solubility and recognition functionality at the upper rim – underpin the versatility of calix[*n*]arenes in supramolecular host–guest chemistry. As discussed in a recent review, these unique structural features enable calixarenes to selectively bind a wide variety of guest molecules within their hydrophobic cavity, while also forming complexes at both the upper and lower rims, a property that is particularly relevant for applications in biology and medicine.[89] Meanwhile, recent studies[90] provide a comprehensive evaluation of calixarenes, highlighting their evolving role as versatile supramolecular platforms for next-generation applications not only in biomedicine, but also in analytical chemistry, medical imaging, environmental science, and industrial chemistry.

2.5 *p*-Sulfonatocalix[*n*]arenes

The first water-soluble calix[*n*]arene derivative was not obtained until 1984. That same year, Shinkai *et al*. reported the first *p*-sulfonatocalix[*n*]arenes (C*n*S) which represented the earliest examples with high solubility in water.[91]

They are obtained by the electrophilic sulfonation of calix[*n*]arene precursors using concentrated sulfuric acid or Sulphur trioxide-based reagents. This transformation selectively introduces sulfonate groups (–SO_3H / –SO_3^-) at the para positions of each phenolic ring, producing polyanionic macrocycles that preserve the characteristic basket-like conformation of the parent calixarenes (Figure 11). The degree of sulfonation corresponds to the ring size, typically producing *p*-sulfonatocalix[4]arene, [6]arene, or [8]arene in high yield.

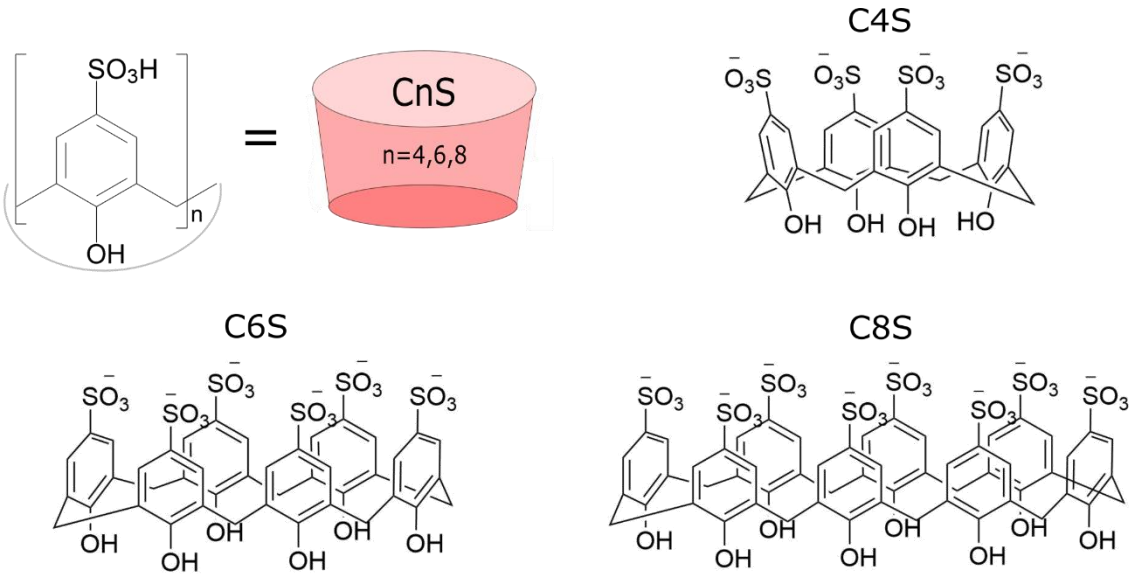

Figure 11. (a) Structures of p-sulfonatocalix[n]arenes with the basket-like conformation: (a) n = 4; (b) n = 6; (c) n = 8.[92]

Electrostatic repulsion between the negatively charged sulfonate groups at the upper rim and the hydroxyl groups at the lower rim stabilizes the cone conformation and limits the conformational flexibility of the macrocycles. This structural rigidity enhances the host–guest binding affinity, particularly for cationic and electron-deficient guests, by providing a preorganized cavity that complements the shape and charge distribution of the guests. This phenomenon has been observed in various studies, including those by Guo *et al*. (2008), who discussed the complex structures and binding behaviors of C*n*S in aqueous solutions.[93]

Since then, C*n*S have demonstrated several advantages over other calixarene derivatives: (1) they can be readily prepared by direct sulfonation of calixarenes at the upper rim; (2) their cavities display strong binding affinity toward guest molecules through hydrophobic and π-stacking interactions, which are more effective in aqueous media than in organic solvents; (3) the sulfonate groups at the upper rim and the hydroxyl at the lower provide binding sites for cations *via* electrostatic interactions, further strengthening host–guest complexation,[94,95] (4) the ability to self-assemble, (5) exhibition of the good water solubility and biocompatibility,[96] both critical for potential biological and pharmaceutical applications.

Because of their distinct water solubility, cavity sizes, framework rigidity, and complexation affinities, C*n*S display unique recognition and assembly behaviors, making them suitable for constructing responsive host–guest systems. C*n*S engage in electrostatic, hydrogen-bonding, and ion–dipole interactions with a broad spectrum of positively charged guests, including alkali metal ions, amino acids,[97,98] alkaloids,[99] peptides,[100] and cationic drug molecules[101]. Although C*n*S were discovered years ago, their functional applications are still being actively studied.

2.5.1 Crystal structure of the *p*-sulfonatocalix[4]arene complexes and assemblies

In 1987, *p*-sulfonatocalix[4]arene (C4S) was first synthesized by Shinkai,[102] and in 1988 Coleman and co-workers[96] reported the first structural investigation of its sodium salt. More than 360 crystal structures (12 of these were determined by me and are described in this dissertation) in the Cambridge Structural Database feature C4S predominantly in the cone conformation, stabilized by circular intramolecular hydrogen bonding at the lower rim (Figure 12a). An interesting exception is a single structure in which C4S adopts the 1,3-alternate conformation, observed in its complex with 4,4-bipyridine crystallized at low pH (Figure 12c).[103] The cone-shaped conformation of C4S may be influenced by guest size and the nature of the host–guest interactions, which can induce "pinching"[104] of the macrocycle (Figure 12b).

C4S, the smallest and most widely studied analogue in the calix[*n*]arene series, possesses a bowl-shaped, π-rich hydrophobic cavity with an anionic hydrophilic sulfonate rim, creating an amphiphilic host that engages in a range of non-covalent interactions, including hydrogen bonding, electrostatic attraction, cation–π, and van der Waals contacts. This dual hydrophobic–hydrophilic character strongly affects host–guest binding: the non-polar cavity facilitates inclusion of suitably sized cationic or neutral guests *via* hydrophobic effects and π-stacking, while the sulfonate groups at the rim promote strong electrostatic and hydrogen bonding interactions with polar and positively charged species. The balance between hydrophobic and hydrophilic interactions influences host–guest recognition, dictating solvent-dependent binding modes and affinities.[101,105–107] Its ease of synthesis, rigid conformation, favorable crystallization properties, and straightforward collection and refinement of single-crystal diffraction data have further contributed to its widespread use.[108,109] C4S participates in diverse supramolecular assemblies, including nanometer-scale spheres and tubules,[110] though it most commonly organizes in bilayers (Figure 12d).[96,111] This versatility has established C4S as a central component in aqueous supramolecular chemistry and crystal engineering, with applications ranging from simple host–guest complexes[112] to advanced drug-delivery systems,[113] sensors,[114] vesicles,[115] crystalline materials,[101] and protein recognition[116].

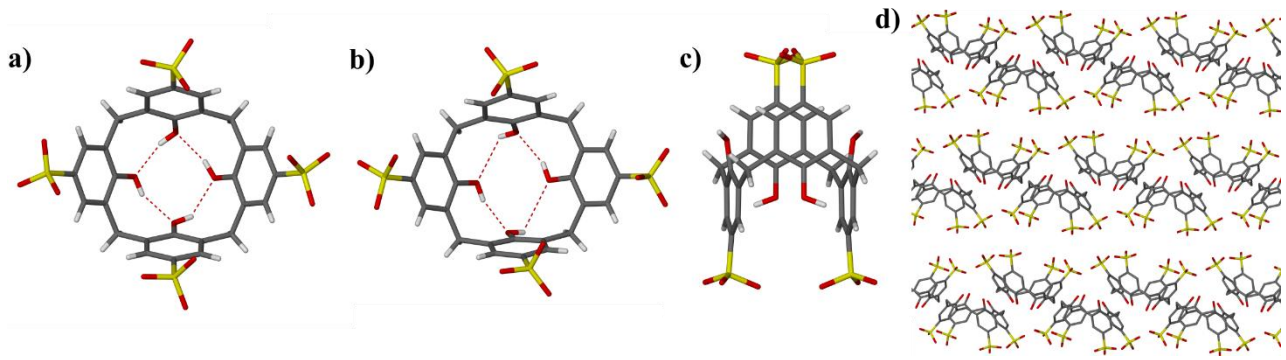

Figure 12. (a) Cone and (b) pinched cone conformations of the C4S with the circular intramolecular hydrogen bonds at the lower rim; (c) 1,3-alternate conformation of the C4S in which this hydrogen bond is absent; (d) bilayer arrangement of the C4S molecules (refcode SAFJEO).[96] *Sodium cations and water molecules omitted for clarity.*

We and others have observed the incorporation of sodium cations, as well as numerous other inorganic ions,[117,118] into C4S crystal complexes with organic cations.[107,119] At neutral to basic pH, C4S exists as a penta-anion and crystallizes as a penta-sodium salt, in which one additional phenolic hydroxyl group is deprotonated (Figure 13a).[96] Two short *O*···*O* distances between oxygen atoms at the lower rim provide clear evidence for the presence of phenol–phenolate charge-assisted hydrogen bonds (Figure 13b). A CSD analysis of phenol–phenolate hydrogen bonds reveals an average *O*···*O*$^-$ distance of 2.528 ± 0.08 Å, which is significantly shorter than the corresponding *O*···*O* distances observed for the phenol–phenol hydrogen-bond homosynthon, averaging 2.812 ± 0.103 Å.[120] Sodium ions bind simultaneously to sulfonate oxygen atoms at the upper rim and phenolic oxygen atoms at the lower rim (Figure 13c). Only a limited number of reported C4S crystal structures exhibit sodium coordination at the lower rim.[121] Such a coordination mode is observed in the ethanol/water solvate of the C4S penta-sodium complex (QADYOK).[122] A similar arrangement is found in the C4S–benzimidazole structure, where sodium coordinates to three phenolic oxygen atoms at the lower rim (JEJMAN).[123] C4S units assemble into bilayers bridged by a Na^+–water coordination network (Figure 13d).

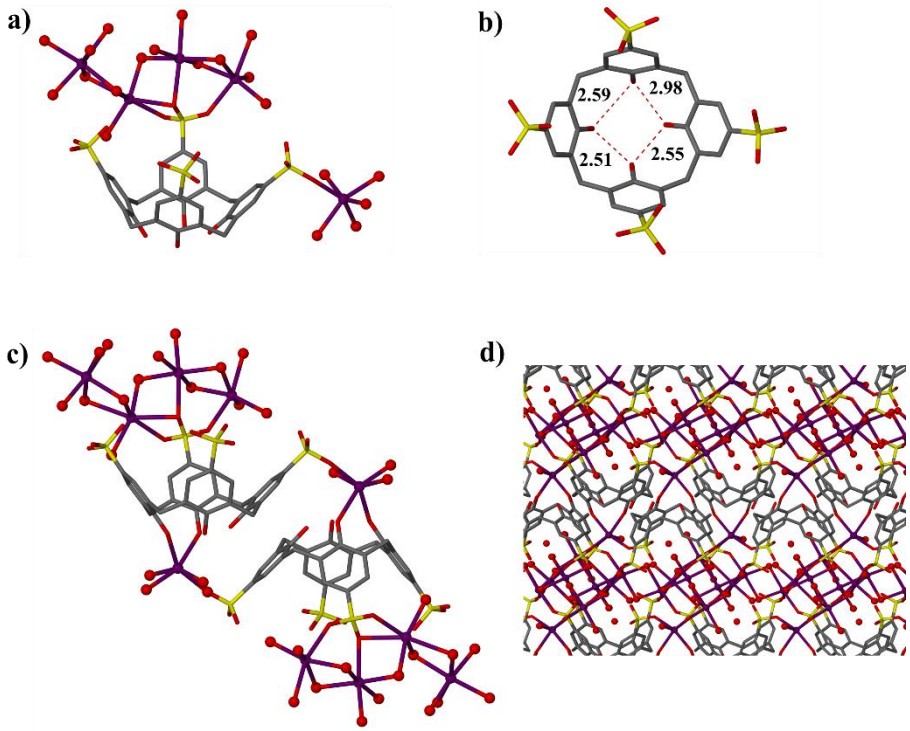

Figure 13. (a) The C4S–5Na⁺ complex (refcode SAFJEO); (b) O–H···O hydrogen bonding at the C4S lower rim with the deprotonation of the one phenolic group; (c) sodium coordination to the upper and lower rims of C4S; (d) crystal packing of the complex along b axis illustrating bilayers of the C4S molecules. Na⁺ cations are colored violet.

Instead, the tetrasodium C4S hydrate exhibits sodium coordination exclusively at the upper rim (Figure 14a).[106] In this structure, the calixarene adopts a pinched conformation and remains fully protonated at the lower rim (phenol–phenol *O···O* distances are in the range 2.77–2.79 Å) (Figure 14b). A single water molecule is included within the hydrophobic C4S cavity (Figure 14c). The primary interaction of this water molecule with C4S occurs through *O–H···π* contacts with the aromatic cavity walls, which are significantly weaker than classical *O–H···O* hydrogen bonds, as reflected by the long contact distances (3.12 and 3.16 Å). Even though the cavity is mostly hydrophobic (aromatic), water can form weak *O–H···π* interactions with the aromatic walls. As observed for the penta-sodium salt, the C4S units assemble into bilayer arrangements, with adjacent layers connected by a Na⁺–water coordination network (Figure 14d).

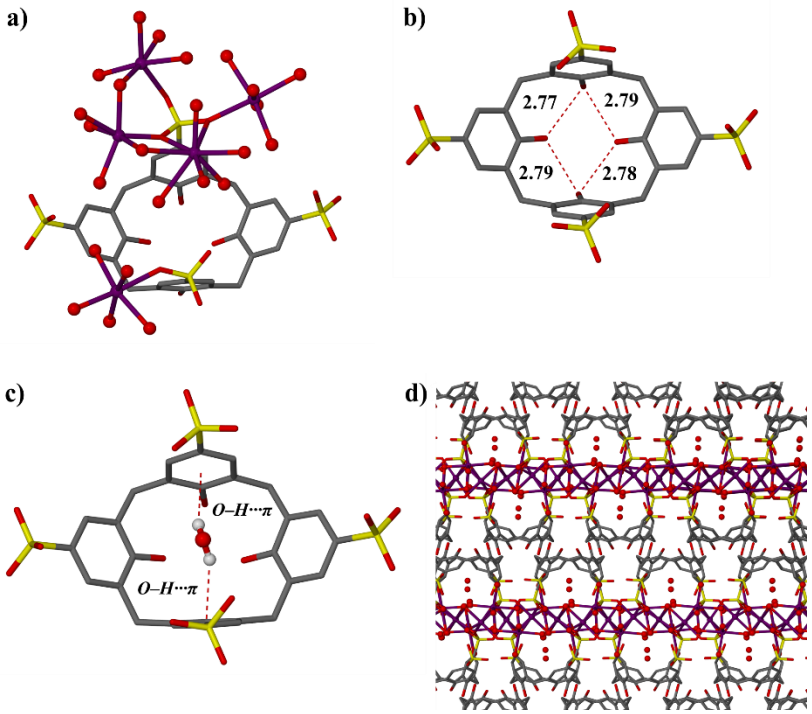

Figure 14. (a) The C4S–4Na$^+$ complex (refcode REBYEE03), four sodium cations are distributed over five sites; (b) O–H···O hydrogen bonding at the C4S lower rim; (c) water inclusion in the C4S hydrophobic cavity via O–H···π interactions; (b)crystal packing of the complex along c axis illustrating bilayers of the C4S molecules. Na$^+$ cations are colored violet.

The C4S cavity can be occupied by water, organic solvent molecules (e.g., ethanol, methanol), or an organic guest, reflecting a competition for the limited cavity space. Danylyuk *et al.* (2015) demonstrated that this competition is controlled by solvent–host and solvent–guest interactions.[124] Crystallization from water favors the formation of an inclusion (endo) complex, in which isoniazid (INH) is encapsulated within the pinched-cone C4S cavity and stabilized by hydrogen bonds with water molecules or the sulfonate groups of the calixarene (Figure 15a). In contrast, crystallization from water–cosolvent (ethanol, methanol, acetone) mixtures leads to exo complexes, in which the cavity is preferentially occupied by the solvent while INH interacts externally with the calixarene through hydrogen bonding and electrostatic interactions (Figure 15b). In this context, the solvent molecules direct the host–guest binding mode.

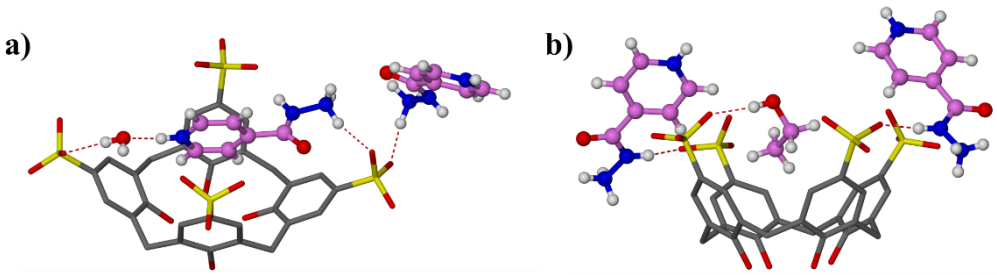

Figure 15. The C4S–isoniazid complexes: (a) C4S–isoniazid complex with the isoniazid molecule included in the cavity; (b) C4S–isoniazid–ethanol complex with the ethanol molecule included in the cavity. The cavity-included solvent and isoniazid molecules are colored pink.

The cup-shaped C4S cavity and the chemical similarity of its endo and exo surfaces enable it to function as a "molecular glue" in protein assembly, allowing multiple proteins to bind simultaneously.[116,125] Crystal structures of protein–C4S complexes offer valuable insights into the interactions between sulfonated (bio)polymers and cationic proteins.[126] C4S has proven to be a particularly versatile host for lysine and arginine recognition in water.[111b,116,127,128] Crystal structure of C4S complex with D-arginine amino acid, revealing a novel packing motif (Figures 16a,b).[128] In this complex, four arginine molecules are included inside the calixarene cavities, while the remaining two occupy independent sites within the cage, still enclosed by the surrounding hosts.

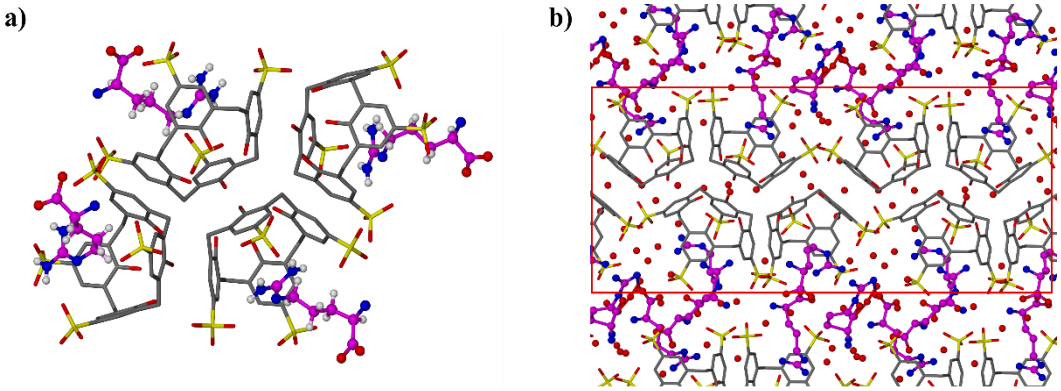

Figure 16. (a) The C4S–D-arginine complex (refcode HAJKIN); (b)crystal packing of the complex along a axis illustrating zig-zag bilayers of the C4S molecules. D-arginine molecules are colored pink.

Xing and co-workers (2018) analyzed the complexation of C4S with the bis-amidine guest terephthalimidamide (Figure 17a).[104] One guest cation sits above the calixarene cavity, forming amidine–sulfonate (*N–H···O*) hydrogen bonds with C4S. Terephthalimidamide cations outside the C4S upper rim link adjacent calixarene units, promoting puckered cationic/anionic layers, within which C4S anions are oriented in opposite directions (Figure 17b).

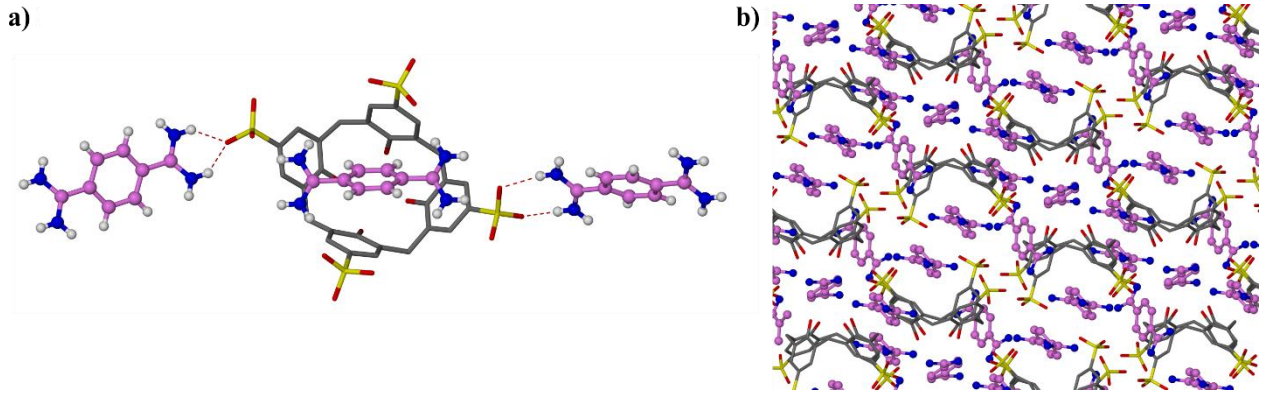

Figure 17. (a) The C4S–terephthalimidamide complex (refcode. HOWHUZ), one terephtalimidamide molecule arranged into the cavity of the calixarene; (b) crystal packing of the complex along c axis. Terephtalimidamide molecules are colored pink.

In the C4S complex with the bis-biguanide antiseptic chlorhexidine, the guest molecule is partially included within the calixarene cavity, adopting a folded, U-shaped conformation (Figure 18a).[129] This conformational change is dictated by the size and shape of the C4S cavity, which

accommodates the central hexyl chain of chlorhexidine molecule while positioning the terminal biguanidinium groups near the upper rim of the host. Stabilization of the folded conformation arises from electrostatic and hydrogen-bonding interactions between the protonated biguanidinium groups of chlorhexidine and the sulfonate groups of C4S. In the crystal packing, the calixarene bowls align in repeating rows to form bilayer-type assemblies, with chlorhexidine molecules occupying the spaces between adjacent layers (Figure 18b).

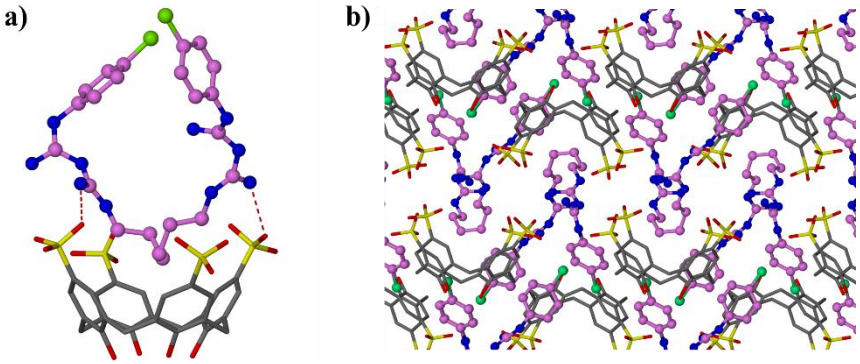

Figure 18. (a) The C4S–chlorhexidine complex (refcode WODGEC), chlorhexidine molecule folding into the cavity of the calixarene; (b) crystal packing of the complex along b axis illustrating host–guest complexation with an "folded" guest in the calixarene bilayers. Chlorhexidine is colored pink.

In C4S complex with the cucurbit[6]uril, two macrocyclicmolecules differ in size and shape, and their co-assembly does not involve direct hydrogen bonding (Figure 19a).[130] Instead, hydrophilic groups on both components are linked indirectly *via* water molecules, which mediate hydrogen-bonding networks and stabilize the structure. When classical $\pi\cdots\pi$ stacking is absent, $C–H\cdots\pi$ interactions support supramolecular assembly (Figure 19b).

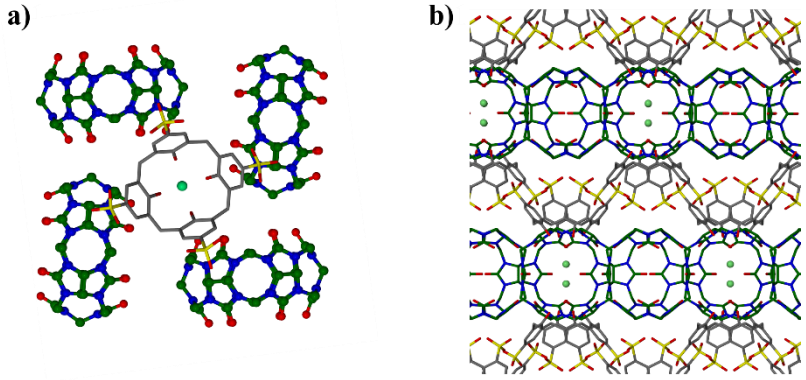

Figure 19. (a) The C4S–cucurbit[6]uril complex (refcode CIYXIS), cucurbit[6]uril molecules surround the calixarene from all sides; (b) crystal packing of the complex along c axis illustrating layered packing. Cucurbit[6]uril molecules are colored green. Water molecule in C4S cavity colored light green.

Two benzimidazole cations are encapsulated by two C4S anions, forming molecular capsules linked *via* sodium cations, as reported by Nichols (2006), shown in Figures 20a,b.[123] Sodium cations connect the adjacent C4S molecules *via* the upper and the lower C4S rims. The typical bilayer

arrangement is absent, as the combination of guest encapsulation and Na^+ coordination disrupts the usual bilayer packing (Figure 20c).

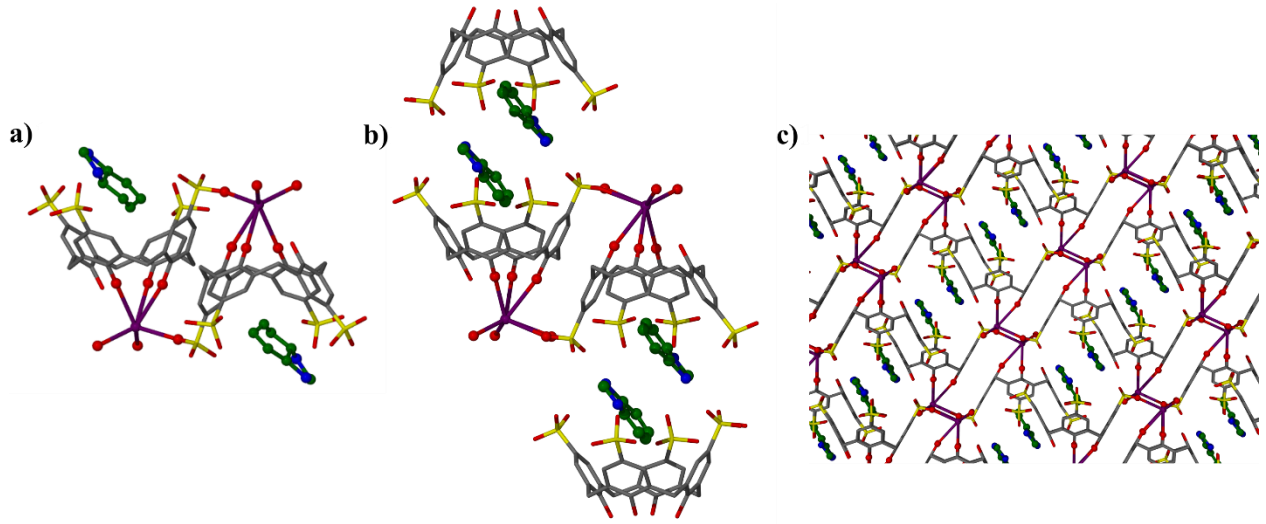

*Figure 20. (a) The C4S–benzimidazole–Na^+ complex (refcode JEJMAN); (b) capsules formed by the calix[4]arene and benzimidazole molecules with the sodium coordination to the upper and lower rims of C4S; (c) crystal packing of the complex along **b** axis. Benzimidazole molecules colored green, Na^+ cations – violet.*

2.5.2 Crystal structure of the *p*-sulfonatocalix[6]arene complexes and assemblies

p-Sulfonatocalix[6]arene (C6S) is the next major member of the *p*-sulfonatocalix[*n*]arene family. Unlike C4S, it is more difficult to assemble into defined supramolecular structures because it carries a higher charge, is more flexible, and crystallizes less readily.[105,131] As a result, the structural behaviour of the larger homologues ($n > 4$) is less predictable, far fewer crystal structures (52 entries, including one reported by me and co-workers), based on C6S have been uploaded to the CSD.

Although the sulfonate and hydroxyl groups of C6S offer multiple oxygen-donor sites that could, in principle, coordinate a wide range of cationic species, this macrocycle has not yet become a common building block in coordination-driven self-assembly. Even so, its structural characteristics make it a promising platform for designing more complex supramolecular architectures. Most advances in C6S chemistry come from the work of Atwood, Raston and co-workers.[132] Although studied far less than C4S, C6S is known to form a variety of structural motifs, including up–down antiparallel bilayers resembling clay-type arrangements,[132a] corrugated bilayers,[132b] extended hydrogen-bonded networks,[132c] molecular capsules,[132d] and ferris-wheel-like aggregates[132e]. These architectures often emerge through interactions with specific guests such as crown ethers, pyridine N-oxide derivatives, 4,4-dipyridine-N,N-dioxide, lanthanide cations, and tetraphenylphosphonium salts. Across the mentioned examples, C6S commonly adopts double cone conformations: an *up–up* double cone conformation or an *up–down* double cone conformation. The *pleated-loop* conformation has been observed in a series of isostructural C6S assemblies with cucurbit[8]uril and metal ions.

The solid-state structure of octa-sodium salt of C6S with two phenolic groups being deprotonated was reported by Atwood *et al*. in 1992 (Figure 21a).[97] In the crystal, the macrocycle adopts an up–down double partial-cone conformation, characterized by a three-up/three-down arrangement of the sulfonate groups. This conformation is stabilized by a network of four strong intramolecular hydrogen bonds between phenolic oxygen atoms (Figure 21c). The Na^+ cations are coordinated to oxygen atoms of the sulfonate groups at the upper rim as well as to phenolate oxygen atoms at the lower rim (Figure 21b). In the crystal packing, the C6S macrocycles are arranged into layers, which are interconnected by Na^+ cations through coordination to sulfonate and phenolate oxygen atoms, thereby linking adjacent layers into a continuous three-dimensional supramolecular network (Figure 21d).

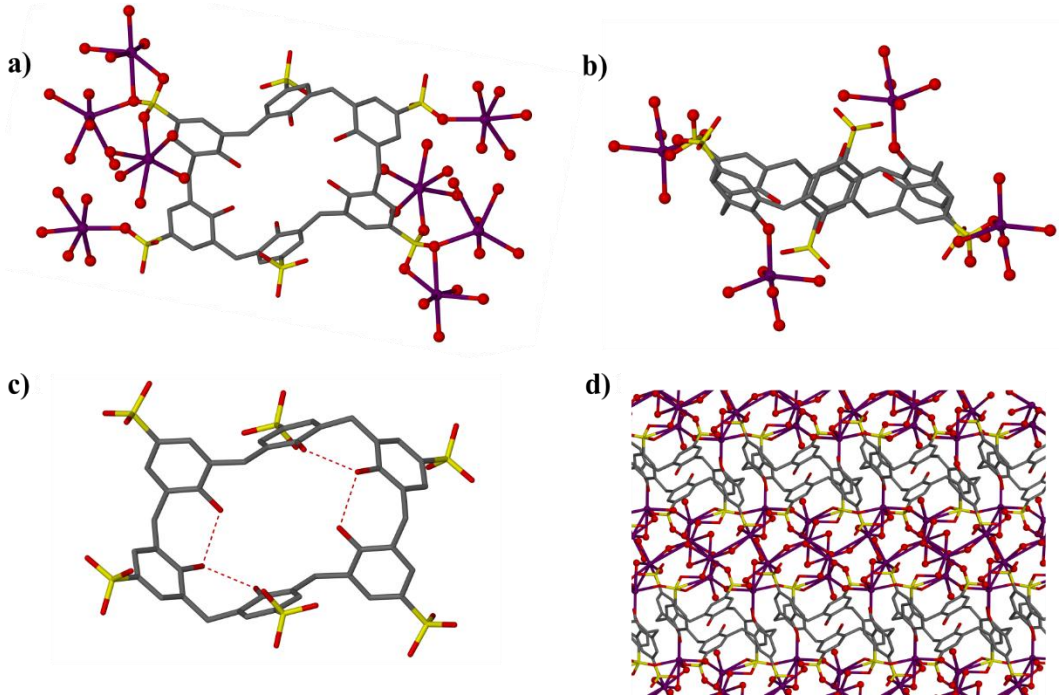

Figure 21. (a) The C6S–Na^+ complex (refcode VUNHAN); (b,c) up–down double partial-cone conformation of the calixarene molecule side and top view; (d) crystal packing of the complex along ***c*** *axis. Sodium cations colored violet.*

Atwood *et al*. (2004) demonstrated that under strongly acidic conditions, C6S selectively incorporates either L- or D-leucine from a racemic mixture to form single crystals. In the crystal, C6S adopts an up–up double cone conformation, in which all aromatic units of the macrocycle tilt upward, forming a symmetrical, open cavity that enables multi-guest inclusion. Two L-leucine molecules are encapsulated, with their hydrophobic side chains extending into opposite cavities of the host, while their polar groups interact with the upper-rim sulfonate functions (Figure 22).[132a]

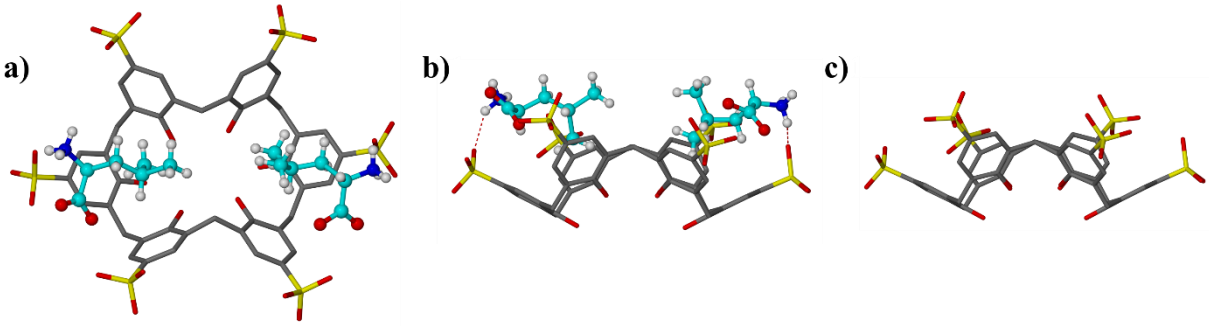

Figure 22. (a) The C6S–leucine complex (refcode FEQYOQ), leucine molecules positioned in the two pseudo calix[3]cavities; (b) leucine molecules connected to the calix[6]arene by N–H···O hydrogen bonds; (c) up–up double cone conformation of the calixarene molecule. Leucine molecules are shown in light blue.

Control over the conformational flexibility of C6S in the solid state is possible in the presence of varied stoichiometric amounts of [18]crown-6 and selected lanthanide(III) chlorides (Figure 23a). Complex **1** with Eu has the C6S in the up–up double cone conformation (Figure 23b) with the two hepta-aqua-europium cations positioned within the two pseudo-calix[3]arene cavities.[132e] One of these cations is coordinated to the calixarene sulfonate group through an Eu–O(S) bond.

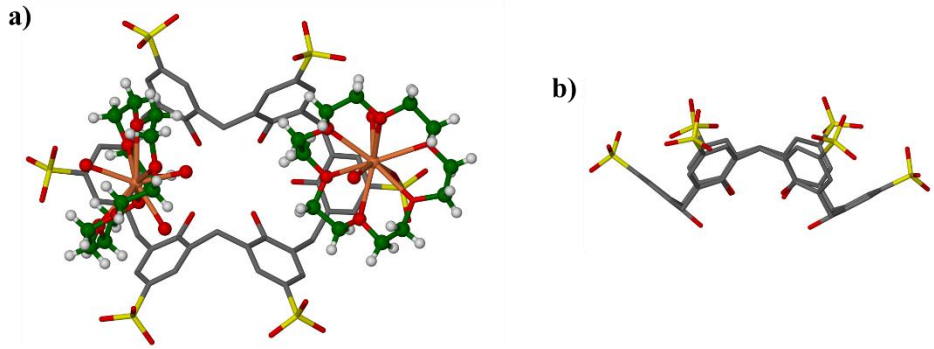

*Figure 23. (a) The C6S–[18]crown-6–Eu complex **1** (refcode TAHDEM), [18]crown-6–Eu molecules are in the grooves of the calixarene; (b) the up–up double cone conformation of the calixarene molecule. [18]crown is colored green, Eu in rude.*

The C6S–[18]crown-6–Eu complex **2** differs from complex 1 (Figure 24a) in that it features [18]crown-6 molecules positioned near both the C6S cavities and the Eu metal centers. The europium ions in complex 2 differ in geometry and coordination preferences from those in the previously described system, causing the C6S host to adopt an up–down double partial-cone conformation, which disrupts the hydrogen-bonding network at the base of C6S required to stabilize the up–up conformation (Figure 24b).

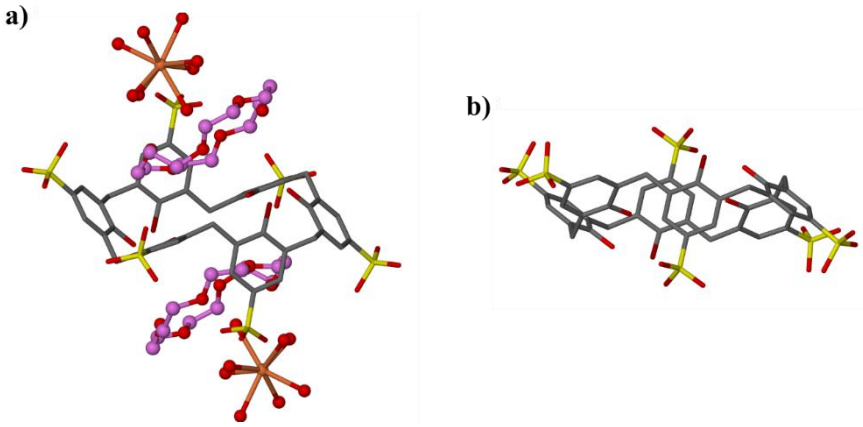

*Figure 24. (a) The C6S–[18]crown-6–Eu complex **2** (refcode TAHDIQ), [18]crown-6–Eu molecules are in the grooves of the calixarene; (b) the up–down double partial-cone conformation of the calixarene molecule. [18]crown-6 is colored pink, Eu in rude.*

Two complexes of C6S with 1,10-phenanthrolinium ($Phen^{+}$) and diazepino-1,10-phenanthroline (PPQ^{2+}) have been reported.[133] In the presence of the $Phen^{+}$ guest, C6S adopts the common centrosymmetric up–down double partial cone conformation and subsequently assembles into polymeric capsule-type structures. In contrast, when complexed with PPQ^{2+}, C6S is induced to assume a previously unobserved, unsymmetric up–down double partial-cone conformation, which further organizes into honeycomb-type aggregates (Figure 25).

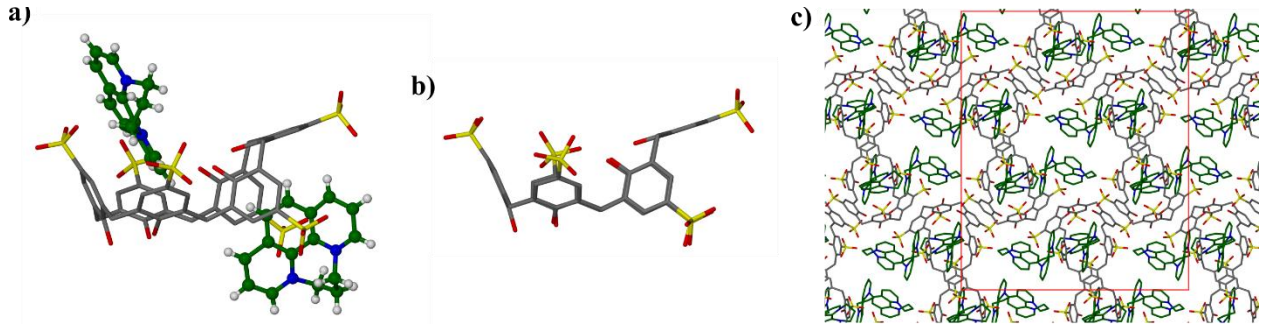

Figure 25. (a) The C6S–diazepino-1,10-phenantroline complex (refcode TIKVOZ), showing guest molecules positioned in the grooves of the calixarene; (b) up–down double partial-cone conformation of the calixarene molecule; (c) honeycomb-type aggregates in complex 2, with phenantroline counterions occupying the hexagonal cavities of the honeycomb. Guest molecules are shown green.

The C6S–cucurbit[8]uril–Ca^{2+} complex belongs to a series of 15 isostructural C6S assemblies with cucurbit[8]uril and various metal ions (Figure 26a). In all complexes, C6S features a flattened pleated-loop conformation, with only minor variations in distortion (Figures 26b–c). The C6S–cucurbit[8]uril–Ca^{2+} crystal packing consists of layered stacks of C6S–cucurbit[8]uril units, with macrocycles oriented to maximize electrostatic and hydrogen-bonding interactions.[130]

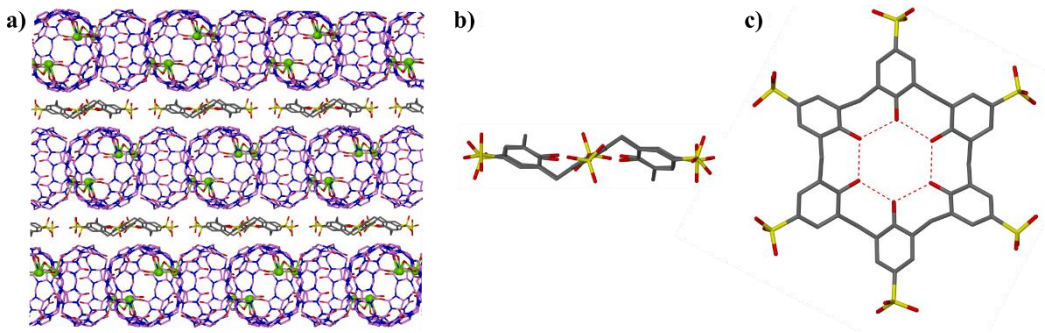

Figure 26. (a) Packing of the C6S–cucurbit[8]uril–Ca^{2+} complex (refcode XAWWOL); (b–c) pleated-loop conformation of the calixarene molecule side and top view.

2.5.3 Crystal structure of the *p*-sulfonatocalix[8]arene complexes and assemblies

Water-soluble C8S contains eight anionic sulfonate groups at the upper rim and eight hydroxyl groups at the lower rim, thus, at neutral pH, C8S exists as a polyanion.[110] Compared to its smaller homologues, C4S and C6S, C8S is larger, more highly charged, and exhibits pronounced conformational flexibility, which complicates crystallization and reduces the probability of obtaining well-ordered crystals suitable for X-ray diffraction. Consequently, only a limited number (26) of coordination and supramolecular structures have been deposited in the CSD database (four reported by me and co-workers), indicating that the structural chemistry of C8S remains less explored.

C8S typically forms complexes with cationic species through metal coordination, charge-assisted hydrogen bonding, and aromatic interactions. Various C8S conformations have been observed in assemblies with porphyrins, metal–phenantroline/bipyridine systems, aromatic N-donor ligands such as phenanthroline, bipyridine, 1,2-bis(4-pyridyl)ethane (BPE), 1,3-bis(4-pyridyl)propane (BPP), 4,4-dipyridine-N,N-dioxide (bpdo), as well as anesthetics drug molecules. Beyond small-molecule crystal structures, more than 30 structures of C8S bound to proteins are available in the PDB demonstrating its capacity for biomolecular recognition and versatile binding behaviour.[134–137]

In a recent study, Flood *et al.*[138] obtained crystals of C8S as an octa-sodium salt from buffered solution (Figure 27a). The molecules stack to form shifted host layers (Figure 27b), with each macrocycle adopting the pleated-loop conformation (Figure 27c). This arrangement is energetically favorable because hydrogen bonds between adjacent hydroxyl groups and the optimized positioning of sulfonate groups reduce steric strain and enhance electrostatic interactions, stabilizing the macrocycle while preserving its conformational flexibility. The staggered arrangement, stabilized by sodium ions, closely resembles packing motifs seen in protein–C8S cocrystals.

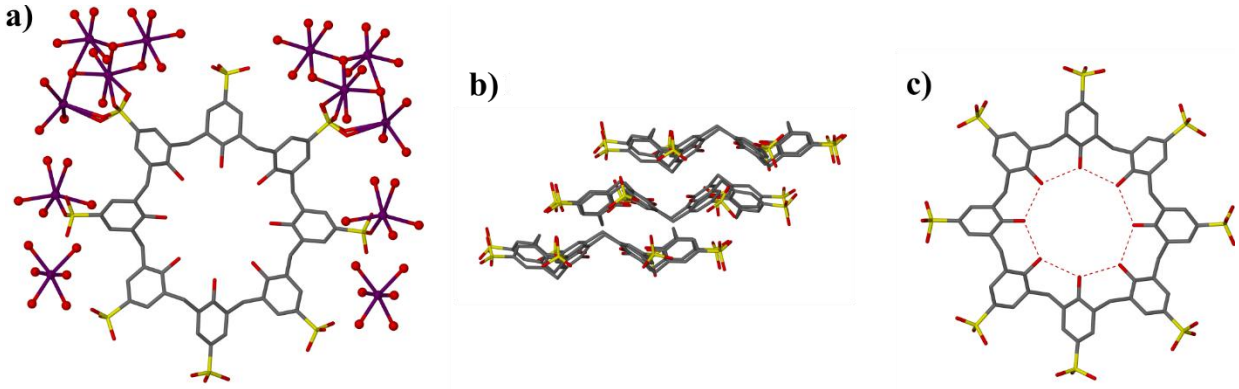

Figure 27. (a) The sclx8–Na complex (refcode KONSAL); (b) crystal packing in a C8S-Na salt structure with calixarene represented as sticks; (c) pleated-loop conformation of the calixarene molecule. Sodium cations colored violet.

In 2005, Dalgarno and co-workers reported the first structural elucidation of C8S as a linking unit within a three-dimensional mixed metal–organic lanthanide coordination polymer (Figure 28a). In this structure, C8S adopts a characteristic pleated-loop conformation (Figure 28b), which provides defined grooves suitable for bpdo guest inclusion. Each of these grooves is occupied by a bpdo molecule whose size and shape complement the host.[139]

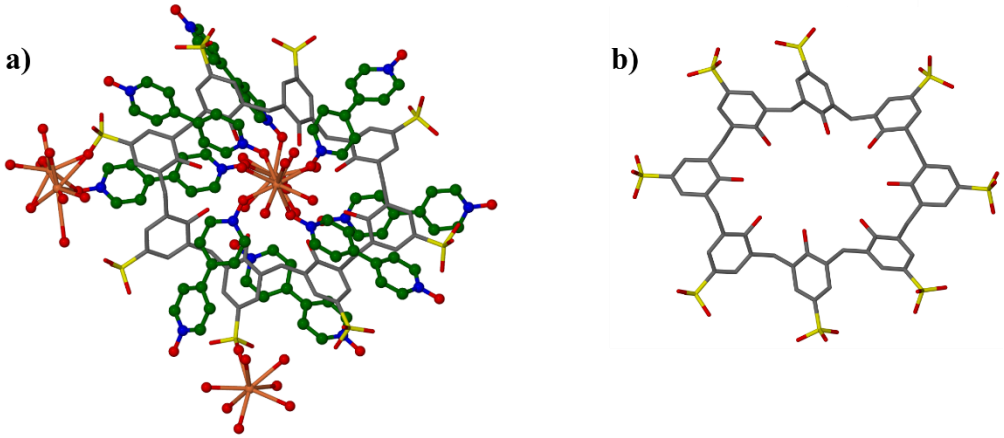

Figure 28. (a) The C8S–bpdo–Eu complex (refcode JAPQIB), bpdo molecules are in the grooves of the calixarene with some of them coordinated with aquated europium(III) ions; (b) the pleated-loop conformation of the calixarene molecule. Bipyridines are colored green.

C8S can also accommodate larger organic guests, such as porphyrins, as shown by Alex *et al.* (2020).[140] In these complexes, the macrocycle exhibits exceptional conformational flexibility, adopting an irregularly folded (distorted pleated-loop) conformation. This generates two internal pockets, resembling calix[3]arene-like and calix[5]arene-like sub-cavities (Figure 29c), which are large enough to host different parts of the porphyrin molecule (Figures 29a,b).

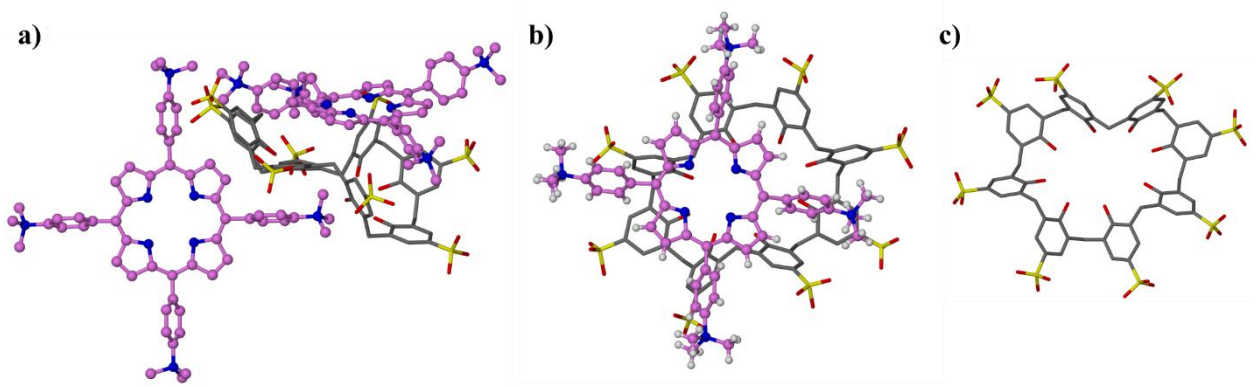

Figure 29. (a) The C8S–porphyrin complex (refcode QUCTIU); (b) the porphyrin molecule close to the C8S following its shape; (c) distorted pleated-loop conformation of the calixarene molecule. Porphyrin is colored pink.

As noted by Leśniewska *et al*. (2014), host–guest complex between C8S and the BPE dipyridyl cation exhibits distinct supramolecular behavior.[141] In this structure, two BPE cations are encapsulated within the C8S pseudo calix[4]arene cavities (Figure 30a), and the double cone conformation of the calixarene molecule was observed for the first time (Figure 30b).

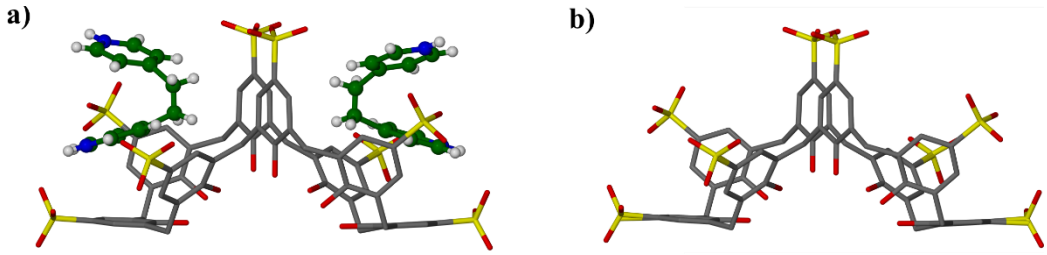

Figure 30. (a) The C8S–BPE (refcode HIZTUH), two guest molecules are in the each of the two-pseudo calix[4]arene cavities; (b) the up–up double cone conformation of the calixarene molecule. BPE molecules are colored green.

In the complex with cyclohexanediammonium, C8S adopts an up–down double cone conformation, in which four sulfonate groups point upward and four downward from the mean plane, forming inverted pseudo calix[4]arene cavities.[142] Hydrogen bonding occurs both between neighboring hydroxyl groups and between sulfonate groups and hydroxyls across the two partial cones (Figure 31b). This geometry resembles two opposing C4S-like cones and is significantly different in size and shape from the planar pleated-loop conformation. In this structure, the guests are oriented vertically, penetrating the partial-cone cavity rather than lying across the grooves (Figure 31a).

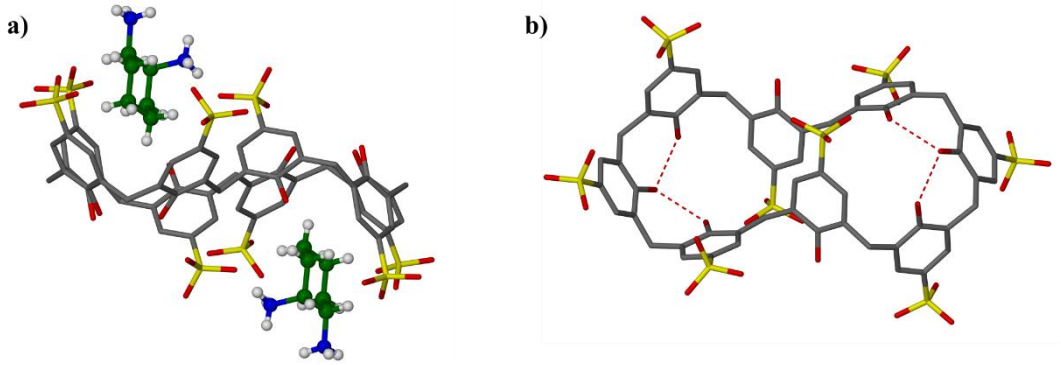

Figure 31. (a) The C8S–cyclohexanediammonium complex (refcode VERBEA), cyclohexanediammonium molecules are in the grooves of the calixarene; (b) up–down double partial-cone conformation of the calixarene molecule. Cyclohexanediammonium molecules are colored green.

An intermediate conformation of C8S between the two extremes (up–up and up–down) was identified in the solid-state structure of the C8S–dimethylammonium complex (Figure 32a).[143] In this structure, the C8S anion adopts a distorted self-closed conformation with two phenolic rings self-included within the cavity (Figure 32b). The typical hydrogen bonding between adjacent phenolic groups is disrupted.

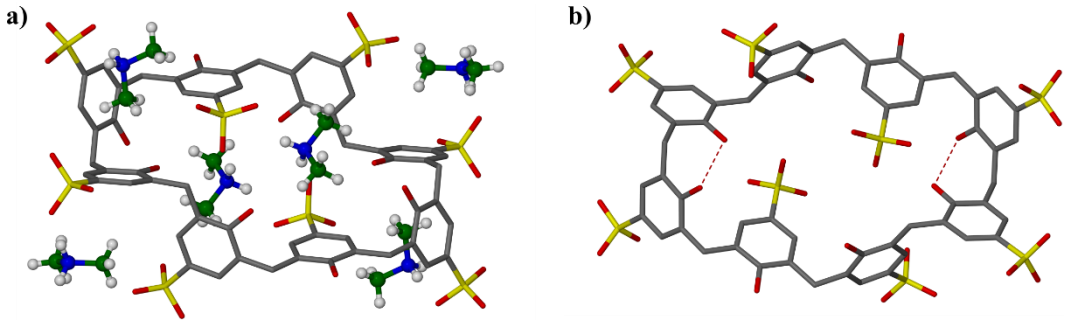

Figure 32. (a) The C8S–dimethylammonium complex (refcode DIZPEI); (b) self-closed conformation of the calixarene molecule. Dimethylammonium is colored green.

A more recent study[144] reported the first rotaxane structure of C8S as part of a supramolecular 3D coordination polymer incorporating a bpdo guest molecule and a Cu^{2+} cation (Figure 33a). In this assembly, bpdo functions as the linear axle, while C8S acts as the wheel. The C8S wheel adopts a self-opened conformation, providing a cavity large enough to accommodate the axle (Figure 33b), with six phenol rings remaining pleated while two adopt “up–down” positions. This conformation is stabilized by a network of hydrogen bonds between the hydroxyl groups located on the planar aromatic rings (Figure 33c).

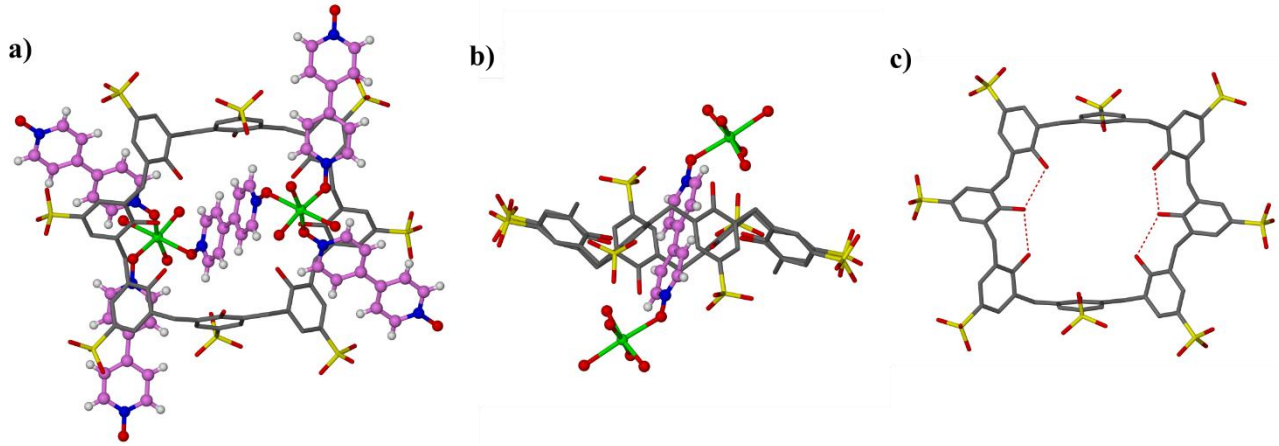

Figure 33. (a) The C8S–bpdo–Cu complex (refcode ZIYSEI); (b)one bpdo molecule is included within the calixarene cavity with the coordinated Cu^{2+} cations; (c) self-opened conformation of the calixarene molecule. Bipyridines are colored pink.

The ability of C8S to interact with phenanthroline and metal ions was demonstrated by Smith *et al*. in 2006.[145] In the solid state, C8S forms a highly distorted, chalice-like cavity (Figures 34a,b) capable of including the coordination complex $[Co(phen)_3]^{3+}$. In the presence of Yb^{3+} ions, a crystalline material is obtained containing large diameter, negatively charged channels extending in three dimensions. Packing on the Figure 34c illustrates the tubular arrangement of the chalice–guest supermolecules and the position of the aquated Yb^{3+} ions within the channel.

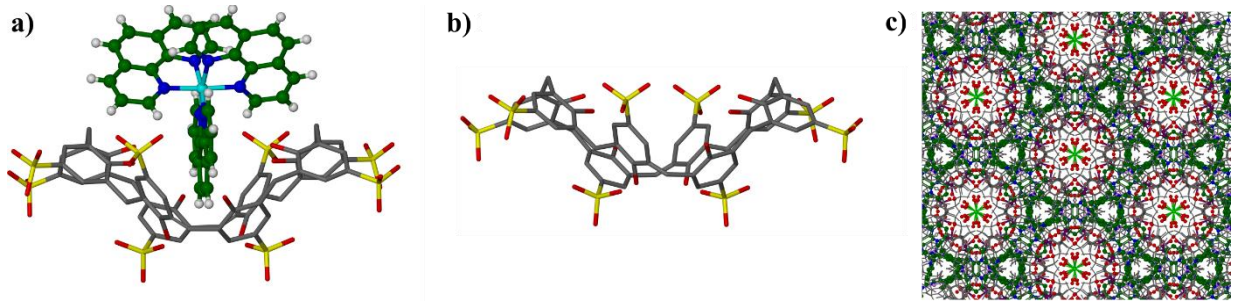

Figure 34. The C8S–$[Co(phen)_3]^{3+}$–Yb^{3+} complex (refcode PEJNUO4); (b) the chalice-like conformation of the calixarene molecule; (c) crystal packing of the complex along the c axis illustrating the tubular arrangement of the chalice–guest supermolecules and the position of the aquated Yb^{3+} ions within the channel. Calixarene is colored in grey, phenantroline in green, Co in light green.

2.6 Structural transformations in the macrocycle-based complexes

Structural transformations in supramolecular solids are generally classified into two main types: *solution-mediated* transformations, which proceed *via* dissolution followed by recrystallization, and *single-crystal-to-single-crystal (SCSC)* transformations, which occur entirely in the solid state.[146] In solution-mediated transformations, a metastable crystalline form dissolves, and nucleation and growth of a more stable phase then take place.[147] Solution-mediated transformations depend on the time that crystal spent in contact with the mother solution.[148] Another aspect rarely discussed in the context of the host–guest crystallization, is the manifestation of Ostwald's rule of stages according to which crystallization often proceeds step by step through the intermediate metastable phases until the most stable phase is formed.[147,149] Or, according to classical nucleation

theory, what one observes is the parallel nucleation and subsequent disappearance of different phases sequentially in the order of their metastability.[150] The different crystal forms or their mixtures can potentially be experimentally detected and harvested from the same crystallization conditions just with the passing of time. The transformations can be associated with the host/guest conformational changes, changes in the non-covalent interactions or hydration pattern, or more generally, the interplay between host, guest and water molecules inside and outside of the macrocyclic cavities. In contrast, SCSC transformations do not require a liquid medium and can involve breaking or reforming noncovalent (and occasionally covalent) interactions, conformational adjustments, or collective molecular motions – rotational or translational within the crystal lattice. These transformations can be triggered by external stimuli such as light, temperature changes, solvent removal or inclusion, solvent exchange, or mechanical force.[151]

The presence of voids in the crystal lattice and the intrinsic flexibility of the molecules are key factors enabling SCSC transformations. Voids provide space for molecular motions, while molecular flexibility allows active sites to rotate and interact. Conformational strain generated during the transformation must be relieved to prevent crystal fragmentation, ensuring a successful SCSC process. Importantly, these structural changes can be examined at the atomic level using routine X-ray crystallography.[152] Although such behavior is well documented for coordination polymers and discrete coordination complexes,[153] comparable examples in purely organic molecular crystals are rare, primarily because these crystals often lose structural integrity during transformation.[154]

In the cucurbit[6]uril–dopamine host–guest system, Danylyuk *et al.*[155] observed two distinct transformations: a solution-mediated transformation and a single-crystal-to-single-crystal transformation. Initially, two crystalline forms, complex I (metastable) and complex II (thermodynamically stable), crystallize simultaneously from aqueous solution (Figure 35). Being metastable, complex I dissolves spontaneously and recrystallizes as complex II over 1–2 days.

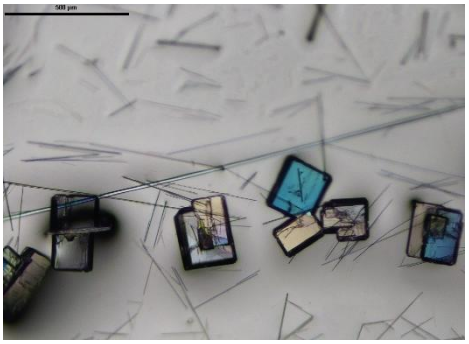

*Figure 35. Photomicrograph of crystals of cucurbit[6]uril–dopamine complex: concomitant crystallization of the metastable complex **I** (forming prismatic crystals) and complex **II** (needle-shaped crystals), observed 24 hours after the start of the crystallization experiment. The scale bar corresponds to 500 µm.*

This solution-mediated transformation is driven by the release of water molecule from the cucurbit[6]uril cavity and results in a change of supramolecular architecture from *zig-zag* strands to hexameric tubular assemblies. Complex II, although stable in solution, undergoes a SCSC transformation when exposed to air, revealing complex III. This process involves partial loss of lattice water, shrinkage of the unit cell and reorientation of dopamine guest molecules. Importantly, the hexametric tubular framework and the depth of dopamine inclusion remain unchanged. Both transformations are associated with water release, either from the macrocyclic cavity (I → II) or from the crystal lattice (II → III), and that supramolecular complexes can undergo structural rearrangements while maintaining crystallinity (Figures 36a–c).

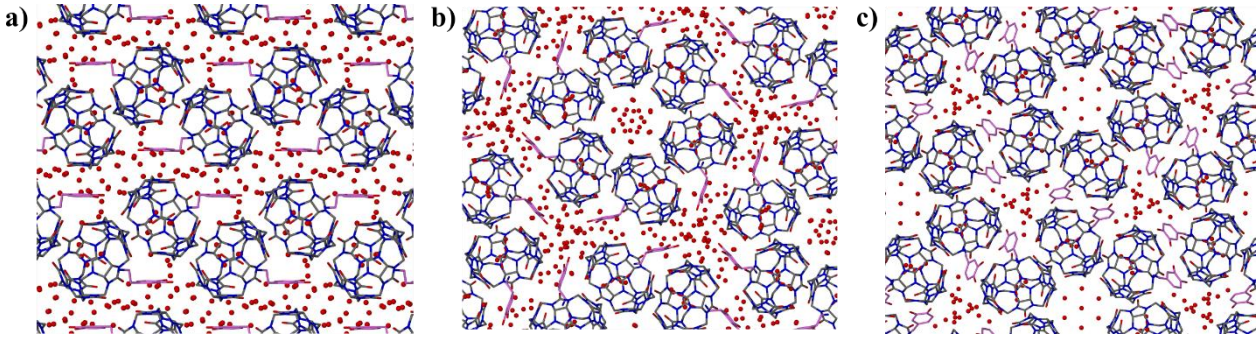

Figure 36. Crystal packing of the cucurbit[6]uril–dopamine complexes: (a) complex I viewed along a axis (refcode PUJYUR); (b) complex II viewed along the c axis (refcode PUJSUL); (c) complex III viewed along the c axis (refcode PUJTAS). Dopamine is colored pink.

2.7 Guest molecules

In the present study, the ability of anionic *p*-sulfonatocalix[*n*]arenes to form host–guest complexes with organic and inorganic cations was examined. The first group comprises cationic amidine derivatives, presented in Figure 37. This group includes benzamidine (**BNZ**),[156,157] 4-methylbenzamidine (**M–BNZ**),[158] 4-hydroxybenzamidine (**H–BNZ**),[159] and 4-aminobenzamidine (**A–BNZ**),[160] all of which are commonly employed as inhibitors of trypsin and serine proteases, or as building blocks in the design of drug delivery systems. Their amidine functional groups provide *N–H* hydrogen-bond donors, enabling interactions with the negatively charged sulfonate groups of calix[*n*]arenes *via* charge-assisted *N–H···O* hydrogen bonds. Substituents such as methyl, hydroxyl, or amino groups further modulate their hydrogen-bonding potential and number of possible hydrogen bonds. Pentamidine (**PT**), a clinically used antimicrobial agent in the treatment of pneumonia, contains two benzamidine groups and is therefore capable of forming up to eight *N–H···O* hydrogen bonds with the sulfonate groups of calix[*n*]arenes, resulting in significantly stronger host–guest interactions compared with monoamidine derivatives.[161]

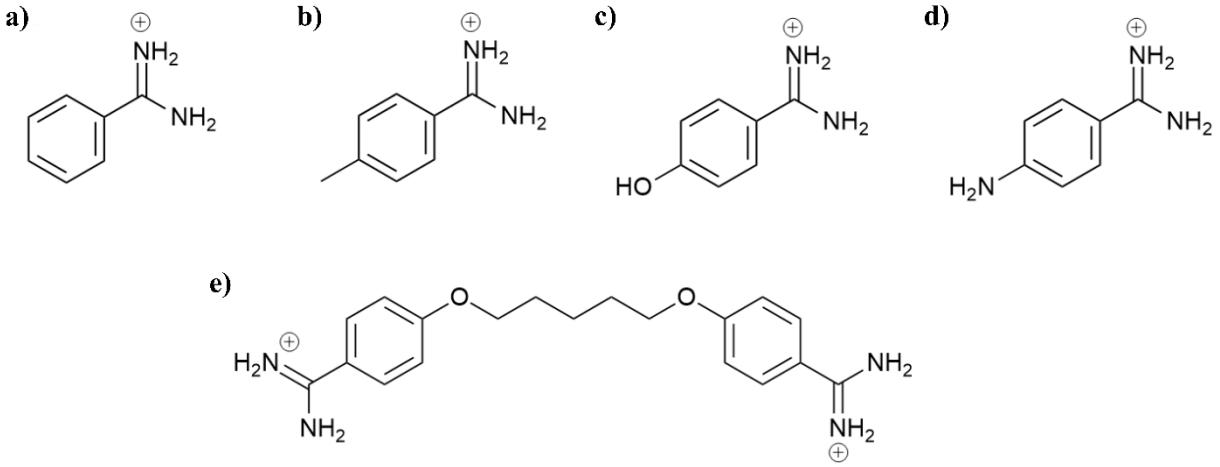

Figure 37. Structural formulas of amidine and selected derivatives: (a) benzamidine; (b) 4-methylbenzamidine; (c) 4-hydroxybenzamidine; (d) 4-aminobenzamidine; (e) pentamidine.

Alexidine (**ALEX**) is a bisbiguanide compound containing two guanidine groups, each providing multiple N–H hydrogen-bond donors for interactions with anionic host molecules (Figure 38). The presence of two guanidine moieties increases the number of potential hydrogen-bonding contacts, allowing alexidine to form multiple *N–H···O* bonds, which can enhance host–guest complex stability compared with mono-cationic derivatives.[162]

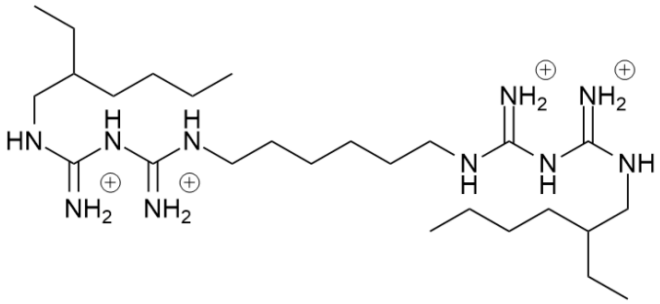

Figure 38. Structural formula of guanidine derivative – alexidine.

The third group comprises macrocyclic pyridinium derivatives, namely pillar[*n*]pyridiniums. These macrocycles consist of positively charged pyridinium units, enabling strong electrostatic interactions with anionic guests (Figure 39). Pillar[*n*]pyridiniums (P[*n*]Ps) are permanently charged, electron-deficient macrocycles currently available as rigid, square-shaped tetramer (**P4P**)[163] and the more flexible, roughly hexagonal hexamer (**P6P**)[164].

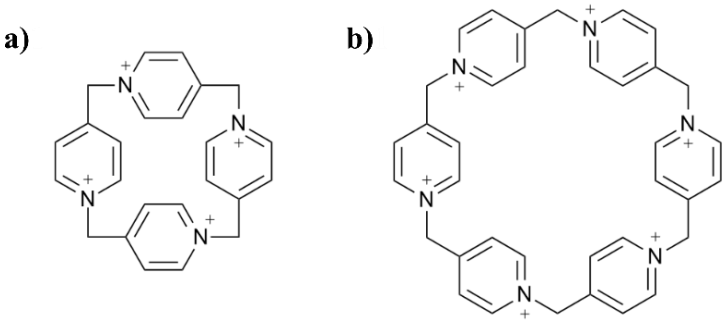

Figure 39. Structural formulas of macrocycles: (a) pillar[4]pyridinium; (b) pillar[6]pyridinium.

Berberine (**Berb**) belongs to the protoberberine group of benzylisoquinoline alkaloids.[165] Berberine weakly inhibits the enzymes CYP2D6 and CYP3A4, which are involved in the metabolism of endogenous compounds and xenobiotics, including many prescription drugs.[165] Recent studies suggest that berberine may have therapeutic potential in a variety of conditions, including metabolic disorders, inflammatory markers, and certain types of cancer.[169] Its structure contains a quaternary ammonium center, which provides a permanent positive charge capable of forming electrostatic interactions with anionic host molecules as shown in the Figure 40.

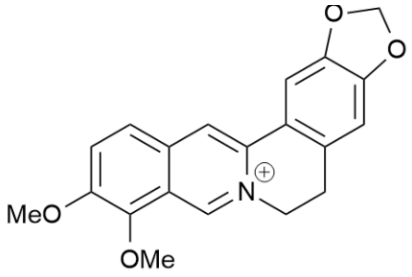

Figure 40. Structural formula of isoquinoline alkaloid – berberine.

The next group comprises hydrazine derivatives, represented by iproniazid (Figure 41). Iproniazid (**IPR**) is a pharmacologically active hydrazide that was historically used as an antituberculosis and antidepressant agent and irreversible monoamine oxidase inhibitor (MAOI) of the hydrazine class, though it was eventually withdrawn due to severe hepatotoxicity.[168] Its structure contains a single hydrazide group (*–NH–NH₂*) and and pyridinium group, which provide four N–H hydrogen-bond donors capable of forming hydrogen-bonding interactions with the sulfonate groups of calix[*n*]arenes.

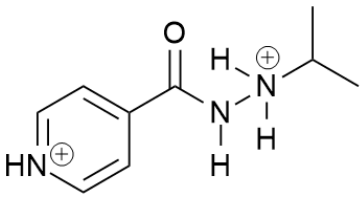

Figure 41. Structural formula of hydrazine derivative – iproniazid.

3. EXPERIMANTAL PART

3.1 Single Crystal X-Ray Diffraction (SXRD)

Single-crystal X-ray diffraction is an important technique for determining the solid-state structure of host–guest complexes. This technique provides crucial information about host–guest complexation, including which atoms are involved, their relative positions, and the bond lengths and angles within the complex. Determining a crystal structure from X-ray diffraction measurements involves several steps, each of which directly affects the quality of the result. In this chapter, I will describe all stages, from the crystal preparations to the final crystal structure.

3.1.1 Preparation of crystalline complexes

Commercially available *p*-sulfonatocalix[*n*]arene sulfonic acids and *p*-sulfonatocalix[4]arene sodium salt were purchased from TCI and Sigma Aldrich, respectively. Benzamidine and its derivatives were ordered from TCI, iproniazid from ABCR. Alexidine, pentamidine, and berberine were purchased from Sigma Aldrich. Pillar[*n*]pyridines were synthesized in the laboratory of Prof. Volodymyr Sashuk at the Institute of Physical Chemistry, Polish Academy of Sciences, by Dr. Sandra Kosiorek, following literature procedures.[163,164] All compounds were used without further modification. The crystals were grown using either water as the solvent or binary solvent mixtures (water–ethanol, water–methanol, water–isopropanol, or water–acetone) in 1:1 or 1:2 ratios, depending on the complex, as specified in the corresponding crystallization section.

Most crystals of the complexes described in this work were obtained by the *slow evaporation method*. In this approach, a nearly saturated solution of a good soluble in solvent compound is allowed to evaporate gradually under controlled conditions, leading to the formation of well-ordered crystals. The following complexes were obtained using different crystallization methods, as their final mixtures had low solubility and precipitated without forming well-defined crystals. The crystals of the ***C8S_Berb*** complex were grown by the slow cooling method in hot glycerin using isothermal equipment. In this method, a saturated solution is gradually cooled under controlled conditions, lowering solubility and inducing supersaturation, which promotes the growth of well-ordered single crystals.[170] The ***C4S_P4P*** complex was obtained by slow *liquid–liquid diffusion in a U-tube* through an agarose gel. Gel crystallization is a simple and effective technique that can improve single-crystal quality, control crystal size and morphology, regulate nucleation, and even influence polymorphic forms.[171] In this experiment, the calixarene solution in water was placed on the left side of the tube and P4P solution on the right; after slow diffusion through the agarose gel, well-formed yellow crystals were obtained. The ***C4S_P6P*** complex was grown by slow *liquid–liquid diffusion in an NMR tube*. Slow diffusion of the two solutions in a narrow NMR tube gradually reduces solubility, inducing

supersaturation and enabling the growth of well-formed single crystals. The crystals of the ***C8S_Na*** complex were obtained by *slow vapor diffusion (gas-phase diffusion)*.[172] In this method, the C8S is first dissolved in a slowly evaporating solvent, such as water. Next, a second, more volatile solvent is selected – one that is miscible with the first solvent but in which the compound has low solubility; in our case, this is ethanol. The experiment is arranged using two nested vials: the inner vial holds the compound solution, while the outer vial contains the antisolvent. Space is left above the liquids to allow vapor exchange between the vials. Gradually, vapors from the outer solvent diffuse into the inner vial, decreasing the solubility of the compound and enabling crystals to form slowly. The process continues until the solution becomes saturated with the second solvent, or the entire pool has transferred, and the duration depends on the choice of solvents and experimental conditions. In contrast, complexes containing pentamidine and alexidine crystallized directly from cloudy solutions containing precipitates, without applying methods to reduce solubility or prevent these perturbations.

For single crystal X-ray diffraction experiment, crystals should ideally be smaller than the diameter of the X-ray beam, exhibit a regular shape, and be free from cracks or twinning. The quality of the obtained crystals was preliminarily evaluated using a Nikon polarizing microscope, which also allowed high-resolution imaging.

3.1.2 Single crystal X-ray diffraction

Selected crystals were mounted on a looped nylon fiber with a minimal amount of PFPAE (perfluoropolyalkylether) oil (viscosity 1800 cSt; ABCR GmbH) to prevent solvent loss from the structure, using Hampton Research Cryoloops, and placed on the goniometer. Measurements were carried out on a SuperNova Agilent X-ray diffractometer for single-crystal studies, equipped with CrysAlisPro[173] software and a two-dimensional Eos CCD detector. The diffractometer is fitted with X-ray sources: molybdenum (MoKα, λ = 0.71073 Å) and copper (CuKα, λ = 1.54178 Å). These sources provide high resolution, generating high-quality data even from small crystals. Additionally, the diffractometer is equipped with a low-temperature attachment, allowing measurements at temperatures above the boiling point of nitrogen. All crystals were flash cooled to 100.0(1) K in a nitrogen gas stream and maintained at this temperature during the experiments to prevent crystal decomposition.

After crystal mounting, the most suitable radiation source was selected. In this work, all measurements were performed using the copper source with a characteristic wavelength (CuKα) of 1.54178 Å. An important factor in selecting the X-ray source is the relative intensity of the two options. Due to the higher focusing efficiency of the copper X-ray optics and the higher diffractive power of copper radiation, diffraction intensity from the same crystal is higher when using copper radiation compared to molybdenum. This allows shorter exposure times per frame while still

obtaining diffraction data at the desired resolution. Diffraction images were recorded using omega-angle scanning, in which the crystal rotates at a constant speed around the ω axis. The incident beam is reflected from lattice planes at the Bragg angle, defined as the angle between the incoming beam and the plane. During measurement, angular positions of the reflected beam from planes perpendicular to the rotation axis are recorded. The detector captures reflections on consecutive frames, allowing precise determination of the shape and symmetry of the diffraction spots. Crystal was carefully centered so that, during any rotation of the goniometer head, it remained exactly at the intersection of all four rotation axes, i.e., in the path of the incident X-ray beam.[174] The next step involved recording several test X-ray frames to assess the crystal's scattering ability, including whether it scattered the incident radiation effectively and whether the resulting reflections were single and symmetrically shaped. For some crystals, achieving the required quality was not possible. Often, crystals scattered over a narrow angular range, and reflections appeared twinned or blurred, reflecting significant disorder and twinning in the structure.

After recording several frames with the established exposure time per frame, the next stage of the diffraction experiment was the pre-experiment. The pre-measurement determines the correct unit cell parameters and the point group, considering the chemical composition of the sample, including the type of radiation, temperature, exposure time per frame, and the distance from the sample to the detector. Based on the pre-experiment results, a measurement strategy for the main experiment was established, specifying the set of reflections whose intensities should be recorded and the corresponding exposure times. This usually involves the asymmetric part of the reflections that fall within the angular range allowed by the diffractometer, excluding systematically absent reflections. Based on the quality of the crystals obtained, most measurements took between several hours and two days. Data was processed using CrysAlisPro[173].

3.1.3 Structure solution and refinement

In X-ray crystallography, the positions of the diffraction spots (reflections) are first used to determine the unit cell parameters and the overall crystallographic system. Once the intensities of these reflections are measured, data reduction is performed to convert the raw intensity measurements into a form that can be used for structure determination. The ability of an atom to scatter X-rays depends on the number of electrons it has. This is quantified by the atomic scattering factor, which measures how strongly an atom scatters X-rays relative to a single electron and depends on the atom's atomic number. Electrons at different positions within the same atom cause differences in the phase of the scattered waves, which can either strengthen or weaken the resulting diffraction signal.

Theoretical scattering factors are calculated assuming the atoms are at absolute zero. At finite temperatures, atoms vibrate around their equilibrium positions, introducing additional phase

differences in the scattered waves. This effect is accounted for using a temperature factor, which adjusts the scattering according to the amplitude of thermal vibrations. The X-ray waves scattered by all atoms in the unit cell interfere with each other, creating phase differences depending on their paths. Only the waves scattered along the direction of the incoming X-rays remain in phase. The total scattering in directions that satisfy the Bragg condition is described by the structure factor, ***F***, which is calculated by summing the amplitudes of waves scattered by all atoms in the unit cell. Waves from different elements have different amplitudes because their atomic scattering factors differ, while waves from atoms of the same element at different positions differ in phase. The experimental data provide only the magnitude of the structure factor, not the phase. This limitation is known as the phase problem, and it cannot be resolved directly from the measured intensities. Solving the phase problem is a central challenge in determining crystal structures.

In the next stage of structure determination, numerical methods such as the heavy-atom method, direct methods, or charge-flipping are used to obtain a preliminary structure model. Structural refinement is the process of systematically adjusting atomic parameters so that the calculated diffraction intensities match the experimental data. This usually requires several refinement cycles until the structural model shows only minimal changes between cycles. The preliminary model is described by parameters such as atomic coordinates, temperature factors (isotropic or anisotropic), and the scale factor (***S***). These parameters are considered preliminary, and further refinement is needed to improve the model. The most used numerical method for this purpose is the least-squares method.

The main criterion for determining the correctness of a model is the discrepancy index, denoted ***R*** and commonly referred to as the ***R*** value. This is the relative average difference between the calculated and experimental structure amplitudes. The ***R*** value can be considered a reference for the degree to which the obtained model reflects the correct structure. Well-measured and refined structures are characterized by an R value of < 5%.[175] Due to the high disorder, relatively large unit cells, and large number of solvent molecules in the structures, the ***R*** value for the described structures in this study ranges from 3.6% to 13.4%. All structures were solved by direct methods and refined using SHELXL-2019/2[176] within the WinGX[177] software.

3.1.4 Details on the structure refinement

Some of the complexes described in this work crystallize as twinned structures. Twinning occurs when two or more individual crystal domains are intergrown in a specific orientation, resulting in a superposition of their diffraction patterns. *Merohedral* twins arise when the twin operation is a symmetrical element of the lattice but not of the crystal structure, leading to perfect overlap of diffraction patterns. *Pseudo-merohedral* twins occur when the lattice metrics are nearly compatible

with a higher symmetry, giving almost perfect overlap. *Non-merohedral* twins arise when the twin operation is not a symmetry of the lattice, resulting in partially overlapping diffraction patterns.[178] In this study, ***C4S_Pt_Ace*** and ***C8S_Na*** exhibit pseudo-merohedral twinning, whereas ***C6S_Pt_MeOH*** shows non-merohedral twinning. Twin analysis was performed using CrysAlis PRO[173] and PLATON[179]. The twin fractions (% contribution of each domain) were refined using **BASF** command. Further details regarding the twinning and refinement of each individual structure are discussed in the discussion section.

Most non-hydrogen atoms were refined anisotropically. Hydrogen atoms were introduced into the structural model at positions that satisfied the required geometric criteria and were subsequently refined as a rigid group (riding refinement). Hydrogen atoms of methyl and hydroxyl groups were refined in calculated geometric positions where the sum of electron density is maximized – so-called "rotating" groups (rotating group refinement). All hydrogen atoms were refined isotropically with temperature factors equal to 120% of the equivalent isotropic displacement parameter of the atom to which the hydrogen is attached, or 150% in the case of hydrogen atoms in methyl or hydroxyl groups. Hydrogen atoms were not added to all water molecules because their positions could not be located from the Fourier difference map. Refinement of the H atoms for each structure will be discussed further in the discussion section.

During the refinement of most structures particularly those based on low-quality diffraction data various geometric restraints were applied, including **SIMU**, **RIGU**, **DELU**, **SADI**, **SAME**, **DANG**, and **DFIX**. The **SIMU** restraint forces neighboring atoms to have similar anisotropic displacement parameters (ADPs). The **RIGU** restraint enforces the rigid-bond model, which assumes that bonded atoms move together along the bond vector. Similarly, **DELU** applies a rigid-bond restraint by ensuring equal components of anisotropic thermal parameters along bond directions. **SADI** and **SAME** restraints were used to make reasonable or equal bond distances between selected pairs of atoms, while **DANG** was applied to define distances between atoms separated by two bonds (1,3-bonds). The **DFIX** restraint was employed to maintain proper *O–H* (0.84 Å or 0.85 Å) and *N–H* (0.88 Å) distances.[180] Additionally, to preserve the correct (hexagonal) geometry of aromatic rings, the **AFIX 66** instruction was used occasionally.

The **SQUEEZE** procedure was applied to remove the contribution of highly disordered water molecules from the diffraction data (***C6S_M–BNZ*** complex). This approach allows for a more accurate refinement of the host framework by effectively "masking out" the electron density arising from solvent molecules that cannot be reliably modeled. Additionally, SQUEEZE helps to identify and characterize solvent-accessible channels and voids (***C8S_IPR_I*** and ***C8S_IPR_II*** complexes) within the crystal lattice, which are often occupied by these disordered solvent molecules. By

estimating the electron count in these voids, the method provides insight into the solvent content and its distribution in the structure.[181]

3.1.5 Structural disorder

Within crystalline systems, three primary types of disorder can be distinguished: substitutional, positional, and solvent disorder. Substitutional disorder arises when different types of atoms occupy the same crystallographic site within the unit cell. Positional disorder, on the other hand, occurs when an atom or group of atoms occupies two or more alternative locations with partial occupancies (*site occupancy factors*, S.O.F.). This type of disorder can be further classified as dynamic, if it reflects actual atomic motion, or static, if atoms remain immobile but are distributed over different positions in various unit cells. The third category, solvent disorder, involves disordered solvent molecules occupying channels or voids within the crystal lattice.[182]

All three types of disorder – substitutional, positional, and solvent are observed across the structures described in this work, with disordered atomic groups or entire molecules frequently present. Substitutional disorder is observed in the ***C4S_P4P*** structure, where nitrogen and carbon atoms of the pyridinium rings in the pillar[4]pyridinium molecule occupy the same crystallographic site. This case will be discussed in more detail in the results and discussion section. Positional disorder of the host is particularly pronounced in the sulfonyl groups attached to the aromatic rings of the calixarene. Guest molecules also exhibit significant disorder in many of the studied structures, affecting both aromatic rings, aliphatic parts etc. Solvent disorder is often observed among the analyzed systems. Several structures (***C4S_P6P*** and ***C8S_IPR*** for example) feature large channels or voids fully occupied by disordered water molecules. In addition to water, other disordered solvent molecules are also observed, including ethanol (e.g., ***C4S_M-BNZ***, ***C4S_A–BNZ***, ***C8S_PT_EtOH***) and acetone (***C4S_Pt_Ace***). The positional and solvent disorder significantly influences the *R-factor*, affecting the overall quality and reliability of the refined structural models. The disorder was treated using the PART commands or by applying the partial occupancies (25%, 50% etc) to the atoms.

3.1.6 Graphical representation of results

Figures were prepared using X-Seed[183] with MSRoll[184] and Mercury CSD[185] software. To maintain structural clarity, in cases of disordered atoms, atom groups, or entire molecules, only those assigned to PART 1 were shown. Where necessary, the disorder corresponding to PART 2 was noted and indicated.

If two or more C*n*S molecules were present in the asymmetric unit, they were numbered consecutively, starting from 1 (for example, 1–24 carbon atoms for one C4S molecule and 25–56 for the second, and so on). For guest molecules, successive letters of the alphabet were used for labeling (e.g., X, Y, Z, K, L, etc.), depending on the number of guests in the structure. Water

molecules were labeled as W, and when present in larger numbers, they were assigned sequential numbers. The atoms of disordered PART 2 were usually labeled with successive letters (e.g., A, B, C, F, etc.) to distinguish between the alternative positions.

Intermolecular interactions were analyzed using PLATON[180] and Mercury CSD[185] software. For hydrogen-bond analysis, the criteria applied were d($D\cdots A$) ≤ 3.2 Å and ∠(D–$H\cdots A$) > 120°.[186] For $\pi\cdots\pi$ aromatic interactions, a distance criterion of d < 4 Å was generally used; in rare cases, slightly higher values were applied when necessary to describe specific host–guest interactions. For C–$H\cdots\pi$ interactions, the criterion d < 4 Å was applied between the carbon atom of a methylene or aromatic group and the centroid of a neighboring aromatic ring. For the identification of *Na–O* coordination interactions, a distance criterion of $d(Na\cdots O)$ ≤ 2.30–3.06 Å was applied, consistent with *Na–O* bond lengths reported for six-coordinated Na by Gagné and Hawthorne (1995).[187]

3.2 Thermogravimetric Analysis and Differential Scanning Calorimetry (TGA–DSC)

Thermal analysis is an important analytical tool for studying the properties of materials as temperature changes. Thermogravimetric Analysis (TGA) and Differential Scanning Calorimetry (DSC) are two of the most widely used techniques for characterizing a variety of materials, including polymorphs, solvates, hydrates, salts, cocrystals, polymers, macromolecules, and amorphous forms.

DSC measures the heat flow into or out of a sample as a function of temperature, providing information on thermal transitions during controlled heating or cooling. These transitions can be physical, such as melting, crystallization, polymorphic conversion, desolvation, or dehydration, or chemical, corresponding to changes in enthalpy. In the case of host–guest complexes, DSC is used to investigate thermal transitions, including stability, host–guest inclusion or release, dehydration, desolvation, and polymorphic changes. TGA measures changes in sample mass as a function of temperature, detecting volatile components such as trapped solvents or water, and monitoring dehydration or desolvation. For host–guest complexes, TGA provides information on thermal stability, solvent content, and host/guest decomposition, complementing the insights obtained from DSC.[188,189]

TGA–DSC measurements were performed simulnateously using a TGA/DSC 3+ instrument (Mettler Toledo). An appropriate amount of each sample analyzed was placed in an aluminum oxide crucible sealed with a lid with a hole to allow controlled gas exchange. The ***C6S_M–BNZ*** complex was heated in the temperature range of 0–500°C, the ***C8S_Berb*** complex was heated in the temperature range of 0–600°C, while the ***C8S_IPR*** complex was heated in the range of 0–600°C, both at a constant rate of 10°C min^{-1} under a nitrogen atmosphere.

The resulting TGA–DSC curves were recorded and analyzed using Mettler Toledo STARe Software to monitor mass loss and thermal transitions associated with the thermal stability and phase behavior of the samples. TGA–DSC measurements described in this study were performed under identical heating conditions by Dr. Karolina Kędra at the Institute of Physical Chemistry, Polish Academy of Sciences.

3.3 Powder X-Ray Diffraction (PXRD)

X-ray powder diffraction (PXRD) is a nondestructive technique widely used to study microcrystalline and nanoscale materials. It provides information on phase composition, sample purity, crystallite size, structural defects, and morphology. Traditionally used for phase identification and quantitative analysis, PXRD is now also applied to determine moderately complex crystal structures and three-dimensional microstructural properties, thanks to modern high-resolution diffractometers and advanced data analysis methods. As a bulk technique, PXRD can confirm whether microscopic observations reflect most of the sample. Proper interpretation of PXRD data is essential, as it is sometimes underutilized or misinterpreted, especially for nanoscale materials.[190,191]

In the case of host–guest complexes, PXRD analysis is widely used to identify the formation of new crystalline phases or to detect structural changes that may arise from the preparation method of the complex or from molecular motion induced by external stimuli such as temperature or organic solvent vapors. PXRD provides information on bulk-phase purity and structural transformations that cannot always be captured by single-crystal X-ray diffraction alone.

Powder X-ray diffraction patterns of the sample prepared by the slurry method. The method is based on combining the solid components in the desired stoichiometric ratio and suspending them in a minimal amount of solvent. The resulting mixture is agitated at room temperature to promote the formation of the stable crystalline phase. The solid product is then isolated by filtration and dried. The air-dried single crystals of the complex ***C6S_M–BNZ_dried*** were recorded using a Panalytical X'Pert PRO diffractometer equipped with Cu Kα radiation (λ = 1.5418 Å). Samples were mounted on a standard glass sample holder, and diffraction data were collected in the 2Θ range of 5–40° at 40 kV and 40 mA under ambient conditions. Data acquisition was performed using X'Pert Data Collector software, and the diffraction patterns were analyzed using X'Pert HighScore Plus[192] to identify characteristic peaks and assess crystallinity. Data Viewer was used for pattern visualization and simple qualitative comparison. Sample preparation, diffraction experiments and the pattern analysis were done at the University of Bologna, Department of Chemistry "Giacomo Ciamician" during my doctoral internship.

3.4 Nuclear Magnetic Resonance (NMR) spectroscopy

Nuclear magnetic resonance (NMR) spectroscopy is a powerful analytical technique widely applied in the investigation of supramolecular host–guest complexes, particularly those involving cavity-containing systems in solution. The size and symmetry of the host and guest molecules substantially influence the dynamics of their interactions, making NMR a valuable tool for elucidating possible binding modes and mechanisms. As a multi-parametric method, NMR provides detailed insights into the structure, size, shape, aggregation state, mutual interactions, and dynamic behavior of the studied systems, as well as their thermodynamic and kinetic stability. Moreover, NMR spectroscopy has been extensively employed in the study of organic cages, porous liquids, and molecular frameworks, both in the solid state and in solution.[193]

This technique distinguishes between various nuclei, most commonly protons, by measuring their chemical shifts during the formation of host–guest complexes. The interaction between two molecular components induces changes in the electronic environment, resulting in characteristic variations in the NMR signals. Complex formation typically causes the guest signals to shift, broaden, or even disappear due to the altered magnetic environment within the host cavity.

In the case of *p*-sulfonatocalix[*n*]arene host–guest systems, the chemical shift of guest protons serves as a key parameter for determining the spatial orientation of the guest relative to the host. This phenomenon arises from the inhomogeneous magnetic field inside the macrocyclic cavity and around the calix[*n*]arene framework. The ring current of the aromatic units in the host molecule induces a shielding effect on the guest protons located within the cavity, resulting in upfield (lower $\boldsymbol{\delta}$ value) shifts in the NMR spectrum.

^{1}H NMR studies of *p*-sulfonatocalix[*n*]arene complexes were performed in solution using an Agilent 400 MHz spectrometer at room temperature. The spectra were analyzed with MestReNova[194] software. Deuterated solvents were purchased commercially from Eurisotop. All the NMR analyses described in this study were performed by Dr. Mykola Kravets at the Institute of Physical Chemistry, Polish Academy of Sciences.

4. RESULTS AND DISCUSSION

4.1 *p*-Sulfonatocalix[*n*]arene complexes with benzamidine derivatives

In this chapter, the complexation, crystallization pathway and crystal structure analysis of C4S and C6S host–guest complexes with benzamidine (BNZ), 4-methylbenzamidine (M–BNZ), 4-hydroxybenzamidine (H–BNZ), and 4-aminobenzamidine (A–BNZ), are described and discussed. Benzamidine-type guests bear cationic amidinium functionalities that are potential donors of four hydrogen bonds. Amidinium groups are strong and directional donors due to their propensity to form robust (paired) hydrogen bonds, offering prospect of predictable self-assembly (at least in theory). Macrocyclic molecules have either four (C4S) or six (C6S) sulfonate substituents arranged at the upper rim. Each anionic sulfonate group of C_{3v} symmetry can accept protons from different directions, forming multiple hydrogen bonds. Thus, the high structural diversity of charged-assisted hydrogen bonding between cationic amidinium groups of the guest molecules and anionic sulfonate rims of calixarenes can be anticipated in the supramolecular assemblies. The hydrogen bonding and electrostatic interactions between cationic benzamidine and anionic macrocycles are certainly influenced by the possibility of host–guest interaction, for example inclusion of aromatic group of benzamidine within macrocyclic cavity. Additionally, the influence of solvent (water) molecules should be considered as part of the supramolecular system. In the wider view of obtaining host–guest architectures of the "open" supramolecular structure featuring channels, pores or discrete pockets, the introduction of additional substituents (methyl, hydroxy and amino) on benzamidine guest have been studied. This can perturb both the inclusion scenario and hydrogen bonding between host and guest, as additional supramolecular synthons hydroxy-sulfonate or ammonium-sulfonate are introduced in the system.

For the host–guest system of C4S with unsubstituted benzamidine, very detailed studies on the time-dependent crystallization pathways have been performed. Namely, two commercially available forms of C4S macrocycle have been used – sulfonic acid and sodium salt. Sodium counterions stemming from C4S sodium salt, are not simple bystanders in the host–guest recognition and complexation. Sodium ions can have both competitive and cooperative effect on the complexation of organic guest molecules. The coordination hetero-ternary complexes between sulfonated calixarenes, organic cations and sodium ions were previously experimentally observed in the solution and solid state, as described in the Literature Review chapter. The additional aspect that has been considered is what happens when initially formed crystals are kept in the mother solution simply over passing of time, allowing slow evaporation. This seems to be not as innocent as it intuitively appears. The "aging" of multi-component crystals exposed to concentration changes of the dissolved

components during crystal growth and partial evaporation of the mother solution can embrace different scenarios, including dissolution-recrystallization transformations. Five different host–guest crystal forms in the C4S-benzamidine system have been identified and structurally characterized, some of the complexes comprise sodium or oxonium ions as part of the supramolecular assembly. The host–guest crystal forms are defined by the C4S counterion and the time that crystals spent in the contact with the mother solution under slow evaporation conditions. These results have been published in *Crystal Growth & Design* titled as **"*Host–Guest Complexes of p-Sulfonato-calix[4]arene and Benzamidine: A Matter of Counterion and Aging in the Mother Liquor*"**.

In the further crystallization and complexation studies, only sulfonic acid form of C4S and C6S have been used. The size of calixarene macrocycle defying the flexibility of the macrocyclic skeleton, has also been considered as a factor in the host–guest supramolecular assembly. Only one host–guest crystal complex of C6S with benzamidine has been identified and described. In the case of 4-methylbenzamidine as a guest, no drastic changes in the supramolecular organization and structure have been anticipated, as there is no perturbation of hydrogen bonding synthons in the system. However, the crystal structure of C6S with 4-methylbenzamidine revealed a beautiful, highly symmetric *supramolecular framework* (or *hydrogen-bonded organic framework*) featuring discrete structural voids filled with disordered solvent molecules. The synthesis of this crystalline material was also performed via slurry method. This part of the study was conducted in the Department of Chemistry "Giacomo Ciamician", University of Bologna, during my foreign fellowship funded by Polish National Agency for Academic Exchange (NAWA).

Unexpectedly, two crystal forms of C6S complexes with 4-hydroxybenzamidine have been identified that drastically differ in the conformation of the macrocyclic host. In the case of 4-aminobenzamidine guest, two C4S complexes have been obtained – one as a metastable kinetic form featuring inclusion of ethanol molecules inside the macrocyclic cavity (while A–BNZ guests are hydrogen bonded to the macrocycle but reside outside the cavity), and a second host–guest inclusion complex that crystallizes later via the dissolution of the first crystal form.

It should be noticed that all benzamidine complexes described in this chapter were obtained from water-ethanolic solution to keep the solvent variable constant. Solvent can definitely influence the crystallization pathway, and even the supramolecular assembly itself, as water and other solvent molecules can be incorporated in the crystal structure, forming hydrogen bonds with macrocyclic host and benzamidine guests. Details of the crystallization setups, along with the refinement procedures, structural analyses and additional experiments for selected complexes (NMR, PXRD, TG-DSC) are described in Section 4.1.

C4S complexes with benzamidine: Forms I–V

Crystallization and microscopic observations for C4S sulfonic acid complexes with benzamidine

20 mg of C4S ***sulfonic acid*** was dissolved in 0.5 mL of H_2O/EtOH (1:1). The solution of 16.8 mg benzamidine hydrochloride in 0.5 mL of H_2O/EtOH (1:1) was combined with the solution of the host (Figure 42).

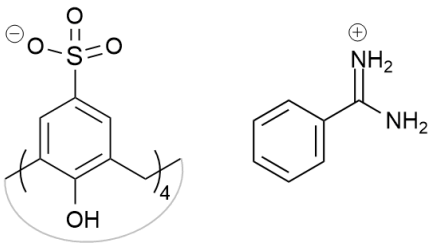

*Figure 42. Chemical structure of C4S **sulfonic acid** host and benzamidine (**BNZ**) guest.*

After one day the colorless rod-shaped crystals of a good diffraction quality appeared (Figure 43a). Single-crystal X-ray diffraction analysis revealed these rod-shaped crystals to be the host–guest complex ***C4S_BNZ_Form I***.

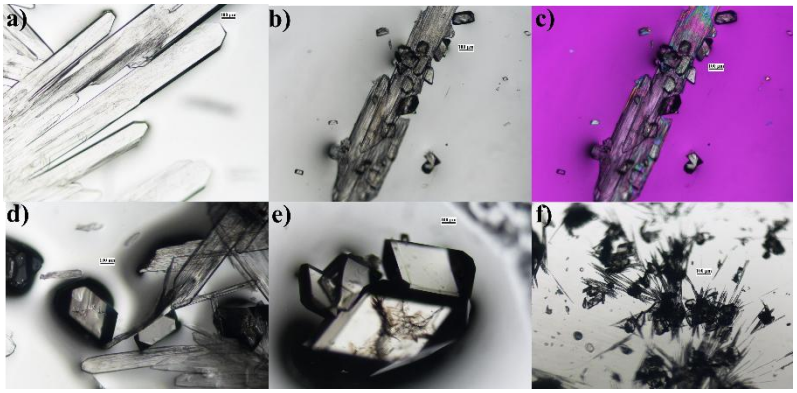

*Figure 43. Photomicrographs of crystals of **C4S_BNZ** complexes: (a) rod-like crystals of **C4S_BNZ_Form I**; (b–d) a mixture of rod-shaped crystals of **C4S_BNZ_Form I** and new prismatic crystals of **C4S_BNZ_Form II**; (e) only large prismatic crystals of **C4S_BNZ_Form II** remain in the mother solution after several days; (f) small prismatic crystals of **C4S_BNZ_Form III** appeared simultaneously with needle-like crystals of benzamidine hydrochloride after aging of **C4S_BNZ_Form II** in the mother solution allowing the solvent to evaporate slowly. The scale bar corresponds to 100 µm.*

The crystals of ***C4S_BNZ_Form I*** are unstable in the contact with the mother solution and dissolve slowly, accompanied by the appearance of new prism-shaped crystals (Figure 43b,c). The dissolution–recrystallization transformation takes place over 1–2 days. During this time spent in solution, the presence of two crystal forms of different morphology is noticed under microscopical observation (Figure 43d). After two days, only colorless prism-like crystals remain in the mother solution. Single-crystal X-ray diffraction analysis showed these crystals to be the host–guest complex ***C4S_BNZ_Form II*** (Figure 43e).

Then, the crystals ***C4S_BNZ_Form II*** were left in the mother solution in the open vial to let the solvent evaporate slowly. Careful examination of the vial with the dry crystals after two weeks

revealed the mixture of needle-like and small prismatic crystals (Figure 43f). Single-crystal X-ray diffraction analysis of a needle-shaped crystal showed the structure of benzamidine hydrochloride monohydrate, which was reported by T.G. Row in 1986 and deposited in the CSD under the code DOHHAJ.[156] Small prismatic crystals corresponded to a new complex ***C4S_BNZ_Form III***.

The refinement details of the C4S_BNZ complexes: Form I, II and III

The asymmetric unit of ***C4S_BNZ_Form I*** consists of two tetra-anionic C4S molecules, eight monocations of benzamidine occupying nine atomic sites, and 16.30 water molecules.

Oxygen atom O26 of C4S sulfonate group is disordered over two positions. The first component of disorder (O26) is refined with PART 1 command (93.5% occupancy), the second O26A is refined with PART 2 (6.5% occupancy). Oxygen atoms O5 > O7 and O9 > O11 of C4S sulfonate groups are disordered over two positions. The first component of disorder O5 > O7 is refined with PART 1 command (54.4% occupancy), the second O5A > O7A is refined with PART 2 (45.6% occupancy). The first component of disorder O9 > O11 is refined with PART 1 command (54.4% occupancy), the second O9A > O11A is refined with PART 2 (45.6% occupancy). O25 > S7 and O29 > S8 sulfonate group are disordered over two positions. The first component of disorder O25 > S7 is refined with PART 1 command (57.8% occupancy), the second O25A > S7A is refined with PART 2 (42.2% occupancy). The first component of disorder O29 > S8 is refined with PART 1 command (57.8% occupancy), the second O29A > S8A is refined with PART 2 (42.2% occupancy).

Benzamidine molecule with atom names C1I > N2I lies close to 2-fold axis of symmetry and is refined with 50% occupancy with the help of PART –1 instruction. Another benzamidine molecule in the general position with atom names C1K > N2K resides in the water channel and is refined with 50% occupancy surrounded with disordered water molecules. The benzamidines with atom names C1X > N2X, C1N > N2N, C1V > N2V are refined as disordered over two positions. The first component C1X > N2X of disordered molecule is refined with PART 1 command (85.9% occupancy), the second C1XA > N2XA is refined with PART 2 (14.1% occupancy). The first component C1N > N2N is refined with PART 1 command (45.5% occupancy), the second C1NA > N2NA is refined with PART 2 (54.5% occupancy). SIMU and RIGU restraints are used to C1X > N2X and C1N > N2N molecules equate atomic displacement parameters of disordered atoms and to make the relative motion of these atoms at right angles to the formed bonds. The first component C1V > N2V is refined with PART 1 command (59.4% occupancy), the second C1VA > N2VA is refined with PART 2 (40.6% occupancy). The majority of the water molecules in the structure are disordered and refined with PART 1 and PART 2 instructions. The hydrogen atoms of the host and guest molecules are placed at calculated positions. Hydrogen atoms of water molecules are not included in the model.

The asymmetric unit of ***C4S_BNZ_Form II*** includes two tetra-anions of C4S molecules, eight monocations of benzamidines, and 10.25 water molecules. Oxygen atom O26 of one of C4S sulfonate group is disordered over two positions. The first component of disorder O26 is refined with PART 1 command (93.5% occupancy), the second O26A is refined with PART 2 (6.5% occupancy). The SADI restraint is applied to fix the proper *S–O* distance.

The benzamidine molecule C1Y > N2Y included in the calix[4]arene cavity is refined as disordered over three positions. The first component of disorder C1Y > N2Y (75% occupancy) is refined with PART 1 command. The last two components C1YA > N1YA and C1YB > N2YB of minor occupancies (12.5% occupancy) lie close to the 2-fold axis, therefore they are refined using PART –2 and PART –3 commands to separate all disordered components including those generated by the symmetry operation.

Most of the water molecules in this structure are disordered. O1W, O2W, O12A and O13A water molecules lie close to the disordered benzamidine molecule. The O1W water molecule, using PART 1 command, is refined with 50% occupancy, since it lies on the 2-fold axis. The O2W molecule in a PART 1, and O12A / O13A in a PART –2 are refined with the partial occupancies of 75%, 25% and 25%, respectively. The O6W water molecule lies close to 2-fold axis and is disordered over two positions. The first component of disorder O6W is refined with PART 1 command (50% occupancy), the second O6WA is refined with PART 2 command (50% occupancy). The O7W water molecule is disordered over two positions. The first component of disorder O7W is refined with PART 1 command (86.2% occupancy), the second O7WA is refined with PART 2 command (13.8% occupancy). O8W, O9W and O10W molecules are positioned close to each other and are disordered over two positions. The first components of disorder O8W, O9W and O10W are refined with PART 1 command (62.9% occupancy), the second components – O8WA, O9WA and O10A are refined with PART 2 command (37.1% occupancy). The O11W water molecule is also disordered over two positions. The first component of disorder O11W is refined with PART 1 command (78.2% occupancy), the second O11A is refined with PART 2 command (21.8% occupancy).

All hydrogen atoms are added geometrically, except H1W atom. H1W hydrogen atom of the O1W molecule is located from a difference Fourier map (semi-free refinement) and the *O–H* distance of 0.85 Å is fixed with DFIX restraint. The O2W, O6W, O7W, O8W, O9W, O10W, O11W, O12A, O13A molecules are refined without hydrogen atoms. Some residual electron density is associated with unaccounted disorder of water solvent molecules in the water channels.

The asymmetric unit of the ***C4S_BNZ_Form III*** complex consists of one tetra-anion C4S molecule, two monocations of benzamidine, two $H_5O_2^+$ Zundel cations and 4.4 water molecules.

The O4W water molecule is disordered over two positions (O4W and O4A) with 60.7% and 39.3% occupancies. The O8W water molecule is disordered over two positions (O8W and O8A) with 62.2% and 37.8% occupancies, respectively. O9W molecules is refined with a partial occupancy of 40%. Hydrogen atoms of the host, guest and O5W, O6W, O7W and O8W water molecules are added geometrically. Hydrogen atoms of the molecules O1W, O2W, O3W, O4W are added from a difference Fourier map, where the *O–H* distance of 0.84 Å is fixed with DFIX restraint. The O9W molecule is refined without hydrogen atoms. The basic crystallographic data of the three discussed structures is provided in Table 2.

*Table 2. Crystal data and structure refinement for **C4S_BNZ** complexes: **Form I**, **II** and **III**.*

Parameters	***Form I***	***Form II***	***Form III***
Formula moiety	$2(C_{28}H_{20}O_{16}S_4)\cdot 8(C_7H_9N_2)\cdot 16.30(H_2O)$	$2(C_{28}H_{20}O_{16}S_4)\cdot 8(C_7H_9N_2)\cdot 10.25(H_2O)$	$(C_{28}H_{20}O_{16}S_4)\cdot 2(C_7H_9N_2)\cdot 2(H_5O_2^+)\cdot 4.4(H_2O)$
Formula weight	2744.29	2635.31	1136.35
Crystal system	Monoclinic	Monoclinic	Triclinic
Space group	*I2/a*	*P2/n*	*P–1*
a / Å	37.8612(3)	24.7113(2)	12.0818(5)
b / Å	20.6340(1)	17.7833(1)	14.1974(5)
c / Å	35.5290(3)	28.4769(2)	16.8985(5)
α / °	90	90	105.079(3)
β / °	113.531 (1)	100.305(1)	109.683(3)
γ / °	90	90	101.030(3)
Volume / Å^3	25448.1(4)	12312.3(2)	2508.2(2)
Z	8	4	2
ρ_{calc} /g·cm^{-3}	1.43	1.42	1.51
Crystal color	Colorless	Colorless	Colorless
Crystal morphology	Rod	Prism	Prism
μ / mm^{-1}	2.12	2.13	2.54
θ_{max} / °	70.5	70.0	70.5
Reflections collected	117251	79229	24812
Independent reflections	24168 [R_{int} = 0.030]	23178 [R_{int} = 0.032]	9536 [R_{int} = 0.033]
Data / Restraints /	24168 / 804 / 2227	23178 / 2 / 1732	9536 / 8 / 725
Observed data [I > 2σ(I)]	21347	20332	8207
Final R indexes [I ≥ 2σ(I)]	R_1 = 0.059, wR_2 = 0.167	R_1 = 0.048, wR_2 = 0.129	R_1 = 0.039, wR_2 = 0.099
Final R indexes [all data]	R_1 = 0.065, wR_2 = 0.176	R_1 = 0.054, wR_2 = 0.135	R_1 = 0.047, wR_2 = 0.105
Goodness-of-fit on F^2	1.05	1.03	1.03
Largest diff. peak and hole / e·Å^{-3}	0.95 / –0.76	1.44 / –0.74	0.80 / –0.53

Structure analysis of the C4S_BNZ_Form I complex

The co-crystallization of C4S ***sulfonic acid*** with benzamidine hydrochloride from water–ethanol solution (1:1) results in the formation of the complex ***C4S_BNZ_Form I*** with the formula $2(C_{28}H_{20}O_{16}S_4)\cdot 8(C_7H_9N_2)\cdot 16.30(H_2O)$. Single-crystal X-ray diffraction analysis shows that this complex crystallizes in a monoclinic crystal system in the space group *I2/a*. The asymmetric part

consists of two C4S, eight benzamidines occupying nine atomic sites, and 16.30 water molecules (Figure 44).

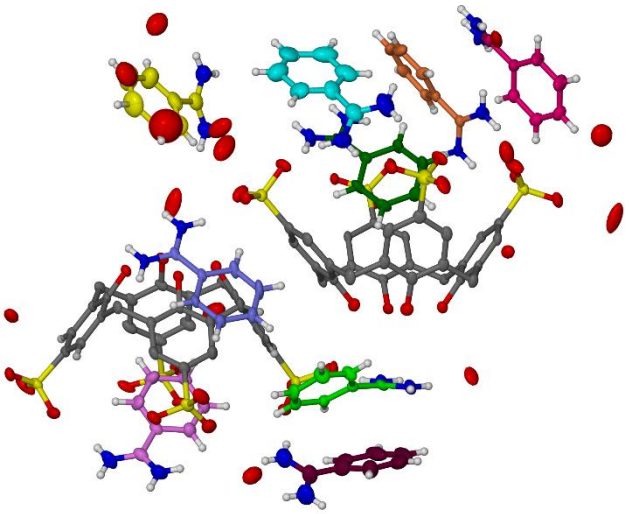

*Figure 44. The asymmetric unit of the host–guest complex **C4S_BNZ_Form I**. Crystallographically unique benzamidine molecules are presented in different colours. Atomic displacement parameters set at 50% probability. Disorder omitted for clarity.*

In the ***C4S_BNZ_Form I*** complex C4S host molecule appears as a tetra-anion (Figure 45a,b). The upper rim is presented by four sulfonate groups providing anchor points for complexing benzamidine guest molecules *via* amidinium–sulfonate hydrogen bonding. Meanwhile, the lower rim of C4S is formed by four hydroxyl groups engaged in the intramolecular hydrogen bonds with the *O···O* distance in the range of 2.644(2)–2.734(2) Å, which is shorter than the standard distance between two water molecules (2.82 Å). The parameters of the intramolecular hydrogen bonds at the C4S lower rims are demonstrated in Table 21, Annex I.

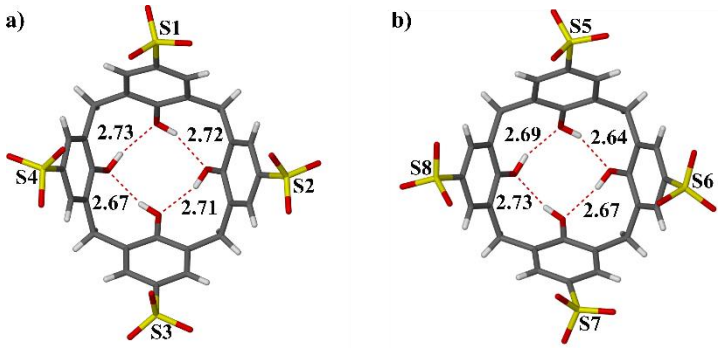

*Figure 45. O–H···O hydrogen bonding at the C4S lower rim in the host–guest complex **C4S_BNZ_Form I**. O···O distances are given in Å.*

Two C4S cavities are occupied by benzamidine molecules. C1Y > N2Y, colored in pink, has the full occupancy. The second benzamidine (green) is disordered over two positions – C1X > N2X (86% occupancy) and C1XA > N2XA (14% occupancy) (Figure 46a,b). The inclusion of the benzamidine molecules into the macrocyclic cavity of C4S occurs at different depth which is defined as the distance between the P plane defined by methylene bridges of C4S and the centroid of the

benzamidine aromatic ring. The depth of inclusion of the C1Y > N2Y and C1X > N2X molecules is 4.33 Å and 4.24 Å, respectively (Figure 47). Differences in inclusion depth result in slight changes of the conformation of the macrocycle. Both C4S molecules are in the pinched cone conformation. The distances between opposite Sulphur atoms are 9.96 and 10.74 Å for C4S molecule including C1Y > N2Y benzamidine, 9.73 and 10.93 Å for C4S including C1X > N2X benzamidine, reflecting a slight cone pinching in both cases.

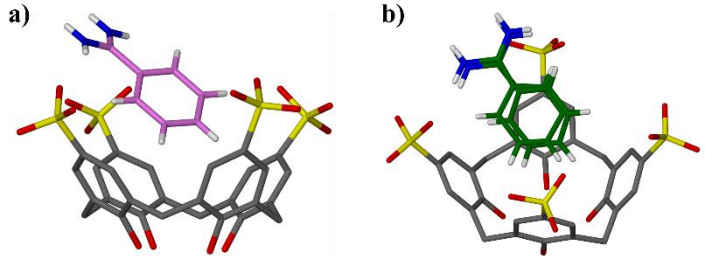

*Figure 46. Inclusion mode of benzamidines in C4S cavity into the host–guest complex **C4S_BNZ_Form I**: (a) inclusion of benzamidine with 100% occupancy; (b) inclusion of benzamidine disordered over two positions.*

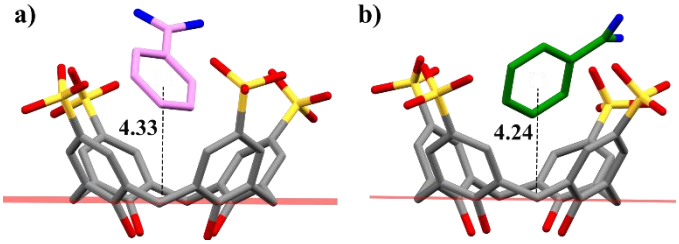

*Figure 47. The depth of inclusion of benzamidine into C4S cavity in the host–guest complex **C4S_BNZ_Form I**: (a) inclusion of benzamidine with 100% occupancy; (b) inclusion of benzamidine disordered over two positions (only C1X > N2X of major occupancy 86% is shown). Distances are given in Å.*

Symmetry expansion *via* inversion centre reveals that 1:1 host–guest ensemble (with ordered pink C1Y > N2Y benzamidine as a guest) is part of *2:2 pseudocapsular associate*. C4S molecules are placed in the *rim-to-rim* position holding two benzamidine cations in antiparallel orientation (Figure 48a). The size of the *pseudocapsule* is 15.1 Å measured as the distance between the planes defined by the hydroxyl groups of two C4S molecules. Located between two C4S molecules in the capsule, benzamidine forms *N–H···O* interactions with both calixarenes and water. The amidinium group donates four *N–H···O* hydrogen bonds: one toward a sulfonate oxygen atom of parent C4S, two toward oxygen atoms of the adjacent C4S, and one toward water molecule (*N···O* distances 2.767(15)–3.111(4) Å). In addition, benzamidine participates in two weak *C–H···O* contacts with the parent calixarene upper rim, and engages in two *C–H···π* interactions with the cavity interiors of the host, with *C···centroid* distances of 3.519(3) and 3.647(4) Å (Figure 48b).

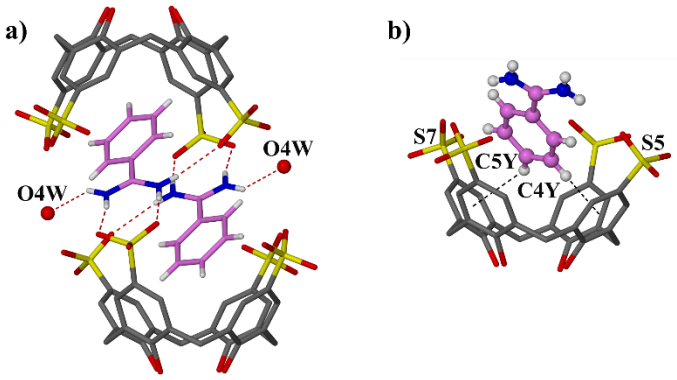

*Figure 48. Host–guest complex **C4S_BNZ_Form I**: (a) N–H···O hydrogen bonds between N–H groups of benzamidine and sulfonate oxygen atoms of C4S / water molecules in the pseudocapsule; (b) C–H···π interactions between benzamidine aromatic ring and cavity interior of C4S molecule.*

In contrast to the C1Y > N2Y benzamidine, which is incorporated into a *2:2 pseudocapsular associate*, the C1X > N2X benzamidine forms an *open inclusion complex* with C4S. Its amidinium group establishes four *N–H···O* hydrogen bonds: two directed toward the parent macrocycles and two toward neighbouring molecules (*N···O* distances 2.912(8)–3.095(10) Å), Figure 49a). In addition, C1X > N2X engages with the cavity interior of C4S through three *C–H···π* interactions, with *C···centroid* distances of 3.595(4), 3.613(4), and 3.618(5) Å (Figure 49b). The parameters of these interactions formed by the benzamidines are summarized in Tables 21,22, Annex I.

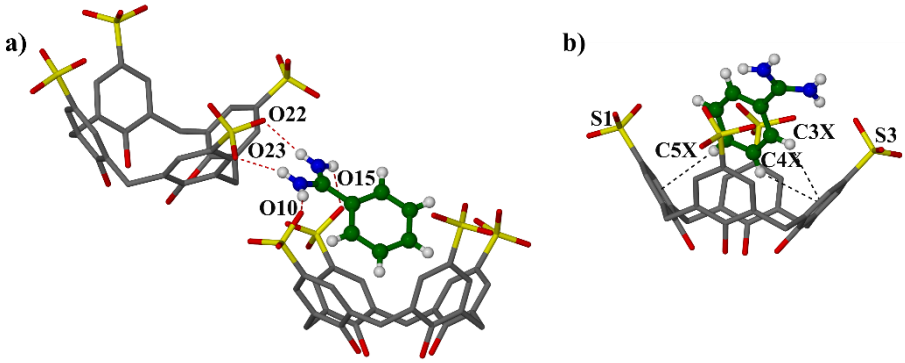

*Figure 49. Host–guest complex **C4S_BNZ_Form I**: (a) N–H···O hydrogen bonds between N–H groups of benzamidine (C1X > N2X of major occupancy 86%) and sulfonate oxygen atoms of C4S; (b) C–H···π interactions between benzamidine aromatic ring and cavity interior of C4S molecule. Disorder of the benzamidine omitted for clarity.*

The hydrogen bonding patterns of all benzamidines residing outside the cavities of C4S are rather intuitive comprising from two to four amidinium–sulfonate hydrogen bonds with C4S, remaining hydrogen bonds are satisfied with water molecules. The Figure 50a shows the example of the *N–H···O* hydrogen bonding between outer benzamidines and C4S / water molecules. C1K > N2K benzamidine interacts *via* hydrogen bonds with C4S and water molecules at the *N···O* distances in the range of 2.745(8)–3.200(9) Å, C1L > N2L – 2.864(3)–3.158(8) Å. The benzamidine molecule C1M > N2M interacts with C4S from the outside through the *π···π* contact, the distance between centroids of the aromatic rings is 3.877(17) Å (Figure 50b). The parameters of *N–H···O* and *π···π* interactions

formed by external benzamidines are shown in Table 21 and Table 23, Annex I.

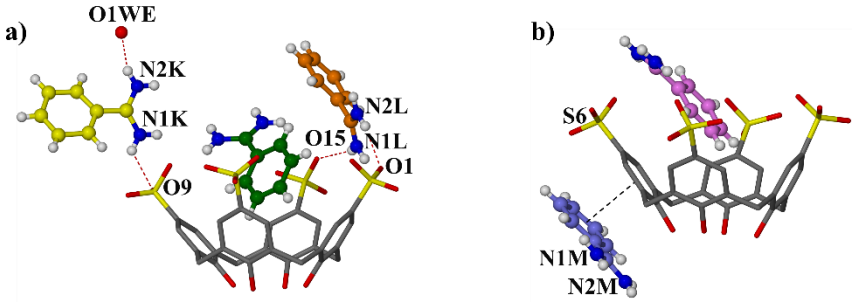

*Figure 50. Host–guest complex **C4S_BNZ_Form I**: (a) N–H···O hydrogen bonds between N–H groups of outer benzamidines and sulfonate oxygen atoms of C4S / water molecules; (b) π···π interaction between aromatic rings of outer benzamidine and C4S.*

The crystal structure expansion reveals that the layers of C4S molecules are stabilized by *C–H···π* and *π···π* interactions. A *C–H···π* contact is formed between the methylene bridge *C–H* groups and the aromatic ring of an adjacent C4S molecule, with a *C···centroid* distances of 3.285(3) Å. Neighbouring C4S molecules engage in *π···π* stacking with an inter-ring distances of 3.680(14) Å. The parameters of these intermolecular interactions are placed in Table 23, Annex I. The crystal packing consists of corrugated antiparallel bilayers of C4S molecules, separated by layers of benzamidines and water molecules (Figures 51a,b). Benzamidine molecules are located both inside the C4S double layers and in the spaces between them together with the water molecules.

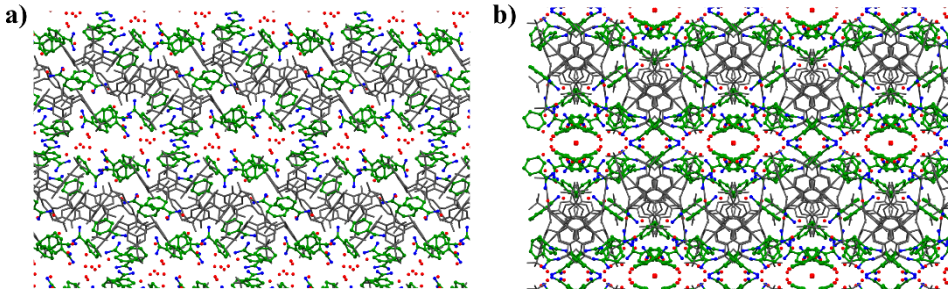

*Figure 51. Crystal packing of the host–guest complex **C4S_BNZ_Form I** viewed along (a) **b** and (b) **c** directions. All benzamidine molecules are colored in green. Disorder omitted for clarity.*

Structure analysis of the C4S_BNZ_Form II complex

The complex ***C4S_BNZ_Form II*** has the formula $2(C_{28}H_{20}O_{16}S_4)\cdot 8(C_7H_9N_2)\cdot 10.25(H_2O)$. Single-crystal X-ray diffraction analysis shows that this complex crystallizes in a monoclinic crystal system in the space group *P2/n*. The asymmetric part consists of two C4S, eight benzamidine molecules, and 10.25 water molecules (Figure 52).

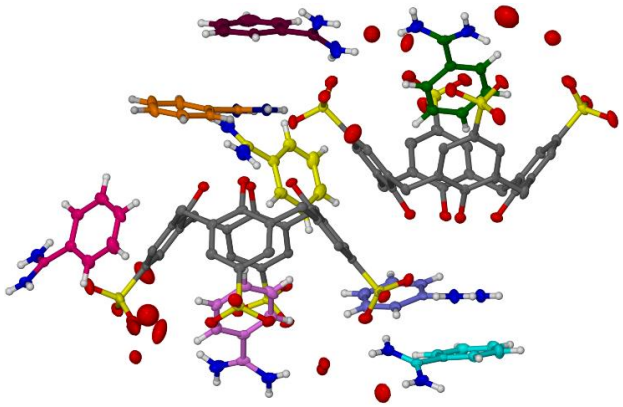

*Figure 52. The asymmetric unit of the host–guest complex **C4S_BNZ_Form II**. Crystallographically unique benzamidine molecules are presented in different colours. Atomic displacement parameters set at 50% probability. Disorder omitted for clarity.*

In the ***C4S_BNZ_Form II*** complex C4S molecule appears as a tetra-anion (Figure 53a,b). The upper rim features four sulfonate groups that anchor benzamidine guest molecules in the C4S cavity through hydrogen bonds. The lower rim consists of four phenolic *–OH* groups forming intramolecular hydrogen bonds with the distance between O atoms in the range of 2.622(2)–2.706(2) Å. The parameters of intramolecular hydrogen bonds in C4S molecules are shown in Table 24, Annex I.

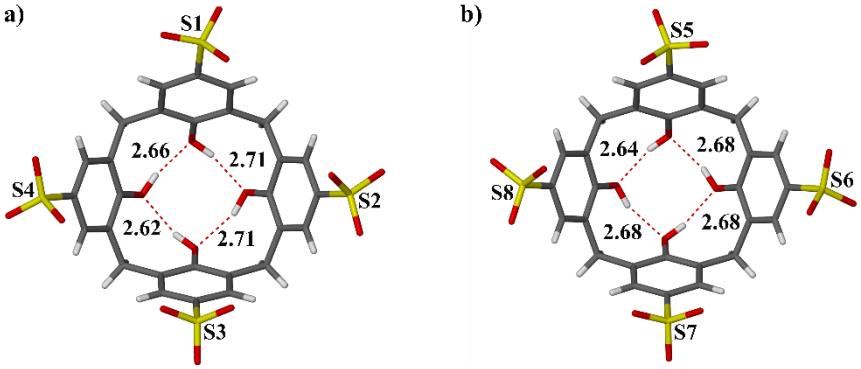

*Figure 53. O–H···O hydrogen bonding at the C4S lower rim in the host–guest complex **C4S_BNZ_Form II**. O···O distances are given in Å.*

Each C4S molecule hosts one benzamidine within its cavity. The C1X > N2X benzamidine, shown in pink, is fully occupied, while the second benzamidine, shown in green, is disordered over three positions with occupancies of 75% for C1Y > N2Y, and 12.5% each for C1YA > N1YA and C1YB > N2YB (Figures 54a–c). The benzamidines are included in the macrocyclic cavities of C4S at different depths, measured as the distance between the plane defined by the C4S methylene bridges (P plane) and the centroid of the benzamidine aromatic ring. The inclusion depths are 4.15 Å for C1X > N2X and 4.23 Å for C1Y > N2Y (Figure 55). Variations in the depth and mode of inclusion lead to

slight differences in the cone conformations of the macrocycles. The distances between opposite sulfur atoms are 9.98 and 10.97 Å for one C4S, and 10.21 and 11.14 Å for another.

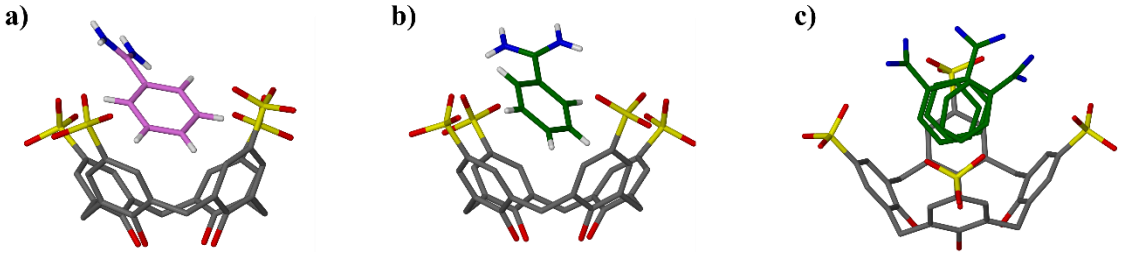

Figure 54. Inclusion mode of benzamidines into C4S cavity in the host–guest complex ***C4S_BNZ_Form II****: (a) inclusion of benzamidine with 100% occupancy; (b) inclusion of benzamidine disordered over three positions (C1Y > N2Y) of major occupancy 75%; (c) inclusion of benzamidine disordered over three positions.*

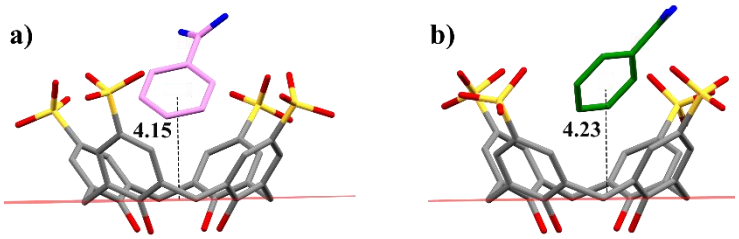

Figure 55. The depth of inclusion of benzamidine in C4S cavity in the host–guest complex ***C4S_BNZ_Form II****: (a) inclusion of benzamidine with 100% occupancy; (b) inclusion of benzamidine disordered over three positions (only C1Y > N2Y of major occupancy 75% is shown). Distances are given in Å.*

Symmetry expansion through a 2-fold axis shows that the 1:1 host–guest ensemble, with the ordered C1X > N2X benzamidine as guest, forms a *2:2 pseudocapsular associate*. The C4S molecules are arranged in a *rim-to-rim* orientation, accommodating two benzamidine cations in an antiparallel position (Figure 56a). The resulting capsule has a size of 15.7 Å, defined by the distance between the planes formed by the hydroxyl groups of C4S. The C1X > N2X benzamidine participates in *N–H···O* hydrogen bonding with C4S and water molecules, donating four hydrogen bonds: two to sulfonate oxygen atoms of adjacent C4S and two to water molecules (2.864(14)–3.119(2) Å). In addition, the benzamidine interacts with the cavity interior of C4S *via* two *C–H···π* contacts, with *C···centroid* distances of 3.507(2) Å and 3.630(3) Å (Figure 56b).

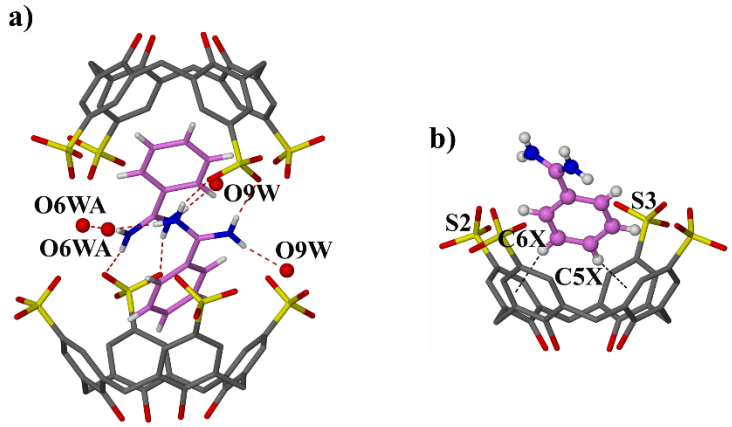

*Figure 56. Host–guest complex **C4S_BNZ_Form II**: (a) N–H···O hydrogen bonds between N–H groups of benzamidine C1X > N2X and sulfonate oxygen atoms of C4S / water molecules in the pseudocapsule; (b) C–H···π interactions between benzamidine aromatic ring and cavity interior of C4S molecule.*

The disordered benzamidine C1Y > N2Y is also incorporated into a *2:2 pseudocapsular associate*, with the capsule size measuring 15.5 Å. This benzamidine forms one *N–H···O* hydrogen bond with the parent C4S, two with neighbouring C4S molecules, and one with water molecule, with *N···O* distances ranging from 2.698(3) to 3.027(4) Å (Figure 57a). C1Y > N2Y molecule is stabilized within the C4S cavity by two *C–H···π* interactions at the 3.775(7) and 3.366(5) Å distances (Figure 57b).

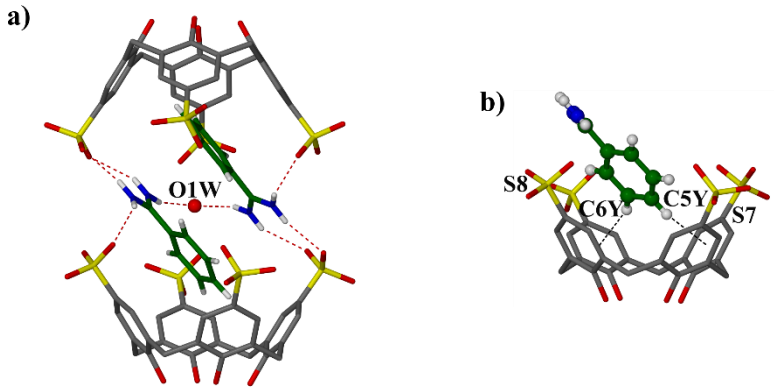

*Figure 57. Host–guest complex **C4S_BNZ_Form II**: (a) N–H···O hydrogen bonds between N–H groups of benzamidine C1Y > N2Y nd sulfonate oxygen atoms of C4S / water molecules; (b) C–H···π interactions between benzamidine aromatic ring and cavity interior of C4S molecule. Disorder of the benzamidine omitted for clarity.*

Benzamidine molecules located outside the cavities of C4S form hydrogen bonds with both C4S and water molecules. Figure 58a illustrates *N–H···O* hydrogen bonds involving two benzamidines and C4S/water molecules. The *N···O* distances range from 2.798(4) to 2.905(13) Å for C1I > N2I and from 2.775(2) to 2.933(2) Å for C1L > N2L. In addition, two benzamidines, C1Z > N2Z and C1K > N2K, engage in *C–H···π* interactions with the outer surface of C4S, with *C···centroid* distances of 3.720(3) and 3.748(3) Å (Figure 58b). Detailed parameters of all non-covalent interactions involving benzamidine molecules are summarized in Tables 24,25, Annex I.

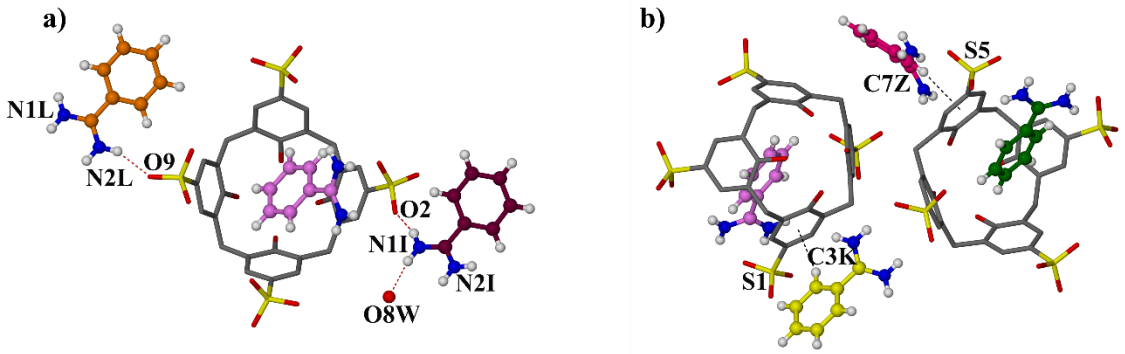

*Figure 58. Host–guest complex **C4S_BNZ_Form II**: (a) N–H···O hydrogen bonds between N–H groups of outer benzamidines and sulfonate oxygen atoms of C4S / water molecules; (b) C–H···π interactions occur between the aromatic rings of the outer benzamidine molecules and the aromatic rings of the C4S molecules.*

Analysis of the expanded crystal structure shows that the layers of C4S molecules are stabilized through *C–H···π* interactions, formed between the methylene bridge *C–H* groups and the aromatic rings of adjacent C4S molecules, at distances of 3.209(2) and 3.232(2) Å (Figure 59). Geometric parameters of these interactions are summarized in Table 25, Annex I.

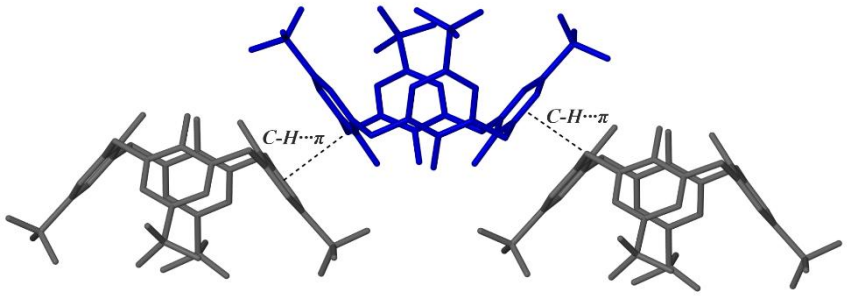

*Figure 59. Host–guest complex **C4S_BNZ_Form II**: C–H···π interactions between C4S molecules. Crystallographically non–equivalent C4S molecules are shown in different colors.*

The overall packing is characterized by bilayers of C4S molecules arranged in alternating *up–down* orientations, separated by layers of benzamidines and water molecules. Benzamidines are distributed both inside the C4S double layers and within the layers (Figure 60).

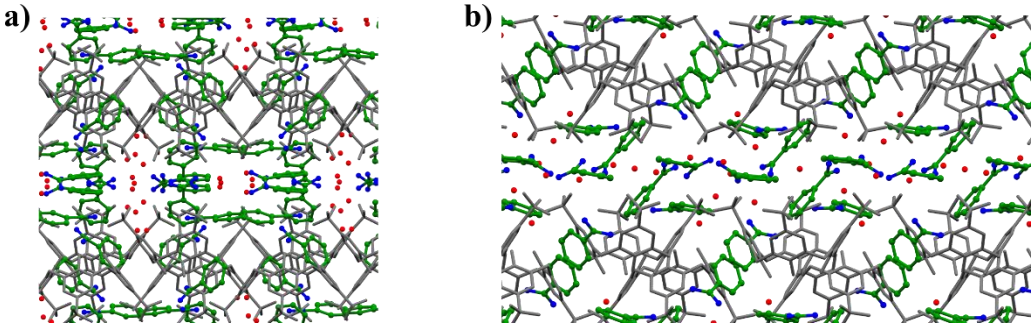

*Figure 60. Crystal packing of the host–guest complex **C4S_BNZ_Form II** viewed along (a) **a** and (b) **b** directions. Benzamidine molecules are colored in green. Disorder omitted for clarity.*

Structure analysis of the C4S_BNZ_Form III complex

The complex ***C4S_BNZ_Form III*** has the formula $(C_{28}H_{20}O_{16}S_4)\cdot 2(C_7H_9N_2)\cdot 2(H_5O_2^+)\cdot 4.4(H_2O)$. Single-crystal X-ray diffraction analysis shows that this complex crystallizes in a triclinic crystal system in the space group *P–1*. The asymmetric part consists of one C4S, two benzamidines, two Zundel cations and 4.4 water molecules (Figure 61).

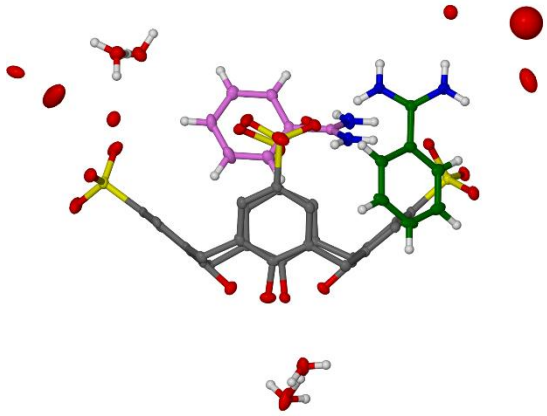

*Figure 61. The asymmetric unit of the host–guest complex **C4S_BNZ_Form III**. Crystallographically unique benzamidine molecules are presented in different colours. Atomic displacement parameters set at 50% probability. Disorder of Zundel cation omitted for clarity.*

In the ***C4S_BNZ_Form III*** complex, the C4S molecule appears as a tetra-anion (Figure 62a). The hydroxyl groups form intramolecular hydrogen bonds, with *O···O* distances ranging from 2.692(2) to 2.894(3) Å; the geometric parameters are listed in Table 26, Annex I. The C4S cavity is occupied by one benzamidine molecule, C1X > N2X, shown in pink (Figures 62b,c). Compared to complexes ***I*** and ***II***, the benzamidine is positioned slightly higher within the cavity. The tilted aromatic ring of benzamidine lies nearly centrally between the S1 and S3 atoms of C4S, at distances of 3.69 and 3.74 Å between the nearest O atoms of the C4S sulfonate group and the benzamidine centroid of the aromatic ring. The amidinium group is close to the three sulfonate groups of the calixarene. The depth of inclusion is 4.85 Å. To accommodate this mode of benzamidine incorporation, the C4S molecule adopts a distinctly pinched conformation, in contrast to the more symmetrical cone shape observed in complexes ***I*** and ***II***. The distances between opposite sulfur atoms are 8.31 and 12.25 Å.

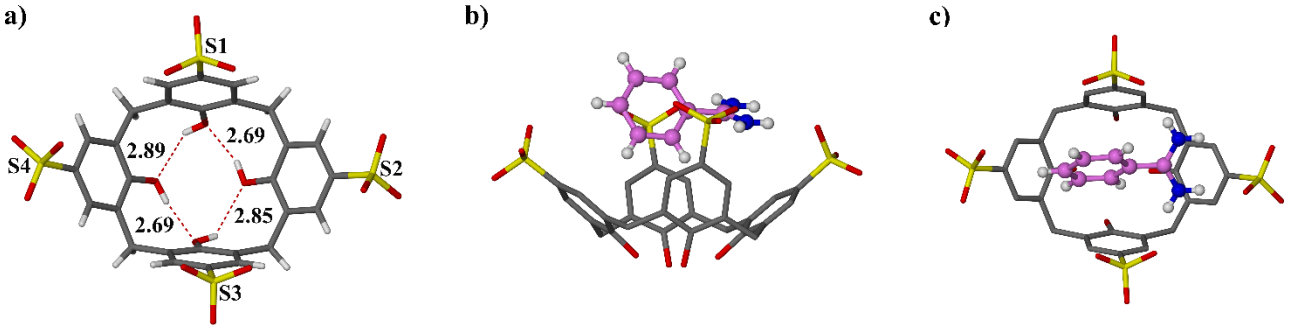

*Figure 62. Host–guest complex **C4S_BNZ_Form III**: (a) O–H···O hydrogen bonding at the C4S lower rim; (b–c) inclusion mode of benzamidine into C4S cavity. Distances are given in Å.*

The C1X > N2X benzamidine forms a *2:2 pseudocapsular* associate. The C4S molecules adopt a *rim-to-rim* arrangement, accommodating two benzamidine molecules in an antiparallel orientation (Figure 63a). The capsule formed by C4S has a size of 15.9 Å, defined as the distance between the planes formed by the hydroxyl groups of the macrocycles. The included C1X > N2X benzamidine participates in non-covalent interactions of the *N–H···O* types with C4S and water molecules. It donates four *N–H···O* hydrogen bonds: three to sulfonate oxygen atoms of the parent C4S and one to water molecule, with *N···O* distances of 2.855(3)–2.904(3) Å. A single *C–H···π* contact is formed between the benzamidine and macrocycle aromatic walls at the 3.546(3) Å (Figure 63b). The second benzamidine molecule, C1Y > N2Y, is located outside the C4S cavity and engages in three *N–H···O* hydrogen bonds with sulfonate oxygen atoms of three C4S molecules and one hydrogen bond with water molecule, with *N···O* distances ranging from 2.819(3) to 2.929(3) Å (Figure 63c).

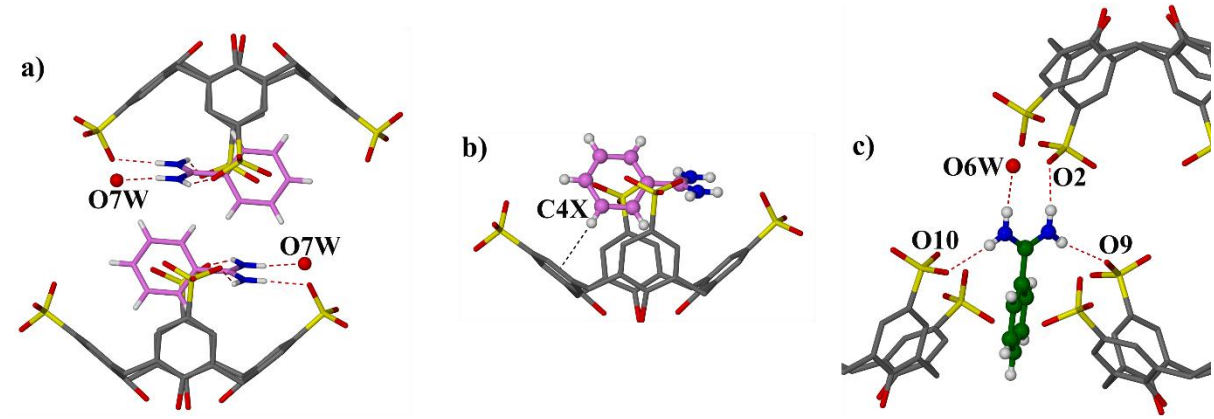

*Figure 63. Host–guest complex **C4S_BNZ_Form III**: (a) N–H···O hydrogen bonds between N–H groups of benzamidine and sulfonate oxygen atoms of C4S / water molecules; (b) C–H···π interaction between benzamidine aromatic ring and aromatic ring of C4S molecule; (c) N–H···O hydrogen bonds between N–H groups of outer benzamidine and sulfonate oxygen atoms of C4S / water molecules.*

The charge balance of the complex is maintained by two oxonium ions, $H_5O_2^+$ Zundel cations. These cations are characterized by short *O–H···O* distances of 2.441(2) Å (O1W–O2W) and 2.557(5) Å (O3W–O4W), indicative of strong hydrogen bonding. One $H_5O_2^+$ cation (O1W–O2W) is

positioned near the upper rim of C4S (Figures 64a,b) and forms four hydrogen bonds with its environment: two to sulfonate oxygen atoms and two to water molecules, with *O···O* distances of 2.573(2)–2.690(2) Å. The second cation (O3W–O4W) resides close to the hydroxyl groups at the lower rim of C4S (Figures 65a,b) and donates four hydrogen bonds to the sulfonate oxygen atoms of adjacent C4S molecules, with *O···O* distances ranging from 2.594(5) to 2.745(3) Å.

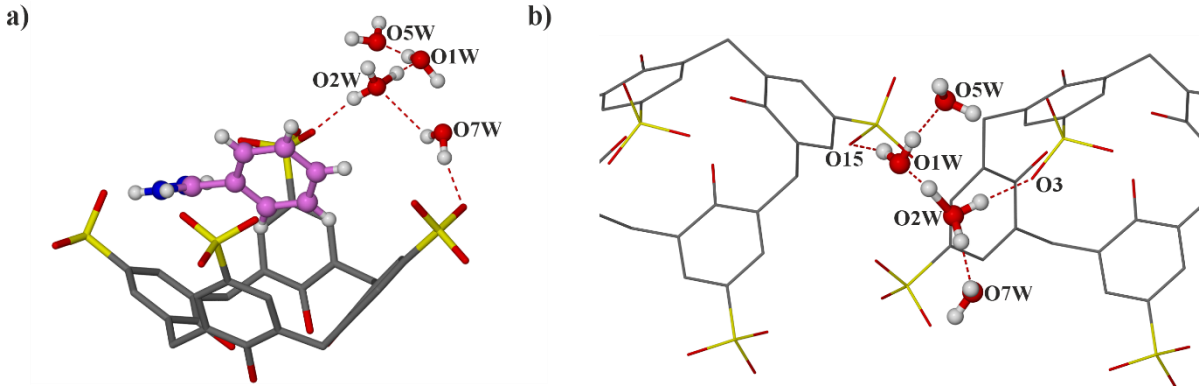

*Figure 64. Host–guest complex **C4S_BNZ_Form III**: (a) interaction between Zundel cation $H_5O_2^+$ formed by O1W and O2W water molecules and the upper rim of the C4S macrocycle; (b) the hydrogen bonding network around Zundel cation.*

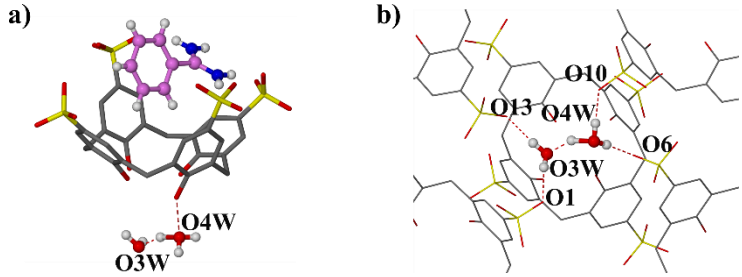

*Figure 65. Host–guest complex **C4S_BNZ_Form III**: (a) interaction between Zundel cation $H_5O_2^+$ formed by O3W and O4W water molecules and the lower rim of the C4S macrocycle; (b) the hydrogen bonding network around Zundel cation.*

As in the case of complexes ***I*** and ***II***, the crystal packing of ***C4S_BNZ_Form III*** is represented by *up–down* C4S bilayers separated by the layers of benzamidine and water molecules (Figures 66a,b). Benzamidine molecules are in the C4S bilayers and the space between them. However, in complexes ***I*** and ***II***, the C4S molecules in these bilayers are bound by *C–H···π* and *π···π* interactions, while in complex ***III*** such types of interactions are absent. The C4S molecules, closer to each other, in the *up–down* positions are connected by *O–H···O* contacts between the *O12–H12* hydroxyl group of the up C4S molecule and the sulfonate oxygen atom O6 of the down calixarene, with a contact distance of 2.911(2) Å. Detailed parameters of the *O–H···O*, *C–H···π* and *π···π* intermolecular interactions in the ***C4S_BNZ_Form III*** complex are written in Tables 26,27, Annex I.

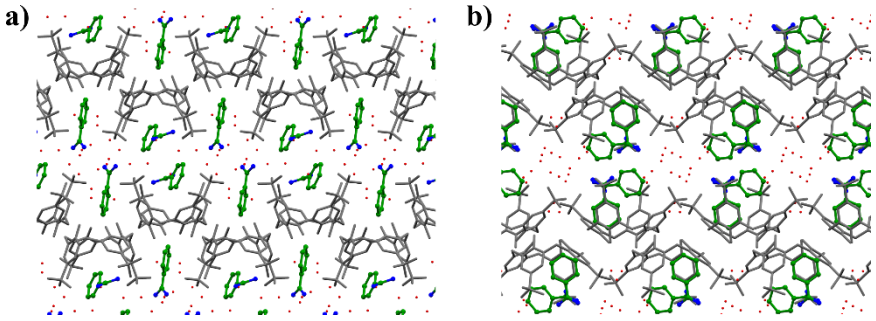

*Figure 66. Crystal packing of the host–guest complex **C4S_BNZ_Form III** viewed along (a) **a** and (b) **b** directions. Benzamidine molecules are colored in green. Disorder omitted for clarity.*

NMR analysis of the C4S_BNZ complex

To gain a better insight into the host–guest system of C4S with benzamidine, the complexation studies in a solution (D_2O) using ^1H NMR spectroscopy were performed (Figure 67). The dissolution of C4S ***sulfonic acid*** in water (4 mM in D_2O) results in a pH value of 1.6, while the pH value of benzamidine chloride is 8.5. Upon mixing host and guest solutions, the pH remained at 1.6. Due to the significant difference in pH between the solutions of benzamidine hydrochloride and C4S ***sulfonic acid***, the spectrum of benzamidine hydrochloride at pH 1.6 was re-checked. The position of aromatic proton resonances in the spectrum at pH 1.6 is identical to that at pH 8.5. As a result of the host–guest complexation, the signals from aromatic protons of benzamidine (signals ***a***, ***b***, and ***c***) showed a noticeable shift towards lower ppm values in the presence of C4S. Specifically, the signal of proton ***a*** shifted from 7.62 ppm to 6.53 ppm (Δδ=1.09 ppm), proton ***b*** shifted from 7.78 ppm to 5.65 ppm (Δδ=2.13 ppm), and proton ***c*** shifted from 7.75 ppm to 5.50 ppm (Δδ=2.25 ppm). This shift of all aromatic proton resonances confirms the inclusion of the benzamidine aromatic ring within the macrocyclic cavity of C4S.

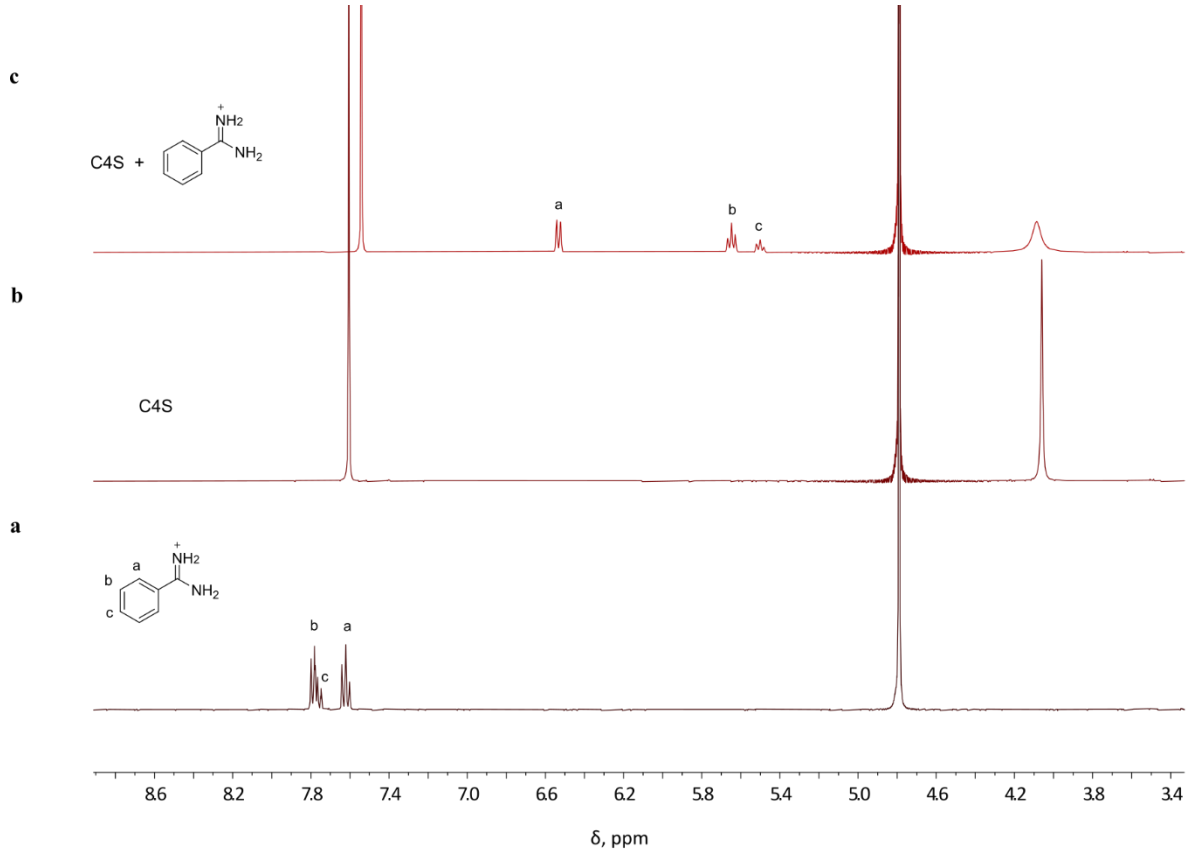

*Figure 67. ^{1}H NMR spectra of (a) benzamidine; (b) C4S **sulfonic acid**; (c) **C4S_BNZ** host–guest complex recorded at RT in D_2O, C (benzamidine) = 4 mM, C (C4S) = 4 mM, pH (**C4S_BNZ**) = 1.6.*

Crystallization and microscopic observations for C4S sodium salt complexes with benzamidine

In the previous section, the crystal structures of three host–guest complexes derived from C4S ***sulfonic acid*** and benzamidine were analyzed. This section presents detailed information on the preparation, refinement, and crystal structure characterization of complexes obtained from the ***sodium salt*** of C4S.

20 mg of C4S ***sodium salt*** was dissolved in 0.5 mL of H_2O/EtOH (1:1). The solution of 16.3 mg benzamidine hydrochloride in 0.5 mL of H_2O/EtOH (1:1) was combined with the solution of the host (Figure 68a). After a month, the colorless prismatic crystals of good diffraction quality appeared. Single-crystal X-ray diffraction analysis revealed these crystals to be the host–guest complex ***C4S_BNZ_Form IV*** (Figure 68b). The crystals of ***C4S_BNZ_Form IV*** were unstable in the contact with the mother solution and dissolved slowly accompanied by the appearance of a colorless elongated prismatic crystals after 10 days. The new crystals were identified concomitantly with ***C4S_BNZ_Form IV*** and corresponded to the complex ***C4S_BNZ_Form V*** (Figure 68c).

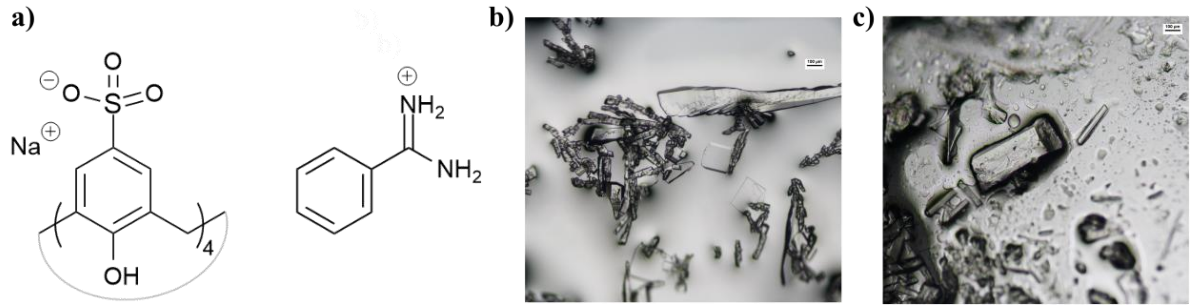

Figure 68. (a) Chemical structure of the C4S ***sodium salt*** *host and the benzamidine (**BNZ**) guest; (b) photomicrographs of prism–like crystals of **C4S_BNZ_Form IV**; (c) small, elongated prismatic crystals of **C4S_BNZ_Form V** appearing after aging of crystals **C4S_BNZ_Form IV** in the mother liquor allowing the solvent to evaporate slowly. The scale bar corresponds to 100 µm.*

The refinement details of the C4S_BNZ complexes: Form IV and V

The asymmetric unit of ***C4S_BNZ_Form IV*** includes one penta-anion of C4S molecule, three monocations of benzamidine, two sodium cations and 8.4 water molecules. One sulfonate group of C4S was modelled and refined as disordered over two positions. The first component of disorder O5 > S2 is refined with PART 1 command (58.3% occupancy), the second O5A > S2A is refined with PART 2 (41.7% occupancy).

The aromatic ring of the benzamidine molecule C1X > N2X included in the calix[4]arene cavity is refined as disordered over two positions. The first component of disorder C2X > C7X is refined with PART 1 command (51% occupancy). Second component of a disorder C2XA > C7XA is refined with the PART 2 (49% occupancy). SIMU and RIGU restraints are used to equate atomic displacement parameters of disordered atoms and to make the relative motion of these atoms at right angles to the formed bonds.

The Na1 cation has the full occupancy, and the second Na2 is disordered over two positions Na2 (58.3% occupancy) and Na2a (41.7% occupancy). O4W, O5W, O6W, O8W, O9W water molecules are coordinated to the Na2 cation and are disordered over two positions with the respect occupancies. The hydrogen atoms in this complex are added in a mixed type – geometrically and from the difference Fourier map. Atoms from the difference Fourier map are added to the O1W, O2W, O3W, O4W, O8W, O9W water molecules and to the O4 atom of the C4S hydroxyl group. DFIX restraints are used to limit the proper *O–H* distances. DANG command is applied to the water molecules O3W and O8W to restraint 1,3 atom distance. O5W, O6W, O7WA molecules are refined without hydrogen atoms.

The asymmetric unit of ***C4S_BNZ_Form V*** consists of one penta-anion of C4S molecule, five monocations of benzamidine and 3.5 water molecules. Atoms of the three C4S sulfonate groups are disordered over two positions. The first component of disorder O1 > O3 is refined with PART 1 command (62% occupancy), the second O1A > O3A is refined with PART 2 (38% occupancy). The first component of disorder O5 > S2 is refined with PART 1 command (65.6% occupancy), the

second O5A > S2A is refined with PART 2 (34.4% occupancy). The first component of disorder O13 > O15 is refined with PART 1 command (65.1% occupancy), the second O13A > O15A is refined with PART 2 (34.9% occupancy).

The benzamidine molecule with atom names C1I > N2I residing outside of the C4S is refined as disordered over two positions. The first component of the disorder C1I > N2I is refined with PART 1 command (63.7% occupancy). Second component of a disorder C1IA > N2IA is refined with the PART 2 (36.3% ccupancy). To equate atomic displacement parameters of disordered atoms and to make the relative motion of these atoms at right angles to the formed bonds, the SIMU and RIGU restraints are used.

The O3W molecule is refined with 50% occupancy. The O4W water molecule lies close to disordered C1I > N2I molecule and is also disordered over two positions. The first component of disorder O4W is refined with PART 1 command (63.7% occupancy), the second O4A is refined with PART 2 command (36.3% occupancy). All hydrogen atoms are added geometrically, except H1KA and H1KB hydrogen atoms of the N1K amidine group. The DFIX restraint is applied to fix the proper *N–H* distance of 0.88 Å. The O4W molecule is refined without hydrogen atoms. The basic crystallographic data of the two discussed structures is provided in Table 3.

*Table 3. Crystal data and structure refinement for **C4S_BNZ** complexes: **Form IV** and **V**.*

Parameters	***Form IV***	***Form V***
Formula moiety	$(C_{28}H_{19}O_{16}S_4Na_2)\cdot 3(C_7H_9N_2)$ $\cdot 8.4(H_2O)$	$(C_{28}H_{19}O_{16}S_4)\cdot 5(C_7H_9N_2)$ $\cdot 3.5(H_2O)$
Formula weight	1300.47	1408.53
Crystal system	Triclinic	Monoclinic
Space group	*P–1*	$P2_1/n$
a / Å	14.1739(2)	17.6557(1)
b / Å	14.1861(3)	17.9135(1)
c / Å	16.4567(3)	20.5080(1)
α / °	64.756(2)	90
β / °	77.269(1)	91.579(1)
γ / °	70.678(2)	90
Volume / Å^3	2812.2(1)	6483.7(1)
Z	2	4
ρ_{calc} /g·cm^{-3}	1.54	1.44
Crystal color	Colorless	Colorless
Crystal morphology	Prism	Prism
μ / mm^{-1}	2.49	2.05
θ_{max} / °	70.0	70.1
Reflections collected	74035	82172
Independent reflections	10611 [R_{int} = 0.025]	12282 [R_{int} = 0.029]
Data / Restraints / Parameters	10611/ 267/ 950	12282/ 362/ 1051
Observed data [I > 2σ(I)]	10181	11466
Final R indexes [I ≥ 2σ(I)]	R_1 = 0.057, wR_2 =0160	R_1 = 0.036, wR_2 =0.096
Final R indexes [all data]	R_1 = 0.058, wR_2 = 0.162	R_1 = 0.038, wR_2 = 0.098
Goodness-of-fit on F^2	1.04	0.99
Largest diff. peak and hole / e·Å^{-3}	1.02 / –0.84	0.42 / –0.43

Structure analysis of the C4S_BNZ_Form IV complex

The co-crystallization of C4S ***sodium salt*** with benzamidine hydrochloride from water–ethanol solution (1:1) results in the formation of the complex ***C4S_BNZ_Form IV*** with the formula $C_{28}H_{20}O_{16}S_4Na_2\cdot 3C_7H_9N_2\cdot 8.4H_2O$. Single-crystal X-ray diffraction analysis shows that this complex crystallizes in a triclinic crystal system in the space group *P–1*. The asymmetric part consists of one C4S, three benzamidine molecules, two sodium cations, and 8.4 water molecules (Figure 69).

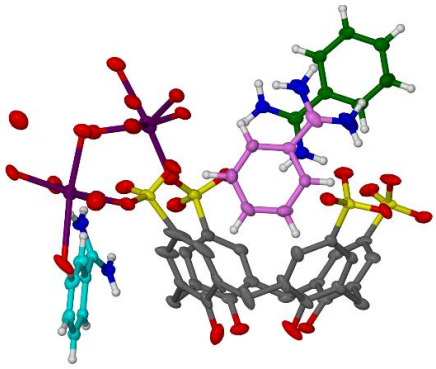

*Figure 69. The asymmetric unit of the host–guest complex **C4S_BNZ_Form IV**. Crystallographically unique benzamidine molecules are presented in different colours. Atomic displacement parameters set at 50% probability. Disorder omitted for clarity.*

The ***C4S_BNZ_Form IV*** complex features a penta-anionic C4S molecule (Figure 70a). Four sulfonate groups define the upper rim, while the lower rim contains three phenolic *–OH* groups and one deprotonated phenolate group. The deprotonated O16 atom participates in two short *phenol–phenolate O···O* hydrogen bonds with O4 and O8 atoms, measuring 2.570(3) and 2.592(3) Å. Detailed intramolecular hydrogen bond parameters are provided in Table 28, Annex I. A single benzamidine molecule, C1X > N2X (pink), occupies the C4S cavity, with an inclusion depth of 4.58 Å (Figures 70b,c). The opposite sulfur atoms are separated by 10.17 and 10.55 Å, indicating a slightly pinched conformation of the macrocycle.

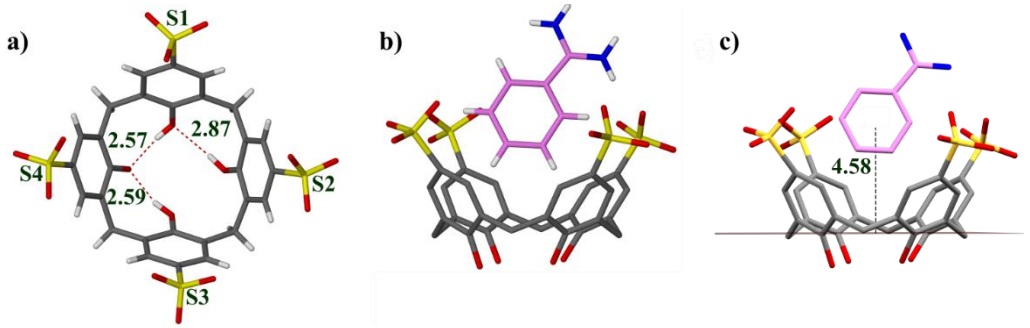

*Figure 70. Host–guest complex **C4S_BNZ_Form IV**: (a) O–H···O hydrogen bonding at the C4S lower rim with the deprotonation of the one phenolic group; (b) inclusion mode of benzamidine into C4S cavity; (c) the depth of benzamidine inclusion in C4S cavity. Distances are given in Å.*

Symmetry expansion through the inversion centre indicates that the 1:1 host–guest ensemble is part of a *2:2 pseudocapsular associate*. The C4S molecules adopt a *rim-to-rim* arrangement, accommodating two benzamidine cations in an antiparallel orientation, with the capsule measuring 16.12 Å. C1X > N2X amidinium groups donates four *N–H···O* hydrogen bonds – one to the parent sulfonate oxygen and three to oxygen atoms of adjacent C4S molecules (2.825(6)–2.969(5) Å) (Figure 71a). Stabilization within the cavity is further achieved through four *C–H···O* interactions (2.692(14)–3.393(8) Å) and one *C–H···π* interaction (3.562(10) Å) (Figures 71b,c). The detailed parameters of these interactions are described in Tables 28 and 30, Annex I.

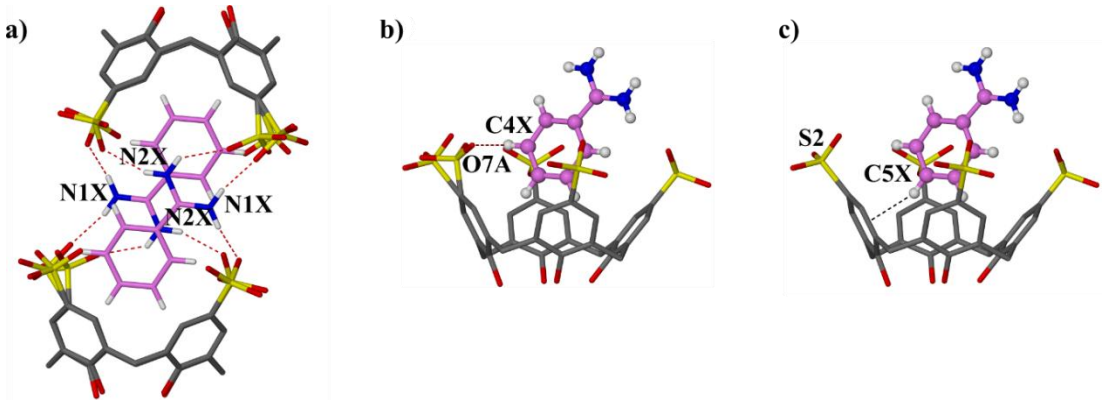

*Figure 71. Host–guest complex **C4S_BNZ_Form IV**: (a) N–H···O hydrogen bonds between N–H groups of benzamidine and sulfonate oxygen atoms of C4S in the pseudocapsule; (b) the shortest C–H···O hydrogen bond between benzamidine aromatic ring and sulfonate oxygen atom of C4S; (c) C–H···π interaction between benzamidine aromatic ring and cavity interior of C4S molecule.*

Benzamidine molecules located outside the C4S cavity are linked to C4S *via* *N–H···O* hydrogen bonds, with *N···O* distances ranging from 2.857(3) to 2.973(3) Å. These benzamidines also participate in *C–H···π* and *π···π* interactions with C4S (Figures 72a,b). Specifically, the C1Z > N2Z benzamidine forms two *C–H···π* interactions with C4S, with distances between the C atom and the centroids of the C4S aromatic rings of 3.757(3) Å and 3.683(3) Å. Also, C1Z > N2Z engages in *π···π* interactions with a symmetry-related C1Z > N2Z molecule, with a *centroid-to-centroid* distance of 3.936(17) Å. The parameters of non-covalent interactions formed by external benzamidine molecules are shown in Table 28,30,31, Annex I.

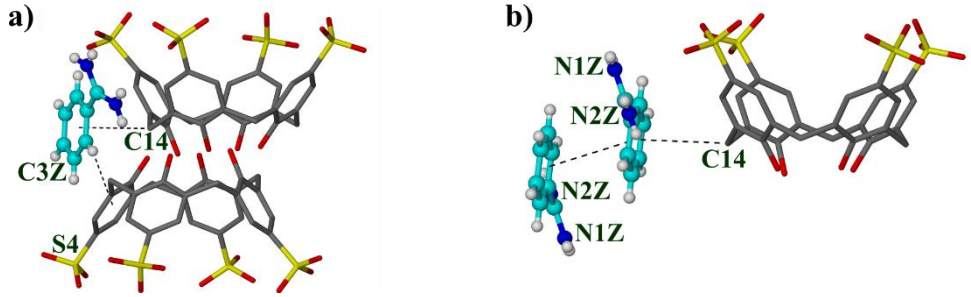

*Figure 72. Host–guest complex **C4S_BNZ_Form IV**: (a) C–H···π and π···π interactions between outer benzamidine and C4S molecule; (b) C–H···π and π···π interactions between outer benzamidine / C4S molecule, outer benzamidine / outer benzamidine.*

The structure contains two sodium cations, Na1 and Na2 (Figure 73a). Na1 is coordinated to the sulfonate oxygen atom of the C4S molecule. Its coordination sphere is completed by five water molecules, giving an overall coordination number of six. The Na1–O distances range from 2.300(3) to 2.620(9) Å. The second cation, Na2, is disordered over two positions, Na2 and Na2a, with occupancies of 58% and 42%, respectively. Na2 is connected to the upper and lower rims of C4S, as indicated in Figure 73a by Na2(1) and Na2(2). Analysis of the expanded crystal structure shows that Na2 is coordinated to three oxygen atoms of C4S (two sulfonate oxygens of the upper rim and one hydroxyl oxygen of the lower rim) and three water molecules (Figure 73b), with Na2–O distances ranging from 2.321(4) to 2.755(3) Å. The minor position, Na2a, coordinates only to water molecules

(2.294(7)–2.465(8) Å) and is omitted from the figure for clarity. Detailed bond parameters of the sodium cations are provided in Table 29, Annex I.

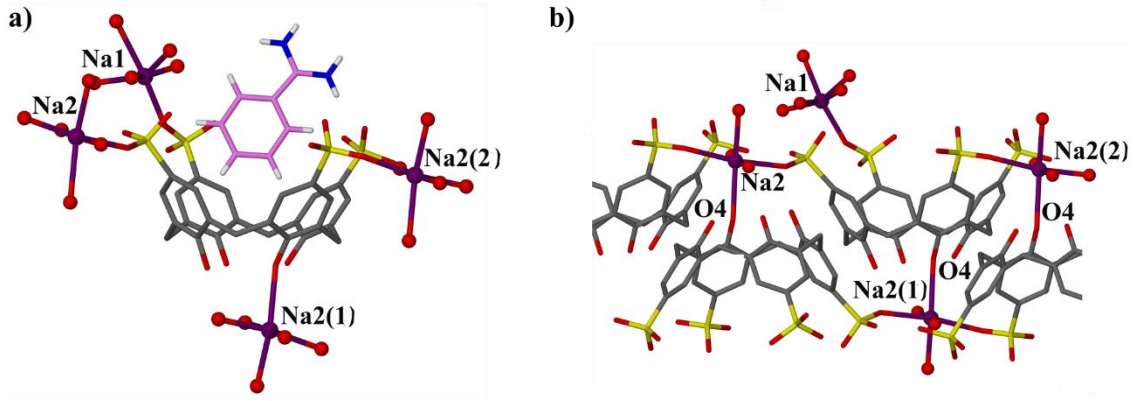

*Figure 73. Host–guest complex **C4S_BNZ_Form V**: (a,b) sodium coordination to the upper and lower rims of C4S. Disorder omitted for clarity.*

Figure 74 shows the packing of the ***C4S_BNZ_Form IV*** structure, consisting of alternating bilayers of C4S molecules coordinated with sodium cations, separated by layers of benzamidine and water molecules. Benzamidine molecules are located both within the C4S layers and in the interlayer spaces.

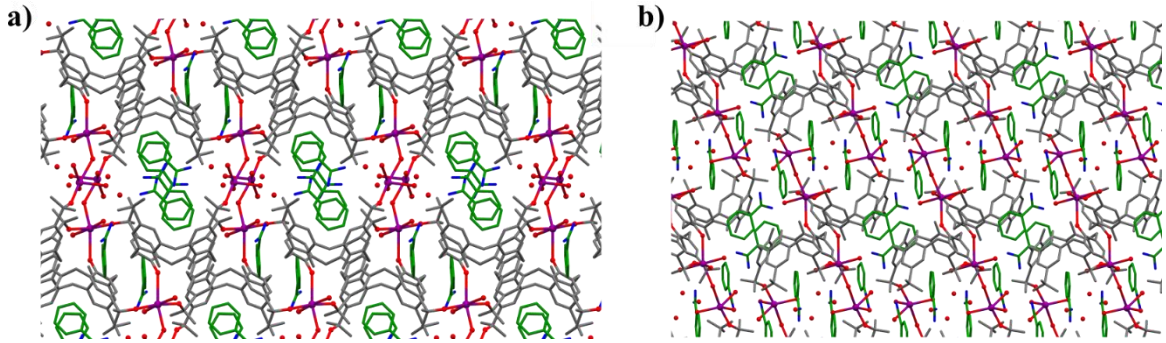

*Figure 74. Crystal packing of the **C4S_BNZ_Form IV** complex viewed along (a) **a** and (b) **b** directions. Benzamidine molecules colored in light green.*

Structure analysis of the C4S_BNZ_Form V complex

The complex ***C4S_BNZ_Form V*** has the formula $C_{28}H_{19}O_{16}S_4 \cdot 5C_7H_9N_2 \cdot 3.5H_2O$. Single-crystal X-ray diffraction analysis shows that this complex crystallizes in a monoclinic crystal system in the space group $P2_1/n$. The asymmetric part consists of one C4S, five benzamidine molecules, and 3.5 water molecules (Figure 75).

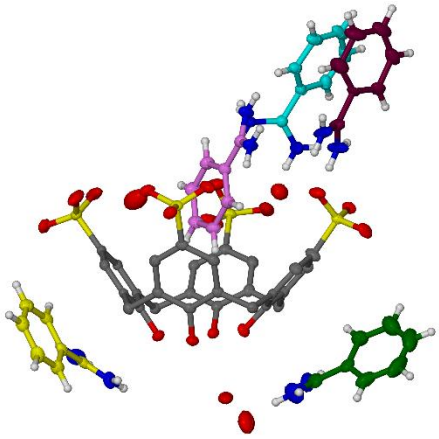

*Figure 75. The asymmetric unit of the host–guest complex **C4S_BNZ_Form V**. Crystallographically unique benzamidine molecules are presented in different colours. Atomic displacement parameters set at 50% probability. Disorder omitted for clarity.*

In the ***C4S_BNZ_Form V*** complex, the C4S molecule exists as a penta-anion (Figure 76a). The upper rim is defined by four sulfonate groups, while the lower rim comprises three protonated phenolic *–OH* groups and one deprotonated. The deprotonated O4 atom forms two short *O···O phenol–phenolate* hydrogen bonds with adjacent O8 and O16 atoms, with distances of 2.508(14) and 2.558(15) Å. Calixarene is occupied by a one benzamidine molecule (C1X > N2X, colored pink in Figure 76b), which is inserted into the cavity to a depth of 4.45 Å (Figure 76c). The size of the C4S cone, defined by the distance between opposite sulfur atoms, is 9.89 and 10.72 Å, indicating that the macrocycle adopts a slightly pinched conformation.

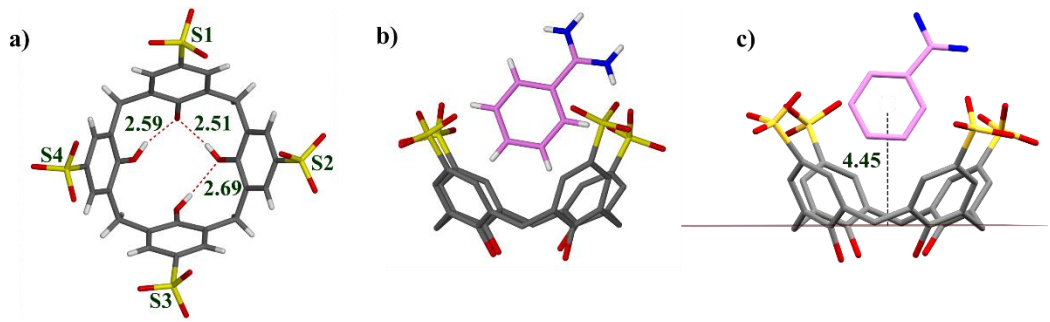

*Figure 76. Host–guest complex **C4S_BNZ_Form V**: (a) O–H···O hydrogen bonding at the C4S lower rim with the deprotonation of the one phenolic group; (b) inclusion mode of benzamidine into C4S cavity; (c) the depth of benzamidine inclusion in C4S cavity. Distances are given in Å.*

The symmetry expansion through the inversion centre demonstrates *2:2 pseudocapsular associate* formed by C4S molecules in the *rim-to-rim* position. These two calixarenes are hosting two benzamidine cations in antiparallel orientation. The *C4S–C4S* capsule measures 15.79 Å. The C1X > N2X benzamidine engages in *N–H···O* interactions with C4S molecules, donating four *N–H···O* hydrogen bonds – one to a parent sulfonate oxygen and three to neighboring C4S oxygens (2.780(18)–3.334(6) Å) (Figure 77a). Two *C–H···π* interactions (3.510(18) and 3.566(18) Å) with the calixarene aromatic walls further stabilize the benzamidine within the cavity (Figure 77b).

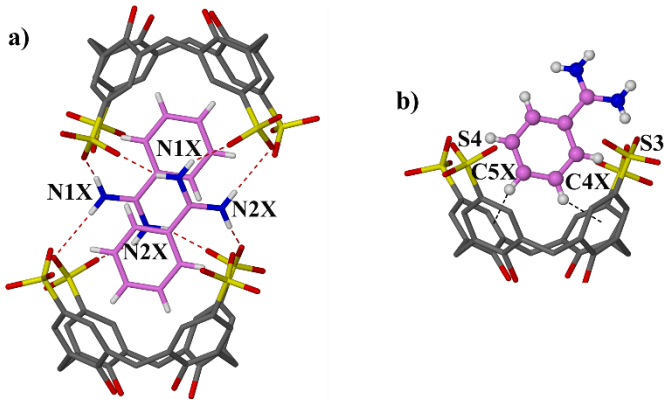

*Figure 77. Host–guest complex **C4S_BNZ_Form V**: (a) N–H···O hydrogen bonds between N–H groups of benzamidine and sulfonate oxygen atoms of C4S; (b) C–H···π interactions between benzamidine aromatic ring and aromatic rings of C4S molecule.*

The four benzamidine molecules located outside the C4S cavity are primarily connected *via* *N–H···O* hydrogen bonds to C4S. C1Y > N2Y forms two hydrogen bonds also with water, with *O···O* distances of 2.649(7)–3.053(3) Å (Figure 78a). Aromatic interactions between benzamidine and C4S are illustrated in Figure 78b, showing *C–H···π* and *π···π* contacts between C1K > N2K and two aromatic rings of C4S. The distances from the benzamidine C atoms to the centroids of the C4S aromatic rings are 3.555(19) Å, while the *centroid···centroid* distance between the benzamidine and C4S rings is 3.960(9) Å.

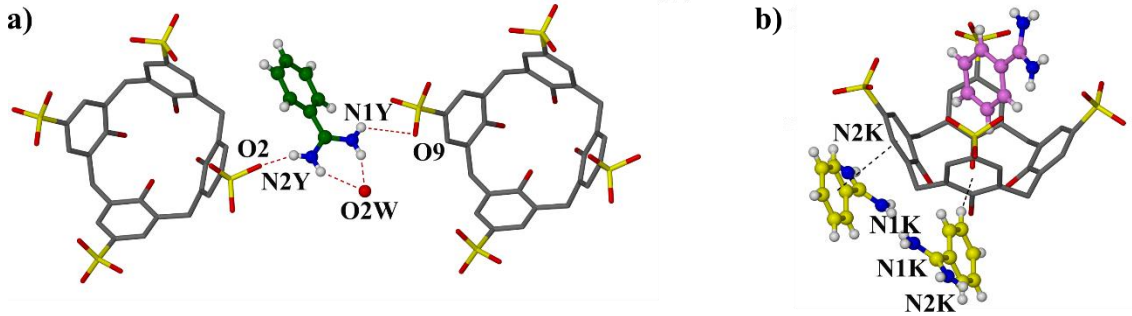

*Figure 78. Host–guest complex **C4S_BNZ_Form V**: (a) N–H···O hydrogen bonds between N–H groups of outer benzamidine and sulfonate oxygen atoms of C4S / water molecules; (b) C–H···π and π···π interactions between outer benzamidines and C4S molecule.*

Meanwhile, the external benzamidines participates in *N–H···π* and *π···π* interactions with each other. Specifically, C1K > N2K and C1Z > N2Z form an *N–H···π* contact at 3.511(17) Å (Figure 79a), while *π···π* interactions between the aromatic rings of C1I > N2I and C1Z > N2Z occur at 3.928(4) Å (Figure 79b).

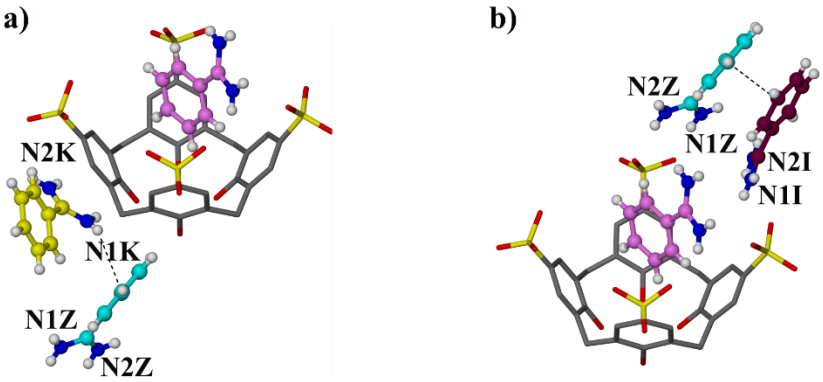

*Figure 79. Host–guest complex **C4S_BNZ_Form V**: (a) N–H···π interactions between N–H group and aromatic ring of outer benzamidines; (b) π···π interactions between aromatic rings of outer benzamidines.*

The layers of C4S molecules in the structure of complex ***V*** hold together by *C–H*···π interactions. The distance between *C–H* group of C4S methylene bridge and C4S aromatic ring is 3.470(15) Å. The classical bilayer organization of C4S is disrupted in ***C4S_BNZ_Form V*** (Figures 80a,b) due to the increased number of benzamidine cations, which interact with the outer surfaces of C4S and with each other. Detailed parameters of the non-covalent interactions in the complex ***C4S_BNZ_Form V*** are provided in Tables 32–34, Annex I.

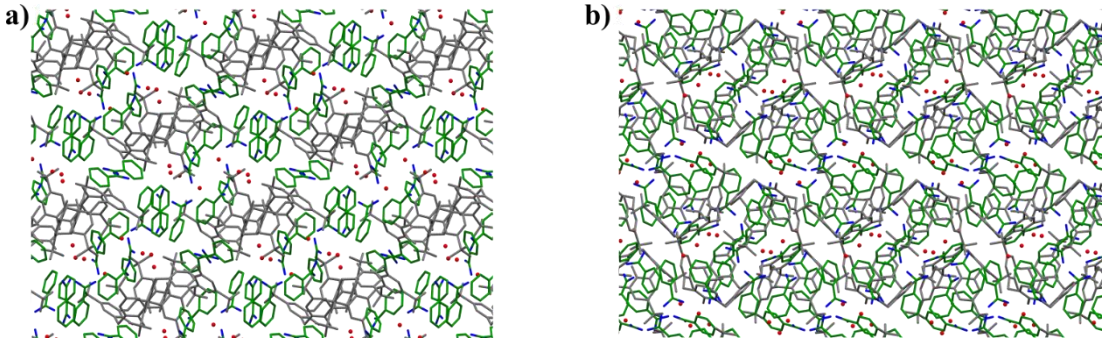

*Figure 80. Crystal packing of the host–guest complex **C4S_BNZ_Form V** viewed along (a) **b** and (b) **c** directions. All benzamidine molecules are colored in green. Disorder omitted for clarity.*

NMR analysis of the C4S_BNZ complex

Analysis of the formation of the C4S ***sodium salt*** – benzamidine complex was carried out in solution (D_2O) using ^1H NMR spectroscopy (Figure 81). C4S ***sodium salt*** was dissolved in water (4 mM in D_2O) and measured pH resulted in 8.5 value, that almost doesn't change after adding benzamidine hydrochloride solution (pH = 8.4). In the presence of C4S, all aromatic proton resonances of benzamidine are strongly shifted towards the upfield region, which indicates a deep location of the guest in the macrocyclic cavity. The shift for the signal of a proton ***a*** is from 7.62 ppm to 6.43 ppm (Δδ=1.19 ppm), for proton ***b*** from 7.78 ppm to 5.71 ppm (Δδ=2.07 ppm) and for proton **c** from 7.75 ppm to 5.76 ppm (Δδ=1.99 ppm.). Complexation in solution confirms the inclusion of benzamidine in the C4S macrocyclic cavity.

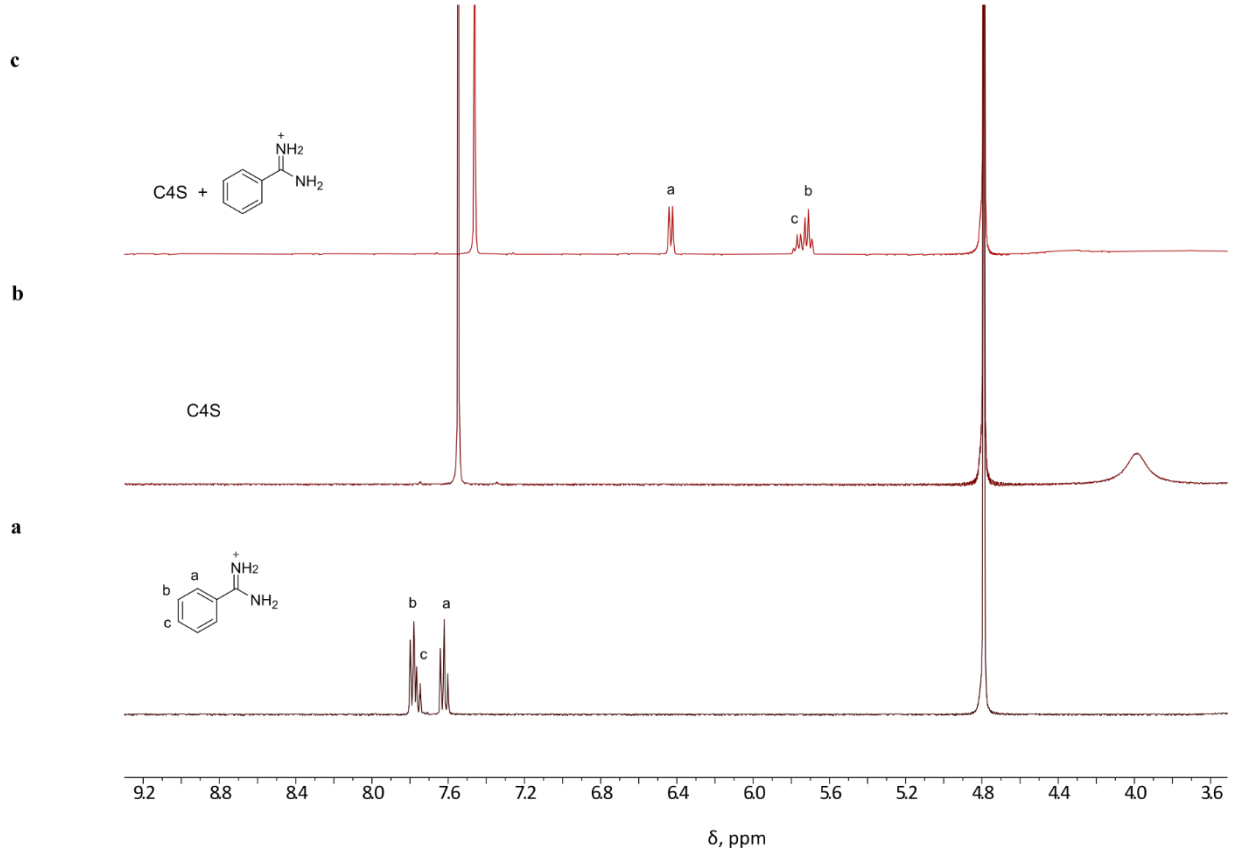

Figure 81. [1]H NMR spectra of (a) benzamidine; (b) C4S ***sodium salt****; (c)* ***C4S_BNZ*** *host–guest complex recorded at RT in D_2O, C (benzamidine) = 4 mM, C (C4S) = 4 mM, pH (****C4S_BNZ****) = 8.4.*

4.1.2 C6S complex with benzamidine

Crystallization and microscopic observations for C6S sulfonic acid complex with benzamidine

5 mg of C6S ***sulfonic acid*** was dissolved in 0.5 mL of H_2O. The solution of 4.2 mg of benzamidine hydrochloride in 0.5 mL of H_2O was combined with the solution of the host (Figure 82a). After approximately ten days, colorless, prism-shaped crystals appeared, as illustrated in Figure 82b. Single-crystal X-ray diffraction analysis confirmed the formation of the host–guest complex ***C6S_BNZ***.

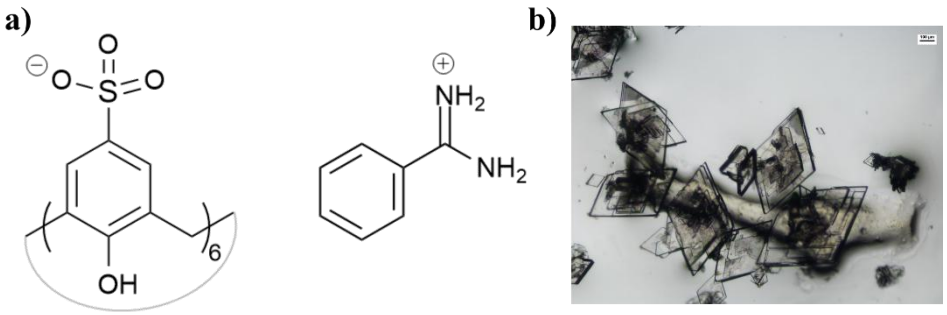

Figure 82. (a) Chemical structure of C6S ***sulfonic acid*** *host and benzamidine (****BNZ****) guest; (b) photomicrograph of crystals of* ***C6S_BNZ*** *complex. The scale bar corresponds to 100 µm.*

The refinement details of the C6S_BNZ complex

The asymmetric unit of ***C6S_BNZ*** consists of half of C6S hexa-anion molecule positioned on the inversion centre, three benzamidine monocations and 4.5 water molecules.

C1Z > N2Z benzamidine molecule is disordered over two positions. The first component of disorder C1Z > N2Z is refined with PART 1 command (53% occupancy), the second C1A > N2A is refined with PART 2 (47% occupancy). SIMU and RIGU restraints are applied. The O2W, O3W and O5W water molecules are close to each other and disordered. The disordered molecules are refined using the common PART 1 and PART 2 commands. The O2W and O3W atoms in PART 1 occupy 49.5%. O2A and O3A atoms in PART 2 occupy 50.5%. The O4W molecule is disordered over three positions. The O4W in the PART 1 occupies 49.5%, O4A in PART 2 occupies 25.2%, O4B in PART 3 occupies 25.2%. The O5W molecule in PART 1 is refined with the 50% occupancy. Hydrogen atoms are added geometrically. Water molecules O2W, O3W, O4W, O5W are refined without hydrogen atoms. The basic crystallographic data of the discussed structure is shown in Table 4.

*Table 4. Crystal data and structure refinement for **C6S_BNZ** complex.*

Parameters	***C6S_BNZ***
Formula moiety	$C_{42}H_{30}O_{24}S_6 \cdot 6(C_7H_9N_2) \cdot 9(H_2O)$
Formula weight	2000.13
Crystal system	Monoclinic
Space group	$P2_1/c$
a / Å	18.6619(2)
b / Å	12.92010(1)
c / Å	20.2173(2)
α / °	90
β / °	108.730(1)
γ / °	90
Volume / Å^3	4616.51(8)
Z	2
ρ_{calc} /g·cm^{-3}	1.44
Crystal color	Colorless
Crystal morphology	Prism
μ / mm^{-1}	2.15
θ_{max} / °	70.0
Reflections collected	28705
Independent reflections	8691 [R_{int} = 0.020]
Data / Restraints / Parameters	8691 / 228 / 738
Observed data [I > 2σ(I)]	8241
Final R indexes [I ≥ 2σ(I)]	R_1 = 0.038, wR_2 = 0.104
Final R indexes [all data]	R_1 = 0.039, wR_2 = 0.106
Goodness-of-fit on F^2	1.03
Largest diff. peak and hole / e·Å^{-3}	0.84 / –0.51

Structure analysis of the C6S_BNZ complex

The co-crystallization of C6S ***sulfonic acid*** with benzamidine hydrochloride from water result in the formation of the complex **C6S_BNZ** with the formula $C_{42}H_{30}O_{24}S_6 \cdot 6(C_7H_9N_2) \cdot 9(H_2O)$. Single-crystal X-ray diffraction analysis shows that this complex crystallizes in monoclinic crystal system in the space group $P2_1/c$. The asymmetric part consists of half of C6S, three benzamidine and 4.5 water molecules (Figure 83) .

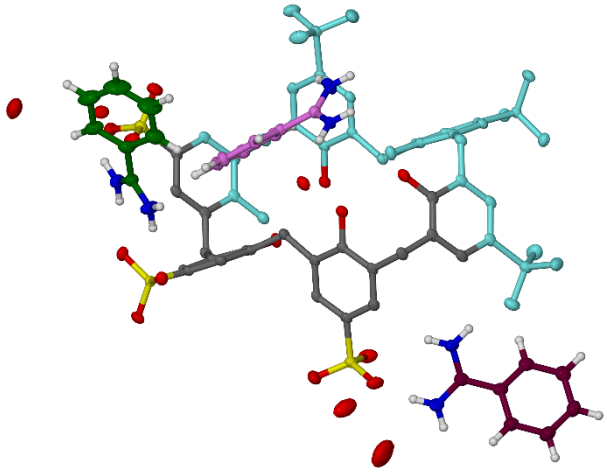

*Figure 83. The asymmetric unit of the **C6S_BNZ** complex with the expanded C6S molecule. The macrocycle lies over an inversion centre, the light blue corresponds to symmetry generated half of the calix[6]arene molecule. Three crystallographically unique benzamidine molecules are presented in different colours. Atomic displacement parameters set at 50% probability. Disorder omitted for clarity.*

The *up–down* double partial-cone conformation (Figure 84a,b) of the C6S macrocycle in this complex is characterized by three rings oriented upwards, while others pointed downwards. Due to the *up–down* geometry of C6S, the lower rim of the macrocycle exhibits intramolecular and intermolecular hydrogen bond interactions involving both the hydroxyl groups of C6S and water molecules (Figure 84c). The donor–acceptor hydrogen bonding distances range from 2.573(18) to 2.826(17) Å. The parameters of the *O–H···O* hydrogen bonds are placed in Table 35, Annex I.

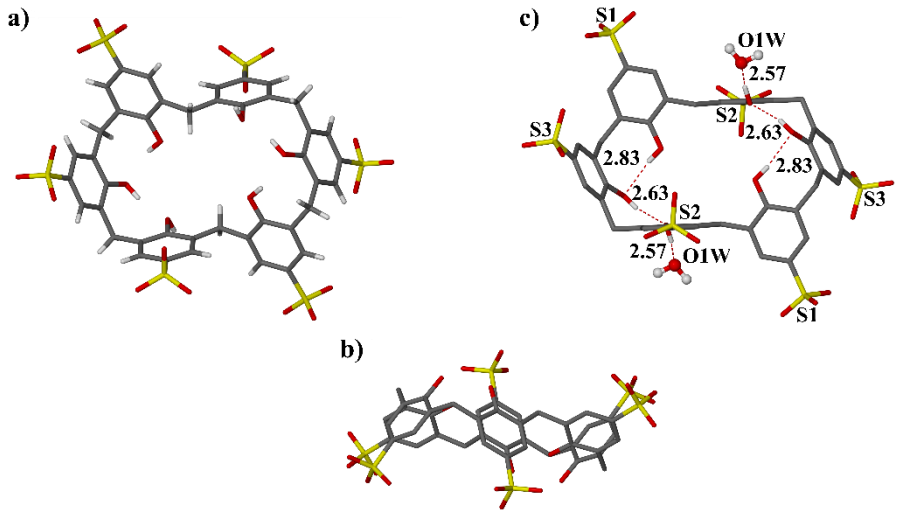

*Figure 84. Host–guest complex **C6S_BNZ**: (a,b) top and side views on up–down double partial-cone conformation of the C6S; (c) O–H···O hydrogen bonding at the C6S lower rim. O···O distances are given in Å.*

The conformation of C6S molecule provides two *pseudo* cavities opened in opposite directions, into which the benzamidine molecules (C1X > N2X) are included. Two other benzamidine are located outside these cavities. All three molecules form four *N–H···O* hydrogen bonds: three with C6S molecules and one with water (Figure 85a). Two benzamidine molecules located outside the C4S cavity are additionally connected to the macrocycle *via C–H···O* hydrogen bonds between their aromatic rings and the sulfonate oxygen atoms of C4S (Figure 85b), whereas the benzamidine included within the cavity does not form *C–H···O* contacts with the macrocycle. The *N···O* distances range from 2.799(2) to 3.140(3) Å, and the *C···O* distances range from 2.906(4) to 3.396(2) Å.

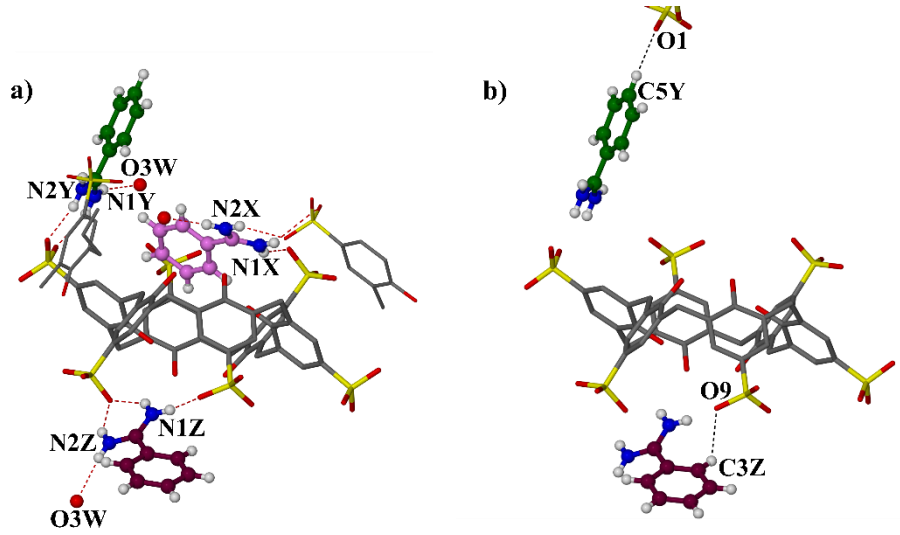

*Figure 85. Host–guest complex **C6S_BNZ**: (a) N–H···O hydrogen bonds between N–H groups of benzamidine and sulfonate oxygen atoms of C6S and water molecules; (b) C–H···O hydrogen bonds between benzamidines and C6S molecules.*

Upon expansion of the crystal structure, two C1X > N2X benzamidine molecules form *C–H···π* interactions with the aromatic rings of the parent C6S at 3.542(2) Å, while two additional

benzamidines interact *via* a *C–H···centroid* contact of 3.786(2) Å (Figure 86). Detailed parameters are provided in Tables 35,36, Annex I.

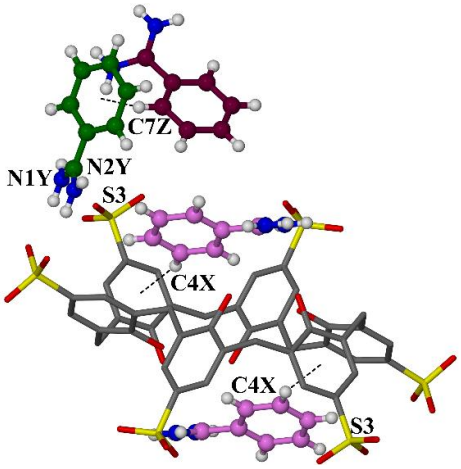

*Figure 86. Host–guest complex **C6S_BNZ**: C–H···π interactions formed by the benzamidine molecules.*

The crystal packing of the complex features a layered arrangement of C6S and benzamidine molecules along the ***c*** axis. Two benzamidine molecules alternate in almost vertical positions, with an additional molecule included within the calixarene cavity (Figures 87a,b). Within the layers, C6S molecules interact through *C–H···O* hydrogen bonds at distances of 3.40 and 3.35 Å. The parameters of the non-covalent interactions involving the calixarene molecules are summarized in Table 35, Annex I.

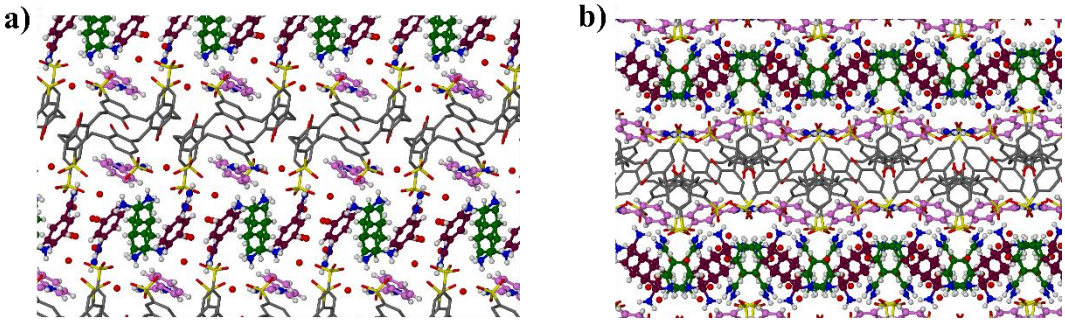

*Figure 87. Crystal packing of the host–guest complex **C6S_BNZ** viewed along (a) **b** and (b) **c** directions.*

Solid-state complexes of C*n*S with benzamidine – discussion of results

The five ***C4S_BNZ*** complexes were obtained from two forms commercially available of calixarene: C4S sulfonic acid (***Forms I–III***) and C4S sodium salt (***Forms IV–V***). Crystallization from water-ethanolic solution using these two forms of macrocycle, combined with aging of the crystals in the mother solution, produces a series of host–guest complexes that exhibit distinct structural changes over time. The crystal complexes differ in the structure, stoichiometry, inclusion mode, hydration, and overall chemical composition. All five crystal complexes contain water molecules, peculiarly one crystal form incorporates water in the form of oxonium ions. The crystal forms that crystallize initially (metastable kinetic complexes) incorporate more water molecules in the crystal

structure, than crystal forms that appear later. One of the crystal complexes contains sodium ions together with benzamidine cations. The clear distinction between C4S sulfonic acid complexes and C4S sodium salt complexes is the charge of C4S host molecule. The C4S is tetra-anionic in all three ***C4S_BNZ*** complexes of C4S sulfonic acid, while penta-anionic in two complexes of C4S sodium salt. The common feature of all five complexes is the amidinium-sulfonate charge-assisted hydrogen bonding between BNZ cations and anionic upper rim of C4S macrocycles.

Three crystal forms of ***C4S_BNZ*** complexes were obtained employing C4S sulfonic acid. Initially, co-crystallization yields ***C4S_BNZ_Form I*** in monoclinic space group *I2/a.* This structure contains two C4S tetra-anions, eight benzamidine cations, and 16.3 water molecules. The rod-shaped crystals of **form I** are metastable in the mother solution and gradually dissolve over two days, while new prismatic crystals of **form II** appear in the crystallization vial. The microscopic observation reveals that dissolution-recrystallization transformation is completed after two days, as only crystals **II** remain in the solution. Form **II** of monoclinic space group *P2/n* comprises two C4S, eight benzamidine and 10.2 water molecules. The chemical composition of **I** and **II** differs only in the number of water molecules. The inclusion mode in the complexes **I** and **II** is similar occurring in the slantway orientation of BNZ guest in the C4S cavity. Such inclusion mode of positioning aromatic ring of BNZ at the bottom of the macrocyclic cavity is also confirmed in the aqueous solution by ^{1}H NMR spectroscopy. Overall, the crystals of complex **II** are quite stable in the mother solution over long period of time (app. two weeks) during its evaporation. However, after complete evaporation, only form **III** in the mixture with benzamidine hydrochloride crystals remains in the sample.

This structure in the triclinic *P-1* space group contains one C4S tetra-anion, two benzamidine molecules, two oxonium (Zundel) cations, and water. The inclusion mode in the longitudinal orientation of BNZ residing above the pinched cone of the macrocycle is strikingly different than in **I** and **II** complexes. The BNZ inclusion is also shallower that in I and II – the depth of inclusion in III is 4.9 Å comparing to 4.2–4.3 Å in complexes I and II. This is also reflected in the number of short *C–H···π* contacts between BNZ aromatic ring and C4S interior. There is only one *C–H···π* interaction between BNZ and C4S cavity in complex III, while there are two such contacts in complexes I and II. The macrocycle is strongly pinched to serve the optimal interaction with BNZ, as there are three hydrogen bonds between BNZ and sulfonate oxygen atoms of C4S. For comparison, there is either one or two such hydrogen bonds in the complexes **I** and **II**, respectively. C4S adopts a more pinched cone conformation compared to the previous forms.

Forms IV and ***V***, obtained from the sodium salt form of C4S, exhibit distinct structural features. ***C4S_BNZ_Form IV*** contains one C4S macrocycle, three benzamidine molecules, two sodium cations, and 8.4 water molecules. One sodium cation is coordinated only to the upper rim of

C4S, while the second connects both upper and lower rims, linking the calixarene molecules within bilayers. The coordination of two sodium cations to C4S does not disturb the host–guest inclusion property of the macrocycle, as BNZ resides in the macrocyclic cavity similarly as in complexes I and II.

C4S_BNZ_Form V forms upon aging form ***IV*** crystals in the mother solution. It contains one C4S macrocycle, five benzamidine molecules, and 3.5 water molecules. The crystals of form ***IV*** and form ***V*** coexist in the mother solution. The reason for the late crystallization of complex V might be the increased relative concentration of benzamidine cations in the solution after the crystal growth of form ***IV*** and further slow evaporation of the mother solution. The starting ratio of C4S and BNZ was 1:4. Thus, the crystallization of form ***IV*** and form ***V*** took place at different compositions of the mother solution. The host–guest inclusion mode in form V is similar as in complexes I, II and IV.

Overall, it is evident that crystallization and complexation pathway in C4S–BNZ system depends on the form of the C4S macrocycle (sulfonic acid or sodium salt), as it affects the charge of the macrocycle itself, defining the chemical composition of the resulting crystals. When initially formed crystals are kept in the mother solution simply over passing of time under slow evaporation conditions, various scenarios are possible, including dissolution-recrystallization transformations. Such solution-mediated transformations can be induced by the concentration changes of the dissolved components (including pH changes) during crystal growth and partial evaporation of the mother solution or can occur spontaneously due to the delicate interplay between kinetically and thermodynamically regulated pathways of the host–guest complexation and crystallization events.

Co-crystallization of the larger C6S with benzamidine yields the ***C6S_BNZ*** complex, which contains one C6S macrocycle, six benzamidine molecules, and water. Here, C6S adopts an up–down double partial-cone conformation, creating two oppositely oriented pseudo-cavities. Two benzamidine molecules are encapsulated within these cavities, while additional guests interact externally. The structure exhibits layered packing, stabilized by an extensive hydrogen-bond network and aromatic stacking between host and guest molecules. The larger size of C6S strongly affects the extent of guest inclusion, the connectivity of the structure, and the packing arrangement, due to the greater number of available hydrogen-bonding sites.

4.1.3 C4S complex with 4-methylbenzamidine

Crystallization and microscopic observations for C4S sulfonic acid complex with 4-methyl benzamidine

10 mg of C4S ***sulfonic acid*** was dissolved in 0.5 mL of H_2O/EtOH (1:1). The solution of 9.2 mg 4-methylbenzamidine hydrochloride in 0.5 mL of H_2O/EtOH (1:1) was combined with the solution of the host (Figure 88a). After approx. 12 days the colorless prism-shaped crystals appeared

(Figure 88b). Single-crystal X-ray diffraction analysis revealed these crystals to be the host–guest complex ***C4S_M–BNZ***.

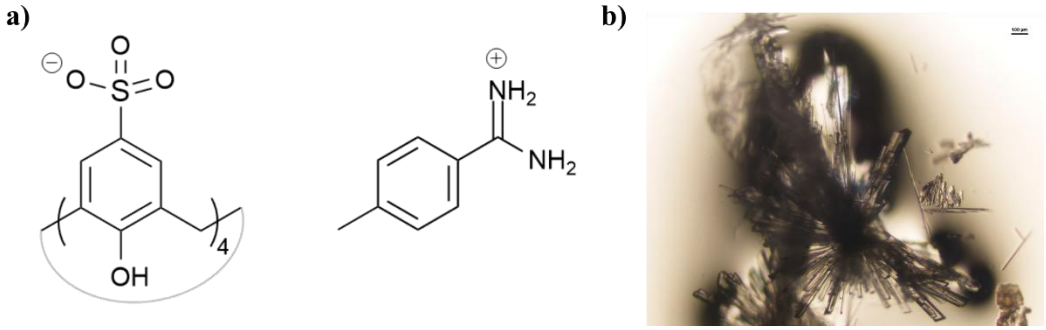

Figure 88. (a) Chemical structure of C4S ***sulfonic acid*** *host and methylbenzamidine (****M–BNZ****) a guest; (b) photomicrograph of crystals of the* ***C4S_M–BNZ*** *complex. The scale bar corresponds to 100 µm.*

The refinement details of the C4S_M–BNZ complex

The asymmetric unit of ***C4S_M–BNZ*** consists of one C4S tetra-anion molecule, four M–BNZ monocations, one ethanol and two water molecules. The C1E > O1E ethanol molecule is disordered over two positions. The first component of the disorder C1E > O1E is refined with the PART 1 command (81.8%). The second component of the disorder C1A > O1A is refined with the PART 2 command (18.2%) using the SIMU, RIGU and SADI restraints. Hydrogen atoms are placed on geometrically calculated positions and refined using a riding model. The basic crystallographic data of the discussed structure is provided in Table 5.

Table 5. Crystal data and structure refinement for ***C4S_M–BNZ*** *complex.*

Parameters	***C4S_M–BNZ***
Formula moiety	$C_{28}H_{20}O_{16}S_4 \cdot 4(C_8H_{11}N_2) \cdot C_2H_6O \cdot 2(H_2O)$
Formula weight	1363.53
Crystal system	Triclinic
Space group	*P–1*
a / Å	10.4856(2)
b / Å	18.5014(6)
c / Å	18.8633(5)
α / °	104.024(2)
β / °	105.419(2)
γ / °	104.061(2)
Volume / Å^3	3232.46(16)
Z	2
ρ_{calc} /g·cm^{-3}	1.40
Crystal color	Colorless
Crystal morphology	Prism
µ / mm^{-1}	2.02
θ_{max} / °	70.0
Reflections collected	36788
Independent reflections	12182 [R_{int} = 0.037]
Data / Restraints / Parameters	12182 / 86 / 872
Observed data [I > 2σ(I)]	10614

Final R indexes [I ≥ 2σ(I)]	R_1 = 0.042, wR_2 = 0.110
Final R indexes [all data]	R_1 = 0.048, wR_2 = 0.116
Goodness-of-fit on F²	1.02
Largest diff. peak and hole / e·Å⁻³	0.73 / –0.42

Structure analysis of the C4S_M–BNZ complex

The co-crystallization of C4S ***sulfonic acid*** with 4-methylbenzamidine hydrochloride from water–ethanol mixture results in the formation of the complex ***C4S_M–BNZ*** with the formula $C_{28}H_{20}O_{16}S_4 \cdot 4(C_8H_{11}N_2) \cdot C_2H_6O \cdot 2(H_2O)$. Single-crystal X-ray diffraction analysis shows that this complex crystallizes in triclinic crystal system in the space group *P–1*. The asymmetric part consists of one C4S, four M–BNZ, one ethanol and two water molecules (Figure 89).

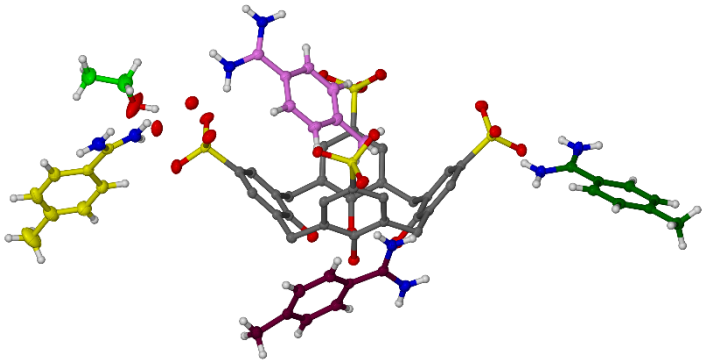

*Figure 89. The asymmetric unit of the host–guest complex **C4S_M–BNZ**. Four crystallographically unique methylbenzamidine molecules are presented in different colours. Atomic displacement parameters set at 50% probability. Disorder omitted for clarity.*

In ***C4S_M–BNZ*** complex, the C4S host adopts a cone conformation with slight cone pinching. The overall cavity size is defined by the distances between opposite Sulphur atoms, resulting in 9.73 and 11.68 Å. The cone geometry at the lower rim is stabilized by a cyclic intramolecular hydrogen-bonds formed by hydroxyl groups. The *O···O* distances between adjacent hydroxyl oxygen atoms range from 2.626(2) to 2.914(19) Å. The parameters of intramolecular interactions at the lower rim of the C4S molecule are shown in Table 37, Annex I.

Among the benzamidine guest molecules, one is located within the C4S cavity, while the remaining three molecules are positioned out of the macrocyclic space. The encapsulated benzamidine (colored in pink) is inserted into the host cavity at the inclusion depth of 5.04 Å. The depth is measured as the distance between the P plane defined by methylene bridges of C4S and the centroid of the benzamidine aromatic ring.

An ethanol molecule is situated outside the C4S cavity. It is linked to the neighbouring benzamidine molecule (C1I > N2I) *via* benzamidine–ethanol *N–H···O* hydrogen bonding and interacts with water molecule. The benzamidine moieties engage in interactions with ethanol, C4S, and water molecules, as illustrated in Figure 90a,b. The *N···O* hydrogen bond distances fall within the range of 2.770(3)–3.284(2) Å. Three benzamidine molecules interact with the C4S *via C–H···O* hydrogen

bonds. The encapsulated benzamidine (C1X > N2X) forms a *C–H···O* contact with the sulfonate oxygen atom of the host at 3.58 Å. Two other benzamidines, C1Y > N2Y and C1Z > N2Z, are in proximity to adjacent calixarene molecules. The *C···O* contact distances for these molecules 3.231(3) and 3.312(3), 3.210(3) and 3.520(3) Å, respectively (Figure 90c). The parameters of hydrogen bonds between the benzamidines and calixarene / water molecules are shown in Table 37, Annex I.

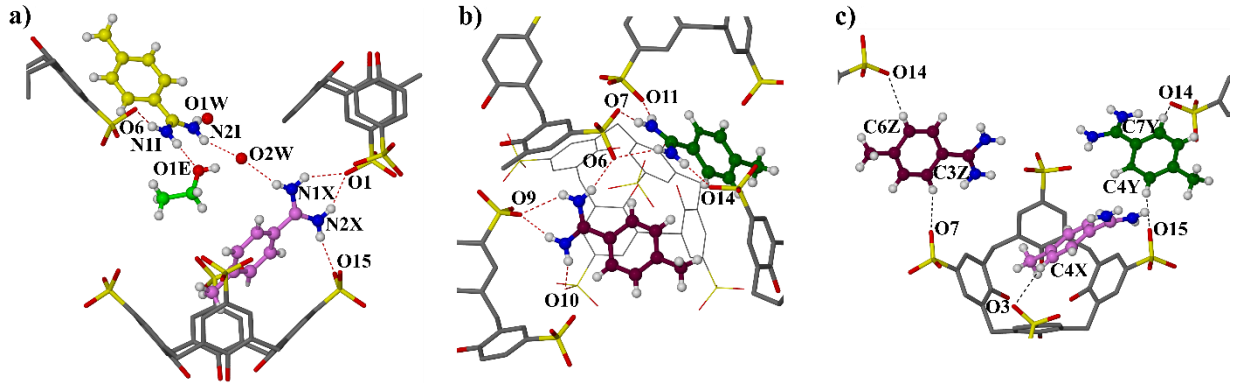

*Figure 90. Host–guest complex **C4S_M–BNZ**: (a,b) the network of N–H···O hydrogen bonds between methylbenzamidines and ethanol, C4S and water molecules; (c) C–H···O hydrogen bonds between C atoms of the methylbenzamidines aromatic rings and C4S molecules.*

The included methylbenzamidine molecule points to the C4S cavity by its methyl group and contact with the host *via C–H···π* interactions. The shortest *C···centroid* distance is 3.599(2) Å. The C1Z > N2Z benzamidine, located outside the C4S cavity, forms with the calixarene an *N–H···π* interaction, where the *N···centroid* distance is 3.570(2) Å (Figure 91a). M–BNZ molecules on opposite sides of the macrocycle interact through *π···π* stacking. For the C1I > N2I and C1Z > N2Z molecules the *centroid···centroid* distance is 3.888(13) Å. The C1Y > N2Y molecules also show a weak *π···π* interaction, *centroid···centroid* distance is 4.06 Å (Figure 91b). The parameters of *N–H···π* and *C–H···π* non-covalent interactions involving the benzamidine molecules are provided in Tables 38,39, Annex I.

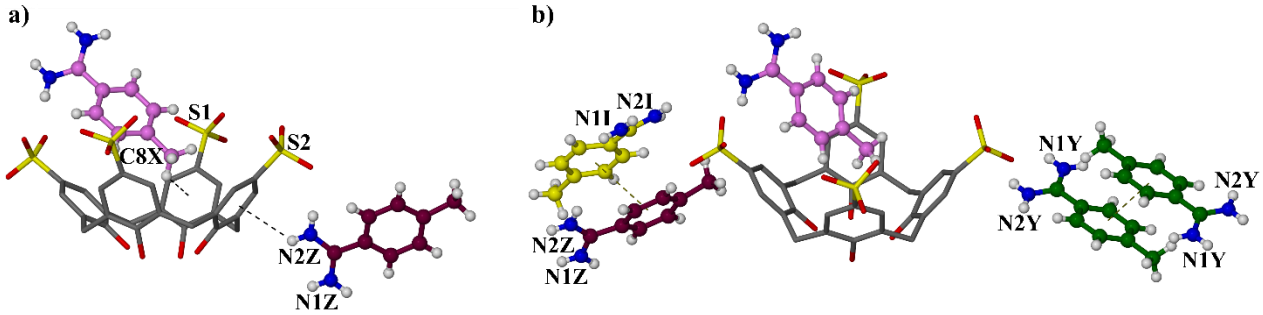

*Figure 91. Host–guest complex **C4S_M–BNZ**: (a) N–H···π and C–H···π interactions between two methylbenzamidines and C4S molecule; (b) π···π interaction between aromatic rings of methylbenzamidine molecules.*

The expanded view of the crystal structure shows that the C4S molecules are connected by *O–H···O* hydrogen bonds between hydroxyl *O8–H8* group of one C4S molecule and sulfonate oxygen atom O11 of adjacent C4S. The benzamidine molecules surround the C4S from almost all sides and

interacting *via* $\pi\cdots\pi$ interactions (Figure 92a,b). Because C4S mainly interacts with methylbenzamidine molecules on the outer surface of the macrocycles, the usual bilayer arrangement in the crystal is disrupted. Instead, the structure is formed by single rows of C4S connected by hydrogen bonds and separated by methylbenzamidine molecules.

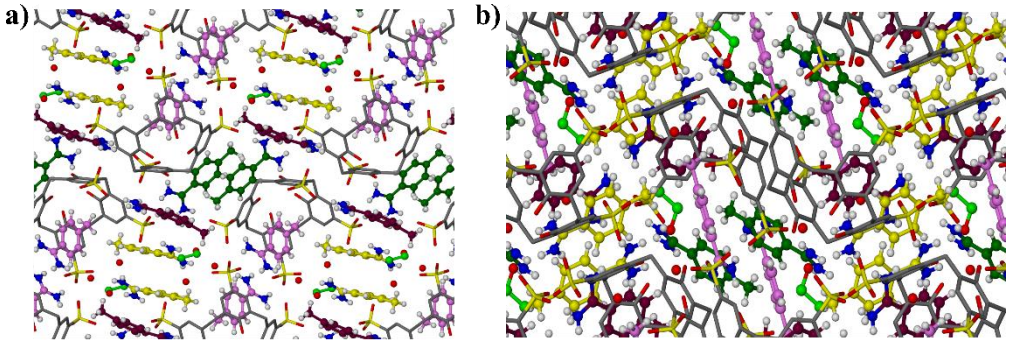

*Figure 92. Crystal packing of the host–guest complex **C4S_M–BNZ** viewed along (a) **a** and (b) **b** directions.*

4.1.4 C6S complex with 4-methylbenzamidine

Crystallization and microscopic observations for C6S sulfonic acid complex with 4-methyl benzamidine

10 mg of C6S ***sulfonic acid*** was dissolved in 0.5 mL of H_2O/EtOH (1:1). The solution of 9.2 mg 4-methylbenzamidine hydrochloride in 0.5 mL of H_2O/EtOH (1:1) was combined with the solution of the host (Figure 93a). After 2 days the colorless prism–shaped crystals of a good diffraction quality appeared (Figure 93b). Single-crystal X-ray diffraction analysis showed these crystals to be the host–guest complex ***C6S_M–BNZ***. The crystals were then removed from the solution and dried on a glass slide at room temperature (25°C) for one day. Single-crystal X-ray diffraction analysis of the dried crystals revealed the host–guest complex structure with negligible differences, referred to as ***C6S_M–BNZ_dried***.

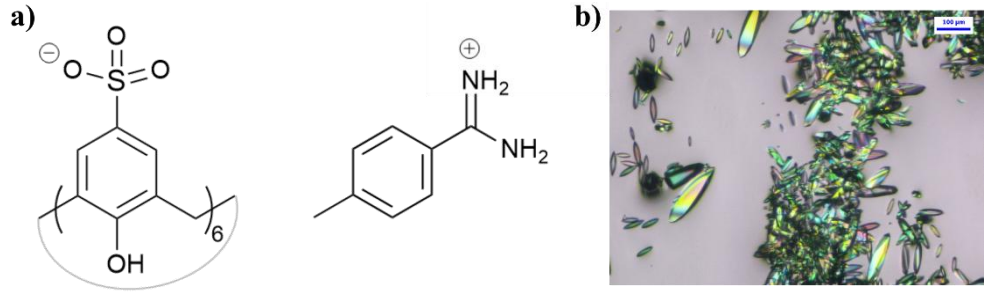

*Figure 93. (a) Chemical structure of C6S **sulfonic acid** host and methylbenzamidine (**M–BNZ**) guest; (b) photomicrograph of crystals of **C6S_M–BNZ** complex. The scale bar corresponds to 100 µm.*

The refinement details of the C6S_M–BNZ complexes

The asymmetric unit of ***C6S_M–BNZ*** includes 1/6 part of C6S hexa-anion, positioned on 3-fold rotoinversion axis, and one monocation of M–BNZ. The asymmetric unit contains heavily disordered water molecules that do not form hydrogen bonds with the C6S or benzamidine molecules.

To address the solvent disorder issue, the SQUEEZE analysis was applied. The SQUEEZE procedure revealed a solvent-accessible volume of 1068 Å^3 and total of 321 electrons are found in these voids (13.7% of the total crystal volume), corresponding to approximately 10.7 water molecules per formula unit (1.78 molecules in the asymmetric unit). C3X > C8X atoms of benzamidine molecule are disordered over two positions. First component of disorder C3X > C8X is refined with PART 1 command (76.7%), second component of disorder C3A > C8A is refined using PART 2 command (23.3%). The disorder is refined using SIMU and RIGU restraints. All hydrogen atoms are added geometrically.

The asymmetric unit of ***C6S_M–BNZ_dried*** includes 1/6 part of C6S hexa-anion, positioned on 3-fold rotoinversion axis, and one monocation of M–BNZ. The asymmetric unit also contains heavily disordered water molecules that do not form hydrogen bonds with the C6S or benzamidine molecules. To address the solvent disorder issue the SQUEEZE analysis was implemented. The SQUEEZE procedure revealed a solvent-accessible volume of 1032 Å^3 and total of 263 electrons (13.3% of the total crystal volume), corresponding to approximately 8.77 water molecules per formula unit (1.46 molecules in the asymmetric unit). C3X > C8X atoms of benzamidine molecule is disordered over two positions. First component of disorder C3X > C8X is refined with PART 1 command (71%), second component of disorder C3A > C8A is refined using PART 2 command (29%). The disorder is refined using SIMU, RIGU and SAME restraints. All hydrogen atoms are added geometrically. The basic crystallographic data of the discussed structures is provided in Table 6.

*Table 6. Crystal data and structure refinement for **C6S_M–BNZ** and **C6S_M–BNZ_dried** complexes.*

Parameters	***C6S_M–BNZ***	***C6S_M–BNZ_dried***
Formula moiety	$C_{42}H_{30}O_{24}S_6 \cdot 6(C_8H_{15}N_2)$ [+ solvent]	$C_{42}H_{30}O_{24}S_6 \cdot 6(C_8H_{15}N_2)$ [+ solvent]
Formula weight	1922.14	1922.14
Crystal system	Trigonal	Trigonal
Space group	*R–3*	*R–3*
a / Å	26.3589(8)	26.3184(7)
b / Å	26.3589(8)	26.3184(7)
c / Å	12.9106(5)	12.8888(4)
α / °	90	90
β / °	90	90
γ / °	120	120
Volume / Å^3	7768.4(6)	7731.5(5)
Z	3	3
ρ_{calc} /g·cm^{-3}	1.23	1.24
Crystal color	Colorless	Colorless
Crystal morphology	Prism	Prism
μ / mm^{-1}	1.83	1.84
θ_{max} / °	67.7	67.7

Reflections collected	7974	8166
Independent reflections	3254 [R_{int} = 0.096]	3245 [R_{int} = 0.090]
Data / Restraints / Parameters	3254 / 204 / 257	3245 / 215 / 257
Observed data [I > 2σ(I)]	2337	2145
Final R indexes [I ≥ 2σ(I)]	R_1 = 0.082, wR_2 = 0.148	R_1 = 0.068, wR_2 = 0.169
Final R indexes [all data]	R_1 = 0.060, wR_2 = 0.166	R_1 = 0.096, wR_2 = 0.198
Goodness-of-fit on F²	0.99	0.97
Largest diff. peak and hole / e·Å⁻³	0.52 / –0.46	0.45 / –0.54

Structure analysis of the C6S_M–BNZ complex

The co-crystallization of C6S ***sulfonic acid*** with 4-methylbenzamidine hydrochloride from water–ethanol solution (1:1) results in the formation of the complex ***C6S_M–BNZ*** with the formula $C_{42}H_{30}O_{24}S_6 \cdot 6(C_8H_{15}N_2)$ [+ solvent]. Single-crystal X-ray diffraction analysis shows that this complex crystallizes in a trigonal crystal system in the space group *R–3*. The asymmetric part consists of 1/6 C6S and M–BNZ (Figure 94a).

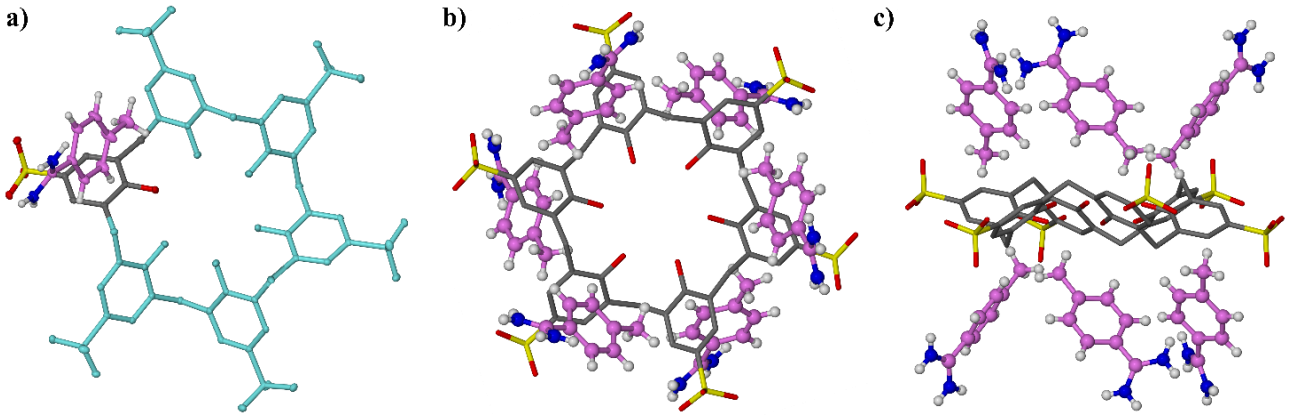

*Figure 94. (a) The asymmetric unit of the **C6S_M–BNZ** complex with the expanded C6S molecule. The macrocycle lies over a 3-fold rotoinversion axis, the light blue corresponds to symmetry generated calix[6]arene atoms. Atomic displacement parameters set at 50% % probability. (b) the C6S molecule is surrounded by six benzamidine molecules, each located in a groove of the macrocycle; (c) side view on the figure (b) illustrating the arrangement of three M–BNZ molecules above and three below the macrocycle. Disorder omitted for clarity.*

The C6S molecule adopts a pleated-loop conformation, in which the phenolic oxygen atoms of the macrocycle are alternately positioned above and below the molecular plane, creating a loop-like structure (Figure 95b). Due to this conformation, the oxygen atoms of the hydroxyl groups are positioned closer together, with an *O···O* distance of 2.554(3) Å (Figure 95a). Each groove of the C6S molecule accommodates one 4-methylbenzamidine, resulting in a total of six benzamidine molecules to complete the charge balance as is shown in Figure 94b,c.

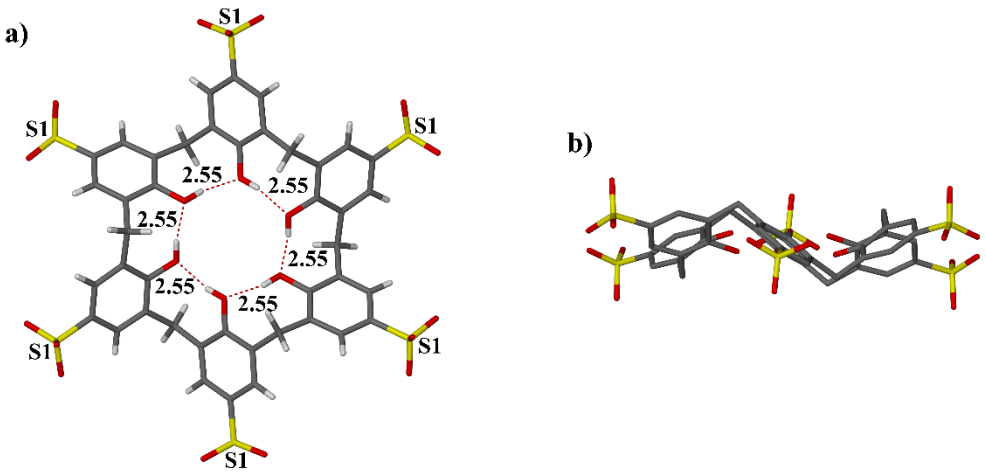

*Figure 95. Host–guest complex **C6S_M–BNZ**: (a) O–H···O hydrogen bonding at the C6S lower rim; (b) side view on the pleated-loop conformation of C6S molecule. O···O distances are given in Å.*

The guest molecule occupies the groove of the macrocycle and is oriented outward toward C6S through its amidinium group. As a result, benzamidine engages in one *N–H···O* hydrogen bond with a sulfonate oxygen atom of the parent C6S molecule and forms three hydrogen bonds with adjacent hosts, as shown in Figure 96. The *N···O* distances for these interactions range from 2.853(3) to 2.892(4) Å.

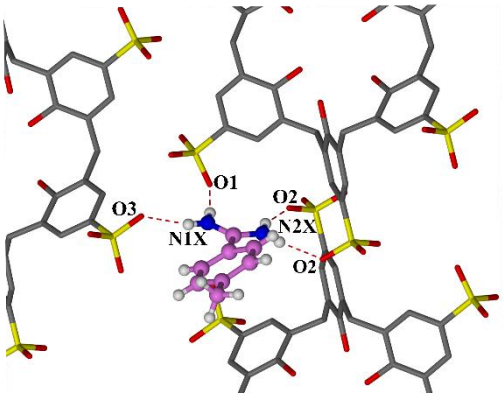

*Figure 96. Host–guest complex **C6S_M–BNZ**: N–H···O hydrogen bonds between N–H groups of methylbenzamidine and sulfonate oxygen atoms of C6S molecules.*

Oriented toward the parent calixarene through its methyl group (Figure 97a), the guest interacts with the macrocycle *via* a weak *C–H···π* interaction between the benzamidine methyl carbon and the calixarene's aromatic ring. The distance between the C8X atom and the centroid of the aromatic ring is 3.46 Å. Further analysis of the crystal structure shows that two benzamidine molecules are arranged in an antiparallel orientation between C6S units, engaging in *π···π* stacking interactions with a *centroid···centroid* distance of 3.836(4) Å, as illustrated in Figure 97b. The details of the intermolecular interactions involving methylbenzamidine molecules are summarized in Tables 40,41, Annex I.

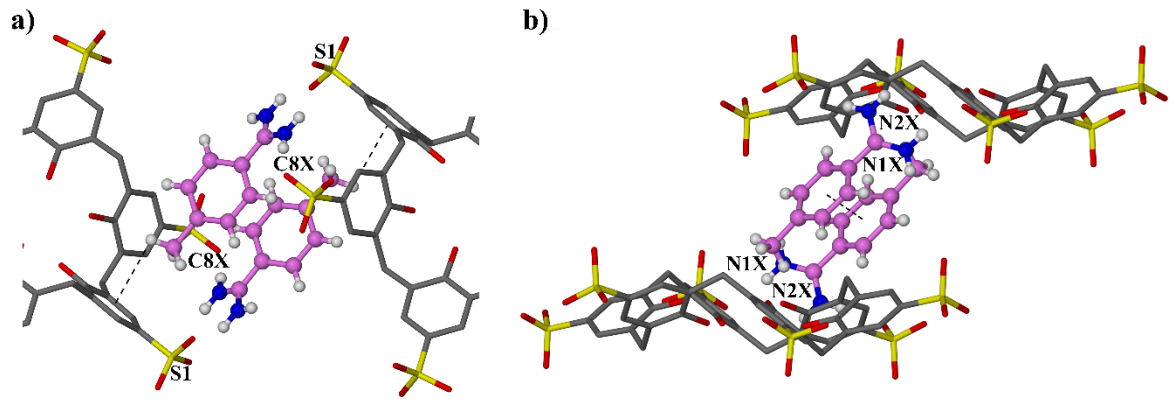

*Figure 97. Host–guest complex **C6S_M–BNZ**: (a) weak C–H···π interaction between methylbenzamidine and C6S molecules; (b) π···π interaction between aromatic rings of two methylbenzamidine molecules.*

In the ***C6S_M–BNZ*** complex, disordered water molecules occupy isolated voids that are not interconnected. The voids are enclosed by two calixarene molecules – at the top and bottom and by six methylbenzamidine molecules on the sides. The void contact surfaces, visualized using MERCURY software with a probe radius of 1.5 Å and grid spacing of 0.3 Å, are highlighted in blue in Figures 98a–d. Because methylbenzamidine is disordered over two positions, void contact surfaces were generated separately for each disorder component. According to the MERCURY analysis, the void associated with the major benzamidine position occupy a volume of 491.4 Å^3 per formula unit (corresponding to 1474.2 Å^3 per unit cell, Z = 3). The voids associated with the minor position have a volume of 338.2 Å^3 per formula unit and 1014.7 Å^3 per unit cell. The voids accommodating the disordered water molecules are enclosed by two calixarene molecules at the top and bottom and by six methylbenzamidine molecules on the sides. The void contact surfaces were also generated using MSROLL/XSEED software with a probe radius of 1.5 Å for each disorder component (Figures 99a,b). According to the MSROLL analysis, the void generated by the major benzamidine position occupies a volume of 538.1 Å^3, whereas that generated by the minor position has a volume of 369.8 Å3. As no significant differences in composition or structure were observed between the ***C6S_M–***

BNZ and ***C6S_M–BNZ_dried*** complexes, their packing arrangements remain essentially unchanged. Within this framework, the host molecules engage in intermolecular C–H···O interactions.

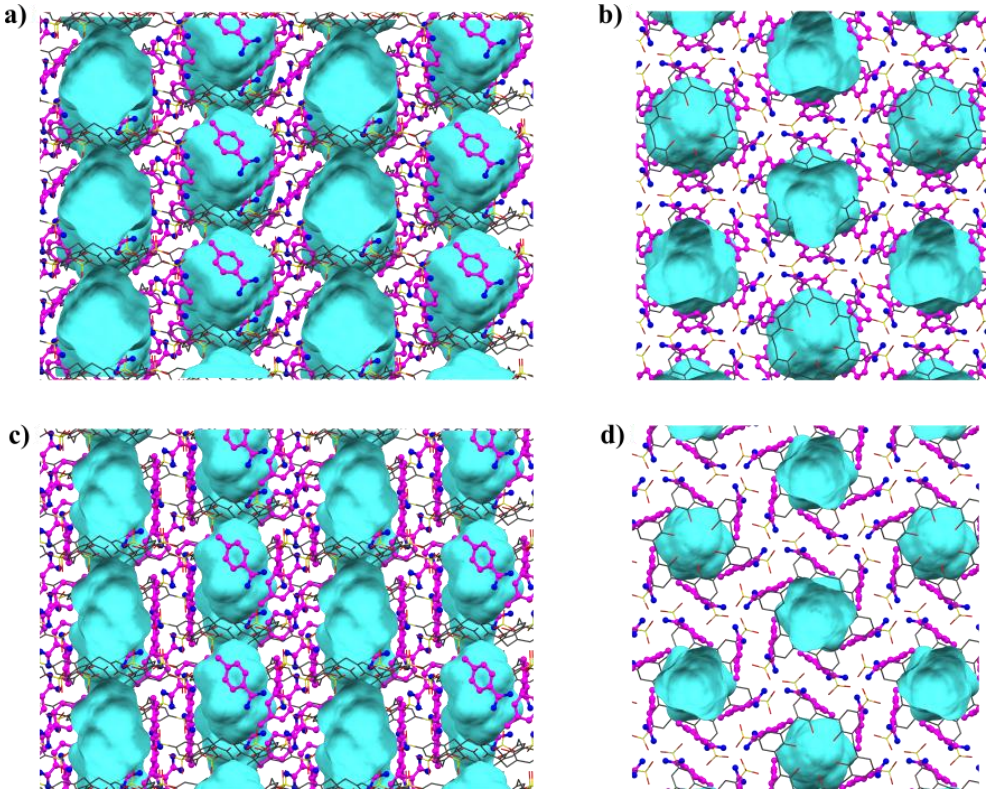

*Figure 98. Host–guest complex **C6S_M–BNZ**: crystal packing of the complex viewed along **a*** (a) and **c** (b) directions for the major benzamidine component (76.3% occupancy), and along **a*** (c) and **c** (d) directions for the minor benzamidine component (23.7% occupancy). Discrete voids are shown as light blue contact surfaces, generated using a probe radius of 1.5 Å in MERCURY.*

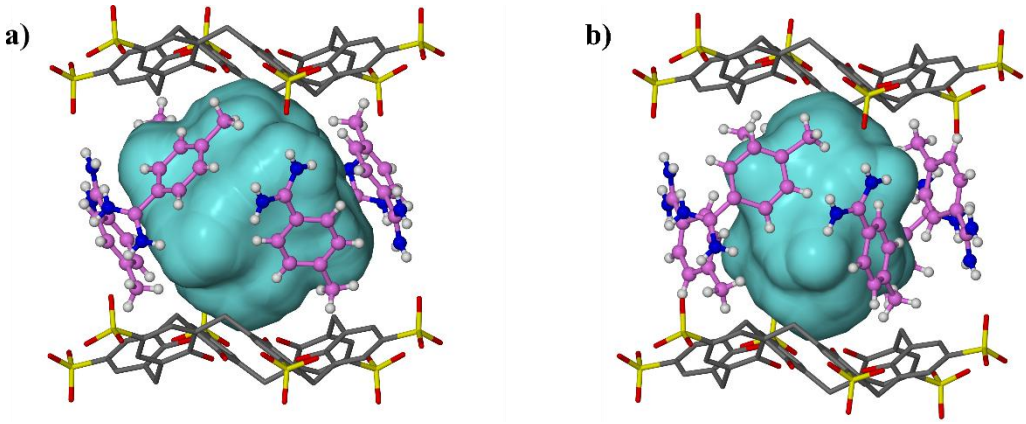

Figure 99. Void cavities enclosed by two calixarene molecules and six methylbenzamidine molecules were generated using a probe radius of 1.5 Å in MSROLL/XSEED. Panels (a) and (b) correspond to the major (76.3% occupancy) and minor (23.7% occupancy) benzamidine, respectively.

The water molecules located within these voids are only weakly associated with the parent supramolecular structure and primarily act as space fillers. This behavior is unusual for *p*-sulfonatocalix[*n*]arene crystal complexes, which typically incorporate large amounts of water into their crystals and are rarely stable outside the mother solution. Dehydration commonly leads to a loss of crystallinity and gradual or rapid decomposition of the crystals. In some cases, desolvation may

proceed *via* a *single-crystal-to-single-crystal* transformation involving reorganization of the supramolecular framework. Thus, it is unique that ***C6S_M–BNZ*** supramolecular framework does not comprise hydrogen bonded water molecules and remains stable and unchanged in air outside the mother solution.

Slurry-method synthesis and PXRD analysis of the C6S_M–BNZ complex

The crystalline complex was prepared using the slurry method and was compared with air-dried crystals of the ***C6S_M–BNZ_dried*** complex obtained through solution crystallization. To achieve this, 30 mg of C6S was combined with 27.5 mg of 4-methylbenzamidine in a 1:6 molar ratio, followed by the addition of 0.5 mL of an H_2O/EtOH (1:1) mixture. The suspension was stirred continuously at room temperature (23–25 °C) for 24 hours using a magnetic stirrer. The resulting solid was then filtered on the filter paper and after dried at room temperature for approximately 1.5 hours. Powder X-ray diffraction was employed to compare the crystallinity and structure of slurry-prepared sample with the single-crystalline phase. The PXRD pattern of the single crystals was theoretically generated ***C6S_M–BNZ_dried*** crystal structure using MERCURY software. The strong agreement between their PXRD patterns confirms that both share the same crystalline phase (Figure 100).

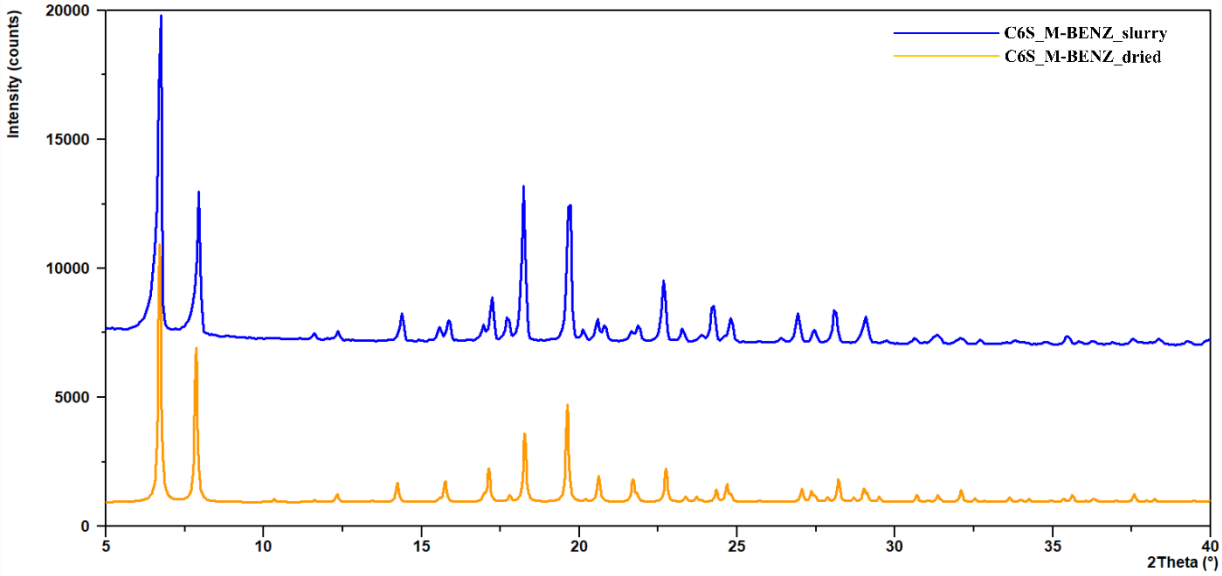

*Figure 100. Powder X-ray diffraction patterns of the **C6S_M–BNZ** complex. The blue pattern corresponds to the sample prepared by the slurry method, while the yellow patterns correspond to the calculated pattern obtained from single crystal X-ray diffraction analysis of the complex **C6S_M–BNZ_dried**.*

TGA–DSC analysis of the C6S_ M–BNZ complex

Since the slurry-prepared sample and the air-dried crystals exhibit the same crystalline material, the next step was to estimate and compare their water content and thermal stability.

The thermogravimetric analysis (TGA) and differential scanning calorimetry (DSC) curves are presented in Figure 101. TGA analysis shows an initial weight loss of 1.98 % below 120 °C,

corresponding to the release of approximately 2.16 molecules per formula unit (MW = 1922.14 g/mol) from the air-dried single crystals (green curve). At higher temperature further weight loss is still visible that might indicate water liberation from the confined space of enclosed voids in the supramolecular framework. In contrast, the slurry-prepared powder sample exhibited negligible mass loss under the same conditions, indicating minimal or no released water.

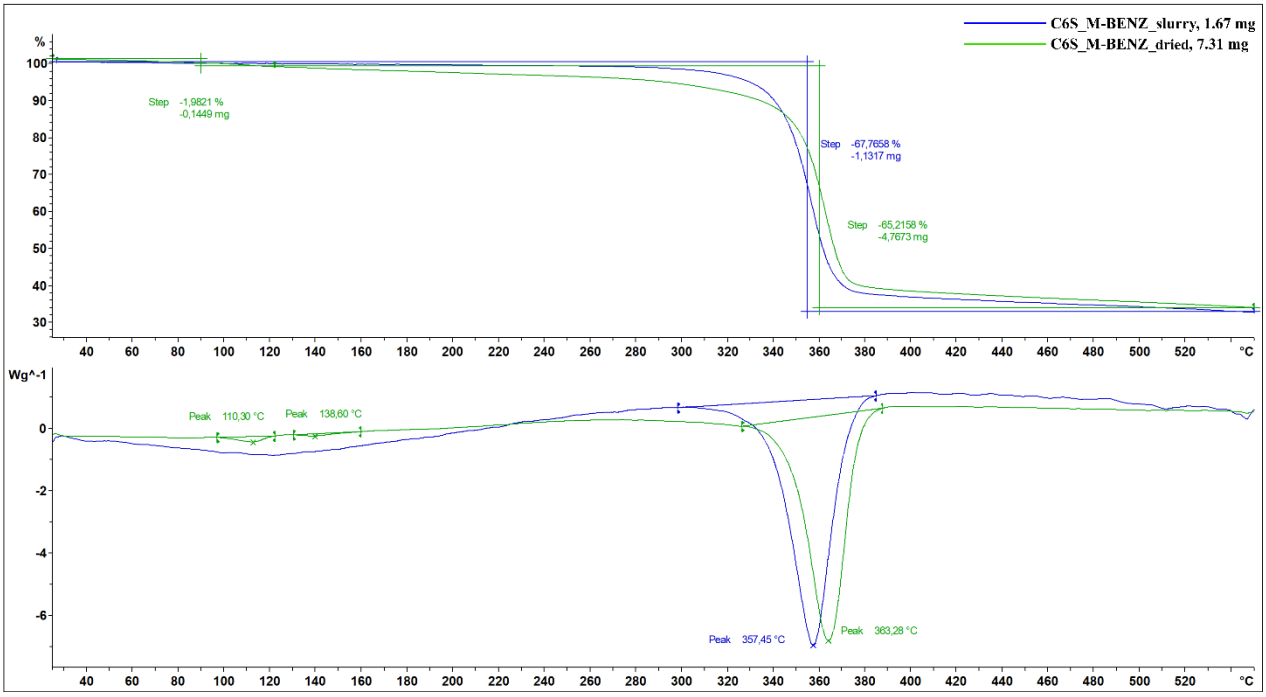

*Figure 101. TGA (top) and DSC (bottom) curves of the **C6S_M–BNZ** complex. The blue curve represents the powder sample prepared by the slurry method, and the green curve represents the dried crystals of the complex **C6S_M–BNZ_dried**.*

Solid-state complexes of C4S and C6S with 4-methylbenzamidine – discussion of results

The host–guest complex ***C4S_M–BNZ***, obtained from C4S and 4-methylbenzamidine, consists of one calixarene molecule and four methylbenzamidine guests, together with one ethanol and two water molecules. One of the four methylbenzamidine molecules is encapsulated within the calixarene cavity and is stabilized by a weak *C–H···π* interaction. Comparing to previously described host–guest complexes with unsubstituted BNZ the inclusion of M-BNZ occurs through the methyl group pivoting to the cavity bottom. While in the complexes with BNZ the inclusion is sustained by *C–H···π* interaction between aromatic carbon atoms of the guest and cavity interior, in the case of M-BNZ inclusion is sustained by the *C–H···π* interaction of methyl group with C4S aromatics. The slantway inclusion geometry in ***C4S_M–BNZ*** is similar as in complexes **I**, **II**, **IV** and **V** with BNZ guest. Interestingly, in the case of ***C4S_M–BNZ*** crystal complex, one ethanol molecule is part of solid state assembly, which was not observed in the complexes with BNZ.

Crystallization of C6S with 4-methylbenzamidine affords complex ***C6S_M–BNZ***. In contrast to many crystalline complexes of *p*-sulfonatocalix[*n*]arenes, crystals of ***C6S_M–BNZ*** are stable in

air outside the mother liquor at room temperature. Single-crystal X-ray diffraction revealed that air-drying the crystal for one day results in ***C6S_M–BNZ_dried*** structure of the same host–guest composition (1/6 of C6S and one benzamidine molecule in the asymmetric unit) and the same pleated-loop conformation of the calixarene, differing only in their disordered water content.

Structural analysis shows that the complex contains large isolated voids accommodating disordered water molecules. These voids are enclosed by two calixarene molecules – one at the top and one at the bottom, and by six methylbenzamidine molecules on the sides. Owing to disorder of the methylbenzamidine over two positions, the voids were analysed separately for each disorder component using both MERCURY and MSROLL/XSEED softwares. According to MERCURY, one void associated with the major benzamidine position occupies a volume of 491.4 $Å^3$, whereas the alternate void associated with the minor M-BNZ position amounts to 338.2 $Å^3$. Analysis using MSROLL/XSEED yields larger void volumes of 538.1 and 369.8 $Å^3$ for the major and minor disorder components, respectively. The differences in the volumes calculated by Mercury and MSROLL arise from the way each program "sees" the space inside a crystal. Mercury uses a grid-based algorithm with a spherical probe to map all regions that a solvent molecule could access. The calculated volume depends on the grid spacing: finer grids give more accurate results but take longer to compute, while coarser grids slightly underestimate cavity sizes. MSROLL, on the other hand, measures the volumes of discrete, enclosed cavities by fitting a smooth molecular surface around the host framework. This method is like using an infinitely fine grid in Mercury, giving highly accurate volumes for isolated voids. However, it cannot handle open channels, because the probe would "fall out" of the continuous space. MSROLL is therefore best for counting and measuring individual cavities, whereas Mercury provides a broader picture of the total free space in the crystal.[195] In addition to crystallization from solution, the ***C6S_M–BNZ*** complex was also obtained using the slurry method. Powder X-ray diffraction confirmed that the resulting material is identical to the air-dried single crystals, indicating the formation of the same crystalline phase.

The host–guest structure ***C6S_M–BNZ*** can be considered as a supramolecular framework based on the charge-assisted hydrogen bonds. The unusual stability of the supramolecular assembly can be attributed to the specific hydrogen bonding between M–BNZ and sulfonate groups of C4S macrocycle, as all amidinium hydrogen bond donors of M–BNZ are engaged in the interaction with C4S. In the complexes of C4S with BNZ and M–BNZ, besides amidinium-sulfonate supramolecular synthons, there are always amidinium-water hydrogen bonds present. Also, in ***C6S_BNZ*** crystal complex, there are ordered water molecules that take part in the hydrogen bonding both with C6S and BNZ molecules. The pleated loop conformation of C6S can also be crucial for the stability of ***C6S_M–BNZ*** assembly, as all phenolic groups of C6S are efficiently engaged in the circular

hydrogen bonding. In the up-down double cone conformation that C6S adopts in ***C6S_BNZ*** complex, the intramolecular hydrogen bonding is disrupted and some phenolic groups become engaged in the hydrogen bonding with water molecules. It seems that the interplay of the host–guest complexation, namely hydrogen bonding, ionic forces and weaker *C–H···π* interaction between M–BNZ and C6S, together with specific pleated loop conformation of the macrocyclic host, promotes ineffective crystal packing featuring discrete structural voids filled with disordered solvent molecules. The ***C6S_M–BNZ*** supramolecular framework can potentially be porous or permeable to additional guests, that will be a subject for future studies.

4.1.5 C4S complexes with 4-aminobenzamidine

Crystallization and microscopic observations for C4S sulfonic acid complexes with 4-aminobenzamidine

10 mg of C4S ***sulfonic acid*** was dissolved in 0.25 mL of H_2O/EtOH (1:1). The solution of 2.8 mg 4-aminobenzamidine dihydrochloride in 0.25 mL of H_2O/EtOH (1:1) was combined with the solution of the host (Figure 102a).

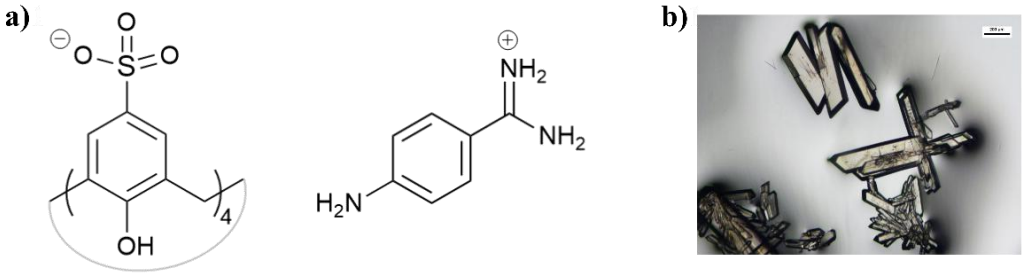

*Figure 102. Chemical structure of C4S **sulfonic acid** host and aminobenzamidine (**A–BNZ**) guest; (b) photomicrographs of crystals of **C4S_A–BNZ_I** complex; (c) small prismatic crystals of **C4S_A–BNZ_I** appeared simultaneously with needle-like crystals of benzamidine hydrochloride after aging of **C4S_A–BNZ_II** in the mother solution allowing the solvent to evaporate slowly. The scale bar corresponds to 200 µm.*

After one day, colorless prism-shaped crystals of good diffraction quality were obtained (Figure 102b). Single-crystal X-ray diffraction analysis confirmed that the crystals corresponded to the host–guest complex ***C4S_A–BNZ_I***. The crystals were then left in the original solution in an open vial to allow the solvent to evaporate slowly. After 10 days, X-ray analysis of the dried crystals showed a new host–guest complex ***C4S_A–BNZ_II***.

The refinement details of the C4S_A–BNZ_I and C4S_A–BNZ_II complexes

The asymmetric unit of ***C4S_A–BNZ_I*** consist of two tetra-anions C4S molecules, four dications of aminobenzamidine, five ethanol and 31.02 water molecules.

The O7 atom of the C4S sulfonate group is disordered over two positions and refined using PART 1 and PART 2 commands (59% of O7 and 41% of O7A) with SIMU and RIGU restraints. The C5E > O3E ethanol molecule is disordered over two positions. The first component of the disorder C5E >

O3E is refined with the PART 1 command (75.7%). The second component of the disorder C5A > O3A is refined with the PART 2 command (24.3%) using the SIMU, RIGU and SADI restraints. The C8E and O4E atoms of C7E > O4E ethanol molecule are disordered over two positions. The first component of the disorder C8E > O4E is refined with the PART 1 command (53%). The second component of the disorder C8A > O4A is refined with the PART 2 command (47%). The SIMU, RIGU and SADI restraints are applied. The atoms of C9E > O5E ethanol molecule are disordered over two positions. The first component of the disorder C9E > O5E is refined with the PART 1 command (38.1%), the second component of the disorder C9A > O5A is refined with the PART 2 command (61.9%) with SIMU, RIGU and SADI restraints. The O20W water molecule, closed to the disordered ethanol molecule, is placed in PART 2 and refined with 50% occupancy. The O14W water molecule is disordered over two positions and refined with PART commands (O14W occupies 23% and O14A occupies 77%). The O22W water molecule is disordered over two positions and refined with PART commands (O22W occupies 78.2% and O22A occupies 21.8%). The O28W water molecule is disordered over two positions and refined with PART commands (O28W occupies 69.5% and O28A occupies 30.5%). The O29W water molecule is disordered over two positions and refined with PART commands (O29W occupies 73.2% and O29A occupies 26.8%). The O30W molecule is close to the disordered O29W molecule and is refined in PART 2 with 26.8% occupancy. The O31W, O32W, and O33W disordered water molecules are positioned close to each other. The disorder is refined with PART 1 and PART 2 commands. O31W and O32W in PART 1 are refined with 75% and 50% occupancies, respectively. O31A and O33W in PART 2 are refined with 50% and 50% occupancies, respectively. All hydrogen atoms are added geometrically. Hydrogen atoms of water molecules are not included in the model. Some residual density is related to the disordered water molecules in the structure.

The asymmetric unit of ***C4S_A–BNZ_II*** consists of one C4S tetra-anion, one sodium cation, one dication of aminobenzamidine, one Zundel ($H_5O_2^+$) cation and 4.26 water molecules.

The Na1 cation is disordered over two positions – Na1 and Na2. The first component of the disorder is refined with the PART 1 command (25.7%). The second component of the disorder is refined with the PART 2 command (74.3%). The O5W water molecule coordinated to the Na1 is also disordered over two positions and refined with PART commands (O5W occupies 25.7% and O5A occupies 74.3%). The O6W is close to the disordered O5W molecule and refined in the same parts with the same occupancies (O6W occupies 25.7% and O6A occupies 74.3%). The O7W molecule in the same PART 1 is refined with the 25.7% occupancy. All hydrogen atoms are added geometrically, except H2WA, H2WB, and H2WC hydrogen atoms of the O2W molecule, which is a part of the Zundel cation. These atoms are located from a difference Fourier map, and the *O–H* distance of 0.84

Å is fixed with a DFIX restraint. The O3W, O4W, O5W, O6W, and O7W molecules are refined without hydrogen atoms. The basic crystallographic data of the discussed structures are provided in Table 7.

*Table 7. Crystal data and structure refinement for **C4S_A–BNZ_I** and **C4S_A–BNZ_II** complexes.*

Parameters	***C4S_A–BNZ_I***	***C4S_A–BNZ_II***
Formula moiety	$2(C_{28}H_{20}O_{16}S_4)\cdot4(C_7H_{11}N_3)\cdot5(C_2H_6O)$ $\cdot31.02(H_2O)$	$C_{28}H_{20}O_{16}S_4Na\cdot C_7H_{11}N_3\cdot H_5O_2^+$ $\cdot4.26(H_2O)$
Formula weight	2819.26	1014.58
Crystal system	Triclinic	Monoclinic
Space group	*P–1*	*P2₁/c*
a / Å	11.8800(2)	13.7304(3)
b / Å	15.2725(2)	18.0014(3)
c / Å	37.3360(4)	17.4205(3)
α / °	90.3740(1)	90
β / °	97.3870(1)	93.766(2)
γ / °	97.5060(1)	90
Volume / Å³	6658.48(16)	4296.46(14)
Z	2	4
ρ_{calc} ***/g·cm⁻³***	1.41	1.57
Crystal color	Colorless	Colorless
Crystal morphology	Prism	Prism
μ / mm⁻¹	2.14	2.93
θ_{max} ***/ °***	70.1	70.2
Reflections collected	77385	25781
Independent reflections	25028 [R_{int} = 0.04]	7025 [R_{int} = 0.04]
Data / Restraints / Parameters	25028 / 105 / 1768	7025 / 2 / 625
Observed data [I > 2σ(I)]	23240	8096
Final R indexes [I ≥ 2σ(I)]	R_1 = 0.072, wR_2 = 0.185	R_1 = 0.056, wR_2 = 0.152
Final R indexes [all data]	R_1 = 0.076, wR_2 = 0.188	R_1 = 0.064, wR_2 = 0.158
Goodnesso-f-fit on F²	1.09	1.04
Largest diff. peak and hole / e·Å⁻³	1.21 / –0.72	0.69 / –0.83

Structure analysis of the C4S_A–BNZ_I complex

The co-crystallization of C4S ***sulfonic acid*** with 4-aminobenzamidine dihydrochloride from water–ethanol solution (1:1) results in the formation of the complex ***C4S_A–BNZ_I*** with the formula $2(C_{28}H_{20}O_{16}S_4)\cdot4(C_7H_{11}N_3)\cdot5(C_2H_6O)\cdot31.02(H_2O)$. Single-crystal X-ray diffraction analysis shows that this complex crystallizes in a triclinic crystal system in the space group *P–1*. The asymmetric part consists of two C4S molecules, four A–BNZ, five ethanol and 31.02 water molecules (Figure 103).

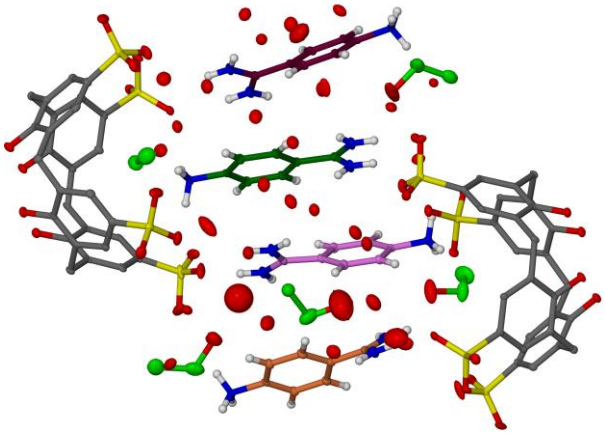

*Figure 103. Asymmetric unit of the **C4S_A–BNZ_I** complex. The crystallographically unique benzamidine molecules are presented in different colours. Atomic displacement parameters set at 50% probability. Some hydrogen atoms and disorder are omitted for clarity.*

In the complex ***C4S_A–BNZ_I***, two calixarene molecules have the typical cone conformation. The C4S cone sizes, measured by the distances between opposite Sulphur atoms, are almost similar – 10.62 Å and 9.86 Å for one macrocycle and 10.64 Å and 9.65 Å for second. The *O···O* distances at the C4S lower rims range from 2.679(3) Å to 2.769(3) Å for the both hosts, showing the formation of cyclic intramolecular *O–H···O* hydrogen bonds. The parameters of the intramolecular hydrogen bonds within the C4S lower rims are placed in Table 42, Annex I.

The cavities of two C4S hosts are occupied by ethanol molecule (shown in light green), other three ethanol molecules are positioned out of the macrocycles (Figure 104). Solvents molecules form hydrogen bonds with sulfonate oxygen atoms of the C4S and water. The *O···O* distances for these interactions fall within hydrogen bonding ranges (2.751(6)–2.953(19) Å). Additionally, *C–H···π* interactions for cavity included molecules are observed between the methylene / methyl groups of ethanol and the *π*–systems of the C4S phenolic rings (Figure 104). The parameters of the intermolecular interactions formed by ethanol molecules are described in in Tables 42,43, Annex I.

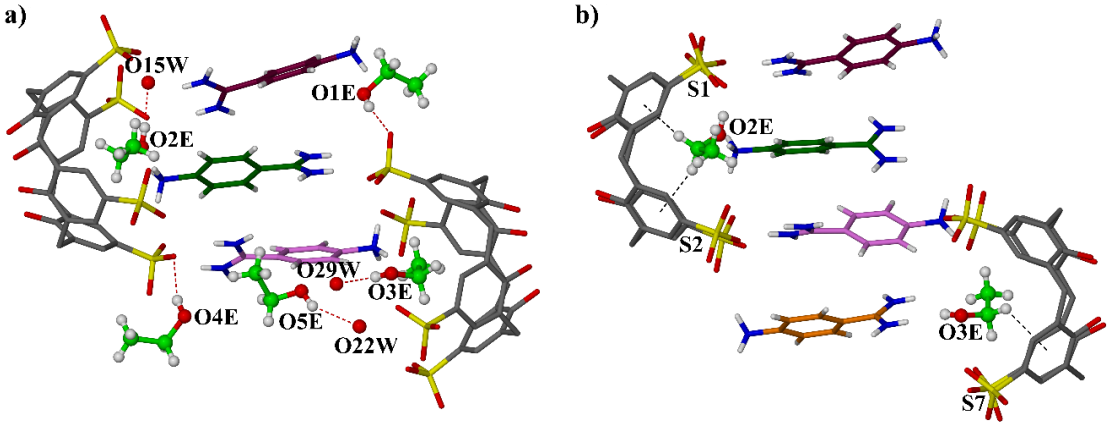

*Figure 104. Host–guest complex **C4S_A–BNZ_I**: (a) O–H···O hydrogen bonding between ethanol and C4S / water molecules; (b) C–H ···π interactions formed methylene / methyl groups of the ethanol molecules and aromatic rings of the C4S.*

Each aminobenzamidine molecule participates in the formation of seven *N–H···O* hydrogen bonds, involving interactions with C4S, ethanol and water molecules. Figure 105 presents representative examples of these *N–H···O* interactions, specifically those involving the C1I > O3I and C1Z > O3Z aminobenzamidines. The *N···O* distances are in the range of 2.651(4)–3.257(4) Å. In addition to the *N–H···O* interactions, the described guest molecules engage in *C–H···O* contacts with the oxygen atoms of the nearby C4S host. The parameters of intermolecular interaction formed by all aminobenzamidines are shown in in Table 42, Annex I.

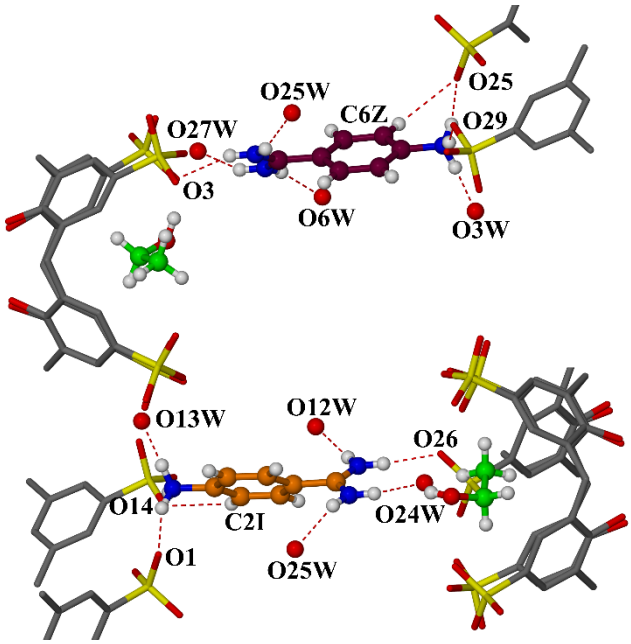

*Figure 105. Host–guest complex **C4S_A–BNZ_I**: an example of N–H···O and C–H···O hydrogen bonds between aminobenzamidine and C4S molecules.*

The crystal packing of the ***C4S_A–BNZ_I*** host–guest complex, viewed along the ***a*** and ***b*** axes, reveals a bilayered arrangement of C4S macrocycles in an alternating *up–down* orientation (Figure 106). The calixarene molecules in layers are connected through *C–H···O* hydrogen bonds and *π···π* stacking. The space between the layers incorporates aminobenzamidine, ethanol (located also within the C4S cavities), and water molecules. The benzamidine molecules adopt a *head-to-tail* parallel orientation. The parameters of the intermolecular interactions formed between C4S molecules are provided in Table 44, Annex I.

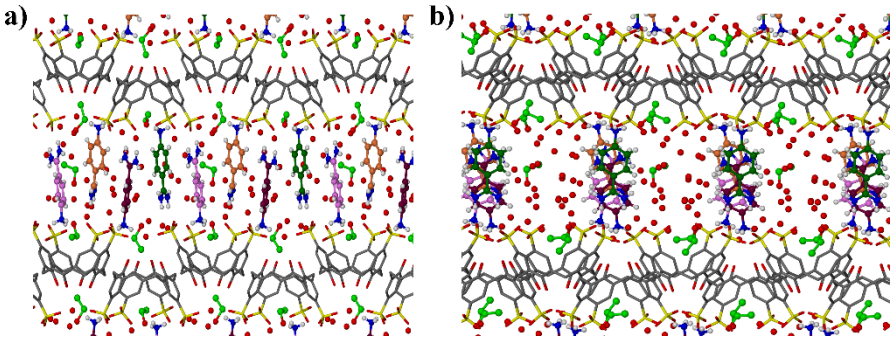

*Figure 106. Crystal packing of the host–guest complex **C4S_A–BNZ_I** viewed along (a) **a** and (b) **b** directions.*

Structure analysis of the C4S_A–BNZ_II complex

The complex ***C4S_A–BNZ_II*** has the formula $C_{28}H_{20}O_{16}S_4Na \cdot C_7H_{11}N_3 \cdot H_5O_2^+ \cdot 4.26(H_2O)$. Single-crystal X-ray diffraction analysis shows that this complex crystallizes in a monoclinic crystal system in the space group $P2_1/c$. The asymmetric part consists of one C4S molecule with one coordinated sodium cation, one A–BNZ molecule, one $H_5O_2^+$ Zundel cation and 4.26 water molecules (Figure 107).

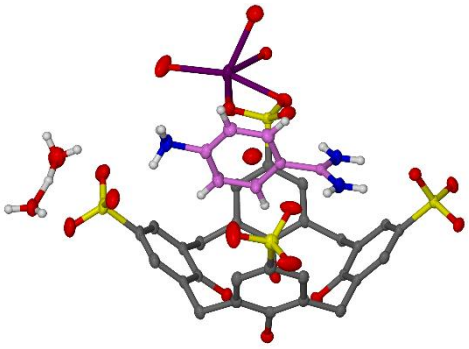

*Figure 107. Asymmetric unit of the **C4S_A–BNZ_II** complex. Atomic displacement parameters set at 50% probability. Disorder omitted for clarity.*

In the complex ***C4S_A–BNZ_II***, a tetra-anion calixarene molecule adopts a typical cone conformation. The size of the C4S cone, measured by the distances between opposite Sulphur atoms, is 8.55 Å and 12.00 Å, indicating a significant pinched shape. Despite this deformation, the *O···O* distances at the C4S lower rim, ranging from 2.718(3) Å to 2.839(3) Å, suggest the formation of circular intramolecular *O–H···O* hydrogen bonds. The parameters of the intramolecular hydrogen bonds within the C4S molecule are shown in Table 45, Annex I.

The cavity of C4S is occupied by a C1X > N3X aminobenzamidine molecule, shown in pink. The inclusion of the guest into the macrocyclic cavity occurs to a depth of 5.33 Å, measured as the distance between the P-plane formed by the methylene bridges of C4S and the centroid of the aromatic ring of aminobenzamidine (Figure 108a).

In addition to the benzamidine cation, the complex contains one oxonium species – a $H_5O_2^+$ Zundel cation formed by O1W and O2W water molecules. The *O1W···O2W* distance is 2.485(4) Å

that is typical for Zundel cation, characterizing the strong hydrogen bond. The oxonium cation is located close to the upper rim of C4S (Figure 108b). The O1W–O2W cation forms four *O–H···O* hydrogen bonds with the parent and adjacent C4S molecules and water. An expansion of the crystal structure also shows the position of the cation near the lower rim of the symmetry-related host. At the lower rim C4S is connected to the cation through O12 oxygen atom of the hydroxyl group. The *O12–H12···O1W* hydrogen bond occurs at the *O···O* distance of 2.724(3) Å. The parameters of the intermolecular interactions involving Zundel cation are summarized in Table 45, Annex I. The charge balance of the complex is achieved through the presence of a third type of cation – the Na^+ ion (Figure 108c). The sodium cation is disordered over two positions, with occupancies of 27.7% (Na1) and 74.3% (Na2). Na1 is coordinated to the upper rim of the C4S molecule by two *Na···O* bonds, to two oxygen atoms from adjacent C4S molecules, and to two water molecules, resulting in an overall coordination number of six and a distorted octahedral coordination geometry. The major site, Na2, is three-coordinate and adopts a distorted trigonal planar geometry, coordinating to the upper rims of two adjacent calixarene units and to a water molecule. The *Na···O* bond distances for Na1 range from 2.358(12) Å to 2.494(6) Å, and for the Na2 – from 2.504(6) Å to 2.576(5) Å, as summarized in Table 46, Annex I.

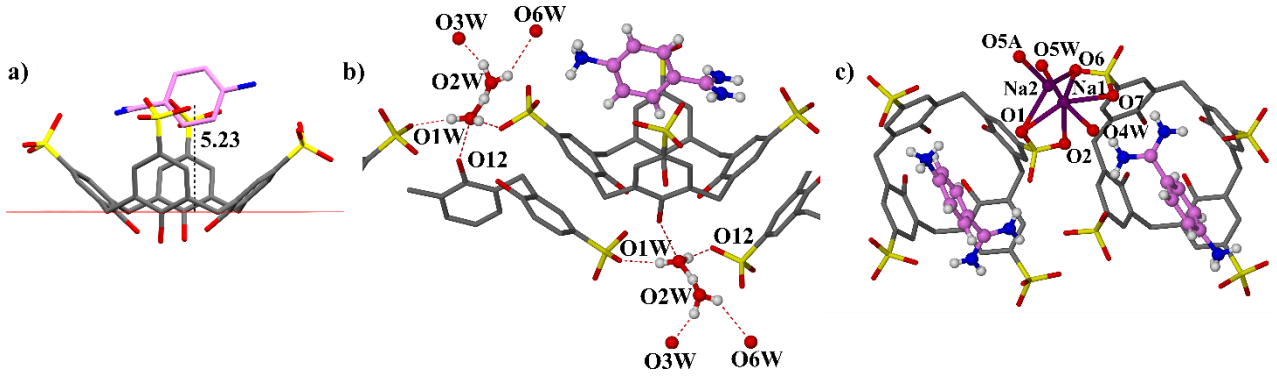

*Figure 108. Host–guest complex **C4S_A–BNZ_II**: (a) the depth of inclusion of aminobenzamidine into C4S cavity; (b) the hydrogen bonding network around Zundel cation formed by O1W and O2W water molecules; (c) the coordination sphere of sodium cation in the host–guest complex. The disordered part of the sodium cation and water molecules are omitted for clarity. Distance is given in Å.*

The aminobenzamidine molecule is encapsulated within the C4S cavity, aligned along the two opposite sulfonate groups. It forms seven *N–H···O* hydrogen bonds involving the parent C4S and water molecules (Figure 109a), with corresponding *N···O* distances ranging from 2.816(4) to 3.080(4) Å. Additionally, one *C–H···π* interaction is observed between the aromatic ring of aminobenzamidine and the C4S, with a *C···centroid* distance of 3.734(4) Å. Further structural analysis reveals *π···π* stacking interactions between adjacent C4S molecules, with *centroid···centroid* distances of 3.541(16)

Å (Figure 109b). Detailed parameters of the intermolecular interactions involving aminobenzamidine molecules are provided in Tables 45, 47, and 48, Annex I.

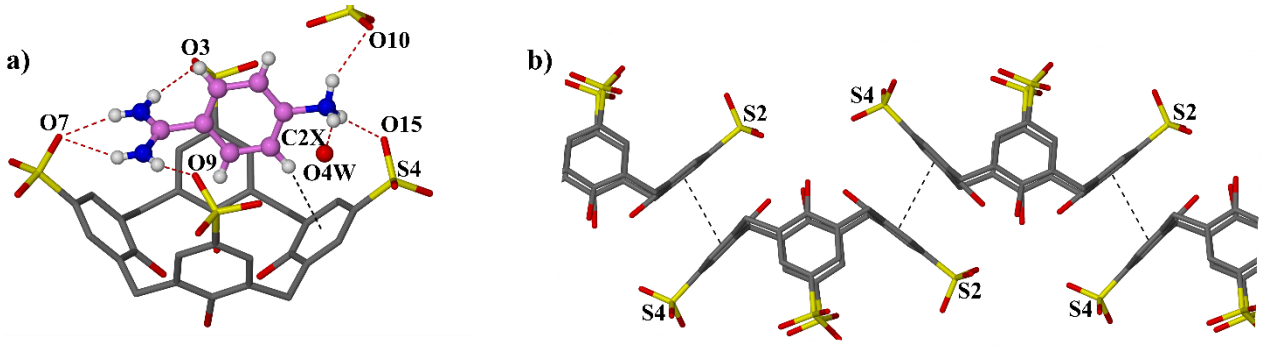

*Figure 109. Host–guest complex **C4S_A–BNZ_II**: (a) N–H···O hydrogen bonds between N–H groups of aminobenzamidine and sulfonate oxygen atoms of C4S / water molecule together with the C–H···π interaction formed between the benzamidine and C4S aromatic rings; (b) π···π interactions between aromatic rings of C4S molecules.*

Expansion of the crystal structure further confirms the presence of separated C4S bilayers. Sodium cations are positioned between these layers, along with both coordinated and free water molecules (Figures 110a,b).

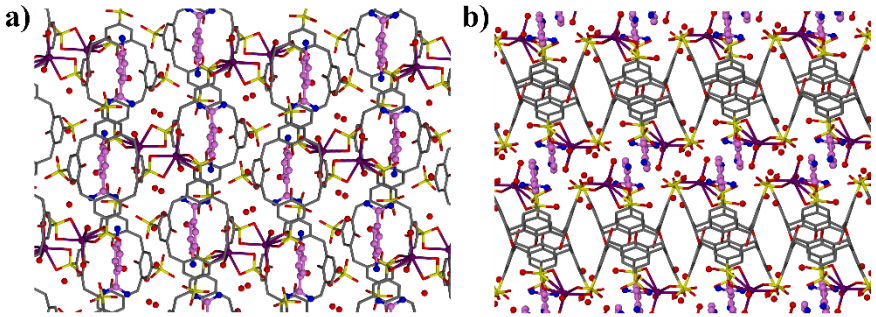

*Figure 110. Crystal packing of the host–guest complex **C4S_A–BNZ_II** viewed along (a) **a** and (b) **b** directions.*

Solid-state complexes of C4S with 4-aminobenzamidine– discussion of results

The co-crystallization of *p*-sulfonatocalix[4]arene with 4-aminobenzamidine yielded two host–guest complexes obtained under different crystallization conditions. Crystals of ***C4S_A–BNZ_I*** formed rapidly within one day after combining the host and guest solutions in a water–ethanol mixture, whereas ***C4S_A–BNZ_II*** appeared only after ten days of slow solvent evaporation from the same crystallization vial. The source of sodium cation in the complex ***C4S_A–BNZ_II*** might stem from the contamination of commercial *p*-sulfonatocalix[4]arene sulfonic acid used for the cocrystallization.

The compositions of the complexes reflect these differences. ***C4S_A–BNZ_I*** contains two C4S, four aminobenzamidine, five ethanol and 31 water molecules per asymmetric unit. In this complex, aminobenzamidine molecules remain outside the C4S cavities, while ethanol occupies the cavity space. This is in contrast to the C4S inclusion complexes with benzamidine (five crystal forms) and methylbenzamidine. All these complexes were crystallized from the same water-ethanol solvent

mixture. Ethanol molecules are known competitors to the organic guests for the place in the C4S macrocyclic cavity. Aminobenzamidinium as a potential guest molecule is more polar than unsubstituted benzamidine and methylbenzamidine, as it carries additional charge and hydrogen bond donors at the ammonium group in the *para* position to amidinium group. Thus, the inclusion of dicationic aminobenzamidinium is less favorable or comparable to the inclusion of ethanol molecules. Despite being outside of the macrocyclic cavity, ABZ molecules as ditopic ligands interact efficiently through hydrogen bonding via both amidinium and ammonium end groups. This propensity is realized as amidinium-sulfonate and ammonium-sulfonate supramolecular synthons with two distant C4S molecules. Every sulfonate group in the structure accepts one or two hydrogen bonds from nitrogen donors of ABZ.

Upon aging in the mother solution, the ethanol molecules are gradually excluded, leading to ***C4S_A–BNZ_II***, which contains one C4S molecule, one aminobenzamidine, one sodium cation, one $H_5O_2^+$ (Zundel) cation, and 4.26 water molecules. Obviously, slow evaporation of the mother solution and concentrational changes of the dissolved components induce dissolution of the crystals of ***C4S_A–BNZ_I***, and crystallization of ***C4S_A–BNZ_II*** complex**.** In this complex, one aminobenzamidine in the *app*. longitudinal orientation resides above the pinched cone of the macrocycle. The amidinium and ammonium substituents of A–BNZ donate hydrogen bonds to all four sulfonate groups of C4S. Due to such multipoint hydrogen bonding between one guest and one host the overall inclusion mode is shallow as the guest prefers to stay near the anionic sulfonate rim of the macrocycle. Only the edge of A–BNZ aromatic ring approaches the entrance to the hydrophobic inner cavity of C4S. The shallow inclusion mode and longitudinal orientation of the guest above the pinched cone of the macrocycle is similar to the structure of ***C4S_BNZ_Form III***, that also crystallize late (preceded by Forms I and II) and contains oxonium ions. However, the inclusion of A–BNZ is even shallower than that of BNZ in Form III, as additional ammonium-sulfonate synthon appear causing ABZ to be positioned higher above the upper rim (the inclusion depth is 5.3 Å for A–BNZ, and 4.9 Å for BNZ in Form III). It is interesting, that these two crystal complexes involving strong pinching of C4S cone shape and longitudinal orientation of the guest above the cavity take long time to form and crystallize, and are preceded by different complexes that form and crystallize rapidly and do not require strong deformation of the macrocycle. Such step-wise crystallization can be considered in the terms of Ostwald's rule of stages according to which crystallization often proceeds step by step *via* intermediate metastable phases until the most stable phase will be formed. However, in the case of multi-component supramolecular complexes and assemblies, the complicated phenomena of crystal nucleation and growth are interlaced with the kinetic factors and induced fit complexation aspects in the host–guest systems.

4.1.6 C6S complexes with 4-hydroxybenzamidine

Crystallization and microscopic observations for C6S sulfonic acid complexes with 4-hydroxybenzamidine

10 mg of C6S ***sulfonic acid*** was dissolved in 0.5 mL of H_2O/EtOH (1:1). The solution of 9.3 mg 4-hydroxybenzamidine hydrochloride in 0.5 mL of H_2O/EtOH (1:1) was combined with the solution of the host (Figure 111a). After approx. two weeks the colorless prism-shaped crystals of a good diffraction quality appeared (Figure 111b). Single-crystal X-ray diffraction analysis revealed these crystals to be the host–guest complex ***C6S_H–BNZ_I***. Crystals of ***C6S_H–BNZ_I*** complex were than left in the mother solution for approximately one month after which newly formed, colorless prism-shaped crystals were identified through microscopic observation. Single-crystal X-ray diffraction analysis showed these crystals to be the host–guest complex of the ***C6S_H–BNZ_II*** (Figure 111c).

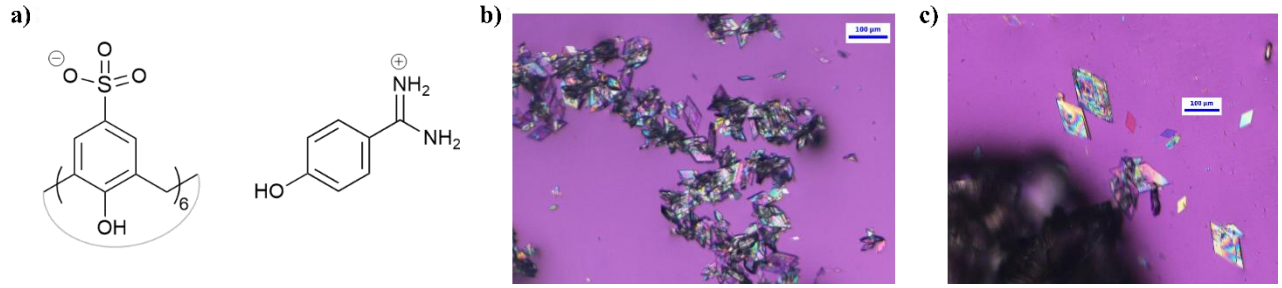

*Figure 111. Chemical structure of C6S **sulfonic acid** host and hydroxybenzamidine (**H–BNZ**) guest; (b) Photomicrograph of prismatic crystals of the **C6S_H–BNZ_I** complex that appeared in the mother solution after two weeks; (c) prismatic crystals of the **C6S_H–BNZ_II** complex appeared in the mother solution after one month of slow solvent evaporation.. The scale bar corresponds to 100 µm.*

The refinement details of the C6S_H–BNZ_I and C6S_H–BNZ_II complexes

The asymmetric unit of ***C6S_H–BNZ_I*** consists of 1/2 molecule of C6S hexa-anion, positioned on 2-fold axis, three monocations of H–BNZ and 2.5 water molecules. Atoms of two C6S sulfonate groups are disordered over two positions. The first component of disordered O1 > O2 atoms is refined with PART 1 command (81% occupancy), the second O1A > O2A is refined with PART 2 command (19% occupancy). The first component of disordered O10 > S3 atoms is refined with PART 1 command (85.5% occupancy), the second O10A > S3A is refined with PART 2 command (14.5% occupancy). Both disorders are refined using SIMU and RIGU restraints. The O2W molecule lies on 2-fold axis and is refined with 50% occupancy. All hydrogen atoms are added geometrically.

The asymmetric unit of ***C6S_H–BNZ_II*** consist of 1/2 molecule of C6S hexa–anion, positioned on inversion centre, three monocations of H–BNZ and 3 water molecules. C1X > O1X benzamidine is disordered over two positions. First component of disorder C1X > O1X is refined with PART 1 command (51.4%), second component of disorder C1A > O1A is refined using PART 2 command (48.6%). The O3W molecule lies close to disordered benzamidine molecule. The first

component of disorder O3W is refined with PART 1 command (51.4% occupancy), the second O3A is refined with PART 2 command (48.6% occupancy). All hydrogen atoms are added geometrically except H1X atom the *O1X–H1X* hydroxyl group which is added from the difference Fourier map, the *O–H* distance of 0.84 Å is fixed with DFIX restraint. The O3W molecule is refined without hydrogen atoms. The basic crystallographic data of the discussed structures is provided in Table 8.

*Table 8. Crystal data and structure refinement for **C6S_H–BNZ_I** and **C6S_H–BNZ_II** complexes.*

Parameters	***C6S_H–BNZ_I***	***C6S_H–BNZ_II***
Formula moiety	$C_{42}H_{30}O_{24}S_6 \cdot 6(C_7H_9N_2O) \cdot 5(H_2O)$	$C_{42}H_{30}O_{24}S_6 \cdot 6(C_7H_9N_2O) \cdot 6(H_2O)$
Formula weight	2024.07	2042.08
Crystal system	Monoclinic	Triclinic
Space group	*C2/c*	*P–1*
a / Å	40.1989(6)	8.8583(4)
b / Å	10.6128(2)	14.6590(1)
c / Å	21.2800(4)	18.7971(11)
α / °	90	107.561(6)
β / °	100.059(2)	94.065(4)
γ / °	90	103.848(5)
Volume / Å^3	8939.0(3)	2232.3(2)
Z	4	1
ρ_{calc} /g·cm^{-3}	1.50	1.52
Crystal color	Colorless	Colorless
Crystal morphology	Prism	Prism
μ / mm^{-1}	2.24	2.26
θ_{max} / °	70.0	71.6
Reflections collected	54366	21363
Independent reflections	8439 [R_{int} = 0.05]	8392 [R_{int} = 0.08]
Data / Restraints / Parameters	8439 / 136 / 667	8392 / 408 / 730
Observed data [I > 2σ(I)]	7284	6011
Final R indexes [I ≥ 2σ(I)]	R_1 = 0.041, wR_2 = 0.110	R_1 = 0.090, wR_2 = 0.235
Final R indexes [all data]	R_1 = 0.049, wR_2 = 0.117	R_1 = 0.113, wR_2 = 0.276
Goodness-of-fit on F^2	1.04	1.02
Largest diff. peak and hole / e·Å^{-3}	0.37 / –0.48	1.19 / –0.81

Structure analysis of the C6S_H–BNZ_I complex

The co-crystallization of C6S ***sulfonic acid*** with 4-hydroxybenzamidine hydrochloride from water–ethanol solution (1:1) results in the formation of the complex ***C6S_H–BNZ_I*** with the formula $C_{42}H_{30}O_{24}S_6 \cdot 6(C_8H_{15}N_2) \cdot 5(H_2O)$. Single-crystal X-ray diffraction analysis shows that this complex crystallizes in a monoclinic crystal system in the space group *C2/c*. The asymmetric part consists of 1/2 C6S molecule, three H–BNZ and 2.5 water molecules (Figure 112).

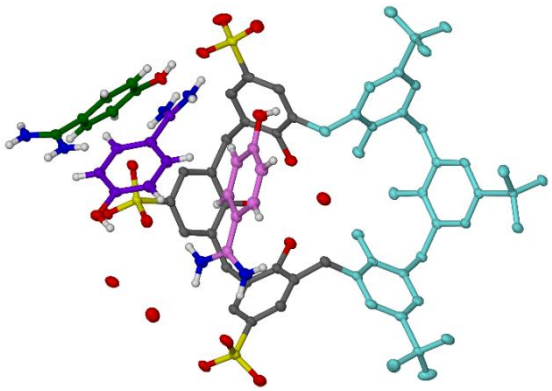

*Figure 112. The asymmetric unit of the **C6S_H–BNZ_I** complex with the expanded C6S molecule. The macrocycle lies over a 2-fold axis, the light blue corresponds to symmetry generated calix[6]arene atoms. Three crystallographically unique benzamidine molecules are are presented in different colours. Atomic displacement parameters set at 50% probability. Disorder omitted for clarity.*

In the H–BNZ complex, the calixarene molecule adopts a *up–up* double cone conformation. (Figure 113b). All six phenolic units are oriented in the same direction, with hydroxyl groups on the lower rim pointing inward, facilitating the formation of intramolecular hydrogen bonds. The *O···O* distances between adjacent hydroxyl groups at the lower rim range from 2.685(2) to 2.797(2) Å (Figure 113a). The C6S molecule in the *up–up* double cone conformation is pinched, creating two pseudo "calix[3]arene" cavities, each holding one H–BNZ guest (Figure 113c). Parameters of the intramolecular interactions at the C6S lower rim are provided in Table 49, Annex I.

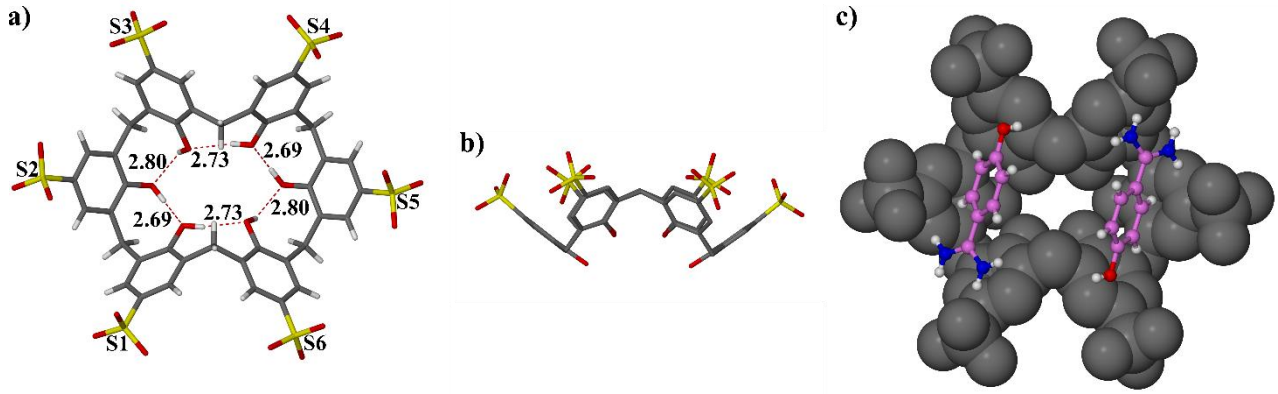

*Figure 113. Host–guest complex **C6S_H–BNZ_I**: (a) O–H···O hydrogen bonding at the C6S lower rim. O···O distances are given in Å; (b) side view on the up–up doble cone conformation of C6S molecule; (c) C6S with two included benzamidine guests shown in space-filled mode in dark grey.*

The crystal structure reveals that hydroxybenzamidine molecules form *O–H···O* hydrogen bonds through multiple modes (Figure 114a). Two guest molecules (pink and violet) interact *via* their hydroxyl groups with the sulfonate oxygen atoms of C6S, while the third molecule (green) forms a hydrogen bond with water molecule (O1W). These interactions occur at *O···O* distances ranging from 2.664(2) to 2.775(5) Å. The hydroxybenzamidine molecules also form *N–H···O* hydrogen bonds with neighboring C6S molecules, the O3W water molecule, and another benzamidine molecule (C1Y > O1Y), at *N···O* distance of 2.838(2) to 3.126(2) Å (Figure 114b).

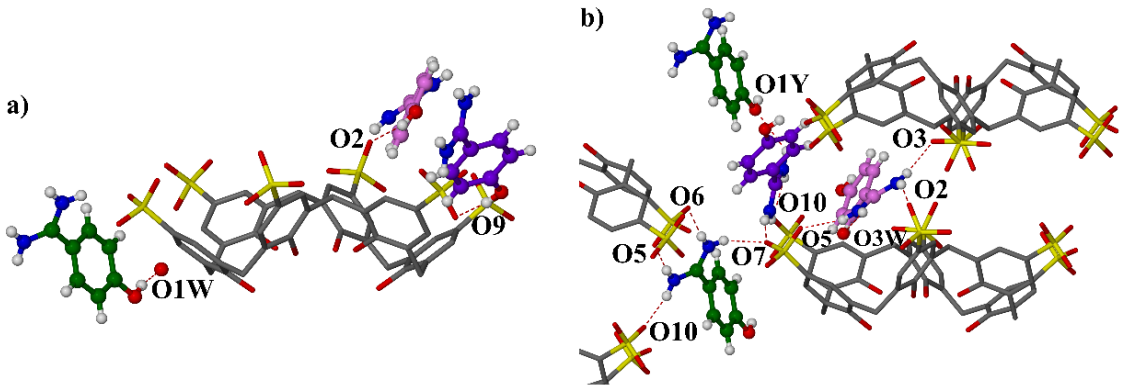

*Figure 114. Host–guest complex **C6S_H–BNZ_I**: (a) O–H···O hydrogen bonds between O–H groups of hydroxybenzamidine and sulfonate oxygen atoms of C6S / water molecule; (b) N–H···O hydrogen bonds between N–H groups of hydroxybenzamidine and sulfonate oxygen atoms of C6S / water molecule.*

In addition to *N–H···O* hydrogen bonding, the C1X > O1X hydroxybenzamidine molecule forms *C–H···O* interactions with adjacent C6S molecules, with *C···O* distances ranging from 3.17(3) to 3.411(5) Å (Figure 115a). The C1X > O1X and C1Z > O1Z benzamidine molecules also engage in *C–H···π* interactions with the aromatic rings of the host, characterized by *C···centroid* distances of 3.390(2) to 3.786(2) Å. Furthermore, the C1Z > O1Z molecule [symmetry code: x, 1+y, z] forms a *C–H···π* contact with a neighboring C1Y > O1Y benzamidine molecule, involving aromatic ring interactions at 3.390(2) Å (Figure 115b). Parameters of the intermolecular interactions formed by hydroxybenzamidine amolecules are provided in Tables 49,50, Annex I.

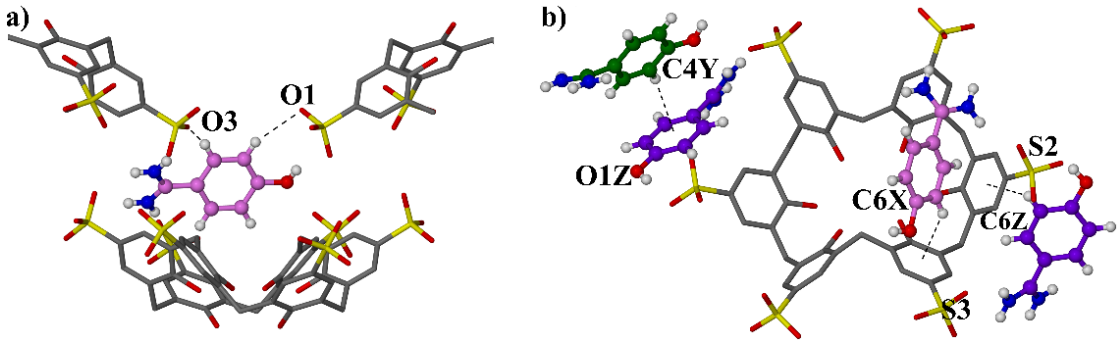

*Figure 115. Host–guest complex **C6S_H–BNZ_I**: (a) C–H···O hydrogen bonds between C–H groups of hydroxybenzamidine aromatic ring and sulfonate oxygen atoms of C6S molecules; (b) the C–H···π interactions between the aromatic rings of hydroxybenzamidine and C6S molecules and neighboring hydroxybenzamidine units.*

The crystal packing shows C6S tapes formed by *C–H···O* and *π···π* interactions, as illustrated in Figure 116c. The individual tapes are separated by H–BNZ molecules complexed outside the macrocyclic cavity. A single water molecule is located at the center of the macrocycle, while additional water molecules occupy positions between the benzamidine molecules (Figures 116a,b). Parameters of these interactions are provided in Tables 49 and 51, Annex I.

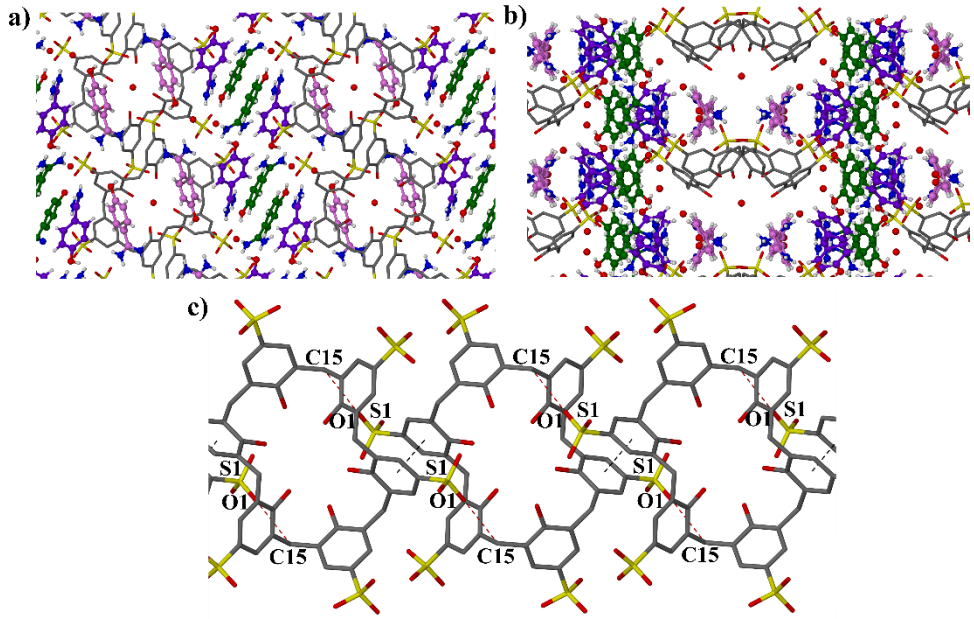

*Figure 116. Crystal packing of the host–guest complex **C6S_H–BNZ_I** viewed along (a) **b** and (b) **c** directions; (c) the network of C–H···O and π···π interactions between C6S molecules.*

Structure analysis of the C6S_H–BNZ_II complex

The complex ***C6S_H–BNZ_II*** has the formula $C_{42}H_{30}O_{24}S_6 \cdot 6(C_7H_9N_2O) \cdot 6(H_2O)$. Single-crystal X-ray diffraction analysis shows that this complex crystallizes in a triclinic crystal system in the space group *P–1*. The asymmetric part consists of 1/2 C6S molecule, three H–BNZ and 3 water molecules (Figure 117).

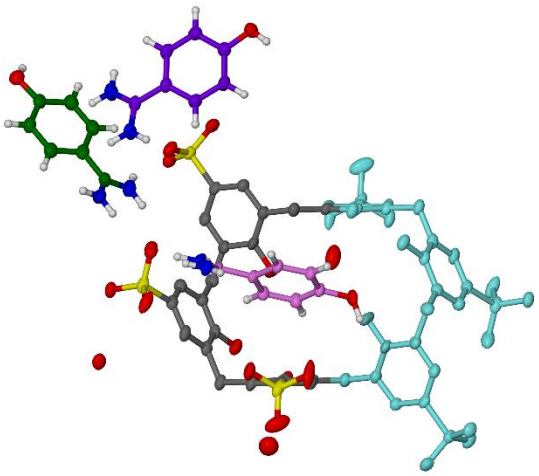

*Figure 117. The asymmetric unit of the **C6S_H–BNZ_II** complex with the expanded C6S molecule. The macrocycle lies over inversion centre, the light blue corresponds to symmetry generated calix[6]arene atoms. Three crystallographically unique benzamidine molecules are presented in different colours. Atomic displacement parameters set at 50% probability. Disorder omitted for clarity.*

In the complex ***C6S_H–BNZ_II***, the calixarene adopts an *up–down* double partial-cone conformation (Figures 118a,b). Due to the disruption of the cone structure, the alignment of the hydroxyl groups no longer supports a complete hydrogen-bonding network. Consequently, intramolecular hydrogen bonds are limited to two hydroxyl groups, while the remaining hydroxyl

groups form *O–H···O* contacts with neighboring calixarene and benzamidine molecules. The *O···O* distances for these interactions range from 2.601(7) to 2.845(7) Å (Figure 118c). Detailed parameters of the intermolecular interactions at the C6S lower rim are listed in Table 52, Annex I.

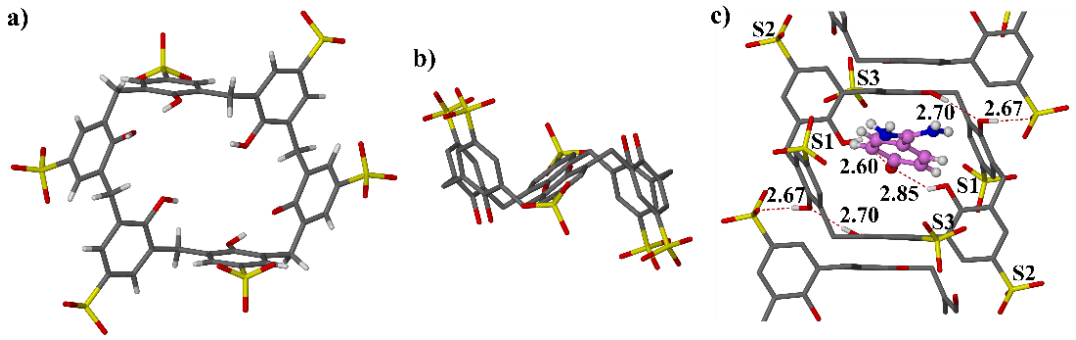

*Figure 118. Host–guest complex **C6S_H–BNZ_II**: (a,b) front and side views on the up–down double partial-cone conformation of C6S molecule; (c) O–H···O hydrogen bonding at the C6S lower rim. O···O distances are given in Å.*

Hydroxybenzamidine molecules form *N–H···O* hydrogen bonds with both C6S and water molecules. Each guest engages in one interaction with water molecule, while the remaining hydrogen bonds involve the calixarene hosts (Figure 119a). The corresponding *N···O* distances range from 2.785(5) to 3.106(6) Å. In addition, the benzamidines participate in *C–H···O* interactions, which occur between their aromatic rings and the sulfonate oxygen atoms of C6S, as well as between the benzamidine hydroxyl groups and the calixarene methylene bridges. These *C···O* contacts fall within the range of 3.202(9)–3.426(10) Å (Figure 119b). Further analysis reveals *π···π* stacking between two pairs of benzamidine molecules, with *centroid···centroid* distances of 3.889(3) Å (C1Y > O1Y) and 3.849(3) Å (C1Z > O1Z) (Figure 119c). The parameters of the intermolecular interactions involving benzamidine molecules are summarized in Tables 52,53, Annex I.

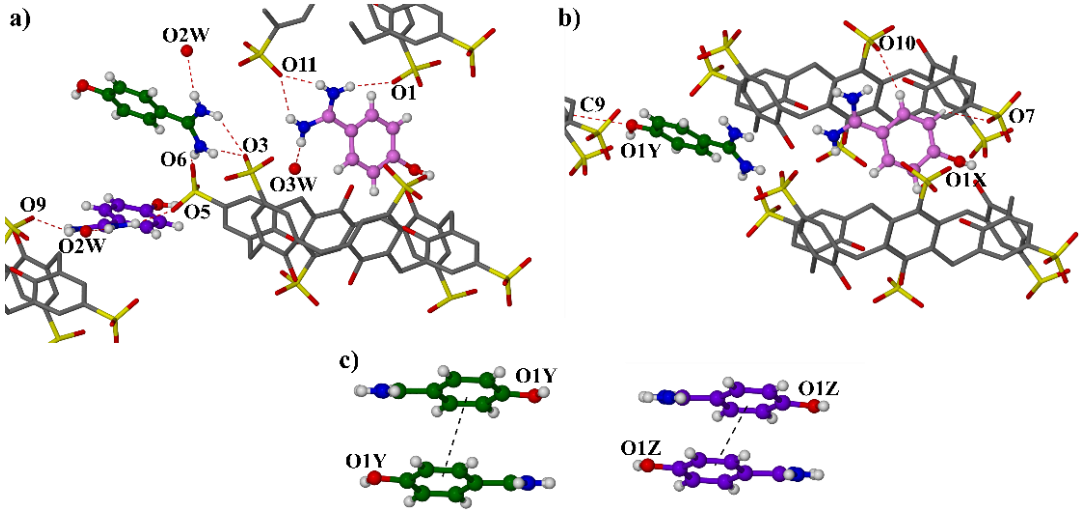

*Figure 119. Host–guest complex **C6S_H–BNZ_II**: (a) N–H···O hydrogen bonds between N–H groups of hydroxybenzamidine and sulfonate oxygen atoms of C6S / water molecules; (b) C–H···O hydrogen bonds between hydroxybenzamidine and C6S molecules; c) π···π interactions between aromatic rings of hydroxybenzamidine molecules.*

In the crystal packing of ***C6S_H–BNZ_II*** *C6S* molecular layers formed through *O–H···O* and *C–H···O* hydrogen bonds, as illustrated in Figure 120c. These layers are separated by layers of hydroxybenzamidine molecules complexed outside the macrocyclic cavities. (Figures 120a,b). The geometric parameters of these hydrogen bonds between C6S molecules are provided in Table 52, Annex I.

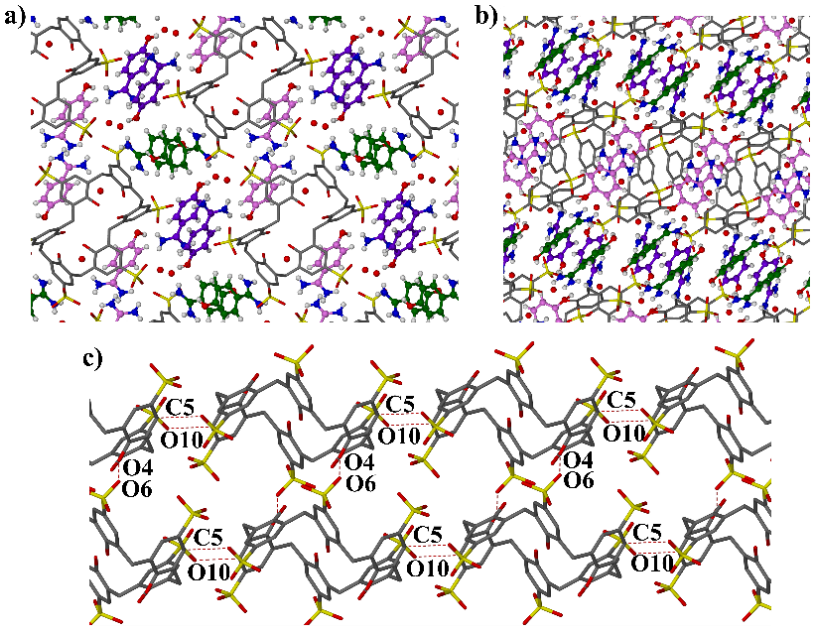

Figure 120. Crystal packing of the host–guest complex ***C6S_H–BNZ_II*** *viewed along (a)* ***a*** *and (b)* ***b*** *directions; (c) the network of O–H···O and C–H···O hydrogen bonds between C6S molecules in the layers.*

Solid-state complexes of C6S with 4-hydroxybenzamidine – discussion of results

Co-crystallization of *p*-sulfonatocalix[6]arene with 4-hydroxybenzamidine yielded two distinct host–guest complexes obtained under different conditions. Crystals of ***C6S_H–BNZ_I*** complex were grown after approximately two weeks of slow crystallization from a water–ethanol mixture, whereas ***C6S_H–BNZ_II*** formed after about one month of aging in the mother solution, indicating that prolonged crystallization promotes structural rearrangement,modification of the host comformation and guest inclusion.

The asymmetric unit of ***C6S_H–BNZ_I*** comprises half a C6S macrocycle, three hydroxybenzamidine molecules, and 2.5 water molecules. The host adopts an up–up double cone conformation, generating two pseudo calix[3]arene cavities, each accommodating one guest molecule, while the other guests are located outside the macrocyclic cavity. The up-up double cone conformation is relatively rare for C6S, of the 52 crystal structures of this calix[6]arene deposited in the CSD, only 8 comprise C6S in up-up conformation. The most common is up-down double partial cone shape, as witnessed by 29 crystal structures having C6S in this conformation. The first structures confirming the possibility of C6S to take up-up double cone conformation were reported by Raston

et al. in 2003. The study describes the successful crystallization and structural characterizations of C6S lanthanide 18-crown-6 complexes. Interestingly, C6S conformation can vary (up-down or up-up) depending on the ratio of the guest used and the nature of the lanthanide metal ion. Also, C6S in the up-up double cone can serve as a host to a pair of either L- or D-leucine guests in the single crystal (refcode FEQYOQ).[132a]

In ***C6S_H–BNZ_II***, the asymmetric unit contains half a C6S macrocycle, three hydroxybenzamidine molecules, and three water molecules. Here, the calixarene adopts an up–down double partial-cone conformation, resulting in disruption of the continuous intramolecular hydrogen-bonding network. Two hydroxybenzamidine molecules are accommodated within inverted pseudo calix[3]arene cavities, while the remaining guest molecules are positioned within the C6S layers. The packing exhibits a layered arrangement of C4S with benzamidine guests included within the macrocyclic cavities, while additional benzamidine molecules are located between adjacent layers. The common feature of ***C6S_H–BNZ_I*** and ***C6S_H–BNZ_II*** complexes is the inclusion of two hydroxybenzamidine guests, as each of two C6S conformations bears two identical pseudo calix[3]arene cavities. In the up-up double cone, two cavities are opened in one direction, while in the up-down conformation two cavities are opened in the opposite direction. For comparison, C6S complex with unsubstituted benzamidine comprises C6S macrocycle in the up-down conformation, though ***C6S_BNZ*** and ***C6S_H–BNZ_II*** are not isostrctural. Peculiarly, the guest methylbenzamidine despite having the same molecular shape as hydroxybenzamidine induces C6S into flattened pleated loop conformation in the complex ***C6S_M–BNZ***.

4.2 *p*-Sulfonatocalix[*n*]arene complexes with alexidine and pentamidine

In this chapter, the complexation, crystallization and crystal structure analysis of C4S, C6S and C8S complexes with pentamidine, together with one C4S complex with alexidine are described and discussed. Pentamidine and alexidine are FDA-approved drug compounds of antimicrobial activity, currently rediscovered as membrane-targeting antibiotic sensitizers, capable of enhancing the activity of antibiotics against multidrug-resistant bacterial pathogens. From the structural viewpoint, pentamidine is a bisbenzamidine derivative, in which two benzamidine groups are connected by a flexible aliphatic linker. Alexidine is a bisbiguanidine with the central hexamethylene chain linking two biguanidines attached to ethyl-hexyl end groups. The guanidine group is similar to amidine, differing in the nature of the substituents of the central carbon atom – amidine group has two nitrogen atoms bonded to this carbon, while guanidine bears three nitrogen atoms. Thus, the supramolecular synthons of charge-assisted amidinium-sulfonate and guanidinium-sulfonate hydrogen bonding can be expected similarly as for calixarene-benzamidine complexes. The presence

of central aliphatic chains connecting either two benzamidine moieties in pentamidine, or two biguanidine moieties in alexidine can also influence host–guest complexation, while defining very high flexibility of drug molecules. The interest in the host–guest crystalline assemblies of C*n*S with pentamidine and alexidine stems from their potential propensity as self-assembled supramolecular framework architectures, as well as exploration of potential supramolecular formulations and/or crystal forms of pentamidine and alexidine as drugs.

For the host–guest system of C4S with pentamidine, very detailed studies on the influence of crystallization solvent have been performed. The first C4S-pentamidine complexation experiments in the solution by ^{1}H NMR spectroscopy have shown a clear difference between aqueous and methanolic media. In water pentamidine forms inclusion complex with C4S entering the macrocyclic cavity via pentyl chain. This is also corroborated by the crystal structure of the complex crystallized from aqueous solution. The addition of other solvents to water alters the interaction in the supramolecular system and the structure of the final host–guest assembly, as has been confirmed by ^{1}H NMR solution experiments, and crystallization of host–guest complexes in the mixed solvent systems. Besides several C4S-pentamidine crystal structures, C6S and C8S complexes with pentamidine have been crystallized and structurally authenticated, to show the effect of the size of the macrocycle on the host–guest complexation and assembly. Only one crystal complex of alexidine with C4S has been obtained, as all crystallization experiments (unsuccessful with larger calixarenes) suffered from significant micro-precipitation.

The results presented in this chapter have been described in the articles entitled "***Alexidine and Pentamidine Fold Inside the Bowl-shaped Cavity of p-Sulfonato-calix[4]arene***", published in *Chemistry – A European Journal*; and "***Host–guest conformational adaptation in the crystal complexes of pentamidine and p-sulfonato-calix[n]arenes***", published in *CrystEngComm*.

C4S complex with alexidine

Crystallization of C4S sulfonic acid complex with alexidine from water–ethanol mixture

6.4 mg of C4S ***sulfonic acid*** was dissolved in 0.5 mL of H_2O/EtOH (1:1). The solution of 10 mg alexidine dihydrochloride in 0.5 mL of H_2O/EtOH (1:1) was slowly combined with the solution of the host (Figure 121). The instant clouding of the solution has been observed followed by the precipitation. The diffraction-quality colorless prism-shape crystals were found within the precipitate after one week. Single-crystal X-ray diffraction analysis revealed these crystals to be the host–guest complex ***C4S_ALEX.***

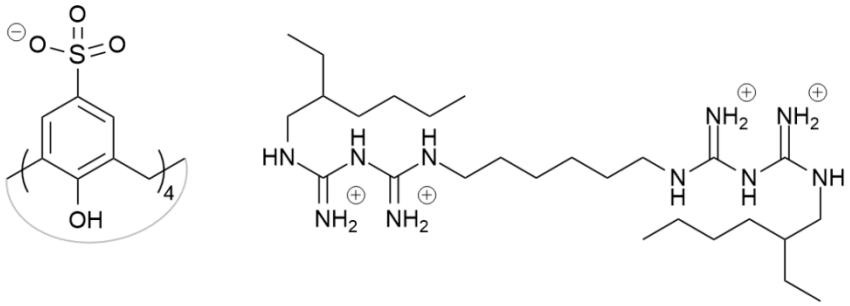

*Figure 121. Chemical structure of C4S **sulfonic acid** host and alexidine (**ALEX**) guest.*

The refinement details of the C4S_ALEX complex

The asymmetric unit of ***C4S_ALEX*** consists of one tetra-anion C4S molecule, one tetracation of alexidine and five water molecules. Oxygen atoms of one of C4S sulfonate group are disordered over two positions. The first component of disorder O5 > O7 is refined with PART 1 command (47% occupancy), the second O5A > O7A is refined with PART 2 (53% occupancy).

The central hexamethylene chain and both ethyl–hexyl side chains of the alexidine molecule have been modelled as disordered. The hexamethylene chain is disordered over two positions. The first component of disorder C1X > C6X is refined with PART 1 command (43.8% occupancy), the second C1XA > C6XA is refined with PART 2 command (56.2% occupancy). To solve the disorder, the SADI and SIMU commands are used. The atoms of one ethyl–hexyl side chain C11C > C21C are disordered over two positions. The first component of disorder C11C > C21C is refined with PART 1 command (51.4% occupancy). The second component of disorder C11D > C21D is refined with PART 2 command (48.6% occupancy). The atoms of the second ethyl–hexyl side chain C10A > C21A are disordered over three positions. The first component of disorder C10A > C21A is refined with PART 1 command (50% occupancy). The second component of disorder C10B > C21B is refined with PART 2 command (25% occupancy). The third component of disorder C10E > C21E is refined with PART 3 command (25% occupancy). The combination of SIMU, DELU, SADI, SAME, DANG and DFIX commands has been used to ensure sensible geometry and displacement parameters of the second ethyl–hexyl alexidine chain.

The O1W molecule is a part of O5 > O7 calixarene disorder. Molecule is disordered over two positions. The first component of disorder O1W is refined with PART 1 command (47% occupancy), the second O1WA is refined with PART 2 command (53% occupancy). The O4W water molecule is disordered over two positions. The first component of disorder O4W is refined with PART 1 command (69% occupancy), the second O4WA is refined with PART 2 command (31% occupancy). The O5W water molecule is also disordered over two positions. The first component of disorder O5W is refined with PART 1 command (39% occupancy), the second O5WA is refined with PART 2 command (61% occupancy). All hydrogen atoms are added geometrically and refined using a “riding model”. The

water molecules are refined without hydrogen atoms. The basic crystallographic data of the discussed structure is provided in Table 9.

*Table 9. Crystal data and structure refinement for **C4S_ALEX** complex.*

Parameters	***C4S_ALEX***
Formula moiety	$C_{28}H_{20}O_{16}S_4 \cdot C_{26}H_{60}N_{10} \cdot 5(H_2O)$
Formula weight	1343.59
Crystal system	Triclinic
Space group	*P–1*
a / Å	12.2069(9)
b / Å	16.3735(10)
c / Å	19.7215(14)
α / °	69.533(6)
β / °	87.206(6)
γ / °	69.152(6)
Volume / Å^3	3438.2(4)
Z	2
ρ_{calc} /g·cm^{-3}	1.30
Crystal color	Colorless
Crystal morphology	Prism
μ / mm^{-1}	1.91
θ_{max} / °	70.8
Reflections collected	24621
Independent reflections	12751 [R_{int} = 0.074]
Data / Restraints / Parameters	12751 / 455 / 988
Observed data [I > 2σ(I)]	5871
Final R indexes [I ≥ 2σ(I)]	R_1 = 0.108, wR_2 = 0.279
Final R indexes [all data]	R_1 = 0.187, wR_2 = 0.373
Goodness-of-fit on F^2	1.02
Largest diff. peak and hole / e·Å^{-3}	0.76 / –0.53

Structure analysis of the C4S_ALEX complex

The co-crystallization of C4S ***sulfonic acid*** with alexidine dihydrochloride from water–ethanol results in the formation of the complex ***C4S_ALEX*** with the formula $C_{28}H_{20}O_{16}S_4 \cdot C_{26}H_{60}N_{10} \cdot 5(H_2O)$. Single-crystal X-ray diffraction analysis shows that this complex crystallizes in a triclinic crystal system in the space group *P–1*. The asymmetric part consists of one C4S, one alexidine and five water molecules (Figure 122).

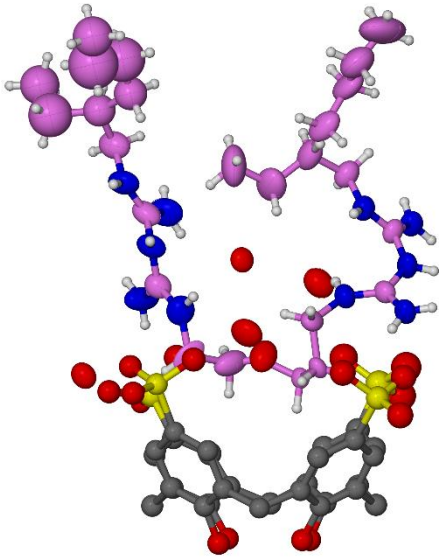

*Figure 122. The asymmetric unit of the host–guest complex **C4S_ALEX.** Atomic displacement parameters set at 50% probability. Disorder omitted for clarity.*

In the structure of the complex ***C4S_ALEX*** the alexidine molecule is included in the C4S cavity by its hexamethylene bridge, two (2-ethylhexyl) bisguanidinium units are located outside the macrocyclic cavity. *p*-Sulfonatocalix[4]arene has a pinched cone conformation, the distances between the opposite Sulphur atoms of the host molecule are 9.81 and 10.96 Å. The lower rim of the C4S cone is presented by four hydroxyl groups which participate in the formation of the *O–H···O* hydrogen bonds (*O···O* distances in the range 2.655(7)–2.711(7) Å). Alexidine follows to the cone shape of C4S and adopts a U-shaped folded conformation (Figure 123). The parameters of the intramolecular interactions at the C4S lower rim are described in the Table 54, Annex I.

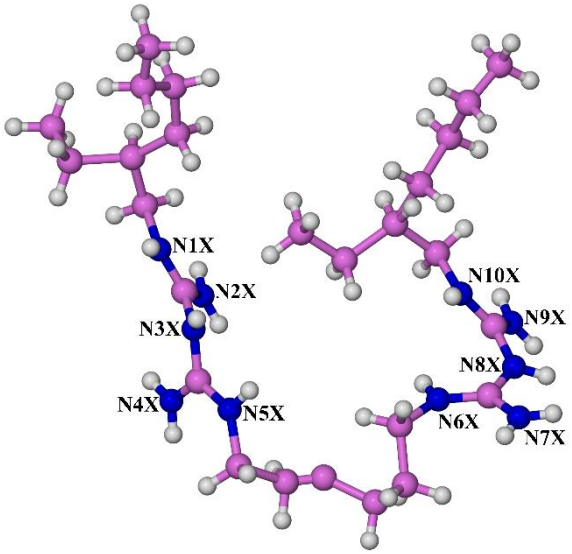

*Figure 123. Host–guest complex **C4S_ALEX**: U–shaped folded conformation of the alexidine molecule.*

Alexidine molecule forms charge-assisted hydrogen bonds with sulfonate oxygen atoms of C4S and water molecules. There are some similarities in the hydrogen binding mode between N atoms of alexidine of both sides (Figure 124). The N5X and N6X atoms connected to the hexamethylene

bridge and don't participate in the formation of *N–H···O* contact with parent C4S molecule, since are turned out from macrocycle. Meanwhile they interact with the O5W and O3W water molecules. The N4X and N7X atoms are connected both to the parent and adjacent C4S *via N–H···O* hydrogen bonds. N3X and N8X interact with the adjacent calixarenes. The N2X and N9X make an *N–H···O* contact with adjacent macrocycle and water molecules. Finally, N1X and N10X atoms, connected to ethyl–hexyl chains, participate in hydrogen bonding with the neighbouring C4S molecules with *N···O* distances in the range 2.729(9)–2.969(18) Å.

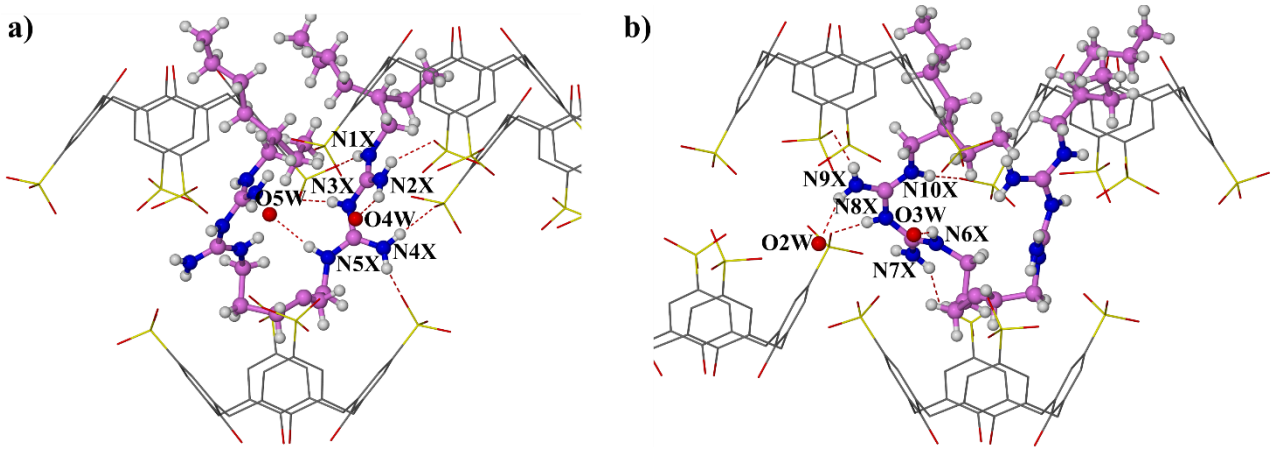

*Figure 124. Host–guest complex **C4S_ALEX**: (a,b) N–H···O hydrogen bonds between N–H groups of two alexidine biguanide units and sulfonate oxygen atoms of C4S / water molecules.*

Alexidine molecule included in the C4S cavity doesn't make *C–H···O* hydrogen bonding with the closest calixarene, otherwise it interacts with adjacent host at the distance 3.51(2) Å and O1W water molecule at 3.54(4) Å (Figure 125a). The alexidine guest participates in two *C–H···π* interactions with macrocyclic hosts. The first interaction occurs with the parent macrocyclic host *via* C atom of alexidine hexamethylene chain and the C4S aromatic ring at the distance 3.591(17) Å. For the second *C–H···π* interaction the distance between C atom of alexidine hexyl chain and C4S aromatic ring is 3.58(6) Å (Figure 125b). The parameters of intermolecular interactions formed by alexidine molecule are described in the Table 54–55, Annex I.

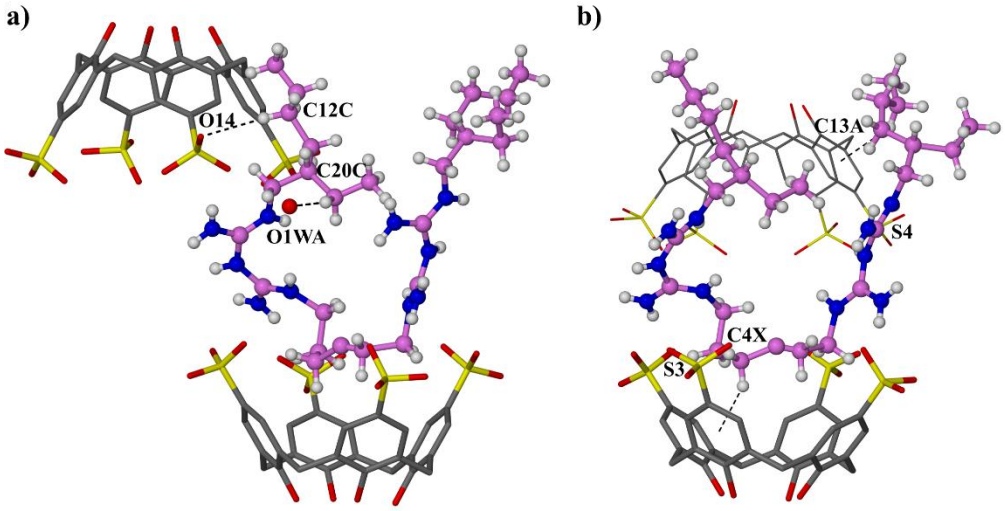

*Figure 125. Host–guest complex **C4S_ALEX**: (a) C–H···O hydrogen bonds between C atoms of alexidine and sulfonate oxygen atoms of C4S / water molecule; (b) C–H···π interactions between C atoms of alexidine and aromatic rings of C4S molecules.*

The packing of the ***C4S_ALEX*** complex is represented by bilayers of C4S molecules additionally penetrated with 2-ethylhexyl groups of ALEX guests. The bilayers are separated by a hydrophilic region comprising biguanidinium groups of ALEX and water molecules (Figure 126).

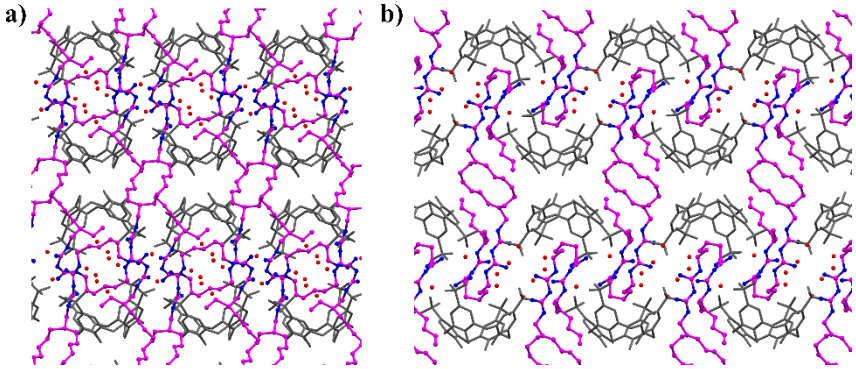

*Figure 126. Crystal packing of the host–guest complex **C4S_ALEX** viewed along **a** direction. Alexidine is colored in pink. Disorder omitted for clarity.*

NMR analysis of the C4S_ALEX complex

To gain a better insight into the host–guest system of C4S with alexidine, the complexation studies in a solution (CD_3OD) using ^1H NMR spectroscopy was performed (Figure 127). The low solubility and immediate precipitation of the ***C4S_ALEX*** complex precluded its characterization by ^1H NMR spectroscopy in aqueous solution (both in the unbuffered D_2O and 0.3 M acetate buffer). The replacement of the host–guest complexation medium to methanol (CD_3OD) improved the solubility and revealed the significant change in the ALEX proton resonances in the presence of the macrocyclic host. Some of the proton resonances of ALEX experience upfield shifts (signals ***e***, ***i***, ***j***) indicating inclusion of the central hexyl chain into the macrocyclic cavity.

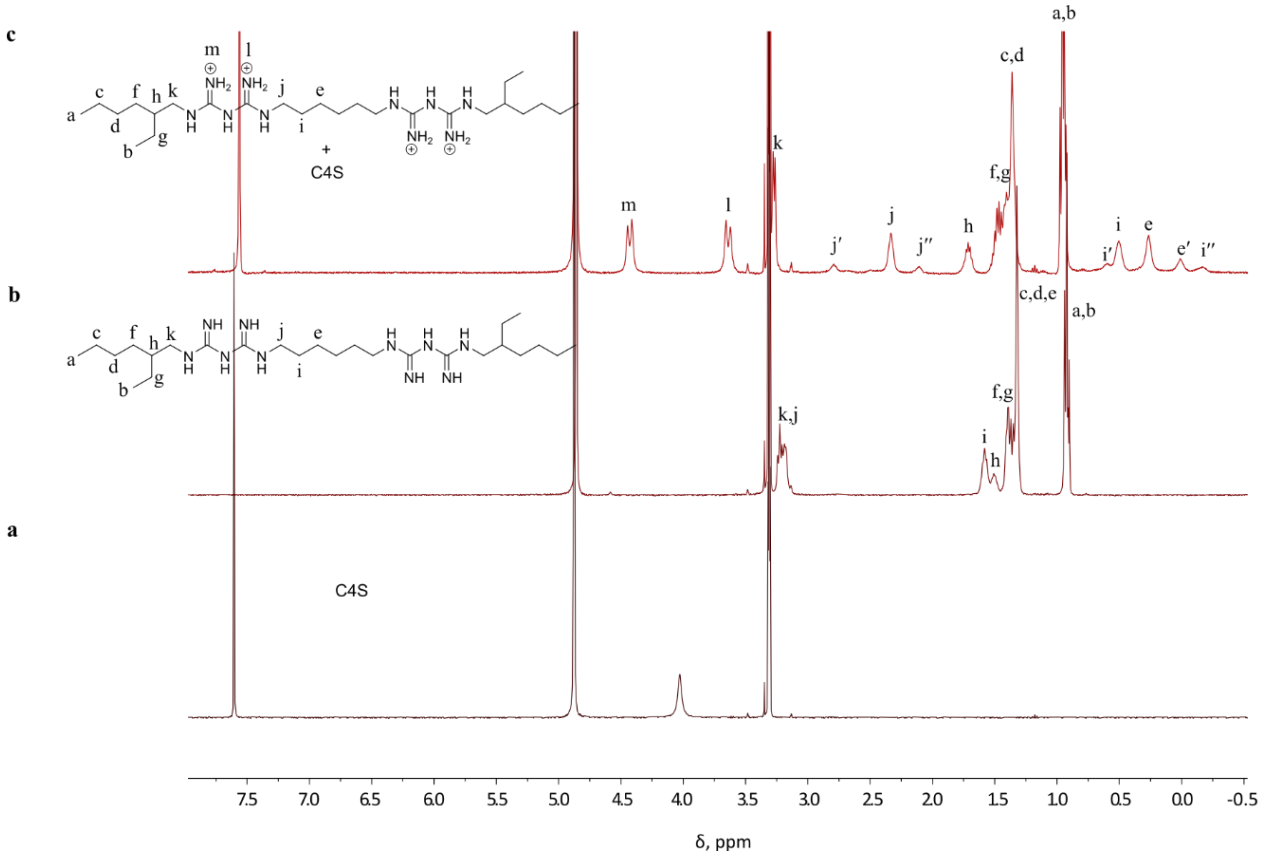

*Figure 127. [1]H NMR spectra of (a) C4S **sulfonic acid**; (b) alexidine hydrochloride; (c) **C4S_ALEX** host–guest complex recorded on Agilent 400 MHz instrument at room temperature in CD_3OD, C(C4S) = 4 mM, C(ALEX) = 4 mM.*

In the presence of C4S, several conformers of ALEX are evident in the ^{1}H NMR spectrum. Two-dimensional correlation NMR spectroscopy was used to assign the signals corresponding to the different conformers of ALEX after complexation (Figure 128).

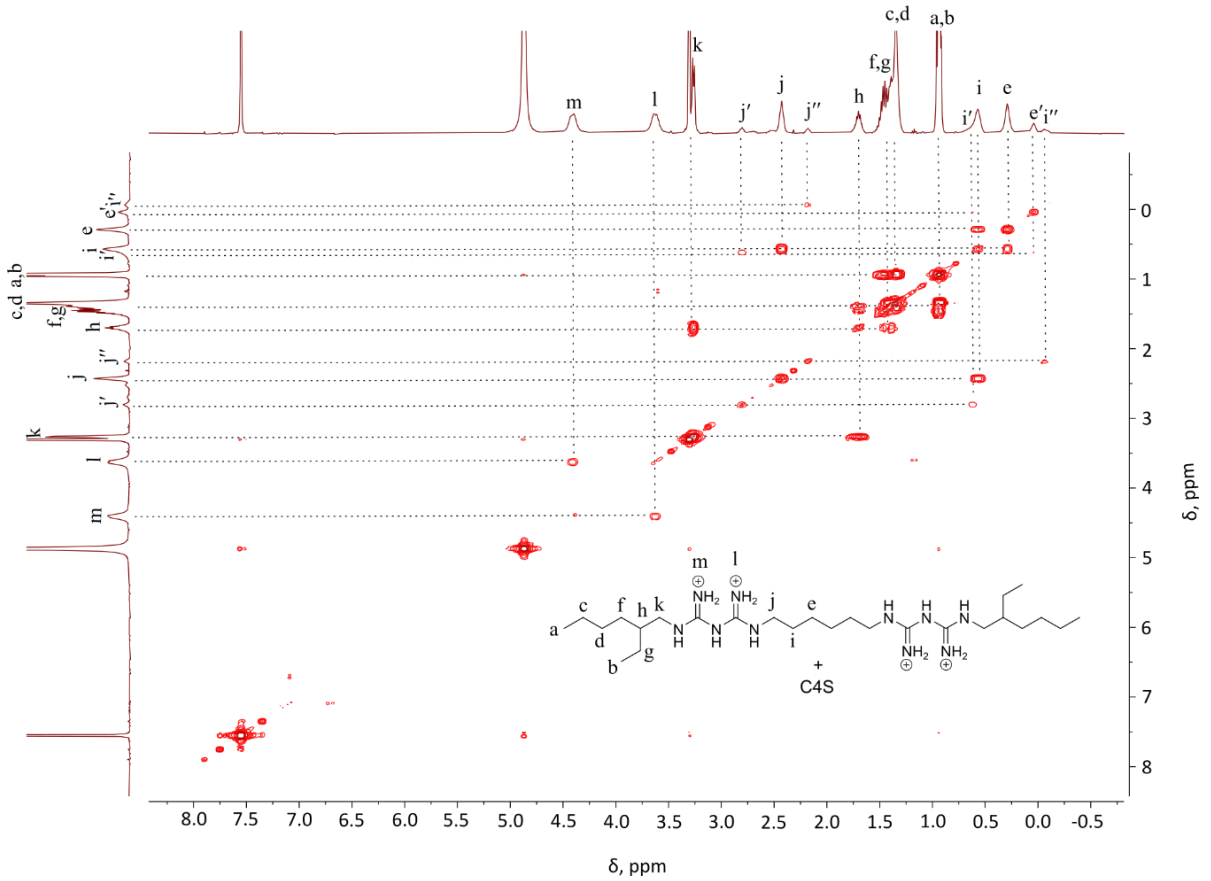

*Figure 128. 2D COSY spectra of **C4S_ALEX** host–guest complex recorded on Agilent 400 MHz instrument at room temperature in MeOD, C(C4S) = 15 mM, C(ALEX) = 15 mM.*

4.2.2 C4S complexes with pentamidine

Crystallization of C4S sulfonic acid complex with pentamidine from water

5 mg of C4S ***sulfonic acid*** was dissolved in 0.5 mL of H_2O. The solution of 4.6 mg pentamidine isethionate in 0.5 mL of H_2O was combined with the solution of the host (Figure 129). The instant clouding of the solution has been observed followed by the precipitation. The diffraction-quality colorless prism-shape crystals were found within the precipitate after several weeks. Single-crystal X-ray diffraction analysis revealed these crystals to be the host–guest complex ***C4S_PT_H2O.***

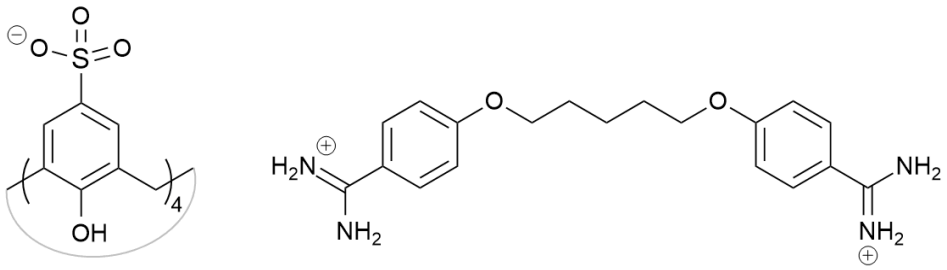

*Figure 129. Chemical structure of C4S **sulfonic acid** host and pentamidine (**PT**) guest.*

The refinement details of the C4S_PT_H2O complex

The asymmetric unit of ***C4S_PT_H2O*** consists of one tetra-anion C4S molecule, two dications of pentamidine and eight water molecules. The aliphatic linker (C8Y > C12Y) of the C1Y

> O2Y pentamidine molecule is disordered over two positions. The first component of disorder is refined with PART 1 command (72.9% occupancy), the second component is refined using PART 2 (27.1% occupancy). SIMU and DELU restraints are used to equate atomic displacement parameters of disordered atoms and restrain the differences in the components of the displacement parameters. All hydrogen atoms are added geometrically. Some residual electron density is associated with unaccounted disorder of water solvent molecules in the water channels. The basic crystallographic data of the discussed structure is provided in Table 10.

*Table 10. Crystal data and structure refinement for **C4S_PT_H2O** complex.*

Parameters	***C4S_PT_H2O***
Formula moiety	$C_{28}H_{20}O_{16}S_4 \cdot 2(C_{19}H_{26}N_4O_2) \cdot 8(H_2O)$
Formula weight	1569.68
Crystal system	Triclinic
Space group	*P–1*
a / Å	10.4611(2)
b / Å	16.1920(3)
c / Å	22.0243(4)
α / °	96.946(2)
β / °	101.704(2)
γ / °	91.090(2)
Volume / Å^3	3622.59(12)
Z	2
ρ_{calc} /g·cm^{-3}	1.44
Crystal color	Colorless
Crystal morphology	Prism
μ / m^{-1}	1.98
θ_{max} / °	70.1
Reflections collected	42974
Independent reflections	13660 [R_{int} = 0.040]
Data / Restraints / Parameters	13660 / 31 / 987
Observed data [I > 2σ(I)]	12094
Final R indexes [I ≥ 2σ(I)]	R_1 = 0.059, wR_2 = 0.159
Final R indexes [all data]	R_1 = 0.065, wR_2 = 0.165
Goodness-of-fit on F^2	1.02
Largest diff. peak and hole / e·Å^{-3}	1.03 / –1.07

Structure analysis of the C4S_PT_H2O complex

The co-crystallization of C4S ***sulfonic acid*** with pentamidine isethionate from water results in the formation of the complex ***C4S_PT_H2O*** with the formula $C_{28}H_{20}O_{16}S_4 \cdot 2(C_{19}H_{26}N_4O_2) \cdot 8(H_2O)$. Single-crystal X-ray diffraction analysis shows that this complex crystallizes in a triclinic crystal system in the space group *P–1*. The asymmetric part consists of one C4S, two pentamidines and eight water molecules (Figure 130).

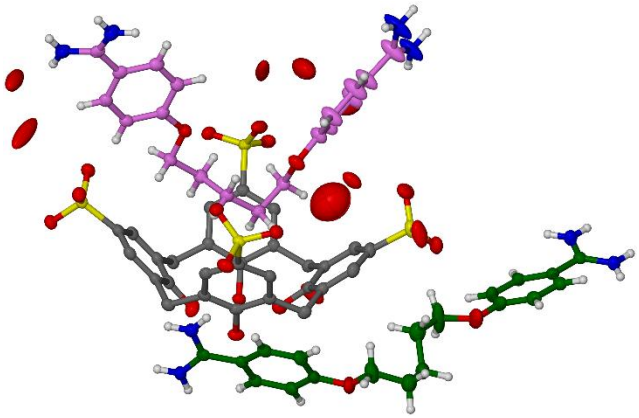

*Figure 130. The asymmetric unit of the host–guest complex **C4S_PT_H2O**. Two crystallographically unique pentamidine molecules are presented in different colours. Atomic displacement parameters set at 50% probability. Disorder omitted for clarity.*

p-Sulfonatocalix[4]arene prefers a cone conformation stabilized by a circular array of hydrogen bonds. The lower rim of C4S (four hydroxyl groups) participates in the formation of the intramolecular hydrogen bonds with *O···O* distances in the range of 2.616(3)–2.782(3) Å. The parameters of the C4S intramolecular interactions are described in the Table 56, Annex I. The distances between the opposite Sulphur atoms of the host molecule are 10.14 and 12.44 Å, indicating the degree of pinching of the C4S cone. In the structure of the ***C4S_PT_H2O*** complex, the first pentamidine C1X > O2X (pink) is included in the macrocyclic cavity by its pentanediol central linker, and the benzamidine groups are located outside the macrocyclic cavity. The pentamidine molecule adopts a U-fold shape. The second pentamidine C1Y > O2Y, located outside the C4S cavity, has a crumpled intermediate shape between the extended and folded conformations. The distances between the *O···O* atoms of pentamidine connected to the central aliphatic chain are 4.45 and 5.57 Å, respectively (Figure 131).

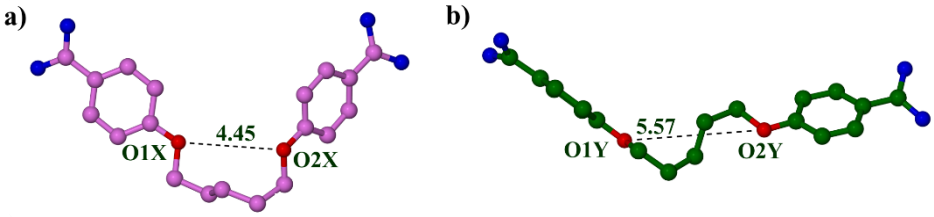

Figure 131. Molecular conformation of pentamidine molecules showing O···O distances between oxygen atoms bound to the central pentyl chain: (a) cavity included C1X > O2X PT (pink) subjected to U-folding; (b) externally complexed C1Y > O2Y PT (green) in the crumpled conformation. O···O distances are given in Å.

Each positively charged amidinium group of pentamidine molecule bears four hydrogen atoms that can form charge-assisted hydrogen bonds with sulfonate anions of C4S or water molecules. There is no hydrogen bonding between amidinium groups of the included C1X > O2X pentamidine and its parent C4S molecule because two benzamidine moieties are directed away from the cavity due to the imposed U-shape of pentamidine. Pentamidine donates eight *N–H···O* hydrogen bonds – five towards

sulfonate oxygen atoms of adjacent C4S and three towards water molecules (*N···O* distances in the range 2.800(3)–3.262(3) Å) (Figure 132a). Being inside of the C4S cavity C1X > O2X guest forms two *C–H···O* interactions with C4S at the *C···O* distances 3.364(4) Å and 3.578 Å (Figure 132b). Pentamidine participates in two *C–H···π* interactions with macrocyclic host. The first interaction occurs with the parent macrocyclic host *via* C atom of pentamidine aliphatic chain and the C4S aromatic ring at the distance 3.783(3) Å. The second *C–H···π* interaction between aromatic rings of pentamidine and adjacent C4S occurs at the distance 3.541(3) Å (Figure 133a). Two symmetrically equivalent C1X > O2X pentamidines contact at the distance of 3.579(16) Å, forming *π···π* interactions (Figure 133b).

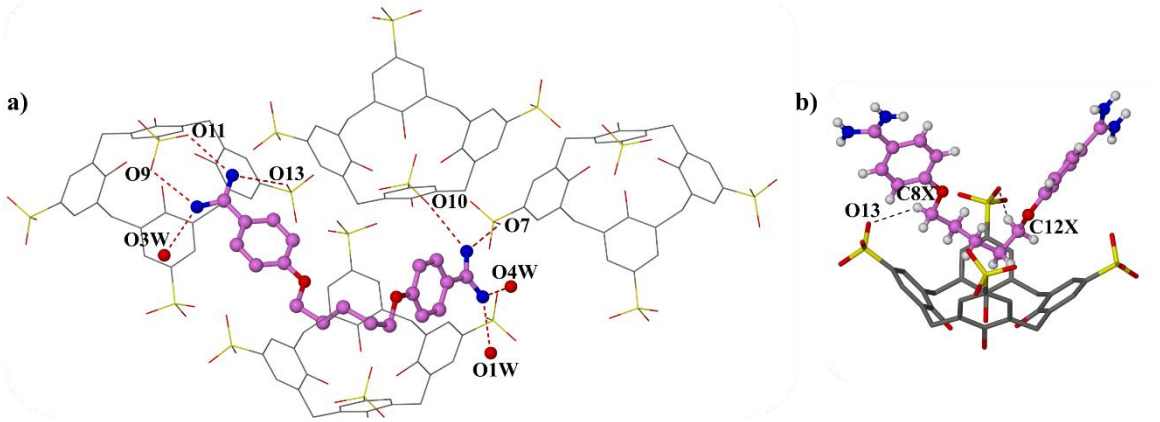

*Figure 132. Host–guest complex **C4S_PT_H2O**: (a) N–H···O hydrogen bonds between N–H groups of pentamidine and sulfonate oxygen atoms of C4S / water molecules; (b) C–H···O hydrogen bonds between C atoms of pentamidine aliphatic chain and sulfonate oxygen atoms of C4S molecule.*

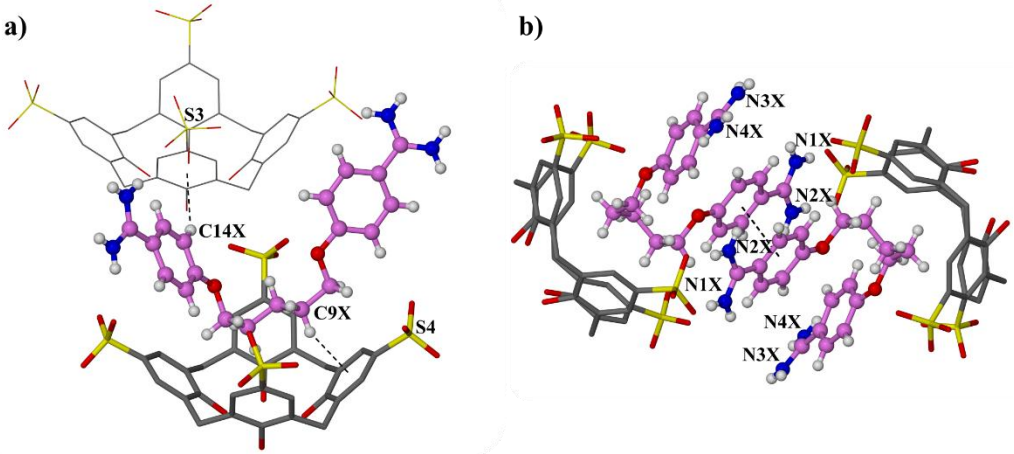

*Figure 133. Host–guest complex **C4S_PT_H2O**: (a) C–H···π interactions between C atoms of pentamidine (aliphatic chain / aromatic ring) and aromatic rings of C4S molecules; (b) π···π interaction between aromatic rings of calixarene included pentamidines.*

The second C1Y > O2Y pentamidine (green) is outside of the C4S cavity. Pentamidine donates eight *N–H···O* hydrogen bonds – seven towards sulfonate oxygen atoms of adjacent C4S molecules and one towards water molecule (*N···O* distances in the range 2.784(3)–3.262(3) Å) (Figure 134). At

the same time there are six *C–H···O* hydrogen bonds between pentamidine and adjacent macrocyclic host/water molecules, *C···O* distances in the range of 3.053(3)–3.413(9) Å (Figure 135).

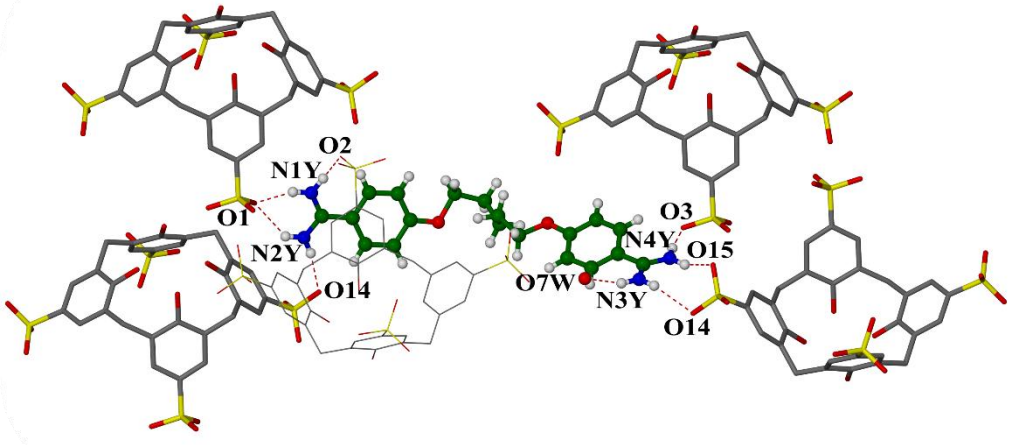

*Figure 134. Host–guest complex **C4S_PT_H2O**: N–H···O hydrogen bonds between N–H groups of outer pentamidine and sulfonate oxygen atoms of C4S molecules.*

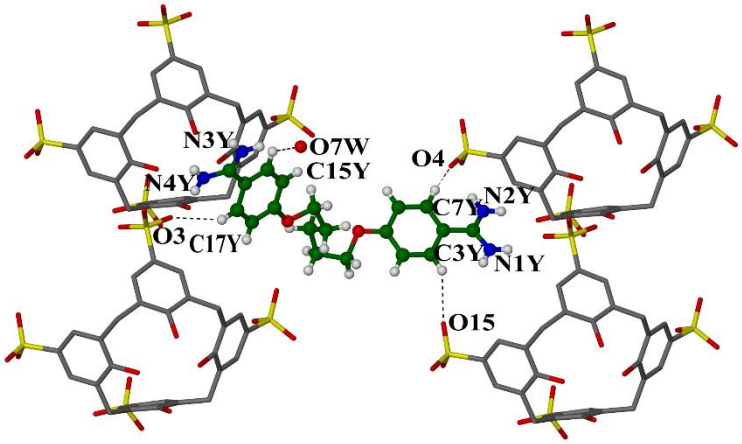

*Figure 135. Host–guest complex **C4S_PT_H2O**: C–H···O hydrogen bonds between aromatic rings of outer pentamidine and sulfonate oxygen atoms of C4S / water molecule.*

The C1Y > O2Y molecule participates in one *N–H···π* and one *π···π* interactions with C4S molecule (Figure 136a). The distance between *N–H* group of pentamidine and centroid of the C4S aromatic ring is 3.535(2) Å. The distance between the centroid of the pentamidine and the C4S aromatic ring is 3.970(15) Å. The parameters of intermolecular interactions formed by pentamidine molecules are described in the Table–58, Annex I. Crystal packing shows alternate up and down orientation of calix[4]arenes, but bilayer organization is diminished due to the extensive insertion of pentamidine molecules between macrocycles (Figure 136b). The host molecules interact *via* hydroxyl–sulfonate *O–H···O* hydrogen bonds, *O16–H16A···O3* bond length is 2.753(3) Å. C1X > O2X pentamidines and water molecules are in between the calixarene bilayers.

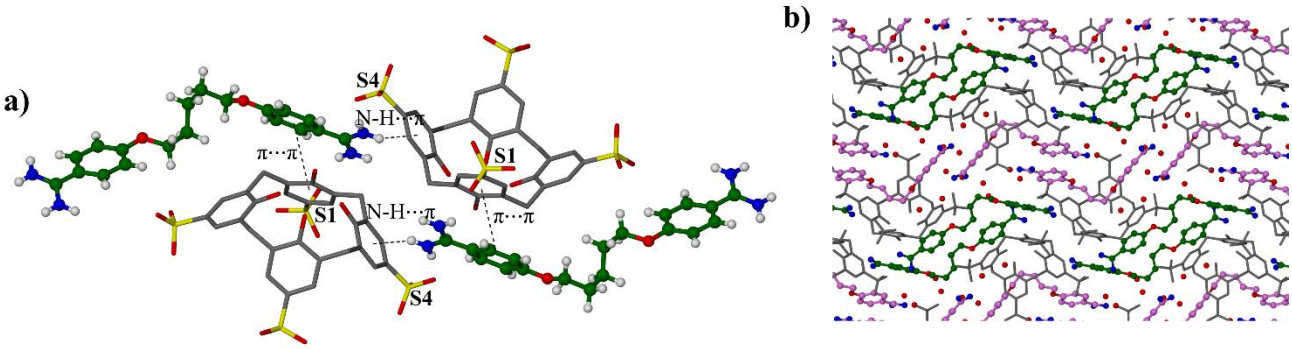

*Figure 136. Host–guest complex **C4S_PT_H2O**: (a) N–H···π hydrogen bonds between N–H group of pentamidine and aromatic ring of C4S molecule, π···π interactions between aromatic ring of outer pentamidine and aromatic ring of C4S molecules; b) crystal packing of the host–guest complex **C4S_PT_H2O** viewed along **a** direction. Two crystallographically non-equivalent pentamidine molecules are colored in pink and green. Disorder omitted for clarity.*

NMR analysis of the C4S_PT_H2O complex

The ^{1}H NMR spectroscopy experiments for the ***C4S_PT*** complexation in aqueous solution were hindered by the low solubility of the host–guest complex. Upon adding pentamidine isethionate to an unbuffered C4S solution, an immediate precipitate formed, preventing the observation of guest proton resonances in the spectrum. Despite some precipitation in the acetate buffer, the host–guest complexation is manifested through the upfield shifts of all proton resonances of pentamidine. The most significant shifts ($\Delta\delta$ = **0.38** and **0.35**) were observed for the central aliphatic linker protons, indicating their positioning within the macrocyclic cavity, consistent with the crystal structure model (Figure 137). The addition of 10% methanol to aqueous solution improved solubility but also hindered the insertion of pentamidine's aliphatic chain into the C4S cavity (Figure 138). ^{1}H NMR experiments in methanolic solution (CD_3OD) revealed only minor shifts in PT aliphatic signals in the presence of C4S, (Figure 139). This indicates that pentamidine complexation is solvent dependent. Additionally, upfield shifts in pentamidine's aromatic proton resonances suggest the potential inclusion of its benzamidine groups into a macrocyclic cavity, which was not observed in the solid-state complex.

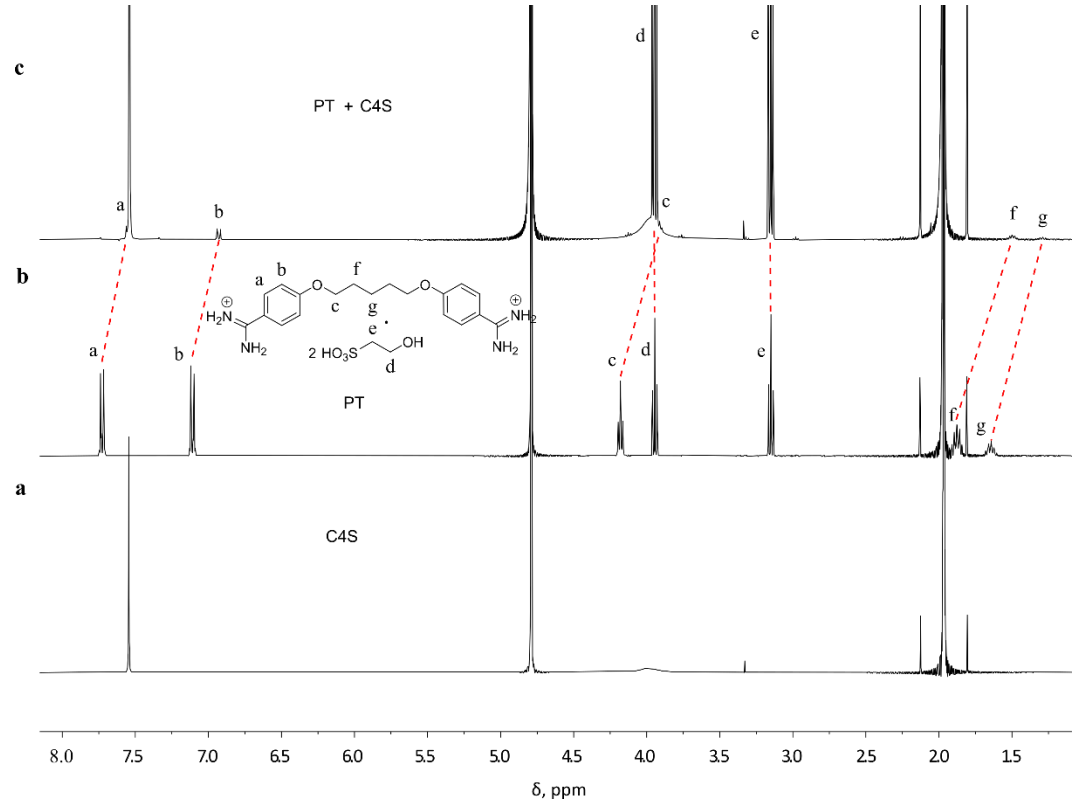

Figure 137. [1]H NMR spectra of (a) C4S ***sulfonic acid****; (b) pentamidine isethionate; (c)* ***C4S_PT*** *host–guest complex – in the presence of the* ***precipitate*** *recorded on Agilent 400 MHz instrument at room temperature in 0.3 M acetate buffer, pH=5.1* ***(D₂O)****. c(C4S)=4 mM, c(PT)=4 mM.*

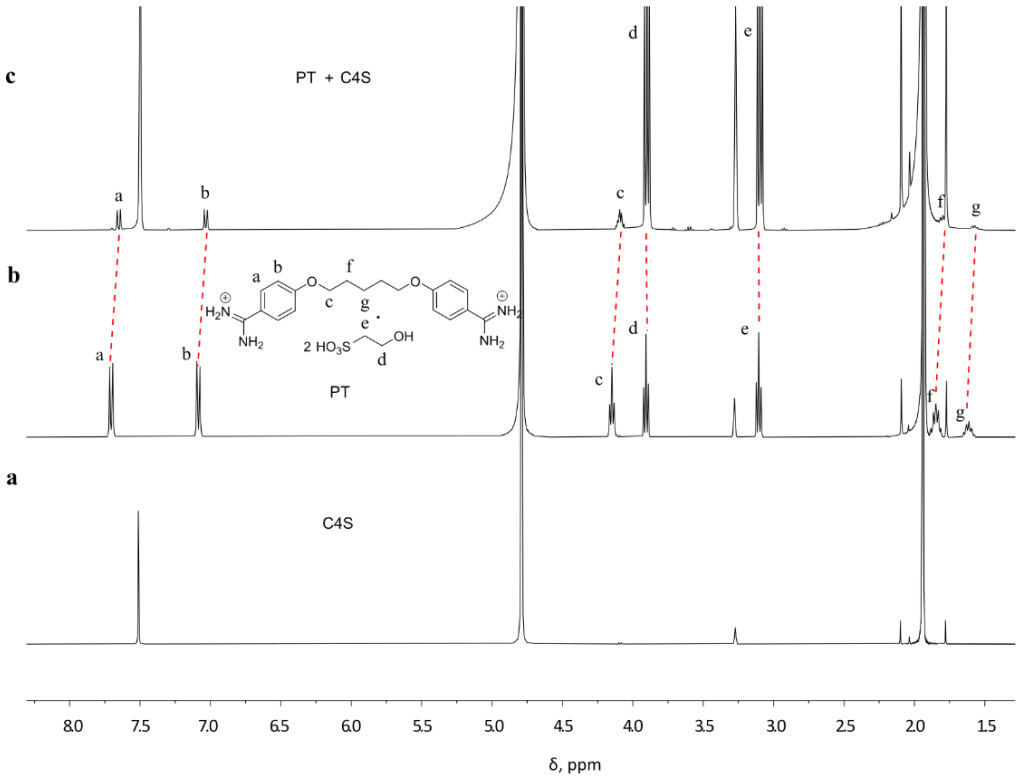

*Figure 138. [1]H NMR spectra of (a) C4S **sulfonic acid**; (b) pentamidine isethionate; (c) **C4S_PT** host–guest complex – in the presence of **slight precipitate** recorded on Agilent 400 MHz instrument at room temperature in 0.3 M acetate buffer, pH = 5.1 **(D_2O/MeOD (v/v=9:1))**, C(C4S) = 4 mM, C(pentamidine) = 4 mM.*

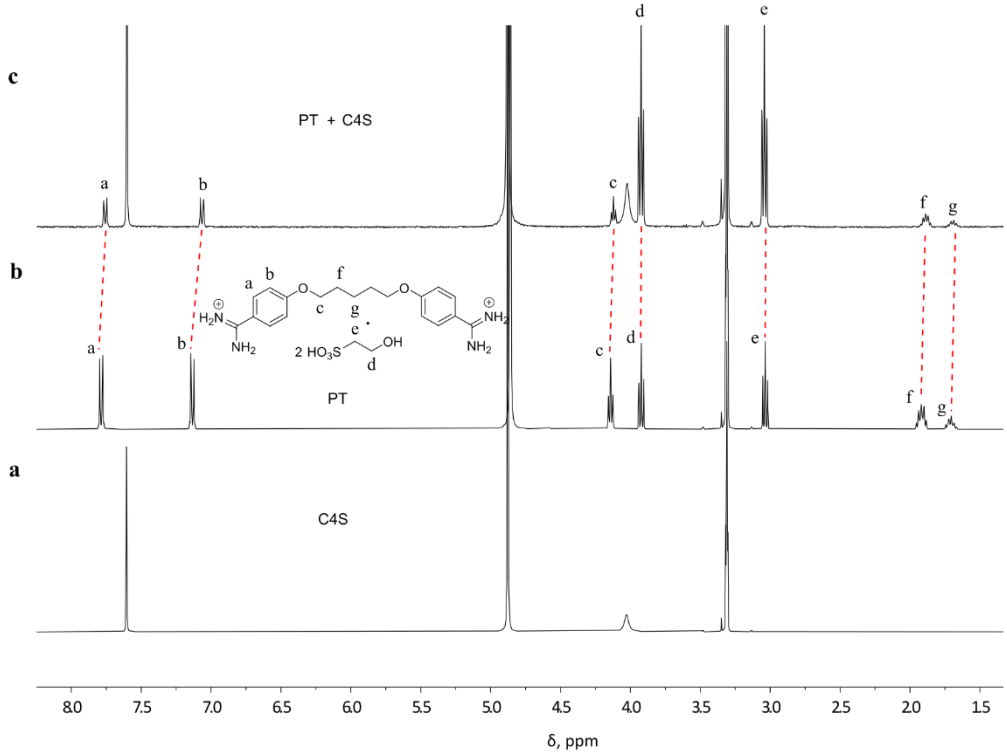

*Figure 139. [1]H NMR spectra of (a) C4S **sulfonic acid**; (b) pentamidine isethionate; (c) **C4S_PT** host–guest complex recorded on Agilent 400 MHz instrument at room temperature in **MeOD**, C(C4S) = 4 mM, C(pentamidine) = 4 mM.*

C4S complex with pentamidine in water–ethanol

Crystallization of C4S sulfonic acid complex with pentamidine from water–ethanol mixture

5 mg of C4S ***sulfonic acid*** was dissolved in 0.5 mL of H_2O/EtOH (1:1). The solution of 4.6 mg pentamidine isethionate in 0.5 mL of H_2O/EtOH (1:1) was combined with the solution of the host. The cloud solution with the precipitation was observed. The diffraction-quality colorless prism-shape crystals were found within the precipitate after several weeks. Single-crystal X-ray diffraction analysis revealed these crystals to be the host–guest complex ***C4S_PT_EtOH***.

The refinement details of the C4S_PT_EtOH complex

The asymmetric unit of ***C4S_PT_EtOH*** consists of one tetra-anion C4S molecule, two dications of pentamidine, one ethanol and 4.2 water molecules. Oxygen atoms of one of C4S sulfonate group are disordered over two positions. The first component of disorder O13 > O15 is refined with PART 1 command (51% occupancy), the second O13A > O15A is refined with PART 2 (49% occupancy). The C1E and C2E atoms of the C1E > O1E ethanol molecule lies close to the disordered sulfonate atoms O13 > O15 of calixarene and refined over two positions with the same occupancy. To solve both disorders SIMU, RIGU and SADI restraints are applied. C10Y > O2Y atoms of C1Y > O2Y pentamidine are disordered over two positions. The first component of disorder C10Y > O2Y is

refined with PART 1 command (63.3% occupancy). The second component of disorder C10A > O2A is refined with PART 2 command (36.7% occupancy). To solve the disorder of pentamidine molecule SIMU and RIGU restraints are applied.

The O2W water molecule is disordered over three positions. The first component of disorder O2W is refined with PART 1 command (50% occupancy), the second O2WA is refined with PART 2 command (25% occupancy) and the third with PART 3 (25% occupancy). The O4W water molecule is disordered over two positions. The first component of disorder O4W is refined with PART 1 command (50.9% occupancy), the second O4WA is refined with PART 2 command (49.1% occupancy). The O5W and O6W water molecules are refined with fixed occupancy 50%. The O6W lies close to the disordered sulfonate atoms O13 > O15 of calixarene. All hydrogen atoms are added geometrically. The O2W, O3W, O4W, O5W and O6W water molecules are refined without hydrogen atoms. Some residual electron density is associated with unaccounted disorder of water solvent molecules in the water channels. The basic crystallographic data of the discussed structure is provided in the Table 11.

*Table 11. Crystal data and structure refinement for **C4S_PT_EtOH** complex.*

Parameters	***C4S_PT_EtOH***
Formula moiety	$C_{28}H_{20}O_{16}S_4 \cdot 2(C_{19}H_{26}N_4O_2) \cdot C_2H_6O \cdot 4.2(H_2O)$
Formula weight	1547.29
Crystal system	Orthorombic
Space group	$P2_12_12_1$
a / Å	10.17420(1)
b / Å	23.0539(2)
c / Å	31.6460(4)
α / °	90
β / °	90
γ / °	90
Volume / Å^3	7422.73(14)
Z	4
ρ_{calc} /g·cm^{-3}	1.39
Crystal color	Colorless
Crystal morphology	Prism
μ / mm^{-1}	1.89
θ_{max} / °	70.2
Reflections collected	51925
Independent reflections	13964 [R_{int} = 0.036]
Data / Restraints / Parameters	13964 / 677 / 1144
Observed data [I > 2σ(I)]	12324
Final R indexes [I ≥ 2σ(I)]	R_1 = 0.062, wR_2 = 0.172
Final R indexes [all data]	R_1 = 0.069, wR_2 = 0.180
Goodness-of-fit on F^2	1.04
Largest diff. peak and hole / e·Å^{-3}	1.27 / –0.45

Structure analysis of the C4S_PT_EtOH complex

The co-crystallization of C4S ***sulfonic acid*** with pentamidine isethionate from water–ethanol mixture results in the formation of the complex ***C4S_PT_EtOH*** with the formula $C_{28}H_{20}O_{16}S_4 \cdot 2(C_{19}H_{26}N_4O_2) \cdot C_2H_6O \cdot 4.2(H_2O)$. Single-crystal X-ray diffraction analysis shows that this complex crystallizes in orthorhombic crystal system in the space group $P2_12_12_1$. The asymmetric part consists of one C4S, two pentamidines, one ethanol and 4.2 water molecules (Figure 140a). In comparison to the structure of the complex ***C4S_PT_H2O***, in the ***C4S_PT_EtOH*** the cavity of C4S is occupied by one ethanol molecule C1E > O1E (Figure 140b). The solvent molecule interacts with the macrocycle *via O–H···O* hydrogen bond at the distance of 2.813(7) Å and the adjacent water molecules O1W at 2.814(6) Å. The parameters of intermolecular interactions formed by ethanol molecule are shown in Table 59, Annex I.

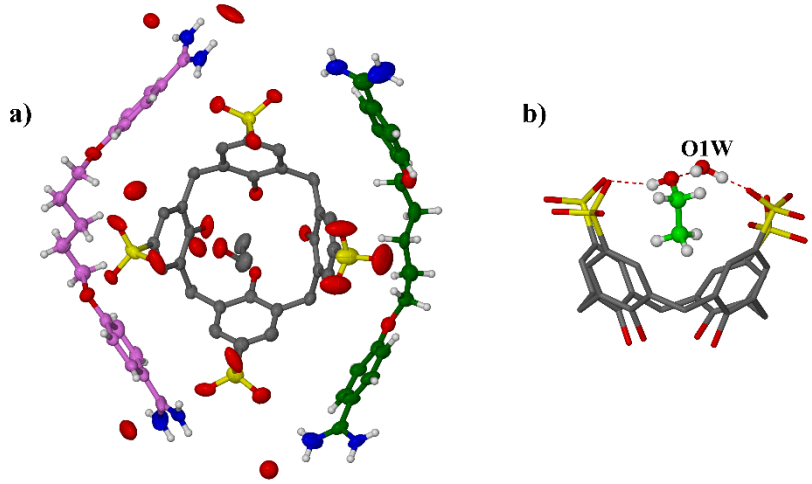

*Figure 140. (a) The asymmetric unit of the host–guest complex **C4S_PT_EtOH**. Two crystallographically unique pentamidine molecules are presented in different colours. Atomic displacement parameters set at 50% probability. Disorder omitted for clarity; (b) O–H···O hydrogen bonding between ethanol included into the C4S cavity and sulfonate oxygen atoms of C4S / water molecules.*

The two pentamidines in the complex are located externally on opposite sides of the macrocycle. The size of the C4S cone is determined by the distance between the opposite Sulphur atoms, which is 9.14 and 10.96 Å, the conformation of the macrocycle is pinched. The two pentamidine molecules accept this C4S shape and adopt *C-shaped* conformations. The distances between the *O···O* atoms, connected to the central aliphatic chain, are 6.01 Å (C1X > O2X) and 6.33 Å (C1Y > O2Y) (

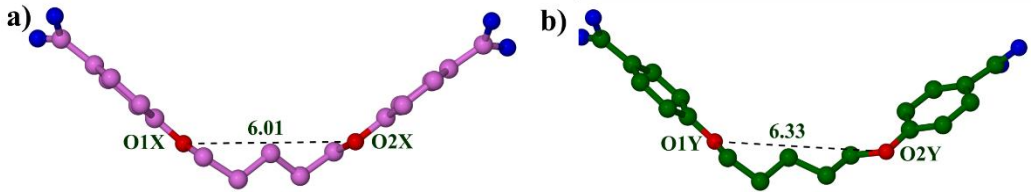

Figure 141. C–shaped conformation of pentamidine molecules showing O···O distances between oxygen atoms bound to the central pentyl chain: (a) C1X > O2X PT (pink); (b) C1Y > O2Y PT (green). O···O distances are given in Å.

Each pentamidine molecule form eight charge-assisted hydrogen bonds with sulfonate oxygens of C4S and water molecules. Pink pentamidine donates eight *N–H···O* hydrogen bonds – two towards sulfonate oxygen atoms of parent C4S, four towards sulfonate oxygen atoms of adjacent C4S and two towards water molecules with *N···O* distances in the range 2.523(17)–2.910(6) Å (Figure 142). At the same time pentamidine forms *C–H···O* hydrogen bonds with C4S, *C···O* distances are 3.115(7) Å, 3.543(7) Å and 3.45(3) Å (Figure 143).

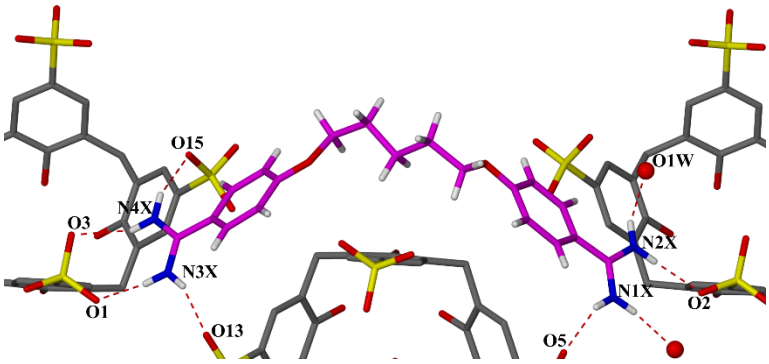

*Figure 142. Host–guest complex **C4S_PT_EtOH**: N–H···O hydrogen bonds between N–H groups of pentamidine and sulfonate oxygen atoms of C4S / water molecules.*

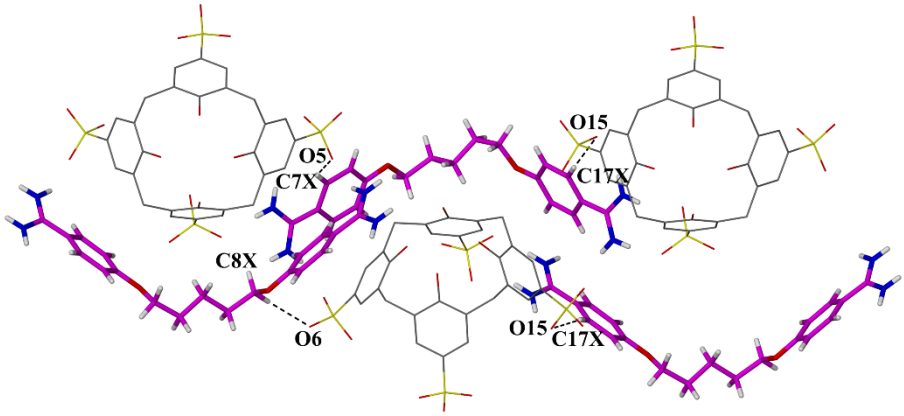

*Figure 143. Host–guest complex **C4S_PT_EtOH**: C–H···O hydrogen bonds between C atom of pentamidine aliphatic chain / pentamidine aromatic ring and sulfonate oxygen atoms of C4S molecules.*

The C1X > O2X pentamidine molecule surrounding the C4S from one side participates in two *C–H···π* interactions with the parent C4S molecule (Figure 144a). The distances between the calixarene carbon atoms of the C4S methylene bridges and the centroids of the pentamidine aromatic rings are 3.704(5) Å and 3.683(5) Å. Additionally, a *π···π* contact between pentamidine and an

adjacent C4S molecule occurs at a distance of 3.963(3) Å between the centroids of the aromatic rings (Figure 144b).

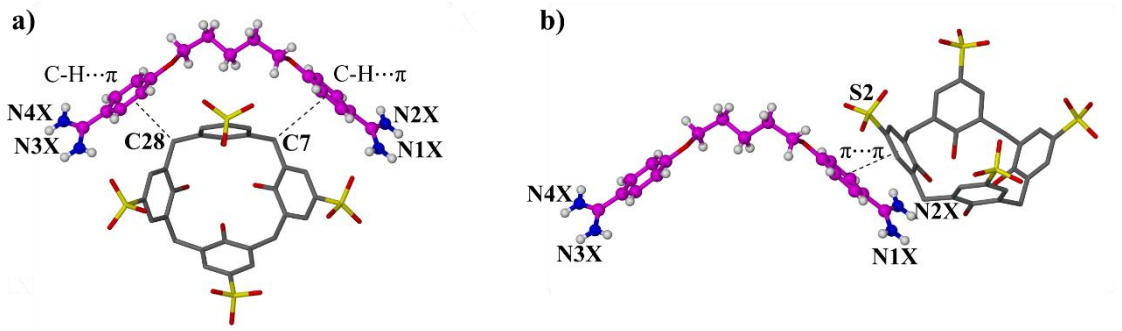

*Figure 144. Host–guest complex **C4S_PT_EtOH**: (a) C–H···π interactions between methylene bridges of C4S and aromatic rings of pentamidine; (b) π···π interaction between aromatic ring of pentamidine and aromatic ring of C4S molecule.*

Since pentamidine C1Y > O2Y (green) surrounds C4S on the side opposite to C1X > O2X, it forms two *N–H···O* hydrogen bonds with the parent C4S molecule. The remaining hydrogen bonds are completed through six interactions with neighboring C4S molecules, with *N···O* distances ranging from 2.82 to 3.07 Å (Figure 145). Pentamidine also interacts with adjacent hosts *via* two *C–H···O* hydrogen bonds, with *C···O* distances of 3.528(17) Å and 3.51(3) Å. The C1Y > O2Y pentamidine molecule is more corrugated, so it does not form *C–H···π* contacts with the methylene bridges of C4S (Figure 146). Instead, a *C–H···π* interaction occurs between a C atom of the pentamidine pentyl chain and the aromatic ring of C4S at a distance of 3.531(14) Å. The parameters of the intermolecular interactions formed by pentamidine molecules are summarized in Tables 59–61, Annex I.

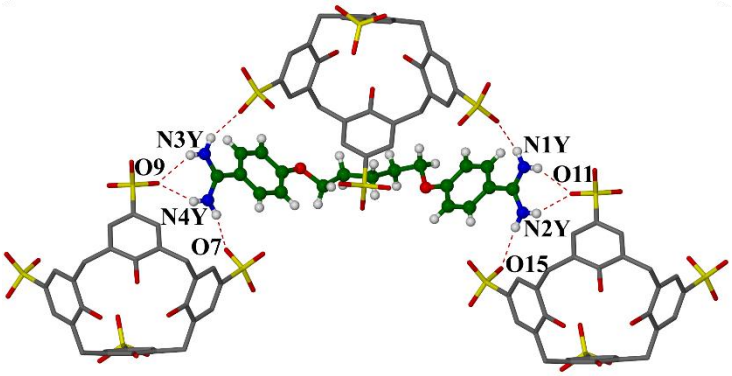

*Figure 145. Host–guest complex **C4S_PT_EtOH**: N–H···O hydrogen bonds between N–H groups of pentamidine and sulfonate oxygen atoms of C4S molecule.*

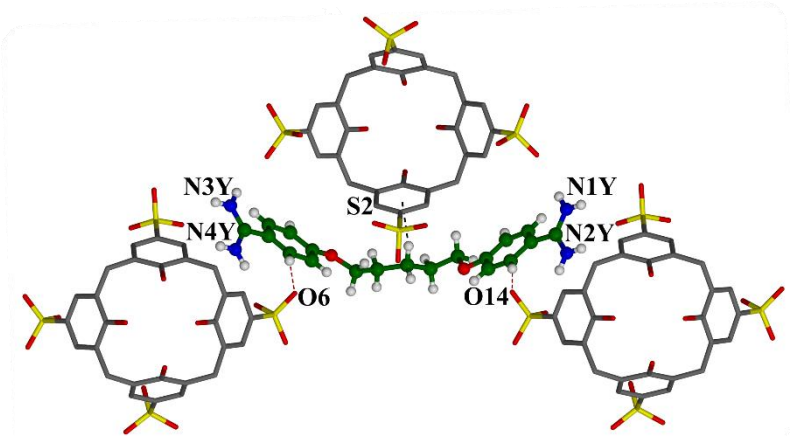

*Figure 146. Host–guest complex **C4S_PT_EtOH**: C–H···O hydrogen bonds between pentamidine aromatic rings and sulfonate oxygen atoms of C4S molecule, C–H···π interaction between C atom of pentamidine aliphatic chain and aromatic ring of C4S molecule.*

The C4S molecules are assembled into columns along ***a*** direction, Figure 147. These columns do not interact directly with one another, as they are well separated by pentamidine molecules. Thus, the classical bilayer organization is perturbed due to multiple interactions between pentamidine molecules and exo-walls of C4S.

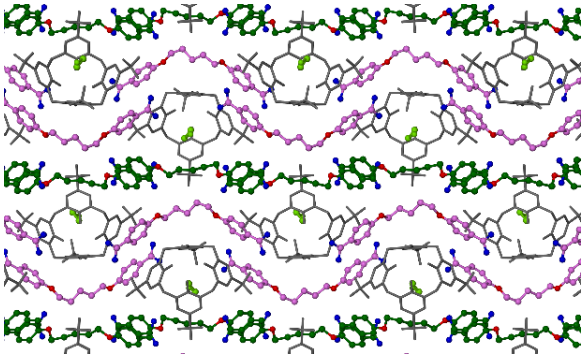

*Figure 147. Crystal packing of the host–guest complex **C4S_PT_EtOH** viewed along **a** direction. Two crystallographically non-equivalent pentamidine molecules are colored in pink and green, ethanol in light green. Disorder and water molecules omitted for clarity.*

C4S complex with pentamidine in water–isopropanol

Crystallization of C4S sulfonic acid complex with pentamidine from water–isopropanol mixture

5 mg of C4S ***sulfonic acid*** was dissolved in 0.5 mL of H_2O/IPA (1:1). The solution of 4.6 mg pentamidine isethionate in 0.5 mL of H_2O/IPA (1:1) was combined with the solution of the host. The slightly cloudy solution with the precipitation was observed. The colorless prismatic-shape crystals suitable for diffraction were observed within the precipitate after three days. Single-crystal X-ray diffraction analysis confirmed these crystals to be the host–guest complex ***C4S_PT_IPA.***

The refinement details of the C4S_PT_IPA complex

The asymmetric unit of ***C4S_PT_IPA*** consists of three tetra-anions C4S molecules, six dications of pentamidine, six isopropanol and eleven water molecules. All hydrogen atoms are added

geometrically. O1W and O2W water molecules are refined without hydrogen atoms. The basic crystallographic data of the discussed structure is provided in the Table 12.

*Table 12. Crystal data and structure refinement for **C4S_PT_IPA** complex.*

Parameters	***C4S_PT_IPA***
Formula moiety	$3(C_{28}H_{20}O_{16}S_4)\cdot 6(C_{19}H_{26}N_4O_2)\cdot 6(C_3H_8O)\cdot 11H_2O$
Formula weight	4835.39
Crystal system	Monoclinic
Space group	$P2_1/c$
a / Å	23.6106(1)
b / Å	30.3731(2)
c / Å	31.5092(2)
α / °	90
β / °	91.424(1)
γ / °	90
Volume / Å^3	22589.1(2)
Z	4
ρ_{calc} /g·cm^{-3}	1.42
Crystal color	Colorless
Crystal morphology	Prism
μ / mm^{-1}	1.89
θ_{max} / °	70.1
Reflections collected	145446
Independent reflections	42467 [R_{int} = 0.052]
Data / Restraints / Parameters	42467/ 0 / 2971
Observed data [I > 2σ(I)]	34396
Final R indexes [I ≥ 2σ(I)]	R_1 = 0.060, wR_2 = 0.163
Final R indexes [all data]	R_1 = 0.075, wR_2 = 0.174
Goodness-of-fit on F^2	1.03
Largest diff. peak and hole / e·Å^{-3}	1.02 / −0.76

Structure analysis of the C4S_PT_IPA complex

The co-crystallization of C4S ***sulfonic acid*** with pentamidine isethionate from water–isopropanol mixture results in the formation of the complex ***C4S_PT_IPA*** with the formula $2(C_{28}H_{20}O_{16}S_4)\cdot 6(C_{19}H_{26}N_4O_2)\cdot 6(C_3H_8O)\cdot 11(H_2O)$. Single-crystal X-ray diffraction analysis shows that this complex crystallizes in the monoclinic crystal system in the space group $P2_1/c$. The asymmetric part consists of two C4S, six pentamidines, six isopropanol and eleven water molecules (Figure 148).

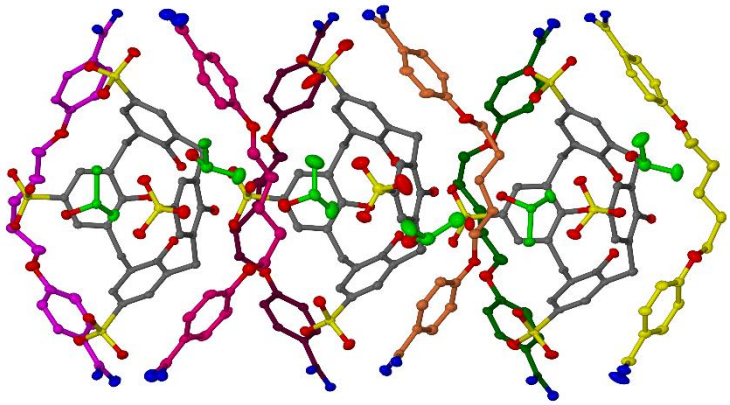

*Figure 148. The asymmetric unit of the host–guest complex **C4S_PT_IPA**. Crystallographically unique pentamidine molecules are presented in different colours. Atomic displacement parameters set at 50% probability. Water molecules and hydrogen atoms are omitted for clarity.*

Three C4S molecules in this complex are surrounded by two pentamidine molecules from opposite sides, as observed in the ethanol complex. The resulting capsule has a size of 15.7 Å, defined of the C4S cone is defined by the distance between the opposite sulfur atoms, resulting in values of 11.38 and 8.87 Å, 11.27 and 8.84 Å, 11.50 and 8.83 Å. The macrocycles adopt distinctly pinched conformations. The C4S cone is constrained at the lower rim by four hydroxyl groups, which participate in the formation of intermolecular hydrogen bonds, with *O···O* distances ranging from 2.690(3) to 2.864(3) Å. One hydroxyl group, *O24–H24*, forms a hydrogen bond with the O8W water molecule at an *O···O* distance of 2.704(2) Å. The parameters of the C4S intramolecular interactions are placed in Table 62, Annex I.

Each calixarene molecule encapsulates one isopropanol in its cavity, while the remaining three isopropanol molecules are located outside the host. These isopropanols form *O–H···O* hydrogen bonds with the host and water molecules, with *O···O* distances ranging from 2.757(2) to 3.146(3) Å. Additionally, two of the six isopropanol molecules interact with pentamidine through *N–H···O* hydrogen bonds. Figure 149a illustrates such an interaction between C1K > O2K pentamidine and C8I > O4I isopropanol, with the *N4K–H4KA···O4I* hydrogen bond measuring 2.982(4) Å. The three isopropanol molecules located within the host cavities also participate in *C–H···π* interactions with C4S, with distances between the carbon atoms of isopropanol and the aromatic rings of C4S in the range 3.548(5) to 3.724(5) Å (Figure 149b). Parameters of the intermolecular interactions formed by the isopropanol molecules are shown in Table 62, Annex I.

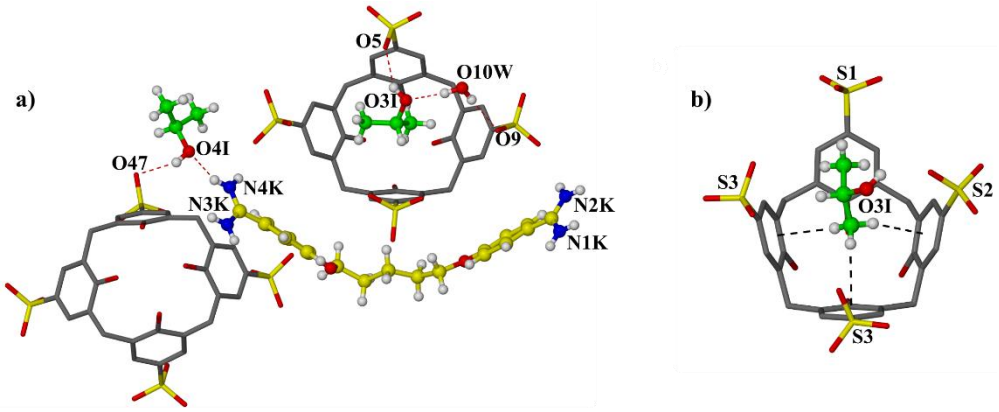

*Figure 149. Host–guest complex **C4S_PT_IPA**: (a) O–H···O and N–H···O hydrogen bonding mode between isopropanol molecules and the components of the crystal structure; (b) C–H···π bonds between isopropanol included into C4S cavity and aromatic rings of C4S molecule.*

All pentamidines engage *in N–H···O* hydrogen bonds with C4S (either the parent or neighboring molecules), as well as with isopropanol and water molecules, with *N···O* distances ranging from 2.71 to 3.26 Å. Figure 150a illustrates an example of these *N–H···O* hydrogen bonds between pentamidine (C1Z > O2Z) and various structural components, including C4S and isopropanol molecules located outside the C4S cavity. *N···O* distances are in the range 2.861(4)–3.258(4) Å. Additionally, pentamidines form *C–H···O* hydrogen bonds with the host molecules, interacting with both the parent and neighboring calixarenes, as shown in Figure 150b.

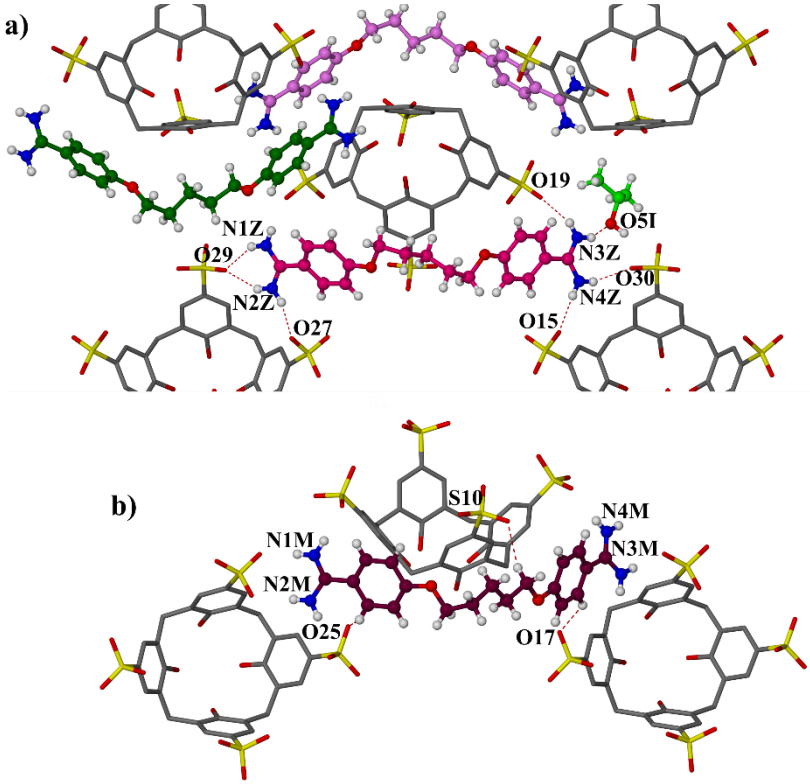

*Figure 150. Host–guest complex **C4S_PT_IPA**: (a) N–H···O hydrogen bonds between N–H groups of pentamidines and sulfonate oxygen atoms of C4S / isopropanol molecules; (b) C–H···O hydrogen bonds between C atoms of pentamidine aliphatic chain / aromatic ring and sulfonate oxygen atoms of C4S molecules.*

The conformation of three of the pentamidine molecules in this complex is similar to that of C1X > O2X pentamidine in the ***C4S_PT_EtOH*** complex with the different degrees of the deformation. These guest molecules participate in *C–H···π* interactions between the *C–H* groups of the C4S methylene bridges and the aromatic rings of pentamidine, as illustrated in Figure 151a. Simultaneously, a *C–H···π* interaction occurs between the aromatic ring of the C1X > O2X pentamidine molecule and the aromatic ring of C4S. Expansion of the crystal structure reveals that the pentamidines also form *π···π* contacts: C1K > O2K interacts with C1Z > O2Z at a distance of 3.774(2) Å, while two symmetrically equivalent C1L > O2L molecules interact at a distance of 3.813(2) Å (Figure 151b). For more details, the parameters of the intermolecular interactions formed by the pentamidine molecules are presented in Tables 62–64, Annex I.

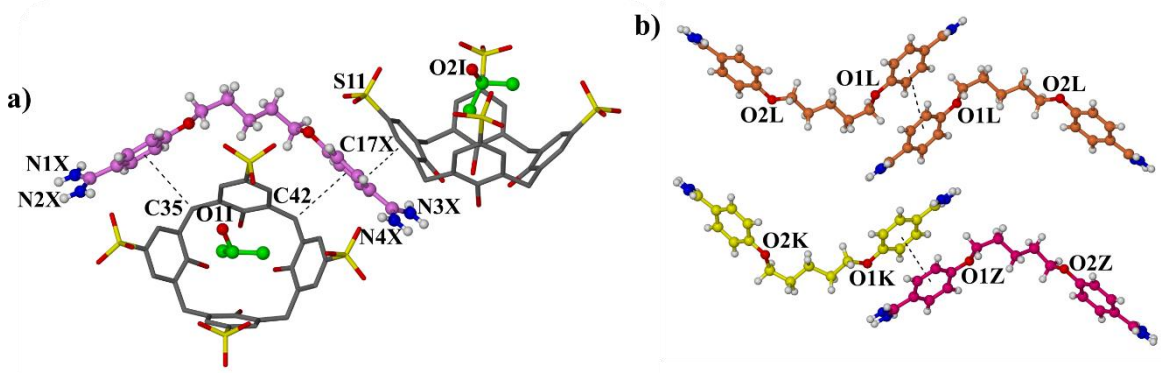

*Figure 151. Host–guest complex **C4S_PT_IPA**: (a) C–H···π interactions between methylene bridges of C4S and aromatic rings of pentamidine and between pentamidine / C4S aromatic rings; (b) π···π interaction between aromatic rings of pentamidine molecules.*

In the ***C4S_PT_IPA*** complex, the C4S molecules are arranged in a columnar manner and interact *via O–H···O* hydrogen bonds, with *O···O* distances ranging from 2.867(3) to 2.907(3) Å (Figure 152a). Detailed parameters of the intermolecular interactions are provided in Table 62, Annex I. The packing of the ***C4S_PT_IPA*** complex reveals the significant perturbation of bilayer organization, instead, the individual C4S columns are well separated by pentamidine bundles (Figure 152b).

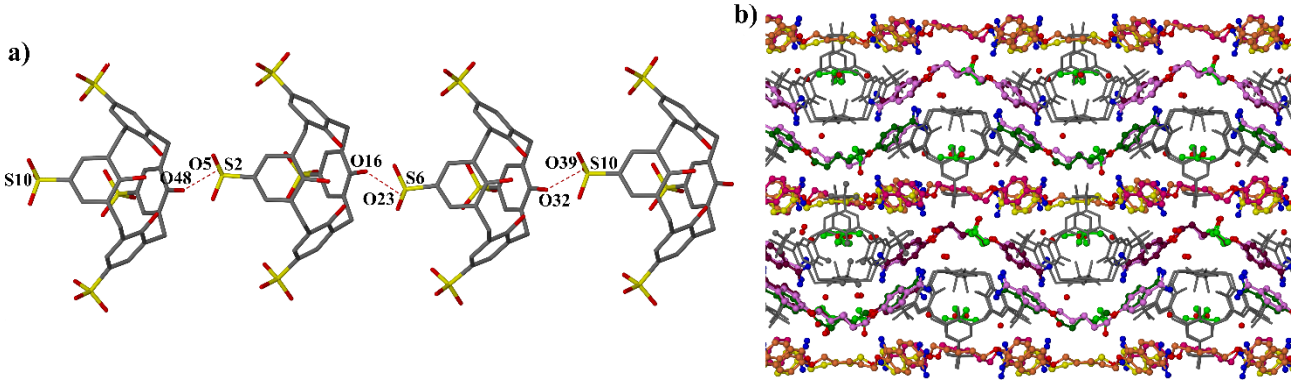

*Figure 152. Host–guest complex **C4S_PT_IPA**: (a) O–H···O hydrogen bonds between C4S molecules; (b) crystal packing of the host–guest complex **C4S_PT_IPA** viewed along **b** direction. Crystallographically non-equivalent pentamidine molecules are colored in different colors.*

C4S complex with pentamidine in water–acetone

Crystallization of C4S sulfonic acid complex with pentamidine from water–acetone mixture

5 mg of C4S ***sulfonic acid*** was dissolved in 0.5 mL of H_2O/Ace (1:1). The solution of 4.7 mg pentamidine isethionate in 0.5 mL of H_2O/Ace (1:1) was combined with the solution of the host. The cloud solution with the precipitation was observed. The colorless prismatic-shape crystals suitable for diffraction were observed within the precipitate after two days. Single-crystal X-ray diffraction analysis confirmed these crystals to be the host–guest complex ***C4S_PT_Ace.***

The refinement details of the C4S_PT_Ace complex

The asymmetric unit of ***C4S_PT_Ace*** consists of one tetra-anion C4S molecule, two dications of pentamidine, two acetone and six water molecules. The structure of the complex is refined as a 2-component twin. The crystal is twinned by pseudo-merohedry with the twin law defined as (1 0 0 1 –1 0 1 0 –1). The twin component was refined using the TWIN and BASF instructions in SHELXL, yielding a refined twin of 11.44%.

C1T > O1T acetone molecule included into C4S cavity is disordered and refined over two positions. The first component of disorder C1T > O1T is refined with PART 1 command (65.1% occupancy), the second C1U > O1U is refined with PART 2 command (34.9% occupancy). SIMU and RIGU restraints are applied to fix this disorder.

O2 > S1 atoms of C4S sulfonate group are disordered over two positions. The first component of disorder O2 > S1 is refined with PART 1 command (65.5% occupancy), the second O2A > S1A is refined with PART 2 command (34.5% occupancy). O10 > S3 atoms of C4S sulfonate group are also disordered over two positions. The first component of disorder O10 > S3 is refined with PART 1 command (50.8% occupancy), the second O10A > S3A is refined with PART 2 command (49.2% occupancy). Two pentamidine molecules in this complex are disordered over two positions and refined with PART commands. The C1X > O2X pentamidine PART 1 occupies 56.5%, PART 2 C1B > O2B occupies 43.5%. Disorder of pentamidine molecule is refined using SIMU, RIGU, SADI and SAME restraints. The first component of disordered C1C > O2C pentamidine molecule – C1C > O2C is refined with PART 1 command (49.3% occupancy), the second C1Y > O2Y is refined with PART 2 command (50.7% occupancy). Disorder is refined using SIMU, RIGU and SAME restraints.

Water molecules O3W, O4W, O5W, O6W are disordered over two positions. The first component of disorder O3W is refined with PART 1 command (64% occupancy), the second O3WA is refined with PART 2 command (36% occupancy). The first component of disorder O4W is refined with PART 1 command (56.2% occupancy), the second O4WA is refined with PART 2 command (43.8% occupancy). The first component of disorder O5W is refined with PART 1 command (66% occupancy), the second O5WA is refined with PART 2 command (34% occupancy). The first

component of disorder O6W is refined with PART 1 command (66% occupancy), the second O6WA is refined with PART 2 command (34% occupancy). All hydrogen atoms are added geometrically. Water molecules are refined without hydrogen atoms. The basic crystallographic data of the discussed structure is provided in 13.

*Table 13. Crystal data and structure refinement for **C4S_PT_Ace** complex.*

Parameters	***C4S_PT_Ace***
Formula moiety	$C_{28}H_{20}O_{16}S_4 \cdot 2(C_{19}H_{26}N_4O_2) \cdot 2(C_3H_6O) \cdot 6(H_2O)$
Formula weight	1649.80
Crystal system	Triclinic
Space group	*P–1*
a / Å	13.5261(12)
b / Å	15.7490(12)
c / Å	21.1794(12)
α / °	83.816(5)
β / °	71.887(6)
γ / °	65.344(8)
Volume / Å^3	3895.9(6)
Z	2
ρ_{calc} /g·cm^{-3}	1.41
Crystal color	Colorless
Crystal morphology	Prism
μ / mm^{-1}	1.86
θ_{max} / °	68.2
Reflections collected	47759
Independent reflections	14262 [R_{int} = 0.086]
Data / Restraints / Parameters	14262 / 2673 / 1590
Observed data [I > 2σ(I)]	8026
Final R indexes [I ≥ 2σ(I)]	R_1 = 0.131, wR_2 = 0.343
Final R indexes [all data]	R_1 = 0. 178, wR_2 = 0.40
Goodness-of-fit on F^2	0.92
Largest diff. peak and hole / e·Å^{-3}	0.90 / –0.64

Structure analysis of the C4S_PT_Ace complex

The co-crystallization of C4S ***sulfonic acid*** with pentamidine isethionate from water–acetone mixture results in the formation of the complex ***C4S_PT_Ace*** with the formula $C_{28}H_{20}O_{16}S_4 \cdot 2(C_{19}H_{26}N_4O_2) \cdot 2(C_3H_6O) \cdot 6(H_2O)$. Single-crystal X-ray diffraction analysis shows that this complex crystallizes in triclinic crystal system in the space group *P–1*. The asymmetric part consists of one C4S, two pentamidines, two acetone and six water molecules (Figure 153a). The C4S molecule in this complex is surrounded by two pentamidines. The pentamidines are positioned in such way that one benzamidine moiety is placed closely to the sulfonate groups of calixarene and one is directed away from C4S cone. The size of calixarene cone is defined by the distance between opposite Sulphur atoms, resulting in 9.87 and 11.22 Å, so the size point on the pinched conformation of the macrocycle. The lower rim of C4S presented by four hydroxyl groups correspond for the

formation of the intramolecular hydrogen bonds, *O···O* distances in the range of 2.706(8)–2.733(8) Å. The parameters of the C4S intramolecular interactions are described in the Table 45, Annex I.

The C4S complex contains one acetone molecule within its cavity, while a second acetone molecule is positioned near the lower rim of the macrocycle. The acetone in the cavity forms a *C–H···π* interaction with C4S, with the distance between the acetone methylene group and the aromatic ring of C4S measuring 3.48(4) Å (Figure 153b). The second acetone, located outside the C4S cavity, interacts with the macrocycle *via O–H···O* hydrogen bonds at a distance of 2.942(13) Å. The two acetone molecules also interact with each other through a *C–H···O* contact at a distance of 3.29(3) Å. Parameters of intermolecular interactions involving acetone molecules are summarized in Table 65, Annex I.

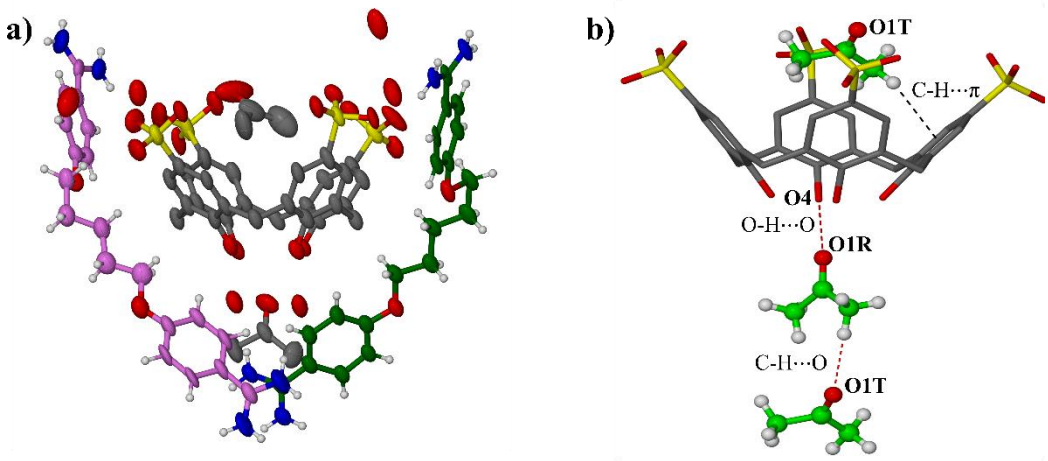

*Figure 153. (a) The asymmetric unit of the host–guest complex **C4S_PT_Ace**. Two crystallographically unique pentamidine molecules are presented in different colours. Atomic displacement parameters set at 40% probability. Disorder omitted for clarity; (b) O–H···O, C–H···O and C–H···π interactions between acetone–acetone and acetone–C4S molecules.*

In this complex, the pentamidine molecules are oriented toward the C4S sulfonate groups via one benzamidine moiety. Its *N–H···O* hydrogen bonding pattern includes one interaction with the parent C4S, while the remaining contacts are formed with adjacent C4S molecules or water. For the pink pentamidine molecule, the *N···O* distances range from 2.60(3) to 3.12(3) Å. For the green pentamidine molecule the *N···O* distances range from 2.61(5) to 3.06(3) Å (Figures 154 and 155).

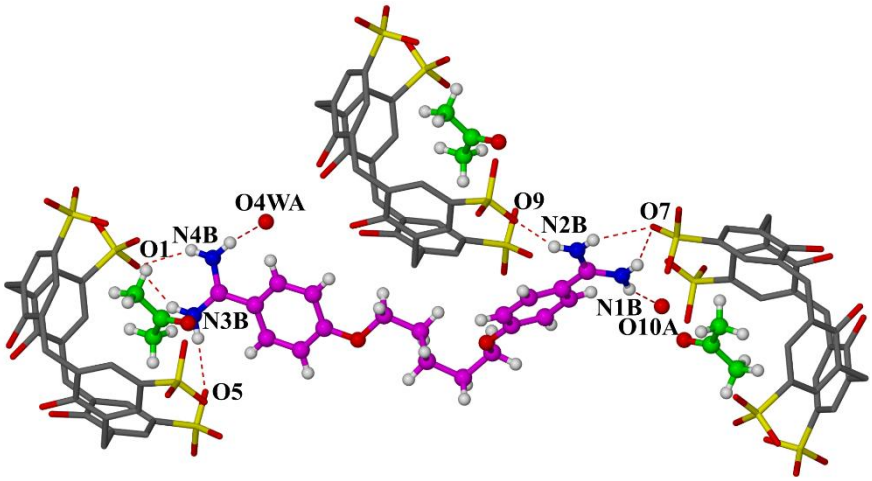

*Figure 154. Host–guest complex **C4S_PT_Ace**: N–H···O hydrogen bonds between N–H groups of pentamidine and sulfonate oxygen atoms of C4S / water molecules.*

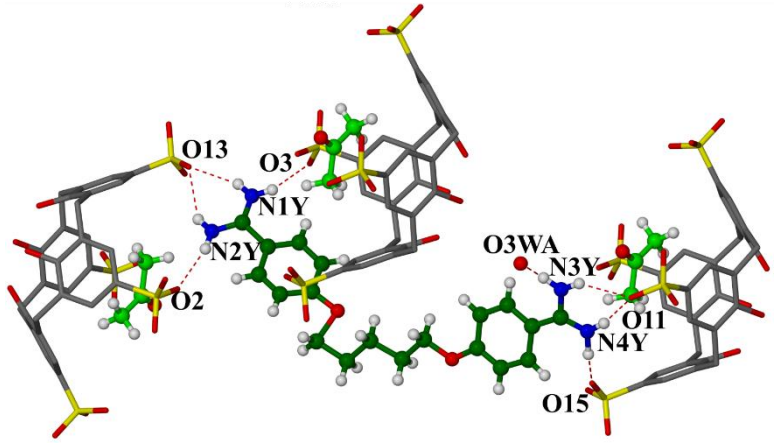

*Figure 155. Host–guest complex **C4S_PT_Ace**: N–H···O hydrogen bonds between N–H groups of pentamidine and sulfonate oxygen atoms of C4S / water molecule.*

In the structure of the complex, certain similarities in the *C–H···π* interaction mode between pentamidine molecules and C4S are observed (Figures 156a,b). These interactions involve the C atoms of the pentamidine aliphatic chain and the aromatic rings of C4S, with contact distances ranging from 3.40(2) to 3.75(2) Å.

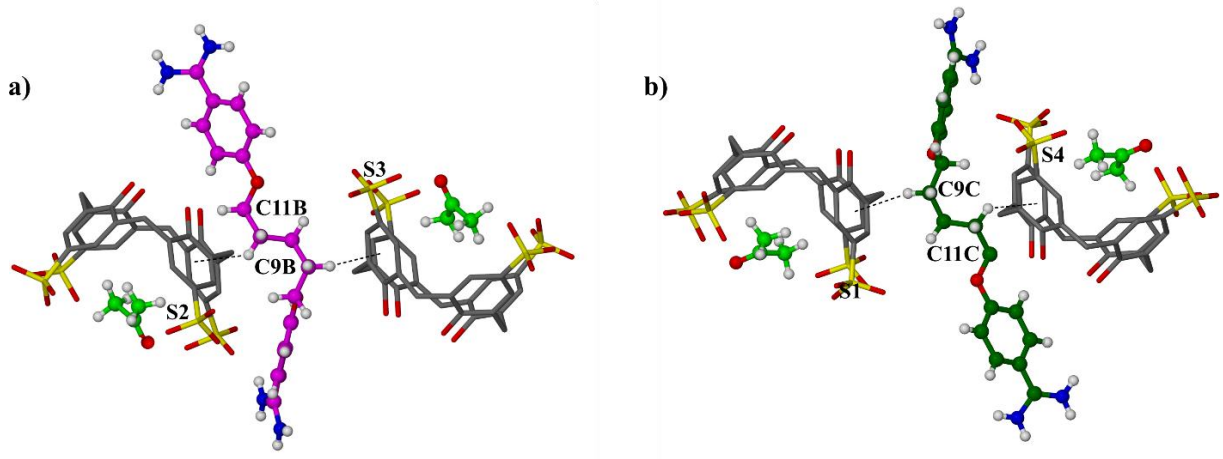

*Figure 156. Host–guest complex **C4S_PT_Ace**: (a) C–H···π interactions between C atoms of the pink pentamidine aliphatic chain and aromatic rings of the C4S molecules; (b) C–H···π interactions between C atoms of the green pentamidine aliphatic chain and aromatic rings of the C4S molecules.*

As shown in Figure 157, the C1Y > O2Y pentamidine molecule, which is extended between two host molecules, forms two *C–H···O* contacts with C4S *via* its aromatic rings. The remaining four interactions occur between pentamidine penthyl chain and water molecules, with *C···O* distances ranging from 2.91(2) to 3.50(2) Å.

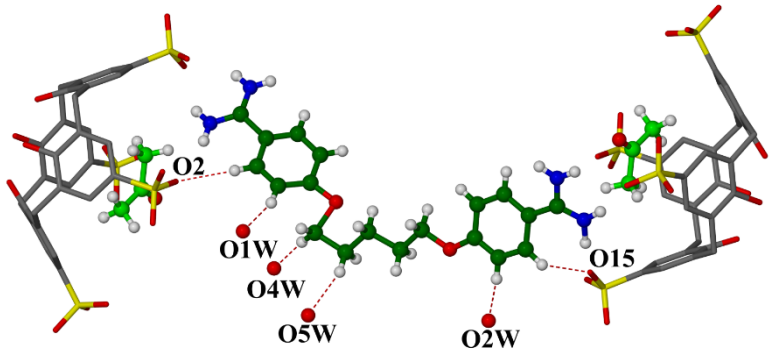

*Figure 157. Host–guest complex **C4S_PT_Ace**: C–H···O hydrogen bonds between C–H group of C1Y > O2Y pentamidine and sulfonate oxygen atoms of C4S / water molecules.*

In the ***C4S_PT_Ace*** complex, two symmetrically equivalent pentamidine molecules participate in *π···π* interactions with each other. For the C1X > O2X and C1C > O2C molecules, the distances between the centroids of the C4S aromatic rings are 3.90(4) Å and 3.745(18) Å, respectively (Figure 158a). Calixarenes are connected *via C–H···O* hydrogen bonds (Figure 158b). Interactions between the aromatic rings and the sulfonate oxygen atoms of C4S occur *at C···O* distances ranging from 3.335(10) to 3.441(11) Å. Detailed parameters of the intermolecular interactions involving pentamidine molecules are provided in Tables 65–67, Annex I.

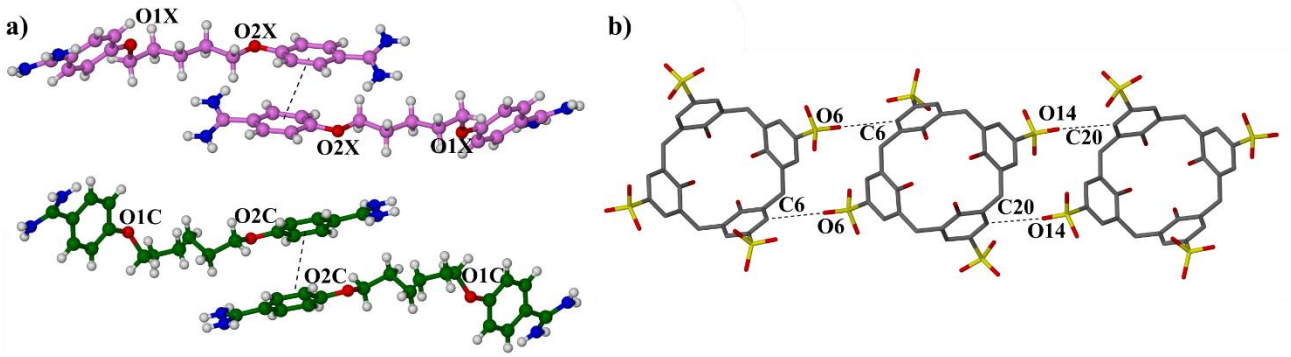

*Figure 158. Host–guest complex **C4S_PT_Ace**: (a) π···π interaction between aromatic rings of pentamidine molecules C1X > O2X, π···π interaction between aromatic rings of pentamidine molecules C1C > O2C; (b) C–H···O hydrogen bonds between C–H groups and sulfonate oxygen atoms of C4S molecules.*

The packing of the ***C4S_PT_Ace*** complex shows columns of C4S molecules, with acetone molecules located both inside the cavities and between adjacent macrocycles (Figure 159). The columns are separated by pentamidine molecules interacting with C4S outer surface.

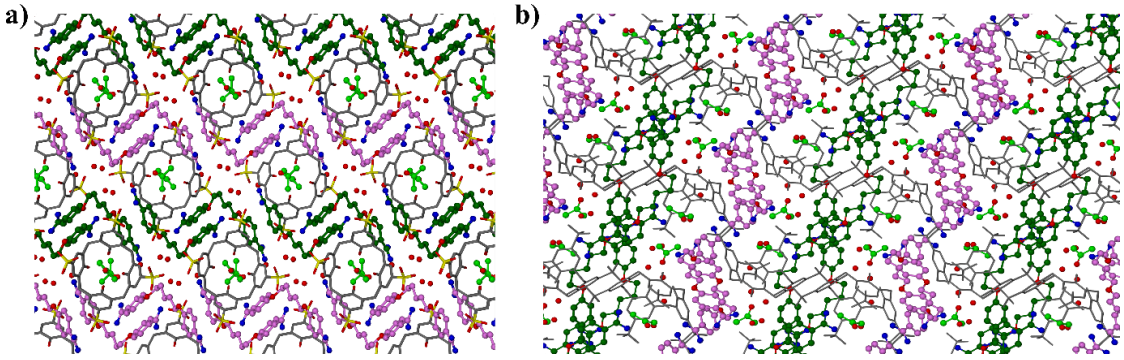

*Figure 159. Crystal packing of the host–guest complex **C4S_PT_Ace** viewed (a) **a** and (b) **b** directions. Crystallographically non–equivalent pentamidine molecules are colored in different colors, acetone in light green.*

4.2.3 C6S complex with pentamidine

Crystallization of C6S sulfonic acid complex with pentamidine from water–methanol mixture

20 mg of C6S ***sulfonic acid*** was dissolved in 0.5 mL of H_2O/MeOH (1:2). The solution of 18.3 mg pentamidine isethionate in 0.5 mL of H_2O/MeOH (1:2) was combined with the solution of the host (Figure 160). The cloud solution with the precipitation was observed. The colorless prismatic-shape crystals suitable for diffraction were observed within the precipitate after approx. 10 days. Single-crystal X-ray diffraction analysis confirmed these crystals to be the host–guest complex ***C6S_PT_MeOH***.

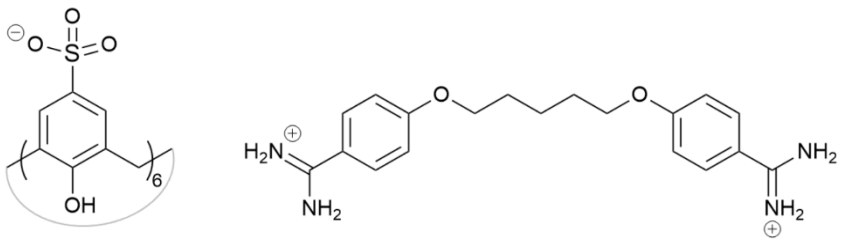

*Figure 160. Chemical structure of C6S **sulfonic acid** host and pentamidine (**PT**) guest.*

The refinement details of the C6S_PT_MeOH complex

The asymmetric unit of ***C6S_PT_MeOH*** consists of one hexa-anion C6S molecule, three dications of pentamidine, two methanol and 8.28 water molecules. The structure of the complex is refined as a 2-component non-merohedral twin. The twin component is refined using BASF instructions in SHELXL, yielding a refined twin 20.47%.

Atoms of three C6S sulfonate groups are disordered over two positions. Disorder of the first group is refined in the next way: O5 > O7 atoms in the PART 1 with 77.6% occupancy, O5A > O7A atoms in the PART 2 with 22.4% occupancy. Disorder of the second sulfinate group is refined in the next way: O13 > O15 atoms in the PART 1 with 77.7% occupancy, O13A > O15A atoms in the PART 2 with 22.3% occupancy. Disorder of the third sulfonate group is refined in the next way: O17 > S6 atoms in the PART 1 with 54.4% occupancy, O17A > S6A atoms in the PART 2 with 45.6% occupancy. The SIMU and RIGU restraints have been applied to fix the disorder of the atoms of the second and the third sulfonate groups.

Two pentamidine molecules in this complex are disordered over two positions and refined with PART commands. The C1X > O2X pentamidine has disordered atoms of aliphatic chain and benzamidine group. C8X > O2X atoms in PART 1 occupy 73.7%, C1B > O2B atoms PART 2 occupy 26.3%. Disorder of pentamidine molecule is refined using SIMU, RIGU and SADI restraints. The C1Z > O2Z pentamidine has also disordered atoms of the aliphatic chain and benzamidine mojety. The first component of disordered pentamidine molecule – C8Z > O2Z is refined with PART 1 command (77.7% occupancy), the second C8C > O2C is refined with PART 2 command (22.3 % occupancy). Disorder is refined using SIMU, RIGU and SADI restraints.

The O4W, O6W and O7W molecules are close to the disordered O5 > O7 atoms of C6S sulfonate group. O4W is disordered over two positions (O4W atom name in PART 1 with 77.6% occupancy and O4A atom name in the PART 2 with 22.4% occupancy). O6W is placed in PART 1 and refined with 77.6% occupancy, O7W in PART 2 is refined with 22.4% occupancy. The O2W, and O8W molecules are close to the disordered O13 > O15 atoms of C6S sulfonate group. O8W is disordered over two positions (O8W atom name in PART 1 with 77.7% occupancy and O8A atom name in the PART 2 with 22.3% occupancy). O2W is placed in PART 1 and refined with 77.7% occupancy. Water molecules O9W and O10W are close to each other. O9W is disordered over two positions. The first component of O9W is refined with PART 1 command (77.6% occupancy), the second O9A is refined with PART 2 command (22.4% occupancy). The O10W is refined with 50% occupancy in PART 1. All hydrogen atoms are added geometrically. Water molecules are refined without hydrogen atoms. The basic crystallographic data of the discussed structure is provided in the Table 14.

*Table 14. Crystal data and structure refinement for **C6S_PT_MeOH** complex.*

Parameters	***C6S_PT_MeOH***
Formula moiety	$C_{42}H_{30}O_{24}S_6 \cdot 3(C_{19}H_{26}N_4O_2) \cdot 2(CH_4O) \cdot 8.28(H_2O)$
Formula weight	2351.54
Crystal system	Triclinic
Space group	*P–1*
a / Å	12.3629(5)
b / Å	16.5072(7)
c / Å	28.5794(17)
α / °	85.914(4)
β / °	85.670(4)
γ / °	74.715(4)
Volume / Å^3	5602.0(5)
Z	2
ρ_{calc} /g·cm^{-3}	1.39
Crystal color	Colorless
Crystal morphology	Prism
μ / mm^{-1}	1.90
θ_{max} / °	60.9
Reflections collected	16703
Independent reflections	16703 [R_{int} = 0.079]
Data / Restraints / Parameters	16703 / 1506 / 1174
Observed data [I > 2σ(I)]	10883
Final R indexes [I ≥ 2σ(I)]	R_1 = 0.117, wR_2 = 0.310
Final R indexes [all data]	R_1 = 0.173, wR_2 = 0.350
Goodness-of-fit on F^2	1.07
Largest diff. peak and hole / e·Å^{-3}	0.95 / –0.50

Structure analysis of the C6S_PT_MeOH complex

The co-crystallization of C6S ***sulfonic acid*** with pentamidine isethionate from water–methanol mixture results in the formation of the complex ***C6S_PT_MeOH*** with the formula $C_{42}H_{30}O_{24}S_6 \cdot 3(C_{19}H_{26}N_4O_2) \cdot 2(CH_4O) \cdot 8.28(H_2O)$. Single-crystal X-ray diffraction analysis shows that this complex crystallizes in triclinic crystal system in the space group *P–1*. The asymmetric part consists of one C6S, three pentamidines, two methanol and 8.28 water molecules (Figure 161).

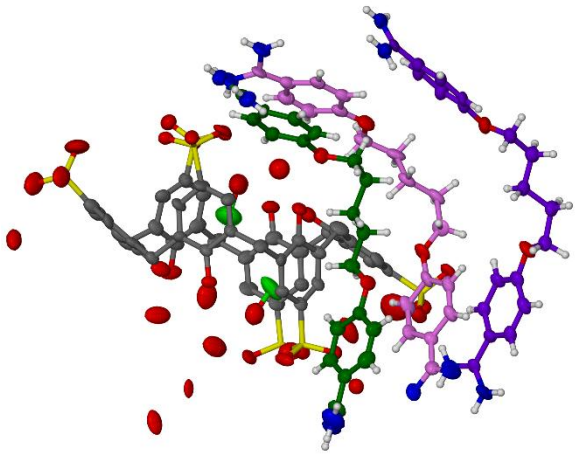

*Figure 161. The asymmetric unit of the host–guest complex **C6S_PT_MeOH**. Three crystallographically unique pentamidine molecules are presented in different colours, methanol in light green. Atomic displacement parameters set at 50% probability. Disorder omitted for clarity.*

In the pentamidine complex, the C6S molecule adopts a up–down double partial-cone conformation, with three rings pointing upward and three rings pointing downward (Figure 162a). In this conformation, *O–H···O* hydrogen bonding is more restricted or "sheltered" due to the tilting of the C6S rings (Figure 162b). Consequently, *O–H··O* hydrogen bonding interactions occur with adjacent calixarene and water molecules, with distances ranging from 2.574(12) to 3.039(12) Å; the corresponding parameters are summarized in Table 68, Annex I. The C6S molecule includes two methanol molecules, which interact with adjacent sulfonate oxygen atoms of C6S at distances of 2.624(13) Å and 2.713(15) Å (Figure 162c).

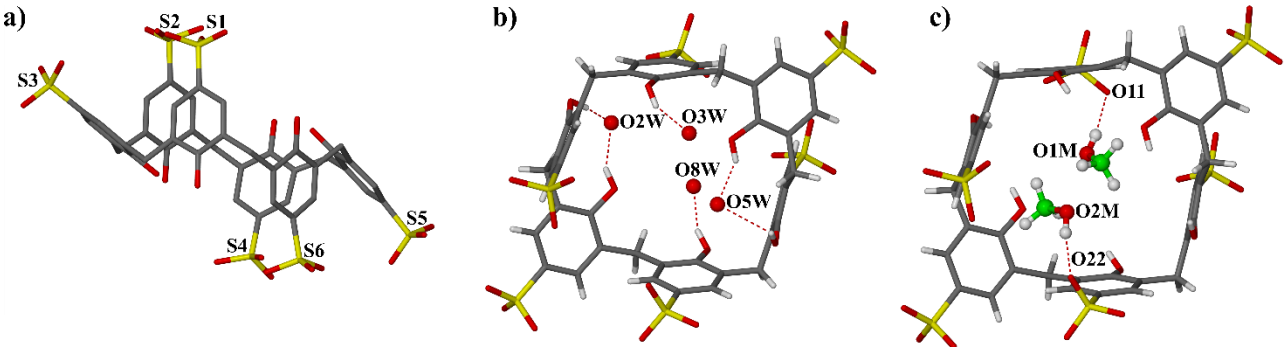

*Figure 162. Host–guest complex **C6S_PT_MeOH**: (a) up–down double partial-cone conformation of C6S molecule; (b) O–H···O hydrogen bonding at the C6S lower rim; (c) O–H···O hydrogen bonds between methanol and sulfonate oxygen atoms of C6S molecule.*

Three pentamidine molecules adopt a *C-shaped* conformation. The distances between the opposite oxygen atoms directly bonded to the pentamidine aliphatic chain are 5.84 Å for C1X > O2X, 5.99 Å for C1Y > O2Y, and 5.86 Å for C1Z > O2Z molecules (Figure 163).

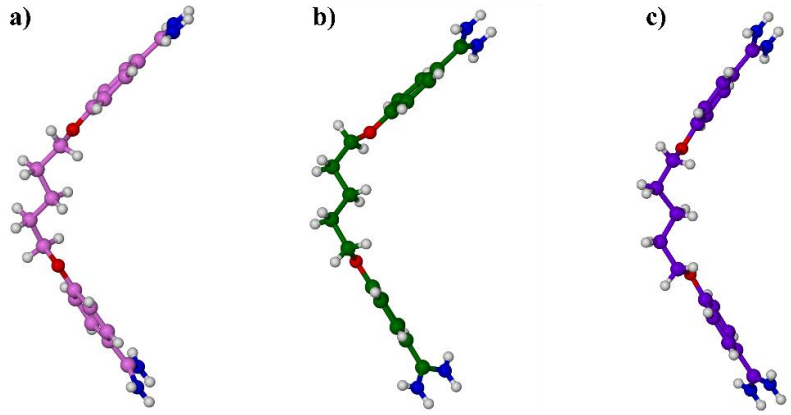

Figure 163. C-shaped conformations of pentamidine molecules.

Hydrogen bonding interactions between pentamidine, calixarene, and water are exemplified by the C1Y > O2Y pentamidine molecule. This guest molecule forms eight *N–H···O* hydrogen bonds: one with the parent C6S, four with neighboring calixarenes, and three with water molecules, with *N···O* distances ranging from 2.84(2) to 3.17(2) Å (Figure 164a). Pentamidine molecules positioned between the C6S units also form *C–H···O* hydrogen bonds with both C6S and water molecules (Figure 164b), primarily involving the C atoms of the pentamidine aromatic rings, with *C···O* distances ranging from 2.987(15) to 3.536(16) Å. Detailed parameters of these non-covalent interactions are summarized in Table 68, Annex I.

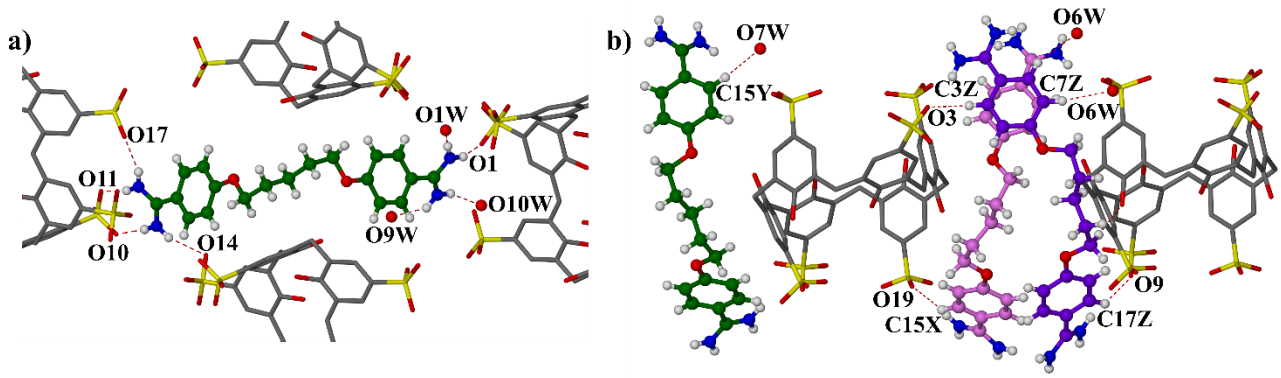

*Figure 164. Host–guest complex **C6S_PT_MeOH**: (a) N–H···O hydrogen bonds between N–H groups of C1Y > O2Y pentamidine and sulfonate oxygen atoms of C6S / water molecules; (b) C–H···O hydrogen bonds between C atoms of pentamidine molecules and sulfonate oxygen atoms of C6S / water molecules.*

The *C–H···π* interaction between the C1Y > O2Y pentamidine molecule and C6S occurs at a *C···centroid* distance of 3.423(12) Å, involving atoms of the pentamidine methylene group and the C6S aromatic rings (Figure 165a). The C1Z > O2Z pentamidine molecule forms two *C–H···π* interactions *via* the C atoms of its aliphatic chains and C1Y > O2Y aromatic rings, at distances of 3.64(2) Å and 3.76(2) Å. It also engages in a *π···π* contact with the C1X > O2X pentamidine molecule, with a *centroid···centroid* distance of 3.733(6) Å (Figure 165b). Furthermore, the C1X > O2X

molecule interacts with another symmetry-related C1X > O2X molecule [1–x, 1–y, –z] at a distance of 3.935(12) Å.

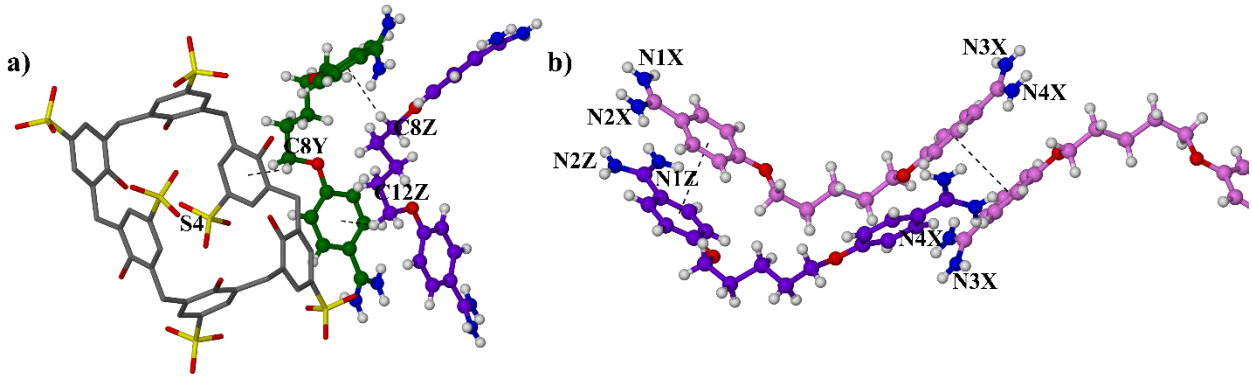

*Figure 165. Host–guest complex **C6S_PT_MeOH**: (a) C–H···π interactions between C6S–pentamidine and pentamidine–pentamidine molecules; (b) π···π interaction between aromatic rings of **C1X > O2X – C1Z > O2Z** and **C1X > O2X – C1X > O2X** pentamidine molecules.*

The *C–H···π* interaction between two C6S molecules involves the methylene bridge of one molecule and the aromatic ring of the other, with a *C···centroid* distance of 3.413(11) Å (Figure 166c). Crystal packing along the ***a*** axis shows that rows of C6S molecules are separated by ordered arrays of pentamidine molecules (Figures 166a,b). Parameters of these intermolecular interactions involving pentamidine molecules are summarized in Tables 68–70, Annex I.

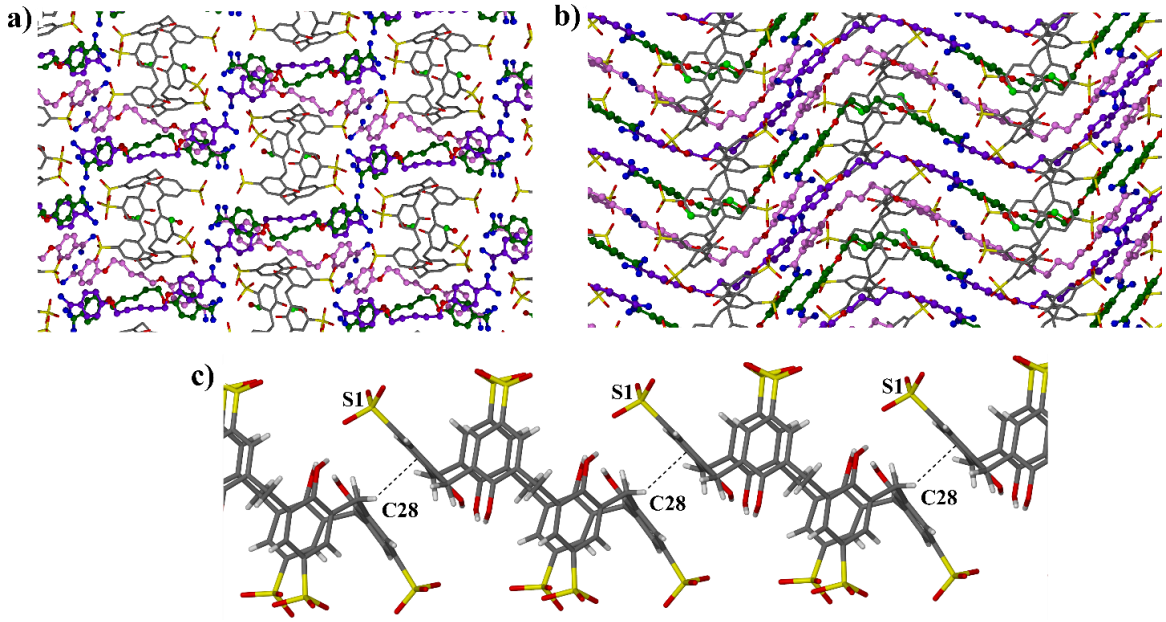

*Figure 166. (a–b) Crystal packing of the host–guest complex **C6S_PT_MeOH** viewed **a** and **b** directions; (c) C–H···π interactions between C atoms of C6S methylene bridges and C6S aromatic rings. Crystallographically non-equivalent pentamidine molecules are colored in different colors, methanol in light green. Disorder and water molecules are omitted for clarity.*

NMR analysis of the C6S_PT_MeOH complex

The host–guest complexation between C6S and pentamidine was investigated in CD_3OD using ^1H NMR spectroscopy (Figure 167). Upon the addition of pentamidine isethionate to the

methanolic solution of C6S, a rapid formation of a suspension/precipitate was observed, which partially dissolved after gentle heating. The ^{1}H NMR spectra revealed minor shifts in the aliphatic proton signals of pentamidine (***f***,***g***) in the presence of C6S, while more pronounced upfield shifts were detected for the aromatic protons of the benzamidinium groups (***a***,***b***). The observed upfield shifts for all pentamidine resonances indicate an inclusion-type host–guest complexation in methanolic solution, in contrast to the exclusion-type complexes identified in the crystal structure.

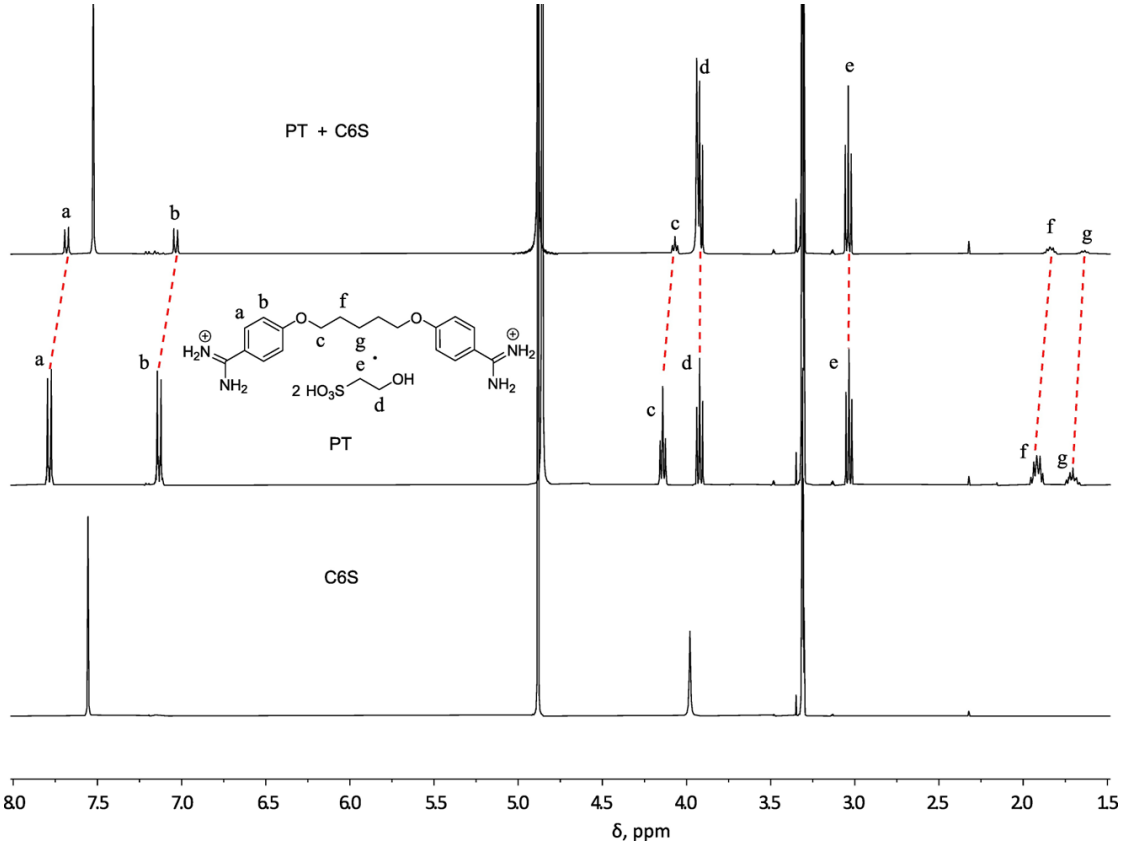

*Figure 167. ^{1}H NMR spectra of (a) C6S **sulfinic acid**; (b) pentamidine isethionate; (c) **C6S_PT_MeOH** host–guest complex – in the presence of slight precipitate, recorded on Agilent 400 MHz instrument at room temperature in CD_3OD, C(**C6S**) = 4 mM, C(pentamidine) = 4 mM.*

4.2.4 C8S complex with pentamidine

Crystallization and microscopic observations for C8S sulfonic acid complexes with pentamidine from water–ethanol mixture

20 mg of C8S ***sulfonic acid*** was dissolved in 1 mL of H_2O/EtOH (1:1). The solution 9.2 mg of pentamidine isethionate in 1 mL of H_2O/EtOH (1:1) was combined with the solution of the host. The cloudy solution was observed. The colorless prismatic-shape crystals suitable for diffraction were observed after 1 day. Single-crystal X-ray diffraction analysis confirmed these crystals to be the host–guest complex ***C8S_PT_EtOH*** (Figure 168).

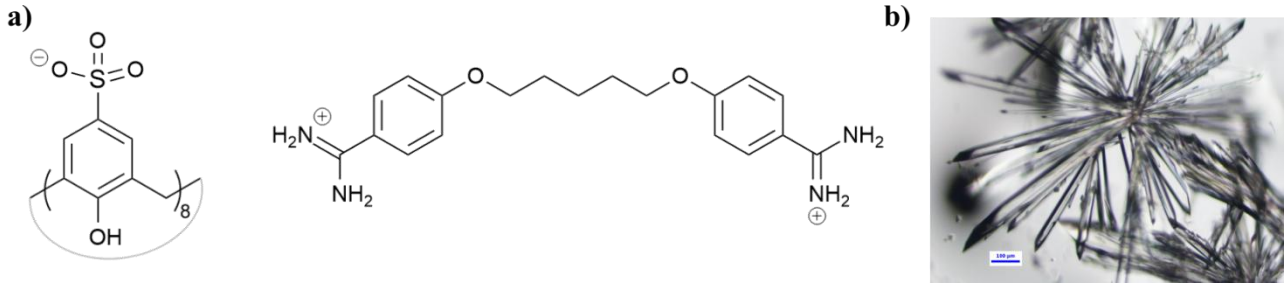

Figure 168. (a) Chemical structure of C8S ***sulfonic acid*** *host and pentamidine (****PT****) guest; (b) photomicrograph of crystals of* ***C8S_PT_EtOH*** *complex. The scale bar corresponds to 100 µm.*

The refinement details of the C8S_PT_EtOH complex

The asymmetric unit of ***C8S_PT_EtOH*** consists of two octa-anion C8S molecules, eight dications of pentamidine, 2.5 ethanol and 35.84 water molecules.

The O1I atom of one ethanol molecule is disordered over two positions and refined with PART commands, PART 1 with 61% occupancy, PART 2 with 39% occupancy. The C1R and C2R atoms of second ethanol molecule lies on the 2-fold axis, so C2R > O1R molecule is refined with 50% occupancy in in PART –1.

Two pentamidine molecules are disordered over two positions and refined with PART commands. The N1N > C19N pentamidine has disordered atoms of aliphatic chain. O1N > C12N atoms in PART 1 occupy 64.9%, O1H > C12H atoms PART 2 occupy 35.1%. The N1M > C19M pentamidine has disordered atoms of aliphatic chain and benzamidine part mojety. The first component of disordered pentamidine molecule – N1M > C19M is refined with PART 1 command (55.4% occupancy), the second N1Z > C19Z is refined with PART 2 command (44.6 % occupancy). The N1V > C19V pentamidine has disordered atoms of aliphatic chain and benzamidine part mojety. The first component of disordered pentamidine molecule – N1V > C19V is refined with PART 1 command (61.4% occupancy), the second N1F > C19F is refined with PART 2 command (38.6 % occupancy).SIMU, RIGU and SAME restraints are applied to the disordered pentamidine molecules. Most of the water molecules are disordered and refined with the PART 1, PART 2 and PART 3 commands. All hydrogen atoms are added geometrically. Water molecules and O1S atom of the ethanol are refined without hydrogen atoms. The basic crystallographic data of the discussed structure is shown in the Table 15.

*Table 15. Crystal data and structure refinement for **C8S_PT_EtOH** complex.*

Parameters	***C8S_PT_EtOH***
Formula moiety	$2(C_{56}H_{40}O_{32}S_8)\cdot 8(C_{19}H_{26}N_4O_2)\cdot 2.5(C_2H_6O)\cdot 35.84(H_2O)$
Formula weight	6462.98
Crystal system	Monoclinic
Space group	*C2/c*
a / Å	33.9061(5)
b / Å	41.7359(5)
c / Å	46.4819(7)
α / °	90
β / °	94.269(2)
γ / °	90
Volume / Å^3	65575.9(17)
Z	8
ρ_{calc} /g·cm^{-3}	1.31
Crystal color	Colorless
Crystal morphology	Prism
μ / mm^{-1}	1.78
θ_{max} / °	66.6
Reflections collected	636921
Independent reflections	57860 [R_{int} = 0.170]
Data / Restraints / Parameters	57860 / 2516 / 4890
Observed data [I > 2σ(I)]	30117
Final R indexes [I ≥ 2σ(I)]	R_1 = 0.134, wR_2 = 0.348
Final R indexes [all data]	R_1 = 0.197, wR_2 = 0.416
Goodness-of-fit on F^2	1.34
Largest diff. peak and hole / e·Å^{-3}	0.85 / –0.77

Structure analysis of the C8S_PT_EtOH complex

The co-crystallization of C8S ***sulfonic acid*** with pentamidine isethionate from water–ethanol mixture results in the formation of the complex ***C8S_PT_EtOH*** with the formula $2(C_{56}H_{40}O_{32}S_8)\cdot 8(C_{19}H_{26}N_4O_2)\cdot 2.5(C_2H_6O)\cdot 35.84(H_2O)$ Single-crystal X-ray diffraction analysis shows that this complex crystallizes in monoclinic crystal system in the space group *C2/c.* The asymmetric part consists of two C8S, eight pentamidines, 2.5 ethanol and 35.84 water molecules (Figure 169).

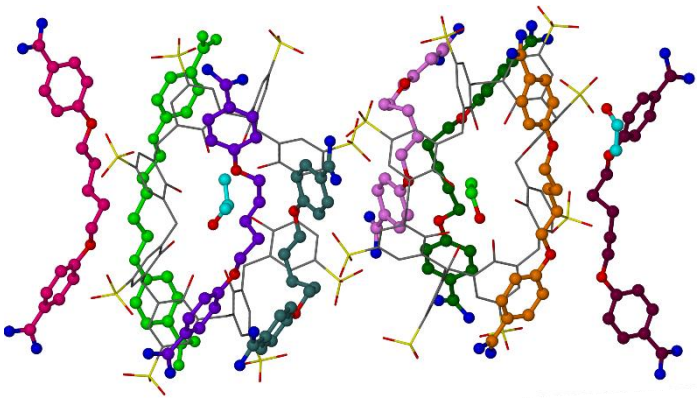

*Figure 169. The asymmetric unit of the host–guest complex **C8S_PT_EtOH**. The crystallographically unique pentamidine molecules are presented in different colours, ethanol in light blue and green. Water molecules, hydrogen atoms and disorder are omitted for clarity.*

The C8S molecules adopt a distorted pleated-loop conformation. The eight hydroxyl groups at the C8S lower rim participate in both intra- and intermolecular hydrogen bonding. Six hydroxyl groups form intramolecular hydrogen bonds, one forms an intermolecular hydrogen bond with an adjacent C8S molecule, and one interacts with an ethanol molecule (Figure 170a). The hydrogen bonding pattern at the lower rim of the second C8S molecule is similar. The *O···O* distances between hydrogen-bonded hydroxyl groups at the lower rim range from 2.594(8) to 2.889(6) Å. Two ethanol molecules occupy the central cavities of two different C8S units (Figure 170b), while one ethanol molecule is located outside the calixarene. These ethanol molecules interact with calixarene and water molecules *via O–H···O* and *C–H···O* hydrogen bonds (Figure 170c). Geometric parameters of the hydrogen bonds at the C8S lower rims are presented in Table 71, Annex I.

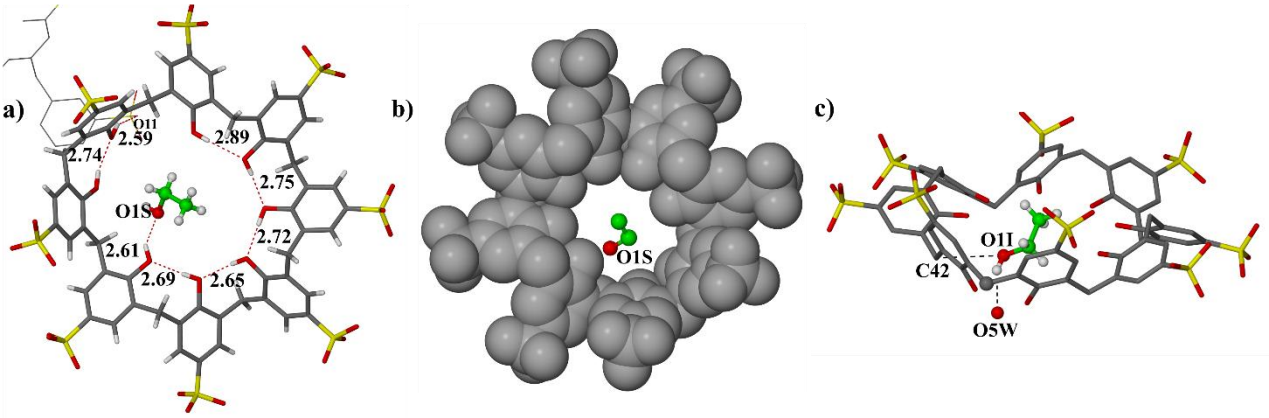

*Figure 170. Host–guest complex **C8S_PT_EtOH**: (a) example of the O–H···O hydrogen bonding at the lower rim of the one C8S molecule. O···O distances are given in Å; (b) the calixarene molecule is shown in space filled mode in grey, the ethanol molecule located in the central hole at the lower rim of the macrocycle; (c) O–H···O and C–H···O hydrogen bonds between ethanol and C8S molecules. Ethanol molecules are colored in green.*

In the ***C8S_PT_EtOH*** complex, the pentamidine molecules are positioned both in front of and behind the C8S macrocycles. All guest molecules adopt similar *C-shaped* conformations, though they exhibit varying degrees of deformation. Figure 171 illustrates the most elongated and the most twisted

pentamidine molecules in the complex. The degree of deformation is quantified by the distance between the oxygen atoms attached to the aliphatic chain of pentamidine, which ranges from 5.60 to 6.65 Å.

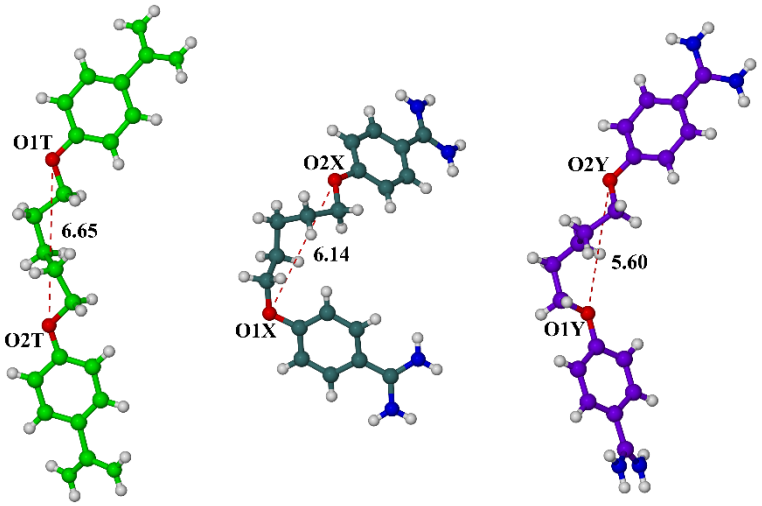

Figure 171. The variety of C-shaped conformations of pentamidine molecules showing O···O distances between oxygen atoms bound to the central pentyl chain. O···O distances are given in Å.

Each pentamidine molecule donates eight *N–H···O* hydrogen bonds to the oxygen atoms of neighboring C8S macrocycles and water molecules, with *N···O* distances ranging from 2.61(2) to 3.308(18) Å (Figure 172a). The pentamidine molecules also form multiple *C–H···O* hydrogen bonds with calixarenes and water molecules, as exemplified by the C1M > O2M pentamidine molecule in Figure 172b. The corresponding *C···O* distances in the structure range from 3.12(2) to 3.500(7) Å. Parameters of both *N–H···O* and *C–H···O* hydrogen bonds involving the pentamidine molecules are summarized in Table 71, Annex I.

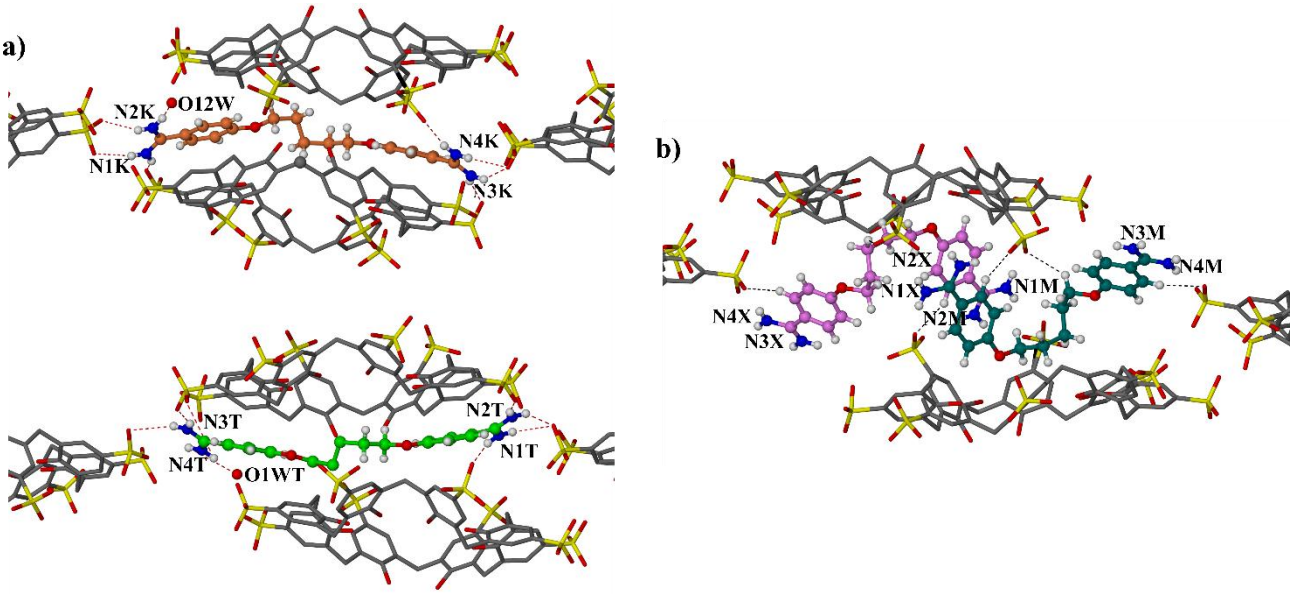

*Figure 172. Host–guest complex **C8S_PT_EtOH**: (a) N–H···O hydrogen bonds between N–H groups of pentamidine molecules and sulfonate oxygen atoms of C8S / water molecules; (b) C–H···O hydrogen bonds between C atoms of pentamidine molecules and sulfonate oxygen atoms of C8S.*

In Figure 173a, the C8S molecules engage in multiple *C–H···π* interactions with surrounding pentamidine molecules, involving both pentamidine aliphatic methylene groups and aromatic rings positioned near the C8S macrocycles. The aliphatic *C–H···π* contacts occur at distances ranging from 3.579(14) to 3.71(3) Å, while the aromatic *C–H···π* contacts are observed at 3.336(8) to 3.909(13) Å. In Figure 173b, six pentamidine molecules, aligned nearly parallel to one another, interact through their aliphatic chains and aromatic rings, with contact distances ranging from 3.555(15) to 3.726(18) Å.

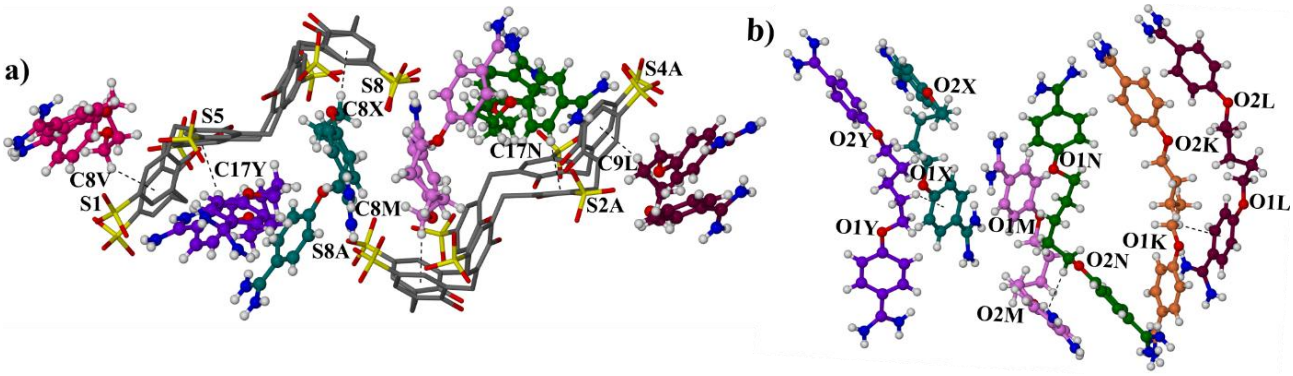

*Figure 173. Host–guest complex **C8S_PT_EtOH**: (a) C–H···π interactions between aromatic rings / methylene bridges of pentamidine and aromatic rings of C8S molecules; (b) C–H···π interactions between pentamidine molecules.*

Four pentamidine molecules positioned near the C8S units form *π···π* interactions with the macrocycles *via* their aromatic rings (Figure 174a). In addition, the pentamidine molecules engage in *π···π* stacking with each other (Figure 174b), with *centroid···centroid* distances ranging from 3.734(9)

to 3.871(6) Å. Parameters of the aromatic interactions involving the pentamidine molecules are summarized in Tables 72,73, Annex I.

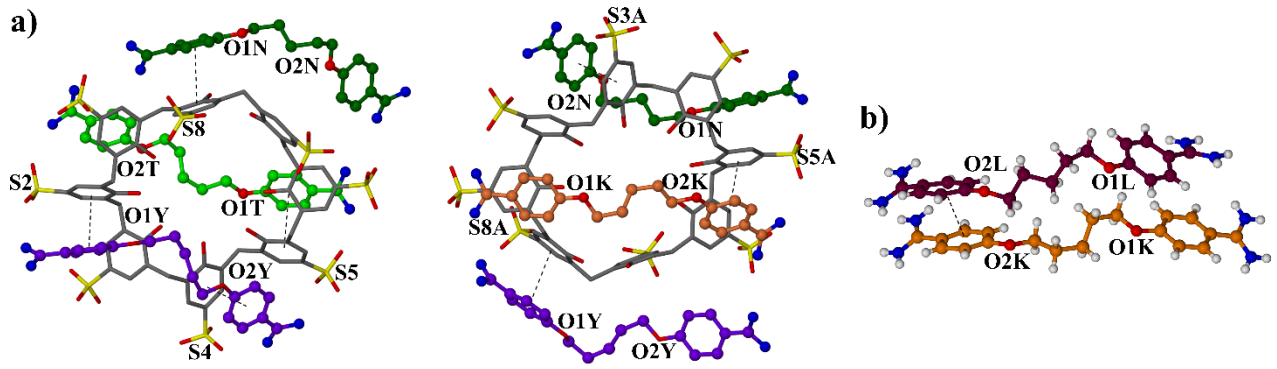

*Figure 174. Host–guest complex **C8S_PT_EtOH**: π···π interactions between aromatic rings of (a) pentamidine and C8S; (b) pentamidine molecules.*

The packing of the ***C8S_PT_EtOH*** complex (Figure 175a) shows that pentamidine molecules surround the C8S macrocycles from all sides. The C8S molecules are interconnected *via O–H···O* hydrogen bonds, with *O···O* distances of 2.594(8) and 2.707(7) Å (Figure 175b). Detailed parameters of these *O–H···O* interactions between C8S molecules are listed in Table 71, Annex I.

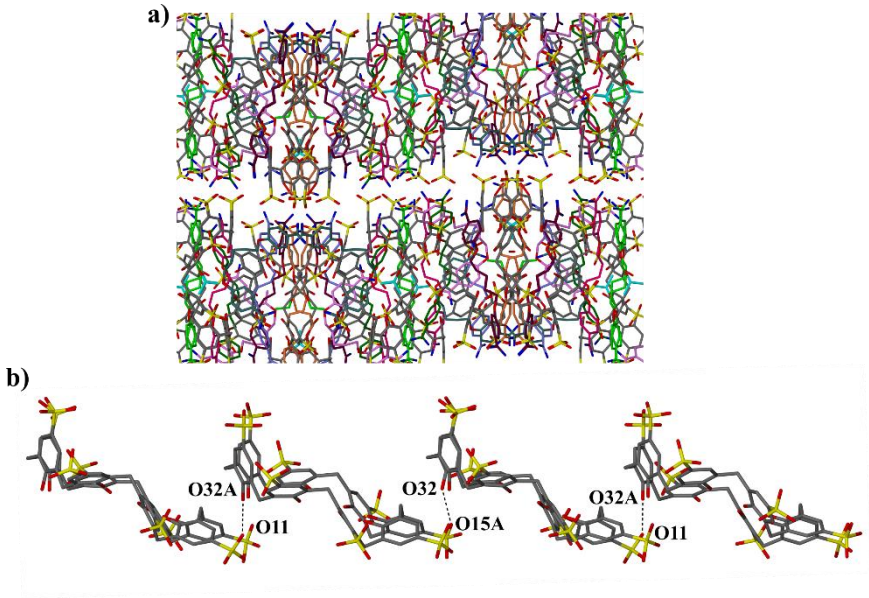

*Figure 175. Crystal packing of the host–guest complex **C8S_PT_EtOH** viewed along (a) **a** direction; (b) O–H···O interactions between C8S molecules. Crystallographically non-equivalent pentamidine molecules are colored in different colors. Disorder and water molecules are omitted for clarity.*

NMR analysis of the C8S_PT_EtOH complex

The host–guest complexation between C8S and pentamidine was investigated in CD_3OD using ^1H NMR spectroscopy (Figure 176). Upon the addition of pentamidine isethionate to the C8S solution, a rapid formation of a precipitate was observed, which partially dissolved after gentle heating.

The ^{1}H NMR spectra displayed minor shifts in the aliphatic proton signals of pentamidine (***f***,***g***) in the presence of C8S. In contrast, significant upfield shifts were observed for the aromatic protons of the benzamidinium groups (***a***,***b***), which were even more significant than those detected in the ***C6S_PT_MeOH*** complex. These substantial shifts indicate a deep inclusion of the pentamidine benzamidinium groups within the host cavity. Consequently, in solution, C8S adopts a distinctly different conformation characterized by a substantial cavity that enables guest inclusion, in contrast to the distorted pleated-loop arrangement observed in the crystalline complex.

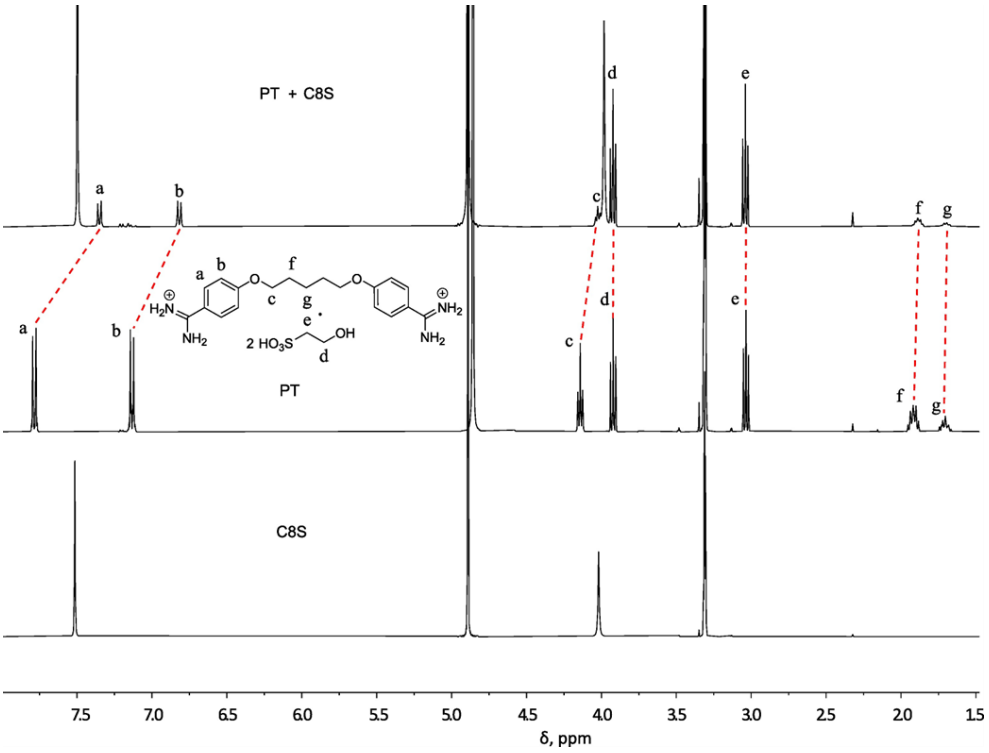

*Figure 176. ^{1}H NMR spectra of (a) C8S **sulfinic acid**; (b) pentamidine isethionate; (c) **C8S_PT_EtOH** host–guest complex – in the presence of slight precipitate, recorded on Agilent 400 MHz instrument at room temperature in CD_3OD, C(**C8S**) = 4 mM, C(pentamidine) = 4 mM.*

Solid-state complexes of C*n*S with alexidine and pentamidine – discussion of results

Sulfonated calixarenes (C4S, C6S, C8S) are versatile macrocyclic hosts that accommodate flexible multicationic guests, such as pentamidine and alexidine, through shape complementarity and extensive networks of noncovalent interactions. The binding behavior of these guests is largely driven by the size, geometry, and conformational flexibility of the calixarene host. Both pentamidine and alexidine contain flexible aliphatic linkers and multiple hydrogen-bonding sites, allowing them to adjust their conformations to fit within the host cavity or interact externally when inclusion is unfavorable. Moreover, the choice of solvent during crystallization strongly affects guest behaviour and determines the overall supramolecular structure of the host–guest assembly.

Alexidine forms a 1:1 complex with *p*-sulfonatocalix[4]arene. Its central hexyl chain folds into the calixarene cavity while two biguanidinium groups form hydrogen bonds with the parent and nearby hosts, and water molecules. The inclusion type host–guest complexation occurs not only in aqueous–ethanolic solvent mixtures but also in methanol, as confirmed by ^{1}H NMR analysis, indicating that alexidine strongly favors inclusion even in another solvent.

Pentamidine as a guest exhibits solvent-dependent binding behavior with *p*-sulfonatocalix[*n*]arenes similar to the C4S–isoniazid complex reported by Danylyuk *et al.* (2015).[124] The cocrystallization of C4S and pentamidine in aqueous solution results in 1:2 host–guest complex ***C4S_PT_H2O*** in which one pentamidine molecule is included within the calixarene cavity, while the second binds externally. The C4S host adopts a typical pinched cone conformation, and the flexible central pentyl linker of pentamidine folds within the cavity. The included pentamidine molecule adopts compact U-shaped conformation.

The cocrystallization of C4S and pentamidine in water–ethanol solvent mixtures affords a 1:2 host–guest complex (***C4S_PT_EtOH***), in which the calixarene cavity is occupied by an ethanol molecule. Both pentamidine molecules remain external, positioned on opposite sides of the C4S scaffold and engaged in multiple noncovalent interactions with the host and surrounding water molecules. Similarly, in water–isopropanol mixtures the complex ***C4S_PT_IPA*** retains the same 1:2 stoichiometry and exclusion binding mode, with the macrocyclic cavity occupied by an isopropanol molecule. In water–acetone mixtures, a 1:2 host–guest complex (***C4S_PT_Ace***) crystallizes in which one acetone molecule resides inside the calixarene cavity, while a second acetone molecule is located below the lower rim; the two pentamidine molecules bind externally through hydrogen bonding interactions with the calixarene and water molecules.

Across all water–cosolvent systems, cocrystallization of C4S with pentamidine consistently results in exclusion complexation of the pentamidine guests, which adopt a C-shaped conformation complementary to the external curvature of the macrocycle, while the C4S cavities are preferentially occupied by solvent molecules (ethanol, isopropanol, or acetone). This behavior highlights a pronounced guest–solvent competition for binding within the C4S cavity, where small solvent molecules outcompete pentamidine for inclusion, thereby enforcing exclusion binding at the macrocyclic exterior. Consequently, the supramolecular binding mode of C4S–pentamidine complexes can be switched from inclusion to exclusion simply by changing the crystallization medium from pure water to water–cosolvent mixtures. In all three exclusion complexes, pentamidine molecules embrace the outer surface of C4S through a combination of charge-assisted amidinium–sulfonate hydrogen bonds with the anionic rim of the macrocycle and *C–H*$\cdots\pi$ interactions. This external association of pentamidine disrupts direct calixarene–calixarene contacts, with the

pentamidine guests separating adjacent macrocycles in the crystal lattice and preventing the formation of the typical bilayer arrangement observed for C4S[96].

Host size also exhibits a significant influence on the binding of pentamidine. In the complex with *p*-sulfonatocalix[6]arene (***C6S_PT_MeOH***) crystallized from water-methanol mixture, the host adopts an up–down double partial-cone conformation.[97] In this conformation C6S accommodates two methanol molecules within its pseudo calix[3]arene cavities. All pentamidine molecules bind externally with the calixarene by amidinium-sulfonate hydrogen bonding and *C–H···π* interaction. Interestingly, ^{1}H NMR analysis in methanolic solution shows endo– type pentamidine complexation, contrasting with the exo– type observed in the crystal structure.

The *p*-sulfonatocalix[8]arene-pentamidine complex (***C8S_PT_EtOH***) crystallized from water-ethanol solvent mixture exhibits increased host flexibility compared to C4S and C6S complexes. In the ideal pleated-loop conformation of C8S, eight hydroxyl groups form an almost planar, cyclic hydrogen-bonded network (Figure 177a). The plane defined by these eight coplanar oxygen atoms generates four identical grooves on both sides of the macrocycle, resulting from the alternating up-and-down orientation of the methylene bridges. In the host–guest complex ***C8S_PT_EtOH***, this regular hydrogen-bonded arrangement is disrupted. The C8S molecule adopts a distorted pleated-loop conformation, where six aryl rings are connected by five intramolecular hydrogen bonds. The distortion involves two adjacent aryl rings (pseudo-calix[2]) oriented upright relative to the plane formed by the six oxygen atoms of the pleated- loop region (Figure 177b). The methylene carbon linking these two rings lies approximately in this plane, while two hydroxyl groups within the pseudo-calix[2] fragment are directed below it. Notably, none of the 25 crystal structures of C8S assemblies deposited in the Cambridge Structural Database exhibit a comparable distorted pleated-loop conformation. Previously reported host–guest complexes show a wide range of geometries, from an extreme chalice-like conformation[145] to a nearly flat pleated-loop conformations of C8S[138,139].

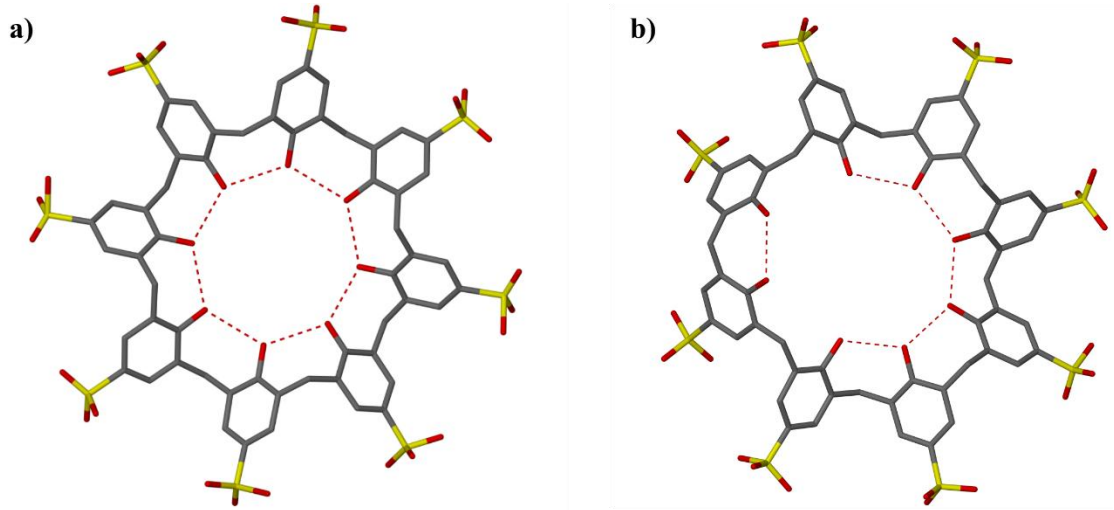

Figure 177. Comparison of the (a) pleated-loop conformation of C8S molecule in ***C8S–butanediammonium*** *complex (refcode VERBAW) and (b) distorded pleated-loop conformation of C8S molecule in* ***C8S_PT_EtOH*** *complex.*

A comparison of pentamidine conformations across described complexes illustrates its structural adaptability. A search of the Cambridge Structural Database (version 2025.2) contains two salt forms of pentamidine isethionate.[161a,b] The pentamidine molecules in both forms adopt extended conformations, with nearly identical *O···O* distances of 7.23 Å (isethionate) and 7.24 Å (diisethionate). Also, three host–guest complexes involving pentamidine and a carboxylated pillar[5]arene (refcodes BAWNEW, BAWNIA, BAWNOG) have been identified.[196] In these structures, pentamidine adapts to the rigid prismatic shape of the host by threading through the macrocycle and interacting with the carboxylate groups of adjacent pillar[5]arene molecules (Figures 178a–c). In BAWNOG, one of the two pentamidine molecules is positioned outside the host (Figure 178c). Within the three complexes mentioned, the *O···O* distances between the two oxygen atoms of pentamidine directly bound to the central pentyl chain range from 7.26 to 7.35 Å. The pillar[6]arene–pentamidine complex (refcode ZESCUZ, Figure 178d) features one pentamidine molecule passing through the pillar[6]arene cavity and another positioned outside.[196] In pentamidine, the *O···O* distances across the central pentyl chain measure 7.17 and 7.39 Å.

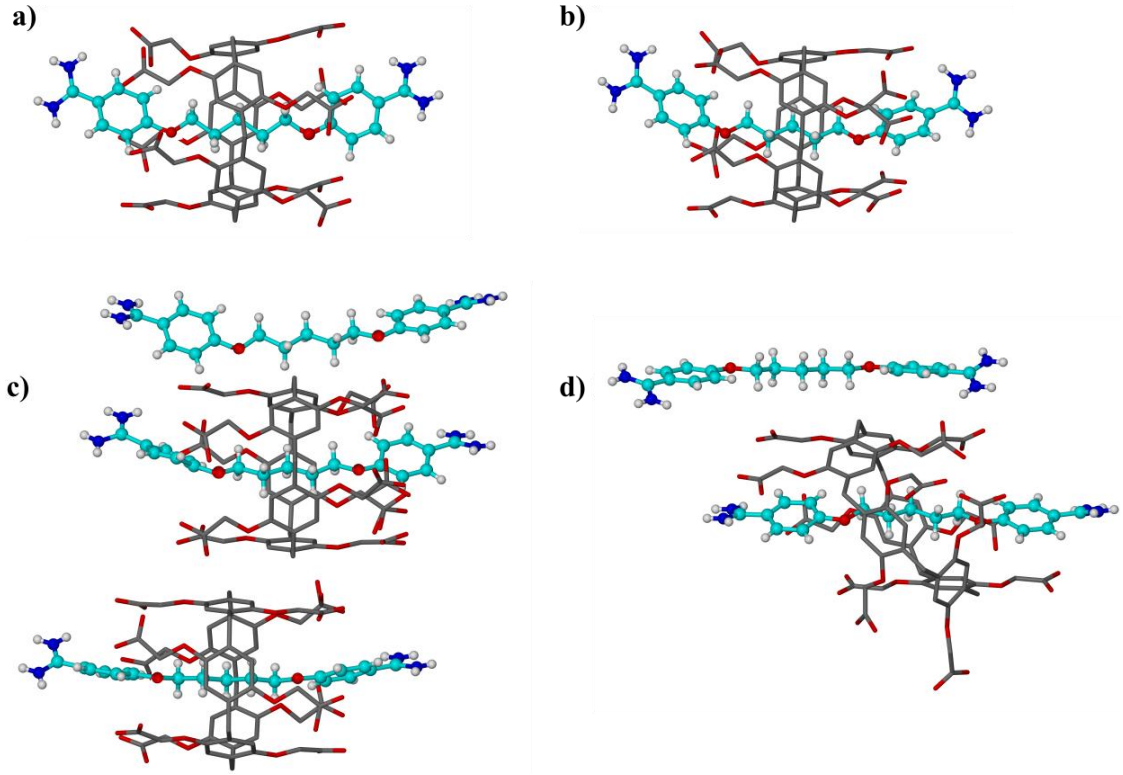

Figure 178. (a–c) Inclusion complexes of pentamidine with pillar[5]arene (refcodes BAWNEW, BAWNIA, BAWNOG) and (d) with pillar[6]arene (refcode ZESCUZ). Pentamidine molecules are colored light blue.

In contrast, within discussed calixarene-based complexes, the pentamidine guests adopt significantly folded conformations, with *O···O* distances ranging from 4.45 to 6.65 Å. These comparisons indicate that pentamidine adapts its conformation to the size and shape of the host, enabling interactions either inside or outside the cavity under favorable conditions. The most folded conformation among the calixarene systems is observed in the ***C4S_PT*** complex, where the *O···O* distance reaches 4.45 Å, whereas the most extended conformation occurs in the ***C8S_PT_EtOH*** complex, with an *O···O* distance of 6.65 Å. Figures 179a,b highlight the pronounced difference between the folded and extended conformations of pentamidine in calixarene and pillar[6]arene complexes.

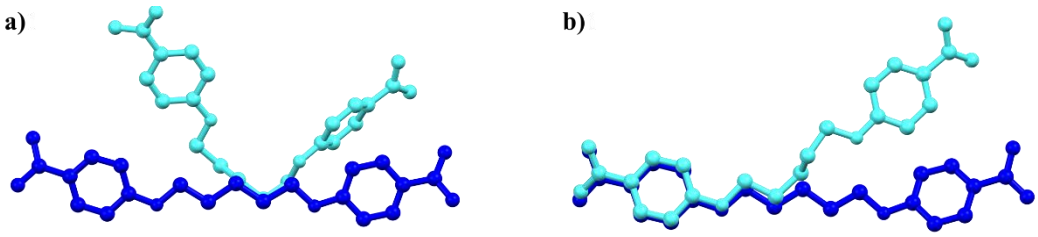

Figure 179. Superposition of pentamidine conformations in different macrocyclic host complexes. (a) The most folded conformation of pentamidine in ***C4S_PT*** *complex and the extended conformation from the carboxylated pillar[6]arene–pentamidine complex (refcode ZESCUZ). (b) The most extended conformation of pentamidine from the* ***C8S_PT_EtOH*** *complex and the extended conformation from the carboxylated pillar[6]arene–pentamidine complex (refcode ZESCUZ). Pentamidine molecules in the* ***C4S_PT*** *and* ***C8S_PT_EtOH*** *complexes are shown in light blue, while pentamidine from the pillar[6]arene complex is dark blue.*

4.3 *p*-Sulfonatocalix[4]arene complexes with pillar[*n*]pyridiniums

In this chapter, inherently cationic macrocycles pillar[*n*]pyridiniums have been considered as partner molecules for the co-assembly with C4S. Since pillar[*n*]pyridinium molecules are devoid of classical hydrogen bond donors, the hybrid supramolecular architectures driven mainly by electrostatic interactions have been anticipated. Pillar[*n*]pyridiniums currently available as tetracationic pillar[4]pyridinium (rigid box-like structure) and hexacationic pillar[6]pyridinium (flexible structure) have good aqueous solubility, as well as *p*-sulfonatocalix[*n*]arenes. Taking into account the complementarity between electron-deficient cavities of pillar[*n*]pyridiniums and electron-rich cavities of *p*-sulfonatocalix[*n*]arenes, the good supramolecular fit between two macrocyclic families of opposite charge is expected. The cocrystallization experiments of C4S with P4P/P6P macrocycles have been challenging, and less common crystallization methods needed to be employed. I have succeeded in the using crystallization gel technique in the U-tube for the C4S–P4P system, and liquid–liquid diffusion in the NMR tube for C4S–P6P complex. The crystal structure of resulting co-assemblies has shown encaging of the cationic pillar[*n*]pyridinium units within/between the capsules that emerge from anionic calix[4]arene pairs.

The co-assembled supramolecular architectures based on C4S complexes with P4P and P6P are described in the article entitled ***"Electrostatic Co-assembly of Pillar[n]pyridiniums and Calix[4]arene in Aqueous Media"***, published in *CrystEngComm*.

4.3.1 C4S complex with pillar[4]pyridinium

Crystallization and microscopic observations for C4S sulfonic acid complex pillar[4]pyridinium

0.73 mg of C4S ***sulfonic acid*** was dissolved in 0.25 mL of H_2O. The solution of 0.5 mg pillar[4]pyridinium hexafluorophosphate in 0.25 mL of H_2O was slowly combined with the solution of the host (Figure 180a). The mixing of the aqueous solutions results in rapid clouding and precipitation of white microcrystals. To obtain good quality single crystals the gel crystallization method has been applied. As a crystallization setup, the U-shaped tube filled with agarose gel was used. The one arm of the tube is filled with an aqueous solution of P4P and the other arm with a solution of C4S. Such crystallization which involves the diffusion of each macrocyclic component through the gel environment yielded yellow single crystals of the product. The diffraction-quality yellow prism-shape crystals (Figure 180b) were found after approx. one month. Single-crystal X-ray diffraction analysis revealed these crystals to be the host–guest complex ***C4S_P4P***.

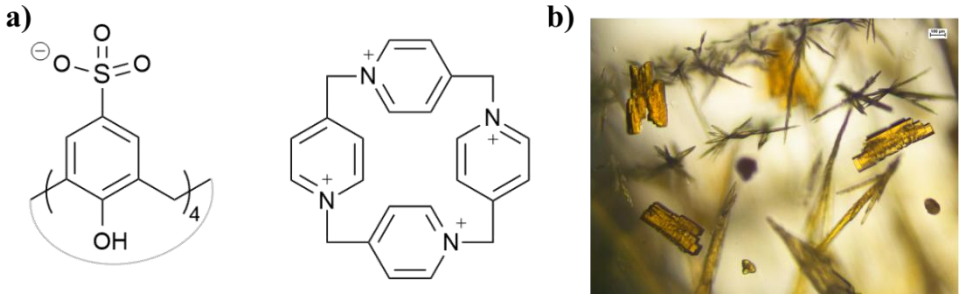

Figure 180. (a) Chemical structure of C4S ***sulfonic acid*** *host and pillar[4]pyridinium (**P4P**) guest; (b) photomicrograph of crystals of **C4S_P4P** complex. The scale bar corresponds to 100 μm.*

The refinement details of the C4S_P4P complex

The asymmetric unit of ***C4S_P4P*** consists of 1/2 of C4S tetra–anion, positioned on a mirror plane, 1/4 part of two pillar[4]pyridinium tetra-cations and seven water molecules. The atoms of O1 > S1 of the sulfonate group lies close to the mirror plane and are refined with 50% of occupancy with the help of PART –1 instruction, SADI restraint is applied to equate the proper *S–O* distance. C4S sulfonate group O5 > S2 is disordered over two positions. The first component of disorder O5 > S2 is refined with PART 1 command (53.5% occupancy), the second O5A > S2A is refined with PART 2 (46.5% occupancy). The S3 > O11 atoms of the sulfonate group lies close to the mirror plane and disordered over two positions. S3 atom is refined with occupancy 50% using PART –1 command. O9 > O11 atoms also are refined with PART –1 command (25% occupancy). The second component of disorder O9A > O11A is refined with PART 2 command (25% occupancy). SADI restraint is applied to the atoms of PART 1 and PART 2 to equate *S–O* distance.

The pillar[4]pyridinium molecule lies on the intersection of the 2-fold axis and the mirror plane. The C1X lies on the mirror plane, C7X atom lies on the 2-fold axis and are refined with the 50% occupancy. The nitrogen atoms of the pyridinium rings of the pillar[4]pyridinium molecule cannot be reliably distinguished from the carbon atoms, so substitutional disorder is introduced into the model. Since no position is clearly favoured over the other, it is equally possible that the nitrogen atoms can be found in either a clockwise or counterclockwise direction around the macrocycle. The disorder model was built using PART 1 and 2 instructions with the 50% occupancy of the C4X and N1X atoms. The positions of the nitrogen and carbon atoms that share the same site are built using the EXYZ (same position) and EADP (same thermal parameters) restraints. The C1Y > N2Y molecule of P4P lies on the intersection of the 2-fold axis and the mirror plane. The C2Y, C3Y, C6Y, C7Y, N1Y and N2Y atoms are refined with 50% occupancy.

The O1W molecule lies on 2-fold axis and a mirror plane and has 25% of occupancy. The O2W molecule lies on 2-fold axis and refined with PART –1 (50% occupancy). The O3W molecule lies on 2-fold axis and a mirror plane with 25% of occupancy. The O4W molecule lies close to a mirror plane and refined with PART –1 command (50% occupancy). O5W molecule is refined with

25% of occupancy. The O6W water molecule is disordered over two positions. The first component of disorder O6W is refined with PART 1 command (25% occupancy), the second O6WA is refined with PART 2 command (25% occupancy). The O7W is refined with 50% occupancy. The O8W component of PART 1 has 25% of occupancy, O9W component of PART 2 has 50% of occupancy. The PART 3 includes 25% of O8WA and 25% of O10W molecules. The O12W, O13W and O14W water molecules are close to the disordered O5 > S2 sulfonate group. The disorder is refined using PART 1 and PART 2 commands. The O1WA, O12W and O13W atoms of PART 1 occupies 53.5% of atomic site. The O11W, O12A and O14W atoms of PART 2 occupies 46.5% of atomic site. The hydrogen atoms are added using mixed mode. Majority of hydrogen atoms are added geometrically, H atoms of the C1X > N1X P4P molecule are located from the Fourier difference map. Water molecules are refined without hydrogen atoms. The basic crystallographic data of the discussed structure is provided in Table 16.

*Table 16. Crystal data and structure refinement for **C4S_P4P** complex.*

Parameters	***C4S_P4P***
Formula moiety	$C_{28}H_{20}O_{16}S_4 \cdot C_{24}H_{24}N_4 \cdot 14(H_2O)$
Formula weight	1360.36
Crystal system	Tetragonal
Space group	$P4_2/m$
a / Å	18.3974(1)
b / Å	18.3974(1)
c / Å	20.6604(2)
α / °	90
β / °	90
γ / °	90
Volume / Å³	6992.81(1)
Z	4
ρ_{calc} ***/g·cm⁻³***	1.29
Crystal color	Yellow
Crystal morphology	Prism
μ / m⁻¹	1.97
θ_{max} ***/ °***	68.24
Reflections collected	41529
Independent reflections	6549 [R_{int} = 0.027]
Data / Restraints / Parameters	6549 / 6 / 588
Observed data [I > 2σ(I)]	5516
Final R indexes [I ≥ 2σ(I)]	R_1 = 0.085, wR_2 = 0.254
Final R indexes [all data]	R_1 = 0.095, wR_2 = 0.270
Goodness-of-fit on F²	1.04
Largest diff. peak and hole / e·Å⁻³	0.63 / –0.34

Structure analysis of the C4S_P4P complex

The co-crystallization of C4S ***sulfonic acid*** with pillar[4]pyridinium hexafluorophosphate in agarose gel results in the formation of the complex ***C4S_P4P*** with the formula

$C_{28}H_{20}O_{16}S_4 \cdot 2(C_{24}H_{24}N_4) \cdot 14(H_2O)$. Single-crystal X-ray diffraction analysis shows that this complex crystallizes in a tetragonal crystal system in the space group $P4_2/m$. The asymmetric part consists of half of C4S tetra-anion, 1/4 part of two pillar[4]pyridinium tetra-cations and seven water molecules (Figure 181a,b).

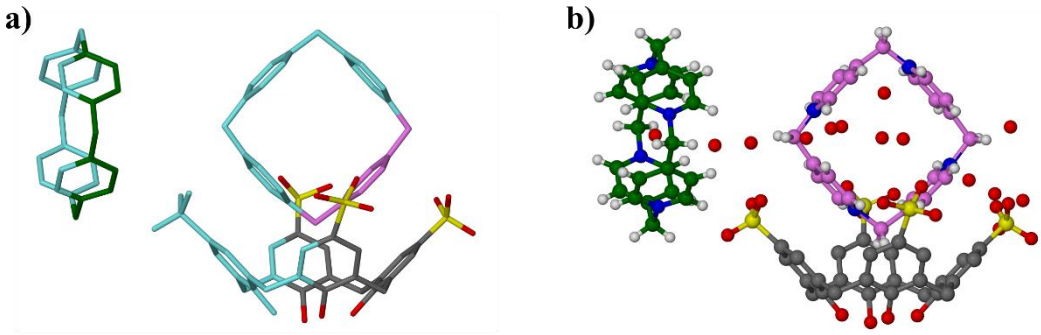

*Figure 181. Host–guest complex **C4S_P4P**: (a) the asymmetric unit of the **C4S_P4P** complex with the expanded C4S and P4P molecules. The macrocycle lies on a mirror plane, the light blue corresponds to symmetry generated half of P4P and C4S molecules, water molecules omitted for clarity; (b) the expanded asymmetric unit of the **C4S_P4P** complex. Two crystallographically unique P4P molecules are presented in different colours. Disorder omitted for clarity.*

In the ***C4S_P4P*** complex, one P4P molecule is included within the C4S cavity, while another resides outside the cavity. The size of the guest molecules is determined as the distance between the carbon atoms of opposite methylene groups. The pink P4P size is 5.71 Å and 5.71 Å, and the green P4P measures 5.71 Å and 5.73 Å, indicating a rigid-square conformation (Figure 182). This geometry allows P4P to fit closely into the pinched cone shape of the C4S host cavity. The size of the calixarene bowl, measured as the distance between opposite sulfur atoms, is 10.01 Å and 11.55 Å. The lower rim of the C4S cavity is restricted by the hydroxyl groups which form intermolecular hydrogen bonds with *O···O* distances in the range 2.557(3)–2.930(3) Å. The parameters of the C4S intramolecular interactions are summarized in Table 74, Annex I.

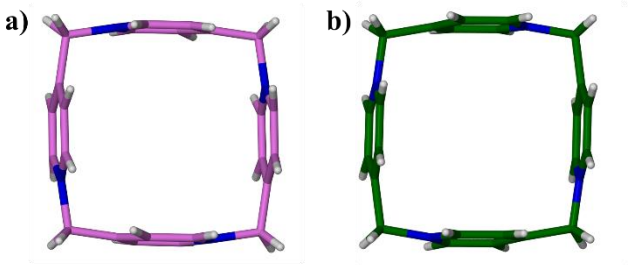

*Figure 182. Host–guest complex **C4S_P4P**: rigid-square conformations of P4P molecules.*

The pink P4P molecule (C1X > N7X) is included within the C4S cavity. Expansion of the crystal structure shows that the P4P molecule is sandwiched between two C4S molecules, forming a *2:1 pseudocapsule* (Figure 183a). The size of the pseudocapsule, measured as the distance between the planes defined by the hydroxyl groups of the two C4S molecules, is 16.01 Å. Within this pseudocapsule, the guest is stabilized by *C–H···O* hydrogen bonds between the carbon atoms of the

P4P aromatic rings and the sulfonate oxygen atoms of the C4S molecules, all occurring at *C···O* distances of 3.235(8)–3.237(12) Å. Water molecule, O1W, is positioned precisely at the center of the small P4P cavity, located at the intersection of the mirror plane and the 2-fold rotation axis (Figure 183b). This water molecule is positioned at the same distance from all four pyridinium walls of P4P, allowing for favorable *O–H···π*$^+$ hydrogen bonds, with *O···centroid* distances of 3.10 Å. Another water molecule, O4W, is located above each edge of the macrocyclic P4P "box", interacting with the intracavity water molecule *via O–H···O* hydrogen bonds (2.78 Å). P4P also interacts with water through *C–H···O* hydrogen bonds, with distances between aromatic carbon atoms and water molecules ranging from 3.110(16) to 3.447(10) Å (Figure 183c).

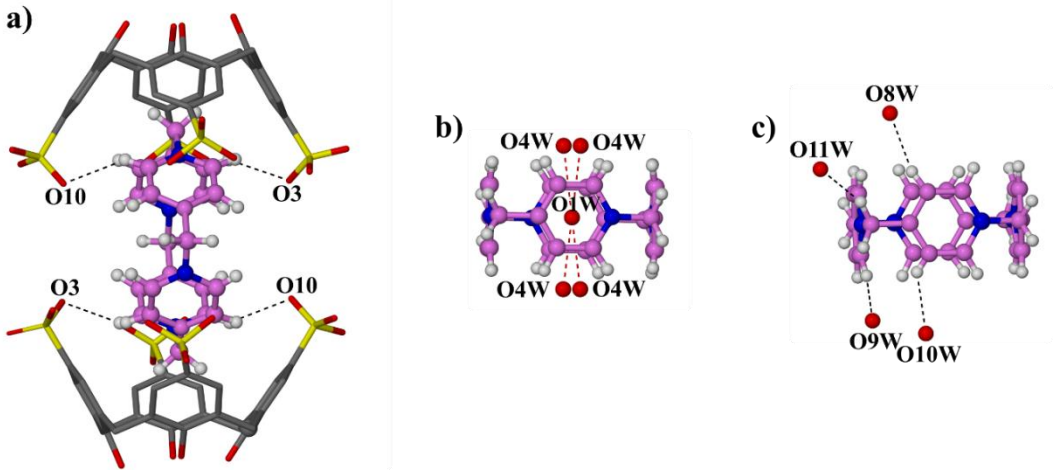

*Figure 183. Host–guest complex **C4S_P4P**: (a) C–H···O hydrogen bonds between C atoms of P4P aromatic rings and sulfonate oxygen atoms of C4S molecules in pseudocapsule; (b) O–H···O hydrogen bonds between water molecule in the exact center of the P4P cavity and outside the cavity; (c) C–H···O hydrogen bonds between C atoms of P4P aromatic rings and water molecules.*

Two *C–H···π* interactions are observed between the carbon atoms of the P4P methylene bridge and the aromatic rings of the C4S molecule within the cavity, with *C···centroid* distances ranging from 3.735(5) to 3.766(5) Å. In addition, a *π···π* interaction occurs between the aromatic walls of C4S and P4P at 3.953(19) Å (Figures 184a,b).

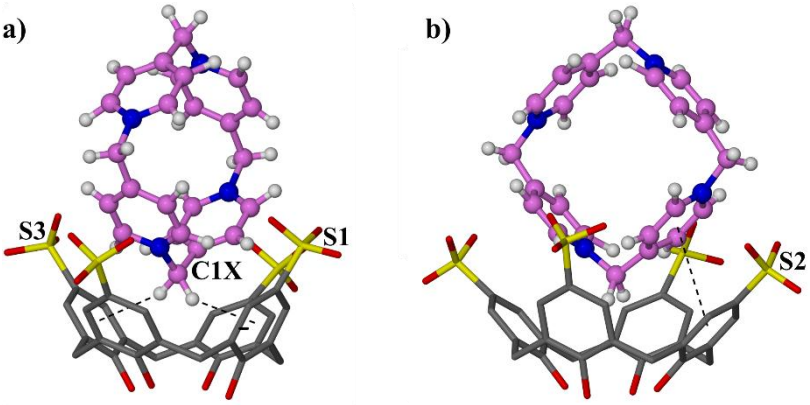

*Figure 184. Host–guest complex **C4S_P4P**: (a) C–H···π interactions between C atoms of P4P methylene bridge and aromatic rings of C4S molecule; (b) π···π interaction between P4P and C4S aromatic rings.*

The second P4P molecule is located outside the C4S cavity. The crystal structure reveals that P4P is surrounded by four C4S molecules, forming *C–H···O* contacts at distances of 3.31 and 3.39 Å (Figure 185a). As in the included P4P, the external P4P cavity contains water molecule, O3W, at the intersection of the mirror plane and 2-fold rotation axis, with distances to the pyridinium centroids of 3.08 and 3.15 Å (Figure 185b). Additional water molecules, O2W and O11W, lie outside the macrocyclic box, interacting with O3W *via O–H···O* hydrogen bonds of 2.76 and 2.59 Å.

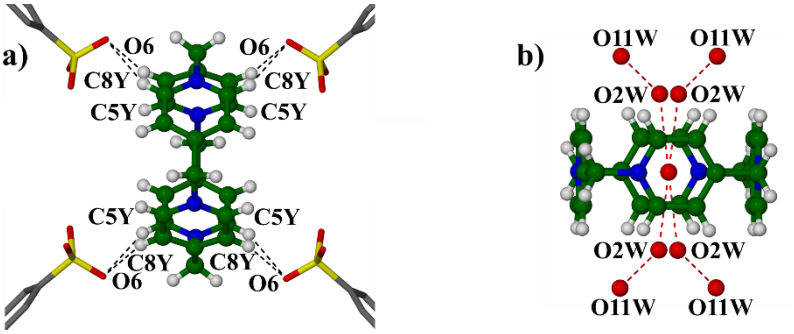

*Figure 185. Host–guest complex **C4S_P4P**: (a) C–H···O hydrogen bonds between C atoms of P4P aromatic rings and sulfonate oxygen atoms of the adjacent C4S molecules; (b) O–H···O hydrogen bonds between water O3W molecule in the center of the external P4P cavity and water molecules outside the cavity.*

The external P4P molecule participates in a single $\pi\cdots\pi$ interaction with a macrocyclic C4S host. The interaction between the aromatic rings of P4P and C4S occurs at a distance of 3.450(2) Å (Figure 186a). The parameters of intermolecular interactions involving P4P molecules are summarized in Tables 74–76, Annex I. The packing of the ***C4S_P4P*** complex presents layers of pseudocapsules formed by C4S and the C1X > C36X P4P molecules. Between these capsules, the C1Y > C36Y P4P guest and water molecules are located (Figure 186b).

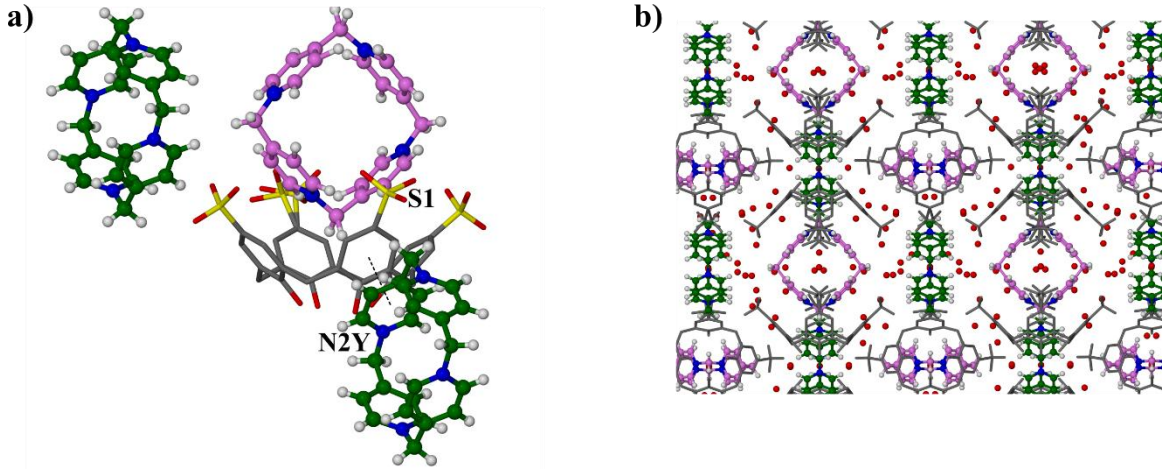

*Figure 186. Host–guest complex **C4S_P4P**: (a) π···π interaction between P4P and C4S aromatic rings; b) crystal packing of the host–guest complex **C4S_P4P** viewed along **–b** direction.*

4.3.2 C4S complex with pillar[6]pyridinium

Crystallization and microscopic observations for C4S sulfonic acid complex pillar[6]pyridinium

0.73 mg of C4S ***sulfonic acid*** was dissolved in 0.25 mL of H_2O. The solution of 0.5 mg pillar[6]pyridinium chloride in 0.25 mL of H_2O was slowly combined with the solution of the host (Figure 187a). The mixing of the aqueous solutions results in rapid clouding and precipitation of white microcrystals. In this case the liquid–liquid diffusion of layered aqueous solutions of C4S and P6P in the NMR tube has been successfully applied to slow down nucleation and obtain single crystals. Such crystallization which involves the slow diffusion of one macrocyclic component into another yielded colorless single crystals of the product. The diffraction-quality colorless prism-shape crystals (Figure 187b) were found after approx. two months. Single-crystal X-ray diffraction analysis revealed these crystals to be the host–guest complex ***C4S_P6P***.

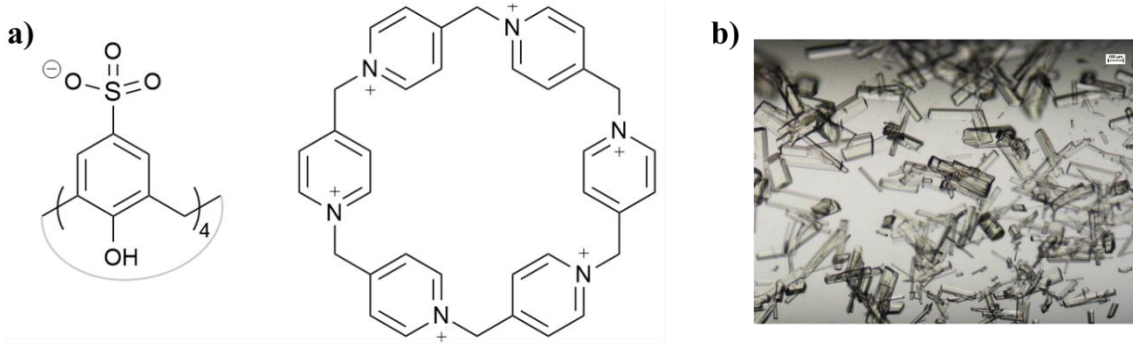

*Figure 187. (a) Chemical structure of C4S **sulfonic acid** host and pillar[6]pyridinium (**P6P**) guest; (b) photomicrograph of crystals of **C4S_P6P** complex. The scale bar corresponds to 100 µm.*

The refinement details of the C4S_P6P complex

The asymmetric unit of ***C4S_P6P*** consists of three tetra-anion C4S molecule, two pillar[6]pyridinium hexa-cations and 56.8 water molecules. The atoms of S2 > O7 sulfonate group are disordered over two positions. The first component of disorder S2 > O7 is refined with PART 1 command (29.5% occupancy), the second S2A > O7A is refined with PART 2 (70.5% occupancy).. The O13 > O15 atoms of S4 > O13 sulfonate group are disordered over two positions. The first component of disorder O13 > O15 is refined with PART 1 command (54.6% occupancy), the second O13A > O15A is refined with PART 2 (45.4% occupancy). The atoms of S11 > O41 sulfonate group are disordered over two positions. The first component of disorder S11 > O41 is refined with PART 1 command (23.2% occupancy), the second S11A > O41A is refined with PART 2 (76.8% occupancy). SADI restraint is applied to atoms of PART 1 and PART 2 to equate *S–O* distance. SIMU and RIGU restraints are applied to the disordered atoms of the C4S sulfonate groups.

C1Y > C36Y P6P molecule is disordered over two positions. The disorder is refined using PART 1 and PART 2 commands. The first component of disorder C1Y > C36Y is refined with PART 1 command (50% occupancy), the second C1A > C36A is refined with PART 2 (50% occupancy).

The disorder is fixed using SIMU, DELU and SAME restraints. The DANG restraint is applied to fix the *C16Y–C18Y* distance. Most of the water molecules in the structure are disordered. All hydrogen atoms are added geometrically and refined using a "riding model". Water molecules are refined without hydrogen atoms. The basic crystallographic data of the discussed structure is provided in Table 17.

*Table 17. Crystal data and structure refinement for **C4S_P6P** complex.*

Parameters	***C4S_P6P***
Formula moiety	$3(C_{28}H_{20}O_{16}S_4)\cdot 2(C_{36}H_{36}N_6)\cdot 56.8(H_2O)$
Formula weight	4350.75
Crystal system	Triclinic
Space group	*P–1*
a / Å	20.9250(7)
b / Å	21.5501(5)
c / Å	28.2109(6)
α / °	102.793(2)
β / °	91.143(2)
γ / °	116.562(3)
Volume / Å^3	10992.4(6)
Z	2
ρ_{calc} /g·cm^{-3}	1.31
Crystal color	Colorless
Crystal morphology	Prism
μ / mm^{-1}	1.96
θ_{max} / °	65.1
Reflections collected	84106
Independent reflections	37424 [R_{int} = 0.064]
Data / Restraints / Parameters	37424 / 2188 / 2979
Observed data [I > 2σ(I)]	19777
Final R indexes [I ≥ 2σ(I)]	R_1 = 0.114, wR_2 = 0.260
Final R indexes [all data]	R_1 = 0.180, wR_2 = 0.310
Goodness-of-fit on F^2	1.02
Largest diff. peak and hole / e·Å^{-3}	0.87 / –0.70

Structure analysis of the C4S_P6P complex

The co-crystallization of C4S ***sulfonic acid*** with pillar[6]pyridinium chloride from water result in the formation of the complex ***C4S_P6P*** with the formula $3(C_{28}H_{20}O_{16}S_4)\cdot 2(C_{36}H_{36}N_6)\cdot 56.8(H_2O)$. Single-crystal X-ray diffraction analysis shows that this complex crystallizes in a triclinic crystal system in the space group *P–1*. The asymmetric part consists of three C4S, two pillar[6]pyridinium and 56.8 water molecules (Figure 188).

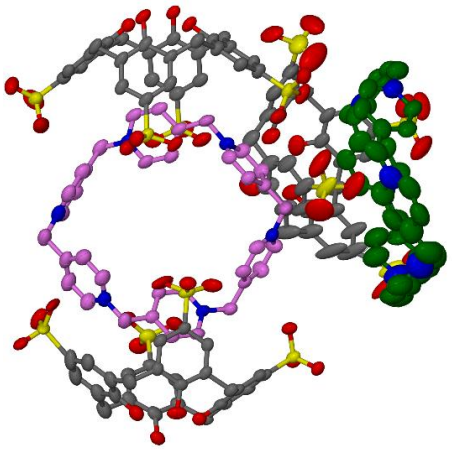

*Figure 188. The asymmetric unit of the host–guest complex **C4S_P6P**. Two crystallographically unique P6P molecules are presented in different colours. Atomic displacement parameters set at 50% probability. Water molecules, hydrogen atoms and disorder are omitted for clarity.*

In the ***C4S_P6P*** complex, one P6P molecule (pink) is sandwiched between two C4S molecules forming a *2:1 pseudocapsule*. The second P6P molecule (green) is part of an *open inclusion* complex. The P6P molecules adopt bent conformations and bind differently within the ***C4S_P6P*** complex, reflecting their varying degrees of deformation. (Figure 189). The six methylene bridges of P6P allow the molecules to bend in various ways, adapting to the conformation of C4S. As in previous complexes, the C4S macrocycle adopts a pinched cone conformation. The two C4S molecules forming the *2:1 pseudocapsule* have bowl sizes of 12.69/7.41 Å and 12.64/7.74 Å, while the C4S of the open inclusion has a size of 12.46 Å and 7.99 Å. All macrocycles exhibit a significantly pinched conformation. Intramolecular interactions at the C4S lower rims occur at *O···O* distances of 2.752(11)–2.872(7) Å (see Table 77, Annex I). The pink P6P is incorporated into the C4S cavities at inclusion depths of 4.49 Å and 4.59 Å, while the green P6P has an inclusion depth of 4.30 Å. Here, the inclusion depth is defined as the distance between the plane defined by the methylene bridges of C4S and the centroid of the pyridinium aromatic ring. Because the green P6P is deeply immersed in the most bent C4S cavity, it is forced to bend more and tilt toward the host molecule.

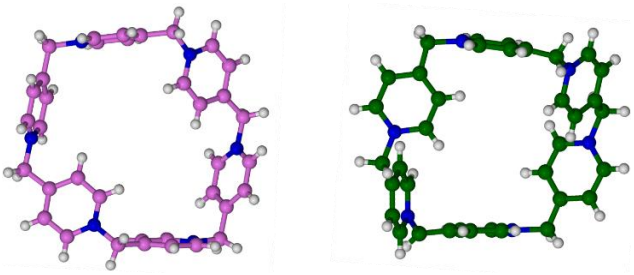

*Figure 189. Host–guest complex **C4S_P6P**: P6P molecules with the different degrees of conformational deformation.*

As part of the *pseudocapsule*, P6P molecules form non-covalent interactions with the parent C4S host molecules, including *C–H···O* and *C–H···π* contacts (Figures 190a,b). The *C–H···O* hydrogen bonds involve the carbon atoms of the P6P aromatic rings or methylene bridges and the

parent or adjacent calixarene molecules, with *C···O* distances ranging from 3.080(9) to 3.327(11) Å. In addition, P6P participates in *C–H···π* interactions with the macrocyclic host, with *C···centroid* distances between 3.352(11) and 3.584(9) Å.

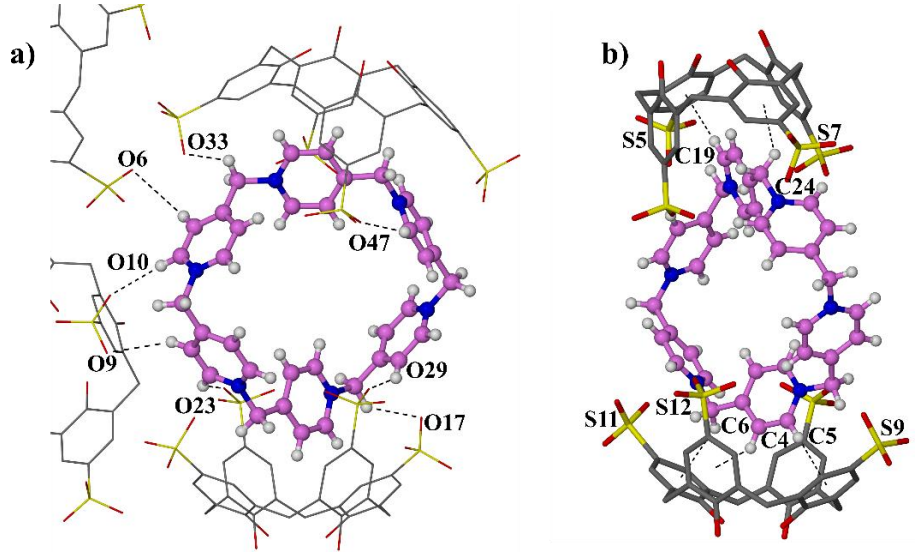

*Figure 190. Host–guest complex **C4S_P6P**: (a) C–H···O hydrogen bonds between C atoms of P6P aromatic rings and sulfonate oxygen atoms of C4S molecules; (b) C–H···π interactions between C atoms of P6P aromatic rings / methylene bridges and aromatic rings of C4S molecules.*

The cavity of P6P accommodates six water molecules arranged in a hexagonal-like pattern (Figure 191). These water molecules form a cluster and engage in hydrogen bonding with each other as well as with the sulfonate oxygen atoms of C4S, contributing to the stabilization of the overall structure. The distances between water molecules are in the range 2.59–2.88 Å.

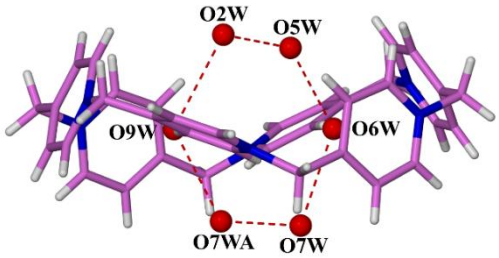

*Figure 191. Host–guest complex **C4S_P6P**: P4P molecule with included hexameric water cluster.*

The C1Y > C36Y P6P molecule, surrounded by C4S on one side, donates five *C–H···O* hydrogen bonds – two to the sulfonate oxygen atoms of the parent C4S and three to the sulfonate oxygen atoms of adjacent C4S molecules, with *C···O* distances ranging from 2.81(4) to 3.37(3) Å (Figure 192a). The P6P molecule located within the host cavity also forms two *C–H···π* contacts with the aromatic walls of the parent C4S and one with the symmetrically equivalent neighboring C4S. The distances between the carbon atoms of the P6P aromatic rings or methylene bridges and the centroids of the C4S aromatic rings are 2.93(4) Å, 3.29(2) Å, and 3.61(2) Å (Figure 192b). Additionally, a *π···π* contact between P6P and an adjacent C4S occurs at a *centroid···centroid* distance

of 3.597(15) Å (Figure 192c). The parameters of the intermolecular interactions involving P6P molecules are summarized in Tables 77–79, Annex I. Packing of the ***C4S_P6P*** complex is presented on the Figure 193.

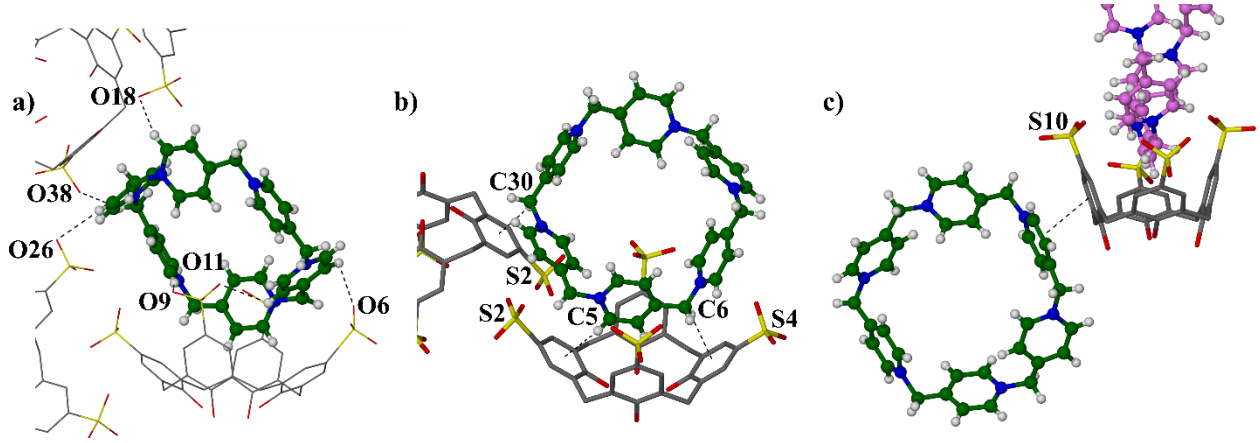

*Figure 192. Host–guest complex **C4S_P6P**: (a) C–H···O hydrogen bonds between C atoms of P6P aromatic rings and sulfonate oxygen atoms of C4S molecules; (b) C–H···π interactions between C atoms of P6P aromatic rings / methylene bridges and aromatic rings of C4S molecules; (c) π···π interactions between P4P and C4S aromatic rings.*

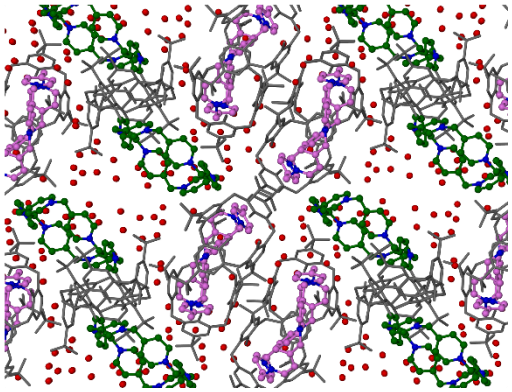

*Figure 193. Crystal packing of the host–guest complex **C4S_P6P** viewed along **–b** direction. Disorder omitted for clarity.*

Solid-state complexes of C4S with pillar[*n*]pyridiniums – discussion of results

The co-crystallization of *p*-sulfonatocalix[4]arene with pillar[*n*]pyridinium cations in aqueous media results in the formation of two distinct host–guest complexes, ***C4S_P4P*** and ***C4S_P6P***. Interestingly, two co-assemblies built from oppositely charged macrocycles are devoid of the classical hydrogen bonds, relying on the electrostatic attraction, and less conventional non-covalent interactions, as *C–H···O*, *C–H···π*, *cation···π* or *anion···π*. Although two components are macrocyclic molecules, C4S can be considered as a host molecule in both co-assemblies, as either P4P or P6P partially enter calix[4]arene cavity through their skeletons. P4P and P6P molecules hold either a single water molecule, or hexameric water cluster within their cavities, respectively. Therefore, they can be considered as macrocyclic hosts towards water molecule(s).

In the complex with the smaller pillar[4]pyridinium guest (***C4S_P4P***), charge and shape complementarity enable one P4P molecule to be included within the cavity of a C4S host. This

inclusion is capped by a second C4S molecule, resulting in the formation of a *2:1 pseudocapsule*. P4P molecule pivots into two C4S cavities through two methylene bridging groups, while pyridinium aromatic rings stay near C4S anionic rims. The pseudocapsule is stabilized by *C–H···O* hydrogen bonds between the host and guest, as well as by a water molecule occupying the cavity of the P4P guest. A second P4P molecule remains outside the calixarene cavity but is linked to the assembly through hydrogen bonding and $\pi\cdots\pi$ interactions involving C4S and water molecules.

In contrast, the ***C4S_P6P*** complex exhibits a more intricate architecture due to the larger size and conformational flexibility of the pillar[6]pyridinium guest. One P6P molecule is encapsulated between two C4S hosts to form a pseudocapsule, while a second P6P participates in an open inclusion complex. In both instances, it is the P6P pyridinium ring that enters the C4S cavity, inducing strong pinching of C4S cones. Both P6P molecules adopt distinct bent conformations to be accommodated within calixarene cavities. Notably, the P6P guest within the pseudocapsule encloses a hexameric water cluster inside its own cavity.

4.4 *p*-Sulfonatocalix[8]arene complexes with sodium cations and berberine

In this chapter, two examples of the successful incorporation of *p*-sulfonatocalix[8]arene into crystalline complexes with cationic species are described: a coordination complex with sodium cations and a host–guest complex with berberine. The aim of this study was to investigate how C8S self-assembles with guests of different nature and to identify the intermolecular forces governing complex formation. Previous studies have reported crystalline sodium complexes of C4S and C6S, as well as solution complexation of C8S and sodium cations, as described in the Literature Review chapter. However, no crystallographic proof of the sodium complexation by C8S has been reported. As part of this dissertation, the structural evidence on the interaction of the sodium counterions with C8S giving rise to 3-D coordination polymer has been provided. Berberine considered as potential guest for C8S macrocycle, possesses a permanent cationic charge as it is a quaternary ammonium cation. From the crystal engineering viewpoint, berberine molecule does not have the reliable supramolecular synthon. However, the combination of its permanent charge and large hydrophobic surface with aromatic systems could have some benefits for the solid state design. It can be anticipated that oligo-anionic macrocyclic host molecule C8S of large hydrophobic cavity and surface can be potential candidate for the berberine complexation in the crystal state.

The C8S complexes with sodium and berberine cations are reported in the article ***"p-Sulfonatocalix[8]arene Coordinates Sodium Cations and Forms Host–Guest Complex with Berberine: Insight from Crystal Structure"***, published in *Supramolecular Chemistry*.

4.4.1 C8S complex with sodium cations

Crystallization and microscopic observations for C8S sodium complex

5 mg of C8S ***sodium salt*** was dissolved in 1 mL of H_2O. To obtain single crystals the slow diffusion method of ethanol vapours into an aqueous solution of C8S has been applied. The colorless prism-shape diffraction-quality crystals were found after one week. Single-crystal X-ray diffraction analysis revealed these crystals to be the host–guest complex ***C8S_Na*** (Figure 194).

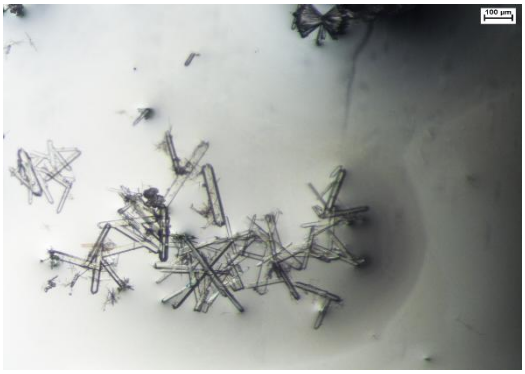

*Figure 194. Photomicrograph of crystals of **C8S_Na** complex. The scale bar corresponds to 100 µm.*

The refinement details of the C8S_Na complex

The determination of the crystal structure presented challenges due to twinning by pseudo–merohedry. Initial indexing of the diffraction pattern suggested a primitive hexagonal unit cell. However, all attempts to solve the structure within hexagonal or trigonal symmetry were unsuccessful. A chemically plausible structural model, featuring four C8S molecules in the asymmetric unit, was identified in the *P–1* space group. A thorough symmetry analysis indicated the possibility of a monoclinic crystal system, and the structure was successfully solved in the *C2/c* space group. The crystal was twinned by pseudo-merohedry with the twin law defined as (–1 0 0 0 –1 0 1 0 1). The twin component was refined using the TWIN and BASF instructions in SHELXL, yielding a refined twin of 13.19%. This correction was essential to achieve a satisfactory refinement and accurate structural model.

The asymmetric unit of ***C8S_Na*** consists of two halves of octa-anionic C8S molecule, positioned on the 2-fold axis, and eight sodium cations distributed over nine sites and 18 water molecules (15 of which are aqua ligands). The Na5 and Na9 sodium cations refined with the 50% occupancy. The O4W water molecule is disordered over two positions. The first component of disorder O4W is refined with PART 1 command (86% occupancy), the second O4A is refined with PART 2 command (14% occupancy). O10W and O12W molecules are disordered over two positions (the component of PART 1 occupies 50%, PART 2 – 50%). The O11W molecule is refined with 50% occupancy in PART 1 with O10W and O12W molecules. The O13W water molecule is disordered over two positions. The first component of disorder O13W is refined with PART 1 command (50%

occupancy), the second O13A is refined with PART 2 command (50% occupancy). The O14W water molecule is disordered over two positions. The first component of disorder O14W is refined with PART 1 command (60.7% occupancy), the second O14A is refined with PART 2 command (39.3% occupancy). The O15W and O16W molecules lies close to the 2-fold axis and refined with 50% occupancy. All hydrogen atoms are added geometrically. Water molecules are refined without hydrogen atoms. Some residual electron density is associated with unaccounted disorder of water solvent molecules in the water channels. The basic crystallographic data of the discussed structure is provided in Table 18.

*Table 18. Crystal data and structure refinement for **C8S_Na** complex.*

Parameters	***C8S_Na***
Formula moiety	$[2(Na_8(C_{56}H_{40}O_{32}S_8)\cdot 15(H_2O)]\cdot 3(H_2O)$
Formula weight	3925.08
Crystal system	Monoclinic
Space group	*C2/c*
a / Å	44.4373(14)
b / Å	9.1248(2)
c / Å	44.5808(15)
α / °	90
β / °	119.828(4)
γ / °	90
Volume / Å^3	15681.9(1)
Z	4
ρ_{calc} /g·cm^{-3}	1.66
Crystal color	Colorless
Crystal morphology	Prism
μ / mm^{-1}	3.51
θ_{max} / °	71.0
Reflections collected	69547
Independent reflections	14925 [R_{int} = 0.073]
Data / Restraints / Parameters	14925 / 0 / 1124
Observed data [I > 2σ(I)]	10153
Final R indexes [I ≥ 2σ(I)]	R_1 = 0.096, wR_2 = 0.258
Final R indexes [all data]	R_1 = 0.129, wR_2 = 0.300
Goodness-of-fit on F^2	1.07
Largest diff. peak and hole / e·Å^{-3}	1.55 / –1.19

Structure analysis of the C8S_Na complex

The crystallization of C8S ***sodium salt*** *via* slow diffusion of ethanol vapours into an aqueous calixarene solution result in the formation of the complex ***C8S_Na*** with the formula $[2(Na_8(C_{56}H_{40}O_{32}S_8)\cdot 15(H_2O)]\cdot 3(H_2O)$. Single-crystal X-ray diffraction analysis reveals that this complex crystallizes in monoclinic crystal system in the space group *C2/c*. The asymmetric unit comprises two halves of the C8S macrocycles, eight sodium cations distributed over nine sites and 18 water molecules (15 of which are aqua ligands) (Figure 195).

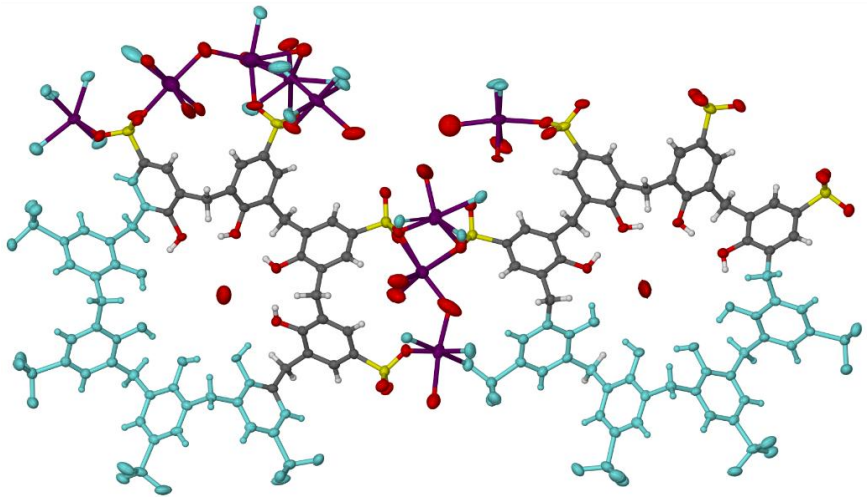

*Figure 195. The asymmetric unit of the **C8S_Na** complex with the expanded C8S and water molecules. Two crystallographically non–equivalent macrocycles reside on the 2-fold axis, the light blue corresponds to symmetry generated part of the structure. Atomic displacement parameters set at 50% probability. Disorder omitted for clarity.*

In the sodium complex, the two macrocycles adopt similar pleated-loop conformations (Figure 196b). The conformation is stabilized by a circular array of intramolecular hydrogen bonds between the oxygen atoms on the lower rims of the macrocycles (Figure 196a). The *O···O* distances of these intramolecular hydrogen bonds range from 2.640(7)–2.691(8) Å for the first C8S molecule and from 2.674(7)–2.727(9) Å for the second (Table 80, Annex I). Each calixarene also contains a disordered water molecule at its center.

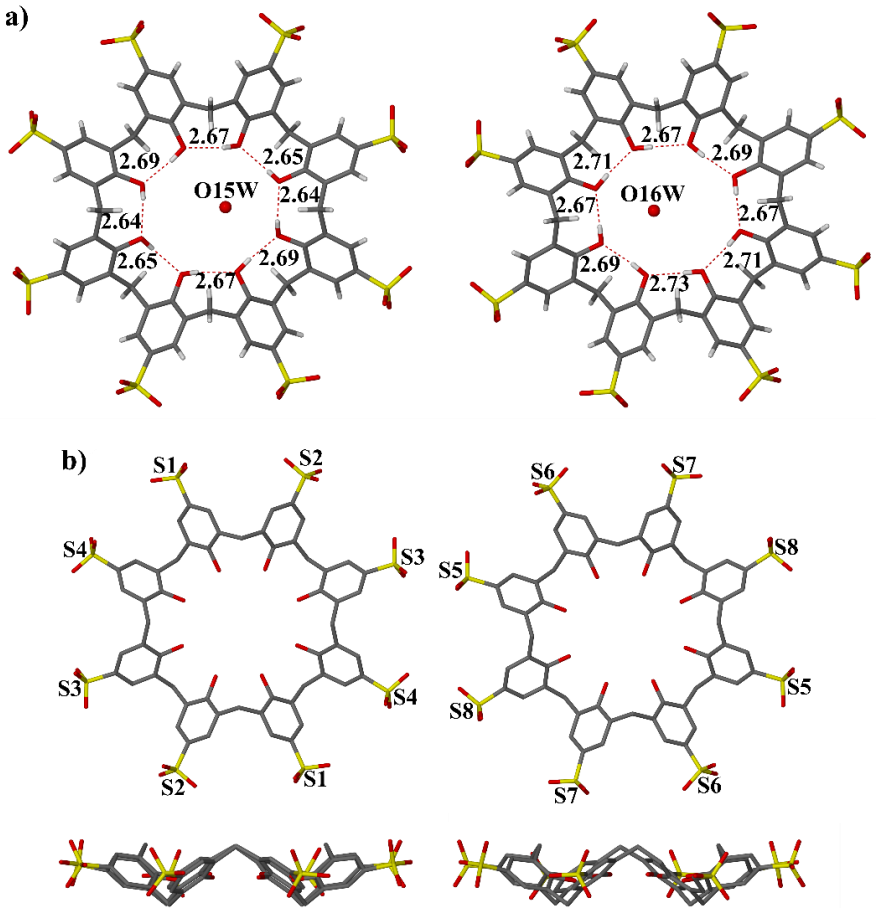

*Figure 196. Host–guest complex **C8S_Na**: (a) O–H···O hydrogen bonding at the C8S lower rims. O···O distances are given in Å; (b) the pleated-loop conformation of the C8S molecules, front (top) and the side (bottom) views.*

The expanded crystal structure demonstrates that the two symmetry-independent calixarene molecules are stacked in a tubular arrangement, positioned one above the other. As shown in Figures 197a,b, macrocycles are slightly offset by approximately 5°.

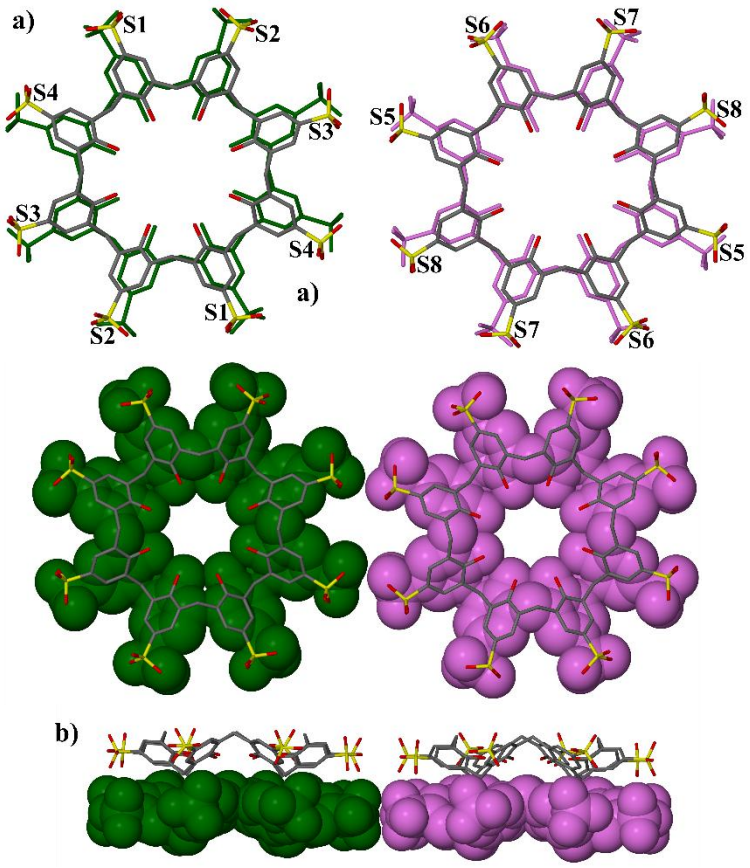

*Figure 197. Host–guest complex **C8S_Na**: the stacking of adjacent macrocycles into tubular structure, the crystallographically non–equivalent C8S molecules (in green and pink) are rotated around 5° in respect to one other, the front (a) and side (b) views.*

Calixarenes stack to form tubular columns that are stabilized by *C–H···π* interactions. These occur between the carbon atoms of the methylene bridges and the aromatic rings within the calixarene framework (Figure 198). The distances between the carbon atoms of the C8S units and the centroids of the aromatic rings range from 3.492(8) to 3.774(9) Å. The geometrical parameters of these interactions between the C8S molecules are summarized in Table 82, Annex I.

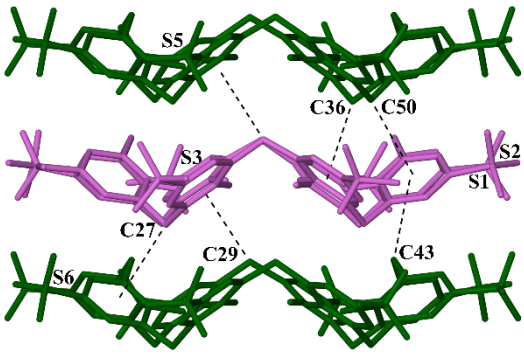

*Figure 198. Host–guest complex **C8S_Na**: the stacking of adjacent C8S molecules into tubular structure sustained by C–H···π interaction between the C atoms of the C8S methylene bridges and macrocycles aromatic rings.*

Each Na^+ ion in the ***C8S_Na*** complex coordinates with six or seven oxygen atoms from sulfonate groups in both parent and neighbouring C8S units and with water molecules, with *Na···O* bond lengths ranging from 2.178(13) to 2.883(11) Å (Table 81, Annex I). These cations surround the

C8S molecules, facilitating the formation of a 3D coordination polymer (Figure 199a). As a result of these interactions, the complex crystallizes in a pseudo-hexagonal arrangement, observed along the ***b*** axis in Figure 199b. Adjacent macrocycles stack on top of each other, with Na^+ ions linking one C8S unit to six surrounding macrocycles. The central cavities of the C8S molecules are filled with water solvent molecules.

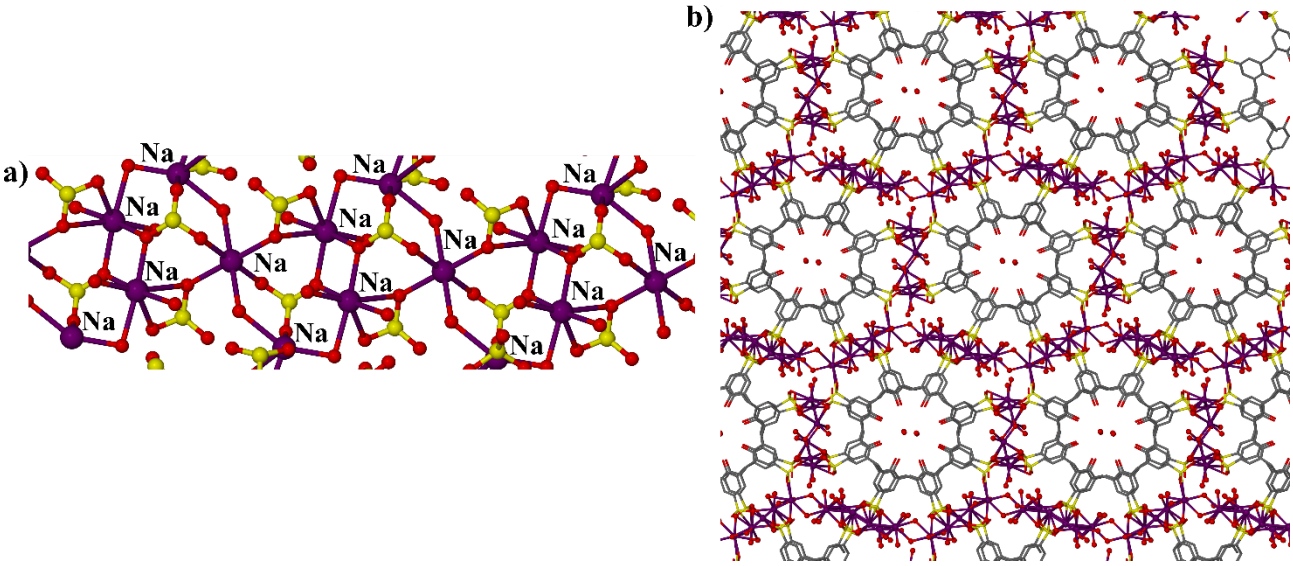

*Figure 199. Host–guest complex **C8S_Na**: (a) a part of the sodium cation network weaved through the tubular stacks of C8S molecules; (b) crystal packing of the host–guest complex viewed along **b** direction.*

4.4.2 C8S complex with berberine

Crystallization and microscopic observations for C8S sulfonic acid complex with berberine

10 mg of C8S ***sulfonic acid*** was dissolved in 0.5 mL of H_2O. The solution of 2.5 mg berberine chloride in 0.5 mL of H_2O was combined with the solution of the host (Figure 200a). The mixing of the aqueous solutions at the room temperature results in rapid yellow clouding and precipitation. In this case, the tube containing the solution was immersed in hot glycerin using isothermal equipment to slow nucleation and facilitate the growth of high-quality single crystals. The yellow plates of diffraction-quality crystals were found after one week. Single-crystal X-ray diffraction analysis revealed these crystals to be the host–guest complex ***C8S_Berb*** (Figure 200b).

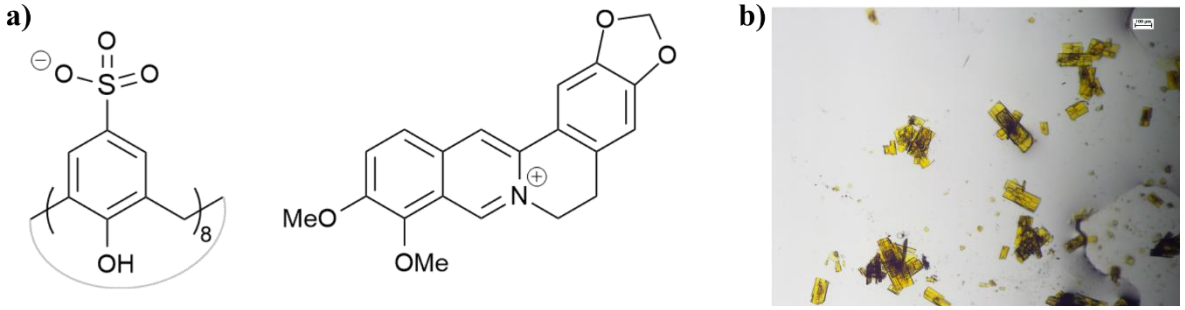

*Figure 200. (a) Chemical structure of C4S **sulfonic acid** host and berberine (**Berb**) guest; (b) photomicrograph of crystals of **C8S_Berb** complex. The scale bar corresponds to 100 µm.*

The refinement details of the C8S_Berb complex

The asymmetric unit of ***C8S_Berb*** consists of half octa-anionic C8S molecule, positioned on the inversion centre, four berberine cations and 12.94 water molecules. Atoms of one of C4S sulfonate group are disordered over two positions. The first component of disorder O5 > S2 is refined with PART 1 command (82.3% occupancy), the second O5A > S2A is refined with PART 2 (17.7% occupancy). Two berberine molecules are disordered over two positions. The first component of the disorder C1I > O4I occupies 73.9% (PART 1 command is applied), the second component of the disorder C1A> O4A occupies 26.1% (PART 2 command is applied). Disorder of berberine C1I > O4I molecule is solved using SIMU, RIGU and SAME restraints. The first component of disordered berberine molecule C1Z > O4Z is refined with PART 1 command (73.6% occupancy), the second C1B > O4B is refined with PART 2 command (26.4% occupancy). SIMU and RIGU restraints are applied.

Water molecules O11W, O12W, O13W and O14W lie close to the disordered C1Z > O4Z berberine molecule. The O11W is disordered over two positions. The first component of disorder O11W is refined with PART 1 command (73.6% occupancy), the second O11A is refined with PART 2 command (26.4% occupancy). The O12W water molecule also is disordered over two positions. The first component of disorder O12W is refined with 50% occupancy and the second O12A is refined with 20% occupancy. O13W and O14W molecules in PART 1 refined with 50%, and 73.6% occupancies respectively. Hydrogen atoms are placed on geometrically calculated positions and refined using a riding model. Water molecules are refined without hydrogen atoms. The basic crystallographic data of the discussed structure is provided in Table 19.

*Table 19. Crystal data and structure refinement for **C8S_Berb** complex.*

Parameters	***C8S_Berb***
Formula moiety	$C_{56}H_{40}O_{32}S_8 \cdot 8(C_{20}H_{18}NO_4) \cdot 25.87(H_2O)$
Formula weight	4638.27
Crystal system	Triclinic
Space group	*P–1*
a / Å	13.5622(8)
b / Å	15.6116(7)
c / Å	25.1821(16)
α / °	93.430(4)
β / °	99.859(5)
γ / °	92.719(4
Volume / Å^3	5234.6(5)
Z	1
ρ_{calc} /g·cm^{-3}	1.47
Crystal color	Yellow
Crystal morphology	Plate
μ / mm^{-1}	1.68
θ_{max} / °	61.2
Reflections collected	31434
Independent reflections	15712 [R_{int} = 0.087]
Data / Restraints / Parameters	15712 / 2682 / 1925
Observed data [I > 2σ(I)]	8344
Final R indexes [I ≥ 2σ(I)]	R_1 = 0.081, wR_2 = 0.187
Final R indexes [all data]	R_1 = 0.156, wR_2 = 0.242
Goodness-of-fit on F^2	1.05
Largest diff. peak and hole / e·Å^{-3}	0.92 / –0.41

Structure analysis of the C8S_Berb complex

The co-crystallization of C4S ***sulfonic acid*** with berberine hydrochloride from water–results in the formation of the complex ***C8S_Berb*** with the formula $C_{56}H_{40}O_{32}S_8 \cdot 8(C_{20}H_{18}NO_4) \cdot 25.87(H_2O)$. Single-crystal X-ray diffraction analysis shows that this complex crystallizes in triclinic crystal system in the space group *P–1*. The asymmetric part consists of half of C8S, four berberine and 12.94 water molecules (Figure 201).

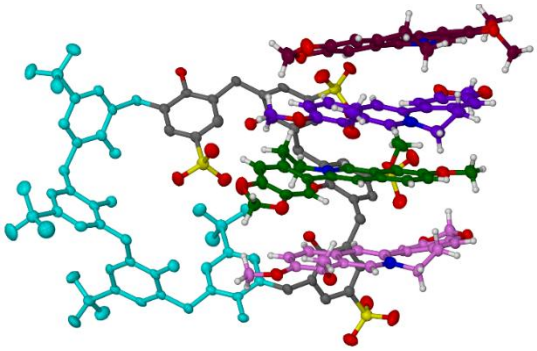

*Figure 201. The asymmetric unit of the **C8S_Berb** complex with the expanded C8S molecule. The macrocycle lies over an inversion centre, the light blue corresponds to symmetry generated half of the calix[8]arene. Four crystallographically unique berberine*

molecules are presented in different colours. Atomic displacement parameters set at 50% probability. Disorder and water molecules omitted for clarity.

In the C8S–berberine complex, the host molecule adopts a self-closed conformation without a large molecular cavity for classical host–guest inclusion (Figure 202a,b). The hydroxyl groups of C8S form four hydrogen bonds with the O1W and O6W molecules, two intramolecular hydrogen bonds between hydroxyl groups as well as two intermolecular hydrogen bonds between hydroxyl and sulfonate calixarene groups (Figure 202c). The *O···O* distances are ranging from 2.609(7) to 2.757(7) (Table 83, Annex I). O2W and O6W water molecules are located in the surface grooves on either side of the macrocycle, where O2W forms hydrogen bonds with the two sulfonate groups (S4) oriented toward the macrocyclic center.

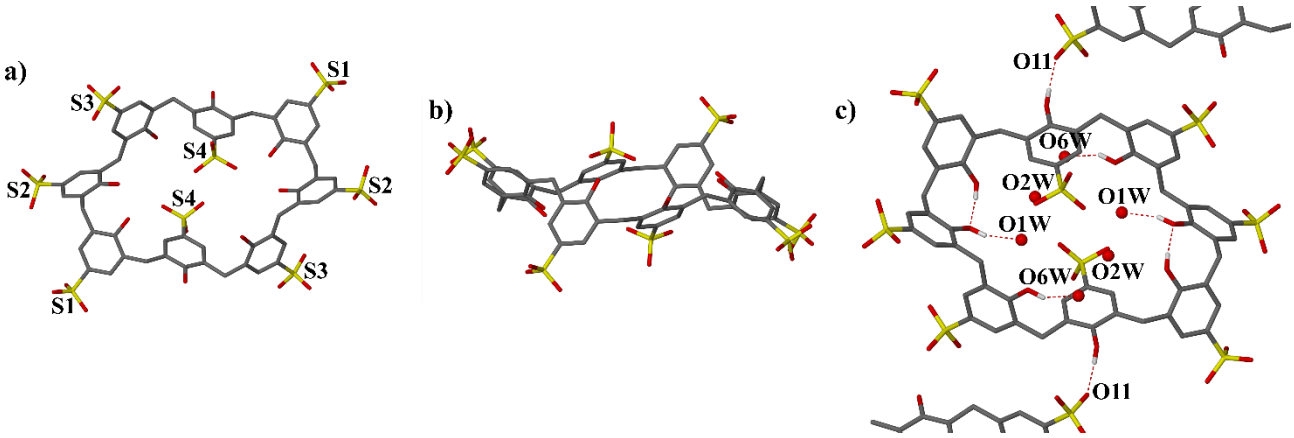

*Figure 202. Host–guest complex **C8S_Berb**: (a,b) views on self-closed conformation of the C8S. Two opposite phenolsulfonate groups are oriented to the centre of the macrocycle thus closing the molecular cavity; (c) O–H···O hydrogen bonding at the C8S lower rim.*

As shown in Figure 203a, the macrocyclic host C8S does not feature a well-defined cavity to accommodate berberines. However, the presence of grooves on its surface facilitates the complexation of eight berberine cations per macrocycle. The edges of the berberine molecules engage in *C–H···O* interactions with the C8S. These interactions occur in various ways. Berberine binds to the host molecule (C8S) through multiple interaction modes. These include contacts *via* both the aromatic and non-aromatic carbon atoms of berberine with the sulfonate groups of calixarene, as well as interactions between the methoxy– group of berberine and the aromatic rings of the host. Additionally, the dioxolo– group of berberine engages with the calixarene aromatic rings. In addition, two berberines (C1I > O4I and C1X > O4X) participate in *C–H···O* interactions with each other by the carbon atom of methylene group and the oxygen atom of the dioxolo– group with a *C···O* distance of 3.232(18) Å, as illustrated in Figure 203b. Positioned within the grooves of C8S, the berberines assemble into stacks oriented approximately perpendicular to the C8S surface. These stacks, when placed *head-to-tail*, interact with neighboring water molecules, as shown in Figure 203c with *C···O* distances in the range 3.291(15)–3.346(11) Å.

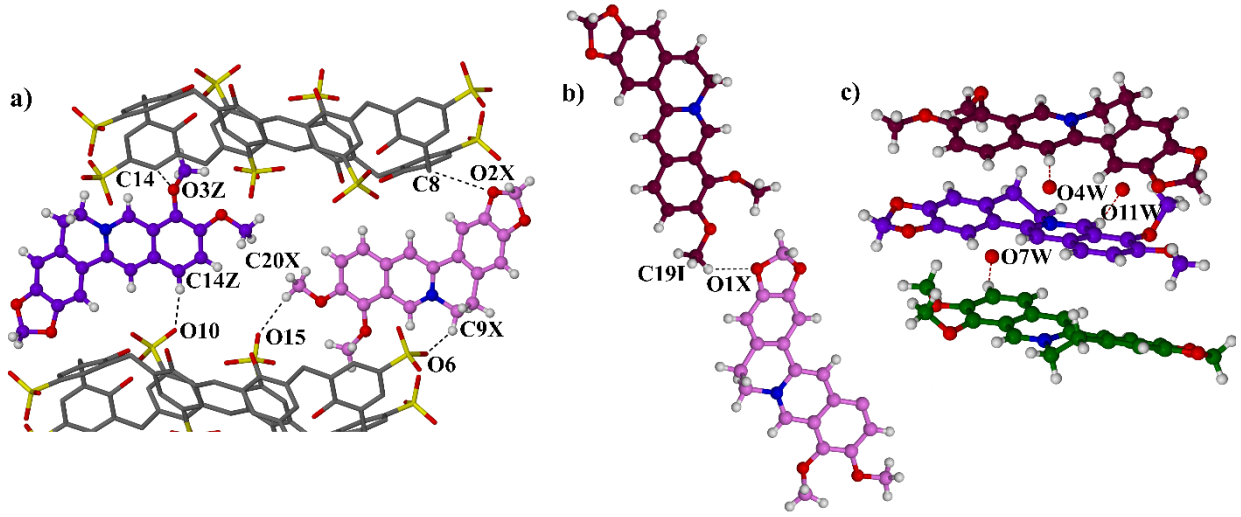

*Figure 203. Host–guest complex **C8S_Berb**: (a) different types of the C–H···O hydrogen bonding between berberine and calixarene molecules; (b) C–H···O hydrogen bond between C atom of C1I > O2I berberine methylene group and O atom of C1X > O2X berberine dioxolo– group; (c) C–H···O hydrogen bonds between berberines and water molecules.*

The berberine molecules which are positioned *head-to-tail*, facilitating *π···π* interactions between their aromatic rings. The distances between the centroids of the aromatic rings are in the range from 3.719(8) to 4.06 Å (Figure 204a). In addition, two berberine molecules C1I > O4I and C1Z > O4Z establish *C–H···π* interactions at distances of 3.396(11) Å and 3.382(13) Å, as depicted in the Figure 204b. The berberines positioned within the C8S layers not only engage in *C–H···O* interactions with the host but also participate in *C–H···π* interactions, formed *via* the carbon atoms of the berberine "edges" and the aromatic rings of the macrocyclic host (Figure 204). The corresponding *C···centroid* distances for these interactions are 3.381(10) Å, 3.633(15) Å and 3.486(7) Å. The detailed overview on the parameters of non-covalent interactions formed by the berberine molecules presented on the Tables 83–85, Annex I.

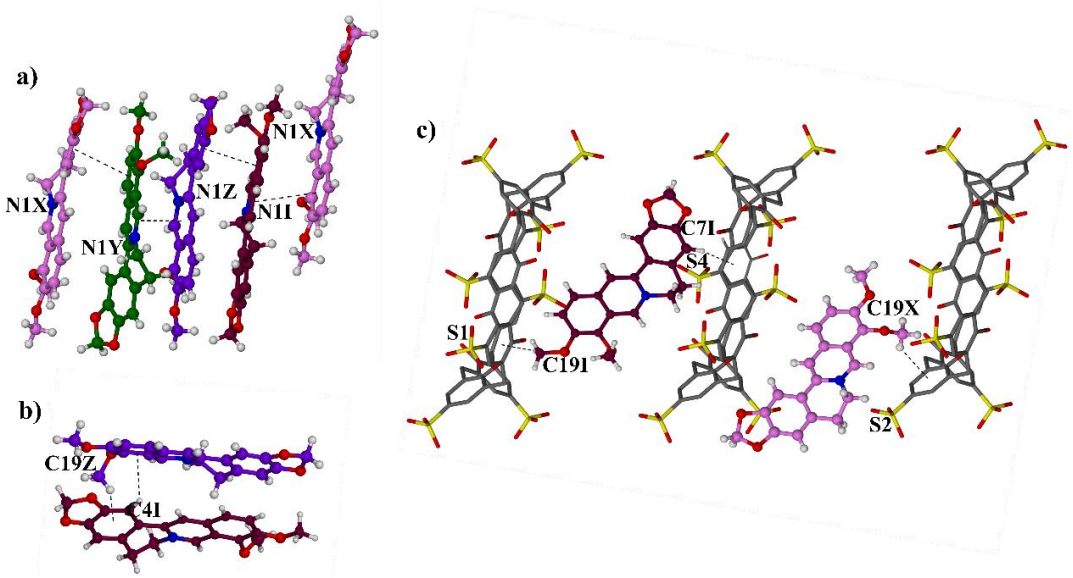

*Figure 204. Host–guest complex **C8S_Berb**: (a) π···π interaction between aromatic rings of berberine molecules; (b) C–H···π interactions between C atoms and aromatic rings of berberine molecules; (c) C–H···π interactions between C atoms of berberine and aromatic rings of C8S molecules.*

The expanded view of the crystal structure shows that the berberine molecules are "sandwiched" between the C8S macrocycles (Figure 205a), that is clearly visible in the crystal packing when viewed along ***a*** and ***b*** directions (Figure 205b,c).

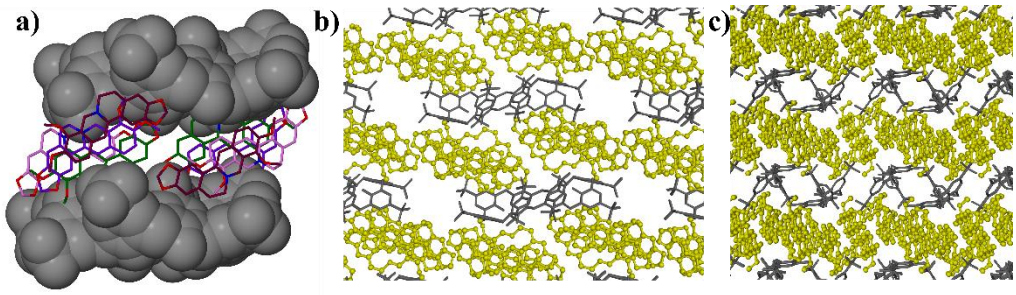

*Figure 205. Host–guest complex **C8S_Berb**: (a) eight berberine molecules stacked between grooves and clefts of adjacent C8S (grey) macrocycles; (b) crystal packing displaying alternating layers of anionic C8S and cationic berberines (yellow) along **a** and **b** directions. Water molecules omitted for clarity.*

TGA–DSC analysis of the C8S_Berb complex

To study the thermal behavior of the host–guest crystals of the ***C8S_Berb*** complex, TGA and DSC measurements were performed on single crystals air-dried for 1 h under ambient conditions (Figure 206). The thermogravimetric curve shows two main weight-loss steps for the ***C8S_Berb*** solid-state complex. Up to 120 °C, the sample loses about 10.4% of its mass due to the removal of water from the crystal lattice. This dehydration occurs in several small steps, which is also reflected in the DSC curve by four exothermic peaks with small areas. The experimental mass loss (10.4%)

agrees well with the calculated value (10%) for water removal from the crystal structure. Decomposition of the complex starts at 322 °C, as indicated by both the TGA and DSC curves.

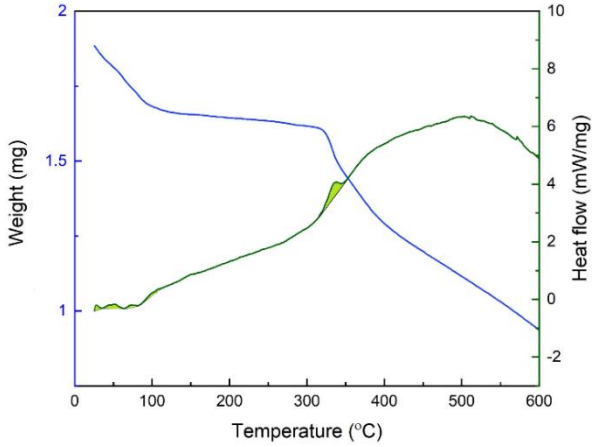

*Figure 206. TGA (blue) and DSC (green) curves of the **C8S_Berb** complex.*

NMR analysis of the C8S_Berb complex

The interaction between berberine and C8S in aqueous solution was further studied using ^{1}H NMR spectroscopy. The inclusion of berberine in the calix[8]arene cavity was confirmed by an upfield shift in all proton resonances of berberine upon the addition of the macrocyclic host (Figure 207). This observation is in good agreement with the crystal structure, where numerous *C–H···O* and *C–H···π* interactions are observed between berberine and the molecular surface of C8S, that nicely confirm the nature of the host–guest interactions.

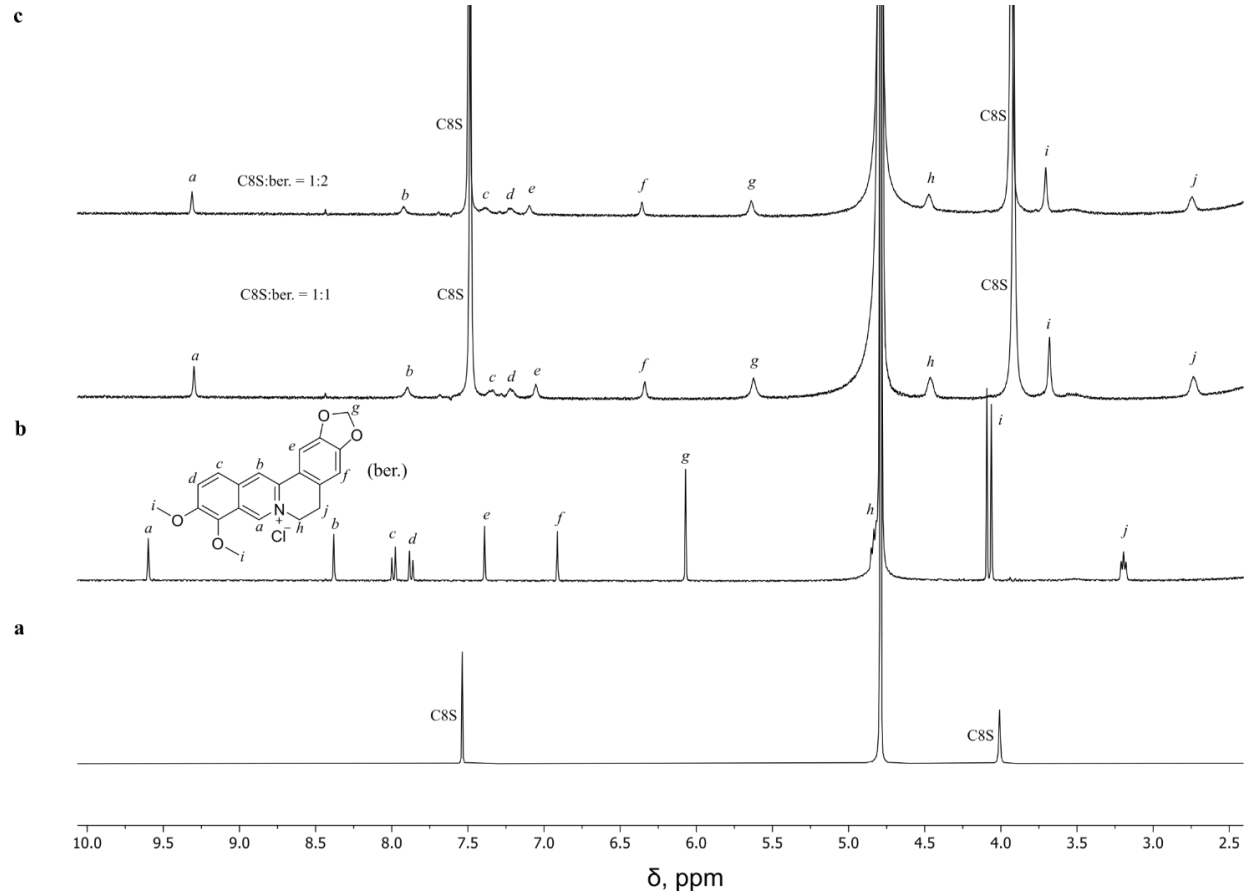

Figure 207. [1]H NMR spectra of (a) C8S ***sulfonic acid****; (b) berberine; (c)* ***C8S_Berb*** *host–guest complex recorded on Agilent 400 MHz instrument at room temperature in 0.5 M Acetate buffer, pH = 5.03 (in D_2O). C(C8S) = 1 mM, C(Berb) = 1 mM; at the host–guest ratio 1:2 the precipitation starts to occur.*

Solid-state complexes of C8S with sodium and berberine – discussion of results

Structural characterization of *p*-sulfonatocalix[8]arene complexes with sodium and berberine cations reveals two distinct modes of host–guest interaction and supramolecular assembly, highlighting the macrocycle's adaptability toward both organic and inorganic species.

Sodium complexes with smaller sulfonated calixarenes, such as C4S and C6S, have been reported previously (refcodes REBYEE and VUNHAN).[106,97] However, the ***C8S_Na*** complex described here represents the first sodium complex involving the larger *p*-sulfonatocalix[8]arene macrocycle. In this structure, the C8S macrocycles adopt a pleated-loop conformation, stabilized by a circular network of intramolecular hydrogen bonds and coordination to sodium ions. Each sodium cation coordinates to sulfonate groups and water molecules, thereby linking neighboring C8S units into a three-dimensional coordination polymer. Sodium ions thus play a central role in the architecture, effectively "stapling" the macrocycles together into a continuous network. The resulting coordination polymer exhibits pseudo-hexagonal crystal packing, characterized by tubular columns of stacked calixarene macrocycles. These columns are further stabilized by *C–H···π* interactions

between adjacent macrocycles. The macrocycles are stacked almost directly on top of one another, forming dense, elongated tubular arrays that extend along *b* axis (Figure 208a).

Flood *et al.*[138] reported crystal structure of C8S sodium salt obtained from sodium citrate at pH 4–6 via hanging drop vapor diffusion. In this structure, the macrocycles adopt the same pleated-loop conformation undergoing a staggered (or staircase) packing arrangements (Figures 208b). The staggered packing motifs observed resemble those in protein–C8S co-crystals, highlighting the versatility of C8S as a supramolecular synthon that can adapt its packing to different guests and environments.

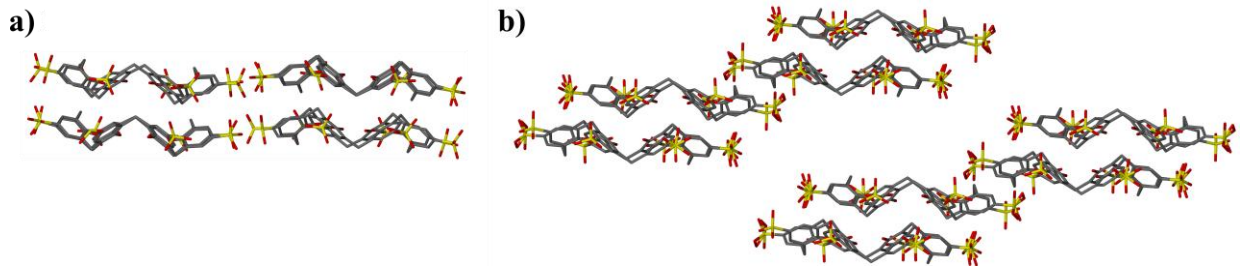

Figure 208. Comparison of C8S arrangements in (a) ***C8S_Na*** *complex along* ***a*** *direction and (b) C8S sodium salt complex (refcode KONSAL) along* ***b*** *direction.*

In the ***C8S_Berb*** complex, the macrocyclic host adopts a self-closed[143] conformation without a traditional macrocyclic cavity. Berberine cations are accommodated within grooves on the host framework, where they engage in various non-covalent interactions, including *C–H···O* and *C–H···π* contacts with the calixarene, as well as *π···π* stacking among themselves. ^{1}H NMR studies in aqueous solution further confirm the effective incorporation of berberine into the surface grooves of the C8S host. Notably, the structure of the ***C8S_Berb*** complex represents the first reported (refcode XEXVAB) example of a host–guest complex with the berberine in the solid state.[197]

4.5 *p*-Sulfonatocalix[8]arene complexes with iproniazid

In this chapter, the crystal complex between C8S and iproniazide featuring "open" supramolecular structure with large water-filled channels is described. Iproniazide as a guest of choice bears two different cationic sites – protonated hydrazine group and pyridinium ring, both are potential hydrogen bond donors. Thus, the supramolecular synthons of charge-assisted hydrogen bonds of pyridinium–sulfonate and hydrazinium–sulfonate type can be expected to guide the complexation and self-assembly with anionic C8S. It can be reasoned that the mismatch between hydrogen bond donors (separated as two hydrazinium donors and one pyridinium) and multiple hydrogen bond acceptors (oxygen atoms of eight sulfonate groups of C8S upper rim) would potentially translate into incorporation of a large number of water molecules into the supramolecular structure. Indeed, it has been found that C8S–iproniazide cocrystallization favors the solid state complex of large water galleries with iproniazide molecules acting as pillars holding open supramolecular framework.

Further dehydration studies have shown that the crystals can undergo single-crystal to single-crystal transformation into close supramolecular structure. The single crystallinity is preserved upon the transformation, a rare observation in the hydrogen bonded organic frameworks.

Crystallization and microscopic observation of C8S sulfonic acid complexes with iproniazid

20 mg of C8S ***sulfonic acid*** was dissolved in 0.5 mL of H_2O,15 mg iproniazid phosphate in 0.5 mL of H_2O was combined with the solution of the host (yellowish solution). After approx. one-week colorless prism-shaped crystals of a good diffraction quality appeared. Single-crystal X-ray diffraction analysis revealed these crystals to be the host–guest complex ***C8S_IPR_I*** (Figure 209).

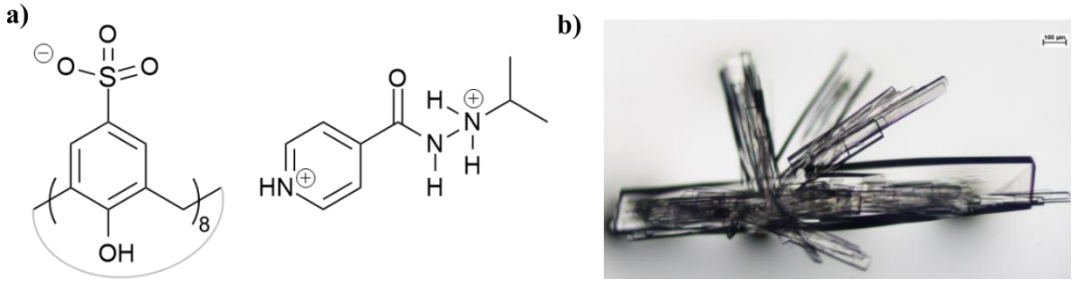

*Figure 209. (a) Chemical structure of C8S **sulfonic acid** host and iproniazid (**IPR**) dication guest; (b) photomicrograph of crystals of **C8S_IPR_I** complex. The scale bar corresponds to 100 µm.*

The crystals of the ***C8S_IPR_I*** complex were then taken from the mother solution and dried on the glass plate at room temperature for approximately one day. Single-crystal X-ray diffraction analysis revealed that the dried crystals correspond to the partially desolvated host–guest complex ***C8S_IPR_II***.

The refinement details of the C8S_IPR complexes

The asymmetric unit of ***C8S_IPR_I*** consist of 1/2 molecule of C8S octa-anion, positioned on the inversion centre, and two dications of iproniazid and 16.45 water molecules. The O17W molecule is refined with PART 1 command (80.9% occupancy), the second component of disorder O17A is refined with PART 2 command (19.1% occupancy). The O11W molecule is refined in PART 1 with 80.9% occupancy. The O12W, O13W, O14W and O18W water molecules are positioned close to each other. The O12W, O13W are disordered over two positions. The first components of disordered O12W and O13W molecules are refined with PART 1 command (56.8% occupancy), the second O12A and O13A are refined with PART 2 command (43.2% occupancy). The O14W molecule is refined in PART 1 with 56.8% occupancy. The O18W molecule is refined in PART 1 with 25% occupancy. The O15W molecule is refined with PART 1 command (81.7% occupancy), the second O15A is refined with PART 2 command (18.3% occupancy). The O16W molecule is refined in PART 1 with 81.7% occupancy. All hydrogen atoms are added geometrically. The O3W, O4W, O5W, O7W, O12W > O17W water molecules are refined without hydrogen atoms. Residual electron density peaks

(~1.3 $e^-/Å^3$) observed near Sulphur atoms are attributed to Fourier truncation effects, common with heavier atoms with no evidence of twinned structure or disorder.

The asymmetric unit of ***C8S_IPR_II*** consist of 1/2 molecule of C8S octa-anion, positioned on the inversion centre, and two dications of iproniazid and 3 water molecules. Atom of one of C8S sulfonate group is disordered over two positions. The O15 atom is refined with PART 1 command (54% occupancy), the second O15A is refined with PART 2 command (46% occupancy). Disorder is refined using SIMU RIGU and SADI restraints. C1Y > O1Y iproniazid N–isopropyl group is disordered over two positions. First component of disorder C7Y > N3Y is refined with PART 1 command (64%), second component of disorder C7A > N3A is refined using PART 2 command (36%). Disorder is refined using SIMU, RIGU and SADI restraints. The O3W is refined with PART 1 command (59.2% occupancy), the second O3A is refined with PART 2 command (40.8% occupancy). Hydrogen atoms in the structure are added geometrically. The O3W water molecule is refined without hydrogen atoms. The residual electron density peak (~1.4 $e^-/Å^3$) corresponds to a disordered water molecule with 25% occupancy and was therefore not included in the crystal structure. The basic crystallographic data of the discussed structures is provided in Table 20.

*Table 20. Crystal data and structure refinement for **C8S_IPR** complexes **I** and **II.***

Parameters	***C8S_IPR_I***	***C8S_IPR_II***
Formula moiety	$C_{56}H_{40}O_{32}S_8 \cdot 4(C_9H_{15}N_3O)$ $\cdot 32.89(H_2O)$	$C_{56}H_{40}O_{32}S_8 \cdot 4(C_9H_{15}N_3O)$ $\cdot 6(H_2O)$
Formula weight	2798.81	2314.41
Crystal system	Triclinic	Triclinic
Space group	*P–1*	*P–1*
a / Å	13.3094(2)	13.1478(5)
b / Å	16.3889(4)	14.1514(7)
c / Å	16.6134(3)	14.9264(8)
α / °	112.951(2)	69.246(5)
β / °	95.9200(1)	85.037(4)
γ / °	100.278(2)	76.271(4)
Volume / Å³	3223.20(12)	2522.8(2)
Z	1	1
ρ_{calc} ***/g·cm⁻³***	1.44	1.52
Crystal color	Colorless	Colorless
Crystal morphology	Prism	Prism
μ / mm⁻¹	2.21	2.50
θ_{max} ***/ °***	68.2	68.3
Reflections collected	37008	16454
Independent reflections	11758 [R_{int} = 0.03]	9056 [R_{int} = 0.04]
Data / Restraints / Parameters	11758 / 0 / 846	9056 / 183 / 760
Observed data [I > 2σ(I)]	11333	7329
Final R indexes [I ≥ 2σ(I)]	R_1 = 0.081, wR_2 = 0.218	R_1 = 0.103, wR_2 = 0.280
Final R indexes [all data]	R_1 = 0.082, wR_2 = 0.218	R_1 = 0.117, wR_2 = 0.295

Goodness-of-fit on F^2	1.07	1.05
Largest diff. peak and hole / e·Å^{-3}	1.31 / –0.77	1.44 / –0.98

Structure analysis of the C8S_IPR_I complex

The complex ***C8S_IPR_I*** has the formula $C_{56}H_{40}O_{32}S_8 \cdot 4(C_9H_{15}N_3O) \cdot 32.89(H_2O)$. Single-crystal X-ray diffraction analysis shows that this complex crystallizes in a triclinic crystal system in the space group *P–1*. The asymmetric part consists of half of C8S, two iproniazid and 16.45 water molecules (Figure 210).

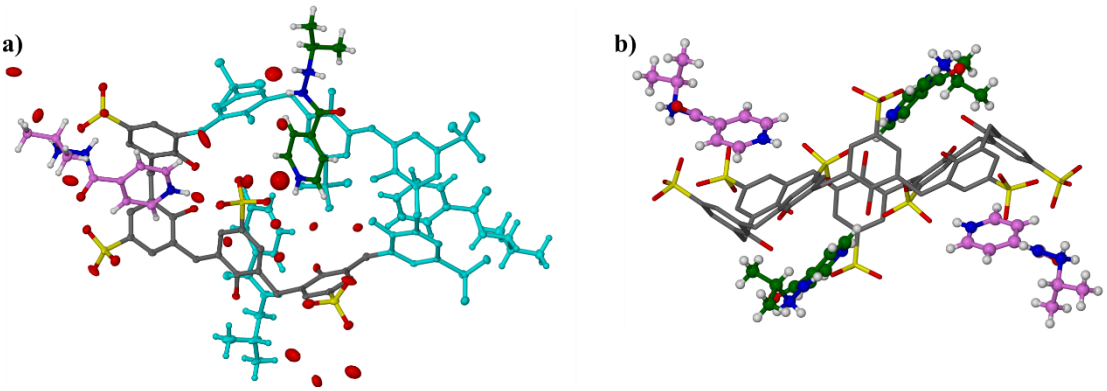

*Figure 210. The asymmetric unit of the **C8S_IPR_I** complex: (a) the macrocycle lies over inversion centre, the light blue corresponds to symmetry generated iproniazid and calix[8]arene molecules. Atomic displacement parameters set at 50% probability. Disorder omitted for clarity; (b) side view on the **C8S_IPR_I** complex. Water molecules omitted for clarity.*

In ***C8S_IPR_I*** complex the calix[8]arene adopts a self-closed conformation. Two phenolic rings fold inward with their sulfonate groups, while the remaining six extend outward. This arrangement creates groove-like cavities between the alternating inward- and outward-oriented aromatic rings, which serve as the binding sites for the guest or water molecules. The self-closed conformation disrupts the formation of a continuous intramolecular hydrogen-bonding network at the lower calixarene rim (Figure 211a). The *O4–H4A* hydroxyl group forms an intramolecular hydrogen bond with the adjacent O16 atom (*O4–H4A···O16*). At the same time, it engages in a hydrogen bond with water molecule O2W (*O4–H4A···O2W*, 2.822(4) Å), thus participating in a bifurcated hydrogen-bonding interaction. One intermolecular hydrogen bond connects the hydroxyl and sulfonate groups of two adjacent C8S molecules (*O8–H8···O15*), and another links a hydroxyl group to water molecule (*O12–H12···O4W*). One intramolecular hydrogen bond occurs between the hydroxyl and sulfonate groups of C8S (*O16–H16A···O6*). The *O···O* distances for these interactions fall within the range of 2.676(5)–3.029 Å. Detailed geometrical parameters are provided in Table 86, Annex I. The two guest iproniazid molecules adopt similar conformations and differ only slightly in the orientation of their N–isopropyl chains (Figure 211b).

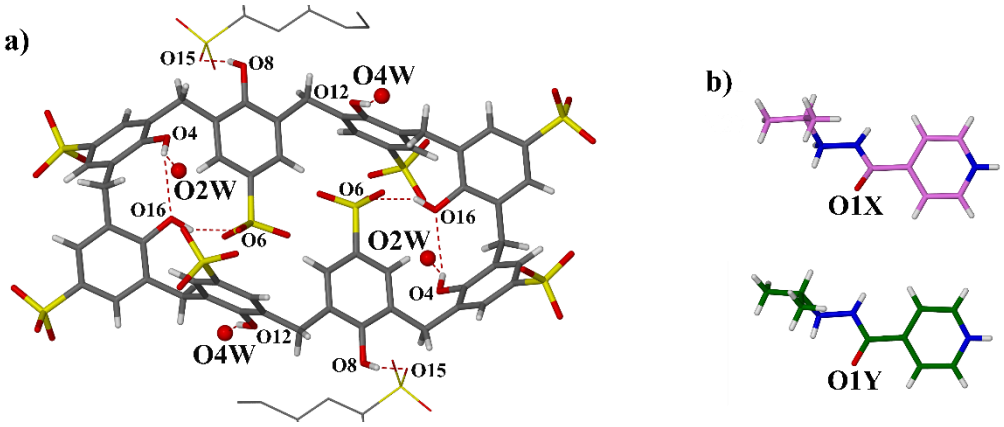

*Figure 211. Host–guest complex **C8S_IPR_I**: (a) O–H···O hydrogen bonding pattern at the calixarene lower rim; (b) conformations of the iproniazid molecules.*

Iproniazid molecules interact with the same self-inclined sulfonate group of the calixarene, but from opposite directions. The pink molecule C1X > O1X (**X**) occupies the groove of the macrocycle and is anchored by two *N–H···O* hydrogen bonds (one pyridinium-sulfonate and one hydrazinium-sulfonate) to sulfonate oxygen atoms of the parent C8S, along with two additional contacts to water molecules, with *O···O* distances of 2.671(6)–2.774(5) Å (Figure 212a). These strong interactions, complemented by one weak *C–H···O* contact with the parent (3.471(6) Å) and neighbouring calixarenes (3.2–3.3 Å), stabilize the guest in the groove site (Figure 212b). The green molecule C1Y > O1Y (**Y**) is positioned closer to two inward-facing sulfonate groups. Its *N–H···O* hydrogen-bonding pattern differs from that of the pink guest. One pyridine *N–H* group forms a bifurcated hydrogen bonds with a parent sulfonate oxygen and water molecule, while the hydrazine part engages in hydrogen bonds with two adjacent calixarenes and water, at *O···O* distances of 2.635(7)–2.878(4) Å (Figure 212a). In addition, the C1Y > O1Y guest forms *C–H···O* contacts with the parent C8S upper rim (with O7 atom is not shown, 3.09 Å) and three with the lower rim by its aromatic ring. Further weak *C–H···O* interactions with neighbouring calixarenes occur at the 3.140(7) and 3.443(7) Å (Figure 212b).

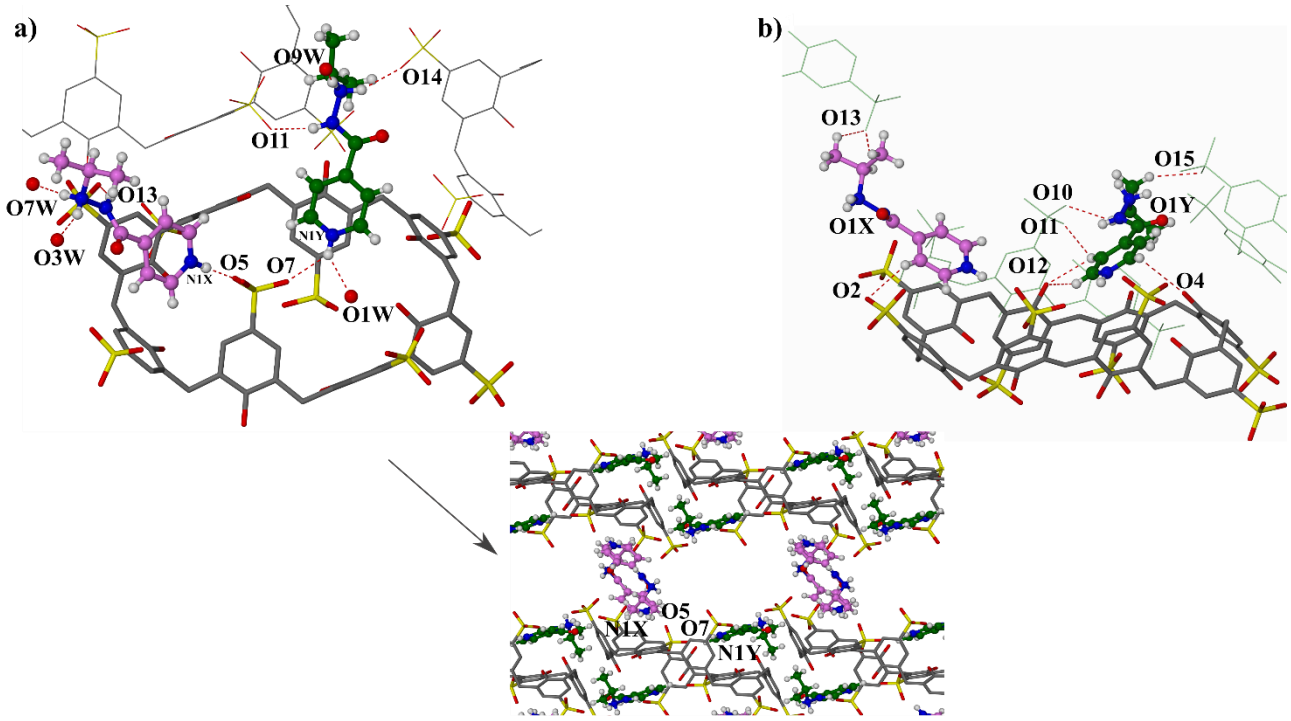

*Figure 212. Host–guest complex **C8S_IPR_I**: (a) N–H···O hydrogen bonds between iproniazid and C8S, water molecules: (b) C–H···O hydrogen bonds between iproniazid and C8S molecules.*

Both iproniazid molecules interact with aromatic rings of the C8S macrocycle through $\pi\cdots\pi$ stacking. The C1X > O1X iproniazid stacks with aromatic ring of the host at 3.865(3) Å, reflecting its groove position. The C1Y > O1Y iproniazid forms interaction with calixarene ring at 3.735(3) Å, above the inward-facing sulfonate groups. Neighbouring calixarene molecules also engage in $\pi\cdots\pi$ interactions at 3.926(3) Å (Figure 213a). All distances and angles of the hydrogen-bonding and aromatic interactions are summarized in Tables 86,87, Annex I. Together, these interactions direct the crystal packing into layered arrangements (Figure 213b). Pink iproniazid molecules occupy the interlayer regions and adopt an almost vertical orientation being surrounded by water molecules, while green iproniazid molecules are embedded within the layers.

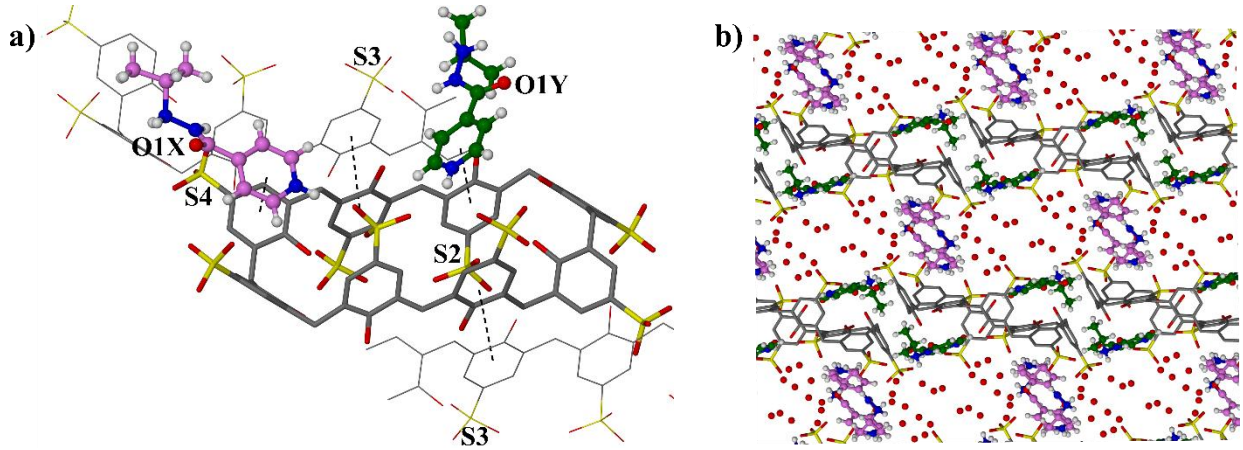

*Figure 213. Host–guest complex **C8S_IPR_I**: (a) π···π interaction between aromatic rings of the iproniazid and C8S molecules and between aromatic rings of adjacent C8S molecules; (b) crystal packing of the host–guest complex **C8S_IPR_I** viewed along **a** direction.*

Structure analysis of the C8S_IPR_II complex

The crystals of ***C8S_IPR_I*** undergo spontaneous *single-crystal-to-single-crystal* desolvation (dehydration) at room temperature outside mother liquor. The structural transformation upon elimination of water solvent molecules from the crystal results in the form ***C8S_IPR_II***. Single-crystal X-ray diffraction analysis shows that the dehydration is not complete, as some water molecules remain in the crystalline complex ***C8S_IPR_II*** with formula $C_{56}H_{40}O_{32}S_8 \cdot 4(C_9H_{15}N_3O) \cdot 6(H_2O)$. The space group *P–1* is retained after the transformation. The dehydration and SCSC transformation led to the total shrinkage of 22 % in unit cell volume and 17.3 % in mass. The asymmetric part consists of half of C8S, two iproniazid and three water molecules (Figures 214a,b).

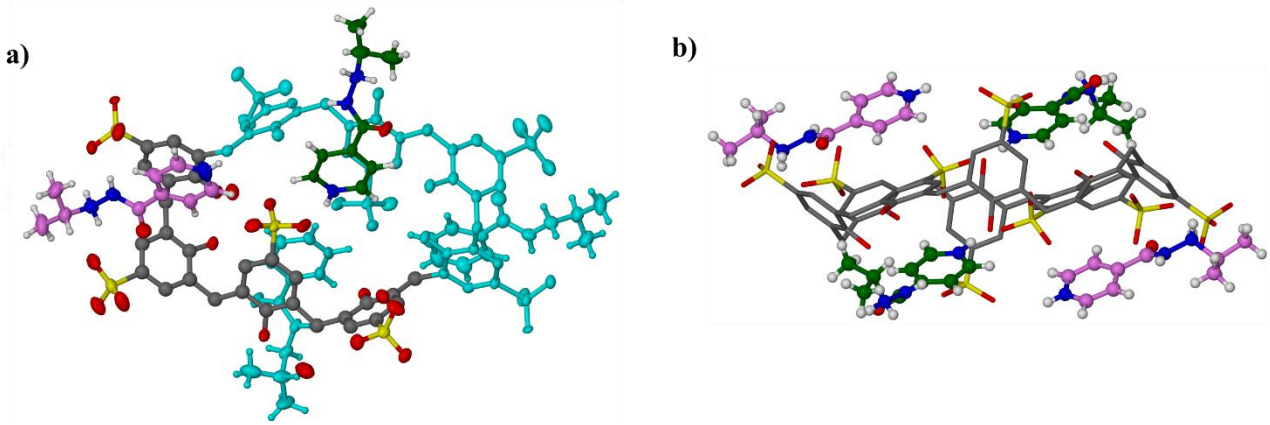

*Figure 214. The asymmetric unit of the **C8S_IPR_II** complex: (a) the macrocycle lies over inversion centre, the light blue corresponds to symmetry generated iproniazid and calix[8]arene molecules. Atomic displacement parameters set at 50% probability. Disorder omitted for clarity; (b) side view on the **C8S_IPR_II** complex. Water molecules omitted for clarity.*

In the ***C8S_IPR_II*** complex calixarene molecule adopts a self-closed conformation. The hydroxyl group *O4–H4A* engages in two hydrogen bonds: one with the neighbouring O16 atom within the same calixarene and another with water molecule O1W, forming a bifurcated interaction (Figure 215a). Two more hydrogen bonds connect adjacent calixarene molecules through their hydroxyl and sulfonate groups (*O8–H8···O15* and *O12–H12···O11*), and an intramolecular bond links *O16–H16A* to the sulfonate O6 atom. The *O···O* distances for these interactions range from 2.701(6) to 2.990(6) Å. The iproniazid molecules adopt conformations different in the orientation of N–isopropyl chains (Figure 215b). Detailed geometrical parameters of the hydrogen bonds at the C8S lower rim are provided in Table 88, Annex I.

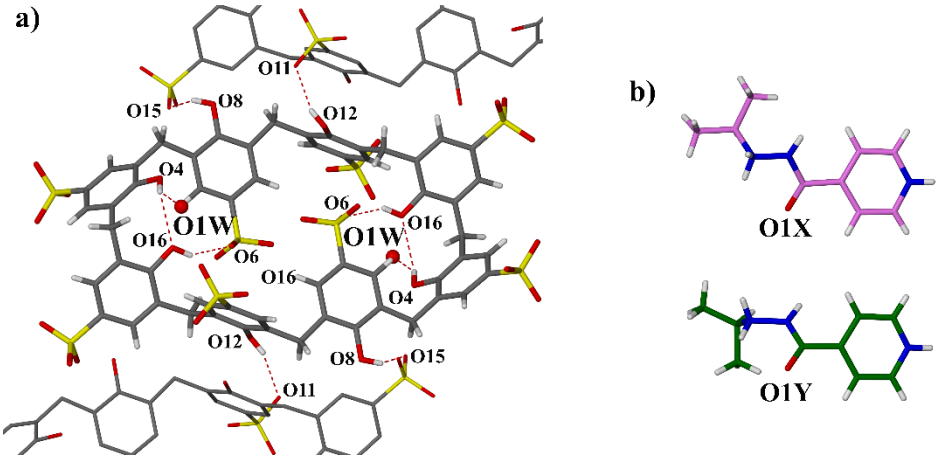

*Figure 215. Host–guest complex **C8S_IPR_II**: (a) O–H···O hydrogen bonding pattern at the calixarene lower rim; (b) conformations of the iproniazid molecules.*

In the host–guest complex, the positions of the iproniazid molecules (pink **X** and green **Y**) differ from those in complex ***C8S_IPR_I***. The pink molecule (C1X > O1X) slightly shifted away from the groove of the macrocycle, whereas the green molecule (C1Y > O1Y) remains in approximately the same location, showing tilting of the pyridine ring and rotation of the N–isopropyl chain. As a result of these positional changes, the hydrogen-bonding pattern in the second structure is altered compared to ***C8S_IPR_I***.

The C1X > O1X molecule is no longer anchored by an *N–H···O* hydrogen bond to the self-included sulfonate group through the pyridine ring but instead interacts with sulfonate group of adjacent C8S molecule (Figure 216a). The remaining hydrazine-sulfonate hydrogen bonds are formed with the parent host, exhibiting *O···O* distances in the range 2.719(9)–2.950(7) Å. These interactions are supported by two *C–H···O* contacts with the parent calixarene both at 3.093(13) and 3.101(10) Å and three additional contacts with a neighbouring calixarenes (3.297(11)–3.458(7) Å) (Figure 216b). The C1Y > O1Y molecule establishes one *N–H···O* hydrogen bond to the parent self-included sulfonate group *via* its pyridine ring, two additional hydrazine-sulfonate *N–H···O* bonds to sulfonate groups of adjacent C8S molecules, and one bond to water molecule, with *O···O* distances in the range 2.578(6)–3.183(17) Å (Figure 216a). Furthermore, the C1Y > O1Y guest forms four *C–H···O* contacts with the lower rim of the parent C8S, at 2.9–3.3 Å and two weak with sulfonate part of the adjacent host (Figure 216b). The interaction with one O8 hydroxyl atom is not shown. The packing fragment illustrates how host–guest interactions lead to differences in molecular orientations.

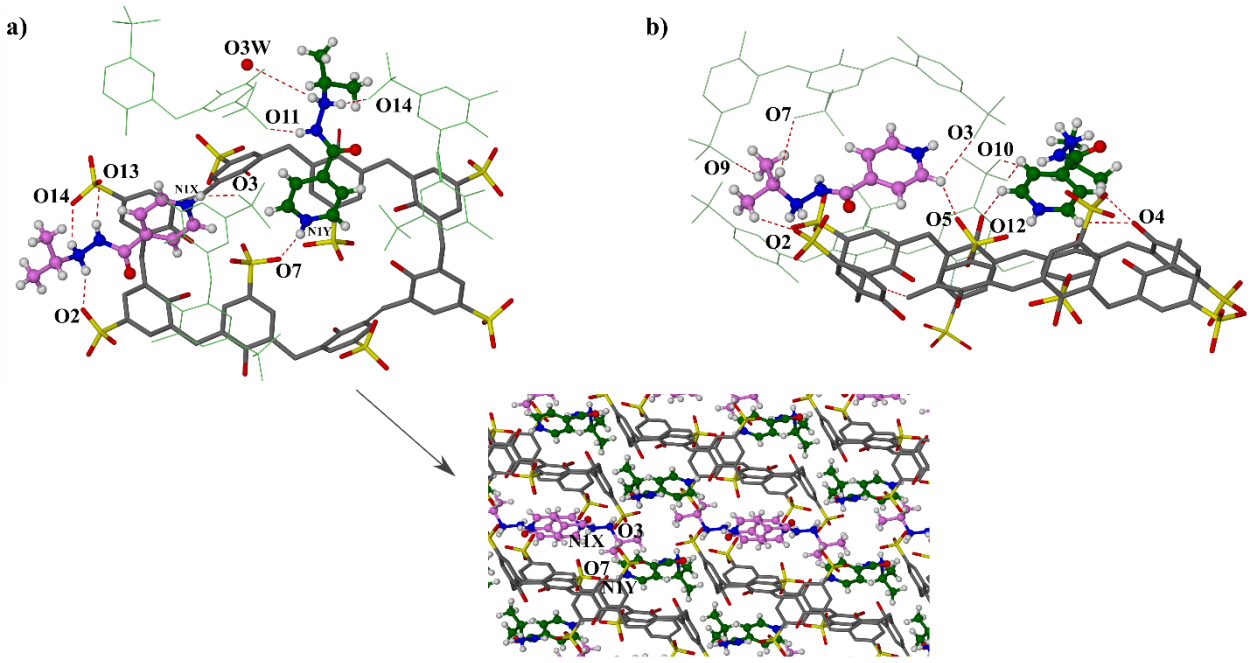

*Figure 216. Host–guest complex **C8S_IPR_II**: (a) N–H···O hydrogen bonds between iproniazid and C8S, water molecules, the adjacent calixarene molecules are shown in light green; (b) C–H···O hydrogen bonds between iproniazid and C8S molecules.*

The aromatic interactions between the host and guests, as well as between neighbouring hosts, remain essentially consistent with those observed in the ***C8S_IPR_I*** complex, showing minor variations in ring orientations and contact distances. The pink C1X > O1X iproniazid is shifted away from the C8S aromatic ring in the groove position by its own aromatic ring and therefore does not form direct *face-to-face* $\pi\cdots\pi$ stacking interactions with the calixarene. C1Y > O1Y iproniazid engages in $\pi\cdots\pi$ stacking with an aromatic ring of the calixarene at 3.752(3) Å. In addition, adjacent calixarene molecules are linked through intermolecular $\pi\cdots\pi$ stacking at 3.670(3) Å (Figure 217a). Geometrical parameters for hydrogen-bonds and aromatic contacts are summarized in Tables 88,89, Annex I. The crystal packing of the ***C8S_IPR_II*** complex is shown in Figure 217b. The calixarene molecules assemble into layers. The pink iproniazid molecules are situated within the interlayer regions, where they adopt an almost horizontal orientation, while the green iproniazid molecules are accommodated directly within the layers. In comparison with the ***C8S_IPR_I*** complex, the number of water molecules occupying the interlayer spaces is reduced notably.

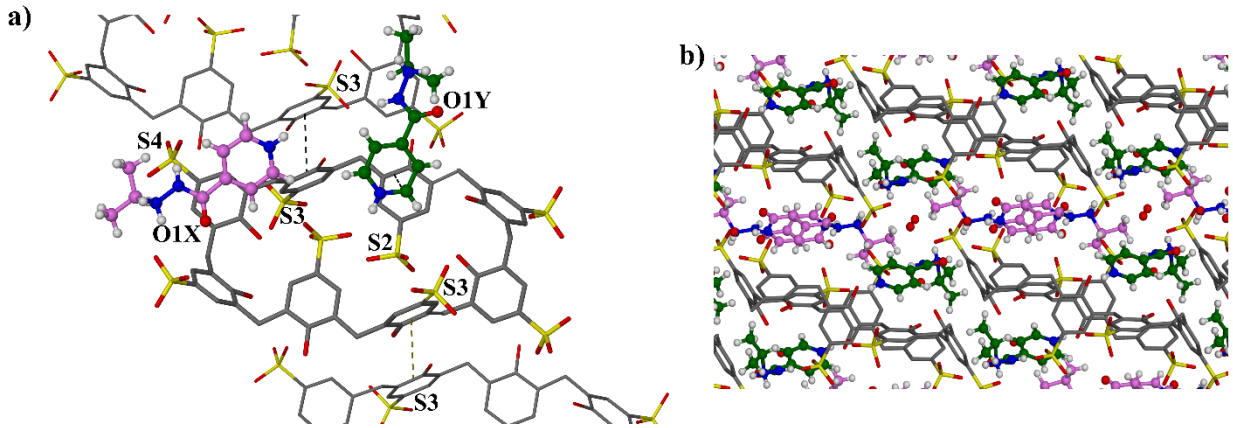

*Figure 217. Host–guest complex **C8S_IPR_II**: (a) π···π interaction between aromatic rings of the iproniazid and C8S molecules and between aromatic rings of adjacent C8S molecules; (b) crystal packing of the host–guest complex **C8S_IPR_II** viewed along **a** direction.*

TGA–DSC analysis of the C8S_ IPR complex

The next step was to compare the water content of the air-dried ***C8S_IPR_II*** crystal structure, determined by single-crystal X-ray diffraction, with that obtained from TGA–DSC measurements. For this purpose, 5.09 mg of ***C8S_IPR_II*** crystals were analysed. The resulting TGA–DSC curves are presented in Figure 218. A two-step weight loss was observed up to 103.2 °C, with a total mass loss of 0.54 mg, corresponding to 10.5% of the initial sample weight.

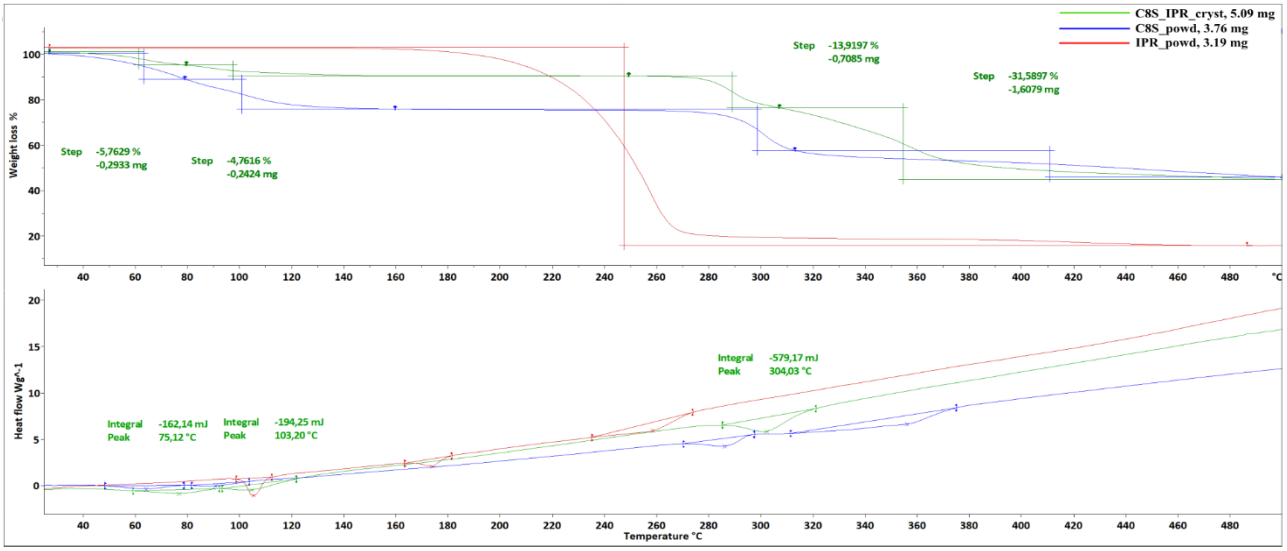

*Figure 218. TGA (top) and DSC (bottom) curves of the **C8S_IPR_II** complex. The green curve represents the crystals of the **C8S_IPR_II** complex, blue and red curves – the powder samples of the C8S and iproniazid, respectively.*

Solid–state complexes of C8S with iproniazid – discussion of results

The co-crystallization of *p*-sulfonatocalix[8]arene with iproniazid produced two distinct complexes: ***C8S_IPR_I***, obtained directly from an aqueous solution, and ***C8S_IPR_II***, formed after air-drying the crystals. Both complexes share the same host–guest stoichiometry. The primary difference between them lies in their water content: ***C8S_IPR_I*** is highly hydrated, containing 32.89 water molecules, whereas ***C8S_IPR_II*** is a low hydrate with only six water molecules.

In both complexes, calixarene adopts a self-closed conformation, in which two phenolic rings fold inward toward the sulfonate groups while the remaining six extend outward similar to C8S–dimethylammonium complex (refcode DIZPEI).[143] Overlaying these conformations in MERCURY highlights these differences and a high RMSD parameter of 3.07 Å and an atomic displacement of 7.23 Å further confirm the conformational variations (Figure 219a). Both ***C8S_IPR_I*** and ***C8S_IPR_II*** complexes display similar hydrogen-bonding patterns at the calixarene lower rim, but some differences arise from partial dehydration and those changes in the C8S conformation. In both structures, the intramolecular hydroxyl-hydroxyl *O4–H4A···O16*, and hydroxyl-water *O4–H4A···water* bifurcated hydrogen bonds are saved. These two hydrogen bonds and hydroxyl-sulfonate *O16–H16A···O6* are slightly shortened in ***C8S_IPR_II*** complex. The hydrogen bonding of the *O12–H12* group is affected the most, changing from interaction with water (*O12–H12···O4W*) in ***C8S_IPR_I*** to interaction with the adjacent C8S molecule (*O12–H12···O11*) in ***C8S_IPR_II***. Regarding the conformations of the iproniazid molecules, they also differ slightly between the two complexes. Molecular overlays performed in MERCURY were used to quantify these conformational differences. The pink (**X**) iproniazid exhibits an RMSD of 0.53 Å with a maximum atomic shift of 1.50 Å, indicating negligible local flexibility in the aliphatic part of the molecule, while the green (**Y**) iproniazid shows a slightly higher RMSD of 0.60 Å with a maximum atomic displacement of approximately 1.05 Å. These results suggest a slightly greater conformational change in the **Y** molecule compared to the **X**, especially in the C1Y > O1Y N–isopropyl chain (Figure 219b).

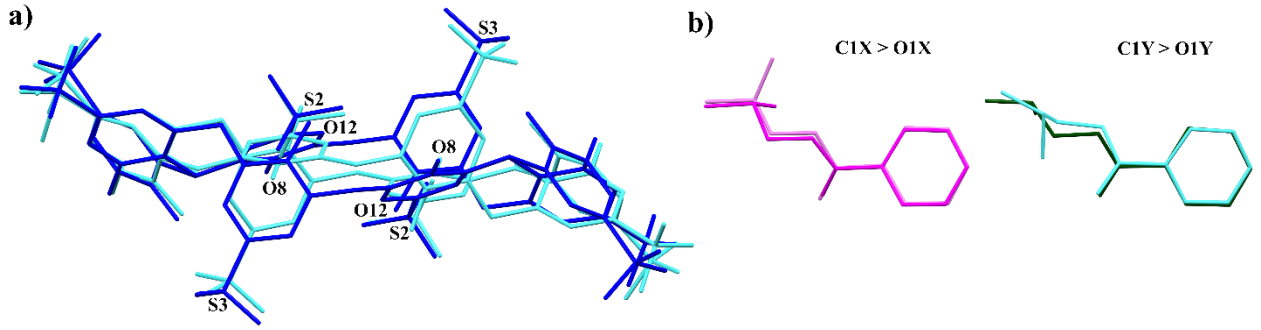

*Figure 219. (a) Molecular overlay of the two C8S conformations: the dark blue structure represents the C8S conformation in the complex **C8S_IPR_I**, while the light blue structure corresponds to the C8S conformation in the complex **C8S_IPR_II**; (b) molecular overlay of the iproniazid molecules. The dark colours represent the iproniazid conformations in the complex **C8S_IPR_I**, while the light colours correspond to the iproniazid conformations in the complex **C8S_IPR_II**.*

To analyse the host–guest binding modes in the two complexes and highlight further differences caused by the partial dehydration, the crystal structures were first overlaid (Figure 220). The host–guest ensemble remains largely similar overall. However, the reorganization of non-covalent interactions results in noticeable differences in guest orientations relative to the calixarene molecule.

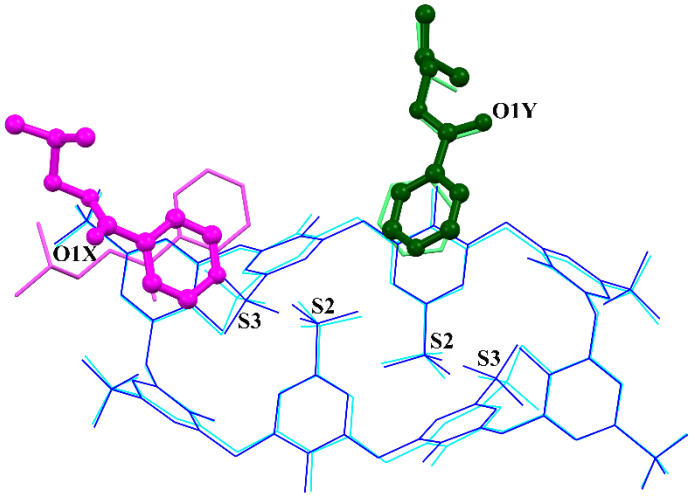

*Figure 220. Molecular overlay of the **C8S_IPR_I** and **C8S_IPR_II** complexes: The dark colours represent the complex **C8S_IPR_I**, while the light colours correspond to the complex **C8S_IPR_II**.*

In complex ***I***, both guests (dark pink and green) are hydrogen bonded *via* pyridinium groups to self-included sulfonate group (S2). The pink molecule experiences the most notable changes upon structural solvent loss, affecting both non-covalent interactions and its position relatively to C8S molecules in the crystal. In complex ***I***, the pyridinium ring of pink molecule is embedded within the calixarene groove and forms one *N–H···O* hydrogen bond with the oxygen atom of S2 sulfonate group. One of its hydrazine nitrogen atoms interacts with a S4 sulfonate oxygen of the parent C8S, and the remaining protonated hydrazine nitrogen is hydrogen bonded with two water molecules. In complex ***II***, *N–H···O* hydrogen bond of the same pyridine ring now connects to a sulfonate group of an adjacent C8S from the above layer. The cationic hydrazine group is positioned between two neighbouring sulfonate groups S1 and S4, and all three hydrogen bond donors of hydrazine are satisfied with these sulfonate oxygen acceptors. Due to the elimination of the majority of water molecules form the crystal and collective reorientation of iproniazid molecules there are no hydrazine-water hydrogen bonds as in form ***I***. In both complexes, the green iproniazid molecule hydrogen bonded to the same sulfonate group through the N atom of the pyridine ring. However, in complex II the molecule lies closer to this group (*N···O* distance of 2.578(6) Å compared to 2.878(4) Å in complex ***I***) and no longer forms the additional bifurcated hydrogen bond with water. The two hydrogen bonds involving the N atoms of the hydrazine group and sulfonate oxygens of adjacent C8S are preserved, with nearly identical distances in both complexes. The hydrazine-water *N–H···O* interaction is still present but weaker in complex ***II***. The most notable changes in *N–H···O* hydrogen bonding between the IPR molecules and the calixarene are presented on the Figure 221.

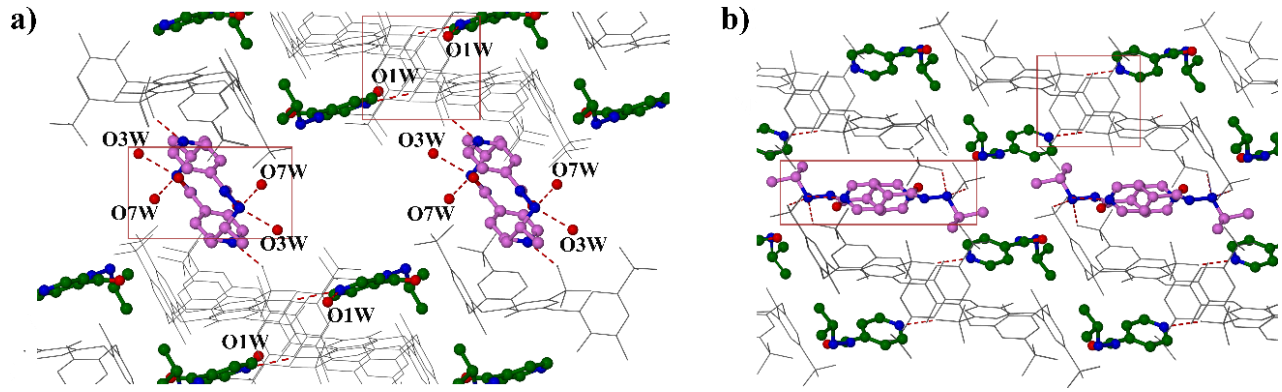

Figure 221. The comparison of the N–H···O hydrogen bonds between the IPR and C8S molecules in the complexes (a) ***C8S_IPR_I*** *and (b)* ***C8S_IPR_II****.*

In both complexes, the pink iproniazid displays different *C–H···O* and *π···π* interaction patterns. In complex ***I***, pink IPR molecule adopts almost vertical position between the layers, with its isopropyl tail anchored to the C8S molecule from adjacent layer through several $C_{(isopropyl)}$–$H\cdots O_{(sulfonate)}$ interactions. In complex ***II***, the pink IPR molecules reorganize to an almost horizontal orientation between the layers. Now the isopropyl tail of IPR (pink) is in close $C_{(isopropyl)}$–$H\cdots O_{(sulfonate)}$ contacts with C8S molecules from both parent and adjacent layers. In complex ***I*** pyridinium ring of pink iproniazid engages in *face-to*-face *π···π* interaction with an aromatic ring of the parent calixarene, the *centroid···centroid* distance is of 3.86 Å. After the dehydration and reorientation of IPR molecules, the same pyridinium ring shows only *edge-to-face* close contacts with C8S aromatic wall, the shortest *C···C* distances are of 3.35 and 3.47 Å.

Structural analysis of the crystal complexes shows significant changes in the interlayer distances and packing arrangement after solvent removal. In the solvated crystal, the interlayer distance, measured between planes through the C8S methyl bridges, is 15.4 Å. Upon drying, this distance decreases to 9.8 Å (Figure 222). As described the overall arrangement of C8S in both structures is layered: the pink molecules occupy the space between the layers, while the green iproniazid molecules are located within the C8S layers. Upon loss of water molecules from the one-dimensional channels in *single-crystal-to-single* crystal fashion, the pink molecules are most affected changing orientation from pillar-like vertical to horizontal. The green molecules undergo more subtle conformational changes.

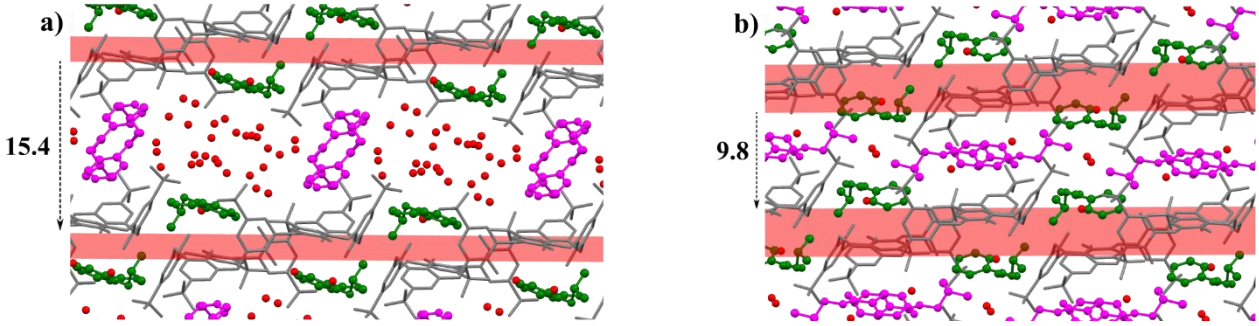

Figure 222. The interlayer distance between the C8S molecules in: (a) ***C8S_IPR_I*** *and (b)* ***C8S_IPR_II*** *complexes measured in Å.*

Computational removal of water solvent molecules from the structure model ***C8S_IPR_I*** and use of Mercury software (probe radius 1.2 Å) show the unidimensional channels of 929 $Å^3$ (*per* unit cell) that take *app.* 28 % of the crystal volume (Figure 223a). The channels propagate along [100] direction. The anionic sulfonate groups of C8S and cationic hydrazine groups of IPR molecules are exposed to the channel walls and take part in the hydrogen bonding with water molecules inside. The maximum pore diameter is 6.2 Å and the limiting diameter is of 3.9 Å, as given by Mercury software. The air-dried dehydrated phase ***C8S_IPR_II*** has practically closed structure with small, isolated voids (5 % of the crystal volume as calculated by Mercury) (Figure 223b).

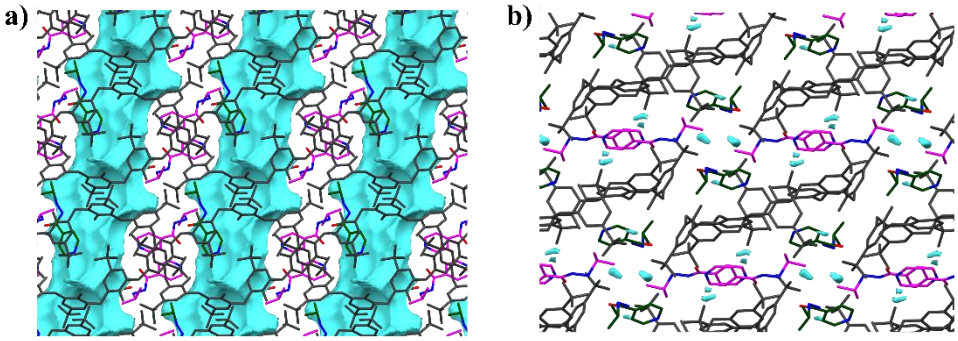

Figure 223. The fragment of the crystal packing of the (a) ***C8S_IPR_I*** *complex with solvent-accessible* ***channels*** *and (b)* ***C8S_IPR_II*** *complex with solvent-accessible* ***voids*** *shown in blue. The boundaries of channels and voids (probe radius 1.2 Å) were calculated using Mercury software.*

5. CONCLUSIONS

The systematic investigation of *p*-sulfonatocalix[*n*]arene (C4S, C6S, and C8S) host–guest complexes demonstrates the pronounced structural adaptability of sulfonated calixarenes toward variety of cationic guests in the solid state. Analysis of 26 crystallographically characterized complexes shows that the resulting supramolecular architectures are governed altogether by host size and charge state, its counterion, guest functionalization, solvent composition, as well as crystallization pathway embracing formation of metastable kinetic host–guest–solvent assemblies. No single parameter is sufficient to predict the final structure; instead, complexation outcomes reflect the balance between the crystallization conditions and the combined interplay of non-covalent interactions between host, guest, and solvent components.

Host size and conformational freedom strongly influence complexation mode. The smallest C4S host, with a restricted cavity, favors single-guest inclusion accompanied by pronounced cone pinching, enabling optimized charge-assisted hydrogen-bonding contacts with benzamidinium derivatives. In contrast, C6S and C8S exhibit significantly higher conformational flexibility while adopting pleated-loop, double partial-cone, up–up, up–down, or self-closed conformations in response to the guest structure and crystallization conditions. These conformations of larger C6S and C8S macrocycles generate pseudo-cavities, grooves, and extended binding surfaces that support multi-guest inclusion, external surface binding, and cooperative host–guest–solvent assemblies.

The counterion of calixarene host can be an important factor determining stoichiometry and supramolecular connectivity in the final assembly. Sodium ions as counterions can act as coordination nodes linking sulfonate groups of calixarenes and water molecules, leading to extended bilayer assemblies or three-dimensional coordination polymers. This behavior positions sulfonated calixarenes at the interface between classical host–guest chemistry and coordination-driven supramolecular assembly.

Minor guest functionalization, as introduction of methyl, hydroxy or amino substitution on benzamidine, significantly influences inclusion geometry and host–guest interactions, also affecting host conformation. The guest molecules themselves can display conformational adaptability in the presence of macrocyclic hosts, particularly flexible multicationic species such as pentamidine and alexidine. These guests undergo various degree of folding or bending to match the shape of the host, adopting U-shaped, C-shaped, or extended conformations depending on the preferred complexation mode and size of the macrocycle. Such assemblies can be considered in terms of mutually induced fit complexation.

Across all amidine and biguanidine complexes, charge-assisted *N–H···O* hydrogen bonding with anionic sulfonate groups of calixarenes constitutes the dominant host–guest interaction. This interaction can be considered as a conserved supramolecular synthon that anchors the guest to the anionic upper rim of the macrocycle and stabilizes both inclusion and exclusion complexation. Variations in the interaction multiplicity, geometry, and cooperativity with secondary contacts – such as *C–H···π* interactions, *π···π* stacking, and water-mediated hydrogen bonds – modulate guest orientation respectively to the host cavity, depth of inclusion, and overall crystal packing.

Some of the studied complexes and assemblies are devoid of the classical hydrogen bonding. In pillar[*n*]pyridinium-based complexes, assembly is driven primarily by strong electrostatic interactions between the anionic sulfonate groups of C4S and cationic pyridinium moieties, together with less common *C–H···π*, *anion···π*$^{+}$, and *π···π*$^{+}$ interactions. Also, in C8S complex with berberine, the supramolecular assembly is driven by ionic interactions supported by multiple *C–H···π* and *C–H···O* contacts between host and guest.

Solvent composition and time that crystals spent in the contact with the mother solution under slow evaporation conditions should also be considered as important variables for the supramolecular and crystal design of host–guest complexes. Water frequently acts as a structural component, bridging, for example, sulfonate and amidinium groups, or occupying calixarene cavities in direct competition with organic guests. In the calixarene–pentamidine complexes, solvent molecules (ethanol, methanol, isopropanol, acetone) preferentially occupy the macrocyclic cavity, enforcing exclusion binding at the calixarene exterior. The crystal structures are corroborated by solution complexation studies, also showing a change of supramolecular regime in response to solvent composition. These results demonstrate pronounced guest–solvent competition and show that binding modes can be switched by changes in the complexation/crystallization medium.

Time-dependent crystallization studies reflect the interplay between kinetic and thermodynamic control in the host–guest–solvent complexation. Initially, highly hydrated host–guest crystal forms crystallize, that further undergo dissolution-recrystallization transformation into less hydrated complexes. Also, initial rapid crystallization can afford cavity inclusion of competitive ethanol molecules with actual guests bound externally via hydrogen bonding, as in the case of C4S complex with amino-benzamidine. Later formed crystalline complex involves inclusion of amino-benzamidine guest within the same macrocyclic cavity that require considerable deformation of the macrocycle. Such step-wise crystallization can be considered in the terms of Ostwald's rule of stages according to which crystallization often proceeds step by step *via* intermediate metastable phases until the most stable phase will be formed. However, in the case of multi-component supramolecular

complexes and assemblies, the complicated phenomena of crystal nucleation and growth are interlaced with the kinetic factors and induced fit complexation aspects in the host–guest systems.

p-Sulfonatocalix[*n*]arene crystal complexes typically incorporate large amounts of water molecules and are rarely stable outside the mother solution, as dehydration commonly causes loss of crystallinity and decomposition. However, in the C8S complex with iproniazid guest, large water channels present in the crystal structure transform into small voids upon dehydration through a single-crystal-to-single-crystal (SCSC) transformation while maintaining crystallinity. In the C6S complex with methyl-benzamidine, large discrete structural voids are observed that contain disordered water molecules even after air-drying. The water molecules within these voids are only weakly associated with the framework and primarily act as space fillers. Thus, the ***C6S_M–BNZ*** framework is unusual among *p*-sulfonatocalix[*n*]arene complexes because it remains stable and unchanged in air despite the presence of weakly bonded disordered water molecules. The persistence of the supramolecular framework upon partial solvent loss indicates notable structural robustness and suggests potential applications in terms of porosity or permeability to additional guests, that will be a subject for future studies.

The results demonstrate that the structural diversity of calixarene-based complexes is not random but arises from the combined influence of multiple factors governing host–guest interactions and assembly in the solid state. These findings establish guiding principles for the future more rational design of calixarene assemblies and highlight the potential of sulfonated calixarenes as tunable building blocks in supramolecular and crystal engineering.

6. REFERENCES

1. Fischer, E. Einfluss der Configuration auf die Wirkung der Enzyme. *Ber. Dtsch. Chem. Ges.* **1894**, *27* (3), 2985–2993.
2. Lehn, J.-M. Supramolecular chemistry. *Science* **1993**, *260* (5115), 1762–1763.
3. Lehn, J.-M. *Supramolecular Chemistry: Concepts and Perspectives*; Wiley-VCH: Weinheim, **1995**.
4. Yang, L. P.; Zhang, L.; Quan, M.; *et al*. A supramolecular system that strictly follows the binding mechanism of conformational selection. *Nat. Commun.* **2020**, *11* (1), 2740.
5. Cram, D. J. Preorganization – From Solvents to Spherands. *Angew. Chem. Int. Ed. Engl.* **1986**, *25* (12), 1039–1057.
6. Leckband, D.; Israelachvili, J. Intermolecular Forces in Biology. *Q. Rev. Biophys.* **2001**, *34* (2), 105–267.
7. Crini, G. Review: A History of Cyclodextrins. *Chem. Rev.* **2014**, *114* (21), 10940–10975.
8. Lagona, J.; Mukhopadhyay, P.; Chakrabarti, S.; Isaacs, L. The Cucurbit[*n*]uril Family. *Angew. Chem. Int. Ed.* **2005**, *44* (31), 4844–4870.
9. Español, E. S.; Villamil, M. M. Calixarenes: Generalities and Their Role in Improving the Solubility, Biocompatibility, Stability, Bioavailability, Detection, and Transport of Biomolecules. *Biomolecules* **2019**, *9* (3), 90.
10. Böhmer, V. Calixarenes, Macrocycles with (Almost) Unlimited Possibilities. *Angew. Chem. Int. Ed. Engl.* **1995**, *34* (7), 713–745.
11. Ogoshi, T.; Yamagishi, T.-A. Pillararenes: Versatile Synthetic Receptors for Supramolecular Chemistry. *Eur. J. Org. Chem.* **2013**, *2013* (15), 2961–2975.
12. Xue, M.; Yang, Y.; Chi, X.; Zhang, Z.; Huang, F. Pillararenes, a New Class of Macrocycles for Supramolecular Chemistry. *Acc. Chem. Res*. **2012**, *45* (8), 1294–1308.
13. Tian, J.-H.; Xu, H.; Hu, X.-Y.; Guo, D.-S. Supramolecular Fluorescence Biosensing Based on Macrocycles. *Supramol. Mater*. **2024**, *3*, 100063.
14. Marcos, P. M.; Berberan-Santos, M. N. Recent Advances in Calixarene-Based Fluorescent Sensors for Biological Applications. *Sensors (Basel)* **2024**, *24* (22), 7181.
15. Wang, C.; Xu, L.; Jia, Z.; Loh, T.-P. Recent Applications of Macrocycles in Supramolecular Catalysis. *Chin. Chem. Lett.* **2024**, *35* (4), 109075.
16. Morimoto, M.; Bierschenk, S. M.; Xia, K. T. *et al*. Advances in Supramolecular Host-Mediated Reactivity. *Nat. Catal*. **2020**, *3*, 969–984.
17. Ma, X.; Xiao, Y.; Li, S.; Du, J.; Wang, J.; Peng, X. Recent Advances in Supramolecular Systems for Precision Medicine: Structural Design, Functional Integration, and Clinical Translation Challenges. *Pharmaceutics* **2025**, *17* (9), 1192.
18. Ma, X.; Zhao, Y. Biomedical Applications of Supramolecular Systems Based on Host–Guest Interactions. *Chem. Rev.* **2015**, *115* (15), 7794–7839.
19. Gravel, J.; Kempf, J.; Schmitzer, A. Host–Guest Strategy to Reversibly Control a Chloride Carrier Process with Cyclodextrins. *Chem. Eur. J.* **2015**, *21* (51), 18642–18646.
20. Liu, J.; Gu, Y.; Lin, R.; Yao, W.; Liu, X.; Zhu, J. Anion encapsulation by Ln(III)/K(I) heterobismetal-capped cucurbit[5]uril. *Supramol. Chem.* **2010**, *22* (2), 130.
21. Anslyn, E. V.; Dougherty, D. A. In *Core Concepts in Supramolecular Chemistry and Nanochemistry*; Steed, J.

W., Ed.; Wiley: Chichester, UK, **2007**; pp 162–168.

22. Schneider, H.-J. Van der Waals Forces. In *Encyclopedia of Supramolecular Chemistry*; Steed, J. W.; Atwood, J. L., Eds.; Marcel Dekker: New York, **2004**; 2, 1550–1556.
23. Hunter, C. A.; Sanders, J. K. M. The Nature of π–π Interactions. *J. Am. Chem. Soc.* **1990**, *112* (14), 5525–5534.
24. Zhuang, W.-R.; Wang, Y.; Cui, P.-F.; Xing, L.; Lee, J.; Kim, D.; Jiang, H.-L.; Oh, Y.-K. Applications of π–π Stacking Interactions in the Design of Drug-Delivery Systems. *J. Controlled Release* **2019**, *294*, 311–326.
25. Pérez, E. M.; Martín, N. π–π Interactions in Carbon Nanostructures. *Chem. Soc. Rev.* **2015**, *44* (18), 6425–6433.
26. Thakuria, R.; Nath, N. K.; Saha, B. K. The Nature and Applications of π–π Interactions: A Perspective. *Cryst. Growth Des.* **2019**, *19* (2), 523–528.
27. Zhao, R.; Zhang, R.-Q. A New Insight into π–π Stacking Involving Remarkable Orbital Interactions. *Phys. Chem. Chem. Phys.* **2016**, *18* (36), 25452–25457.
28. Wheeler, S. E. Local Nature of Substituent Effects in Stacking Interactions. *J. Am. Chem. Soc.* **2011**, *133* (26), 10262–10274.
29. Martinez, C. R.; Iverson, B. L. Rethinking the Term "π-Stacking". *Chem. Sci.* **2012**, *3* (7), 2191–2201.
30. Janiak, C. A Critical Account on π–π Stacking in Metal Complexes with Aromatic Nitrogen-Containing Ligands. *J. Chem. Soc., Dalton Trans.* **2000**, 21, 3885–3896.
31. Hunter, C. A.; Lawson, K. R.; Perkins, J.; Urch, C. J. Aromatic Interactions. *J. Chem. Soc., Perkin Trans. 2* **2001**, 5, 651–669.
32. Xu, X.; Jia, K.; Qi, Q.; Tian, G.; Xiang, D. Regulation of π–π interactions between single aromatic molecules by bias voltage *Phys. Chem. Chem. Phys.* **2024**, *26* (20), 14607–14612.
33. Samanta, S.; Sanyal, S.; Maity, M.; Chaudhury, M.; Ghosh, S. Unusual Solvent Effect of Molecular Charge Transfer Complexes: Stacking/Non-Stacking Interaction Revealed by Characterization of Structure and Photophysical Aspects. *J. Lumin.* **2017**, *190*, 403–412.
34. Timmer, B. J. J.; Mooibroek, T. J. Intermolecular π–π Stacking Interactions Made Visible. *J. Chem. Educ.* **2021**, *98* (2), 540–545.
35. Blokzijl, W.; Engberts, J. B. F. N. Hydrophobic Effects. Opinions and Facts. *Angew. Chem., Int. Ed. Engl.* **1993**, *32* (11), 1545–1579.
36. Jeffrey, G. A.; Saenger, W. *Hydrogen Bonding in Biological Structures*; Springer-Verlag: Berlin; New York, **1991**.
37. Jeffrey, G. A. *An Introduction to Hydrogen Bonding*; Oxford University Press: New York, **1997**.
38. Desiraju, G. R.; Steiner, T. *The Weak Hydrogen Bond in Structural Chemistry and Biology*; Oxford University Press: New York, **1999**.
39. Arunan, E.; Desiraju, G. R.; Klein, R. A.; Sadlej, J.; Scheiner, S.; Alkorta, I.; Clary, D. C.; Crabtree, R. H.; Dannenberg, J. J.; Hobza, P.; Kjaergaard, H. G.; Legon, A. C.; Mennucci, B.; Nesbitt, D. J. Defining the Hydrogen Bond: An Account (IUPAC Technical Report). *Pure Appl. Chem.* **2011**, *83* (8), 1619–1636.
40. Arunan, E.; Desiraju, G. R.; Klein, R. A.; Sadlej, J.; Scheiner, S.; Alkorta, I.; Clary, D. C.; Crabtree, R. H.; Dannenberg, J. J.; Hobza, P.; Kjaergaard, H. G.; Legon, A. C.; Mennucci, B.; Nesbitt, D. J. Definition of the Hydrogen Bond (IUPAC Recommendations 2011). *Pure Appl. Chem.* **2011**, *83* (8), 1637–1641.
41. Gilli, G.; Gilli, P. Towards a Unified Hydrogen-Bond Theory. *J. Mol. Struct.* **2000**, *552* (1–3), 1–15.
42. Feldblum, E. S.; Arkin, I. T. Strength of a Bifurcated H Bond. *J. Phys. Chem. B* **2007**, *111* (11), 4085–4090.

43. Pople, J. A. Molecular Association in Liquids II. A Theory of the Structure of Water. *Proc. R. Soc. A.* **1951**, *205* (1081), 163–178.
44. Satange, R.; Hou, M. H. The Role of Water in Mediating DNA Structures with Epigenetic Modifications, Higher-Order Conformations, and Drug-DNA Interactions. *RSC Chem. Biol*. **2025**, *6* (5), 699–720.
45. Bianco, V.; Iskrov, S.; Franzese, G. Understanding the Role of Hydrogen Bonds in Water Dynamics and Protein Stability. *J. Biol. Phys*. **2012**, *38* (1), 27–48.
46. Desiraju, G. R. Hydrogen Bridges in Crystal Engineering: Interactions without Borders. *Acc. Chem. Res.* **2002**, *35* (7), 565–573.
47. MacLeod, J. M.; Rosei, F. Directed Assembly of Nanostructures. In *Comprehensive Nanoscience and Technology*, Vol. 1; Andrews, D. L.; Scholes, G. D.; Gary, P., Eds.; Elsevier: Amsterdam, **2011**; pp 13–68.
48. Schmidt, G. M. J. Photodimerization in the Solid State. *Pure Appl. Chem.* **1971**, *27* (4), 647–678.
49. Moulton, B.; Zaworotko, M. J. From Molecules to Crystal Engineering: Supramolecular Isomerism and Polymorphism in Network Solids. *Chem. Rev.* **2001**, *101* (6), 1629–1658.
50. Braga, D.; Brammer, L.; Champness, N. R. New Trends in Crystal Engineering. *Cryst. Eng. Commun.* **2005**, *7* (1), 1–19.
51. Pepinsky, R. Crystal Engineering: New Concepts in Crystallography. *Phys. Rev.* **1955**, *100*, 971.
52. Stojakovic, J.; MacGillivray, L. R. Cocrystals and Templates to Control Solid-State [2+2] Photodimerizations. In *Comprehensive Supramolecular Chemistry II*, 2nd ed., Vol. 7; Atwood, J. L.; Gokel, G. W.; Barbour, L. J., Eds.; Elsevier: Amsterdam, **2017**; pp 73–87.
53. Desiraju, G. R. Supramolecular Synthons in Crystal Engineering – A New Organic Synthesis. *Angew. Chem. Int. Ed.* **1995**, *34* (21), 2311–2327.
54. Russell, V. A.; Etter, M. C.; Ward, M. D. Layered Materials by Molecular Design: Structural Enforcement by Hydrogen Bonding in Guanidinium Alkane- and Arenesulfonates. *J. Am. Chem. Soc.* **1994**, *116*(5), 1941–1952.
55. Liu, Y.; Chang, G.; Zheng, F.; Chen, L.; Yang, Q.; Ren, Q.; Bao, Z. Hybrid Hydrogen-Bonded Organic Frameworks: Structures and Functional Applications. *Chem. – Eur. J.* **2023**, *29* (14), e202202655.
56. Housecroft, C. E.; Sharpe, A. G. *Inorganic Chemistry*, 3rd ed.; Wiley: Chichester, U.K., **2022**; pp 147–149.
57. Yin, C.; Du, J.; Olenyuk, B.; Stang, P.; Sun, Y. The Applications of Metallacycles and Metallacages. *Inorganics* **2023**, *11* (2), 54.
58. Cook, T. R.; Zheng, Y.-R.; Stang, P. J. Metal–Organic Frameworks and Self-Assembled Supramolecular Coordination Complexes: Comparing and Contrasting the Design, Synthesis, and Functionality of Metal–Organic Materials. *Chem. Rev.* **2013**, *113* (1), 734–777.
59. Cook, T. R.; Stang, P. J. Recent Developments in the Preparation and Chemistry of Metallacycles and Metallacages *via* Coordination. *Chemical Reviews* **2015**, *115* (15), 7001–7045.
60. Yoshizawa, M.; Fujita, M. Development of Unique Chemical Phenomena within Nanometer-Sized, Self-Assembled Coordination Hosts. *Bull. Chem. Soc. Jpn.* **2010**, *83* (6), 609–618.
61. Zhang, R.; Li, R.; Huang, F.; Zhang, M. Metallacycle/Metallacage-Cored Supramolecular Networks. *Prog. Polym. Sci.* **2023**, *141*, 101680.
62. Xu, J.; Wang, J.; Ye, J.; Jiao, J.; Liu, Z.; Zhao, C.; Li, B.; Fu, Y. Metal-Coordinated Supramolecular Self-Assemblies for Cancer Theranostics. *Adv. Sci.* **2021**, *8* (16), e2101101.
63. Li, R.; Zhang, H.; Hou, Y.; Gao, L.; Chu, D.; Zhang, M. Metallacage-Crosslinked Free-Standing Supramolecular

Networks *via* Photo-Induced Copolymerization for Photocatalytic Water Decontamination. *Nat. Commun.* **2025**, *16* (1), 2733.

64. Saputra, M. F. N.; Nursofia, Y.; Tarigan, I. L. The Role of Macrocyclic Compounds as Supramolecular Drug Delivery Systems: A Review. *ChemPublish* **2021**, *9* (1), 141–166.
65. Yue, L.; Yang, K.; Lou, X.-Y.; Yang, Y.-W.; Wang, R. Versatile Roles of Macrocycles in Organic-Inorganic Hybrid Materials for Biomedical Applications. *Matter* **2020**, *3* (5), 1557– 1588.
66. Kali, G.; Haddadzadegan, S.; Bernkop-Schnürch, A. Cyclodextrins and Derivatives in Drug Delivery: New Developments, Relevant Clinical Trials, and Advanced Products. *Carbohydr. Polym.* **2024**, *324*, 121500.
67. Astray, G.; Gonzale-Barreiro, C.; Mejuto, J. C.; Rial-Otero, R.; Simal-Gándara, J. A Review on the Use of Cyclodextrins in Foods. *Food Hydrocolloids* **2009**, *23* (7), 1631–1640.
68. Fouda-Mbanga, B. G.; Tywabi-Ngeva, Z.; Badawy, W. M.; Ebite, C.; Onotu, O. P.; Abogidi, C.; Uzordinma, A. P.; Kaba, S. Green Cyclodextrin Derivatives for Sustainable Remediation of Pesticides and Heavy Metals: A Review. *J. Mol. Struct.* **2025**, *1328*, 141326.
69. Chen, Y.; Liu, Y. Cyclodextrin-Based Bioactive Supramolecular Assemblies. *Chem. Soc. Rev.* **2010**, *39* (2), 495–505.
70. Healy, B.; Yu, T.; da Silva Alves, D. C.; Okeke, C.; Breslin, C. B. Cyclodextrins as Supramolecular Recognition Systems: Applications in the Fabrication of Electrochemical Sensors. *Materials* **2021**, *14* (7), 1668.
71. Assaf, K. I.; Nau, W. M. Cucurbiturils: From Synthesis to High-Affinity Binding and Catalysis. *Chem. Soc. Rev.* **2015**, *44* (2), 394–418.
72. Barrow, S. J.; Kasera, S.; Rowland, M. J.; del Barrio, J.; Scherman, O. A. Cucurbituril-Based Molecular Recognition. *Chem. Rev.* **2015**, *115* (22), 12320–12406.
73. Alabrahim, O. A.; Fahmy, S. A.; Azzazy, H. M. El-S. Stimuli-Responsive Cucurbit[*n*]uril-Based Supramolecular Nanocarriers for Delivery of Chemotherapeutics. *ACS Appl. Nano Mater.* **2023**, *6* (5), 3139–3158.
74. Walker, S.; Oun, R.; McInnes, F. J.; Wheate, N. J. The Potential of Cucurbit[*n*]urils in Drug Delivery. *Bioorg. Med. Chem.* **2011**, *19* (5–6), 616–624.
75. Ogoshi, T.; Yamagishi, T.-A.; Nakamoto, Y. Pillar-Shaped Macrocyclic Hosts Pillar[*n*]arenes: New Key Players for Supramolecular Chemistry. *Chem. Rev.* **2016**, *116* (14), 7937–8002.
76. Gómez-González, B.; García-Río, L.; Basílio, N.; Mejuto, J.; Simal-Gandara, J. Molecular Recognition by Pillar[5]arenes: Evidence for Simultaneous Electrostatic and Hydrophobic Interactions. *Pharmaceutics* **2021**, *14* (1), 60.
77. Wei, S.; Cui, X.; Li, T.; Ma, X.; Liu, L. Pillar[*n*]arene-Based Supramolecular Nanodrug Delivery Systems for Cancer Therapy. *Supramol. Mater.* **2025**, *20* (7), e202400822.
78. Tan, X.; Zhang, Z.; Cao, T.; Zeng, W.; Huang, T.; Zhao, G. Control Assembly of Pillar[6]arene-Modified Ag Nanoparticles on Covalent Organic Framework Surface for Enhanced Sensing Performance toward Paraquat. *ACS Sustainable Chem. Eng.* **2019**, *7* (24), 20051–20059.
79. Hercigonja, M.; Milovanović, B.; Etinski, M.; Petković, M.; Kumar, S.; Ram, B. ER (Phase Transfer Catalyst) Concentration Effect on Kinetics and Product Yield in the Reaction between Solid Potassium p-Nitrobenzoate and Benzyl Bromide. *Rasayan J. Chem.* **2017**, *10* (3), 929–934.
80. Hercigonja, M.; Milovanović, B.; Etinski, M.; Petković, M. Decorated Crown Ethers as Selective Ion Traps: Solvent's Role in Crown's Preference toward a Specific Ion. *J. Mol. Liq.* **2023**, *381*, 121791.

81. Liu, C.; Walter, D.; Neuhauser, D.; Baer, R. Molecular Recognition and Conductance in Crown Ethers. *J. Am. Chem. Soc.* **2003**, *125* (46), 13962–13963.
82. Li, X.; Jin, Y.; Zhu, N.; Jin, L. Y. Applications of Supramolecular Polymers Generated from Pillar[*n*]arene-Based Molecules. *Polymers* **2023**, *15* (23), 4543.
83. Shinkai, S. Calixarenes: The Third Generation of Supramolecules. *Tetrahedron* **1993**, *49* (40), 8933–8968.
84. Zinke, A.; Ziegler, E. Über Kondensationen des Acetessigesters mit Aldehyden. *Ber. Dtsch. Chem. Ges.* **1941**, *74*, 1729–1805; **1944**, *77*, 264–272.
85. Gutsche, C. D.; Muthukrishnan, R. Analysis of the Product Mixtures Produced by the Base-Catalyzed Condensation of Formaldehyde with Para-Substituted Phenols. *J. Org. Chem.* **1978**, *43*(25), 4905–4906.
86. Lhoták, P. Upper Rim-Bridged Calixarenes. *RSC Adv.* **2024**, *14* (32), 23303–23321.
87. Deligöz, H.; Karakuş, Ö.; Koyundereli Çilgi, G. A Brief Review on the Thermal Behaviors of Calixarene-Azocalixarene Derivatives and Their Complexes. *J. Macromol. Sci., Part A: Pure Appl. Chem.* **2012**, *49* (3), 259–274.
88. Isik, A.; Oguz, M.; Kocak, A.; *et al*. Calixarenes: Recent Progress in Supramolecular Chemistry for Application in Cancer Therapy. *J. Incl. Phenom. Macrocycl. Chem.* **2022**, *102*, 439–449.
89. Muley, S.; Dhila H.; Gote, M. Calixarene–Guest Complexes: The Next Innovation in Delivery of Drugs and Biologics. *Adv. Ther.* **2024**, *7* (10), 2400207.
90. Srinivasan, G.; Anaikutti, P.; Mohan, S.; Arukkani, M. Versatile Application of Calixarenes and Their Derivatives: From Drug Delivery to Industrial Catalysis and Environmental Remediation. *Crit. Rev. Anal. Chem.* **2024**, 1–58.
91. Shinkai, S.; Mori,S.; Tsubaki, T.; *et al*. New Water-Soluble Host Molecules Derived from Calix[6]arene. *Tetrahedron Lett.* **1984**, *25* (46), 5315–5318.
92. *re3data.org: SupraBank*; editing status 2024-11-21; *re3data.org – Registry of Research Data Repositories*. https://doi.org/10.17616/R31NJMQ9 (accessed Nov 22, **2025**).
93. Guo, D.-S.; Wang, K.; Liu, Y. Selective Binding Behaviors of *p*-Sulfonatocalixarenes in Aqueous Solution. *J. Incl. Phenom. Macrocycl. Chem.* **2008**, *62* (1), 1–21.
94. Zhao, H.-X.; Guo,D.-S.; Liu, Y. Binding Behaviors of *p*-Sulfonatocalix[4]arene with Gemini Guests. *J. Phys. Chem. B* **2013**, *117* (6), 1978–1987.
95. Cui, J.; Uzunova, V. D.; Guo, D.-S.; Wang, K.; Nau, W. M.; Liu, Y. Effect of Lower-Rim Alkylation of *p*-Sulfonatocalix[4]arene on the Thermodynamics of Host–Guest Complexation. *Eur. J. Org. Chem.* **2010**, *2010* (9), 1704–1710.
96. Coleman, A. W.; Bott, S. G.; Morley, S. D.; Means, C. M.; Robinson, K. D.; Zhang, H.; Atwood, J. L. Novel Layer Structure of Sodium Calix[4]arenesulfonate Complexes – A Class of Organic Clay Mimics? *Angew. Chem., Int. Ed.* **1988**, *27*, 1361–1362.
97. Atwood, J. L.; Clark, D. L.; Juneja, R. K.; Orr, G. W.; Robinson, K. D.; Vincent, R. L. Double Partial Cone Conformation for Na8{Calix[6]arene Sulfonate}·20.5H2O and Its Parent Acid. *J. Am. Chem. Soc.* **1992**, *114*, 7558–7559.
98. Douteau-Guével, N. Coleman, A. W.; Morel, J.-P.; Morel-Desrosiers, N. Complexation of Basic Amino Acids by Water-Soluble Calixarene Sulphonates as a Study of the Possible Mechanisms of Recognition of Calixarene Sulphonates by Proteins. *J. Phys. Org. Chem.* **1998**, *11*, 693–696.

99. Wang, L.-H.; Du, P.; Yang, J.; *et al*. Binding Behaviour and Solubilisation of *p*-Sulfonatocalixarenes to Cinchona Alkaloids. *Supramol. Chem.* **2014**, *26* (10–12), 809–816.

100. Heydari, M.; Salehi, N.; Zadmard, R.; Nau, W. M.; Khajeh, K.; Azizi, Z.; Norouzy, A. *p*-Sulfonatocalix[4]arene Turns Peptide Aggregates into an Efficient Cell-Penetrating Peptide. *Sci. Adv.* **2024**, *14* (44), 32460–32470.

101. Danylyuk, O.; Suwinska, K. Solid-State Interactions of Calixarenes with Biorelevant Molecules. *Chem. Commun.* **2009**, 39, 5799–5813.

102. Shinkai, S.; Araki, K.; Tsubaki, T.; Arimura, T.; Manabe, O. New Syntheses of Calixarene-*p*-sulphonates and *p*-Nitrocalixarenes. *J. Chem. Soc., Perkin Trans. 1* **1987**, 2297–2299.

103. Barbour, L. J.; Atwood, J. L. Non-Covalent Interactions Exert Extraordinary Influence over Conformation and Properties of a Well-Known Supramolecular Building Block: Host–Guest Chemistry of *p*-Sulfonatocalix[6]arene Complexes. *Chem. Commun.* **2001**, 19, 2020–2021.

104. Xing, G.; Bassanetti, I.; Ben, T.; Bracco, S.; Sozzani, P.; Marchiò, L.; Comotti, A. Multifunctional Organosulfonate Anions Self-Assembled with Organic Cations by Charge-Assisted Hydrogen Bonds and the Cooperation of Water. *Cryst. Growth Des.* **2018**, *18* (4), 2082–2092.

105. Atwood, J. L.; Barbour, L. J.; Hardie, M. J.; Raston, C. L. Metal Sulfonatocalix[4,5]arene Complexes: Bi-Layers, Capsules, Spheres, Tubular Arrays and Beyond. *Coord. Chem. Rev.* **2001**, *222* (1), 3–32.

106. Edkins, K.; Anderson, K. M.; Filby, M. H.; Henry, M.; Wright, J.; Mason, S. A.; Gutmann, M. J.; Barbour, L. J.; Oliver, C.; Coleman, A. W.; Atwood, J. L.; Howard, J. A. K.; Steed, J. W. The Structure of Water in *p*-Sulfonatocalix[4]arene. *Chem. – Eur. J.* **2011**, *17* (37), 10259–10271.

107. Zheng, G.-L.; Li, Y.-Y.; Guo, H.-D.; Song, S.-Y.; Zhang, H.-J. Constructing Channel Structures Based on the Assembly of *p*-Sulfonatocalix[4]arene Nanocapsules and $[M(bpdo)_3]^{2+}$ (M = Cu, Zn). *Chem. Commun.* **2008**, 40, 4918–4920.

108. Dalgarno, S. J.; Hardie, M. J.; Makha, M.; Raston, C. L. Controlling the Conformation and Interplay of *p*-Sulfonatocalix[6]arene as Lanthanide Crown Ether Complexes. *Chem. – Eur. J.* **2003**, *9* (12), 2834–2839.

109. Dalgarno, S. J.; Raston, C. L. Capture of Di-Protonated [2.2.2] Cryptand in the Cavity of Two *p*-SulfonatedCalixarenes as Part of 2-D Bi-Layer Lanthanide Coordination Polymers. *Chem. Commun.* **2002**, 19, 2216–2217.

110. Orr, G. W.; Barbour, L. J.; Atwood, J. L. Controlling Molecular Self-Organization: Formation of Nanometer-Scale Spheres and Tubules. *Science* **1999**, *285* (5430), 1049–1052.

111.

a) Liu, Y.; Ward, M. D.; Atwood, J. L.; Barbour, L. J.; Dawson, E. S.; Junk, P. C.; Kienzle, J. X-Ray Structure of the Water-Soluble [Adeninium]–[*p*-Sulfonatocalix[4]arene] Which Displays Cationic and Anionic Bilayers. *Supramol. Chem.* **1996**, *7* (4), 271–274.

b) Selkti, M.; Coleman, A. W.; Nicolis, I.; Douteau-Guével, N.; Villain, F.; Tomas, A.; De Rango, C. The First Example of a Substrate Spanning the Calix[4]arene Bilayer: The Solid-State Complex of *p*-Sulfonatocalix[4]arene with L-Lysine. *Chem. Commun.* **2000**, 2, 161–162.

112. Guo, D.-S.; Liu, Y. Supramolecular Chemistry of *p*-Sulfonatocalix[*n*]arenes and Its Biological Applications. *Acc. Chem. Res.* **2014**, *47* (7), 1925–1934.

113. Geng, W.-C.; Sessler, J. L.; Guo, D.-S. Supramolecular Prodrugs Based on Host–Guest Interactions. *Chem. Soc. Rev.* **2020**, *49* (8), 2303–2315.

114.

a) Guo, D.-S.; Uzunova, V. D.; Su, X.; Liu, Y.; Nau, W. M. Operational Calixarene-Based Fluorescent Sensing Systems for Choline and Acetylcholine and Their Application to Enzymatic Reactions. *Chem. Sci.* **2011**, *2* (9), 1722–1734.

b) Dai, L.; Feng, W.-X.; Zheng, S.-P.; Jiang, J.-J.; Wang, D.; van der Lee, A.; Dumitrescu, D.; Barboiu, M. Progressive Folding and Adaptive Multivalent Recognition of Alkyl Amines and Amino Acids in *p*-Sulfonatocalix[4]arene Hosts: Solid-State and Solution Studies. *J. Org. Chem.* **2020**, *85* (8), 1623–1631.

115. Peng, S.; Wang, K.; Guo, D.-S.; Liu, Y. Supramolecular Polymeric Vesicles Formed by *p*-Sulfonatocalix[4]arene and Chitosan with Multistimuli Responses. *Soft Matter* **2015**, *11* (2), 290–296.

116. McGovern, R. E.; McCarthy, A. A.; Crowley, P. B. Protein Assembly Mediated by Sulfonatocalix[4]arene. *Chem. Commun.* **2014**, *50* (72), 10412–10415.

117. Ling, I.; Sobolev, A. N.; Dalgarno, S. J. Cationic Guests Direct Molecular Capsule Formation and the Impact towards the Extended Self-Assembly in Combinatorial Supramolecular Systems. *Supramol. Chem.* **2021**, *33* (4), 71–79.

118. Ling, I.; Raston, C. L. Primary and Secondary Directing Interactions of Aquated Lanthanide(III) Ions with p-Sulfonated Calix[*n*]arene. *Coord. Chem. Rev.* **2018**, *375* (15), 80–105.

119. Zheng, G.; Fan, W.; Song, S.; Guo, H.; Zhang, H. Guests Inducing *p*-Sulfonatocalix[4]arenes into Nanocapsule and Layer Structure. *J. Solid State Chem.* **2010**, *183*, 1457–1463.

120. Jin, S.; Sanii, R.; Song, B.-Q.; Zaworotko, M. J. Crystal Engineering of Ionic Cocrystals Sustained by the Phenol–Phenolate Supramolecular Heterosynthon. *Cryst. Growth Des.* **2022**, *22* (7), 4582– 4591.

121. Groom, C. R.; Bruno, I. J.; Lightfoot, M. P.; Ward, S. C. The Cambridge Structural Database. *Acta Crystallogr., Sect. B: Struct. Sci., Cryst. Eng. Mater.* **2016**, *72* (Pt 2), 171–179.

122. Asfari, Z.; Harrowfield, J.; Thuéry, P.; Vicens, J. Calixarenes as Polyhapto-Aromatic Ligands: Alkali Metal Ions and Sulfonated Calixarenes. *Supramol. Chem.* **2003**, *15* (1), 69–77.

123. Nichols, P. J.; Makha, M.; Raston, C. L. Confinement of Nucleic Acid Bases and Related Compounds Using Tetra-*p*-Sulfonatocalix[4]arene. *Cryst. Growth Des.* **2006**, *6* (5), 1161–1167.

124. Danylyuk, O.; Butkiewicz, H.; Coleman, A. W.; Suwińska, K. Solvent Control in the Formation of Supramolecular Host–Guest Complexes of Isoniazid with *p*-Sulfonatocalix[4]arene. *CrystEngComm* **2015**, *17* (8), 1745–1749.

125. Gordo, S.; Martos, V.; Santos, E.; Menéndez, M.; Bo, C.; Giralt, E.; de Mendoza, J. Stability and Structural Recovery of the Tetramerization Domain of the p53-R337H Mutant Induced by a Designed Templating Ligand. *Proc. Natl. Acad. Sci. U.S.A.* **2008,** *105* (43), 16426–16431.

126. Morfin, I.; Bühler, E.; Cousin, F.; Grillo, I.; Boué, F. Rodlike Complexes of a Polyelectrolyte (Hyaluronan) and a Protein (Lysozyme) Observed by SANS. *Biomacromolecules* **2011,** *12* (4), 859–870.

127. Beshara, C. S.; Jones, C. E.; Daze, K. D.; Lilgert, B. J.; Hof, F. A Simple Calixarene Recognizes Post-Translationally Methylated Lysine. *ChemBioChem* **2010,** *11* (1), 63–66.

128. Lazar, A.; Da Silva, E.; Navaza, A.; Barbey, C.; Coleman, A. W. A New Packing Motif for Para-Sulfonatocalix[4]arene: The Solid-State Structure of the Para-Sulfonatocalix[4]arene d-Arginine Complex. *Chem. Commun.* **2004**, 19, 2162–2163.

129. Dupont, N.; Lazar, A. N.; Perret, F.; Danylyuk, O.; Suwińska, K.; Navaza, A.; Coleman, A. W. Solid-State Structures of the Complexes between the Antiseptic Chlorhexidine and Three Anionic Derivatives of Calix[4]arene. *CrystEngComm* **2008**, *10* (8), 975–977.

130. Lin, R.-G.; Long, L.-S.; Huang, R.-B.; Zheng, L.-S. Directing Role of Hydrophobic–Hydrophobic and Hydrophilic–Hydrophilic Interactions in the Self-Assembly of Calixarenes/Cucurbiturils-Based Architectures. *Cryst. Growth Des.* **2008**, *8* (3), 791–794.

131. Perret, F.; Lazar, A. N.; Coleman, A. W. Biochemistry of the para-Sulfonato-Calix[*n*]arenes. *Chem. Commun.* **2006**, 23, 2425–2438.

132.

a) Atwood, J. L.; Dalgarno, S. J.; Hardie, M. J.; Raston, C. L. Selective Single Crystal Complexation of l-or d-Leucine by *p*-Sulfonatocalix[6]arene. *Chem. Commun.* **2005**, 3, 337–339.

b) Dalgarno, S. J.; Hardie, M. J.; Atwood, J. L.; Raston, C. L. Bilayers, Corrugated Bilayers, and Coordination Polymers of *p*-Sulfonatocalix[6]arene. *Inorg. Chem.* **2004**, *43* (20), 6351–6356.

c) Atwood, J. L.; Dalgarno, S. J.; Hardie, M. J.; Raston, C. L. Hydrogen-Bonded Arrays of a Ytterbium(III) *p*-Sulfonatocalixarene Complex. *New J. Chem.* **2004**, *28* (2), 326–328.

d) Makha, M.; Raston, C. L.; Sobolev, A. N.; White, A. H. Molecular Capsules Based on *p*-Sulfonatocalix[6]arene Shrouding Two Tetraphenylphosphonium Cations. *Chem. Commun.* **2005**, 15, 1962–1964.

133. Liu, Y.; Li, Q.; Guo, D.-S.; Chen, K. Polymeric Capsules and Honeycomb Aggregates Formed by *p*-Sulfonatocalix[6]arene with Phenanthrolinium Compounds. *Cryst. Growth Des.* **2007**, *7* (9), 1672–1675.

134. Alex, J. M.; Rennie, M. L.; Engilberge, S.; Lehoczki, G.; Dorottya, H.; Fizil, Á.; Batta, G.; Crowley, P. B. Calixarene-Mediated Assembly of a Small Antifungal Protein. *IUCrJ* **2019**, *6* (Pt 2), 238–247.

135. Ramberg, K. O.; Engilberge, S.; Skorek, T.; Crowley, P. B. Facile Fabrication of Protein–Macrocycle Frameworks. *J. 5Am. Chem. Soc.* **2021**, *143* (4), 1896–1907.

136. Flood, R. J.; Cerofolini, L.; Fragai, M.; Crowley, P. B. Multivalent Calixarene Complexation of a Designed Pentameric Lectin. *J. Am. Chem. Soc.* **2024**, *25* (2), 1303–1309.

137. Rennie, M. L.; Fox, G. C.; Pérez, J.; Crowley, P. B. Auto-Regulated Protein Assembly on a Supramolecular Scaffold. *Angew. Chem. Int. Ed.* **2018**, *57* (42), 14246–14250.

138. Flood, R. J.; Mockler, N. M.; Thureau, A.; Malinska, M.; Crowley, P. B. Supramolecular Synthons in Protein-Ligand Frameworks. *Cryst. Growth Des.* **2024**, *24* (5), 2149–2156.

139. Dalgarno, S. J.; Hardie, M. J.; Atwood, J. L.; Warren, J. E.; Raston, C. L. A Complex 3D "Wavy Brick Wall" Coordination Polymer Based on *p*-Sulfonatocalix[8]arene. *J. Chem.* **2005**, *29* (5), 649–652.

140. Alex, J. M.; McArdle, P.; Crowley, P. B. Supramolecular Stacking in a High-Z′ Calix[8]arene–Porphyrin Assembly. *CrystEngComm* **2020**, *22* (14), 14–17.

141. Leśniewska, B.; Perret, F.; Suwinska, K.; Coleman, A. W. Structural Characterization of Inclusion Complexes of para-Sulfonato-Calix[8]arene with 1,2-Bis(4-Pyridyl)-Ethane and 1,3-Bis(4-Pyridyl)-Propane. New "Double Cone" and "Up–Flat–Down" Conformations of para-Sulfonato-Calix[8]arene. *CrystEngComm* **2014**, *16* (21), 4399.

142. F. Perret, V. Bonnard, O. Danylyuk, K. Suwinska, A. W. Coleman. Conformational extremes in the supramolecular assemblies of para-sulfonato-calix[8]arene. *New J. Chem.* **2006**, *30* (7), 987–990.

143. Danylyuk, O.; Perret, F.; Coleman, A. W.; Suwińska, K. The Solid-State Complex of *p*-Sulfonato-Calix[8]arene with Dimethylammonium Cations. *Open Crystallogr. J.* **2008**, *1*, 18–23.

144. Fang, H.; Li, G.; Jiang, D.; Zheng, G. A Channel Rotaxane Coordination Polymer Based on *p*-Sulfonatocalix[8]arene and 4,4′-Bipyridine-N,N′-Dioxide. *Polyhedron* **2019**, *160* (1), 53–57.

145. Smith, C. B.; Barbour, L. J.; Makha, M.; Raston, C. L.; Sobolev, A. N. Unlocking the Elusive Binding Cavity in *p*-Sulfonatocalix[8]arene: Chalice Conformation with $[Co(phen)_3]Cl_3$ and $YbCl_3$. *New J. Chem.* **2006**, *30* (7), 991–996.

146. Croker, D. M.; Davey, R. J.; Rasmuson, Å. C.; Seaton, C. C. Solution-Mediated Phase Transformations between Co-Crystals. *CrystEngComm* **2013**, *15* (11), 2044–2047.

147. Cardew, P. T.; Davey, R. J. The Ostwald Ratio, Kinetic Phase Diagrams, and Polymorph Maps. *Cryst. Growth Des.* **2019**, *19* (10), 5798–5810.

148. Assouma, C. D.; Crochet, A.; Chrmond, Y.; *et al*. Kinetics of Ion Transport through Supramolecular Channels in Single Crystals. *Angew. Chem., Int. Ed.* **2013**, *52* (17), 4682–4685.

149. Ostwald W. Ostwald, W. Studien über die Bildung und Umwandlung fester Körper. 1. Abhandlung: Übersättigung und Überkaltung. *Z. Phys. Chem.* **1897**, *22*, 289–330.

150. Cardew, P. T. Ostwald Rule of Stages – Myth or Reality? *Cryst. Growth Des.* **2023**, *23* (6), 3958–3969.

151. Chaudhary, A. M.; Mobin, S. M. Recent Advances in Single-Crystal-to-Single-Crystal Transformation at the Discrete Molecular Level. *Cryst. Growth Des.* **2017**, *17* (5), 2893–2905.

152. Zhang, P.; Liao, P.-Q.; Zhou, H.-L.; Lin, R.-B.; Chen, X.-M. Single-Crystal X-ray Diffraction Studies on Structural Transformations of Porous Coordination Polymers. *Chem. Soc. Rev.* **2014**, *43*(16), 5789–5814.

153.

a) Zhou, H.; Li, C.-P.; Du, M. Mechanisms of Solvent-Mediated Structural Transformations for Dynamic Crystals of Supramolecular Coordination Systems. *CrystEngComm* **2018**, *24* (50), 13072–13077.

b) Aggarwal, H.; Bhatt, P. M.; Bezuidenhout, C. X.; Barbour, L. J. Direct Evidence for Single-Crystal-to-Single-Crystal Switching of Degree of Interpenetration in a Metal–Organic Framework. *J. Am. Chem. Soc.* **2014**, *136* (10), 3776–3779.

154.

a) Meli, E.; Acedi, F. D.; Riccardis, V. J.; Smith, L. J.; Barbour, I.; Izzo, C.; Tedesco, C. Solid-State Conformational Flexibility at Work: Zipping and Unzipping within a Cyclic Peptoid Single Crystal. *Angew. Chem., Int. Ed.* **2016**, *55* (15), 4679–4682.

b) Little, M. A.; Briggs, M. E.; Jones, J. T. A.; Schmidtmann, M.; Hasell, T.; Chong, S. Y.; Jelfs, K. E.; Chen, L.; Cooper, A. I. Trapping Virtual Pores by Crystal Retro-Engineering. Nat. Chem. **2015**, *7* (2), 153–159.

c) Thomas, J.; Reekmans, G.; Adriaensens, P.; Van Meervelt, L.; Smet, M.; Maes, W.; Dehaen, W.; Dobrzańska, L. Actuated Conformational Switching in a Single Crystal of a Homodithiacalix[4]arene. Angew. Chem., Int. Ed. **2013**, *52* (39), 10237–10240.

155. Danylyuk, O.; Worzakowska, M.; Osypiuk-Tomasik, J.; Sashuk, V.; Kedra-Krolik, K. Solution-Mediated and Single-Crystal-to-Single-Crystal Transformations of Cucurbit[6]uril Host–Guest Complexes with Dopamine. *CrystEngComm* **2020**, *22* (4), 634–638.

156. Thailambal, V. G.; Pattabhi, V.; Row, T. N. G. Structure of benzamidine hydrochloride monohydrate. *Acta Crystallogr.*, **1986**, *C42*, 587–589.

157.

a) Mogaki, R.; Okuro, K.; Aida, T. Molecular Glues for Manipulating Enzymes: Trypsin Inhibition by Benzamidine-Conjugated Molecular Glues. *Chem. Sci.* **2015**, *6* (5), 2802–2805.

b) Tanizawa, K.; Ishii, S.; Hamaguchi, K.; Kanaoka, Y. Proteolytic Enzymes. VI. Aromatic Amidines as Competitive Inhibitors of Trypsin. *J. Biochem.* **1971**, *69* (5), 893–899.

158. Solomin, V. V.; Zaharova, D.; Jirgensons, A. Synthesis of 2-Arylquinazolines by Chan–Evans–Lam Coupling of 2-Formylphenylboronic Acids with Amidines. *Chemistry of Heterocyclic Compounds* **2024**, *60* (3–4), 169–174.

159. Boller, A.; Cereghetti, M.; Schadt, M.; Scherrer, H. Synthesis and Some Physical Properties of Phenylpyrimidines. *Molecular Crystals and Liquid Crystals* **1977**, *42* (1), 215–231.

160. Markwardt, F.; Landmann, H.; Walsmann, P. Comparative Studies on the Inhibition of Trypsin, Plasmin, and Thrombin by Derivatives of Benzylamine and Benzamidine. *Eur. J. Biochem.* **1968**, *6* (4), 502–506.

161.

a) Srikrishnan, T.; De, N. C.; Alam, A. S.; Kapoor, J. Crystal and molecular structure of pentamidine diisethionate: an anti-protozoal drug used in AIDS related pneumonia. *J. Chem. Crystallogr.* **2004**, *34*, 813–818.

b) Lowe, P. R.; Sansom, C. E.; Schwalbe, C. H.; Stevens, M. F. G. Crystal structure and molecular modelling of the antimicrobial drug pentamidine. *J. Chem. Soc., Chem. Commun.* **1989**, 16, 1164–1165.

c) Liew, Y. X.; Ho, A. Y. L.; Wong, G. C.; Chung, S. J.; Tan, T. T.; Tan, B. H. A Retrospective Study of Intravenous Pentamidine for *Pneumocystis jirovecii* Pneumonia Prophylaxis in Adult Patients with Hematologic Malignancies – Its Utility during Respiratory Virus Pandemics. *Int. J. Infect. Dis.* **2024**, *143*, 107059.

162. Barrios, R.; Ferrer-Luque, C.; Arias-Moliz, M. T.; Ruiz-Linares, M.; Bravo, M.; Baca, P. Antimicrobial Substantivity of Alexidine and Chlorhexidine in Dentin. *J. Endod.* **2013**, *39* (11), 1413–1415.

163. Kosiorek, S.; Rosa, B.; Boinski, T.; Butkiewicz, H.; Szymański, M. P.; Danylyuk, O.; Szumna, A.; Sashuk, V. Pillar[4]pyridinium: A Square-Shaped Molecular Box. *Chem. Commun.* **2017**, *53* (100), 13320–13323.

164. Kosiorek, S.; Butkiewicz, H.; Danylyuk, O.; Sashuk, V. Pillar[6]pyridinium: A Hexagonally Shaped Molecular Box That Selectively Recognizes Multicharged Anionic Species. *Chem. Commun.* **2018**, *54* (49), 6316–6319.

165. Zhang, Q.; Cai, L.; Zhong, G.; Luo, W. Simultaneous Determination of Jatrorrhizine, Palmatine, Berberine, and Obacunone in *Phellodendri Amurensis* Cortex by RP-HPLC. *Zhongguo Zhong Yao Za Zhi* **2010**, *35* (16), 2061–2064.

166. Hermann, R.; von Richter, O. Clinical Evidence of Herbal Drugs as Perpetrators of Pharmacokinetic Drug Interactions. *Planta Med.* **2012**, *78* (13), 1458–1477.

167. Chakraborty, S.; Ghosh, B. N. Berberine and Its Impact on Breast Cancer: Unveiling Key Signalling Pathways. *Mol. Biol. Rep*. **2025**, *52* (1), 719.

168. Maxwell, R. A.; Eckhardt, S. B. Iproniazid. In *Drug Discovery*; Humana Press: New York, **1990**; pp 143–154.

169. Chakraborty, S.; Ghosh, B. N. Berberine and Its Impact on Breast Cancer: Unveiling Key Signalling Pathways. *Mol. Biol. Rep.* **2025**, *52* (1), 719.

170. Aggarwal, M. D.; Currie, J. R.; Penn, B. G.; Batra, A. K.; Lal, R. B. *Solution Growth and Characterization of Single Crystals*; NASA Technical Reports Server: **2007**.

171. Kumar, D. K.; Steed, J. W. Supramolecular Gel Phase Crystallization: Orthogonal Self-Assembly under Non-Equilibrium Conditions. *Chem. Soc. Rev.* **2014**, *43* (7), 2080–2088.

172. Sommer, R. D. How to Grow Crystals for X-ray Crystallography. *Acta Crystallogr. C Struct. Chem.* **2024**, *80*(8),

337–342.

173. Agilent. *CrysAlis PRO*; Agilent Technologies Ltd.: Yarnton, UK, **2014**.

174. Berger, H.; Bradaczek, H. A.; Bradaczek, H. Omega-Scan: An X-ray Tool for the Characterization of Crystal Properties. *J. Mater. Sci. Mater. Electron.* **2008**, *19* (Suppl. 1), 1–7.

175. Ladd, M. F. C.; Palmer, R. A. *Structure Determination by X-ray Crystallography: Analysis by X-rays and Neutrons*, 4th ed.; Springer: New York, **2013**.

176. Sheldrick, G. M. Crystal Structure Refinement with SHELXL. *Acta Crystallogr. C Struct. Chem.* **2015**, *71* (Pt 1), 3–8.

177. Farrugia, L. J. WinGX and ORTEP for Windows: An Update. *J. Appl. Crystallogr.* **2012**, *45* (4), 849–854.

178. Yeates, T. O. Detecting and Overcoming Crystal Twinning. *Methods Enzymol.* **1997**, *276*, 344–358.

179. Spek, A. L. Structure Validation in Chemical Crystallography. *Acta Crystallogr. D* **2009**, *65* (Pt 2), 148–155.

180. Hermann, F. In *International Tables for Crystallography*, Vol. C; Kluwer Academic Publishers: Dordrecht, **2006**; pp 763–795.

181. Spek, A. L. PLATON SQUEEZE: A Tool for the Calculation of the Disordered Solvent Contribution to the Calculated Structure Factors. *Acta Crystallogr. C Struct. Chem.* **2015**, *71* (Pt 1), 9–18.

182. Müller, P.; Herbst-Irmer, R.; Spek, A. L.; Schneider, T. R.; Sawaya, M. R. *Crystal Structure Refinement: A Crystallographer's Guide to SHELXL*; Oxford University Press: Oxford, **2006**.

183. Barbour, L. J. X-seed – A Software Tool for Supramolecular Crystallography. *J. Supramol. Chem.* **2001**, *1* (4–6), 189–191.

184. Connolly, M. L. Solvent-Accessible Surfaces of Proteins and Nucleic Acids. *Science* **1983**, *221* (4612), 709–713.

185. Macrae, C. F.; Edgington, P. R.; McCabe, P.; Pidcock, E.; Shields, G. P.; Taylor, R.; Towler, M.; van de Streek, J. Mercury: Visualization and Analysis of Crystal Structures. *J. Appl. Crystallogr.* **2006**, *39*, 453–457.

186. Wood, P. A.; Allen, F. H.; Pidcock, E. Hydrogen-Bond Directionality at the Donor H Atom – Analysis of Interaction Energies and Database Statistics. *CrystEngComm* **2009**, *11* (8), 1563–1571.

187. Gagné, O. C.; Hawthorne, F. C. Bond-Length Distributions for Ions Bonded to Oxygen: Alkali and Alkaline-Earth Metals. *Acta Crystallogr. B* **2016**, *72* (4), 602–625.

188. Byrn, S. R.; Zografi, G.; Chen, X. Differential Scanning Calorimetry and Thermogravimetric Analysis. In *Solid State Properties of Pharmaceutical Materials*; John Wiley & Sons, Ltd.: Hoboken, NJ, **2017**; pp 124–141.

189. Zainal, N. F. A.; Saiter, J. M.; Halim, S. I. A.; Lucas, R.; Chan, C. H. Thermal Analysis: Basic Concept of Differential Scanning Calorimetry and Thermogravimetry for Beginners. *Chemistry Teacher Int.* **2021**, *3* (2), 59–75.

190. Louër, D. Powder X-ray Diffraction, Applications. In *Encyclopedia of Spectroscopy and Spectrometry*, 3rd ed.; Lindon, J. C.; Tranter, G. E.; Koppenaal, D. W., Eds.; Academic Press: London, **2017**; pp 723–731.

191. Holder, C. F.; Schaak, R. E. Tutorial on Powder X-ray Diffraction for Characterizing Nanoscale Materials. *ACS Nano* **2019**, *13* (7), 7359–7365.

192. Degen, T.; Bron, E.; Sadki, M. *Introduction to HighScore Plus*; PANalytical B.V.: Almelo, The Netherlands, **2019**.

193. Cohen, Y.; Slovak, S.; Avram, L. Solution NMR of Synthetic Cavity-Containing Supramolecular Systems: What Have We Learned On and From? *Chem. Commun.* **2021**, *57* (71), 8856–8884.

194. Willcott, M. R. MestRe Nova. *J. Am. Chem. Soc.* **2009**, *131* (36), 13180–13180.

195. Vicatos, A. I.; Loots, L.; Mathada, G.; Drwęska, J.; Janiak, A. M.; Barbour, L. J. Inflatable Porous Organic Crystals. *Nat. Mater*. **2025**, *24*, https://doi.org/10.1038/s41563-025-02393-6.

196. Butkiewicz, H.; Kosiorek, S.; Sashuk, V.; Zimnicka, M.; Danylyuk, O. Inclusion of Pentamidine in Carboxylated Pillar[5]arene: Late Sequential Crystallization and Diversity of Host–Guest Interactions. *Cryst. Growth Des.* **2022**, *22* (5), 2854–2862.

197. Kravets, K.; Kravets, M.; Kędra, K.; Danylyuk, O. *p*-Sulfonatocalix[8]arene Coordinates Sodium Cations and Forms a Host–Guest Complex with Berberine: Insight from the Crystal Structure. *Supramol. Chem.* **2023**, *33* (12), 666–676.

7. ANNEX I – the parameters of intermolecular interactions

Structure of the complex C4S_BNZ_Form I

Table 21. The parameters of hydrogen bonds. Distances (d) are given in Å, angles in °.

D – H	d(D – H)	d(D···A)	d(H···A)	<D – H···A	A
O–H···O intramolecular hydrogen bonds at C4S lower rim					
O4–H4A	0.84	2.734(2)	1.93	159	O16
O8–H8	0.84	2.724(3)	1.92	161	O4
O12–H12	0.84	2.712(3)	1.89	166	O8
O16–H16A	0.84	2.670(2)	1.88	156	O12
O20–H20	0.84	2.692(2)	1.90	157	O32
O24–H24	0.84	2.644(2)	1.84	160	O20
O28–H28	0.84	2.672(2)	1.85	165	O24
O32–H32A	0.84	2.732(3)	1.91	166	O28
N–H···O interactions between benzamidine and C4S / water molecules					
N1X–H1XA	0.88	2.939(10)	2.07	168	O22
N1X–H1XB	0.88	3.095(10)	2.49	127	O15[1]
N2X–H2XA	0.88	2.912(8)	2.06	162	O23
N2X–H2XB	0.88	2.993(9)	2.15	161	O10[1]
N1Y–H1YA	0.88	2.767(15)	1.89	174	O30[2]
N1Y–H1YB	0.88	3.111(4)	2.31	151	O17
N2Y–H2YA	0.88	2.923(10)	2.05	170	O29[2]
N2Y–H2YB	0.88	2.898(6)	2.14	143	O4W[2]
N1Z–H1ZA	0.88	3.132(7)	2.45	134	O7W[3]
N1Z–H1ZB	0.88	3.079(7)	2.20	174	O8W[3]
N2Z–H2ZA	0.88	2.811(5)	1.97	160	O3W[3]
N2Z–H2ZB	0.88	2.795(7)	2.05	142	O26
N1I–H1IA	0.88	2.272(9)	2.01	144	O4W[2]
N1I–H1IB	0.88	2.860(11)	2.00	165	O25A
N2I–H2IA	0.88	2.645(9)	1.91	144	O4WK
N2I–H2IB	0.88	2.886(12)	2.03	165	O8WK[3]
N1K–H1KA	0.88	2.745(8)	1.97	146	O23[4]
N1K–H1KB	0.88	3.200(9)	2.61	126.3(3)	O9
N2K–H2KA	0.88	3.009(7)	2.16	163	O21[4]
N2K–H2KB	0.88	2.799(10)	1.98	153	O1WE[5]
N1L–H1LA	0.88	2.975(3)	2.41	123	O14[6]
N1L–H1LB	0.88	2.864(3)	2.12	142	O15[1]
N2L–H2LA	0.88	2.916(3)	2.12	150	O1[1]
N2L–H2LB	0.88	3.158(8)	2.30	165	O8W[2]
N1M–H1MA	0.88	2.947(3)	2.08	170	O1[6]
N1M–H1MB	0.88	2.857(3)	2.00	164	O13[1]
N2M–H2MA	0.88	2.941(3)	2.19	143	O2[6]
N2M–H2MB	0.88	2.951(4)	2.09	165	O11
N1NA–H1NC	0.88	2.743(8)	1.92	154	O18[7]
N1NA–H1ND	0.88	3.020(12)	2.15	172	O5A[8]
N2NA–H2NC	0.88	2.894(9)	2.03	169	O19[7]
N2NA–H2ND	0.88	2.801(13)	1.99	153	O26A
N1V–H1VA	0.88	2.761(15)	2.42	103	O2WE

N1V–H1VB	0.88	2.905(12)	2.08	156	O9W[9]
N2V–H2VA	0.88	2.849(15)	2.16	134	O7A[4]
N2V–H2VB	0.88	2.978(10)	2.19	148	O10[4]
C–H···O interactions between benzamidine and C4S / water molecules					
C3Y–H3Y	0.95	3.483(4)	2.56	163	O17
C6Y–H6Y	0.95	3.367(5)	2.42	176	O25
C6Z–H6Z	0.95	3.426(9)	2.57	149	O10W
C3I–H3I	0.95	2.897(15)	2.03	151	O8WK
C6I–H6I	0.95	3.129(12)	2.59	117	O25[3]
C6I–H6I	0.95	2.980(15)	2.20	139	O3WA[3]
C3K–H3K	0.95	2.710(12)	2.30	105	O5WK
C6K–H6K	0.95	2.747(16)	2.25	112	O8WK[4]
C3L–H3L	0.95	3.061(11)	2.49	119	O10B[2]
C3L–H3L	0.95	2.954(9)	2.46	112	O8WA[2]
C4L–H4L	0.95	3.058(10)	2.48	119	O10B[2]
C3M–H3M	0.95	3.342(5)	2.42	164	O11
C7M–H7M	0.95	3.242(3)	2.33	160	O13[1]
C6NA–H6NA	0.95	2.735(15)	2.31	107	O2WN[1]
C7NA–H7NA	0.95	3.146(12)	2.23	161	O5A[8]
C3V–H3V	0.95	3.26(3)	2.41	148	O9WA[9]
C6V–H6V	0.95	3.264(13)	2.54	134	O9W

Symmetry operations: [1](x,–1/2+y,1/2–z), [2](1/2–x,1/2–y,1/2–z), [3](1/2–x,y,1–z), [4](–x,1/2+y,1/2–z), [5](–1/2+x,1–y,z), [6](x,1/2–y,–1/2+z), [7](x,1/2–y,1/2+z), [8](–x,–y,1–z), [9](1/2–x,3/2–y,1/2–z).

Table 22. The parameters of X–H···π interactions. Distances (d) are given in Å, angles in °.

D – H	d(D – H)	d(D···A)	d(H···A)	<D – H···A	A
N–H···π interactions between benzamidine molecules					
N1X–H1XB	0.88	3.606(9)	2.92	136	Cg (C2L–C7L)
C–H···π interactions between benzamidine and C4S molecules					
C3X–H3X	0.95	3.613(4)	2.96	127	Cg(C15–C20)[1]
C4X–H4X	0.95	3.618(5)	2.97	127	Cg(C15–C20)[1]
C5X–H5X	0.95	3.595(4)	2.88	133	Cg(C1–C6)[1]
C4Y–H4Y	0.95	3.519(3)	2.78	135	Cg(C29–C34)
C5Y–H5Y	0.95	3.647(4)	2.94	132	Cg(C43–C48)
C49–H49A	0.99	3.500(3)	2.67	142	(C2M–C7M)[2]
C–H···π interactions between benzamidine molecules					
C3N–H3N	0.95	3.257(7)	2.92	102	Cg(C2I–C7I)
C3N–H3N	0.95	3.403(8)	2.99	108	Cg(C2I–C7I)[3]
C–H···π interactions between C4S molecules					
C7–H7B	0.99	3.521(3)	2.95	118	Cg(C8–C13)[4]
C21–H21A	0.99	3.285(3)	2.75	114	Cg(C43–C48)

Symmetry operation: [1](–x,–1/2+y,1/2–z), [2](–x,1/2+y,1/2–z), [3](1/2–x,y,1–z). [4](–x,–y,1–z).

Cg – centroid of benzamidine / C4S aromatic ring

Table 23. The parameters of π···π interactions. Distances (d) are given in Å.

CgA	d(CgA···CgB)	CgB
π···π interactions between benzamidine and C4S molecules		

Cg(C2M–C7M)	3.877(17)	Cg(C36–C41)
π···π interactions between C4S molecules		
Cg(C29–C34)	3.680(14)	Cg(C1–C6)[1]

Symmetry operation: [1](x,1/2–y,–1/2+z).

Cg – centroid of benzamidine / C4S aromatic ring.

Structure of the complex C4S_BNZ_Form II

Table 24. The parameters of hydrogen bonds. Distances (d) are given in Å, angles in °.

D – H	d(D – H)	d(D···A)	d(H···A)	<D – H···A	A
O–H···O intramolecular hydrogen bonds at C4S lower rim					
O4–H4A	0.84	2.665(2)	2.03	132	O8
O8–H8	0.84	2.706(2)	2.05	134	O12
O12–H12	0.84	2.707(2)	1.90	161	O16
O16–H16A	0.84	2.622(2)	1.80	167	O4
O20–H20	0.84	2.679(2)	1.89	156	O24
O24–H24	0.84	2.683(2)	2.04	132	O28
O28–H28	0.84	2.679(2)	1.86	164	O32
O32–H32A	0.84	2.637(2)	1.82	164	O20
N–H···O interactions between benzamidine and C4S / water molecules					
N1X–H1XA	0.88	3.119(2)	2.28	158	O10[1]
N1X–H1XB	0.88	3.107(3)	2.25	164	O6W
N1X–H1XB	0.88	2.864(14)	2.02	159	O6WA[1]
N2X–H2XA	0.88	2.865(2)	2.00	167	O11[1]
N2X–H2XB	0.88	2.875(4)	2.05	155	O9W
N1Y–H1YA	0.88	3.027(4)	2.22	153	O26[2]
N1Y–H1YB	0.88	2.879(4)	2.03	160	O1W
N2Y–H2YA	0.88	3.009(3)	2.17	160	O25[2]
N2Y–H2YB	0.88	2.698(3)	2.05	130	O18
N1Z–H1ZA	0.88	2.810(2)	1.93	175	O5[4]
N1Z–H1ZB	0.88	3.098(2)	2.53	123	O20[4]
N2Z–H2ZA	0.88	3.033(2)	2.18	164	O7[4]
N2Z–H2ZB	0.88	2.744(2)	1.89	164	O19[5]
N1I–H1IA	0.88	2.798(4)	1.93	168	O8W[7]
N1I–H1IB	0.88	2.800(2)	1.95	163	O2[7]
N2I–H2IA	0.88	2.814(13)	1.99	156	O11A[5]
N2I–H2IB	0.88	2.905(3)	2.10	151	O30
N1K–H1KA	0.88	2.985(3)	2.14	161	O22[4]
N1K–H1KB	0.88	2.731(2)	1.89	159	O1[9]
N2K–H2KA	0.88	2.819(3)	1.94	176	O23[4]
N2K–H2KB	0.88	3.049(2)	2.45	126	O4
N1L–H1LA	0.88	2.785(2)	1.92	166	O31
N1L–H1LB	0.88	2.787(2)	2.00	148	O23[4]
N2L–H2LA	0.88	2.933(2)	2.08	162	O30
N2L–H2LB	0.88	2.775(2)	1.95	155	O9[5]
N1M–H1MA	0.88	2.869(3)	2.03	159	O14[3]
N1M–H1MB	0.88	2.764(3)	1.96	152	O5
N2M–H2MA	0.88	2.886(3)	2.01	172	O15[3]

N2M–H2MB	0.88	2.771(3)	1.97	151	O27[8]
N1V–H1VA	0.88	2.832(2)	2.07	144	O3W
N1V–H1VB	0.88	2.951(2)	2.12	157	O7[5]
N2V–H2VA	0.88	2.796(3)	1.95	162	O7W
N2V–H2VB	0.88	3.002(3)	2.16	159	O25[6]
C–H···O interactions between benzamidine and C4S / water molecules					
C3Y–H3Y	0.95	3.379(4)	2.49	157	O2W[3]
C4Z–H4Z	0.95	3.486(3)	2.57	162	O4W[5]
C3I–H3I	0.95	3.291(3)	2.44	149	O29[1]
C3M–H3M	0.95	3.062(3)	2.57	112	O28
C6I–H6I	0.95	3.26(2)	2.43	145	O7WA[7]
C6K–H6K	0.95	3.374(3)	2.44	170	O5W[9]
C5L–H5L	0.95	3.493(3)	2.60	157	O19[4]
C6L–H6L	0.95	3.175(3)	2.47	131	O18[4]
C5V–H5V	0.95	3.421(3)	2.54	155	O13[3]

Symmetry operations: [1](1/2–x,y,1/2–z), [2](1/2–x,y,3/2–z), [3](x,1+y,z), [4](x,–1+y,z), [5](1–x,2–y,1–z), [6](1/2+x,3–y,–1/2+z), [7](1/2+x,2–y,1/2+z), [8](–x,3–y,1–z), [9](–x,2–y,1–z).

Table 25. The parameters of X–H···π interactions. Distances (d) are given in Å, angles in °.

D – H	d(D – H)	d(D···A)	d(H···A)	<D – H···A	A
C–H···π interactions between benzamidine and C4S molecules					
C5X–H5X	0.95	3.507(2)	2.59	163	Cg(C15–C20)
C6X–H6X	0.95	3.630(3)	2.70	165	Cg(C8–C13)
C5Y–H5Y	0.95	3.775(7)	2.96	144	Cg(C43–C48)
C6Y–H7Y	0.95	3.366(5)	2.49	153	Cg(C50–C55)
C5YA–H5YA	0.95	3.770(3)	2.84	168	Cg(C36–C41)
C6YA–H6YA	0.95	3.400(2)	2.45	171	Cg(C43–C48)
C4YB–H4YB	0.95	3.520(4)	2.98	117	Cg(C36–C41)[1]
C4YB–H4YB	0.95	3.660(4)	2.93	134	Cg(C43–C48)[1]
C5YB–H5YB	0.95	3.570(3)	2.71	152	Cg(C50–C55)[1]
C7Z–H7Z	0.95	3.720(3)	2.80	164	Cg(C29–C34)[1]
C3K–H3K	0.95	3.748(3)	2.84	161	Cg(C1–C6)
C–H···π interactions between C4S molecules					
C7–H7A	0.99	3.209(2)	2.75	109	Cg(C50–C55)
C7–H7B	0.99	3.209(2)	2.85	102	Cg(C50–C55)
C35–H35B	0.99	3.232(2)	2.62	120	Cg(C22–C27)[2]

Symmetry operations: [1](x,–1+y,z), [2](x,1+y,z).

Cg – centroid of C4S aromatic ring.

Structure of the complex C4S_BNZ_Form III

Table 26. The parameters of hydrogen bonds. Distances (d) are given in Å, angles in °.

D – H	d(D – H)	d(D···A)	d(H···A)	<D – H···A	A
O–H···O intramolecular hydrogen bonds at C4S lower rim					
O4–H4	0.84	2.894(3)	2.31	127	O16
O8–H8	0.84	2.692(2)	1.88	161	O4
O12–H12	0.84	2.846(2)	2.27	126	O8

O16–H16A	0.84	2.693(2)	1.87	168	O12
O–H···O interactions between C4S molecules					
O12–H12	0.84	2.911(2)	2.26	135	O6[1]
O–H···O interactions between water molecules (Zundel cations)					
O1W–H1WC	1.23(4)	2.441(2)	1.21(4)	177(4)	O2W
O1W–H1WA	0.88(3)	2.605(3)	1.73(3)	173(3)	O5W
O1W–H1WB	0.88(3)	2.690(2)	1.83(3)	167(3)	O15[4]
O2W–H2WA	0.88(3)	2.573(2)	1.69(2)	177(3)	O7W
O2W–H2WB	0.87(3)	2.630(3)	1.77(3)	169(4)	O3[5]
O3W–H3WA	0.85(4)	2.745(3)	1.91(4)	168(3)	O1[6]
O3W–H3WB	0.86(4)	2.687(3)	1.84(4)	171(3)	O13[8]
O4–H4	0.84	2.840(3)	2.24	128	O3W[2]
O4W–H4WA	0.87(4)	2.594(5)	1.73(4)	171(3)	O6
O4W–H4WB	0.88(3)	2.649(5)	1.81(3)	160(4)	O10[7]
O4W–H4WC	1.22(4)	2.557(5)	1.42(5)	150(4)	O3W
N–H···O interactions between benzamidine and C4S / water molecules					
N1X–H1XA	0.88	2.873(3)	1.99	177	O15
N1X–H1XB	0.88	2.904(3)	2.13	146	O2
N2X–H2XA	0.88	2.872(3)	2.06	154	O7W[3]
N2X–H2XB	0.88	2.855(3)	2.02	157	O11
N1Y–H1YA	0.88	2.849(2)	2.01	159	O9[3]
N1Y–H1YB	0.88	2.819(3)	2.03	148	O2[6]
N2Y–H2YA	0.88	2.847(2)	1.97	173	O6W[1]
N2Y–H2YB	0.88	2.929(3)	2.09	159	O10

Symmetry operations: [1](1–x,–y,1–z), [2](1–x,–y,–z), [3](–1+x,y,z), [4](1–x,1–y,1–z), [5](2–x,1–y,1–z), [6](x,–1+y,z), [7](1+x,y,z), [8](1+x,–1+y,z).

Table 27. The parameters of X–H···π interactions. Distances (d) are given in Å, angles in °.

D – H	**d(D – H)**	**d(D···A)**	**d(H···A)**	**<D – H···A**	**A**
C–H···π interactions between benzamidine and C4S molecules					
C4X–H4X	0.95	3.546(3)	2.71	147	Cg(C8–C13)

Cg – centroid of C4S aromatic ring.

Structure of the complex C4S_BNZ_Form IV

Table 28. The parameters of hydrogen bonds. Distances (d) are given in Å, angles in °.

D – H	**d(D – H)**	**d(D···A)**	**d(H···A)**	**<D – H···A**	**A**
O–H···O intramolecular hydrogen bonds at C4S lower rim					
O4–H4A	0.80(4)	2.570(3)	1.78(4)	168(5)	O16
O8–H8A	0.84	2.866(4)	2.04	168	O4
O12–H12A	0.84	2.592(3)	1.77	164	O16
N–H···O interactions between benzamidine and C4S / water molecules					
N1X–H1XA	0.88	2.825(6)	1.96	168	O6[1]
N1X–H1XB	0.88	2.969(5)	2.28	135	O15
N2X–H2XA	0.88	2.897(7)	2.19	137	O6A[1]
N2X–H2XB	0.88	2.897(5)	2.06	158	O3[1]
N1Y–H1YA	0.88	2.960(3)	2.18	147	O11
N1Y–H1YB	0.88	2.935(4)	2.08	163	O13

N2Y–H2YA	0.88	2.946(3)	2.17	148	O11
N2Y–H2YB	0.88	2.903(3)	2.05	164	O1[1]
N1Z–H1ZA	0.88	2.973(3)	2.19	148	O1W[2]
N1Z–H1ZB	0.88	2.857(3)	2.01	161	O14[3]
N2Z–H2ZA	0.88	2.961(3)	2.13	157	O2[4]
N2Z–H2ZB	0.88	2.855(3)	2.03	155	O16[5]
C–H···O interactions between benzamidine and C4S molecules					
C3X–H3X	0.95	3.393(8)	2.47	165	O3[1]
C4X–H4X	0.95	2.692(14)	1.95	133	O7A
C3Y–H3Y	0.95	3.146(4)	2.38	138	O1[1]
C5Y–H5Y	0.95	3.395(4)	2.50	157	O8[6]
C7Y–H7Y	0.95	3.257(4)	2.33	165	O13
C7Z–H7Z	0.95	3.339(3)	2.55	141	O14[3]

Symmetry operations: [1](1–x,1–y,1–z), [2](–x,2–y,1–z), [3](x,1+y,z), [4](–1+x,1+y,z), [5](–x,1–y,2–z), [6](x,y,–1+z).

Table 29. The coordination distances between sodium cations and C4S, water molecules. Distances (d) are given in Å.

Metal	d(Na···O)	O
Na1	2.300(3)	O9
	2.381(3)	O1W
	2.382(3)	O2W
	2.620(9)	O4W[1]
	2.433(6)	O6W
	2.365(5)	O7WA[1]
Na2	2.458(3)	O2[2]
	2.755(3)	O4[3]
	2.410(5)	O5
	2.321(4)	O3W
	2.431(9)	O4W
	2.380(4)	O5W
Na2a	2.294(7)	O1WA
	2.406(15)	O4WA
	2.329(8)	O5WA
	2.465(8)	O5WA[1]
	2.428(6)	O6WA
	2.337(6)	O7WA

Symmetry operations: [1](1–x,2–y,1–z), [2](x,1+y,z), [3](1–x,1–y,2–z).

Table 30. The parameters of X–H···π interactions. Distances (d) are given in Å, angles in °.

D – H	d(D – H)	d(D···A)	d(H···A)	<D – H···A	A
C–H···π interactions between benzamidines and C4S molecules					
C5X–H5X	0.95	3.562(10)	2.75	144	Cg(C8–C13)
C3Z–H3Z	0.95	3.683(3)	2.89	142	Cg(C22–C27)[1]
C14–H14B	0.99	3.757(3)	2.77	173	Cg(C2Z–C7Z)

Symmetry operations: [1](–x,1–y,2–z).

Cg – centroid of benzamidine / C4S aromatic ring.

Table 31. The parameters of π···π interactions. Distances (d) are given in Å.

CgA	d(CgA···CgB)	CgB
π···π interactions between benzamidine molecules		
Cg(C2Z–C7Z)	3.936(17)	Cg(C2Z–C7Z)[1]

Symmetry operations: [1](x,1+y,z).

Cg – centroid of benzamidine aromatic ring.

Structure of the complex C4S_BNZ_Form V

Table 32. The parameters of hydrogen bonds. Distances (d) are given in Å, angles in °.

D – H	d(D – H)	d(D···A)	d(H···A)	<D – H···A	A
O–H···O intramolecular hydrogen bonds at C4S lower rim					
O8–H8	0.84	2.508(14)	1.68	167	O4
O12–H12	0.84	2.685(15)	1.87	163	O8
O16–H16A	0.84	2.558(15)	1.73	171	O4
N–H···O interactions between benzamidine and C4S / water molecules					
N1X–H1XA	0.88	3.334(6)	2.45	178	O13[1]
N1X–H1XB	0.88	2.907(18)	2.20	137	O10
N2X–H2XA	0.88	2.955(5)	2.20	144	O15[1]
N2X–H2XB	0.88	2.780(18)	1.94	158	O11[1]
N1Y–H1YA	0.88	2.910(2)	2.10	152	O2W
N1Y–H1YB	0.88	2.876(2)	2.03	160	O9[2]
N2Y–H2YA	0.88	3.053(3)	2.29	145	O2W
N2Y–H2YB	0.88	2.649(7)	1.83	155	O2[3]
N1Z–H1ZA	0.88	2.738(9)	1.87	170	O3[4]
N1Z–H1ZB	0.88	3.035(4)	2.34	136	O14[5]
N2Z–H2ZA	0.88	2.873(4)	2.00	170	O1[4]
N2Z–H2ZB	0.88	2.952(16)	2.08	169	O9[6]
N1I–H1IA	0.88	2.918(4)	2.21	138	O4W[1]
N1I–H1IB	0.88	2.937(5)	2.08	164	O14[7]
N2I–H2IA	0.88	2.961(4)	2.26	137	O7[1]
N2I–H2IB	0.88	2.965(7)	2.13	159	O15
N1K–H1KA	0.885(18)	2.811(3)	2.00(19)	152.5(17)	O5[2]
N1K–H1KB	0.853(17)	2.983(18)	2.48(2)	118.6(17)	O16
N2K–H2K1	0.88	3.036(3)	2.30	141	O5[2]
N2K–H2K2	0.88	2.932(3)	2.13	152	O6[8]
C–H···O interactions between benzamidine and C4S molecules					
C7X–H7X	0.95	3.443(2)	2.59	150	O11[1]
C7Z–H7Z	0.95	3.369(2)	2.42	176	O11[6]
C4Y–H4Y	0.95	2.814(4)	2.37	108	O5A
C3I–H3I	0.95	2.953(13)	2.19	137	O13A[7]
C5I–H5I	0.95	3.234(6)	2.57	127	O12[6]
C7I–H7I	0.95	2.905(13)	2.04	150	O15

Symmetry operations: [1](1–x,1–y,1–z), [2](3/2–x,1/2+y,3/2–z), [3](3/2–x,–1/2+y,3/2–z), [4](1+x,y,z), [5](1/2+x,3/2–y,1/2+z), [6](2–x,1–y,1–z), [7](3/2–x,–1/2+y,1/2–z), [8](1/2+x,3/2–y,–1/2+z).

Table 33. The parameters of X–H···π interactions. Distances (d) are given in Å, angles in °.

D – H	d(D – H)	d(D···A)	d(H···A)	<D – H···A	A
N–H···π interactions between benzamidine molecules					
N1K–H1KA	0.853(17)	3.511(17)	2.95(2)	125.4(16)	Cg(C2Z–C7Z)
C–H···π interactions between benzamidine and C4S molecules					
C4X–H4X	0.95	3.510(18)	2.86	126	Cg(C15–C20)
C5X–H5X	0.95	3.566(18)	2.96	123	Cg(C1–C6)
C5IA–H5IA	0.95	3.516(4)	2.95	120	Cg(C2X–C7X)
C4K–H4K	0.95	3.555(19)	2.67	156	Cg(C15–C20)[1]
C–H···π interactions between C4S molecules					
C14–H14A	0.99	3.470(15)	2.52	162	Cg(C1–C6)[2]

Symmetry operation: [1](2–x,1–y,1–z), [2](3/2–x,–1/2+y,3/2–z).

Cg – centroid of benzamidine / C4S aromatic ring.

Table 34. The parameters of π···π interactions. Distances (d) are given in Å.

CgA	d(CgA···CgB)	CgB
π···π interactions between benzamidine and C4S molecules		
Cg(C2K–C7K)	3.960(9)	Cg(C22–C27)
π···π interactions between benzamidine molecules		
Cg(C2I–C7I)	3.928(4)	Cg(C2Z–C7Z)

Cg – centroid of benzamidine / C4S aromatic ring.

Structure of the complex C6S_BNZ

Table 35. The parameters of hydrogen bonds. Distances (d) are given in Å, angles in °.

D – H	d(D – H)	d(D···A)	d(H···A)	<D – H···A	A
O–H···O hydrogen bonds at C6S lower rim					
O4–H4	0.84	2.826(16)	2.04	156	O12[1]
O8–H8	0.84	2.573(18)	1.79	153	O1W
O12–H12	0.84	2.628(17)	1.80	167	O8
N–H···O interactions between BNZ and C6S / water molecules					
N1X–H1XA	0.88	2.830(2)	2.05	147	O2[2]
N1X–H1XB	0.88	2.901(2)	2.11	149	O7[1]
N2X–H2XA	0.88	2.909(18)	2.16	142	O2[2]
N2X–H2XB	0.88	2.929(19)	2.06	172	O1W
N1Y–H1YA	0.88	2.880(2)	2.03	162	O1
N1Y–H1YB	0.88	2.907(4)	2.10	153	O3W
N2Y–H2YA	0.88	2.823(2)	1.97	163	O3
N2Y–H2YB	0.88	2.799(2)	2.05	142	O9[3]
N1Z–H1ZA	0.88	3.140(3)	2.36	147	O7[4]
N1Z–H1ZB	0.88	2.878(3)	2.05	157	O9[3]
N2Z–H2ZA	0.88	3.089(10)	2.30	150	O7[4]
N2Z–H2ZB	0.88	2.990(10)	2.17	154	O3W[5]
C–H···O interactions between BNZ and C6S molecules					
C3Z–H3Z	0.95	2.906(4)	2.49	106	O9[3]
C5Y–H5Y	0.95	3.388(4)	2.48	160	O1[6]
C–H···O interactions between C6S molecules					

C1–H1B	0.99	3.396(2)	2.48	154	O2[7]
C17–H17	0.95	3.354(2)	2.45	159	O3[8]

Symmetry operations: [1](1–x,1–y,1–z), [2](x,–1+y,z), [3](x,3/2–y,1/2+z), [4](1–x,1/2+y,3/2–z), [5](2–x,1/2+y,3/2–z), [6](2–x,–1/2+y,3/2–z), [7](1–x,2–y,1–z), [8](1–x,–1/2+y,3/2–z).

Table 36. The parameters of X–H···π interactions. Distances (d) are given in Å, angles in °.

D – H	d(D – H)	d(D···A)	d(H···A)	<D – H···A	A
C–H···π interactions between BNZ and C6S molecules					
C3X–H3X	0.95	3.856(2)	2.97	156	Cg(C9–C14)[1]
C4X–H4X	0.95	3.543(2)	2.64	159	Cg(C16–C21–C20–C19a[1]–C18a[1]–C17a[1])
C4X–H4X	0.95	3.543(2)	2.64	159	Cg(C17–C18–C19–C20a–C21a–C16a)[1]
C–H···π interactions between BNZ molecules					
C7Z–H7Z	0.95	3.786(2)	2.52	147	Cg(C2Y–C7Y)[2]

Symmetry operation: [1](1–x,1–y,1–z), [2](2–x,1/2+y,3/2–z).

Cg – centroid of BNZ / C6S aromatic ring.

Structure of the complex C4S_M–BNZ

Table 37. The parameters of hydrogen bonds. Distances (d) are given in Å, angles in °.

D – H	d(D – H)	d(D···A)	d(H···A)	<D – H···A	A
O–H···O intramolecular hydrogen bonds at C4S lower rim					
O4–H4	0.84	2.688(2)	1.92	151	O16
O8–H8	0.84	2.914(19)	2.49	113	O4
O12–H12	0.84	2.626(2)	1.82	152	O8
O16–H16A	0.84	2.691(18)	1.88	163	O12
O–H···O hydrogen bonds between ethanol and C4S molecules					
O1E–H1E	0.84	3.005(4)	2.17	179	O13[1]
N–H···O interactions between M–BNZ and ethanol / C4S / water molecules					
N1I–H1I1	0.88	2.793(5)	1.91	177	O1E[2]
N1I–H1I2	0.88	2.902(3)	2.11	149	O6[3]
N2I–H2I1	0.88	2.907(2)	2.10	153	O2W[4]
N2I–H2I2	0.88	2.770(3)	1.93	158	O1W[4]
N1X–H1XA	0.88	2.942(2)	2.20	142	O1[1]
N1X–H1XB	0.88	3.026(2)	2.22	153	O2W[3]
N2X–H2XA	0.88	2.789(3)	1.99	151	O1[5]
N2X–H2XB	0.88	2.969(3)	2.10	167	O15
N1Y–H1Y1	0.88	2.845(2)	1.99	163	O7[6]
N1Y–H1Y2	0.88	2.953(2)	2.09	166	O11[7]
N2Y–H2Y1	0.88	3.080(2)	2.32	145	O6[6]
N2Y–H2Y2	0.88	2.846(2)	1.98	169	O14[8]
N1Z–H1ZA	0.88	2.789(2)	1.93	166	O9[9]
N1Z–H1ZB	0.88	2.878(2)	2.23	130	O10
N2Z–H2ZA	0.88	3.284(2)	2.59	136	O9
N2Z–H2ZB	0.88	3.053(2)	2.19	166	O6[6]
C–H···O interactions between M–BNZ and C4S molecules					
C4Y–H4Y	0.95	3.312(3)	2.39	164	O15[7]
C7Y–H7Y	0.95	3.231(3)	2.45	139	O14[8]

C3Z–H3Z	0.95	3.210(3)	2.32	155	O7[9]
C6Z–H6Z	0.95	3.520(3)	2.57	176	O14[9]
C–H···O interactions between C4S molecules					
C13–H13	0.95	3.292(2)	2.37	165	O10[9]

Symmetry operations: [1](3–x,2–y,2–z), [2](3–x,2–y,1–z), [3](1+x,y,z), [4](2–x,2–y,1–z), [5](3–x,2–y,2–z), [6](1–x,1–y,1–z), [7](–1+x,y,z), [8](2–x,1–y,2–z), [9](2–x,1–y,1–z).

Table 38. The parameters of X–H···π interactions. Distances (d) are given in Å, angles in °.

D – H	d(D – H)	d(D···A)	d(H···A)	<D – H···A	A
N–H···π interactions between M–BNZ and C4S molecules					
N2Z–H2ZA	0.95	3.570(2)	2.99	125	Cg(C8–C13)[1]
C–H···π interactions between M–BNZ and C4S molecules					
C8X–H8XA	0.95	3.599(2)	2.95	125	Cg(C1–C6)

Symmetry operation: [1](1–x,1–y,1–z).

Cg – centroid of C4S aromatic ring.

Table 39. The parameters of π···π interactions. Distances (d) are given in Å.

CgA	d(CgA···CgB)	CgB
π···π interactions between M–BNZ molecules		
Cg(C2I–C7I)	3.888(13)	Cg(C2Z–C7Z)[1]

Symmetry operations: [1](2–x,1–y,1–z).

Cg – centroid of M–BNZ aromatic ring.

Structure of the complex C6S_M–BNZ

Table 40. The parameters of hydrogen bonds. Distances (d) are given in Å, angles in °.

D – H	d(D – H)	d(D···A)	d(H···A)	<D – H···A	A
O–H···O intramolecular hydrogen bonds at C6S lower rim					
O4–H4	0.84	2.554(3)	1.74	163	O4[1]
N–H···O hydrogen bonds between M–BNZ and C6S molecules					
N1X–H1XA	0.88	2.868(13)	2.01	169	O2[1]
N1X–H1XB	0.88	2.853(3)	2.03	164	O2[2]
N2X–H2XA	0.88	2.853(3)	2.02	158	O1[3]
N2X–H2XB	0.88	2.892(4)	2.02	170	O3
C–H···O hydrogen bonds between C6S molecules					
C1–H1B	0.99	3.512(4)	2.55	163	O3[3]
C7–H7	0.95	3.253(4)	2.33	164	O1[4]

Symmetry operations: [1](1/3+x–y,–1/3+x,2/3–z), [2](–1/3+y,1/3–x+y,1/3–z), [3](1–x,1–y,1–z), [4](4/3–y, 2/3+x–y,–1/3+z).

Table 41. The parameters of π···π interactions. Distances (d) are given in Å.

CgA	d(CgA···CgB)	CgB
π···π interactions between M–BNZ molecules		
Cg(C2X–C7X)	3.836(4)	Cg(C2X–C7X)[1]

Symmetry operations: [1](1–x,1–y,–z).

Cg – centroid of M–BNZ aromatic ring.

Structure of the complex C4S_A–BNZ_I

Table 42. The parameters of hydrogen bonds. Distances (d) are given in Å, angles in °.

D – H	d(D – H)	d(D···A)	d(H···A)	<D – H···A	A
O–H···O intramolecular hydrogen bonds at C4S lower rim					
O4–H4A	0.84	2.725(3)	1.90	165	O16
O8–H8	0.84	2.686(3)	1.90	156	O4
O12–H12	0.84	2.769(3)	1.97	158	O8
O16–H16A	0.84	2.730(3)	1.95	153	O12
O20–H20A	0.84	2.723(3)	1.89	169	O24
O24–H24	0.84	2.679(3)	1.92	151	O28
O28–H28	0.84	2.736(3)	1.92	164	O32
O32–H32	0.84	2.743(3)	1.97	152	O20
O–H···O hydrogen bonds between ethanol and C4S / water molecules					
O1E–H1E	0.84	2.751(6)	1.93	167	O22
O2E–H2E	0.84	2.766(4)	1.93	176	O15W
O3E–H3E	0.84	2.750(5)	1.92	172	O29W
O4E–H4E	0.84	2.953(19)	2.14	162	O7[1]
N–H···O interactions between benzamidine and C4S / ethanol / water molecules					
N1I–H1IA	0.91	2.759(4)	1.85	172	O14[2]
N1I–H1IB	0.91	2.750(3)	1.88	159	O1[3]
N1I–H1IC	0.91	2.651(4)	1.74	179	O13W
N2I–H2IA	0.88	2.885(4)	2.01	174	O26[4]
N2I–H2IB	0.88	2.952(4)	2.10	164	O12W[2]
N3I–H3IA	0.88	2.924(4)	2.09	158	O24W[3]
N3I–H3IB	0.88	2.949(4)	2.12	156	O25W[3]
N1X–H1XA	0.91	2.875(3)	2.03	154	O18
N1X–H1XB	0.91	2.803(3)	1.93	160	O23[5]
N1X–H1XC	0.91	2.720(5)	1.81	173	O3E[5]
N2X–H2XA	0.88	3.257(4)	2.56	137	O5
N2X–H2XB	0.88	2.860(4)	2.01	161	O5W
N3X–H3XA	0.88	2.944(4)	2.14	152	O5
N3X–H3XB	0.88	2.841(5)	1.96	174	O19W[1]
N1Y–H1YA	0.91	2.724(4)	1.82	175	O2E
N1Y–H1YB	0.91	2.882(4)	2.01	160	O5
N1Y–H1YC	0.91	2.925(3)	2.09	152	O11[5]
N2Y–H2YA	0.88	2.807(3)	1.99	154	O2W
N2Y–H2YB	0.88	2.839(4)	2.00	160	O5W
N3Y–H3YA	0.88	3.062(4)	2.32	142	O23[5]
N3Y–H3YB	0.88	2.896(4)	2.02	171	O6W[5]
N1Z–H1ZA	0.88	2.980(4)	2.16	155	O3
N1Z–H1ZB	0.88	2.894(4)	2.08	154	O25W
N2Z–H2ZA	0.88	2.972(4)	2.28	136	O27W[5]
N2Z–H2ZB	0.88	2.951(4)	2.10	163	O6W[5]
N3Z–H3ZA	0.91	2.678(3)	1.77	176	O3W
N3Z–H3ZB	0.91	2.758(3)	1.87	166	O29[6]
N3Z–H3ZC	0.91	2.853(3)	1.96	167	O25[7]
O–H···O hydrogen bonds between C4S and ethanol molecules					
C6Y–H6Y	0.95	3.250(4)	2.54	132	O2E

C–H···O interactions between benzamidine and C4S / water molecules					
C2I–H2I	0.95	3.254(4)	2.53	134	O14[2]
C3I–H3I	0.95	3.30(17)	2.48	145	O14W[2]
C2X–H2X	0.95	3.165(4)	2.39	139	O18
C5Z–H5Z	0.95	3.174(10)	2.50	128	O33W[5]
C6Z–H6Z	0.95	3.225(4)	2.58	125	O25[7]
C–H···O interactions between C4S molecules					
C23–H23	0.95	3.484(4)	2.53	177	O2[8]
C35–H35B	0.99	3.404(4)	2.52	148	O19[9]
C55–H55	0.95	3.532(4)	2.58	176	O27[5]
C56–H56A	0.99	3.486(4)	2.53	163	O30[10]

Symmetry operations: [1](1–x,–y,1–z), [2](2–x,1–y,1–z), [3](1–x,1–y,1–z), [4](2–x,–y,1–z), [5](–1+x,y,z), [6](x,1+y,z), [7](–1+x,1+y,z), [8](1+x,y,z), [9](1–x, y,–z), [10](1–x,–1–y,–z).

Table 43. The parameters of X–H···π interactions. Distances (d) are given in Å, angles in °.

D – H	d(D – H)	d(D···A)	d(H···A)	<D – H···A	A
C–H···π interactions between ethanol and C4S molecules					
C4E–H4EA	0.99	3.718(5)	2.79	157	Cg(C8–C13)
C4E–H4EB	0.99	3.729(5)	3.00	132	Cg(C1–C6)
C6E–H6EB	0.99	3.632(7)	2.96	126	Cg(C43–C48)

Cg – centroid of C4S aromatic ring.

Table 44. The parameters of π···π interactions. Distances (d) are given in Å.

CgA	d(CgA···CgB)	CgB
π···π interactions between C4S molecules		
Cg(C8–C13)	3.7663(19)	Cg(C8–C13)[1]
Cg(C22–C27)	3.6675(19)	Cg(C22–C27)[2]
Cg(C36–C41)	3.8503(18)	Cg(C36–C41)[3]
Cg(C50–C55)	3.6614(19)	Cg(C50–C55)[4]

Symmetry operation: [1](1–x,–y,1–z), [2](2–x,1–y,1–z), [3](2–x,–y,–z), [4](1–x,–1–y,–z).

Cg – centroid of C4S aromatic ring.

Structure of the complex C4S_A–BNZ_II

Table 45. The parameters of hydrogen bonds. Distances (d) are given in Å, angles in °.

D – H	d(D – H)	d(D···A)	d(H···A)	<D – H···A	A
O–H···O intramolecular hydrogen bonds at C4S lower rim					
O4–H4A	0.84	2.839(3)	2.29	123	O16
O8–H8A	0.84	2.807(3)	1.99	163	O4
O12–H12	0.84	2.786(3)	2.05	146	O8
O16–H16A	0.84	2.718(3)	1.94	153	O12
O–H···O interactions between water molecules (Zundel cation)					
O2W–H2WA	1.18(5)	2.485(4)	1.32(4)	165(2)	O1W[1]
O–H···O interactions between water molecules and C4S					
O1W–H1WA	0.87	2.708(3)	1.85	169	O5[2]
O1W–H1WB	0.87	2.720(4)	1.86	171	O13[5]
O12–H12	0.84	2.724(3)	2.26	115	O1W[6]

O2W–H2WB	0.87(2)	3.148(18)	2.40(2)	144.2(9)	O6W
O2W–H2WC	0.87(3)	2.467(5)	1.65(3)	155(2)	O3W[1]
N–H···O interactions between A–BNZ and C4S molecules / water molecules					
N1X–H1XA	0.91	2.816(4)	1.95	159	O15
N1X–H1XB	0.91	2.841(4)	1.99	156	O4W[2]
N1X–H1XC	0.91	3.080(4)	2.25	152	O10[3]
N2X–H2XA	0.88	3.030(3)	2.25	147	O7[4]
N2X–H2XB	0.88	3.030(3)	1.96	166	O9
N3X–H3XA	0.88	3.045(3)	2.28	146	O7[4]
N3X–H3XB	0.88	2.885(4)	2.03	164	O3

Symmetry operations: [1](–x,1/2+y,1/2–z), [2](–x,1–y,1–z), [3](–x,1–y,–z), [4](x,1/2–y,–1/2+z), [5](–x,–1/2+y,1/2–z), [6](1+x,y,z).

Table 46. The coordination distances between sodium cations and C4S, water molecules. Distances (d) are given in Å.

Metal	d(Na···O)	O
Na1	2.451(6)	O1
	2.421(6)	O2
	2.494(6)	O6
	2.486(6)	O7
	2.476(6)	O4W
	2.358(12)	O5W
Na2	2.570(5)	O1
	2.576(5)	O6
	2.504(6)	O5A

Table 47. The parameters of X–H···π interactions. Distances (d) are given in Å, angles in °.

D – H	d(D – H)	d(D···A)	d(H···A)	<D – H···A	A
C–H···π interactions between benzamidines and C4S molecules					
C2X–H2X	0.95	3.734(4)	2.82	163	Cg(C22–C27)[1]

Cg – centroid of C4S aromatic ring.

Table 48. The parameters of π···π interactions. Distances (d) are given in Å.

CgA	d(CgA···CgB)	CgB
π···π interactions between C4S molecules		
Cg(C8–C13)	3.541(16)	Cg(C22–C27)[1]

Symmetry operations: [1](1–x,–1/2+y,1/2–z).

Cg – centroid of C4S aromatic ring.

Structure of the complex C6S_H–BNZ_I

Table 49. The parameters of hydrogen bonds. Distances (d) are given in Å, angles in °.

D – H	d(D – H)	d(D···A)	d(H···A)	<D – H···A	A
O–H···O intramolecular hydrogen bonds at C6S lower rim					
O4–H4	0.84	2.728(2)	1.90	168	O12[1]
O8–H8	0.84	2.685(2)	1.90	156	O4
O12–H12	0.84	2.797(2)	2.10	140	O8
O–H···O hydrogen bonds between H–BNZ and C6S / water molecules					
O1X–H1X	0.84	2.775(5)	1.98	157	O2[2]

O1Y–H1Y	0.84	2.664(2)	1.84	166	O1W[3]
O1Z–H1Z	0.84	2.719(2)	1.91	162	O9[4]
O–H···O hydrogen bonds between water and C6S molecules					
O1W–H1WA	0.87	2.721(2)	1.88	163	O9[5]
O1W–H1WB	0.87	2.765(19)	1.92	164	O6
O2W–H2WA	0.87	3.026(6)	2.20	157	O3[3]
O2W–H2WB	0.87	3.026(6)	2.26	146	O3[6]
O3W–H3WA	0.87	2.966(3)	2.11	169	O1
N–H···O interactions between H–BNZ and H–BNZ / C6S / water molecules					
N1X–H1XA	0.88	2.913(4)	2.09	156	O2
N1X–H1XB	0.88	3.053(3)	2.19	166	O3[7]
N2X–H2XA	0.88	3.052(2)	2.36	136	O3W
N2X–H2XB	0.88	2.859(3)	2.04	155	O5
N1Y–H1YA	0.88	2.942(2)	2.07	171	O5[8]
N1Y–H1YB	0.88	2.960(3)	2.11	163	O10[10]
N2Y–H2YA	0.88	2.908(2)	2.04	171	O6[8]
N2Y–H2YB	0.88	2.847(2)	2.05	149	O7
N1Z–H1ZA	0.88	2.838(2)	2.04	151	O10
N1Z–H1ZB	0.88	2.886(2)	2.04	162	O7
N2Z–H2ZA	0.88	3.009(3)	2.27	141	O10
N2Z–H2ZB	0.88	3.126(2)	2.48	131	O1Y[9]
C–H···O interactions between H–BNZ and C6S molecules					
C3X–H3X	0.95	3.177(3)	2.56	123	O8[9]
C3X–H3X	0.95	3.348(3)	2.54	144	O3[7]
C4X–H4X	0.95	3.411(5)	2.54	153	O1[2]
C–H···O interactions between H–BNZ molecules					
C3Y–H3Y	0.95	3.421(2)	2.48	173	O1Z[8]
C–H···O interactions between C6S molecules					
C15–H15A	0.99	3.228(4)	2.45	135	O1[11]

Symmetry operations: [1](1–x,y,3/2–z), [2](x,–y,1/2+z), [3](x,1–y,1/2+z), [4](x,–y,–1/2+z), [5](x,1–y,–1/2+z), [6](1–x,1–y,1–z), [7](1–x,–y,1–z), [8](1/2–x,1/2–y,1–z), [9](x,–1+y,z), [10](1/2–x,1/2+y,3/2–z), [11](x,1–y,1/2+z).

Table 50. The parameters of X–H···π interactions. Distances (d) are given in Å, angles in °.

D – H	**d(D – H)**	**d(D···A)**	**d(H···A)**	**<D – H···A**	**A**
C–H···π interactions between H–BNZ and C6S molecules					
C6X–H6X	0.95	3.535(2)	2.76	140	Cg(C16–C21)
C6Z–H6Z	0.95	3.786(2)	2.97	144	Cg(C9–C14)[1]
C–H···π interactions between H–BNZ molecules					
C4Y–H4Y	0.95	3.390(2)	2.69	131	Cg(C2Z–C7Z)[2]

Symmetry operation: [1](x,–1+y,z), [2](x,1+y,z).

Cg – centroid of H–BNZ / C6S aromatic ring.

Table 51. The parameters of π···π interactions. Distances (d) are given in Å.

CgA	**d(CgA···CgB)**	**CgB**
π···π interactions between C6S molecules		
Cg(C2–C7)	3.9509(12)	Cg(C2–C7)[1]

Symmetry operations: [1](1–x,1–y,1–z).

Cg – centroid of C6S aromatic ring.

Structure of the complex C6S_H–BNZ_II

Table 52. The parameters of hydrogen bonds. Distances (d) are given in Å, angles in °.

D – H	d(D – H)	d(D···A)	d(H···A)	<D – H···A	A
O–H···O hydrogen bonds at C6S lower rim					
O4–H4	0.84	2.666(4)	1.83	173	O6[1]
O8–H8	0.84	2.601(7)	2.04	124	O1A[2]
O8–H8	0.84	2.845(7)	2.18	136	O1A[3]
O12–H12A	0.84	2.701(4)	1.86	176	O4
O–H···O hydrogen bonds between H–BNZ and C6S / water molecules					
O1Y–H1Y	0.84	2.787(5)	2.01	153	O2[4]
O1Z–H1Z	0.84	2.653(5)	1.84	163	O1W[5]
O–H···N hydrogen bond between H–BNZ molecules					
O1X–H1X	0.94	3.553(7)	2.60	176	N2Z[6]
N–H···O interactions between H–BNZ and C6S / water molecules					
N1X–H1XA	0.88	3.066(12)	2.36	138	O11[7]
N1X–H1XB	0.88	2.883(15)	2.04	161	O3W
N2X–H2XA	0.88	2.826(8)	2.03	149	O11[7]
N2X–H2XB	0.88	3.099(8)	2.28	154	O1[7]
N1Y–H1YA	0.88	2.852(6)	2.04	154	O3[1]
N1Y–H1YB	0.88	2.966(6)	2.20	145	O6[1]
N2Y–H2YA	0.88	3.106(6)	2.38	140	O3[1]
N2Y–H2YB	0.88	3.046(5)	2.23	153	O2W[10]
N1Z–H1ZA	0.88	2.896(5)	2.02	174	O2W
N1Z–H1ZB	0.88	2.874(5)	2.03	162	O5[8]
N2Z–H2Z1	0.88	2.785(5)	2.09	135	O9[3]
C–H···O interactions between H–BNZ and C6S molecules					
C6X–H6X	0.95	3.202(9)	2.52	129	O7[9]
C7X–H7X	0.95	3.426(10)	2.50	164	O10
C9–H9	0.95	3.290(5)	2.59	131	O1Y[4]
C10–H10A	0.99	3.393(8)	2.51	148	O1X[3]
C–H···O interactions between H–BNZ molecules					
C4X–H4X	0.95	3.262(13)	2.53	134	O1A
C–H···O interactions between C6S molecules					
C5–H5	0.95	3.295(7)	2.40	158	O10[7]

Symmetry operations: [1](1+x,y,z), [2](–1+x,y,z), [3](1–x,1–y,1–z), [4](–x,–y,–z), [5](1–x,1–y,–z), [6](2–x,1–y,1–z), [7](–x,–y,1–z), [8](–x,1–y,–z), [9](–x,1–y,1–z), [10](–1+x,–1+y,z).

Table 53. The parameters of π···π interactions. Distances (d) are given in Å.

CgA	d(CgA···CgB)	CgB
π···π interactions between H–BNZ molecules		
Cg(C2Y–C7Y)	3.889(3)	Cg(C2Y–C7Y)[1]
Cg(C2Z–C7Z)	3.849(3)	Cg(C2Z–C7Z)[2]

Symmetry operations: [1](–x,–y,–z), [2](–x,1–y,–z).

Cg – centroid of H–BNZ aromatic ring.

Structure of the complex C4S_ALEX

Table 54. The parameters of hydrogen bonds. Distances (d) are given in Å, angles in °.

D – H	d(D – H)	d(D···A)	d(H···A)	<D – H···A	A
O–H···O intramolecular hydrogen bonds at C4S lower rim					
O4–H4	0.84	2.711(7)	1.99	144	O16
O8–H8	0.84	2.664(7)	1.99	136	O4
O12–H12	0.84	2.663(8)	1.86	160	O8
O16–H16A	0.84	2.655(7)	1.99	135	O12
N–H···O interactions between alexidine and C4S / water molecules					
N1X–H1X	0.88	2.815(10)	1.94	170	O14[2]
N2X–H2X5	0.88	2.853(12)	2.06	150	O10[3]
N2X–H2X6	0.88	2.969(18)	2.19	148	O5W
N3X–H3X	0.88	2.774(9)	1.90	171	O13[2]
N4X–H4X5	0.88	2.82(4)	2.10	138	O7
N4X–H4X6	0.88	2.82(2)	1.97	161	O6[1]
N5X–H5X	0.88	2.962(17)	2.09	170	O4W[2]
N6X–H6X	0.88	2.858(10)	2.09	146	O3W
N7X–H7X1	0.88	2.774(8)	2.04	141	O15
N7X–H7X2	0.88	2.844(8)	1.98	166	O2[4]
N8X–H8X	0.88	2.729(9)	1.85	173	O1[4]
N9X–H9X1	0.88	2.84(4)	2.00	161	O5[3]
N9X–H9X2	0.88	2.782(9)	2.03	144	O2W
N10X–H10X	0.88	2.864(8)	2.02	159	O2[2]
C–H···O interactions between alexidine and C4S / water molecules					
C12C–H12A	0.99	3.51(2)	2.53	170	O14[6]
C1XA–H1X3	0.99	3.49(6)	2.51	173	O7A
C1XA–H1X3	0.99	3.30(6)	2.32	171	O7
C1XA–H1X4	0.99	3.252(19)	2.53	130	O1
C1XA–H1X4	0.99	3.24(2)	2.48	134	O2W[5]
C20C–H20A	0.99	3.54(4)	2.56	166	O1WA[3]

Symmetry operations: [1](1–x,2–y,–z), [2](–x,3–y,–z), [3](–x,2–y,–z), [4](–1+x,y,z), [5](1+x,y,z), [6](–1–x,3–y,–z).

Table 55. The parameters of X–H···π interactions. Distances (d) are given in Å, angles in °.

D – H	d(D – H)	d(D···A)	d(H···A)	<D – H···A	A
C–H···π interactions between alexidine and C4S molecules					
C13A–H13F	0.99	3.58(6)	2.72	146	Cg(C22–C27)[1]
C4X–H4X2	0.99	3.591(17)	2.92	128	Cg(C15–C20)

Symmetry operation: [1](–x,3–y, –z), [2](–x,2–y,–z).

Cg – centroid of C4S aromatic ring.

Structure of the complex C4S_PT_H2O

Table 56. The parameters of hydrogen bonds. Distances (d) are given in Å, angles in °.

D – H	d(D – H)	d(D···A)	d(H···A)	<D – H···A	A
O–H···O intramolecular hydrogen bonds at C4S lower rim					
O4–H4	0.84	2.616(3)	1.85	151	O16

O8–H8	0.84	2.621(3)	1.84	155	O4
O12–H12	0.84	2.633(3)	1.88	149	O8
O16–H16A	0.84	2.782(3)	2.09	140	O12
O–H···O hydrogen bond between C4S molecules					
O16–H16A	0.84	2.753(3)	2.23	121	O3[1]
N–H···O interactions between pentamidine and C4S / water molecules					
N1X–H1XA	0.88	2.848(3)	2.00	161	O11[9]
N1X–H1XB	0.88	2.848(3)	2.20	141	O13[2]
N2X–H2XA	0.88	2.880(3)	2.01	170	O9[1]
N2X–H2XB	0.88	2.815(3)	1.99	156	O3W
N3X–H3XA	0.88	3.005(4)	2.17	158	O7[3]
N3X–H3XB	0.88	2.929(4)	2.07	164	O10[2]
N4X–H4XA	0.88	2.810(4)	1.95	167	O4W[4]
N4X–H4XB	0.88	2.907(4)	2.04	167	O1W[9]
N1Y–H1YA	0.88	2.784(3)	1.94	161	O1
N1Y–H1YB	0.88	2.843(3)	2.10	141	O2[5]
N2Y–H2YA	0.88	3.262(3)	2.58	135	O1
N2Y–H2YB	0.88	2.998(3)	2.13	170	O14[2]
N3Y–H3YA	0.88	2.985(3)	2.20	148	O14[6]
N3Y–H3YB	0.88	2.800(3)	1.96	159	O7W[6]
N4Y–H4YA	0.88	2.994(3)	2.18	153	O15[6]
N4Y–H4YB	0.88	2.956(3)	2.08	172	O3[7]
C–H···O interactions between pentamidine and C4S / water molecules					
C15X–H15X	0.95	3.364(4)	2.59	138	O10[2]
C17X–H17X	0.95	3.288(4)	2.54	136	O1W[9]
C3Y–H3Y	0.95	3.381(4)	2.58	142	O15
C7Y–H7Y	0.95	3.267(4)	2.44	146	O14[2]
C12Y–H12A	0.99	3.413(9)	2.43	172	O5[5]
C15Y–H15Y	0.95	3.053(3)	2.46	120	O7W[6]
C17Y–H17Y	0.95	3.211(3)	2.46	136	O3[7]
C18Y–H18Y	0.95	3.310(3)	2.55	137	O6W[6]
C16–H16	0.95	3.242(3)	2.35	156	O1W[8]
C21–H21A	0.99	3.235(3)	2.52	129	O1[9]
C27–H27	0.99	3.416(3)	2.51	160	O2[5]

Symmetry operations: [1](1+x,y,z), [2](–1+x,y,z), [3](–x,1–y,2–z), [4](x,1+y,1+z), [5](–x,–y,1–z), [6](–x,–y,–z), [7](x,y,–1+z), [8](1+x,y,1+z), [9](–x,1–y,1–z).

Table 57. The parameters of X–H···π interactions. Distances (d) are given in Å, angles in °.

D – H	**d(D – H)**	**d(D···A)**	**d(H···A)**	**<D – H···A**	**A**
N–H···π interactions between pentamidine and C4S molecules					
N2Y–H2YA	0.88	3.535(2)	2.98	123	Cg(C22–C27)[1]
C–H···π interactions between pentamidine and C4S molecules					
C9X–H9XB	0.99	3.783(3)	2.97	140	Cg(C22–C27)
C14–H14X	0.95	3.541(3)	2.75	141	Cg(C15–C20)[1]

Symmetry operation: [1](–1+x,y,z).

Cg – centroid of C4S aromatic ring.

Table 58. The parameters of π···π interactions. Distances (d) are given in Å.

CgA	d(CgA···CgB)	CgB
π···π interactions between pentamidine and C4S molecules		
Cg(C2Y–C7Y)	3.970(15)	Cg(C1–C6)[1]
π···π interactions between pentamidine molecules		
Cg(C2X–C7X)	3.579(16)	Cg(C2X–C7X)[2]

Symmetry operation: [1](–x,–y,1–z), [2](–x,1–y,1–z).

Cg – centroid of pentamidine / C4S aromatic ring.

Structure of the complex C4S_PT_EtOH

Table 59. The parameters of hydrogen bonds. Distances (d) are given in Å, angles in °.

D – H	d(D – H)	d(D···A)	d(H···A)	<D – H···A	A
O–H···O intramolecular hydrogen bonds at C4S lower rim					
O4–H4	0.84	2.829(7)	2.00	171	O16
O8–H8	0.84	2.661(7)	1.92	146	O4
O12–H12	0.84	2.690(5)	1.86	168	O8
O16–H16A	0.84	2.743(5)	2.03	142	O12
O–H···O hydrogen bonds between ethanol and C4S / water molecules					
O1E–H1E	0.84	2.813(7)	2.02	158	O3
O1W–H1WB	0.87	2.814(6)	1.96	168	O1E
N–H···O interactions between pentamidine and C4S / water molecules					
N1X–H1XA	0.88	2.779(14)	2.01	145	O4W[1]
N1X–H1XB	0.88	2.795(6)	2.01	148	O5
N2X–H2XA	0.88	2.815(7)	1.95	166	O2[2]
N2X–H2XB	0.88	2.790(7)	1.96	157	O1W[2]
N3X–H3XA	0.88	2.910(6)	2.04	168	O1[3]
N3X–H3XB	0.88	2.71(2)	1.92	147	O13
N4X–H4XA	0.88	2.894(10)	2.10	150	O3[3]
N4X–H4XB	0.88	2.523(17)	1.81	137	O6W[3]
N1Y–H1YA	0.88	2.919(9)	2.18	141	O11[5]
N1Y–H1YB	0.88	2.937(7)	2.34	125	O6
N2Y–H2YA	0.88	2.861(12)	2.10	144	O11[5]
N2Y–H2YB	0.88	3.07(4)	2.21	167	O15[5]
N3Y–H3YA	0.88	2.958(15)	2.22	141	O9[4]
N3Y–H3YB	0.88	2.90(2)	2.28	128	O14
N4Y–H4YA	0.88	2.865(19)	2.10	145	O9[4]
N4Y–H4YB	0.88	2.824(17)	1.96	167	O7[4]
C–H···O interactions between pentamidine and C4S / water molecules					
C7X–H7X	0.95	3.115(7)	2.39	132	O5[2]
C8X–H8XA	0.99	3.543(7)	2.58	165	O6[1]
C17X–H17X	0.95	3.45(3)	2.52	167	O15[3]
C7Y–H7Y	0.95	3.536(17)	2.59	174	O14[5]
C17Y–H17Y	0.95	3.51(3)	2.59	164	O6[4]
C14–H14C	0.99	3.384(7)	2.51	146	O1W[6]

Symmetry operations: [1](–1/2+x,1/2–y,1–z), [2](1/2+x,1/2–y,1–z), [3](1/2+x,3/2–y,1–z), [4](1–x,1/2+y,1/2–z), [5](1–x,–1/2+y,1/2–z), [6](1+x,y,z).

Table 60. The parameters of X–H···π interactions. Distances (d) are given in Å, angles in °.

D – H	d(D – H)	d(D···A)	d(H···A)	<D – H···A	A
C–H···π interactions between pentamidine and C4S molecules					
C10Y–H10B	0.99	3.529(14)	2.55	168	Cg(C15–C20)
C7–H7B	0.99	3.704(5)	2.72	170	Cg(C2X–C7X)
C28–H28A	0.99	3.684(5)	2.71	169	Cg(C13X–C18X)
C–H···π interactions between ethanol and C4S molecules					
C1E–H1EA	0.98	3.723(19)	2.79	159	Cg(C1–C6)
C1E–H1EB	0.98	3.679(18)	2.81	149	Cg(C15–C20)

Cg – centroid of pentamidine / C4S aromatic ring.

Table 61. The parameters of π···π interactions. Distances (d) are given in Å.

CgA	d(CgA···CgB)	CgB
π···π interactions between pentamidine and C4S molecules		
Cg(C2X–C7X)	3.963(3)	Cg(C8–C13)[1]

Symmetry operation: [1](–1/2+x,1/2–y,1–z).

Cg – centroid of pentamidine / C4S aromatic ring.

Structure of the complex C4S_PT_IPA

Table 62. The parameters of hydrogen bonds. Distances (d) are given in Å, angles in °.

D – H	d(D – H)	d(D···A)	d(H···A)	<D – H···A	A
O–H···O intramolecular hydrogen bonds at C4S lower rim					
O4–H4	0.84	2.690(3)	1.88	162	O16
O8–H8	0.84	2.864(3)	2.55	104	O4
O12–H12	0.84	2.704(3)	1.88	167	O8
O16–H16A	0.84	2.804(3)	2.13	137	O12
O20–H20A	0.84	2.709(3)	1.89	165	O24
O28–H28	0.84	2.707(3)	1.90	161	O32
O32–H32	0.84	2.790(3)	2.07	144	O20
O36–H36	0.84	2.738(3)	1.93	162	O40
O40–H40	0.84	2.807(3)	2.52	101	O44
O44–H44	0.84	2.721(3)	1.90	165	O48
O48–H48A	0.84	2.769(3)	2.05	144	O36
O–H···O hydrogen bond between C4S and water molecule					
O24–H24	0.84	2.704(2)	1.95	148	O8W
O–H···O interactions between isopropanol and C4S / water molecules					
O1I–H1I	0.84	2.878(3)	2.04	177	O23
O2I–H2IA	0.84	2.881(3)	2.04	174	O39
O3I–H3I	0.84	2.870(4)	2.18	140	O5
O4I–H4I	0.84	3.131(3)	2.47	137	O46[4]
O4I–H4I	0.84	2.860(4)	2.07	157	O47[4]
O5I–H5IA	0.84	3.146(3)	2.57	126	O30[1]
O5I–H5IA	0.84	2.772(3)	1.96	164	O31[1]
O6I–H6I	0.84	2.859(5)	2.09	152	O14[1]
O6I–H6I	0.84	3.103(4)	2.58	121	O15[1]
O4W–H4WA	0.87	2.757(2)	1.89	172	O1I

O9W–H9WB	0.87	2.766(3)	2.03	164	O2I[2]
O10W–H10P	0.87	2.775(3)	1.91	173	O3I
O–H···O interactions between C4S molecules					
O16–H16A	0.84	2.867(3)	2.35	121	O23
O32–H32	0.84	2.907(3)	2.46	114	O39[9]
O48–H48A	0.84	2.874(3)	2.44	113	O5
N–H···O interactions between pentamidine and C4S / isopropanol / water molecules					
N1X–H1XA	0.88	2.902(4)	2.09	153	O5[3]
N1X–H1XB	0.88	2.796(6)	1.93	167	O2W[3]
N2X–H2XA	0.88	2.995(4)	2.15	160	O6[3]
N2X–H2XB	0.88	2.884(4)	2.06	156	O17
N3X–H3XA	0.88	2.877(4)	2.02	166	O7[2]
N3X–H3XB	0.88	2.713(3)	1.90	153	O10W[2]
N4X–H4XA	0.88	2.934(3)	2.18	144	O5W[2]
N4X–H4XB	0.88	2.756(4)	1.95	152	O25
N1Y–H1YA	0.88	2.880(3)	2.01	171	O37[2]
N1Y–H1YB	0.88	2.794(3)	1.95	160	O9W
N2Y–H2YA	0.88	2.873(3)	2.08	149	O8W
N2Y–H2YB	0.88	2.841(3)	2.11	140	O10
N3Y–H3YA	0.88	2.913(3)	2.07	159	O39[3]
N3Y–H3YB	0.88	2.832(3)	1.97	165	O11W
N4Y–H4YA	0.88	2.890(3)	2.02	168	O38[3]
N4Y–H4YB	0.88	2.823(3)	1.97	163	O2
N1Z–H1ZA	0.88	2.870(4)	2.09	147	O29[5]
N1Z–H1ZB	0.88	3.258(4)	2.58	134	O1Y[2]
N2Z–H2ZA	0.88	2.864(4)	2.08	148	O29[5]
N2Z–H2ZB	0.88	2.869(4)	2.02	161	O27[5]
N3Z–H3ZA	0.88	2.861(4)	2.07	149	O5I[3]
N3Z–H3ZB	0.88	2.864(3)	2.09	146	O19
N4Z–H4ZA	0.88	2.869(3)	2.13	140	O30[10]
N4Z–H4ZB	0.88	2.976(3)	2.10	172	O18[10]
N1K–H1KA	0.88	2.894(4)	2.16	141	O45[7]
N1K–H1KB	0.88	2.868(4)	2.01	164	O43[7]
N2K–H2KA	0.88	2.803(4)	2.04	145	O45[7]
N2K–H2KB	0.88	2.909(4)	2.32	124	O11
N3K–H3KA	0.88	2.882(4)	2.11	147	O46[4]
N3K–H3KB	0.88	2.857(4)	1.99	169	O33[4]
N4K–H4KA	0.88	2.892(4)	2.05	159	O4I
N4K–H4KB	0.88	2.796(4)	2.03	145	O1
N1L–H1LA	0.88	2.844(4)	2.07	146	O15[7]
N1L–H1LB	0.88	2.868(4)	1.99	176	O9[7]
N2L–H2LA	0.88	2.883(5)	2.07	153	O6I[6]
N2L–H2LB	0.88	2.834(4)	2.18	131	O42
N3L–H3LA	0.88	2.874(5)	2.13	142	O13[4]
N3L–H3LB	0.88	2.890(4)	2.04	162	O3[4]
N4L–H4LA	0.88	2.816(4)	2.05	145	O13[4]
N4L–H4LB	0.88	2.993(4)	2.38	126	O35
N1M–H1MA	0.88	2.875(4)	2.00	174	O21[9]
N1M–H1MB	0.88	2.887(4)	2.05	158	O41[3]

N2M–H2MA	0.88	2.989(4)	2.18	152	O23[9]
N2M–H2MB	0.88	3.120(4)	2.35	146	O27[9]
N3M–H3MA	0.88	2.867(4)	2.00	168	O22
N3M–H3MB	0.88	2.762(3)	1.92	161	O4W
N4M–H4MA	0.88	2.829(3)	2.03	151	O3W
N4M–H4MB	0.88	2.835(4)	2.09	142	O34[3]
C–H···O interactions between pentamidine and C4S molecules					
C3X–H3X	0.95	3.213(4)	2.48	134	O2[3]
C15X–H15X	0.95	3.241(4)	2.41	146	O10[2]
C3Y–H3Y	0.95	3.294(4)	2.55	135	O41[2]
C15Y–H15Y	0.95	3.286(4)	2.43	150	O34[3]
C7Z–H7Z	0.95	3.406(4)	2.50	159	O26[5]
C17Z–H17Z	0.95	3.227(4)	2.48	135	O18[10]
C15K–H15K	0.95	3.083(4)	2.51	119	O33[4]
C3L–H3L	0.95	3.121(4)	2.52	121	O9[7]
C7M–H7M	0.95	3.196(4)	2.50	130	O25[9]
C7M–H7M	0.95	3.489(4)	2.55	168	O27[9]
C12M–H12K	0.99	3.285(4)	2.54	132	O38[3]
C15M–H15M	0.95	3.238(4)	2.48	137	O17
C–H···O interactions between pentamidine and isopropanol / water molecules					
C3X–H3X	0.95	3.128(6)	2.58	117	O2W[3]
C4K–H4K	0.95	3.124(5)	2.42	131	O6I[8]
C17K–H17K	0.95	3.445(4)	2.52	166	O2M
C8L–H8LB	0.95	3.152(4)	2.57	117	O10W
C14L–H14L	0.95	3.384(5)	2.60	140	O4I[4]
C18L–H18L	0.95	3.345(7)	2.51	146	O2W
C–H···O interactions between C4S and water molecules					
C7–H7B	0.99	3.479(3)	2.51	165	O3W
C28–H28A	0.99	3.363(4)	2.51	144	O4W
C42–H42B	0.99	3.486(3)	2.53	162	O8W[2]
C49–H49B	0.99	3.473(4)	2.60	147	O9W[2]
C70–H70A	0.99	3.371(3)	2.40	166	O5W

Symmetry operations: [1](x,5/2–y,–1/2+z), [2](1–x,–1/2+y,1/2–z), [3](–x,–1/2+y,1/2–z), [4](–x,3–y,1–z), [5](1–x,2–y,1–z), [6](1–x,1/2+y,1/2–z), [7](1–x,3–y,1–z), [8](x,5/2–y,1/2+z), [9](–1+x,y,z), [10](–x,2–y,1–z).

Table 63. The parameters of X–H···π interactions. Distances (d) are given in Å, angles in °.

D – H	**d(D – H)**	**d(D···A)**	**d(H···A)**	**<D – H···A**	**A**
C–H···π interactions between pentamidine and C4S molecules					
C17X–H17X	0.95	3.297(3)	2.94	104	Cg(C71–C76)[1]
C10K–H10G	0.99	3.607(4)	2.65	164	Cg(C22–C27)
C10L–H10J	0.99	3.571(4)	2.59	171	Cg(C78–C83)
C7–H7A	0.99	3.689(3)	2.71	170	Cg(C13Y–C18Y)
C14–H14A	0.99	3.783(3)	2.79	176	Cg(C2Y–C7Y)
C35–H35A	0.99	3.810(3)	2.83	172	Cg(C2X–C7X)
C42–H42A	0.99	3.614(3)	2.63	171	Cg(C13X–C18X)
C63–H63B	0.99	3.589(3)	2.60	174	Cg(C13M–C18M)[2]
C70–H70B	0.99	3.828(3)	2.85	171	Cg(C2M–C7M)[2]
C–H···π interactions between isopropanol and C4S molecules					

C3I–H3IA	0.98	3.742(4)	2.79	165	Cg(C36–C41)
C3I–H3IB	0.98	3.526(4)	2.81	130	Cg(C29–C34)
C3I–H3IC	0.98	3.621(4)	2.69	159	Cg(C50–C55)
C4I–H4IA	0.98	3.617(4)	2.75	148	Cg(C78–C83)
C4I–H4IB	0.98	3.497(4)	2.71	138	Cg(C71–C76)
C4I–H4IC	0.98	3.563(4)	2.62	162	Cg(C64–C69)
C7I–H7IA	0.98	3.685(5)	2.78	154	Cg(C22–C27)
C7I–H7IB	0.98	3.548(5)	2.86	128	Cg(C15–C20)
C7I–H7IC	0.98	3.724(5)	2.78	163	Cg(C8–C13)

Symmetry operations: [1](1–x,–1/2+y,1/2–z), [2](–x,1/2+y,1/2–z).

Cg – centroid of pentamidine / C4S aromatic ring.

Table 64. The parameters of π···π interactions. Distances (d) are given in Å.

CgA	d(CgA···CgB)	CgB
π···π interactions between pentamidine molecules		
Cg(C2K–C7K)	3.774(2)	Cg(C2Z–C7Z)[1]
Cg(C13L–C18L)	3.813(2)	Cg(C13L–C18L)[2]

Symmetry operation: [1](1–x,2–y,1–z), [2](–x,3–y,1–z).

Cg – centroid of pentamidine aromatic ring.

Structure of the complex C4S_PT_Ace

Table 65. The parameters of hydrogen bonds. Distances (d) are given in Å, angles in °.

D – H	d(D – H)	d(D···A)	d(H···A)	<D – H···A	A
O–H···O intramolecular hydrogen bonds at C4S lower rim					
O4–H4	0.84	2.733(8)	1.90	173	O16
O8–H8	0.84	2.699(8)	2.12	126	O4
O12–H12	0.84	2.683(8)	1.90	155	O8
O16–H16A	0.84	2.706(8)	2.01	140	O12
O–H···O hydrogen bond between C4S and acetone molecule					
O4–H4	0.84	2.942(13)	2.57	108	O1R
N–H···O interactions between pentamidine and C4S / water molecules					
N1B–H1BA	0.89	2.95(3)	2.12	154	O7[1]
N1B–H1BB	0.88	3.12(3)	2.28	159	O10A[1]
N2B–H2BA	0.88	3.10(4)	2.32	146	O7[1]
N2B–H2BB	0.88	2.60(3)	1.80	151	O9
N3B–H3BA	0.88	2.84(4)	2.05	149	O1[2]
N3B–H3BB	0.88	2.99(4)	2.13	167	O5[2]
N4B–H4BA	0.87	2.89(5)	2.14	144	O1[2]
N4B–H4BB	0.89	2.71(5)	2.07	128	O4WA
N1Y–H1YA	0.88	2.93(4)	2.18	144	O13[3]
N1Y–H1YB	0.88	2.95(3)	2.16	149	O3
N2Y–H2YA	0.88	3.01(3)	2.28	141	O13[3]
N2Y–H2YB	0.88	2.95(3)	2.10	161	O2[3]
N3Y–H3YA	0.88	3.06(3)	2.30	145	O11[2]
N3Y–H3YB	0.88	2.61(5)	1.94	131	O3WA
N4Y–H4YA	0.88	2.85(4)	2.00	163	O11[2]

N4Y–H4YB	0.88	3.01(4)	2.16	163	O15[2]
C–H···O interactions between pentamidine and C4S / water molecules					
C6Y–H6Y	0.95	3.50(2)	2.59	159	O1W
C7Y–H7Y	0.95	3.46(3)	2.56	158	O2[3]
C8Y–H8YB	0.99	2.91(2)	1.94	166	O4W[6]
C9Y–H9YA	0.99	3.09(3)	2.46	121	O5W[5]
C17Y–H17Y	0.95	2.98(4)	2.29	129	O15[2]
C18Y–H18Y	0.95	3.25(3)	2.35	157	O2W[2]
C–H···O interactions between acetone molecules					
C3R–H3RA	0.98	3.29(3)	2.33	166	O1T[2]
C–H···O interactions between C4S molecules					
C6–H6	0.95	3.441(11)	2.52	163	O6[4]
C20–H20	0.95	3.335(11)	2.40	167	O14[5]
C23–H23	0.95	3.335(10)	2.58	137	O15[5]

Symmetry operations: [1](–x,–y,2–z), [2](1+x,y,z), [3](–x,1–y,1–z), [4](–x,1–y,2–z), [5](1–x,–y,1–z), [6](1–x,1–y,1–z).

Table 66. The parameters of X–H···π interactions. Distances (d) are given in Å, angles in °.

D – H	d(D – H)	d(D···A)	d(H···A)	<D – H···A	A
C–H···π interactions between pentamidine and C4S molecules					
C9B–H9BA	0.99	3.55(2)	2.57	168	Cg(C15–C20)[2]
C11B–H11D	0.99	3.661(18)	2.93	131	Cg(C8–C13)
C9C–H9CA	0.99	3.75(2)	2.79	163	Cg(C1–C6)[1]
C11C–H1E	0.99	3.52(2)	2.78	132	Cg(C22–C27)
C12C–H12F	0.99	3.40(2)	2.95	109	Cg(C22–C27)
C–H···π interactions between acetone and C4S molecule					
C1T–H1TC	0.98	3.48(4)	2.73	133	Cg(C8–C13)

Symmetry operations: [1](1–z,1–y,1–z), [2](1–x,–y,2–z).

Cg – centroid of C4S aromatic ring.

Table 67. The parameters of π···π interactions. Distances (d) are given in Å.

CgA	d(CgA···CgB)	CgB
π···π interactions between pentamidine molecules		
Cg(C13Y–C18Y)	3.876(19)	Cg(C13Y–C18Y) [1]
Cg(C13Y–C18Y)	3.793(18)	Cg(C13C–C18C) [1]
Cg(C13C–C18C)	3.745(18)	Cg(C13C–C18C) [1]
Cg(C13X–C18X)	3.90(4)	Cg(C13X–C18X)[2]

Symmetry operation: [1](2–x,–y,1–z), [2](1–x,1–y,2–z).

Cg – centroid of pentamidine aromatic ring.

Structure of the complex C6S_PT_MetOH

Table 68. The parameters of hydrogen bonds. Distances (d) are given in Å, angles in °.

D – H	d(D – H)	d(D···A)	d(H···A)	<D – H···A	A
O–H···O hydrogen bonds at C6S lower rim					
O4–H4	0.84	2.626(12)	1.92	142	O2W
O8–H8	0.84	2.574(12)	1.75	168	O2W
O12–H12	0.84	2.763(13)	1.98	154	O3W

O16–H16A	0.84	2.601(13)	1.86	145	O5W
O20–H20A	0.84	2.753(10)	2.04	143	O2[1]
O20–H20A	0.84	3.039(12)	2.47	126	O5W
O24–H24A	0.84	2.624(14)	1.83	157	O8W
O–H···O hydrogen bonds between methanol and C6S molecules					
O1M–H1M	0.84	2.624(13)	1.79	170	O22
O2M–H2M	0.84	2.713(15)	1.88	169	O11
N–H···O hydrogen bonds between pentamidine and C6S / water molecules					
N1X–H1XA	0.88	2.829(16)	1.99	159	O6[2]
N1X–H1XB	0.88	2.929(11)	2.15	147	O1W[2]
N2X–H2XA	0.88	3.105(13)	2.24	167	O7[2]
N2X–H2XB	0.88	2.880(14)	2.19	134	O7[3]
N3X–H3XA	0.88	2.80(3)	2.10	136	O17[4]
N3X–H3XB	0.88	2.98(3)	2.45	119	O18
N4X–H4XA	0.88	2.56(3)	1.78	146	O17[4]
N4X–H4XB	0.88	2.88(4)	2.06	154	O13[4]
N1Y–H1YA	0.88	2.737(14)	1.87	169	O11[5]
N1Y–H1YB	0.88	3.04(2)	2.20	161	O17[5]
N2Y–H2YA	0.88	2.933(13)	2.06	175	O10[5]
N2Y–H2YB	0.88	3.17(2)	2.49	134	O14
N3Y–H3YA	0.88	2.965(14)	2.15	154	O1[6]
N3Y–H3YB	0.88	2.905(13)	2.06	159	O1W[6]
N4Y–H4YA	0.88	3.01(3)	2.17	159	O10W[7]
N4Y–H4YB	0.88	2.84(2)	2.12	139	O9W[1]
N1Z–H1ZA	0.88	2.874(11)	2.02	163	O21[6]
N1Z–H1ZB	0.88	2.850(12)	1.99	166	O3[8]
N2Z–H2ZA	0.88	3.230(14)	2.49	142	O21[6]
N2Z–H2ZB	0.88	3.243(15)	2.59	131	O1[9]
N3Z–H3ZA	0.88	3.18(2)	2.65	119.75	O8W[10]
N3Z–H3ZB	0.88	3.43(3)	2.57	166	O19[10]
N4Z–H4ZA	0.88	3.22(3)	2.36	166	O14A[5]
N4Z–H4ZB	0.88	2.83(2)	1.99	157	O10
C–H···O hydrogen bonds between pentamidine and C6S / water molecules					
C15X–H15X	0.95	3.19(3)	2.42	138	O19
C15Y–H15Y	0.95	3.43(3)	2.52	161	O7W
C3Z–H3Z	0.95	3.290(13)	2.42	152	O3[8]
C4Z–H4Z	0.95	3.463(12)	2.52	171	O20[11]
C6Z–H6Z	0.95	3.536(16)	2.59	172	O9W
C7Z–H7Z	0.95	3.467(17)	2.58	156	O6W[6]
C12Z–H12A	0.99	3.31(2)	2.34	166	O8
C17Z–H17Z	0.95	2.987(15)	2.32	127	O9
C–H···O hydrogen bonds between C6S and water molecules					
C7–H7B	0.99	3.419(15)	2.59	142	O2W
C21–H21A	0.99	3.376(17)	2.46	154	O3W
C28–H28A	0.99	3.313(15)	2.52	136	O5W

Symmetry operations: [1](1+x,y,z), [2](1–x,1–y,1–z), [3](x,–1+y,z), [4](2–x,1–y,–z), [5](2–x,2–y,–z), [6](1–x,2–y,1–z), [7](2–x,2–y,1–z), [8](x,1+y,z), [9](–x,2–y,1–z), [10](1–x,2–y,–z), [11](–1+x,1+y,z).

Table 69. The parameters of X–H···π interactions. Distances (d) are given in Å, angles in °.

D – H	d(D – H)	d(D···A)	d(H···A)	<D – H···A	A
C–H···π interactions between methanol and C6S molecule					
C1M–H1MB	0.98	3.586(18)	2.79	139	Cg(C8–C13)
C–H···π interactions between pentamidine and C6S molecules					
C8Y–H8YA	0.99	3.423(12)	2.65	135	Cg(C15–C20)
C–H···π interactions between pentamidine and C6S molecules					
C8Z–H8ZA	0.99	3.76(2)	2.87	150	Cg(C13Y–C18Y)[2]
C12Z–H12B	0.99	3.64(2)	2.89	133	Cg(C2Y–C7Y)[2]
C–H···π interactions between C6S molecules					
C28–H28B	0.99	3.413(11)	2.94	110	Cg(C1–C6)[1]

Symmetry operations: [1](1+x,y,z), [2](–1+x,y,–z).

Cg – centroid of C6S / pentamidine aromatic ring.

Table 70. The parameters of π···π interactions. Distances (d) are given in Å.

CgA	d(CgA···CgB)	CgB
π···π interactions between pentamidine molecules		
Cg(C2X–C7X)	3.733(6)	Cg(C2Z–C7Z)[1]
Cg(C13X–C18X)	3.935(12)	Cg(C13X–C18X)[2]

Symmetry operations: [1](x,–1+y,z), [2](1–x,1–y,–z).

Cg – centroid of pentamidine aromatic ring.

Structure of the complex C8S_PT_EtOH

Table 71. The parameters of hydrogen bonds. Distances (d) are given in Å, angles in °.

D – H	d(D – H)	d(D···A)	d(H···A)	<D – H···A	A
O–H···O hydrogen bonds at C8S lower rim					
O4–H4	0.84	2.707(7)	1.93	153	O8
O8–H8	0.84	2.773(7)	1.94	170	O12
O12–H12	0.84	2.756(6)	1.94	163	O16
O16–H16	0.84	2.727(5)	1.90	169	O20
O20–H20	0.84	2.773(6)	2.04	145	O24
O24–H24	0.84	2.703(9)	2.07	131	O1I
O28–H28	0.84	2.722(6)	1.89	171	O32
O32–H32	0.84	2.710(8)	1.96	149	O15A[1]
O4A–H4A	0.84	2.889(6)	2.08	163	O8A
O8A–H8A	0.84	2.745(6)	1.91	171	O12A
O12A–H12A	0.84	2.721(5)	1.90	167	O16A
O16A–H16A	0.84	2.645(6)	1.84	159	O20A
O20A–H20A	0.84	2.686(7)	1.86	169	O24A
O24A–H24A	0.84	2.610(6)	1.88	145	O1S[2]
O28A–H28A	0.84	2.737(6)	1.93	160	O32A
O32A–H32A	0.84	2.594(8)	1.85	146	O11[2]
O–H···O hydrogen bonds between ethanol / isopropanol and C8S / water molecules					
O1R–H1R	0.84	2.91(3)	2.23	138	O18W[8]
O1R–H1R	0.84	2.86(2)	2.05	162	O180[8]
N–H···O hydrogen bonds between pentamidine and C8S / water molecules					

N1X–H1XA	0.88	2.928(13)	2.12	151	O29A
N1X–H1XB	0.88	3.06(2)	2.24	156	O14W
N2X–H2XA	0.88	2.61(2)	1.88	140	O29A
N2X–H2XB	0.88	2.890(8)	2.02	171	O26A
N3X–H3XA	0.88	2.951(9)	2.13	156	O23A^{2}
N3X–H3XB	0.88	2.857(8)	2.00	164	O25A^{2}
N4X–H4XA	0.88	3.144(10)	2.38	145	O23A^{2}
N4X–H4XB	0.88	2.929(7)	2.09	160	O5A^{3}
N1Y–H1YA	0.88	2.96(2)	2.12	158	O23W^{2}
N1Y–H1YB	0.88	2.88(2)	2.35	118	O5
N2Y–H2YA	0.88	2.725(19)	1.89	157	O30W^{2}
N2Y–H2YB	0.88	2.849(15)	2.02	157	O30A^{2}
N3Y–H3YA	0.88	3.060(11)	2.30	144	O3A^{3}
N3Y–H3YB	0.88	2.841(14)	1.99	163	O15
N4Y–H4YA	0.88	2.868(16)	2.06	153	O2W
N4Y–H4YB	0.88	2.930(7)	2.09	159	O6A^{3}
N1K–H1KA	0.88	2.989(7)	2.13	166	O22A^{4}
N1K–H1KB	0.88	2.960(7)	2.17	149	O5A^{2}
N2K–H2KA	0.88	2.966(7)	2.15	153	O21A^{4}
N2K–H2KB	0.88	2.797(15)	2.01	149	O12W
N3K–H3KA	0.88	3.127(13)	2.37	144	O2A^{5}
N3K–H3KB	0.88	2.911(10)	2.11	150	O19A^{2}
N4K–H4KA	0.88	3.062(11)	2.28	148	O2A^{5}
N4K–H4KB	0.88	2.969(15)	2.10	167	O15
N1L–H1LA	0.88	3.06(3)	2.28	147	O36W^{8}
N1L–H1LB	0.88	3.18(2)	2.43	142	O5W^{8}
N2L–H2LA	0.88	3.06(4)	2.20	167	O33W^{6}
N2L–H2LB	0.88	2.779(17)	1.91	168	O9^{6}
N3L–H3LA	0.88	3.003(17)	2.16	161	O3A^{9}
N3L–H3LB	0.88	3.14(2)	2.34	152	O141^{8}
N4L–H4TA	0.88	2.990(19)	2.12	168	O1A^{9}
N4L–H4TB	0.88	2.94(3)	2.13	155	O1WL^{10}
N1M–H1MA	0.88	2.84(2)	2.04	151	O271
N1M–H1MB	0.88	2.88(2)	2.05	159	O3W
N2M–H2MA	0.88	2.894(12)	2.11	148	O271
N2M–H2MB	0.88	3.11(3)	2.25	164	O29
N3M–H3MA	0.88	3.096(16)	2.35	143	O21^{1}
N3M–H3MB	0.88	2.803(16)	1.94	164	O261^{1}
N4M–H4MA	0.88	2.952(11)	2.15	150	O21^{1}
N4M–H4MB	0.88	2.798(10)	1.93	169	O19^{4}
N1N–H1NA	0.88	2.87(2)	2.07	150	O38W
N1N–H1NB	0.88	2.835(12)	1.98	164	O30
N2N–H2NA	0.88	3.220(17)	2.43	149	O1
N2N–H2NB	0.88	2.845(13)	2.15	136	O18A^{1}
N3N–H3NA	0.88	2.914(6)	2.12	150	O22^{8}
N3N–H3NB	0.88	2.862(6)	2.07	149	O11A^{1}
N4N–H4NA	0.88	2.924(18)	2.13	149	O1W^{8}
N4N–H4NB	0.88	2.915(7)	2.14	147	O18^{8}
N1T–H1TA	0.88	2.906(6)	2.13	147	O23^{8}

N1T–H1TV	0.88	2.815(7)	1.96	162	O19
N2T–H2TA	0.88	2.998(7)	2.35	131	O23
N2T–H2TB	0.88	2.813(6)	1.97	161	O11A[1]
N3T–H3TA	0.88	3.16(2)	2.48	135	O2[9]
N3T–H3TB	0.88	2.89(3)	2.04	160	O1WT
N4T–H4TA	0.88	3.308(18)	2.55	144	O1[9]
N4T–H4TB	0.88	2.788(19)	1.99	150	O6
N1V–H1VA	0.88	3.08(3)	2.35	141	O1WV
N1V–H1VB	0.88	2.94(2)	2.13	154	O19W
N2V–H2VA	0.88	2.83(3)	2.01	155	O1WV
N2V–H2VB	0.88	2.95(2)	2.08	169	O6W
N3V–H3VA	0.88	3.021(12)	2.19	157	O22[8]
N3V–H3VB	0.88	2.832(14)	2.06	146	O9A[5]
N4V–H4VA	0.88	2.827(10)	1.96	167	O21[8]
N4V–H4VB	0.88	2.809(13)	2.06	142	O1WZ
C–H···O hydrogen bonds between pentamidine and isopropanol molecules					
C6L–H6L	0.95	3.417(17)	2.50	162	O1R
C–H···O hydrogen bonds between C8S and ethanol, isopropanol molecules					
C14A–H14A	0.99	3.187(15)	2.30	149	O1R
C42A–H42T	0.99	3.367(8)	2.44	156	O1S[2]
C42–H42B	0.99	3.408(10)	2.43	169	O1I
C–H···O hydrogen bonds between pentamidine and C8S / water molecules					
C3X–H3X	0.95	3.270(10)	2.54	134	O26A
C7X–H7X	0.95	3.177(18)	2.58	121	O14W
C12X–H12J	0.99	3.287(11)	2.57	129	O27A
C15X–H15X	0.95	3.361(9)	2.45	161	O25A[2]
C17X–H17X	0.95	3.391(11)	2.45	171	O5A[3]
C7Y–H7Y	0.95	3.477(17)	2.53	174	O9W
C3K–H3K	0.95	3.500(7)	2.58	162	O5A
C15K–H15K	0.95	3.355(15)	2.59	138	O15
C14L–H14L	0.95	3.27(2)	2.44	145	O170
C3M–H3M	0.95	3.29(2)	2.47	145	O31
C10M–H10N	0.99	3.42(2)	2.58	144	O31A
C12M–H12O	0.99	3.21(2)	2.52	132	O14W
C17M–H17M	0.95	3.12(2)	2.26	151	O19[4]
C15T–H15T	0.95	3.37(2)	2.58	141	O1WT
C–H···O hydrogen bonds between C8S molecules					
C21–H21B	0.99	3.481(9)	2.59	150	O28A[2]
C23A–H23A	0.95	3.092(9)	2.39	130	O28[1]

Symmetry operations: [1](1/2–x,3/2–y,–z), [2](1–x,y,1/2–z), [3](1/2+x,1/2+y,z), [4](–1/2+x,–1/2+y,z), [5](1/2–x,3/2–y,–z), [6](3/2–x,3/2–y,–z), [7](–1/2+x,1/2+y,z), [8](1–x,2–y,–z), [9](1–x,1–y,–z), [10](x,1–y, –1/2+z).

Table 72. The parameters of X–H···π interactions. Distances (d) are given in Å, angles in °.

D – H	**d(D – H)**	**d(D···A)**	**d(H···A)**	**<D – H···A**	**A**
C–H···π interactions between pentamidine and C8S molecules					
C8X–H8XB	0.99	3.569(10)	2.58	177	Cg(C43–C48)
C6Y–H6Y	0.95	3.909(13)	2.96	176	Cg(C15–C20)
C17Y–H17Y	0.95	3.336(8)	2.76	120	Cg(C29–C34)

C9L–H9LB	0.99	3.58(3)	2.73	143	Cg(C22A–C27A)
C8M–H8MA	0.95	3.579(14)	2.61	167	Cg(C50A–C55A)
C17N–H17N	0.95	3.407(6)	2.58	145	Cg(C8A–C13A)
C8V–H8VB	0.99	3.71(3)	2.91	139	Cg(C22–C27)
C9V–H9VA	0.99	3.586(16)	2.86	131	Cg(C15–C20)
C–H···π interactions between pentamidine molecules					
C9Y–H9YB	0.99	3.548(17)	2.85	128	Cg(C2X–C7X)
C8K–H8KB	0.99	3.726(8)	2.93	138	Cg(C2L–C7L)[1]
C12N–H12C	0.99	3.555(15)	2.83	131	Cg(C13M–C18M)

Symmetry operations: [1](–x,y,1/2–z).

Cg – centroid of pentamidine / C8S aromatic ring.

Table 73. The parameters of π···π interactions. Distances (d) are given in Å.

CgA	d(CgA···CgB)	CgB
π···π interactions between C8S and pentamidine molecules		
Cg(C8–C13)	3.995(6)	Cg(C13T–C18T)
Cg(C22–C27)	3.943(5)	Cg(C13Y–C18Y)
Cg(C29–C34)	3.756(3)	Cg(C2T–C7T)
Cg(C50–C55)	3.693(5)	Cg(C2N–C7N)[1]
Cg(C15A–C20A)	3.841(4)	Cg(C13N–C18N)
Cg(C29A–C34A)	3.886(4)	Cg(C13K–C18K)
Cg(C50A–C55A)	3.719(6)	Cg(C2Y–C7Y)[2]
π···π interactions between pentamidine molecules		
Cg(C13L–C18L)	3.871(6)	Cg(C13K–C18K)[3]
Cg(C2T–C7T)	3.734(9)	Cg(C13V–C18V)[4]

Symmetry operations: [1](1/2–x,3/2–y,–z), [2](1–x,y,1/2–z), [3](–x,y,1/2–z), [4](1/2–x,3/2–y,–z).

Cg – centroid of pentamidine / C8S aromatic ring.

Structure of the complex C4S_P4P

Table 74. The parameters of hydrogen bonds. Distances (d) are given in Å, angles in °.

D – H	d(D – H)	d(D···A)	d(H···A)	<D – H···A	A
O–H···O intramolecular hydrogen bonds at C4S lower rim					
O4–H4	0.84	2.705(3)	1.90	161	O8
O4–H4	0.84	2.905(4)	2.55	106	O12[1]
O8–H8	0.84	2.567(3)	1.76	162	O12
O12–H12	0.84	2.567(3)	1.84	144	O8
O12–H12	0.84	2.930(3)	2.49	114	O8[1]
C–H···O interactions between P4P and C4S molecules					
C2X–H2X	0.97(7)	3.237(12)	2.45(7)	139(6)	O10[2]
C6X–H6X	0.99(4)	3.235(8)	2.39(4)	144(3)	O3[2]
C5Y–H5Y	0.95	3.31(2)	2.42	157	O6[3]
C8Y–H8Y	0.95	3.39(2)	2.52	153	O6
C–H···O interactions between P4P and water molecules					
C3X–H3X	0.85(6)	3.381(10)	2.54(6)	169(5)	O9W[2]
C3X–H3X	0.85(6)	3.110(16)	2.44(6)	136(5)	O10W[2]
C5X–H5X	0.99(6)	3.447(10)	2.48(6)	166(5)	O9W[4]

C5X–H5X	0.99(6)	3.38(3)	2.43(6)	163(5)	O8W[4]
C7X–H7X	1.04(6)	3.205(12)	2.23(6)	157(4)	O11W[3]
C1Y–H1Y	0.95	3.409(19)	2.52	156	O6W
C4Y–H4Y	0.95	3.210(13)	2.45	137	O11W

Symmetry operations: [1](1–x,1–y,z), [2](x,y,–z), [3](1–x,–y,z), [4](1–x,–y,–z).

Table 75. The parameters of X–H···π interactions. Distances (d) are given in Å, angles in °.

D – H	d(D – H)	d(D···A)	d(H···A)	<D – H···A	A
C–H···π interactions between P4P and C4S molecules					
C1X–H1XA	0.99	3.766(5)	2.84(6)	159(5)	Cg(C1–C2–C3–C4–C3_a[1]–C2_a[1])
C1X–H1XB	1.02	3.735(5)	2.75(5)	164(4)	Cg(C13–C14–C15–C16–C15_a[1]–C14_a[1])

Symmetry operations: [1](x,y,–z)

Cg – centroid of C4S aromatic ring.

Table 76. The parameters of π···π interactions. Distances (d) are given in Å.

CgA	d(CgA···CgB)	CgB
π···π interactions between P4P and C4S molecules		
Cg(C6–C11)	3.953(19)	Cg(N1X–C2X–C3X–C4A–C5X–C6X)
Cg(C1–C2–C3–C4–C3_a[1]–C2_a[1])	3.450(2)	Cg(N2Y–C5Y–C4Y–C3Y–C4Y_g[2]–C5Y_g[2])[3]

Symmetry operations: [1](x,y,–z), [2](–y,x,1/2–z), [3](–y,x,–1/2+z).

Cg – centroid of P4P / C4S aromatic ring.

Structure of the complex C4S_P6P

Table 77. The parameters of hydrogen bonds. Distances (d) are given in Å, angles in °.

D – H	d(D – H)	d(D···A)	d(H···A)	<D – H···A	A
O–H···O intramolecular hydrogen bonds at C4S lower rim					
O4–H4	0.84	2.764(10)	1.99	154	O8
O8–H8	0.84	2.752(11)	2.09	136	O12
O12–H12	0.84	2.791(15)	2.14	134	O16
O16–H16B	0.84	2.771(8)	1.98	157	O4
O20–H20B	0.84	2.736(7)	1.92	163	O32
O24–H24	0.84	2.872(7)	2.20	137	O20
O28–H28	0.84	2.733(6)	1.91	165	O24
O32–H32	0.84	2.898(7)	2.31	128	O28
O36–H36	0.84	2.746(9)	1.99	150	O40
O40–H40	0.84	2.803(8)	2.23	126	O44
O44–H44	0.84	2.733(9)	2.03	135	O48
O48–H48	0.84	2.820(7)	2.23	127	O36
O–H···O hydrogen bonds between C4S molecules					
O24–H24	0.84	2.770(6)	2.16	130	O34[1]
O40–H40	0.84	3.08(3)	2.47	130	O41[2]
O–H···O hydrogen bonds between C4S and water molecules					
O4–H4	0.84	2.837(18)	2.43	111	O20W[3]
O8–H8	0.84	3.05(3)	2.40	135	O48W
O32–H32	0.84	2.654(11)	1.99	136	O4W[4]
C–H···O interactions between P6P and C4S molecules					

C7X–H7X	0.95	3.293(12)	2.47	145	O47
C14X–H14X	0.95	3.113(12)	2.32	141	O29
C18X–H18A	0.99	3.104(11)	2.34	133	O17
C25X–H25X	0.95	3.080(9)	2.26	144	O31
C26X–H26X	0.95	3.199(10)	2.46	135	O46[5]
C29X–H29X	0.95	3.328(11)	2.58	136	O23
C32X–H32X	0.95	3.243(10)	2.35	157	O45
C34X–H34X	0.95	3.26(3)	2.52	135	O5[6]
C35X–H35X	0.95	3.234(17)	2.32	161	O10
C36X–H36B	0.99	3.183(10)	2.43	133	O33
C11Y–H11Y	0.95	3.05(3)	2.19	149	O9
C12Y–H12C	0.99	3.37(3)	2.44	156	O38[7]
C16Y–H16Y	0.95	3.28(3)	2.56	133	O26
C23Y–H23Y	0.95	3.11(3)	2.24	153	O18[7]
C32Y–H32Y	0.95	3.19(3)	2.60	120	O11
C34Y–H34Y	0.95	2.81(4)	2.39	106	O6
C–H···O interactions between P6P and water molecules					
C12X–H12A	0.99	3.22(3)	2.59	121	O17W
C13X–H13X	0.95	3.21(18)	2.26	178	O32W
C17X–H17X	0.95	3.36(2)	2.44	162	O42W
C22X–H22X	0.95	3.334(10)	2.41	165	O9W
C31X–H31X	0.95	3.354(15)	2.50	150	O12W[5]
C36X–H36A	0.99	3.306(12)	2.51	137	O8W
C1A–H1A	0.95	3.28(7)	2.26	162	O72W[6]
C6A–H6AB	0.99	3.25(4)	2.29	164	O71W[8]
C7Y–H7Y	0.95	2.93(3)	2.02	161	O71W[8]
C13Y–H13Y	0.95	3.16(3)	2.50	126	O21W[7]
C13A–H13A	0.95	3.18(3)	2.53	126	O21W[7]
C14A–H14A	0.95	3.18(4)	2.59	120	O21W[7]
C16A–H16A	0.95	3.21(4)	2.43	139	O23W
C18Y–H18C	0.99	3.06(4)	2.08	173	O23W
C19Y–H19Y	0.95	2.99(3)	2.08	161	O24W
C20Y–H20Y	0.95	3.11(4)	2.30	143	O36W
C22Y–H22Y	0.95	3.29(3)	2.50	141	O55W[7]
C24Y–H24C	0.99	3.58(7)	2.60	170	O50W[7]
C26A–H26A	0.95	3.03(5)	2.11	163	O64W[6]
C28Y–H28Y	0.95	2.65(3)	1.97	126	O29W
C29Y–H29Y	0.95	2.88(4)	2.45	107	O29W
C29Y–H29Y	0.95	2.49(3)	1.56	165	O51W[5]
C34A–H34A	0.95	3.49(3)	2.56	166	O40W[6]
C–H···O interactions between C4S and water molecules					
C20–H20	0.95	3.397(17)	2.45	176	O18W
C23–H23	0.95	3.332(13)	2.59	136	O18W
C49–H49B	0.99	3.411(11)	2.44	166	O4W[4]
C–H···O interactions between C4S molecules					
C9–H9	0.95	3.372(14)	2.51	150	O35[6]
C13–H13	0.95	3.13(3)	2.30	146	O7[6]
C14–H14B	0.99	3.10(3)	2.21	149	O7[6]
C28–H28B	0.99	3.262(14)	2.30	165	O22[8]

C35–H35B	0.99	3.472(12)	2.50	169	O1[8]
C49–H49A	0.99	3.493(10)	2.54	163	O48[5]
C70–H70A	0.99	3.452(12)	2.48	168	O26[9]
C77–H77A	0.99	3.353(10)	2.53	141	O25[5]

Symmetry operations: [1](x,1+y,z), [2](2–x,2–y,–z), [3](2–x,3–y,1–z), [4](1–x,3–y,–z), [5](1–x,2–y,–z), [6](1–x,2–y,1–z), [7](–1+x,–1+y,z), [8](1–x,3–y,1–z), [9](1+x,y,z).

Table 78. The parameters of X–H···π interactions. Distances (d) are given in Å, angles in °.

D – H	d(D – H)	d(D···A)	d(H···A)	<D – H···A	A
C–H···π interactions between P6P and C4S molecules					
C4X–H4X	0.95	3.456(8)	2.90	118	Cg(C78–C83)
C5X–H5X	0.95	3.514(8)	2.57	172	Cg(C57–C62)
C6X–H6XA	0.99	3.352(11)	2.63	130	Cg(C71–C76)
C19X–H19X	0.95	3.584(9)	2.64	176	Cg(C29–C34)
C24X–H24B	0.99	3.470(12)	2.85	122	Cg(C43–C48)
C5Y–H5Y	0.95	3.29(2)	2.35	170	Cg(C8–C13)
C6Y–H6YB	0.99	3.61(2)	2.80	140	Cg(C22–C27)
C30Y–H30C	0.99	2.93(4)	2.28	122	Cg(C8–C13)[1]
C13–H13	0.95	3.31(2)	2.86	110	Cg(N6Y–C35Y)[1]
C–H···π interactions between P6P molecules					
C10Y–H10Y	0.95	3.51(3)	2.85	128	Cg(N3Y–C17Y)
C20Y–H20Y	0.95	3.50(3)	2.82	129	Cg(N5Y–C29Y)

Symmetry operation: [1](1–x,2–y,1–z).

Cg – centroid of P6P / C4S aromatic ring.

Table 79. The parameters of π···π interactions. Distances (d) are given in Å.

CgA	d(CgA···CgB)	CgB
π···π interactions between P6P and C4S molecules		
Cg(N3Y–C17Y)	3.597(15)	Cg(C64–C69) [1]
π···π interactions between C4S molecules		
Cg(C22–C27)	3.744(5)	Cg(C22–C27)[2]
Cg(C36–C41)	3.654(4)	Cg(C1–C6)[2]
Cg(C57–C62)	3.637(4)	Cg(C29–C34)[3]
Cg(C71–C76)	3.607(6)	Cg(C71–C76)[4]

Symmetry operations: [1](–1+x,y,z), [2](1–x,3–y,1–z),[3](x,–1+y,z), [4](2–x,2–y,–z).

Cg – centroid of P6P / C4S aromatic ring.

Structure of the complex C8S_Na

Table 80. The parameters of hydrogen bonds. Distances (d) are given in Å, angles in °.

D – H	d(D – H)	d(D···A)	d(H···A)	<D – H···A	A
O–H···O intramolecular hydrogen bonds at C8S lower rim					
O4–H4	0.84	2.691(8)	1.86	173	O16[1]
O8–H8A	0.84	2.672(9)	1.97	141	O4
O12–H12A	0.84	2.651(8)	1.96	139	O8
O16–H16	0.84	2.640(7)	1.99	133	O12

O20–H20	0.84	2.706(8)	1.87	174	O24
O24–H24	0.84	2.727(9)	1.89	174	O28
O28–H28	0.84	2.688(8)	1.85	172	O32
O32–H32A	0.84	2.674(7)	1.87	160	O20[2]

Symmetry operations: [1](–x,y,1/2–z), [2](1–x,y,1/2–z).

Table 81. The coordination distances between sodium cations and C8S, water molecules. Distances (d) are given in Å.

Metal	d(Na···O)	O
Na1	2.283(9)	O10[1]
	2.323(7)	O15
	2.392(7)	O17[1]
	2.416(8)	O29[2]
	2.602(9)	O2W
	2.322(12)	O18W
Na2	2.325(7)	O1
	2.366(7)	O3[3]
	2.739(7)	O21[4]
	2.381(6)	O22[4]
	2.321(8)	O23[5]
	2.385(9)	O5W[3]
Na3	2.361(9)	O6[4]
	2.844(7)	O25[5]
	2.633(10)	O27[5]
	2.435(8)	O1W
	2.356(8)	O3W
	2.502(15)	O11W
Na4	2.278(7)	O2[4]
	2.462(7)	O21[6]
	2.340(9)	O22
	2.416(9)	O9W
	2.369(10)	O10W
	2.45(3)	O12W
Na5	2.292(8)	O7
	2.292(8)	O7[7]
	2.385(7)	O25[6]
	2.385(7)	O25[8]
	2.483(11)	O6W
	2.483(11)	O6W[7]
Na6	2.399(8)	O11
	2.591(8)	O14[1]
	2.518(7)	O15[1]
	2.367(8)	O18
	2.564(8)	O29[5]
	2.350(13)	O17W
Na7	2.267(8)	O5
	2.399(8)	O31[6]
	2.792(12)	O1W
	2.435(16)	O4W

	2.490(12)	O6W[7]
	2.178(13)	O11W
Na8	2.422(9)	O3
	2.46(2)	O14A
	2.385(15)	O4W
	2.343(11)	O5W
	2.768(14)	O9W[4]
	2.60(3)	O13W
Na9	2.361(10)	O10
	2.883(11)	O11
	2.386(11)	O18
	2.397(14)	O7W
	2.397(14)	O8W
	2.237(15)	O18W

Symmetry operations: [1](1/2–x,1/2+y,1/2–z), [2](1–x,y,1/2–z), [3](–1/2–x,1/2–y,–z), [4](–x,–y,–z), [5](–1/2+x,–1/2+y,z), [6](1/2–x,1/2–y,–z), [7](–x,1–y,–z), [8](–1/2+x,1/2+y,z).

Table 82. The parameters of X–H···π interactions. Distances (d) are given in Å, angles in °.

D – H	d(D – H)	d(D···A)	d(H···A)	<D – H···A	A
C–H···π interactions between C8S molecules					
C20–H20A	0.99	3.727(8)	2.97	134	Cg(C30–C35)[1]
C27–H27A	0.99	3.492(8)	2.73	134	Cg(C37–C42)[2]
C29–H29B	0.99	3.712(8)	2.98	131	Cg(C14–C19)[1]
C36–H36A	0.99	3.638(8)	2.95	128	Cg(C21–C26)[2]
C43–H43A	0.99	3.774(9)	2.97	139	Cg(C1–C28_a[5])[3]
C43–H43A	0.99	3.773(9)	2.97	139	Cg(C28–C1_a[5]–C2_a[5]–C3_a[5]–C4_a[5]–C5_a[5])[1]
C50–H50B	0.99	3.537(8)	2.81	131	Cg(C7–C12)[4]

Symmetry operations: [1](1/2–x,1/2+y,1/2–z), [2](1/2–x,–1/2+y,1/2–z), [3](1/2+x,1/2+y,z), [4](1/2+x,–1/2+y,z), [5](–x,y,1/2–z).
Cg – centroid of C8S aromatic ring.

Structure of the complex C8S_Berb

Table 83. The parameters of hydrogen bonds. Distances (d) are given in Å, angles in °.

D – H	d(D – H)	d(D···A)	d(H···A)	<D – H···A	A
O–H···O hydrogen bonds at C8S lower rim					
O4–H4	0.84	2.703(6)	1.87	172	O8
O8–H8	0.84	2.609(7)	1.85	150	O1W
O12–H12	0.84	2.757(7)	2.16	128	O6W
O16–H16	0.84	2.685(6)	1.85	174	O11[1]
C–H···O interactions between Berb and C8S molecules					
C9I–H9IB	0.99	3.519(11)	2.57	159	O1
C4X–H4X	0.95	3.368(9)	2.44	165	O2[2]
C9X–H9XB	0.99	3.130(10)	2.42	128	O6[3]
C20X–H20I	0.98	3.194(10)	2.38	140	O15
C8–H8B	0.99	3.366(9)	2.42	160	O2X
C1Y–H1YA	0.99	3.432(8)	2.59	143	O12[3]
C4Y–H4Y	0.95	3.239(9)	2.40	146	O15

C14Y–H14Y	0.95	3.194(10)	2.34	149	O7[3]
C18Y–H18Y	0.95	3.263(11)	2.44	145	O7[3]
C14Z–H14Z	0.95	3.303(15)	2.50	142	O10
C18Z–H18Z	0.95	3.176(12)	2.25	165	O9
C20Z–H20O	0.98	3.308(16)	2.58	131	O12[3]
C14–H14	0.95	3.091(11)	2.40	130	O3Z[3]
C–H···O interactions between Berb molecules					
C19I–H19A	0.98	3.232(18)	2.46	136	O1X[4]
C–H···O interactions between Berb and water molecules					
C11I–H11I	0.95	3.335(13)	2.39	172	O4W[5]
C17Y–H17Y	0.95	3.346(11)	2.42	164	O7W
C11Z–H11Z	0.95	3.291(15)	2.43	150	O11W[3]
C–H···O interactions between C8S and water molecules					
C15–H15A	0.99	3.259(9)	2.59	125	O1W

Symmetry operations: [1](2–x,1–y,1–z), [2](2–x,–y,–z), [3](–1+x,y,z), [4](1–x,–y,–z), [5](1–x,–y,1–z).

Table 84. The parameters of X–H···π interactions. Distances (d) are given in Å, angles in °.

D – H	d(D – H)	d(D···A)	d(H···A)	<D – H···A	A
C–H···π interactions between Berb and C8S molecules					
C7I–H7I	0.95	3.381(10)	2.51	153	Cg(C23–C28)[1]
C19I–H19B	0.98	3.633(15)	2.78	145	Cg(C2–C7)[2]
C19X–H19I	0.98	3.486(7)	2.76	131	Cg(C9–C14)[3]
C–H···π interactions between Berb molecules					
C19Z–H19O	0.98	3.396(11)	2.61	137	Cg(C2I–C7I)[4]
C4I–H4I	0.95	3.382(13)	2.91	111	Cg(C12Z–C18Z)[5]

Symmetry operation: [1](2–x,–y,1–z), [2](–1+x,y,z), [3](1+x,y,z), [4](1+x,1+y,z), [5](–1+x,–1+y,z).

Cg – centroid of Berb / C8S aromatic ring.

Table 85. The parameters of π···π interactions. Distances (d) are given in Å.

CgA	d(CgA···CgB)	CgB
π···π interactions between Berb molecules		
Cg(N1I–C14I)	3.856(6)	Cg(C12X–C18X)[1]
Cg(C12I–C18I)	3.778(6)	Cg(C12X–C18X)[1]
Cg(C12I–C18I)	3.719(8)	Cg(C2Z–C7Z)[2]
Cg(C2X–C7X)	3.784(4)	Cg(C12Y–C18Y)

Symmetry operations: [1](–1+x,y,z), [2](1+x,1+y,z).

Cg – centroid of Berb ring.

Structure of the complex C8S_IPR_I

Table 86. The parameters of hydrogen bonds. Distances (d) are given in Å, angles in °.

D – H	d(D – H)	d(D···A)	d(H···A)	<D – H···A	A
O–H···O hydrogen bonds at C8S lower rim					
O4–H4	0.84	2.822(4)	2.09	145	O2W[1]
O8–H8	0.84	2.720(4)	1.89	170	O15[2]
O12–H12	0.84	2.676(5)	1.91	150	O4W[3]
O16–H16	0.84	2.760(4)	2.00	150	O6

N–H···O interactions between iproniazid and C8S / water molecules					
N1X–H1X1	0.88	2.715(5)	1.86	165	O5
N2X–H2X1	0.88	2.741(5)	1.96	147	O13
N3X–H3X1	0.91	2.774(5)	1.89	162	O3W[4]
N3X–H3X2	0.91	2.671(6)	1.77	174	O7W
N1Y–H1Y1	0.88	2.812(5)	2.10	138	O1W
N1Y–H1Y1	0.88	2.878(4)	2.19	135	O7
N2Y–H2Y1	0.88	2.768(5)	1.93	159	O11[5]
N3Y–H3Y1	0.91	2.838(6)	1.88	155	O14[6]
N3Y–H3Y2	0.91	2.635(7)	1.75	163	O9W
C–H···O interactions between iproniazid and C8S molecules					
C2X–H2X	0.95	3.471(6)	2.60	153	O2
C1Y–H1Y	0.95	3.010(5)	2.36	125	O12[3]
C2Y–H2Y	0.95	3.277(5)	2.53	136	O11[5]
C2Y–H2Y	0.95	3.094(6)	2.55	117	O12[3]
C4Y–H4Y	0.95	3.473(6)	2.58	157	O2[6]
C7Y–H7Y	1.00	3.140(7)	2.38	132	O10[5]
C9Y–H9Y2	0.95	3.443(7)	2.54	153	O15[6]

Symmetry operations: [1](x,–1+y,z), [2](1+x,y,z), [3](2–x,–y,2–z), [4](2–x,1–y,3–z), [5](–1+x,y,z)), [6](x,y,–1+z).

Table 87. The parameters of π···π interactions. Distances (d) are given in Å.

CgA	**d(CgA···CgB)**	**CgB**
π···π interactions between C8S and IPR molecules		
Cg(C22–C27)	3.865(3)	Cg(N1X–C5X)
Cg(C8–C13)	3.735(3)	Cg(N1Y–C5Y)[1]
π···π interactions between C8S molecules		
Cg(C15–C20)	3.926(3)	Cg(C15–C20)[2]

Symmetry operations: [1](2–x,–y,2–z), [2](3–x,–y,2–z).

Cg – centroid of IPR / C8S aromatic ring.

Structure of the complex C8S_IPR_II

Table 88. The parameters of hydrogen bonds. Distances (d) are given in Å, angles in °.

D – H	**d(D – H)**	**d(D···A)**	**d(H···A)**	**<D – H···A**	**A**
O–H···O hydrogen bonds at C8S lower rim					
O4–H4A	0.84	2.990(6)	2.52	116	O16
O4–H4A	0.84	2.763(6)	2.03	146	O1W[1]
O8–H8	0.84	2.838(14)	2.53	103	O15[2]
O12–H12	0.84	2.840(6)	2.05	157	O11[3]
O16–H16A	0.84	2.701(6)	1.96	146	O6
N–H···O interactions between iproniazid and C8S / water molecules					
N1X–H1XA	0.88	2.719(9)	1.94	147	O3[4]
N2X–H2XA	0.88	2.918(8)	2.26	132	O13
N3X–H3X1	0.91	2.821(8)	1.99	152	O2
N3X–H3X2	0.91	2.950(7)	2.19	140	O14
N1Y–H1YA	0.88	2.578(6)	1.73	159	O7
N2Y–H2Y1	0.88	2.773(6)	1.92	164	O11[5]
N3Y–H3Y1	0.91	2.810(13)	1.95	157	O14[6]

N3Y–H3Y2	0.91	3.183(17)	2.57	125	O3W[7]
C–H···O interactions between iproniazid and C8S molecules					
C5X–H5X	0.95	3.101(10)	2.39	131	O5
C8X–H8XB	0.98	3.297(11)	2.56	133	O9[4]
C9X–H9XC	0.98	3.093(13)	2.29	139	O2
C4Y–H4Y	0.95	3.017(8)	2.35	127	O4[1]
C–H···O interactions between C8S molecules					
C7–H7B	0.99	3.326(12)	2.46	146	O15[2]
C14–H14A	0.99	3.458(7)	2.50	163	O11[3]

Symmetry operations: [1](1–x,1–y,1–z), [2](–1+x,y,z), [3](–x,1–y,1–z), [4](1–x,2–y,1–z), [5](1+x,y,z), [6](x,–1+y,1+z), [7](1–x,1–y,2–z).

Table 89. The parameters of π···π interactions. Distances (d) are given in Å.

CgA	**d(CgA···CgB)**	**CgB**
π···π interactions between C8S and IPR molecules		
Cg(C8–C13)	3.752(3)	Cg(N1Y–C5Y)[1]
π···π interactions between C8S molecules		
Cg(C15–C20)	3.670(3)	Cg(C15–C20)[2]

Symmetry operations: [1](1–x,1–y,1–z), [2](–x,1–y,1–z).

Cg – centroid of IPR / C8S aromatic ring.